UNIVERSIDAD COMPLUTENSE DE MADRID
FACULTAD DE FARMACIA

TESIS DOCTORAL

New multitarget theranostic compounds against proteinopathies and infectious diseases

Nuevos compuestos teranósticos multidiana contra proteinopatías y enfermedades infecciosas

MEMORIA PARA OPTAR AL GRADO DE DOCTOR

PRESENTADA POR

Marta Piquero Martí

Directores

José Carlos Menéndez Ramos
M. Pilar López-Alvarado Gutiérrez

Madrid

UNIVERSIDAD COMPLUTENSE DE MADRID
FACULTAD DE FARMACIA
Unidad Docente de Química Orgánica y Farmacéutica,
Departamento de Química en Ciencias Farmacéuticas

TESIS DOCTORAL

NEW MULTITARGET THERANOSTIC COMPOUNDS AGAINST PROTEINOPATHIES AND INFECTIOUS DISEASES

NUEVOS COMPUESTOS TERANÓSTICOS MULTIDIANA CONTRA PROTEINOPATÍAS Y ENFERMEDADES INFECCIOSAS

Marta Piquero Martí

Directores:
José Carlos Menéndez Ramos
M. Pilar López-Alvarado Gutiérrez

Madrid, 2020

There is no gate, no lock, no bolt
that you can set upon the freedom of my mind.
Virginia Woolf

Index

ABBREVIATIONS

Aβ	Amyloid β
AChE	Acetylcholinesterase
AD	Alzheimer´s disease
ALS	Amyotrophic Lateral Sclerosis
APP	Amyloid protein precursor
ARE	Antioxidant response element
BACE-1	β-Site amyloid cleaving enzyme 1
BBB	Blood brain barrier
BLA	Bond length alternation
BODIPY	Boron dipyrromethane
BuChe	Butyrylcholinesterase
CAN	Cerium(IV) ammonium nitrate
CAT	Catalase
CDK5	cyclin-dependent-like kinase 5
CNS	Central nervous system
COX	Cyclooxygenase
CR	Congo Red
CRD	Carbohydrate recognition domain
CT	Computed Tomography
DANIR	Donor-Acceptor Near-Infrared
DCF	Dichlorofluorescein
DFCA	2,7-Dichlorofluorescin acetate
DMAQ	Demethylasterriquinone
DMP	Dess Martin Periodinane
DOTA	1,4,7,10-Tetraazacyclododecane-1,4,7,10-tetraacetic acid
DS-TB	Drug-susceptible tuberculosis
DTPA	2-[Bis[2-[bis(carboxymethyl)amino]ethyl]amino]acetic acid
EMB	Etambutol
FI	Fluorescence imaging
FRI	Fluorescence reflectance imaging
FMT	Fluorescence molecular tomography
HAS	Human serum albumin
hIAPP	Human Islet amyloid polypeptide
HIV	Human immunodeficiency virus
HOMO	Highest occupied molecular orbital
HSVM	High speed vibration milling
HYNIC	Hydrazinonicotinic acid
IAPP	Islet amyloid polypeptide
IDP	Intrinsically disordered protein
INH	Isoniazid
kDNA	Kinetoplastid DNA
LDH	Lactate dehydrogenase
LUMO	Lowest unoccupied molecular orbital
MBFT	Multiple bond-forming transformations
MCRs	Multicomponent reactions

MDR-TB	Multidrug resistance tuberculosis
MmpL	*Mycobacterium* membrane protein large
MRI	Magnetic resonance Imaging
MS	Multiple sclerosis
MSOT	Multispectral optoacoustic tomography
MTDL	Multitarget directed ligands
Mtb	*Mycobacterium tuberculosis*
MTR	MitoTracker Red
MVB	Multivesicular bodies
NAT	*N*-acetyltransferase
NIRF	Near-infrared fluorescence
NDD	Neurodegenerative diseases
NGF	Nerve growth factor
NIR-I	First near-infrared
NIR-II	Second near-infrared
NMR	Nuclear magnetic resonance
NOS	Reactive nitrogen species
NTDs	Neglected tropical diseases
OI	Optical Imaging
PAI	Photo Acoustic Imaging
PAMPA	Parallel artificial membrane permeability assay
PAS	*Para*-aminosalicylic acid
PBM	Planetary ball milling
PET	Positron emission tomography
PKA	Protein kinase A
PMDs	Protein misfolding diseases
PMF	Proton motive force
PP2A	Protein phosphatase 2A
PZA	Pyrazinamide
rIAPP	Rodent Islet amyloid polypeptide
RIF	Rifampicin
RND	Resistance nodulatiom division
ROS	Reactive oxygen species
SAR	Structure activity relationship
SI	Selectivity index
SM	Streptomycin
SOD	Superoxide dismutase
SPECT	Single Photon Emission Computed Tomography
T1DM	Type II Diabetes mellitus
T2DM	Type II Diabetes mellitus
TB	Tuberculosis
TDM	Trehalose dimycolate
ThS	Thioflavin S
ThT	Thioflavin T
TMH	Transmembrane α helices
TMM	Trehalose monomycolate
TNF	Tumoral necrosis factor

TPAP	Tetrapropylammonium perruthenate
USI	Ultrasound Imaging
WT	Wild type
XDR-TB	Extremely multidrug resistance tuberculosis

SUMMARY OF THE THESIS "NEW MULTITARGET THERANOSTIC COMPOUNDS AGAINST PROTEINOPATHIES AND INFECTIOUS DISEASE"

Introduction

Drug innovation is a long and high-cost process with no guarantee for success. Paradoxically, despite the great investment and innovations applied in the drug discovery field during the past decades, fewer successful drugs against etiologically complex maladies, such as neurodegenerative and cardiovascular diseases or cancer have been reported. Thus, new approaches in the drug discovery process need to be considered. In multifactorial pathologies, where several receptors or signalling pathways are involved, the inhibition of a single target often does not lead to successful drugs. In this context, the use of multitarget drugs inhibiting several checkpoints of the same disease appears as an attractive alternative. On the other hand, the failure of several drug candidates has been associated to their administration when the pathology is too advanced. In this scenario, theranostic compounds able to combine the modalities of therapy and diagnostic imaging under the same dose appear as a good option to optimize the efficacy and safety of the therapy. Moreover, combining both strategies in a single molecule appears as a promising approach for the treatment of these pathologies.

Objectives

- Design, synthesis and characterization of a family of small-molecule theranostic agents based on the 2-stryrylquinoline scaffold bearing a push-pull system in order to improve their spectroscopic properties.
- Design, synthesis and characterization of a family of 2-styrylquinolines decorated with polyamine chains in position 4 of the quinoline scaffold, increasing this way their basicity and consequently preferential mitochondrion accumulation.
- Development of a new one-pot mechanochemical methodology for the obtention of bis-indolylquinones, an interesting scaffold to develop MSOT probes.
- Design, synthesis and characterization of a family of multitarget directed ligands based on pyrrole isoniazid hybrids, able to inhibit MmpL3 and InhA, two different essential proteins for *Mycobacterium tuberculosis* survival.

Results and discussion

A family of theranostic styrylquinolines bearing a push-pull architecture has been designed and synthesized *via* a good-yielding four-step procedure. Their pharmacological profiles were studied by Drs. Paloma Bermejo and Sagrario Martín-Aragón, showing their ability to inhibit tau aggregation and neuroprotective effects in okadaic acid models. Their full spectroscopic characterization has been carried out with the collaboration of Drs. María Antonia Martín and Ana Isabel Olives, showing that the compounds have native fluorescence in the NIR region.

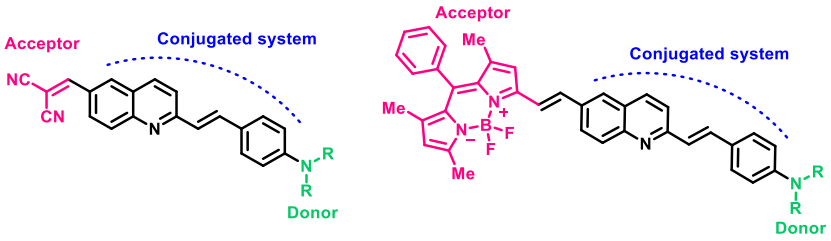

Further their ability to act as amyloid sensors has been verified with different amyloidogenic proteins. First, they were used for *ex-vivo* imaging, showing the capacity to selectively detect β-amyloid plaques in the somatosensory cortex of APP/PS1 transgenic mice and in the temporal cortex of human Alzheimer's disease samples. Due to the ability to interact with amyloidogenic proteins, styrylquinolines were also used to detect amylin, a pancreatic protein overexpressed in type II Diabetes mellitus that may be involved in the development of Alzheimer's disease. These studies were done in collaboration of Drs. Gonzalo León and Manuel Benito, respectively.

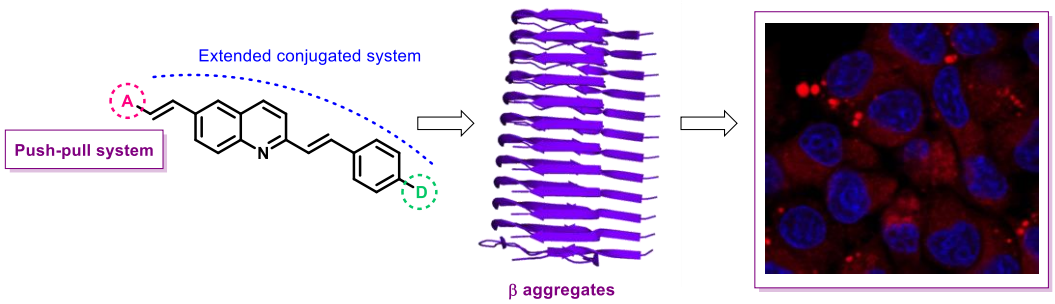

The leishmanicidal activity of a family of 4-amino-2-styrylquinolines was tested thanks to Dr. Luis Rivas, showing good activities and selectivity indexes for the best compounds.

Further mechanistical studies were carried out, pointing out their ability to cause mitochondrial disruption.

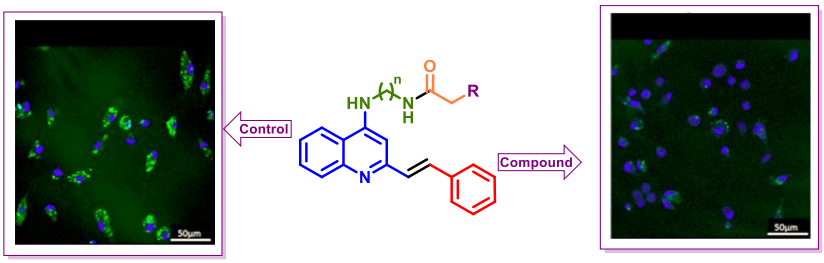

In order to achieve our goal of developing novel push-pull multi-spectral optoacoustic tomography (MSOT) probes, a new one-pot mechanochemical methodology to obtain dihalo-bis-indolylquinones as starting scaffolds has been developed.

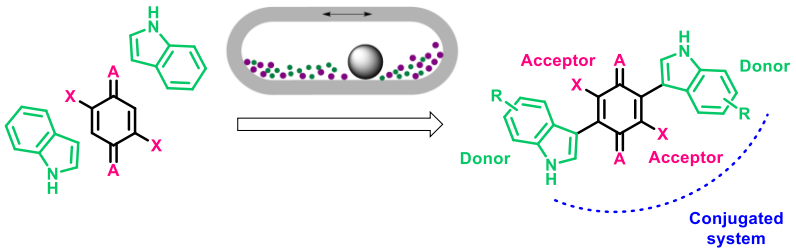

Finally, a novel family of pyrrole-isoniazid hybrid compounds have been synthesised. Their antitubercular activities have been studied, showing interesting activities against *Mycobacterium tuberculosis*, including multidrug-resistant tuberculosis. Further, their ability to inhibit MmpL3 and InhA was verified, proving that they act through a metabolism-activated multitargeting (MAMUT) mechanism.

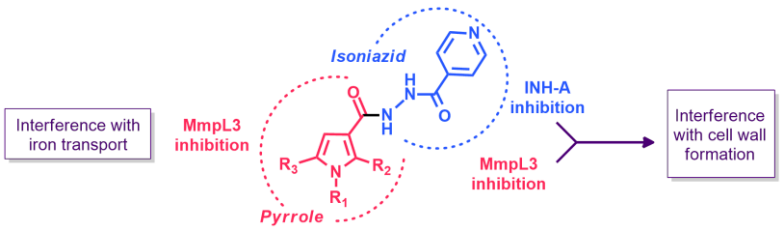

Conclusions

The work performed in this thesis shows that the theranostic and multitarget strategies are promising approaches towards the discovery of molecules that can be used as hits in the development of new drugs for the treatment of proteinopathies or infectious diseases.

RESUMEN DE LA TESIS "NUEVOS COMPUESTOS TERANÓSTICOS MULTIDIANA CONTRA PROTEINOPATÍAS Y ENFERMEDADES INFECCIOSAS"

Introducción

El proceso de descubrimiento de nuevos fármacos es un camino largo y costoso en el que el éxito no siempre está garantizado. Las grandes inversiones y nuevas tecnologías aplicadas en este proceso durante las últimas décadas, no se han visto reflejadas en el número de fármacos comercializados, especialmente en el caso de enfermedades de etiología compleja, como las neurodegenerativas las cardiovasculares o el cáncer. Por estos motivos, es necesario empezar a aplicar nuevas estrategias en el diseño de fármacos. En el caso de las enfermedades multifactoriales, que involucran diversos receptores y vías de señalización, la inhibición de una sola diana no conlleva un significativo efecto terapéutico. De esta manera, una estrategia prometedora sería el empleo de compuestos multidiana capaces de inhibir diferentes vías de señalización de manera simultánea. Por otro lado, la ineficacia de muchos fármacos en fases clínicas se achaca a su administración tardía, cuando las enfermedades están demasiado desarrolladas. En este contexto, el empleo de compuestos teranósticos capaces de detectar y tratar la enfermedad de manera simultánea parece una herramienta prometedora. La suma de ambas estrategias en una sola entidad química parece una metodología prometedora para el desarrollo de nuevos fármacos contra enfermedades neurodegenerativas.

Objetivos

En la presente tesis se han planteado los objetivos de desarrollar diferentes familias de compuestos basados en algunas de las estrategias anteriormente comentadas, frente a proteinopatías, entre las que se incluyen las enfermedades de Alzheimer y la diabetes mellitus tipo 2, o enfermedades infecciosas como la tuberculosis o leishmaniasis.

- En primer lugar, se planteó el diseño, síntesis y caracterización de una familia de agentes teranósticos basados en un núcleo de estirilquinolina. Para mejorar sus propiedades espectroscópicas se ha planteado el uso de una estrategia *push-pull*.

- En segundo lugar, se planteó el diseño, síntesis y caracterización de una familia de estirilquinolinas que posean cadenas poliamínicas en la position 4 del núcleo de quinolina, con el fin de incrementar así su basicidad y favorecer su acumulación mitocondrial, lo que resulta especialmente toxico para este tipo de parásitos.
- En tercer lugar, nos planteamos el desarrollo de una nueva metodología *one-pot* en condiciones mecano-químicas para el desarrollo de bis-indolilquinonas, compuestos interesantes para el posible desarrollo de sondas MSOT.
- Finalmente, nos planteamos el diseño, síntesis y caracterización de una quimioteca de compuestos multidiana con actividad antituberculosa, basados en estructuras hibridas pirrol-isoniazida, capaces de inhibir simultáneamente MmpL3 e InhA, ambas proteínas esenciales para la supervivencia de *Mycobacterium tuberculosis*.

Resultados y discusión

La familia de estirilquinolinas teranósticas ha sido sintetizada gracias a una ruta en cuatro pasos que nos permite obtener los compuestos deseados con buenos rendimientos. En primer lugar, sus propiedades farmacológicas han sido estudiadas gracias a la colaboración de las Drs. Paloma Bermejo y Sagrario Martín Aragón, que han confirmado sus propiedades neuro protectoras en un modelo de toxicidad celular por ácido okadaico, así como su capacidad de inhibir la agregación de la proteína tau. En segundo lugar, su complete caracterización espectroscópica, así como su capacidad para detectar agregados de distintas proteínas amiloidogénicas, ha sido realizada por las Dras. María Antonia Martín y Ana Isabel Olives.

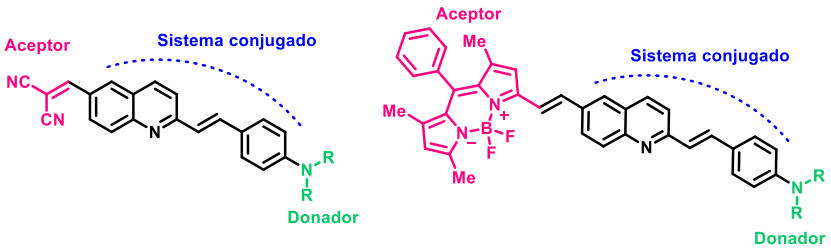

Finalmente, su capacidad de actuar como sensores de distintos tipos de agregados ha sido verificada. En primer lugar, gracias al Dr. Gonzalo León se evaluó su capacidad para detectar agregados de β-amiloide en muestras de corteza somatosensorial en un modelo transgénico de ratón (APP/PS1). Seguidamente, su capacidad para actuar como

sensores *ex-vivo* de β-amiloide fue evaluada en muestras humanas de corteza temporal de pacientes con la enfermedad de Alzheimer.

Debido a su capacidad de interactuar con agregados amiloides, las estiririlquinolinas fueron empleadas para detectar agregados de amilina, proteína sobreexpresada en diabetes mellitus tipo II que podría estar relacionada con el desarrollo de la enfermedad de Alzheimer en este tipo de pacientes. Este estudio se llevó a cabo en colaboración con el grupo dirigido por el Dr. Manuel Benito.

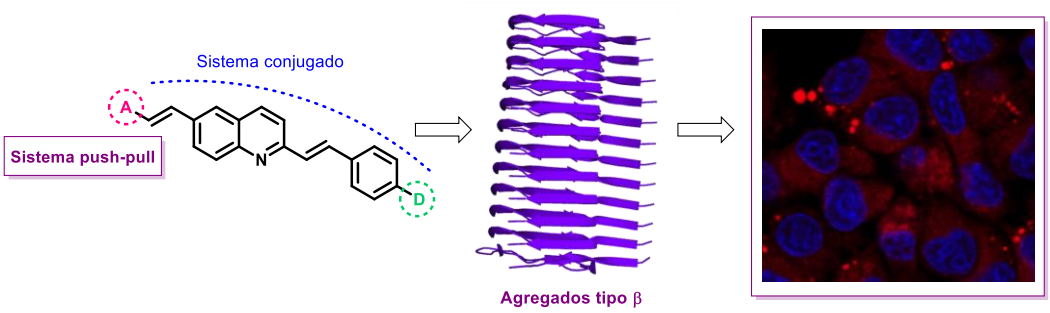

La actividad leishmanicida de la quimioteca de 4-amino-2 estirilquinolinas, fue evaluada gracias al grupo del Dr. Luis Rivas, presentando actividades e índices de selectividad prometedores. Debido a estos resultados, se realizaron diversos estudios mecanísticos que permitieron verificar la habilidad de estos compuestos para alterar la polarización de la membrana mitocondrial.

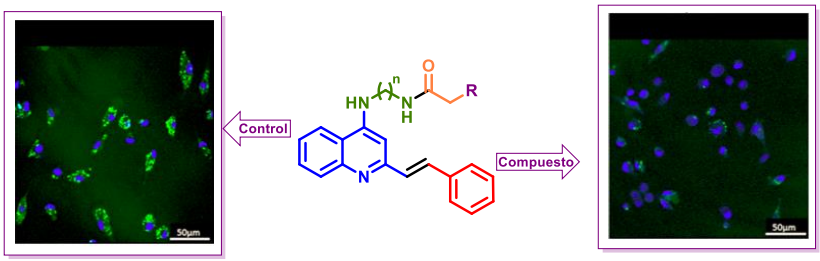

Con el fin de desarrollar compuestos con estructuras tipo push-pull que sirvan como sondas MSOT, hemos desarrollado una nueva metodología *one-pot* en condiciones mecanoquímicas que nos permite la obtención de los núcleos de bis-indolilquinonas en un solo paso.

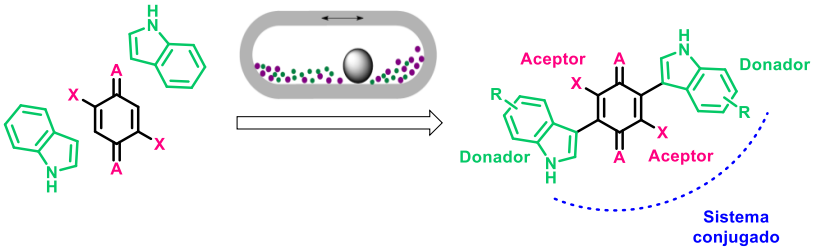

Finalmente, la quimitoteca de compuestos híbridos pirrol-isoniazida fue sintetizada y debidamente caracterizada. Su actividad antituberculosa fue evaluada mostrando resultados prometedores contra *Mycobacterium tuberculosis*. Posteriores estudios mecanísticos corroboraron su habilidad para inhibir tanto MmpL3 como InhA, probando así que su acción tiene lugar a través de un mecanismo multidiana activado por el metabolismo (*metabolism-activated multitargeting*, MAMUT).

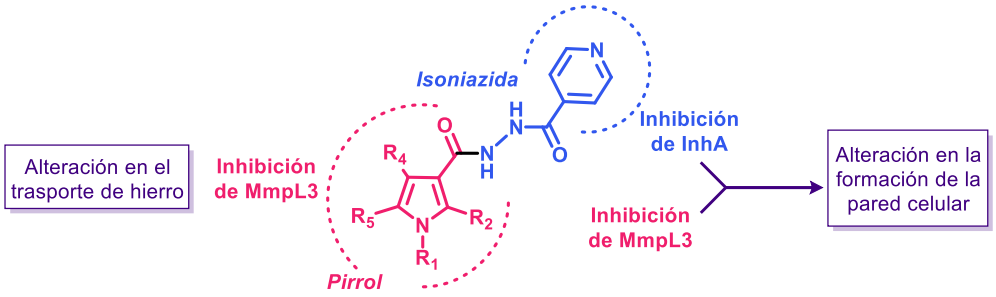

Conclusiones

El trabajo desarrollado en la presente tesis doctoral verifica que el empleo de compuestos teranósticos y multidiana, resulta una estrategia prometedora para el desarrollo de nuevos fármacos contra proteinopatías y enfermedades infecciosas.

CHAPTER 1. INTRODUCTION

1.1. What is a theranostic agent?

The "theranostic" concept was firstly proposed in 2002 by Funkhouser [1] to describe a material that combines the modalities of therapy and diagnostic imaging, providing therapeutic effects and diagnostic imaging simultaneously under the same dose.[2] **(Figure 1.1)**

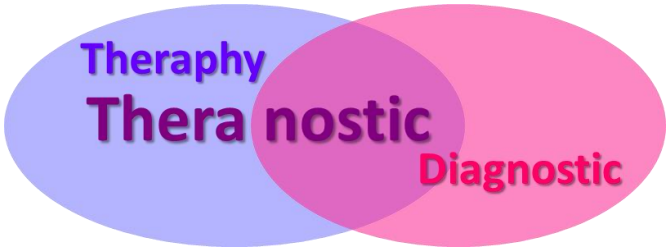

Figure 1.1. Theranostic concept.

In many different pathologies such as infections, cardiovascular diseases, neurodegenerative and inflammation-related disorders or cancer,[3] before starting any kind of treatment it is fundamental to carry out imaging diagnostic tests to evaluate the stage of advancement of the disease. The current approach of using different agents for diagnosis and therapy usually provides several drawbacks in terms of selectivity and biodistribution.

Against this backdrop, the idea of combining these two different objectives in one chemical entity brings the opportunity of overcoming these undesirable side effects. Over the last decades the concept of individualized medicine is gaining more relevance as an approach that can afford more effective and personalize treatments.[4]

Simultaneously, as the data show **(Figure 1.2)**, the theranostic field is also becoming a topic of broad interest as one of its main goals is to provide real time information of the diseased tissues and drug efficacy and kinetics. This technology not only allows to save time and decrease costs, but also enables physicians to make well informed decisions

[1] Funkhouser, J. *Curr. Drug Discovery* **2002**, *2*, 17.
[2] Kelkar, S. S.; Reineke, T. M. *Bioconjug. Chem.* **2011**, *22*, 1879.
[3] Shetty, Y.; Prabhu, P.; Prabhakar, B. *Int. J. Pharm.* **2019**, *558*, 29.
[4] Warenius, H. M. *Expert Opin. Med. Diagn.* **2009**, *3*, 381.

regarding dose adjustment, variations of delivery routes or discontinuation of treatments, obtaining better patient outcomes.[5,6,7,8]

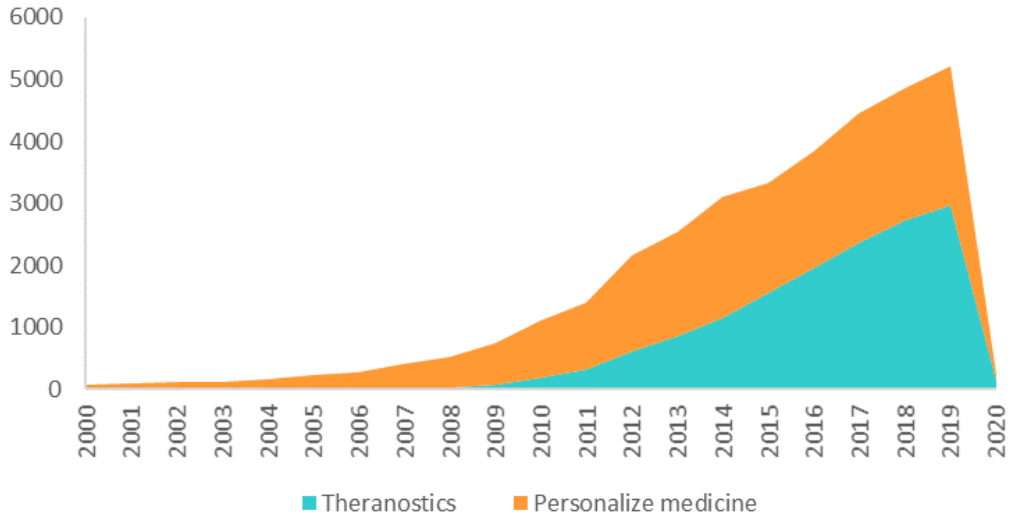

Figure 1.2. Number of publications per year in the corresponding fields. Data obtained from SciFinder.

Progress in molecular biology, material science and imaging techniques are essential to propel the development of theranostics.

1.2. Non-invasive diagnosis techniques

Since the theranostic approach needs non- invasive molecular imaging technologies to facilitate the visualization of different *in vivo* phenomena, current imaging techniques, such as computed tomography (CT), magnetic resonance imaging (MRI), ultrasound imaging (US), single photon emission computed tomography (SPECT), positron emission tomography (PET), optical imaging (OI) and fluorescence imaging (FI) are under study.[9] One important aspect in the choice of technique is the need for a contrast agent, which requires a pre-scan in order to detect the amount of signal preceding the contrast agent administration, thus no background signal is detected and consequently anatomical information is not provided.

[5] Shetty, Y.; Prabhu, P.; Prabhakar, B. *Int. J. Pharm.* **2019**, *558*, 29.
[6] Lammers, T.; Kiessling, F.; Hennink, W. E.; Storm, G. *Mol. Pharm.* **2010,** 7, 1899.
[7] Duncan, R. *Nat. Rev. Drug Discov.* **2003**, *2*, 347.
[8] Peer, D.; Karp, J. M.; Hong, S.; Farokhzad, O. C.; Margalit, R.; Langer, R. *Nat. Nanotechnol.* **2007**, *2*, 751.
[9] Kunjachan, S.; Ehling, J.; Storm, G.; Kiessling, F.; Lammers, T. *Chem. Rev.* **2015**, *115*, 10907.

Among the technologies mentioned above, CT, US and MRI do not need to be used with a contrast agent, while SPECT, PET, OI and FI need the presence of a contrast agent to achieve suitable detection, For this reason, hybrid techniques such as PET-CT, SPECT-CT or PETC-MRI have been developed. These technologies afford the possibility of locating the contrast agents in the correct organs or tissues.[9] It is important to consider that each of these imaging techniques is used for different purposes, depending on its capabilities. Since each of them has different advantages and disadvantages is better to have a deeper understood. **(Figure 1.3)**

IMAGING TECHNIQUE	FORM OF ENERGY	SPATIAL RESOLUTION (mm)	APPLICATIONS	ADVANTAGES	LIMITATIONS
PET SPECT 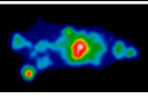	Photons annihilation	4-6	• Drug targeting • Biodistribution • Blood pool imaging	• High sensitivity • Quantitative results • Unlimited penetration	• Limited spatial resolution • No anatomical information • Radiactive probes
CT 	X-rays	0.3-1	• Anatomical information • Hybrid imaging • Perfusion monitoring	• High spatial resolution • Dynamic imaging • Quantitative results	• Low contrast agenr sensitivity • Poor soft tissue contrast • Radiation exposure
MRI 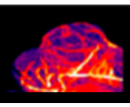	Radio frequency waves	0.2	• Drug reléase • Drug efficacy • Cell tracking	• High spatial resolution • High soft tissue contrast • High versatility	• Low throughput • Low contrast agent sensitivity • Difficult quantification
OI 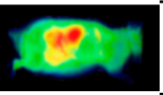	Light	<1	• Drug targeting • Hybrid imaging • Nucleic acid delivery	• High throughput • High sensitivity • High probe versatility	• Poor penetration Depth • No anatomical information • Difficult quantification
US 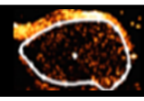	High frequency sound	0.1-1	• Drug targeting • Perfusion monitoring • Sonoporation	• High throughput • High sensitivity • Dynamic imaging	• Low probe versatility • High user dependency • No whole-body imaging

Figure 1.3. Reproduced with permission from reference. [9]

1.2.1. Computed tomography (CT)

Computed tomography is an X-ray-based imaging technique that allows the visualization of cross-section images from the organs and tissues of interest. High-resolution images are obtained in the presence of highly radiopaque contrast agents, such as iodine or barium.

CT is mainly used for visualizing high electron density tissues, such as bones, consequently, is mainly used for orthopaedic applications. Its main drawback is associated with the low sensitivity of the contrast agents, requiring high doses and the consequent toxicity-associated problems.[9]

1.2.2. Magnetic resonance imaging (MRI)

Magnetic resonance imaging and nuclear magnetic resonance (NMR) are based on the same principle, in which the spin states of certain atomic nuclei are detected.

As MRI can be done in the presence or absence of contrast agents, it is widely used for diagnosis, therapy monitoring, biodistribution or pharmacokinetic assays. Thus, MRI is a versatile tool for (pre)clinical diagnosis and therapy monitoring.[9]

The contrast generation depends on freely diffusing water molecules, meaning that the signals of a tracer would be different inside or outside a nanocarrier. Thus, MRI is a perfect technique to monitor drug release and efficacy. [10]

On the other hand, MRI has several disadvantages usually associated with low contrast agent sensitivity and difficulties in quantification.

1.2.3. Positron emission tomography (PET)

During a positron emission tomography (PET) experiment, positron-emitting isotopes, such as ^{11}C, ^{13}N, ^{15}O, ^{18}F, ^{44}Sc, ^{62}Cu, ^{64}Cu, ^{68}Ga, ^{72}As, ^{74}As, ^{76}Br, ^{82}Rb, ^{86}Y, ^{89}Zr or ^{124}I, are administered. These radionuclides emit positrons that annihilate with nearby electrons, generating two photons that shoot off in opposite directions and can be detected by the PET scanners. Thanks to the exceptional penetration depth of these photons and the high sensitivity of PET scanners, radionuclides can generate useful and quantitative information even when administered below picomolar concentrations. Due to these properties PET is widely used in clinic for diagnosis, disease staging, and therapy monitoring. Moreover, is an interesting technique to monitor drug pharmacokinetics, biodistribution, and accumulation at its target site.

The radionuclide necessary for PET probes can be encapsulate via chelating groups such as 2-[bis[2-[bis(carboxymethyl)amino]ethyl]amino]acetic acid (DTPA), 1,4,7,10-tetraazacyclododecane-1,4,7,10-tetraacetic acid (DOTA) or hydrazinonicotinic acid

[10] Terreno, E.; Castelli, D. D.; Viale, A.; Aime, S. *Chem. Rev.* **2012**, *110*, 3019.

(HYNIC). Drugs incorporating ^{11}C or ^{18}F can also be synthesized immediately before their administration.

The main disadvantages associated with PET are the low spatial resolution, the need for radioactive probes and the fact that no anatomical information is obtained. [9]

1.2.4. Single photon emission computed tomography (SPECT)

The main difference between PET and SPECT is the type of radiotracers used, some of the radionuclides most commonly employed in SPECT are ^{99m}Tc, ^{111}In, ^{123}I, and ^{201}Tl. Also, while the first technique measures coincident γ-rays, the second one is based on noncoincident γ-rays. For this reason, SPECT sensitivity is one order of magnitude lower than PET and consequently its quantification is more difficult.

The main advantage of SPECT is that while in PET all emitted γ-photons have the same energy, energies used in SPECT are different. This energy-dependent imaging enables the use of different probes at the same time. As in the case of PET. SPECT provides high sensitivity, quantitative results and high penetration depth but it lacks anatomical information and spatial resolution. In both cases, the need for radioactive probes can be regarded a disadvantage. [9]

1.2.5. Optical imaging (OI)

Due to its simplicity compared to PET or SPECT, interest in the use of optical imaging (OI) techniques has increased during the past decades.

Fluorescence reflectance imaging (FRI) is the most widely employed technique for drug delivery monitoring. It allows comparison between free *vs.* bound ligand, giving valuable semiquantitative information about the location of fluoresecence-labeled compounds in tissue. The accessibility, sensitivity, low-cost and the possibility of using multiple fluorophores at the same time are the main advantages of OI.

Fluorescence molecular tomography (FMT) enables deeper and more quantitative information of the probe biodistribution by using optical measurements through

different illumination and detection paths around the tissue of interest and mathematically combines this information to reconstruct three-dimensional images.[11,12,13] Despite the improvements made by FMT, its fundamental limitation is that fluorescence signals cannot be precisely localized. For this reason, hybrid approaches such as OI-MRI[14] or OI-CT[15,16] have been developed that offer highly versatile tools with clinical applications.

The main drawbacks of optical imaging are associated with autofluorescence and poor penetration depth, but it is important to remark that these problems can be improved by using the appropriate probes. These probes should emit fluorescence in the first near-infrared (NIR-I) or second near-infrared (NIR-II) regions (600-1700 nm),[17] which afford deeper penetration, higher spatial resolution, non-invasive operation, lower optical absorption and scattering from biological substrates with minimal tissue autofluorescence.[18] **(Figure 1.4)**

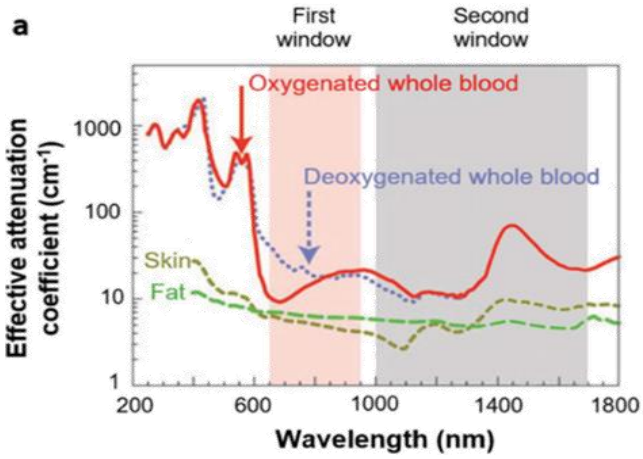

Figure 1.4. Reproduced with permission from reference.[17]

[11] Ntziachristos, V.; Weissleder, R. *Opt. Lett.* **2001**, *26*, 893.
[12] Kunjachan, S.; Pola, R.; Gremse, F.; Theek, B.; Ehling, J.; Moeckel, D.; Hermanns-Sachweh, B.; Pechar, M.; Ulbrich, K.; Hennink, W. E.; Storm, G.; Lederle, W.; Kiessling, F.; Lammers, T. *Nano Lett.* **2014**, *14*, 972.
[13] Ntziachristos, V.; Bremer, C.; Weissleder, R. *Eur. J. Radiol.* **2003**, *13*, 195.
[14] Davis, S. C.; Pogue, B. W.; Springett, R.; Leussler, C.; Mazurkewitz, P.; Tuttle, S. B.; Gibbs-Strauss, S. L.; Jiang, S. S.; Dehghani, H.; Paulsen, K. D. *Rev. Sci. Instrum.* **2008**, *79*, 10.
[15] Hyde, D.; de Kleine, R.; MacLaurin, S. A.; Miller, E.; Brooks, D. H.; Krucker, T.; Ntziachristos, V. *Neuroimage* **2009**, *44*, 1304.
[16] Schulz, R. B.; Ale, A.; Sarantopoulos, A.; Freyer, M.; Soehngen, E.; Zientkowska, M.; Ntziachristos, V. *IEEE Trans. Med. Imaging* **2010**, *29*, 465.
[17] Kenry, D. Y.; Liu, B. *Adv. Mater.* **2018**, *30*, 1.
[18] Staderini, M.; Martín, M. A.; Bolognesi, M. L.; Menéndez, J. C. *Chem. Soc Rev.* **2015**, *44*, 1807.

1.2.6. Ultrasound imaging (sonography)

Ultrasound imaging (USI) is based on the principle of back-scattering, which is the reflection of waves, particles or signals back to the direction from where they came. US can provide real-time and highly spatially resolved images of the area of interest and can be carried out with or without contrast agents, usually formed by 1−5 μm sized bubbles filled with gas or air.

Even though US is an inexpensive, fast, versatile and well-established technique, its main drawbacks rely on the low versatility of the contrast agent, the impossibility to perform whole body images and the high dependency of the quality of the study from the operator performing the scan.[9]

1.2.7. Photo Acoustic Imaging (PAI)

Photo acoustic imaging is a hybrid technique based on the detection of acoustic waves produced as consequence of the absorption of light pulses of ultrashort duration. In 1880 Alexander Graham Bell described for first time the optoacoustic phenomenon,[19] but its applications were not considered until more recently.[20,21,22]

In the past decades, the availability of pulsed laser technology and the sensitive of acoustic detectors, created the possibility of developing optoacoustic technologies, which enable the visualization of subsurface blood vessels with high resolution.[23]

As PAI detection measures the acoustic waves generated by the imaged targets after light excitation, it is capable to overcome the problems associated with optical diffusion and depth penetration. This way PAI has emerged as one of the most promising imaging techniques.[17] The main limitation of this type of detection is the light scattering created by biological tissues. Several endogenous species, such as haemoglobin and deoxyhaemoglobin, are PAI-active because they absorb light significantly in the desired

[19] Bell, A. G. *Am. J. Sci.* **1881**, *20*, 305.
[20] Rosencwaig, A. *Science* **1973**, *181*, 657.
[21] Bowen, T.; Nasoni, L.; Pifer, A. E.; Sembroski, G. H. *Proc. IEEE Ultrasonics Symp.* **1981**, *2*, 823.
[22] Oraevsky, A. A.; Jacques, S. L.; Esenaliev, R. O.; Tittel, F. K. *Proc. SPIE* **1994**, *2134A*, 122.
[23] Wang, X.; Pang, Y.; Ku, G.; Xie, X.; Stoica, G.; Wang, L. *Nat. Biotechnol*. **2003**, *21*, 803.

wavelength range, but unfortunately, they do not produce a sufficiently strong PA signal.[24]

PA imaging is usually performed in the NIR-I region (700-900 nm), so that deeper penetration can be achieved, and unwanted background signals can be avoided. For this purpose, the best option is the use of exogenous PA probes. The detection of these probes usually requires its differentiation from background absorption, and this has led to the development of multispectral optoacoustic tomography (MSOT), which measures chromophores over background tissue absorption. In this technique pulses of different wavelengths, selected to excite the PA agent, are used simultaneously. In response to absorption the PA agent undergoes a thermoelastic expansion that emits ultrasound waves, which can then be detected by acoustic detectors. Afterwards, using appropriate mathematical methods, images of the tissues are obtained.[25] One of the main advantages of this technique is that by scanning at different bands, multiple chromophores can be detected in the same imaging session. To summarize, PA emerges as a new, fast, versatile technique that needs to be explored more deeply. On the other hand, its main drawbacks are once again the limitations of the existing contrast agents and on the operator performing the scan. **(Figure 1.5)**

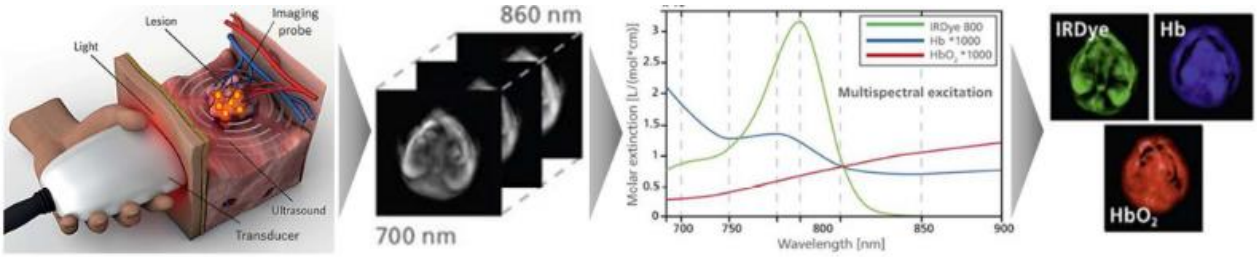

Figure 1.5. Reproduced with permission from reference.[26]

[24] Kenry, D. Y.; Liu, B. *Adv. Mater.* **2018**, *30*, 1.
[25] Ntziachristos, V.; Razansky, D. *Chem. Rev*. **2010**, *110*, 2783.
[26] Gujrati, V.; Mishra, A.; Ntziachristos, V. *Chem. Commun.* **2017**, *53*, 4653.

1.3. Design of imaging probes

As previously mentioned, one of the limiting factors in both OI and PAI is the selection of the appropriate probes. Thus, when it comes to the design of imaging probes several considerations should be taken into account. In the next section the essential characteristics that they should exhibit will be discussed.

1.3.1. Design of fluorescence probes

When a determined amount of energy is given to a molecule, electrons promote from an occupied, low-energy molecular orbital to an empty, higher-energy one, and that transition corresponds to an absorption band in the spectrum. In many cases this energy is dissipated by collision with the solvent, but in the case of fluorescent compounds the excited electrons return to the ground state by emission of photons. This phenomenon is known as fluorescence.

The difference in energy between the highest occupied molecular orbital (HOMO) and the lowest unoccupied molecular orbital (LUMO) is the smallest difference of energy that can be found between a full and an empty orbital. This is the so-called HOMO-LUMO gap, which is correlated with the emission and absorption wavelengths.

As previously mentioned, *in vivo* fluorescence probes should ideally possess certain spectral properties, such as: emission in the NIR-I or NIR-II regions, high fluorescence quantum yields and a large Stokes shift. Smaller HOMO-LUMO gaps are associated with longer absorption and emission wavelengths, and for this reason, NIR probes must be designed with the aim of reducing the HOMO–LUMO gap. **(Figure 1.6)**

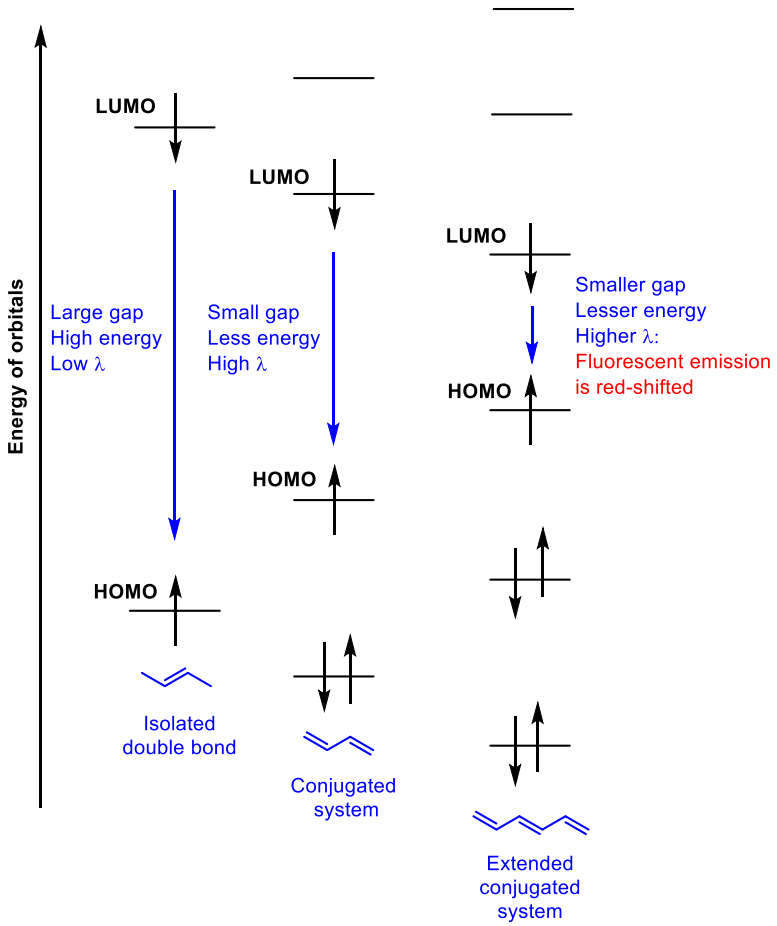

Figure 1.6.

Apart from suitable spectral properties, fluorescence probes should present: high specificity, sensitivity and affinity, the ability to change their fluorescence properties upon target binding, minimum interference with human serum albumin (HSA) allowing *in vivo* applications, suitable lipophilicity to cross membranes and low toxicity.

For this purpose, there are two potential approaches: the use of fluorescence nanoparticles (quantum dots) or small organic molecules. The main advantages of nanoparticles are their spectral properties, since they present narrower emission spectra and higher Stokes shifts. However, these inorganic nanoparticles usually present a high number of health risks, low biocompatibility, low clearance and long-term toxicological problems.[17,18,27] For these reasons, organic molecules appear as an attractive alternative for developing NIR-I and NIR-II probes.

[27] Hardman, R. *Environ. Health Perspect.* **2006**, *114*, 165.

Focusing our attention on small organic molecules, NIR emission can be achieved by following several strategies:

- Introduction of extended conjugation systems: changes in the conjugation length are an effective approach for reducing the HOMO-LUMO energy gap. For this reason, the use of extended π-systems is a good option for probe construction.[18]
- Introduction of push-pull systems: Another approach to reduce the HOMO-LUMO gap is the introduction of electron donors (D) and electron acceptor groups (A) as terminal moieties of the conjugated system, leading to the so-called push-pull systems. In the past years, several authors have also introduced D-A-D systems in order to obtained longer absorption and emission wavelengths. Moreover, to achieve NIR-II probes, dialkyl fluorenes were introduced in these structures as shielding (S) groups, obtaining S-D-A-D-S sturctures.[24]

  The reason why these push-pull systems works is that D-A molecules can be described by two resonance forms: one neutral and one zwitterionic, the latter of which mimics the excited state better. Thus, due to the presence of this kind of D-A systems the whole molecule is more polarized and consequently the ground state is closer to the excited state, meaning that less energy is needed for excitation.[18]

  On one hand, the electron donor group has to bear a lone pair of electrons in a π-orbital that can be shared with the π-molecular orbital of the conjugated system. On the other hand, the electron-acceptor group must have antibonding free π-orbitals. This way, the energy of the HOMO is increased and the LUMO is stabilized. **(Figure 1.7)**

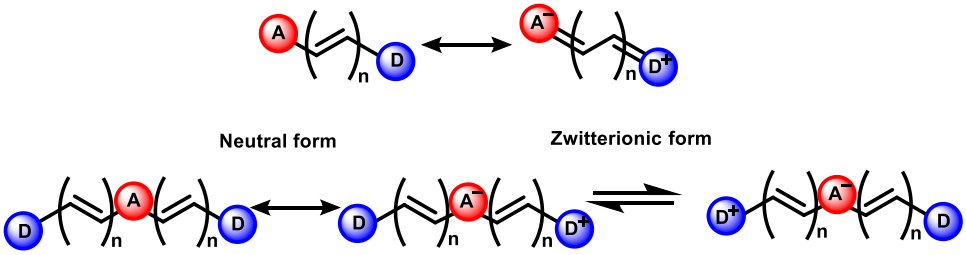

Figure 1.7.

- Bond length alternation (BLA): BLA is the difference in length between consecutive single and double bonds. Its value quantifies the delocalization of electrons across a molecule.

  A standard single bond measures 154 pm and a double bond 134 pm. In a conjugated system a C-C single bond has slightly shorter length and consequently a partial double character. For this reason, these bonds are harder to rotate and molecular structures tend to adopt planar conformations. BLA values close to zero means that the overlap is great, the system is highly conjugated, and the electrons are very delocalized. Push-pull systems also increase the double bond character and consequently reduce the BLA value.[18]
- Planarity: In planar molecules π-orbitals overlap and combine better. As previously mentioned, this allows strong π conjugation and better electron delocalization. This explains why fluorescence emission of solid compounds takes place at longer wavelengths. Planarity is a common structural character but is not essential.[18]

1.3.2. Design of MSOT probes

As with fluorescence probes, to design MSOT probes for *in vivo* imaging, they must have some general characteristics such as: low toxicity, bio-compatibility, high specificity, sensitivity and affinity, suitable lipophilicity to cross membranes and good clearance values.

Several inorganic nanoparticles have been described as MSOT probes, but even though they commonly present better spectroscopic profiles, their toxicity and low clearance make them inappropriate candidates for *in vivo* imaging. In this context, small organic molecules appear again as a better alternative.[26]

When it comes to the spectral properties, although many fluorophores present absorption spectra suitable for MSOT, they do not have the proper characteristics for

optoacoustic detection. This kind of probes should ideally present the following properties:[26,28]

- Absorbance maximum (λ abs) should be between 680 and 950 nm in order to achieve minimal interference from tissues.
- High absorption, meaning a high molar extinction coefficient (>10^4 M^{-1} cm^{-1}) to maximize the amount of light absorbed.
- Low fluorescence quantum yield in order to minimize the emission of light energy and maximize the production of acoustic waves. Apart from quantum yield, other parameter such as solubility, triplet state contributions, excited state absorption, relaxation kinetics can affect the photoacoustic signal strength.
- Efficient conversion of heat energy to produce acoustic waves.
- Narrow spectral profiles, leading to more accurate and sensitive measurements and avoid overlapping spectral responses.
- Resistant to photodynamic damage of bleaching following excitation.
- Contrast agent efficiency: to accurately measure the probe efficiency it should be concentration-normalized (cm^{-1}/(mg/mL)). This value shows the optical absorption coefficient (in cm^{-1}) that can be created in the target volume by using a 1 mg/mL concentration of the contrast agent. For example, some inorganic compounds, such as gold nanoparticles, present high molar extinction values but compared to other chromophores they are quite large and heavy. Thus, after normalizing by molecular weight, organic dyes may have higher absorptivity.[11]

Depending on their specificity, MSOT probes can be divided in two main groups:[26]

- Non-specific imaging probes, which provide contrast wherever they are delivered. Thus, successful imaging depends on compound biodistribution.
- Specific imaging probes target tissue sites or moieties. In this case the imaging not only depends on biodistribution, but also on target binding. They can be divided in two main categories:
  - Probes binding to specific receptors or preferentially encapsulated by specific uptake mechanism.

[28] Knox, H. J. *Acc. Chem. Res.* **2018**, *51*, 2897.

- Activatable probes, which change their spectral properties (shift in the absorption peak wavelength) upon changes in molecular or biochemical parameters (enzymes, pH, ROS, analytes…). This kind of probes minimize the influence of the background signal from endogenous chromophores, appearing as the most attractive alternative due to their higher specificity and sensitivity.

From a chemical point of view, the structure of these probes can be tuned in order to optimize their properties. The main problems of organic MSOT probes are associated with low molar extinction coefficients, tendency to aggregate, low solubility and photobleach. To avoid these issues an ideal MSOT dye must possess:[26,29]

- Conjugated double bonds or aromatic systems in order to present higher molar extinction coefficient in the NIR region.
- D-A or D-A-D push-pull structures, to produce sharp absorption bands in the NIR region.
- Hydrophilic groups to present better solubility and avoid aggregation issues.
- Introduction of triplet state quenchers to inhibit fluorescence.[30,31]
- Integration of stabilizing groups to solve photobleach problems.[32]

[29] Weber, J.; Beard, P. C.; Bohndiek, S. E. *Nat. Publ. Gr.* **2016**, *13*, 639.
[30] Onoe, S.; Temma, T.; Kanazaki, K.; Ono, M.; Saji, H. *J. Biomed. Opt.* **2015**, *20*, 096006.
[31] Gong, W.; Das, P.; Samanta, S.; Xiong, J.; Pan, W.; Gu, Z.; Zhang, J.; Qu, J.; Yang, Z. *Chem. Commun.* **2019**, *55*, 8695.
[32] Reynolds, G. A.; Drexhage, K. H. *J. Org. Chem.* **1977,** *42*, 885.

1.4. Protein misfolding diseases (PMDs)

Proteins are one of the most versatile macromolecules. Mammalian proteomes include between 10.000 and 20.000 proteins, and to maintain its integrity there must be a balance between protein synthesis, folding and degradation.

The number of conformations that a small polypeptide (about 100 amino acids) can adopt is about 1030.[33] However, the biologically active conformation is usually only stable under physiological conditions. Thus, is not surprising that errors frequently take place during the folding process, giving misfolded states and aggregates.[34] These aggregates cause the loss of function or toxicity of the proteins leading to the so-called proteinopathies.

In 1854, Rudolph Virchow introduced the term amyloid, from the Latin *amylum* and meaning "starch-like", to describe a macroscopic tissue abnormality that, like starch, could be stained with iodine. It was in 1859 when Friedreich and Kekulé identified proteins as the real molecular main component of the amyloid deposits.[35] The abnormalities that Virchow described are the main hallmark of proteinopathies. Depending on the aggregated protein and the tissue of accumulation, this misfolding can lead to several diseases. Moreover, these kinds of diseases can be separated into two main groups:[36]

1. ***Loss-of-function:*** characterized by protein dysfunction resulting from mutations that produce metastable proteins prone to degradation. Examples of these diseases are: cystic fibrosis, Gaucher's disease, hypogonadotropic hypogonadism, nephrogenic diabetes insipidus or retinitis pigmentosa.
2. ***Toxic gain-of-function:*** characterized by the formation of metastable proteins that lead to toxic oligomers or aggregates that affect cell functions. Examples of such diseases are: Alzheimer's disease, Type II diabetes, Parkinson's disease, Amyotrophic Lateral Sclerosis (ALS, Lou Gehrig's disease), Huntington's disease,

[33] Dobson, C.M.; Sali, A.; Karplus, M. *Angew. Chem.* **1998**, *37*, 868.
[34] Hartl, F. U. *Annu. Rev. Biochem.* ***2017****, 86,* 21.
[35] Bayer, T. A. P *Eur. Neuropsychopharmacol.* **2015**, *25*, 713.
[36] Denny, R. A.; Gavrin, L. K.; Saiah, E. *Bioorg. Med. Chem. Lett.* **2013**, *23*, 1935.

Creutzfeldt-Jakob disease (mad cow's disease) or Familial amyloid polyneuropathy

This list is by far not complete, but they reflect the heterogeneity of different proteinopathies. Some of them are characterized by a single type of aggregate, while others can present two or more aggregated proteins. **(Figure 1.8)**

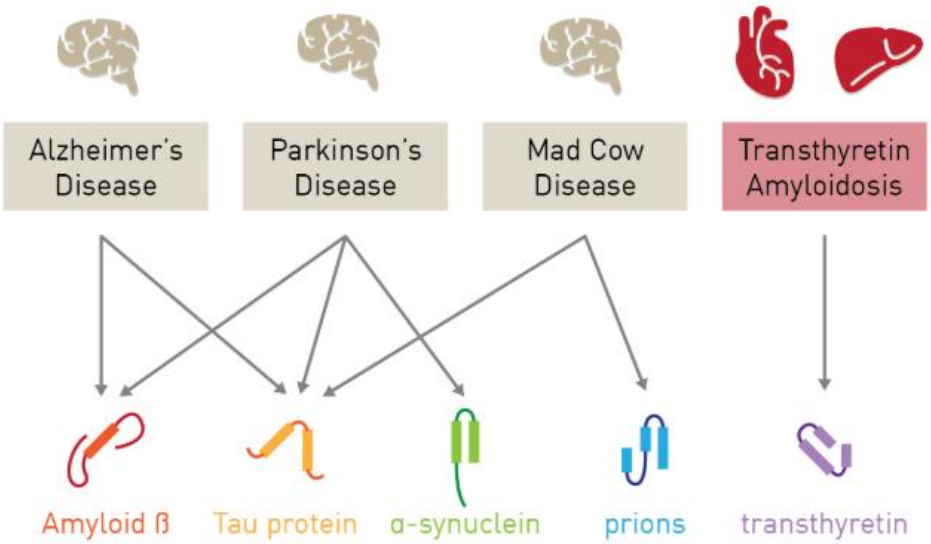

Figure 1.8.

Under physiological conditions, aggregation-prone proteins are usually soluble and lack pathogenic properties, but their conformational change and its consequent change in its aggregation properties is the key step to trigger pathogenic aggregation. There are several factors that can alter the conformational stability and initiate the aggregation processes:[35,37,38]

- Genetic mutations on structural regions of the protein can change their physicochemical properties and make them more prone to aggregation processes.
- Mutations in regulatory regions can activate their transcription increasing their concentration and shifting the equilibrium toward the aggregation products.

[37] Shelkovnikova, T.A.; Kulikova, A.A.; Tsvetkov, Ph.O.; Peters, O.; Bachurin, S.O.; Buchman, V.L.; Ninkina, N.N. *Mol. Biol.* **2012**, *46*, 362.
[38] Melki, R. *The multitude of therapeutic targets in neurodegenerative proteinopathies*. *Disease-Modifying Targets in Neurodegenerative Disorders: Paving the Way for Disease-Modifying Therapies*, Elsevier Inc. 2017. doi:10.1016/B978-0-12-805120-7.00001-4.

- Truncation and/or post-translational modifications of the protein, which change their physicochemical properties.
- Interaction with another aberrant protein that acts as a template and triggers conformation change. This can also be consider a propagation pathway, and a wide range of recent experimental evidence suggest that protein aggregates can spread in such a prion like manner.
- Several environmental changes as: oxidative stress, metal ions, neurotoxins or virus infections can also alter protein conformation.

Once the aggregation-prone protein changes its conformation, the first aggregation step is oligomerization, and next these oligomers form soluble protofibrils. Both processes take place in a functionally active space of the cell and are cytotoxic. Most frequently this kind of structures produce membrane damage, as they have exposed sticky surfaces (hydrophobic amino acid residues), which have the ability to disturb phospholipid bilayers. The most frequently damaged organelle is the mitochondrion, whose membrane permeability is changed, leading to alterations in electron transport and overproduction of reactive oxygen species. Usually these soluble oligomers and protofibrils contribute considerably to cell degeneration, and therefore the subsequent steps of the aggregation pathway are considered as elements of protective mechanisms. Protofibrils are transformed into insoluble fibrils and later into larger packed fibrillar structures. These denser packs act as a trap for other proteins or even organelles. This last product of protein aggregation does not have a direct toxic effect and it may form deposits if cells fail to eliminate it in previous steps.

The integrated cellular machinery that regulates the synthesis, proper folding, degradation and clearance of proteins is known as proteostasis. The proteostatic system is regulated by two main components, the chaperones that refold proteins into a stable conformation and two proteolytic pathways, namely the ubiquitinproteasome and the lysosome-autophagy system. **(Figures 1.9 and Figure 1.10)**

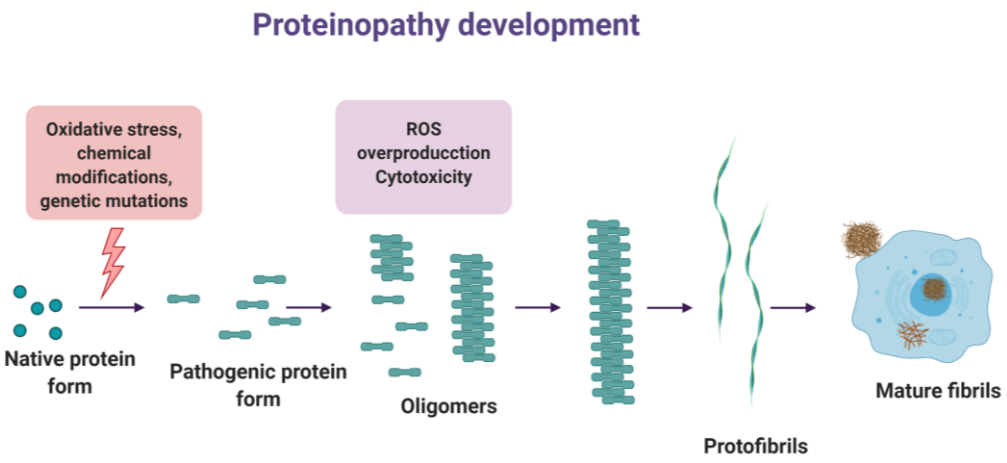

Figure 1.9. Stages in protein aggregation.

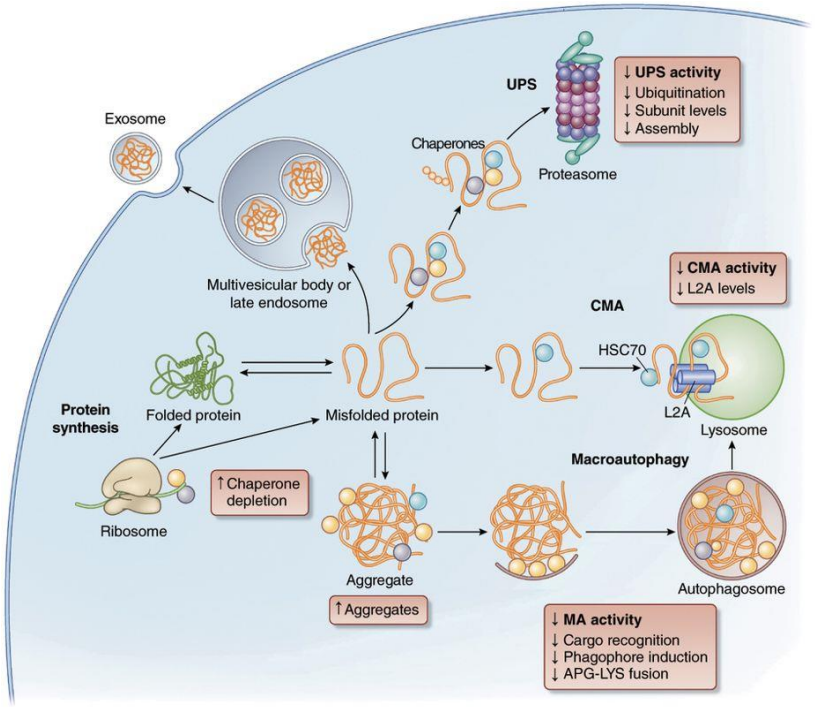

Figure 1.10. The proteostatic system. Reproduced with permission from reference. [39]

1.4.1. Alzheimer's disease (AD)

In 1906 Auguste Deter died at the age of 51, she had been internalized in a mental asylum after experimenting progressive changes in her personality, loss of memory and hallucinations. Auguste ended up completely apathetic and losing the ability to speak.

[39] Kaushik, S.; Cuervo, A. M. *Nat. Med.* **2015**, *21*, 1406.

After her death, Dr. Alois Alzheimer examined her brain, finding pathological hallmarks and introducing the term Alzheimer´s disease (AD).[40]

During the last decades the population above 65 has increased exponentially, thus leading to an associated surge in age-related diseases, such as dementia. Nowadays, AD is the most common form of dementia, forming between 60 to 70 % of the cases.[41] In 2018, the number of people diagnosed with dementias was estimated to be about 50 million, in 2030 it is projected to be 65 million, and 115 million by 2050. These data show the important socio-economic impact of these diseases.[42]

AD is described as a chronic and progressive neurodegenerative disease, with a still unclear etiopathology, that is known to appear several years before the clinical symptoms. The severity of these symptoms is a reflection of the neuronal damage that the disease produces. Depending on the onset of the disease it can be classified into different stages:[43]

1. Predementia: no symptomatology.
2. Mild cognitive impairments: recent memory loss.
3. Early-moderate dementia: difficulty in daily tasks, communication, changes in personality, reasoning difficulties and poor judgment.
4. Late stage dementia: social isolation, disorientation and complete dependency.

Nowadays, diagnosis is mainly base on cognitive, physical and neurobiological tests.[42] Even though significant advances in different fields as molecular biology or genetics have been made, the specific causes of AD remain unclear. Currently, the main hypothesis is that Alzheimer's has a multi-factorial etiology, in which several biochemical pathways are involved including: beta-amyloid aggregation, forming amyloid plaques, intracellular neurofibrillary tangles, containing hyperphosphorylated tau protein, calcium homeostasis deregulation, mitochondrial dysfunction, oxidative stress,

[40] Cipriani, G.; Dolciotti, C.; Picchi, L.; Bonuccelli, U. *Neurological Sciences,* **2011**, *32*, 275.
[41] Association, A. *Alzheimer´s & Dementia: The Journal of the Alzheimer´s Association*, **2018**, *14*, 367.
[42] Dementia: a public health priority. World Health Organization. *World Health Organization* **2012.**
[43] Early signs and symptoms of Alzheimer´s. hhttps:// alz.org/alzheimers-dementia/10_sign?lang=en-US2019 checked on the 22/01/2020.

neuroinflammation and deterioration of synaptic transmission, particularly at cholinergic neurons. **(Figure 1.11)**

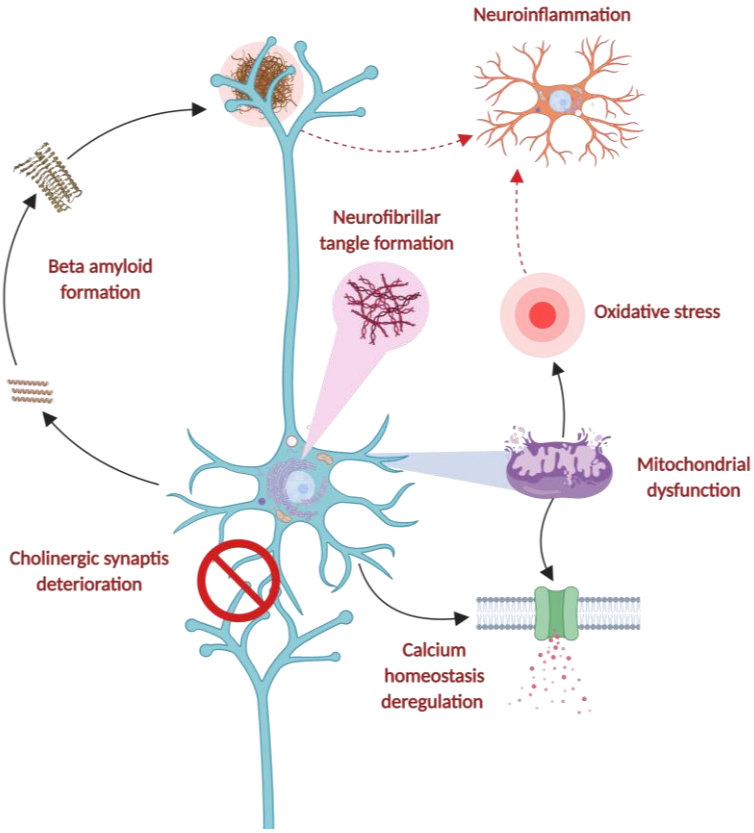

Figure 1.11.

1.4.2. Type II Diabetes mellitus (T2DM)

Diabetes mellitus (DM) is probably one of the oldest diseases known to man, as it was first reported in Egyptian manuscript about 3000 years ago.[44] Is a chronic disease characterized by hyperglycaemia, insulin resistance, and relative insulin deficiency. T2DM is much more common (more than 90% of all cases) than either type 1 diabetes mellitus (T1DM) or gestational diabetes. Even if the exact aetiology of T2DM remains unclear, it is known that it results from an interaction between genetic, environmental and behavioural risk factors. Further, T2DM patients are more vulnerable to various microvascular complications, such as retinopathy, nephropathy and neuropathy or

[44] Ahmed, A. M. *Saudi Med. J.* **2002**, *23*, 373.

macrovascular complications, as a heart attack and stroke, which often lead to their premature death.[45]

Usually, T2DM starts with insulin resistance in skeletal muscle, liver and adipose tissue, follow by a progressive impairment of insulin secretion by pancreatic β-cells. The prediabetic stage is characterized by fasting plasma glucose levels that are higher than normal but do not meet the criteria for the diagnosis of diabetes. The clinical presentation of patients with diabetes can vary considerably among individuals, making the classification of T2DM difficult. Moreover, at the diagnosis time, many patients are asymptomatic, while others present severe hyperglycaemia or even diabetic ketoacidosis. For this reason, screening risk individuals is important, as is common than around of 30% of T2DM patients are undiagnosed.[46]

In the past decades, T2DM has become a major global public health concern. In 2013 the International Diabetes Federation estimated that there were 382 million T2DM patients worldwide, and this number is expected to increase to 592 million by 2035. Surprisingly, particularly affected areas are China and India, where the prevalence of it has dramatically increased despite the relatively low obesity prevalence, this is due to the fact that, with the same body mass index, Asians tend to have a higher percentage of body fat mass, greater abdominal obesity and less muscle mass.[46]

During recent years, epidemiological studies have improved our understanding of T2DM risk factors. Increasing adiposity is the most important one. In addition, good dietary habits, enough physical activity, sleeping habits and no cigarette smoking are also associated with a reduced risk of T2DM. Although genetics plays a key role in T2DM development, the ongoing diabetes epidemic cannot be explained by just by genetic mutations.[46]

From a molecular point of view, after a meal insulin secretion is stimulated and glucagon secretion is inhibited. Together, the changes in glucagon, glucose and insulin levels

[45] Olokoba, A. B.; Obateru, O. A.; Olokoba, L. B. *Oman Med. J.* **2012**, *27*, 269.
[46] DeFronzo, R. A.; Ferrannini, E.; Groop, L.; Henry, R.R.; Herman, W. H.; Holst, J. J.; Hu, F.B.; Kahn, C. R.; Raz, I.; Shulman, G.I.; Simonson, D. C.; Testa, M. A.; Weiss, R.
Nat. Rev. Dis. Prim. **2015**, *1*, 1.

suppress hepatic glucose production, stimulate muscle glucose uptake and inhibit lipolysis. In type 2 diabetes all these processes are altered. Insulin secretion is impaired, plasma glucagon levels are increased, failing to suppress normally after a meal; analogy hepatic glucose production and plasma free fatty acid levels, also increase instead of being inhibited and finally muscle glucose uptake fails. **(Figure 1.12)**

As shown, T2DM is a complex chronic disorder which should be viewed and treated as a multifactorial disease with multiple physio pathological abnormalities. This way, to find a ¨true cure¨' for T2DM requires the elucidation of its molecular aetiology.[46]

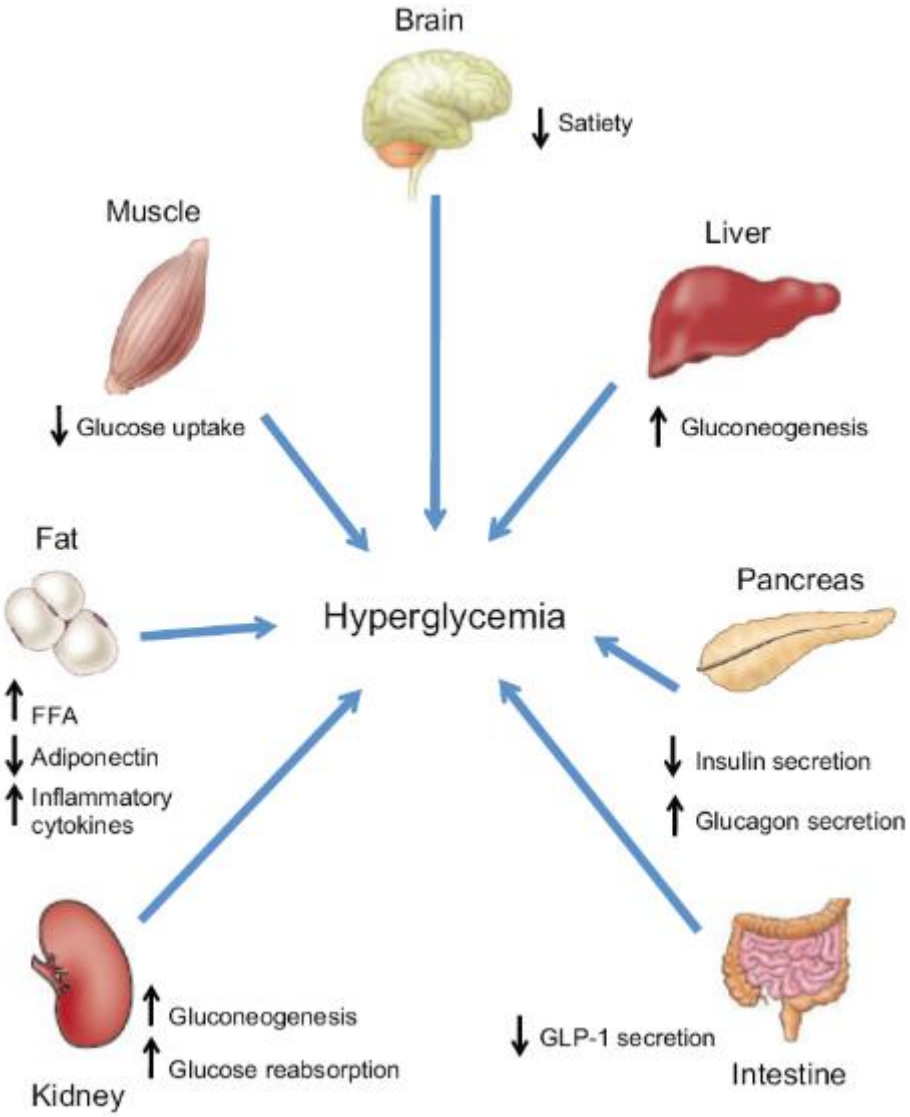

Figure 1.12. Reproduced with permission from reference.[47]

[47] Cornell, S. *Ther. Clin. Risk Manag.* **2015***, 11,* 621.

1.5. Neglected tropical diseases (NTDs)

Neglected tropical diseases are a diverse group of infections, commonly from tropical or sub-tropical low-income regions of Asia, Africa or America. **(Figure 1.13)** NTDs can be considered to arise a result of poverty and they contribute to develop further poverty. Moreover, the prevalence of some of them has been proposed as an indicator of underdevelopment. It is estimated that more than 1 billion people is infected with one or more NTDs and another billion is at risk. This group of diseases share some characteristics, including:[48]

- Slow development which becomes progressively worse.
- Usually they are chronic and can cause irreversible damages.
- Patients with NTDs are often stigmatised and excluded.
- Usually affect people without access to sanitation, safe water or basic heath.
- Can cause life disabilities or severe pains.

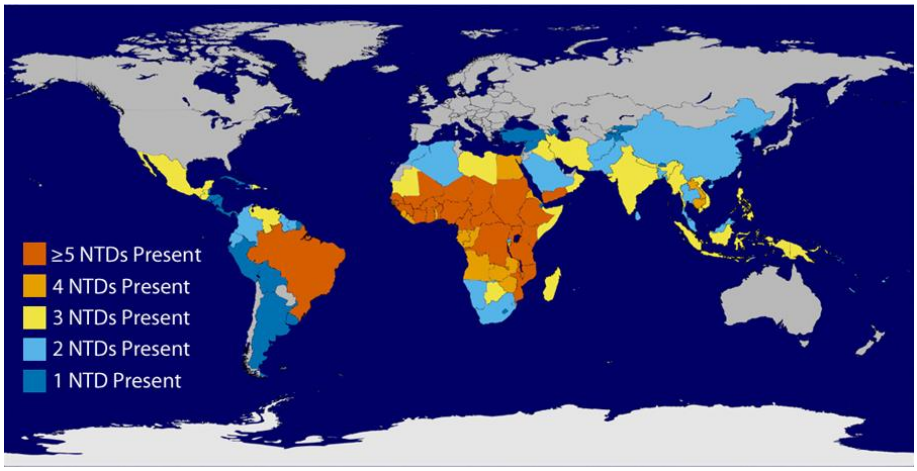

Figure 1.13.

NTDs are mainly caused by viruses, bacteria, protozoa and helminths. The main examples in each category are:[48]

- Viruses: dengue and rabies.
- Bacteria: leprosy, tuberculosis, trachoma and Buruli ulcer.
- Protozoa: leishmaniasis and trypanosomiases.

[48] Molyneux, D.; Foster, A.; Sightsavers, K. H. *Community Eye Health Journal*, **2013**, *26*, 21.

- Helminths: lymphatic filariasis, onchocerciases, intestinal worms and schistosomiasis.

Depending on the infectious agent the transmission is diverse, including:[48]

- Vectors like flies or snails.
- Faeco-oral route or food-related transmission.
- Fomites or direct contact.

Currently available drugs for NTDs present several drawbacks as: low efficacy, high toxicity with important side effects, limited number of available treatments, long treatments needed and the appearance of resistant strains. For this reason, the research for new drugs for the treatment of these diseases is still an imperative.

1.5.1. Leishmaniasis

Leishmaniases are a group of protozoal diseases, caused by over 20 species of the gender *Leishmania.* These parasites are transmitted to the main host, humans or other mammals, by the bites of their infected vectors, female *Phlebotomus* or *Lutzomyia* sand-flies. There are between 12 and 15 million people infected worldwide, and 350 million are at risk of acquiring the disease. It is estimated that around 1.5 to 2 million patients acquire leishmaniasis each year, and it causes 70.000 deaths per year. There are three main forms of leishmaniasis.[49] **(Figure 1.14)**

1. ***Cutaneous* leishmaniasis** is endemic in more than 70 countries around Central and South America, Middle East, Central Asia and Africa.
2. ***Mucocutaneous* leishmaniasis** is observed mostly in Latin America and rarely in Africa.

   Their mains symptoms are:

   - Single or multiple lesions on skin, starting with an erythematous papule with the sand-fly bite, which enlarge to a nodule and extends in surface and depth, ending in ulcers. These ulcers are usually painless and can heal spontaneously leaving a scar.

- Lesions can also spread into mucosa, giving rise to the mucocutaneous form of the disease, which can cause severe disfigurements.

3. ***Visceral* leishmaniasis or Kala-Azar** occurs in more than 60 countries around Africa, Asia, Central and South America and South Europe. Its symptoms leishmaniasis are more severe, ending in pancytopenia, immunosuppression and death if left untreated. The starting symptomatology involves irregular fever for around 2 weeks, splenomegaly, hepatomegaly, anaemia, diarrhoea, epistaxis, lymphadenopathy and weight loss. It is also common that patients develop co-infections like bacterial diarrhoea, pneumonia or tuberculosis.

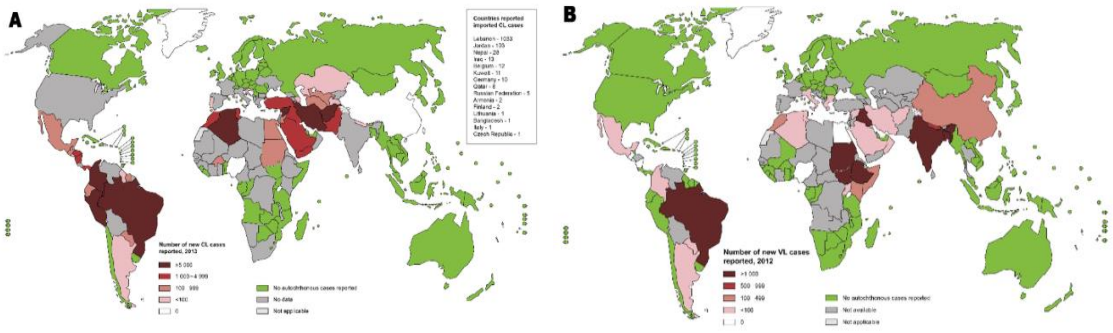

Figure 1.14: Distribution of leishmaniasis: (A) show cutaneous leishmania distribution while (B) shows visceral leishmaniasis distribution. Both data were reported by WHO in 2013.

It is also worth noting that many infected patients do not develop any symptoms throughout their lives, remaining as asymptomatic reservoirs of the disease.[49]

As regards the biological cycle of *Leishmania*, the infectious agent is always a unicellular protozoon of the *Trypanosomatidae* family and *Leishmania* genus. There are two stages in its life cycle:[50] **(Figure 1.15)**

- Amastigotes are non-flagelated intracellular forms, measuring between 2.5-3.5 µm, which are located in the phagocytic cells of the host. When the uninfected female of the phlebotomus bites an infected animal, it absorbs the amastigote forms from their blood. During their time in the insect's gut (between 4-25 days)

[49] https://medicalguidelines.msf.org/viewport/CG/english/leishmaniases-16689769.html checked on the 29/01/2020.
[50] Ocampo, V. D; Gladman, D. *F1000Research* **2019**, *8*, 1.

the parasite begins its transformation into procyclic amastigote, which finally evolves into metacyclic amastigotes. The latter have infectious capacity and after biting a healthy mammal, the vector infects it with the regurgitated promastigotes.

- Promastigotes are the flagellated form that measures between 12-20 µm and is mainly found in the vectors. When the mammal host is infected, the promastigotes are phagocytized by epidermal Langerhans cells or macrophages. Even though the mechanism of amastigote uptake is poorly understood, it is known that they bind the Fc human receptor, and thus the macrophage infection is an immunoglobulin-mediated process. Once inside the phagolysosome, promastigotes evolve into amastigotes and proliferate by binary fission.

The whole biological cycle lasts between 53 to 100 days.

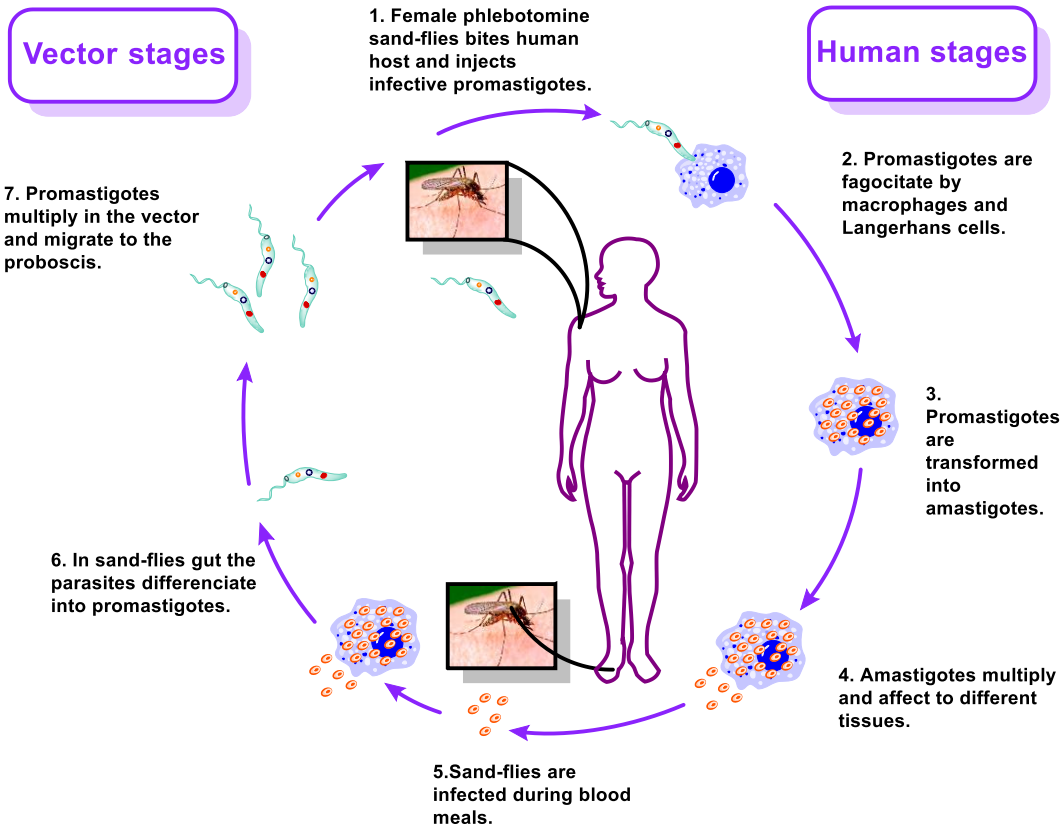

Figure 1.15.

Regarding the treatments, usually cutaneous lesions heal spontaneously in 3 to 6 months. If they persist more than 6 months, leading to ulceration, dissemination or

disfiguration, pharmacological treatment is needed. First the cutaneous lesions are treated with local pentavalent antimonials such as sodium stibogluconate or meglumine antimoniate, in more severe cases miltefosine is given orally or a pentavalent antimonial is administered intramuscularly or intravenously.

In the case of visceral leishmaniasis, intramuscular or intravenous pentavalent antimonial + paromomycin or paromomycin are administered. In case of relapse or for specific vulnerable groups such as pregnant women, patients over 45 years or severe disease, liposomal amphotericin B is given by intravenous infusion.

All the available treatments present serious drawbacks such as low safety, a high rate of resistance and cost. As mentioned, these drugs are used as monotherapy or under combinations, usually with low tolerability, with long treatment durations and difficult administration routes.

1.5.2. Tuberculosis (TB)

In 1882, Robert Koch identified *Mycobacterium tuberculosis* as the causative agent of tuberculosis. Nowadays, it is known that tuberculosis is caused by different members of this family, which includes: *Mycobacterium tuberculosis (*Mtb), the main etiologic agent of TB in humans; *M. africanum*, which causes TB in humans only in certain regions of Africa; *M. bovis, M. caprae* and *M. pinnipedii*, which cause TB in wild and domesticated mammals.

Mtb is an obligated aerobe, a non-motile and non-spore forming bacillum, which is classified as weakly gram positive. *Mycobacterium tuberculosis* owes its high virulence to the fact that is an intracellular bacterium, with a high latent capacity, a slow generation time (15-20 h) and its major feature is the peculiar cell wall structure, which provides an exceptionally strong impermeable barrier to noxious compounds and drugs. Moreover, over the last decades the rate of appearance of multiresistant (MDR-TB) and extremely multiresistant (XDR-TB) strains has considerably increased, making TB one of

the top 10 causes of death worldwide and the leading cause of death from a single infectious agent, already above HIV.[51,52]

About one quarter of the world's population is infected with tuberculosis and hence at risk of developing the disease. In 2018, about 10 million people developed TB, and 1.2 million HIV-negative and 251.000 HIV-positive patients died because of it. TB is mainly localized in South-East Asia, Africa and the Western Pacific region, even if some cases are developed in the Eastern Mediterranean, the Americas or Europe.[53]

TB is mainly spread from person to person through the air. When a patient with lung TB coughs, sneezes or spits, the TB bacilli are propelled and only a low infectious dose is needed to be inhaled to become infected. When a bacillus reaches the alveoli of the lungs it is phagocyted by alveolar macrophages. Inside them, most of these bacteria are destroyed; but some of them may multiply and be released upon macrophage death. This initial stage of the disease is characterized by an innate immune response that involves the recruitment of inflammatory cells to the lungs.

The remaining alive bacilli will spread through bloodstream or lymphatic channels, reaching other organs where the disease can be developed, such as: brain, larynx, lymph node, lung, spine, bone, or kidney. This dissemination process provokes an adaptative immune systemic response, and in 2 to 8 weeks the formed effector T cells and other leukocytes migrate to the infectious area, where they digest and surround Mtb forming a barrier called granuloma. Granulomas are organized structures where the bacilli are controlled that contain macrophages, lymphocytes and fibroblasts. In this stage, patients remain as asymptomatic reservoirs of the disease, but are not infectious. This stage can last during the whole life of some patients. If the immune system fails to control the bacilli, they begin to multiply rapidly, and patients will suffer tuberculosis.

Among all infected persons without any treatment, about 5% of the infected will develop the disease in the first 2 years after infection, and another 5% will develop it at some point of their life. It is also well known that several factors can trigger tuberculosis development, the most common example is HIV coinfection, which affects CD4 T cells

[51] Singh, A.; Budhraj, A.; Shrivastava, A.; Satyavana, A.; Gupta, A.; Gupta, M.; Wadhwa, G.; Sharma, S. K.; Jain, C. J. *Recent. Pat. Anti-infec. Drug Discov.* **2014**, *9*, 25.
[52] Koul, A.; Arnoult, E.; Lounis, N.; Guillemont, J.; Andries, K. *Nature* **2011**, *469*, 483.
[53] Global tuberculosis report, WHO, **2019.**

that play a pivotal role in controlling Mtb replication. Moreover, biological therapies with anti-TNF, corticosteroids, vitamin D deficiencies and any other conditions affecting T cell function may also increase the risk of developing the disease. **(Figure 1.16)** [54,55,56] The most common type of tuberculosis is the pulmonary disease, which courses with cough up to blood or sputum, chest pain, weight loss, weakness, no appetite, fever and nigh sweating.

More rarely extrapulmonary tuberculosis can be developed, usually affecting the larynx, lymph nodes, pleura, kidneys, bones or even brain, producing tuberculous meningitis. In the most severe cases tubercle bacilli can enter the bloodstream and disseminate to all parts of the body, where they grow and cause the disease in multiple sites causing miliary tuberculosis, which is fatal if untreated.[56]

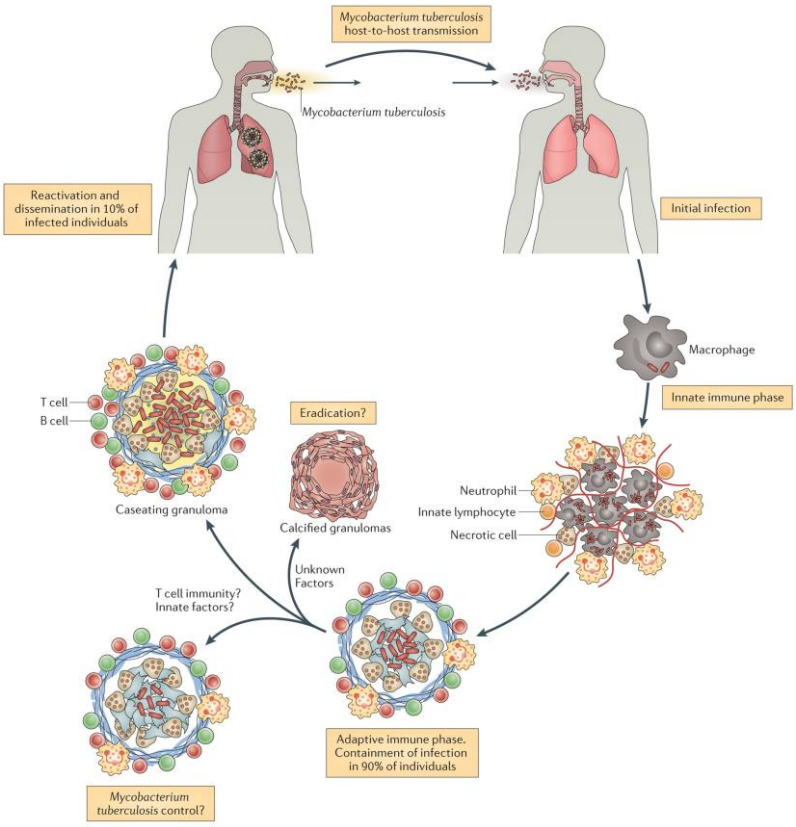

Figure 1.16. Reproduced with permission from reference. [55]

[54] Delogu, G.; Sali, M.; Fadda, G. *Mediterr. J. Hematol. Infect. Dis.* **2013**, *5*, e2013070.
[55] Nunes-Alves, C.; Booty, M. G.; Carpenter, S. M.; Jayaraman, P.; Rothchild A. C.; Behar. S. M. *Nat. Rev. Microbiol.* **2014**, *12*, 289.
[56] Farhat, M. R.; Shapiro, B. J.; Kieser, K. J.;Sultana, R.; Jacobson, K. R.; Victor, T. C.; Warren, R. M.; Streicher, E. M.; Calver, A.; Sloutsky, A.; Kaur, D.; Posey, J. E.; Plikaytis, B.; Oggioni, M. R.; Gardy, J. L.; Johnston, J. C.; Rodrigues, M.;Tang, P. K.C.; Kato-Maeda, M.; Borowsky, M.L.; Muddukrishna, B.; Kreiswirth, B. N.; Kurepina, N.; Galagan, J.; Gagneux, S.; Birren, B.; Rubin, E.J.; Lander, E. S.; Sabeti, P. C.; Murray, M. *Nat. Genet.* **2013**, *45,* 1183.

Current antitubercular therapy depends on the type of strain causing the infection. In the case of drug-susceptible tuberculosis (DS-TB) the first line antitubercular agents can be used. This treatment involves isoniazid, rifamycin, pyrazinamide, streptomycin and ethambutol. Usually a combination of four of them is taken for 2 months, rapidly killing the actively dividing bacteria and resulting in the negativization of sputum. This is followed by a continuation phase in which isoniazid and rifamycin are administered for another 4 to 7 months, in order to kill any remaining or dormant bacilli and prevent recurrence. With this regimen about 95% of DS-TB are cured in about 6 to 9 months.
The most popular second-line treatments for tuberculosis involve: fluoroquinolones as moxifloxacin, levofloxacin and gatifloxacin, aminoglycosides such as kanamycin and amikacin the polypeptide capreomycin, cycloserine and the thioamides ethionamide and prothionamide.

MDR-TB are usually resistant to at least isoniazid and rifampicin, while XDR-TB are resistant to these two drugs and usually to fluoroquinolones. In these cases, second-line antitubercular drugs need to be used. It is worth nothing that some of them are injectable forms and usually the treatments last between 9 to 20 months, making then long and tedious. Moreover, the cure rates for MDR-TB are quite low, typically ranging from 50% to 70%; in the case of XDR-TB, the prognosis is even worse.[56]

A further complication comes from the existence of several drug-drug interactions that restrain the coadministration of some anti TB agents with certain treatments, such as anti-HIV or antidiabetics. For these reasons, to control the diseases there is an urgent need to develop new antitubercular agents able to: [57]

- Target MDR and XMDR strains.
- Lower dosing frequency and simplify day posology.
- Shorten treatments.
- Be co-administered with other drugs, such as HIV medications.

[57] Koul, A.; Arnoult, E.; Lounis, N.; Guillemont, J.; Andries, K. *Nature* **2011***, 469,* 483.

1.6. Multitarget drugs

During the 20th century, the "one molecule, one target, one disease" was the main approach for drug discovery in pharmaceutical industry. [58] This paradigm helped to develop variety of successful selective drugs against certain diseases. However, this mindset started to change in 2005 after the publication of the perspective article entitled "Designed multiple ligands. An emerging drug discovery paradigm".[59]

In multifactorial pathologies, such as neurodegenerative, cancer, cardiovascular or infectious diseases, several receptors or signalling pathways are involved. Thus, the inhibition of a single target does not lead to successful drugs. In this context, inhibition of several checkpoints of the same disease appears as an attractive alternative. Moreover, the mentioned strategy would have the possibility of overcoming resistance to single-target agents in chemotherapy.[60]

The polypharmacology approach can be achieved by three different strategies:[60]

1. *Mixture of monotherapies*, or *drug cocktails:* several drugs, each with a single active ingredient.
2. *Drug combination:* one formula with multiple active ingredients.
3. *Multitarget Directed Ligands (MTDL):* one chemical entity with multiple pharmacological activities. **(Figure 1.17)**

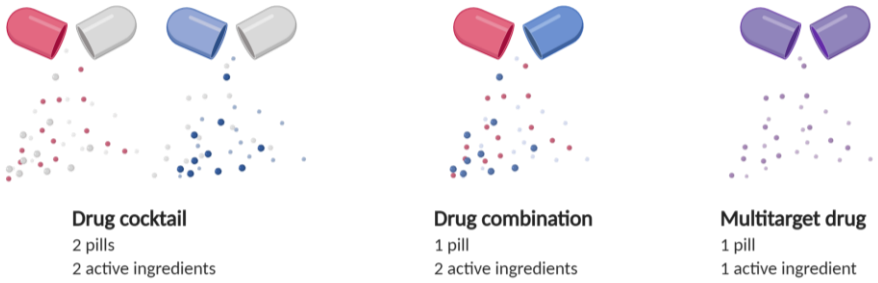

Figure 1.17.

[58] Medina-Franco, J. L.; Giulianotti, M. A.; Welmaker, G. S.; Houghten, R. A. *Drug Discovery Today* **2013**, *18*, 495.
[59] Morphy, R.; Rankovic, Z. *J. Med. Chem.* **2005**, *48*, 6523.
[60] Bolognesi, M. L. *Curr. Med. Chem.* **2013**, *20*, 1639.

While a mixture of monotherapies can offer a better dose flexibility, sequential administration due to clinical experience and lower treatments cost. Multiple directed ligands offer easier development and regulatory procedures, reduced adverse effects, drug-drug interactions and wider therapeutic windows, higher efficacy due to synergic effects, easier pharmacokinetic and pharmacodynamic profiles, resistance development prevention and the avoidance of poor patient compliance issues compared to drug cocktails.

On the other hand, developing balanced and multiselective ligands towards multiple targets is not an easy process.[61]

From an economical point of view, even if the starting hit identification and optimization processes would be more expensive, MTDL are more efficient in cost terms. As previously mentioned, pharmacodynamic and pharmacokinetic profiles would be significantly simpler to study. Formulation and manufacturing would be easier and cheaper; and in terms of regulatory approval processes there would be advantages also, making them more cost-effective.[60]

Depending on their design strategy, MTDL can be classified into three groups:[61] **(Figure 1.18)**

1. ***Hybrid or linked:*** two or more pharmacophores separated by a linker. The position, length and composition of the linker must be rationally designed in order to maintain the activity of the pharmacophores. This linker can be metabolically stable or both fragments can be cleaved *in vivo* acting like mutual prodrugs. Usually linked pharmacophores are not the best choice due to their high molecular weight and consequently poor bioavailability.
2. ***Fused:*** the pharmacophores are partially overlapped.
3. ***Merged:*** with this strategy the highest level of pharmacophore overlapping is achieved. For this reason, even if is the most complicated one is the most attractive approach in terms of drug-likeness properties.

[61] Junting, Z.; Xueyang, J.; Siyu, H.; Hongli, J.; Feng, F.; Wenyuan, L.; Wei, Q.; Haopeng, S. *J. Med. Chem.* **2019**, *62*, 8881.

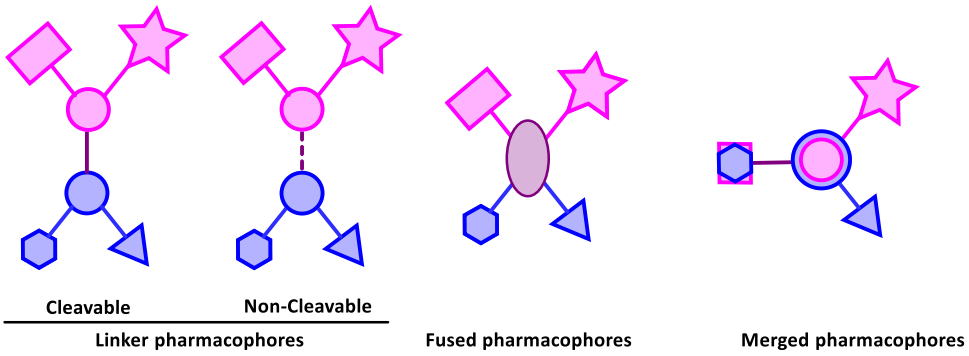

Figure 1.18: Different types of multitarget directed ligands.

Finally, a different design strategy is the use of metabolism-activated multitarget ligands (MAMUT), based on the combination of synergistic effects of a parent drug and its active metabolite(s).[62]

1.6.1. Multitarget drug discovery for Alzheimer´s and neglected tropical diseases

As previously mentioned, the multitarget approach is particularly suitable for the treatment of multifactorial diseases. In this kind of diseases is rare to find one single physiological pathway altered, instead the histopathological pathways are usually interconnected as networks. These networks have evolved to be very robust and reductant. Thus, it is very unlikely that the disease can be stopped by modulating one single check-point. This way is clear that a multimodal approach needs to be used to impact the disease pathogenesis.

Apparently, drug discovery approaches for Alzheimer´s and neglected diseases may seem the opposite, however nowadays both are mayor worldwide health problems without available effective treatments.

There are about 50 million Alzheimer patients worldwide, and every year 7.7 million new cases are diagnosed. It is estimated that this value will increase to 115.4 million in 2050. In parallel drug research has accelerated, but no effective drugs have been found.

Neglected tropical diseases are another of the main health global problems. It is estimated that over one billion people are affected worldwide, mainly in low-income

[62] Mátyus, P.; Chai, C. L. L. *ChemMedChem, **2016**, 11,* 1197.

countries. Nowadays, all the available drugs suffer from toxic side effects, resistance or poor efficacy. For these reasons new strategies are needed to beat these diseases.

In this scenario, MTDL able to inhibit different targets of Alzheimer or neglected diseases appear as an attractive alternative, which could be more efficacious, simple and adequate.[63]

[63] Prati, F.; Uliassi, E.; Bolognesi, M. L. *Med. Chem. Commun.,* **2014,** *5*, 853.

CHAPTER 2. OBJECTIVES

Objective 1

The word "theranostic" describes a compound or material that provides therapeutic effects and diagnostic imaging under the same dose. The first objective of this thesis is to develop small-molecule theranostic agents for optical detection based on the 2-styrylquinoline framework. The ideal *in vivo* fluorescence probe should show emission in the near infrared region, high fluorescence quantum yields and a large Stokes shift. These features can be achieved by reducing the HOMO-LUMO energy gap by the presence of an extended conjugation system and the introduction of an electron donor and electron acceptor groups as terminal moieties of the conjugated system. Thus, the first objective becomes the preparation and spectral characterization of compounds with the following general structures:

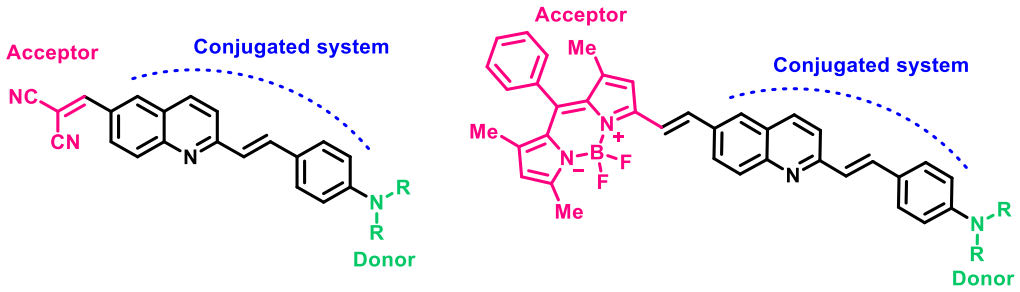

Objective 2

Protein-misfolding diseases are due to errors that take place during the protein folding process, giving misfolded states and the so-called amyloid aggregates. They are increasingly important and include most of the neurodegenerative diseases (Alzheimer's disease, Parkinson's disease, amyotrophic lateral sclerosis, Huntington's disease, Creutzfeldt-Jakob disease, etc.) and type II diabetes, among others. In this context, our second objective was to test the styrylquinoline derivatives as theranostic agents in the context of Alzheimer's disease, by studying their neuroprotective properties in parallel with their use for the imaging of β-amyloid protein. Furthermore, the use of these molecules as markers for amylin, an amyloidogenic protein involved in diabetes, was also examined.

Objective 3

Quinolines have shown a high potential to develop effective and affordable oral treatments as leishmanicidal agents. Using as a starting point the activities of 8-aminoquinoline-based polyamines, we reasoned that an increase in the positive charge of quinoline core would enable the molecules to have a preferential mitochondrial accumulation because mitochondria present a high electrochemical potential ($\Delta\psi_m$). In this context, we designed a library of 2-substituded styrylquinolines, which were decorated with polyamine chains in the C-4 position of the quinoline scaffold. The presence of the 2-styryl fragment, besides potentially increasing activity according to some literature precedent, was expected to confer fluorescence to the molecules and, ideally, allow imaging of the parasite mitochondrion.

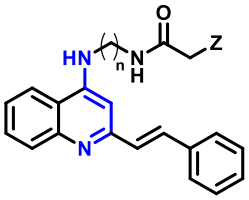

Objective 4

Besides fluorescence-based optical imaging, multi-spectral optoacoustic tomography (MSOT) is appealing as an alternative imaging technique, but its main problem lies on the difficulty of developing adequate molecules acting as MSOT probes. These probes should exhibit absorbance maxima in the NIR range but a low fluorescence quantum yield. To achieve this goal, conjugated structures bearing aromatic systems with push-pull architectures and fluorescence quenchers can be viewed as a good strategy. We envisioned the use of dihalo-bis-indolylquinones for this purpose.

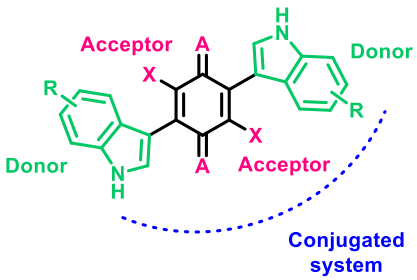

Objective 5

Finally, we undertook the preparation and study of antitubercular compounds acting by a mechanism designed to involve the synergistic effects of the compound itself and an active metabolite. This is an emerging type of multitarget strategy described as metabolism-activated multitargeting (MAMUT). More specifically, our compounds are meant to act at the MmpL3 mycobacterial membrane transport protein and the InhA enzyme, necessary for the biosynthesis of mycobacterial mycolic acids, following activation by the katG peroxidase. These compounds are based on a pyrrole framework, structurally related to known MmpL3 inhibitors, and an isoniazid moiety.

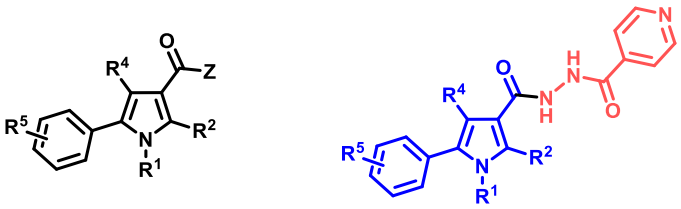

CHAPTER 3. STYRYLQUINOLINE DERIVATIVES AS THERANOSTIC AGENTS FOR ALZHEIMER'S DISEASE

3.1. A more detailed view of Alzheimer´s disease etiopathology

As previously mentioned, Alzheimer´s disease has a complex and multifactorial ethology, in which several factor as: β-amyloid aggregates, neurofibrillary tangles, calcium homeostasis deregulation, mitochondrial dysfunction, oxidative stress, chronic neuroinflammation and cholinergic disbalance, are involved. Some of these factors will be analysed below.

3.1.1. β-amyloid hypothesis

As its name shows, the amyloid protein precursor (APP) is the protein that initiates the cascade of events ending in β-sheet aggregation (Aβ). Its physiological function is still unknown, although it is thought to be involved in synaptogenesis, neural maturation, differentiation and viability. APP is a transmembrane glycoprotein, which under physiological conditions is easily metabolized. During the normal process, α-secretase metabolizes APP into sAPPα, an extracellular soluble fragment, and a transmembrane C-terminal fragment (CTFα), which is further split into P3 and APP intracellular domain (AICD) by γ-secretase; it is worth highlighting that none of these products is toxic. On the other hand, under pathological conditions, APP is metabolized by β-secretase (β-site amyloid cleaving enzyme 1, BACE1), leading to sAPPβ, that is further excised by γ-secretase, giving AICD and Aβ, which is able to form oligomers, fibrils and finally plaques.[64] **(Figure 3.1)**

This hypothesis was postulated in 1992 by Hardy and Higgins and has been corroborated by the studies done in patients with familiar AD, in which mutations in APP, Psen1 or Psen2 (genes codifying secretases) were found.[65]

Even though no correlation between Aβ plaques and cognitive damage has been found yet, it is known that Aβ accumulation precede in 15-20 years the clinical symptoms.

[64] Coronel, R.; Bernabeu-Zornoza, A.; Palmer, C.; Muñiz-Moreno, M.; Zambrano, A.; Cano, E.; Liste, I. *Mol. Neurobiol.* **2018**, *55*, 7107.
[65] Hardy, J. A.; Higgins, G. A. *Science*, **1992**, *256*, 184.

Nowadays, it is accepted that β aggregation contributes to disease development, even if is not its cause.[66]

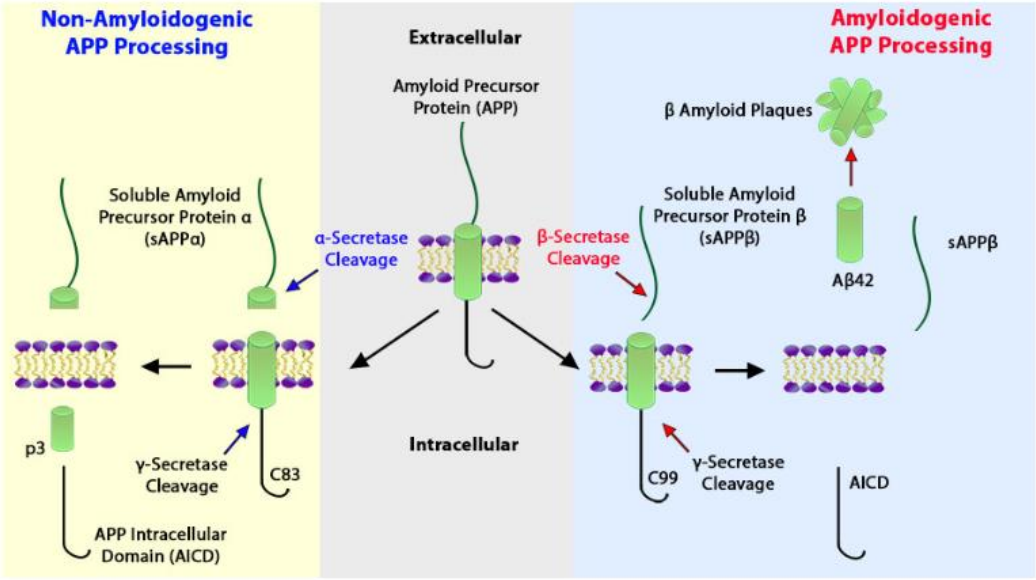

Figure 3.1: Physiological and amyloidogenic pathways of IAPP.

3.1.2. Tau hypothesis

Under physiological conditions, tau oversees the stability and assembly of microtubules, it also affects axonal transport and synapses and is involved in protein trafficking and signalling.[67]

From a structural point of view, tau possess three domains:[68]

1. N-terminal or projection domain.
2. Proline-rich domain, which is the target of serine/proline and threonine/proline directed kinases (PDPKs) that regulate the binding to tubulin by phosphorylation/dephosphorylation equilibria.
3. C-terminal or assembly domain, which interacts with microtubules and stabilizes them.

[66] Herrup, K. *Nat. Neurosci.* **2015**, *18*, 794.
[67] Iqbal, K. Alonso, A.; Chen, S.; Chohan, M. O.; El-Akkad, E.; Gong, C.; Khatoon, S.; Li, B.; Liu, F.; Rahman, A.; Tanimukai, H.; Grundke-Iqbal, I. *Biochimica et Biophysica Acta* **2005**, *1739,* 198.
[68] Rao, S.S.; Adlard, P. A. *Frontiers in molecular neuroscience* **2018***, 11,* 276.

The enzyme in charge of modulating tau phosphorylation is glycogen synthase kinase 3β (GSK3β), protein kinase A (PKA), serine/threonine protein phosphatase 2A (PP2A) and cyclin-dependent-like kinase 5 (CDK5), which are therefore essential for microtubule regulation. In AD patients, the activity of some of these enzymes is compromised and as a result the levels of phosphorylated tau increase. Phospho-tau is considered an aggregation-prone protein, which generates helical filaments that finally lead to neurofibrillary tangles. Moreover, this phosphor-tau accumulation disrupts microtubule assembly, which leads to neuronal death.[69] **(Figure 3.2)**

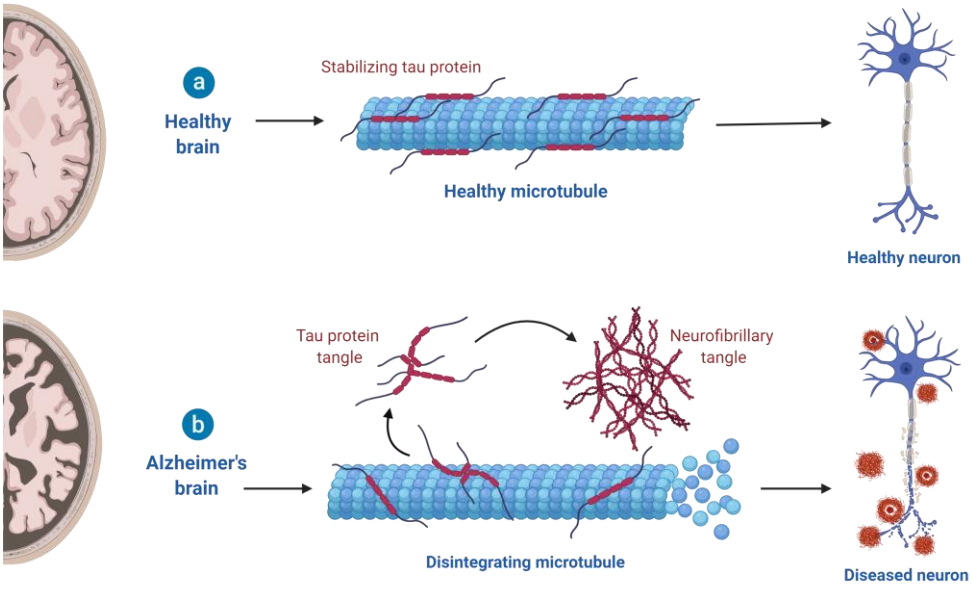

Figure 3.2: Physiological and pathological pathways of tau.

3.1.3. Oxidative stress hypothesis

A radical is a chemical species that contains one or more unpaired electrons in an atomic or molecular orbital, usually coming (in biological settings) from the reduction of an oxygen molecule. Reactive oxygen species (ROS) comprise two oxygen radicals, namely superoxide anion (O2•-) and the hydroxyl radical (•OH), and hydrogen peroxide (H_2O_2).[70]

[69] Iqbal, K.; Liu, F., Gong, C. X. *Nature Reviews. Neurology,* **2016**, *12,* 15.
[70] D'Autréaux, B.; Toledano, M. B. *Nat. Rev. Mol. Cell Biol.* **2007**, *8*, 813.

While under moderate concentrations ROS play key roles in physiological signaling pathways, an increase in ROS activity induces oxidative stress, which in turn leads to senescence, which is correlated with pathological processes. Moreover, the main characteristics of neuronal tissues are their rich lipid content, high energy demand, weak antioxidant capacity and low regenerative ability. For these reasons, the hyperproduction of ROS specifically in these tissues causes neuronal death and brain damage.[71,72]

ROS can be generated through different pathways. In the first place, molecular oxygen is transformed into $O_2^{\bullet-}$ by accepting one electron through mitochondrial oxidative phosphorylation or through the action of several enzymes such as cyclooxygenase (COX) and others. Once superoxide anion is formed it can be eliminated by different pathway such as superoxide dismutase enzymes (SOD) giving H_2O_2. This hydrogen peroxide can be transformed into O_2 and H_2O by different enzymes as peroxidase catalase (CAT). H_2O_2 can also be a substrate of the Fenton reaction, giving $^{\bullet}OH$, a highly reactive radical with short half-life. The deregulation of these redox-equilibriums can lead to ROS overproduction; moreover, β-amyloid aggregates contain Cu^{2+} or Fe^{2+}, which can catalyze the Fenton reaction and contribute to ROS formation.[73,74]

Once these oxygen reactive species are formed, they can be toxic in through different pathways, such as lipid peroxidation, [75,76] DNA oxidative damage [77] or calcium overload,[78,79] all of them leading into cytotoxicity and cell death. **(Figure 3.3)**

[71] Lotharius, J.; Brundin, P. *Nat. Rev. Neurosci.* **2002**, *3*, 932.
[72] Barnham, K. J.; Masters, C. L.; Bush, A. I. *Nat. Rev. Drug Discov.* **2004**, *3*, 205.
[73] Salim, S. *J. Pharmacol. Exp. Ther.* **2017**, *360*, 201.
[74] Prousek, J. *Pure appl. Chem.y* **2007**, *79*, 2325.
[75] Selley, M. L.; Close, D. R.; Stern, S. E. *Neurobiol. Aging* **2002**, *23*, 383.
[76] Dexter, D. T.; Carter, C. J.; Wells, F. R.; Javoy-Agid, F.; Agid, Y.; Lees, A.; Marsden, C. D. *J. Neurochem.* **1989**, *52*, 381.
[77] Alam, Z. I.; Jenner, A.; Daniel, S. E.; Lees, A. J.; Cairns, N.; Marsden, C. D.; Jenner, P.; Halliwell, B. *J. Neurochem.* **1997**, *69*, 1196.
[78] LaFerla, F. M. *Nat. Rev. Neurosci.* **2002**, *3*, 862.
[79] Gibson, G. E. *Free Radic. Biol. Med.* **2002**, *32*, 1061.

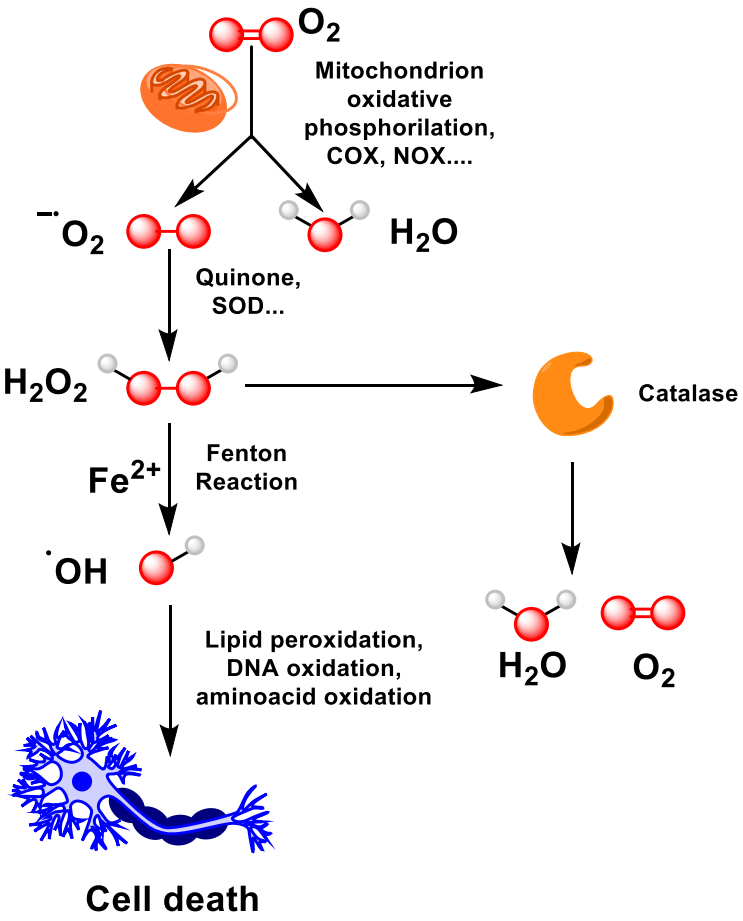

Figure 3.3: ROS formation.

3.1.4. Multifactorial hypothesis

A model based on five of biomarkers has been proposed for tracking the temporal evolution of Alzheimer´s disease. In the first stage, 10-5 years before the dementia is diagnosed, a steep increase in $A\beta_{42}$ can be detected, while level of phospho-tau in cerebrospinal fluid increases in a more progressive way.[80,81] The increases of $A\beta_{42}$ and tau levels are an early even that precedes hypometabolism and finally atrophy, neurodegeneration and clinical symptoms.[82] **(Figure 3.4)**

[80] Jack Jr, C. R.; Knopman, D. S.; Jagust, W. J.; Petersen, R. C.; Weiner, M. W.; Aisen, P. S.; Shaw L. M.; Vemuri, P.; Wiste, H. J.; Weigand, S. D.; Lesnick, T. G.; Pankratz, V. S.; Donohue, M. C.; Trojanowski, J. Q. *Lancet Neurol.* **2013**, *12*, 207.
[81] Buchhave, P.; Minthon, L.; Zetterberg, H.; Wallin, Å. K.; Blennow, K.; Hansson, O. *JAMA Psychiatry* **2012**, *69*, 98.
[82] Pawlowski, M.; Meuth, S. G.; Duning, T. *Diagnostics,* **2017**, *7*, 42.

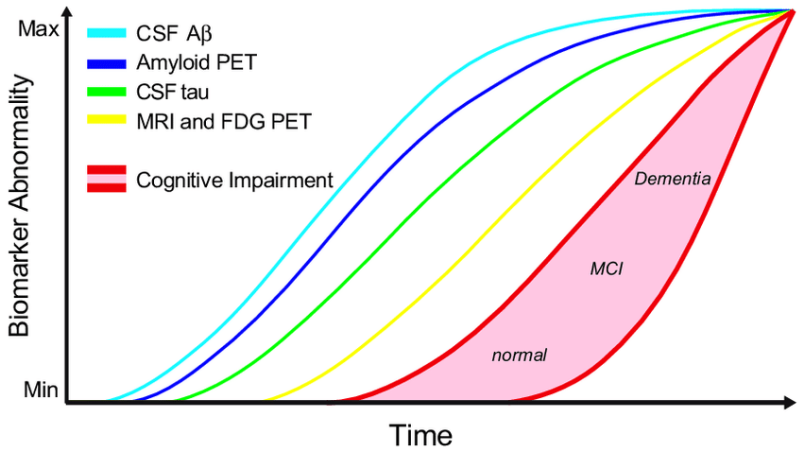

Figure 3.4. MCI: mild cognitive impairment, CSF Aβ: β-amyloid in cerebrospinal fluid, CSF: tau in cerebrospinal fluid, MRI: magnetic resonance imaging, FDG: fluorodeoxyglucose uptake, PET: positron-emission tomography

Even though it seems that some sequential order can be elucidated, is also known that all these hallmarks are interconnected, and it is not clear if they are causes or consequences. For instance, protein misfolding may cause oxidative stress, calcium overloads, neuroinflammation or mitochondrial dysfunction. However, this pathway is bidirectional cause oxidative stress may cause modifications in DNA, lipids and proteins, which may lead to the misfolding and aggregation of the latter. Several of these factors can also trigger the formation of oligomers.[83, 84]

In this context, we can highlight that:

- ✓ Trying to develop new methodologies that allow an early visualization of $A\beta_{42}$ deposits would be a good approach for an early diagnosis of the disease.
- ✓ The development of new drugs that act selectively on one of the hallmarks seems an unsuccessful strategy, and thus the multitarget approach appears as a more efficient alternative.

3.2 Theranostic agents for Alzheimer's disease.

In spite of the great therapeutic advances achieved for many diseases in the last decades, AD and other neurodegenerative diseases remain incurable and are extremely

[83] Angelova, P. R.; Abramov, A. Y. *Biochem. Biophys. Res. Commun.* **2017**, *483*, 1110.
[84] Höhn, A.; Weber, D.; Jung, T.; Ott, C.; Hugo, M.; Kochlik, B.; Kehm, R.; König, J.; Grune, T.; Castro, J. P. *Redox Biol.* **2016**, *11*, 482.

challenging for medicinal chemists.[85] Moreover, although the investment in drug discovery against these maladies has increased, this effort has paradoxically led to fewer successful drugs, and there are still no treatments able to stop the course of the disease.[86]

This situation has been associated with several difficulties related to neurodegenerative diseases in general:

1. As mentioned above, the understanding of their aetiology remains poor, and the fact that many pathways are involved leads to the existence of no truly validated targets.[86]
2. The poorly predictive animal models available for these diseases complicate the development of effective drugs.[87]
3. Finally, the failure of many drug candidates has been associated to their administration when the pathology is too advanced.[88]

In this scenario, the theranostic approach appears as a good option to optimize the efficacy and safety of the therapy, as well as to streamline the whole drug discovery process. [89, 90]

Aβ deposits are the main pathological hallmark of Alzheimer's disease and they are believed to precede clinical symptoms by several years. Therefore, the imaging of fibrillar aggregates is particularly suitable to diagnose the onset of the disease in its early stage and monitor its progression.[91] Thus, the use of theranostics agents targeting amyloid plaques appears as a particularly suitable approach.[92,93] An ideal theranostic agent would have the ability to simultaneously allow real time evaluation of the amount

[85] Chen, B.; Thompson, M.; Louth, J.; Guo, K. *Curr. Top. Med. Chem.* **2013**, *13*, 2441.
[86] Pangalos, M. N.; Schechter, L. E.; Hurko, O. *Nat. Rev. Drug Discov.* **2007**, *6*, 521.
[87] Enna, S. J.; Williams, M. *J. Pharmacol. Exp. Ther.* **2009**, *329*, 404.
[88] Markou, A.; Chiamulera, C.; Geyer, M. A.; Tricklebank, M.; Steckler, *Neuropsychopharmacology* **2009**, *34*, 74.
[89] Kelkar, S. S.; Reineke, T. M. *Bioconjug. Chem.* **2011**, *22*, 1879.
[90] Lammers, T.; Aime, S.; Hennink, W. E.; Storm, G.; Kiessling, F. *Acc. Chem. Res.* **2011**, *44*, 1029.
[91] Aulić, S.; Bolognesi, M. L.; Legname, G. Int. *J. Cell Biol.* **2013**, *2013*, 150952.
[92] Bongarzone, S.; Staderini, M.; Bolognesi, M. L. *Future Med. Chem.* **2014**, *6*, 1017.
[93] Schulz-Schaeffer, W. J.; Tschoke, S.; Kranefuss, N. et al. *Am. J. Pathol.* **2000**, *156*, 51.

of drug reaching the pathological area, while visualizing the molecular changes caused by its therapeutic effects.

During the past years, several molecules able to stain Aβ fibrils and inhibit their aggregation have been reported, as summarized in the following Section.

3.3 NIR probes for the detection of amyloid plaques

NIR fluorescent probes have been mainly used in the oncology field although, as mentioned above, they are extremely useful to visualize and monitor amyloid plaque formation and to evaluate the effectiveness of drug treatment in animal models, therefore they are considered a promising tool for AD early diagnosis.

The clinical application of NIR imaging in AD is specially challenging, since amyloid deposits are formed inside the skull-shielded brain and optical imaging resolution decreases with increasing depth of penetration due to fluorescence scattering in the biological environment. Indeed, traditional fluorescence-based optical imaging of the brain of small animals relied on craniotomy or cranial windows techniques. However, the development of novel techniques such as fluorescent molecular tomography (FMT) or FMT-CT has enabled the *in vivo* visualization of Aβ plaques in mice with an intact cranium.[94] Although these techniques are still in need of technological improvements and it is most likely that the human brain cannot be entirely visualized by optical methods, it has nevertheless been proposed that it will be feasible to image the brain cortex at depths up to 3‑5 cm.[95, 96] Considering that most of the amyloid depositions are located on the neocortical surface, this should be enough to obtain information from AD patients.

Another approach for *in vivo* AD NIR imaging could be based on the use of parts of the central nervous system that are not skull-shielded. Some examples are the retina or the olfactory ephytellium. The retina turns out to be equivalent to a physiological skull

[94] Jucker, M. *Nature Medicine* **2010**, *16*, 1210.
[95] Ntziachristos, V. *Nature Methods* **2010**, *7*, 603.
[96] Hyde, D.; de Kleine, R.; MacLaurin, S. A.; Miller, E.; Brooks, D. H.; Krucker, T.; Ntziachristos, V. *Neuroimage.* **2009**, *44*, 1304.

window, easily accessible for non-invasive direct imaging. Even though there are controversies in the results, some authors have demonstrated the presence of Aβ plaques in the retina of AD patients, while others were able to detect fibrillar tau aggregates in transgenic mice retina and hyperphosphorylated tau AD human retina.[97,98] On the other hand, it is also worth noting that neurofibrillary tangles have been detected in the olfactory epithelium.[99]

Although several fluorescent probes with high affinity for amyloid plaques have been reported through the years, most of them cannot be translated into clinically useful agents due to their low sensitivity and specificity, toxicity or inability to cross the blood brain barrier.[100]

To overcome these drawbacks, it has been proposed that an ideal NIR probe for amyloid deposits imaging should:[18]

- Emit fluorescence in the NIR region.
- Present specificity to amyloid plaques.
- Be able to change fluorescence properties upon fibrils binding.
- Present a high binding affinity.
- Have a high fluorescence quantum yield and large Stokes shift.
- Shown minimum binding with human serum albumin (HSA).
- Be able to cross the BBB.
- Show low toxicity.

During the past years several families of NIRF probes have been reported. Depending on their structures they can be classified as follows:[101]

Curcumin and derivatives: Curcumin is a yellow pigment obtained from *Curcuma longa* rhizomes. Due to its highly delocalized π-electron system and symmetric structure, curcumin itself has been considered as a potential NIRF probe for imaging Aβ deposits

[97] Koronyo, Y.; Salumbides, B. C.; Black, K. L.; Koronyo-Hamaoui, M. *Neurodegener. Dis.* **2012**, *10*, 285.
[98] Schon, C.; Hoffmann, N. A.; Ochs, S. M.; Burgold, S.; Filser, S.; Steinbach, S.; Seeliger, M. W.; Arzberger, T.; Goedert, M.; Kretzschmar, H. A.; Schmidt, B.; Herms, J. *Plos One* **2012**, *7*, e53547.
[99] Gu, J.; Anumala, U. R.; Heyny-von Haußen, R.; Hölzer, J.; Goetschy-Meyer, V.; Mall, G.; Hilger, I.; Czech, C.; Schmidt, B. *ChemMedChem* **2013**, *8*, 891.
[100] Hong, Y.; Meng, L.; Chen, S.; Leung, C. W.; Da, L. T.; Faisal, M.; Silva, D. A.; Liu, J.; Lam, J.W.; Huang, X.; Tang, B. Z. *J. Am. Chem. Soc*. **2012**, *134*, 1680.
[101] Gyasi, Y. I.; Pang, Y.P.; Li, X. R.; Gu, J. X.; Cheng, X. J.; Liu, J.; Xu, T.; Liu, Y. *Eur. J. Med. Chem.* **2020**, *187*, 111982.

and tau fibrils. However, its short emission wavelength and low quantum yield frustrated the use of curcumin as a NIR probe. In an effort to improve these properties, several authors reported curcumin derivatives, named CRANAD, presenting chemical modifications as the introduction of difluoroboronate and *p*-dimethylamino phenyl groups based on a donor-acceptor-donor design, which enhanced the emission wavelength and led to successful bio-imaging probes.[101] **(Figure 3.5)**

BODIPY and derivatives: Since Treibs and Kreuzer described for first time BODIPY (boron dipyrromethane or 4,4-difluoro-4-bora-3a,4a-diaza-s-indacene) dye in 1968, it has gained much popularity among fluorescent probes.[102] It is known that BODIPY dyes present high quantum yield and are biocompatible, although they possess low BBB permeability and emission wavelength. For this reason, several modifications on the BOPIPY core have been reported to overcome these issues, resulting in different functional NIR probes.[101] **(Figure 3.5)**

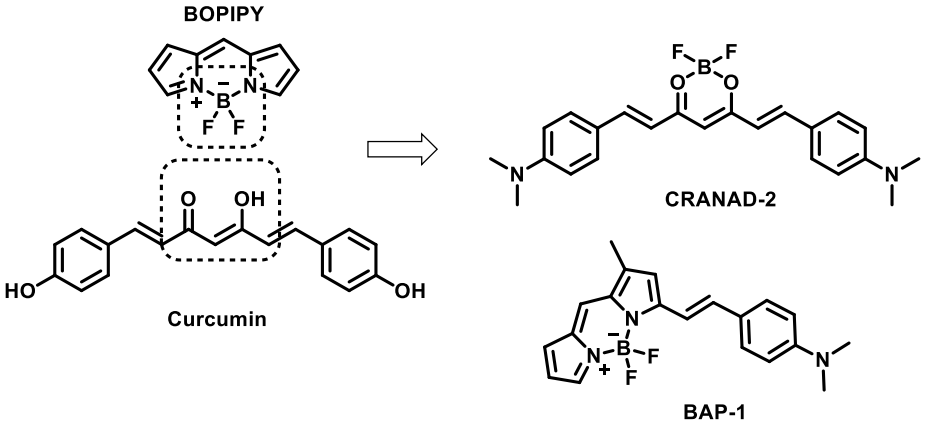

Figure 3.5.

***NIAD dyes*:** The design of NIAD probes is based on Thioflavin T (ThT) and Congo Red (CR), **(Figure 3.6)** which are based on planarized or easily planarized π-systems. NIADs present several donor-acceptor structures to enhance longer excitation/emission wavelengths, while their central core is based on hydrophilic groups (thiophene) which avoid high lipophilicity. Moreover, hydroxyl groups are frequently introduced to balance the BBB permeability and amyloid fibrils affinity.[101] **(Figure 3.6)**

[102] Treibs, A.; Kreuzer, F.H. *Justus Liebigs. Ann. Chem.* **1968**, *718*, 208.

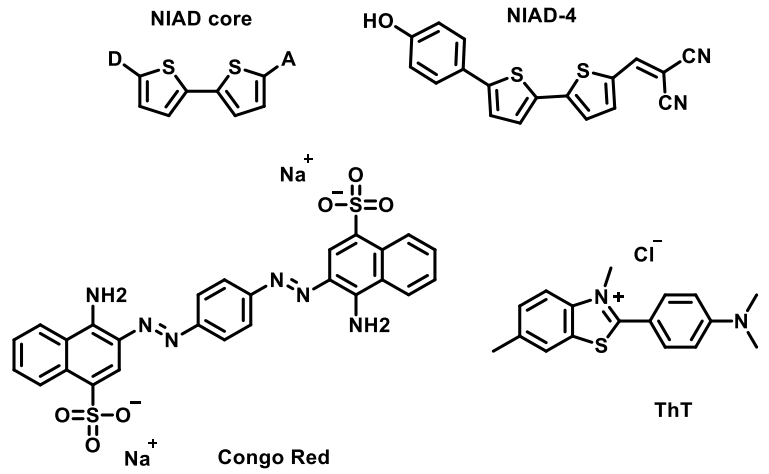

Figure 3.6.

***Oxazines*:** Oxazines presents oxygen and nitrogen atoms in a doubly unsaturated six-membered ring. Their design is based on *p*-benzoquinone imines or diimines and they are mainly characterized by their solvatochromism, which makes them sensitive to their environment and is an important feature of good probes.[101] **(Figure 3.7)**

DANIR (Donor-Acceptor Near-Infrared): In 2014, Cui et al. employed the Donor-Acceptor approach and the extension of π-conjugation to increase electron delocalization and consequently the emission wavelength, reporting this way three novel NIR fluorescence probes to detect Aβ deposits, named DANIR. These dyes exhibited a high affinity for Aβ plaques in AD patients and double transgenic mice. Moreover, they were able to penetrate the BBB while presenting fast kinetics of washout.[103] **(Figure 3.7)**

THK-265: was developed in 2011 by Okaruma and coworkers, the dye was able to label Aβ deposits and it exhibited high quantum yields, molar absorption and binding affinity. Unfortunately, when it came to *in vivo* imaging THK-265 was unable to cross the BBB.[104] **(Figure 3.7)**

[103] Cui, M.; Ono, M.; Watanabe, H.; Kimura, H.; Liu, B.; Saji, H.; *J. Am. Chem. Soc.* **2014**, *136,* 3388.
[104] Okamura, N.; Mori, M.; Furumoto, S.; Yoshikawa, T.; Kudo, Y. *J. Alzheimer's Dis*. **2010**, *23*37.

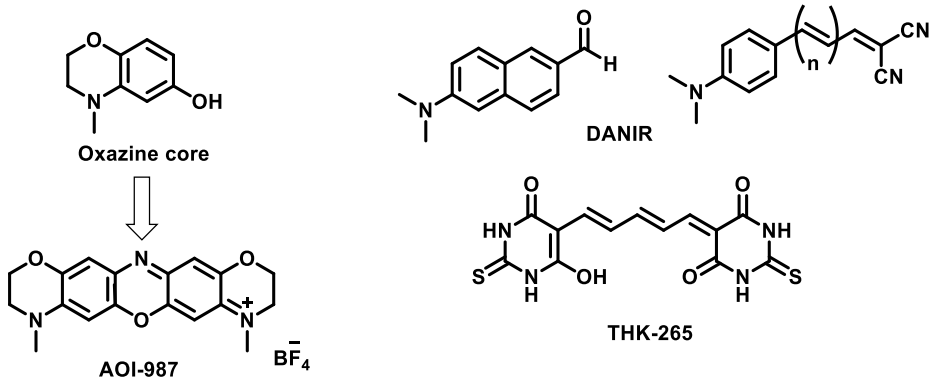

Figure 3.7.

Coumarin derivatives: Shin and co-workers reported iminocoumarin probe IRI-1,[105] designed by combining IBC-2, a large two-photon coumarin-based dye, with ThT. This compound presents large signal-to-background ratios and near-infrared emission, resulting in a dye with excellent properties for *in vivo* and *ex vivo* imaging.[101] **(Figure 3.8)**

Cyanine derivatives: Yang and co-workers presented a few years ago a representative example of a family of theranostic agents against Alzheimer's disease, based on a family of carbazole-based cyanidine derivatives. Among them, SLOH **(Figure 3.8)** was the most attractive candidate, showing selective binding towards $A\beta_{(1\text{-}40)}$ peptides, aggregates and plaques, with strong fluorescence enhancement. Moreover, it was able to inhibit Aβ aggregation and fibrinogenesis, while being non-toxic to neuronal cells. A neuroprotector effect of SLOH against $A\beta_{(1\text{-}40)}$ induced toxicity was also demonstrated. Finally, in vivo experiments verified the ability of the compound to cross the BBB and target Aβ plaques. [106] The related SLM, another carbazole-based quinolinium cyanine dye,[106] has also been reported as an effective theranostic agents for *in vivo* imaging of Aβ in AD mouse models.[101]

Quinoline-malononitrile*:* TM-1 and TM-2 were synthesized in order to improve NIR probes solubility, by introducing a sulfonate group and replacing a naphthalene with a phenyl moiety. These probes present the typical D-A architecture and exhibit maximum

[105] Shin, J.; Verwilst, P.; Choi, H.; Kang, S.; Han, J.; Kim, N.H.; Choi, J.G.; Oh, M.S.; Hwang, J.S.; Kim, D. *Angew. Chem.* **2019**, *58,* 5648.
[106] Yang, W.; Wong, Y.; Ng, O. T. W.; Bai, L.; Kwong, D. W. J.; Ke, Y.; Jiang, Z.; Li, H.; Yung, K. K. L.; Wong, M. S. *Angew. Chem. Int. Ed.* **2012**, *51*, 1804.

emission wavelengths at 680-650 nm. TM-1 and TM-2 were able to bound amyloid fibrils and exhibited significant fluorescence enhancement upon detection.[101] **(Figure 3.8)**

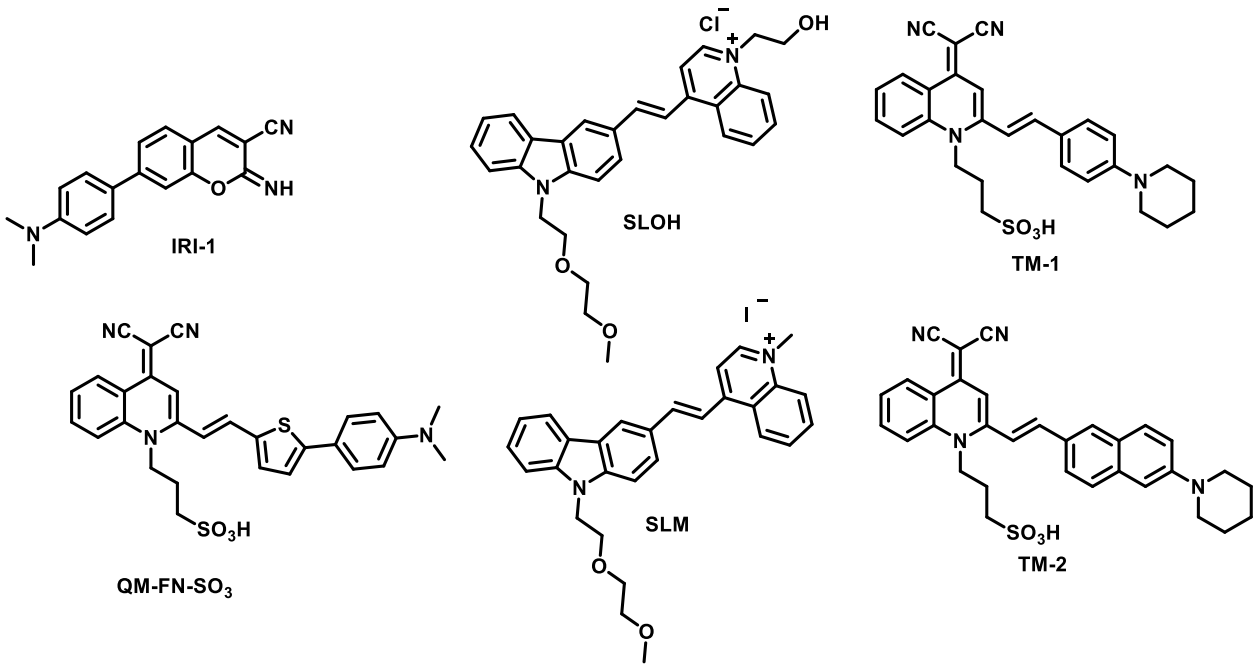

Figure 3.8.

Although many efforts to design better *in vivo* amyloid imaging NIR probes have been done in recent years, most of these compounds still present several drawbacks, usually associated with their solubility, toxicity, inability to cross the BBB, poor sensitivity or sub-optimal spectroscopic properties. Thus, the goal of development ideal amyloid-NIR fluorescence probes is a field that still needs to be improved. For a review of this area, reference [101101] can be perused.

3.4. Design of NIR styrylquinolines as theranostic agents

Some years ago, our group disclosed **styrylquinoline A**, which exhibited excellent properties as a starting point for developing theranostic agents against protein misfolding diseases. This compound showed the ability cross the BBB in a parallel artificial membrane permeability assay (PAMPA). Then its ability to inhibit $A\beta_{42}$ aggregation was assessed by a ThT-based fluorometric assay, behaving as a moderate fibrillization inhibitor and amyloid binder. To investigate the binding mode of **styrylquinoline A** to Aβ, displacement studies in the presence of aggregated $A\beta_{42}$ were

carried out using a fixed concentration of $A\beta_{42}$ and ThT and an increasing concentration of **A**. As a conclusion from these experiments it was proposed that **styrylquinoline A** may have a primary high affinity binding site distinct from ThT and a secondary low-affinity binding site in common with ThT. Moreover, **compound A** was able to detect $A\beta_{42}$ while no interaction with human seric albumin (HSA) was observed. Afterwards, its antiprion activity was tested. In a first assay, **compound A** was able to delay prion fibril formation. Then, in cell-based models of prion disease (ScGT1 cells), **compound A** showed remarkable antiprion activity in nontoxic concentrations. Finally, PrPSc specific binding was confirmed by fluorescent staining with **styrylquinoline A** carried out using ScGT1 living cells.

From a spectroscopic point of view, the native fluorescence of **styrylquinoline A** greatly depended on solvent polarity and its fluorescence emission in ethanol, whose polarity mimics the protein environment, was red-shifted compared to more polar solvents. Moreover, the emission spectra of **styrylquinoline A** showed a hypsochromic shift (from 528 to 490 nm) and a hyperchromic effect upon binding to $A\beta_{42}$. Finally, the solid state fluorescence spectrum of **styrylquinoline A**, as a hydrochloride salt, exhibited an emission maximum above 600 nm.[107]

Xiao-Qin Wang and collaborators [108] also reported a family of 2-styrylquinoline derivatives as multitarget agents for the treatment of Alzheimer's disease. These compounds were able to inhibit Aβ1-42 aggregation, they also acted as potential antioxidant and biometal chelators, moreover, some of them were able to inhibit acetylcholinesterase (AChE) and butyrylcholinesterase (BuChE).

In this scenario, we viewed **styrylquinoline A** as a good starting point, which can be easily manipulated for developing theranostic agents for protein misfolding diseases. On one hand, it has been proved that the styrylquinoline core can inhibit several pathological pathways involved in Alzheimer's disease, and thus they can be considered multitarget-directed ligands. On the other hand, from an imaging point of view the

[107] Staderini, M.; Aulić, S.; Bartolini, M.; Tran, H.N.; González-Ruiz, V.; Pérez, D. I.; Cabezas, N.; Martínez, A.; Martín, M. A.; Andrisano, V.; Legname, G.; Menéndez, J. C.; Bolognesi. M. L. *ACS Med. Chem. Lett*. **2012**, *4*, 225.
[108] Wang, X. Q.; Xia, C. L.; Chen, S. B.; Tan, J. H.; Ou, T. M.; Huang, S. L.; Li, D.; Gu, L. Q.; Huang, Z. S. *Eur. J. Med. Chem.* **2015**, *89*, 349.

absorbance and emission maxima could be easily modified by introducing a push-pull architecture, thus reinforcing the electron-donating/accepting ability of the molecule to enhance the spectral bathochromic shift.

For this purpose, we designed a family of styrylquinoline derivatives, in which different amines bearing diverse substituents were use as electron-donor groups, while a dicyanomethylene groups was chosen as electron acceptor. We also started building a second family of derivatives, this time using the well-known BODIPY core as the electron acceptor part of the molecule. **(Figure 3.9A and 3.9B)**

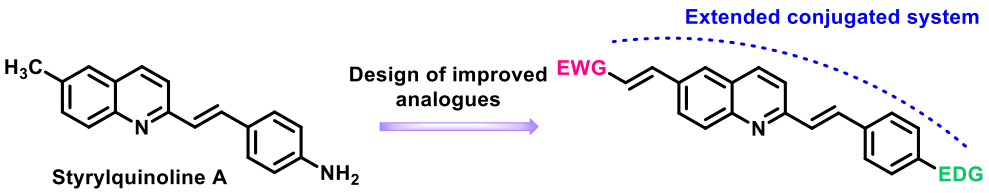

Figure 3.9.A. Design of theranostic derivatives.

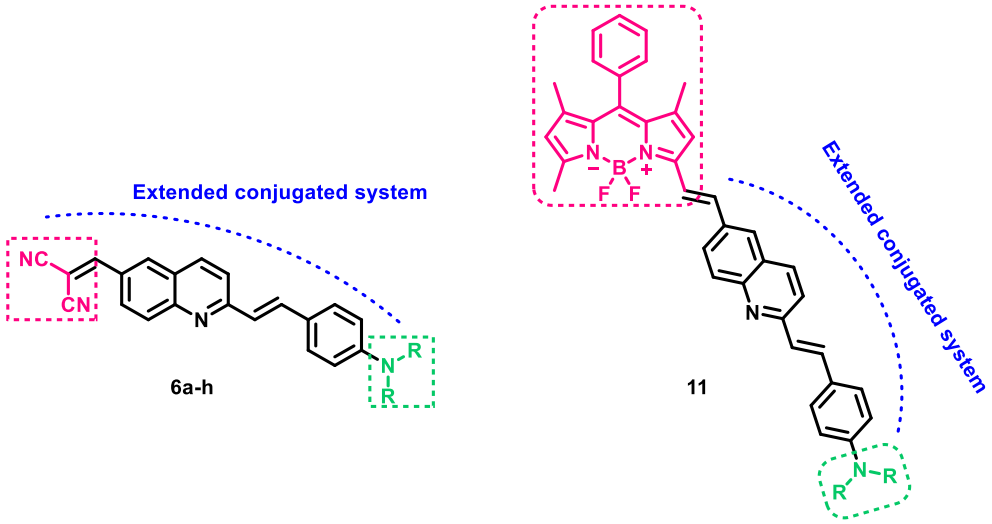

Figure 3.9.B.

3.5. Synthesis of stryrilquinoline derivatives

For the synthesis of the dicyanomethylene derivatives some difficulties needed to be faced, and the beginning different alternative pathways were explored. **(Scheme 3.1)**

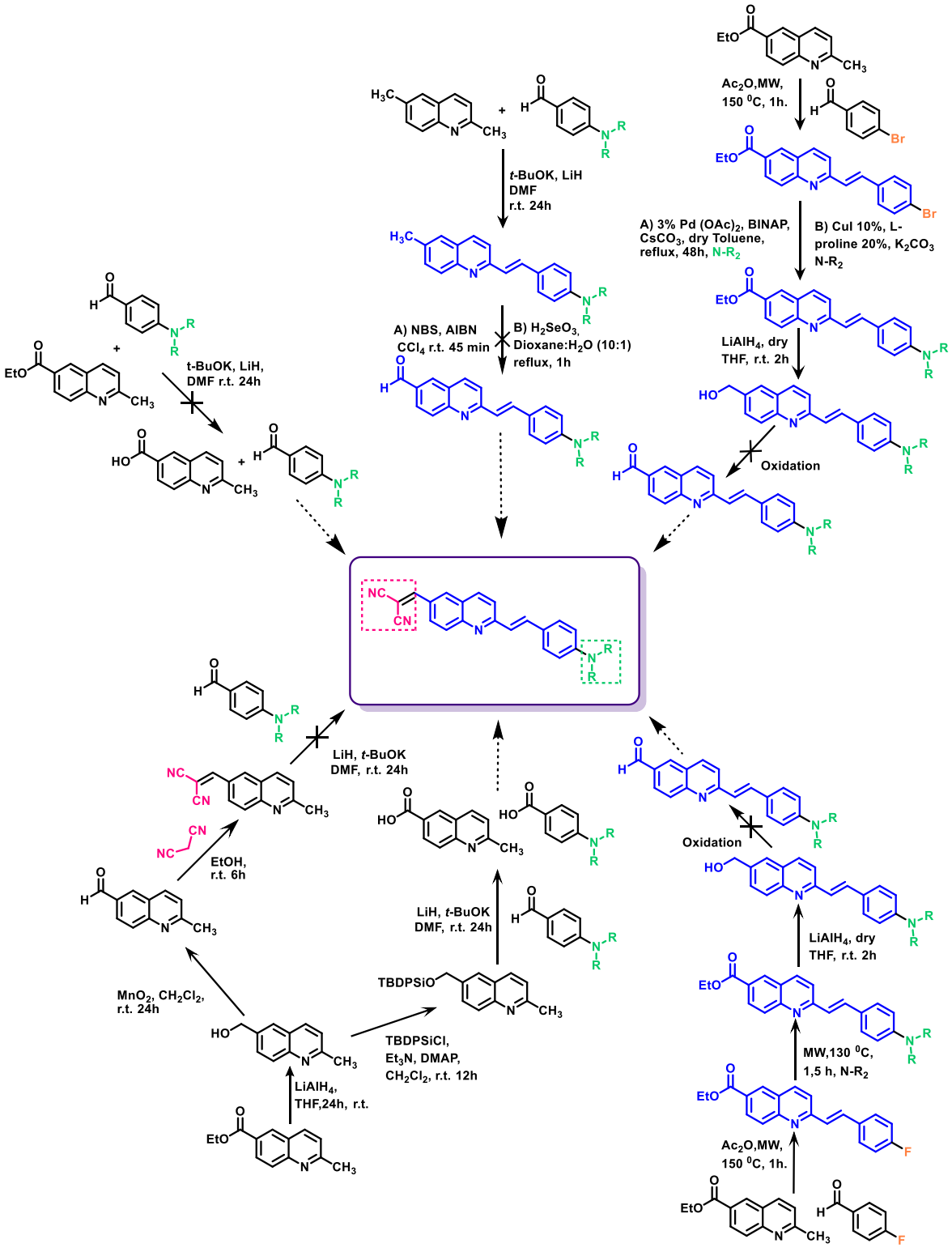

Scheme 3.1.

Finally, we were able to devise a simple four-step route **(Scheme 3.2)** that allowed us to introduce the variability at the final step, thus yielding the eight-compound library. **(Table 3.1)**

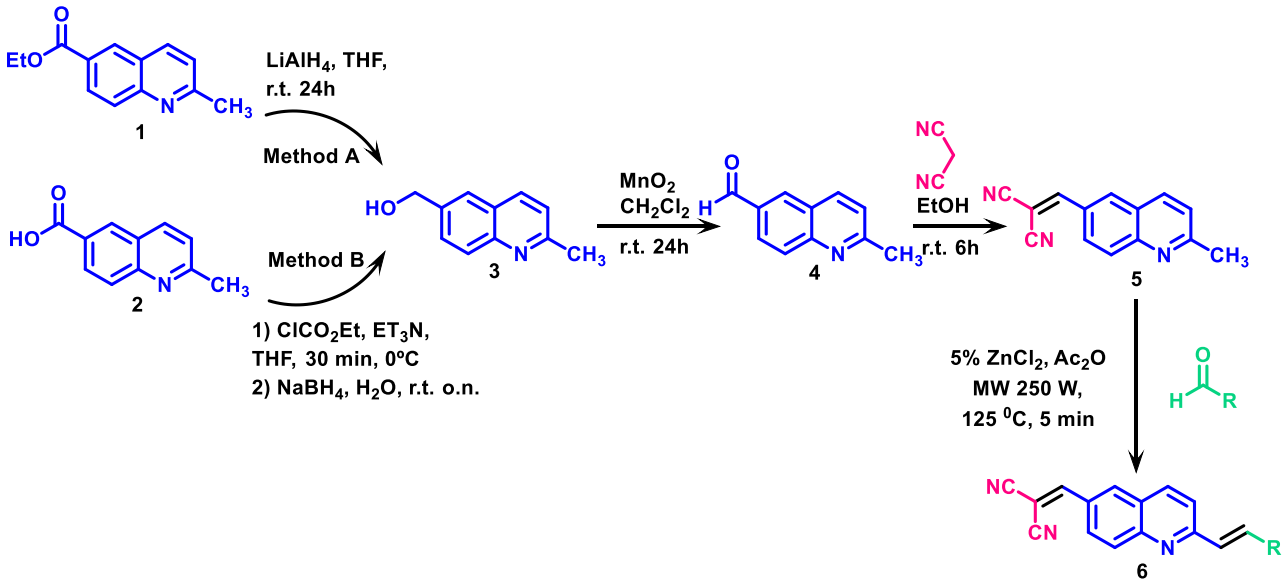

Scheme 3.2.

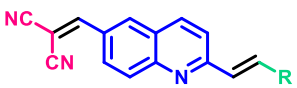

Cpd.	6a	6b	6c	6d
R	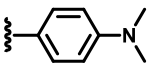	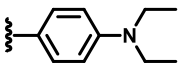	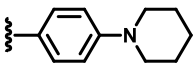	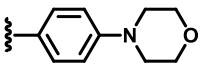
Yield (%)	85	55	40	58
Cpd.	**6e**	**6f**	**6g**	**6h**
R	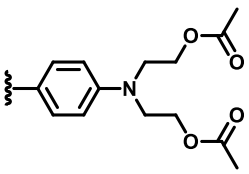	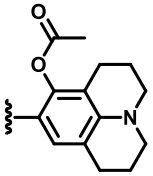	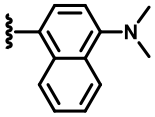	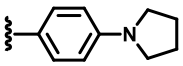
Yield (%)	20	40	56	76

Table 3.1.

Unfortunately, this route did not allow us to obtain compounds **6i-m**. **(Table 3.2)** Derivatives **6i-k** resulted unstable, while all the attempts to obtain compounds **6l** and **6m** from their analogues **6e** and **6f** respectively, resulted in compound decomposition.

Cmpd.	6i	6j	6k	6l	6m
R	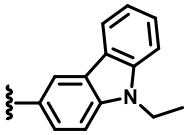	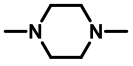	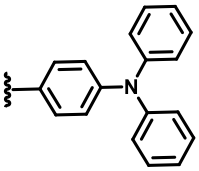	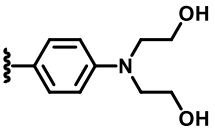	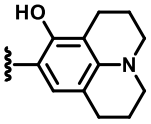

Table 3.2.

Depending on the starting commercial quinoline, two different reduction methodologies were carried out. In the case of the ester derivative **1**, a direct reduction to alcohol **3** with lithium aluminium hydride in THF was performed. For the carboxylic acid derivative **2**, an initial activation step to form a mixed anhydride was needed. After this activation, the reduction was directly performed with $NaBH_4$ yielding the desired alcohol **3** without the need for further purification. In a second step, this alcohol was directly oxidized in dichloromethane in the presence of manganesum oxide to give the aldehyde **4**. All attempts to directly transform the ester **1** into **4** by treatment with DIBAL were unsuccessful.

With the aldehyde **4** in our hands, we next carried out its Knoevenagel condensation with malononitrile, obtaining intermediate **5**, which was finally reacted with different commercially available aldehydes through an aldol condensation promoted by acetic anhydride to give the desire derivatives. It is worth highlighting that this reaction had been previously carried out in our group on a simpler substrate.[109,110] In most cases, the simple presence of acetic anhydride under microwave irradiation was enough to promote the condensation, but in the case of aromatic aldehydes bearing electron-donor groups this reaction did not take place, due to the low reactivity of the aldehyde. After trying several conditions, we established that the presence of zinc chloride as a Lewis acid catalyst for aldehyde activation allowed the aldol condensation. **(Scheme 3.3)**

[109] Staderini, M.; Cabezas, N.; Bolognesi, M. L.; Menéndez, J. C. *Synlett.* **2011**, 2577.
[110] Doctoral tesis, Matteo Staderini, Universidad Complutense de Madrid, February, 2015.

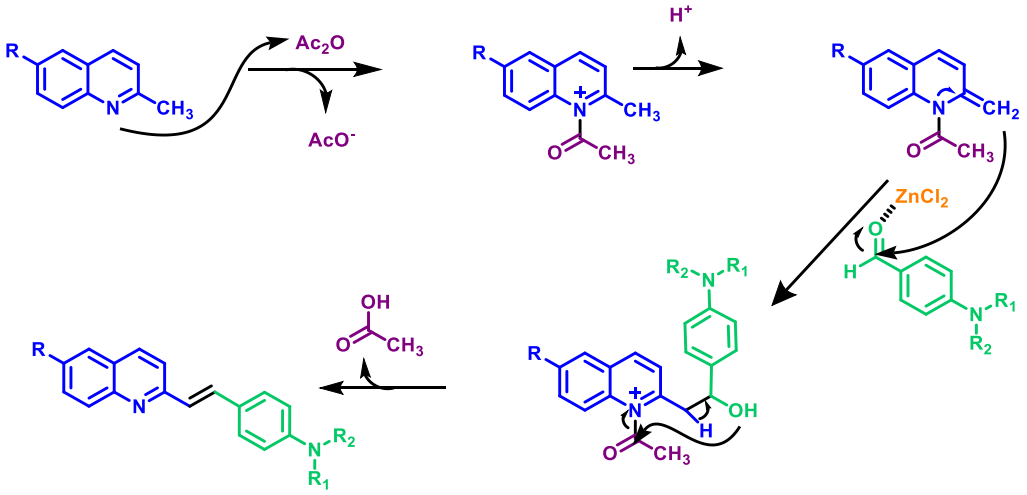

Scheme 3.3. Condensation mechanism.

For the synthesis of the second family of derivatives we altered the order of steps of the sequence. **(Scheme 3.4)** First the condensation with the starting quinoline with the corresponding aldehydes was performed using the Ac_2O-$ZnCl_2$ protocol, yielding the desired styrylquinolines **7**. The ester group was then treated with lithium aluminium hydride, and this reduction took place in much shorter time (1 h *vs* 24 h), probably due to the fact that the substrate has a push-pull structure, which a lower HOMO-LUMO gap, increasing this way the reactivity of the molecule. When it came to the oxidation step, several conditions had to be tried. **(Scheme 3.5)**

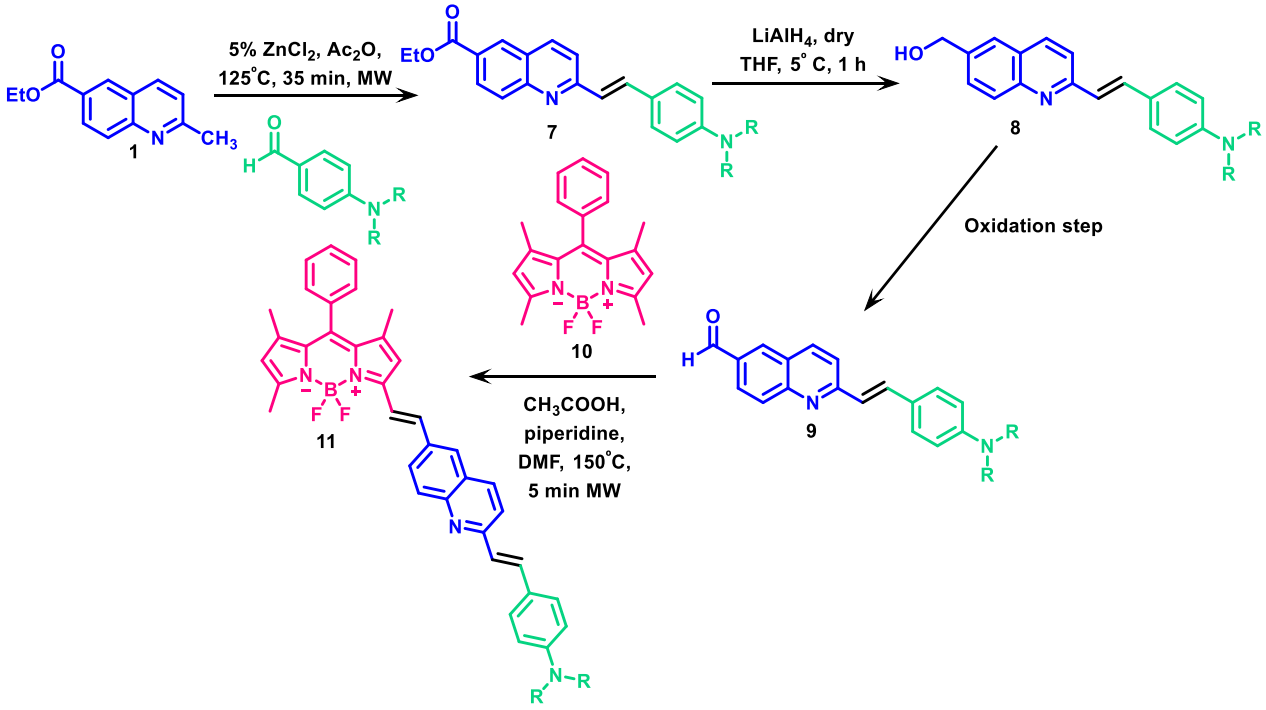

Scheme 3.4.

In a first attempt, we tried the same oxidation conditions previously described, MnO_2 in dichloromethane, but observed a complete decomposition of the starting material. We next decided to use the Dess Martin periodinane, and in this case we were able to isolate the desired product **9** in 32% yield. It is worth highlighting that the reaction time and temperature needed to be precisely controlled, since longer times or higher temperatures led to compound decomposition. Moreover, when we tried to scale up the reaction, the yields dropped to 15 %.

In our next attempt, we used pyridinum chlorocromate supported on alumina. This time, no product was observed after several hours of reaction, and after 72 h the maximum amount of aldehyde found was an 18%, showing that PCC was not a better alternative.
In a next attempt, a Swern oxidadation was also tried, yielding only traces of the desired product, and consequently being discarded as an alternative.
Finally, an oxidation with the Ley-Griffith reagent or tetrapropylammonium perruthenate (TPAP) was also performed, yielding the desired aldehyde **9** in a 40% yield, which decreased to 33% at a higher scale.

The yields obtained in each condition are summarized in **Scheme 3.5** and **Table 3.3.** In order to improve these results, further studies are needed, although the low chromatographic stability of the aldehyde is also a factor to be considered

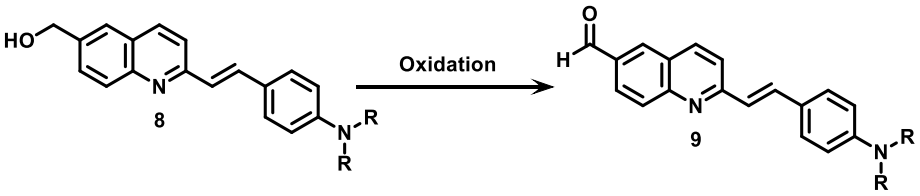

Scheme 3.5.

R	Conditions	Yield %
Me	MnO_2, r.t.,6 h	Decomposition
Me	Dess Martin periodinane, 0°C, 20 min	15-32
Et	PCC-alumina, r.t., 72 h	18
Me	1) Oxalyl bromide, DMSO, - 78 °C 2) Et_3N, CH_2Cl_2, r.t., 1 h	Traces
Et	TPAP, NMO, CH_3CN, r.t., 3.5 h	33-40

Table 3.3.

The BODIPY core **10** was synthesized in parallel by treatment of benzaldehyde with two equivalents of 2,4-dimethylpyrrole in the presence of trifluoroacetic acid and DDQ. **(Scheme 3.6)** Using the small amounts of aldehyde **9** previously obtained, we used typical Knoevenagel condensation conditions under microwave irradiation to carry out the final coupling. This way we were able to isolate the desired compound, albeit in poor yield. **(Scheme 3.7)**

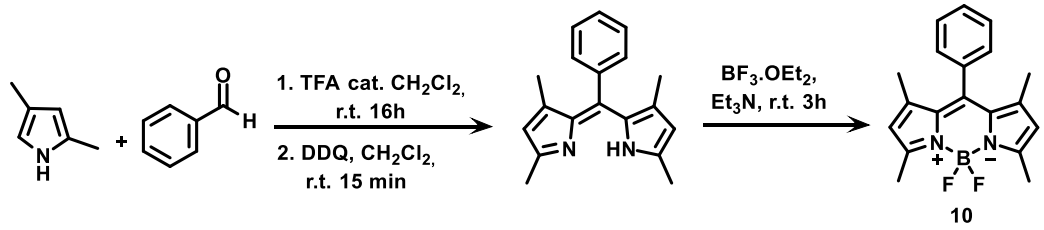

Scheme 3.6.

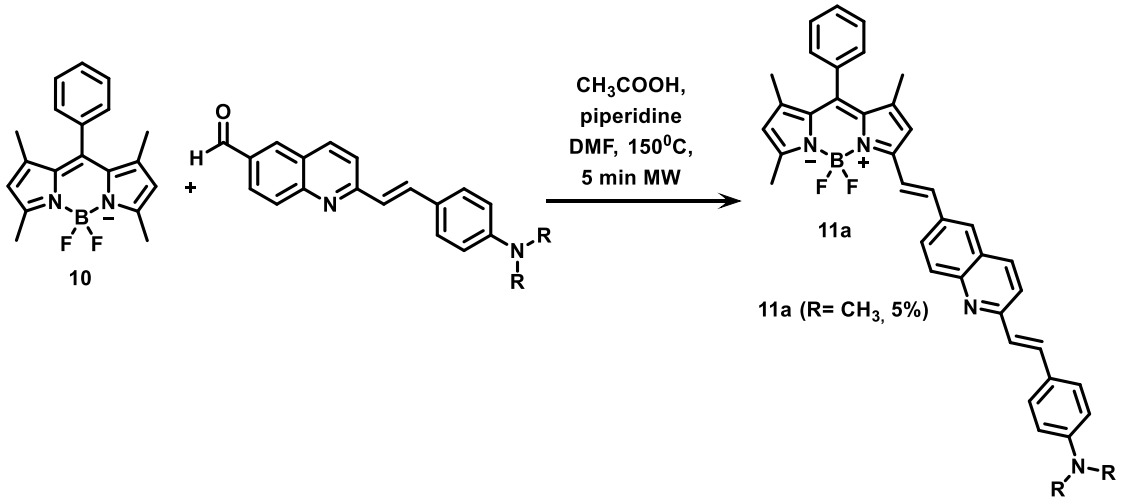

Scheme 3.7.

In order to be able to obtain and study more BOPIPY-quinoline derivatives two different alternative pathways were tried, unfortunately any of them led into the desire compounds **Scheme 3.8** and **Scheme 3.9.** Thus, further efforts to optimize the synthetic route are needed.

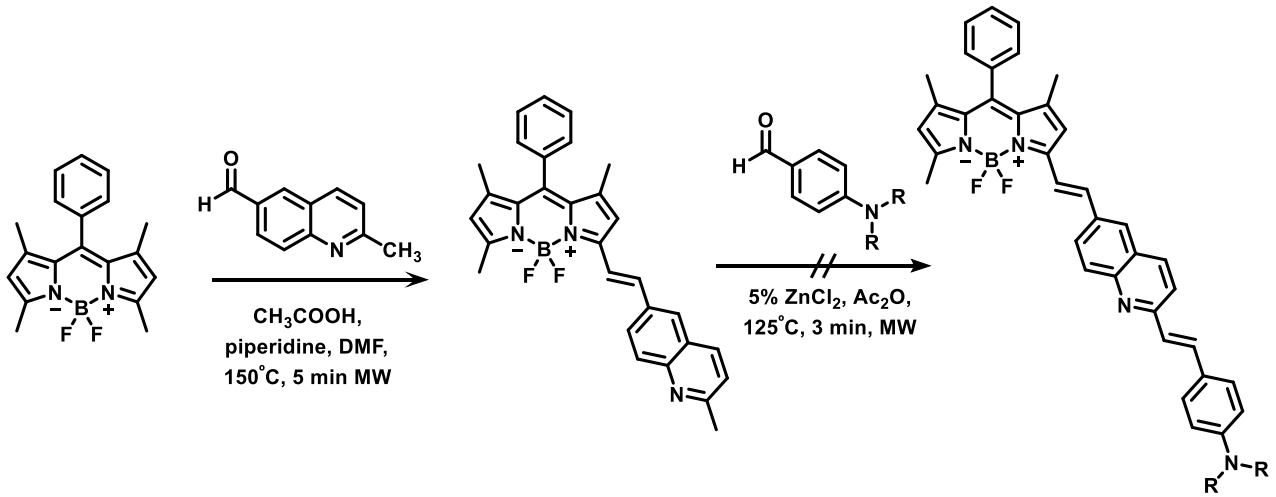

Scheme 3.8.

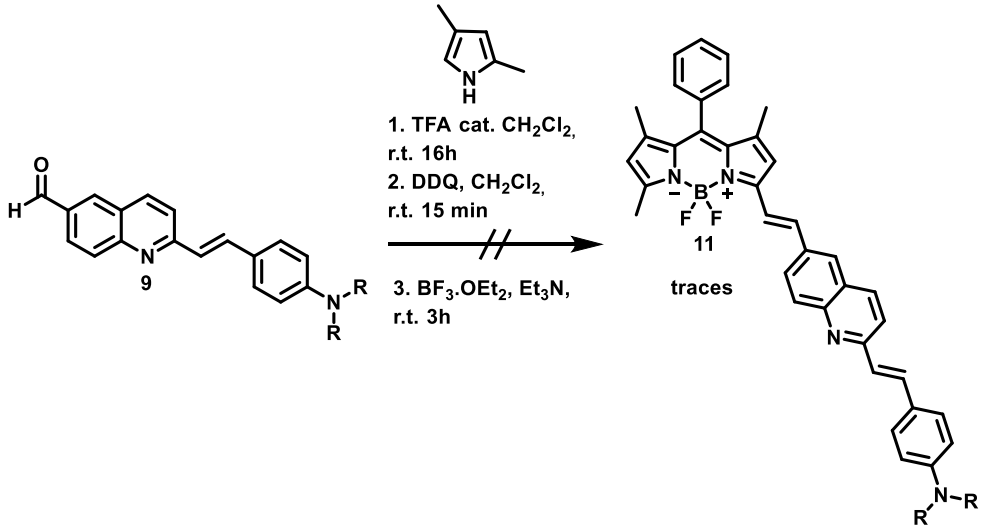

Scheme 3.9.

3.6. Styrylquinoline pharmacological evaluation

The initial pharmacological evaluation of compounds **6a-h** was carried out by Macarena Hernández and Drs. Paloma Bermejo and Sagrario Martín-Aragón, at the Departamento de Farmacología, Facultad de Farmacia, Universidad Complutense. Further characterization of the pharmacological profile of these compounds is in progress.

(a) Cellular viability in the Hek-Tau cell line (MTT)

Firstly, neurotoxicity for compounds **6a-h** was determined by MTT assay in HEK293-Tau3R cells, which are characterized by the overexpression of tau protein. Compounds **6a-h** were tested between 1-10 µM concentrations for 24 h and then cellular viability was determined. No toxicity was detected at concentrations lower than 5 µM. As it is

shown in **Figure 3.9**, at 5-10 µM concentrations compounds **6a-h** start to produce some neurotoxic effect.

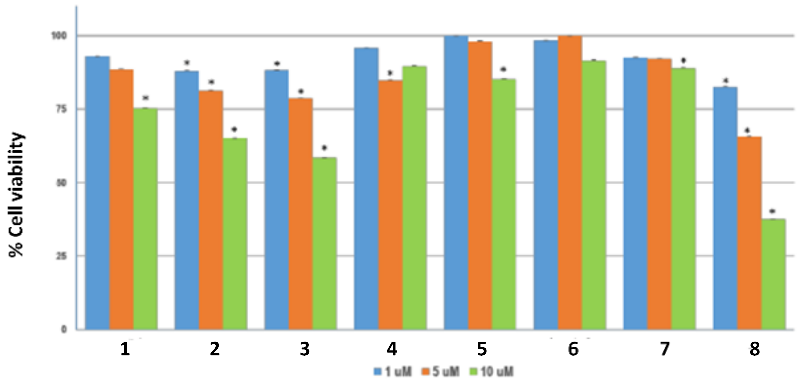

Figure 3.9. Cell viability assay of compounds **6a-h**; $p < 0.05$ indicates statistically significative differences with the control, using the Newman-Keuls test.

(b) Free radical scavenging in the Hek-Tau cell line (DCFA-DA)

Radical oxygen scavenging was tested in HEek293-Tau3R cells using a cellular antioxidant activity assay. The cells were exposed to hydrogen peroxide (200 µM) and treated with the non-fluorescent compound 2,7-dichlorofluorescin acetate (DFCA), a probe that is captured by cells and further hydrolysed by cellular esterase. The resulting 2,7-dichlorofluorescin (DFCH) is still non-fluorescent, but upon oxidation by ROS becomes dichlorofluorescein (DCF) which is highly fluorescent. Thus, the fluorescence measured in the assay is inverse to the scavenging ability of the tested compounds. **(Figure 3.10)**

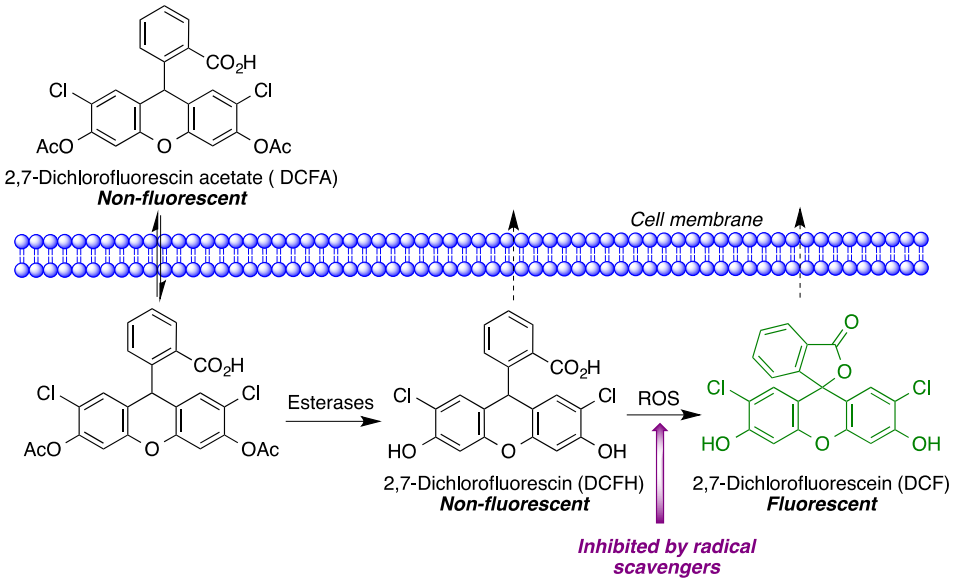

Figure 3.10.

With this essay, variations in the fluorescence signal after 50 min of treatment with compounds **6a-h** were measured. Concentrations lower than 1 µM showed a moderate antioxidant activity of the compounds. **(Figure 3.11)**

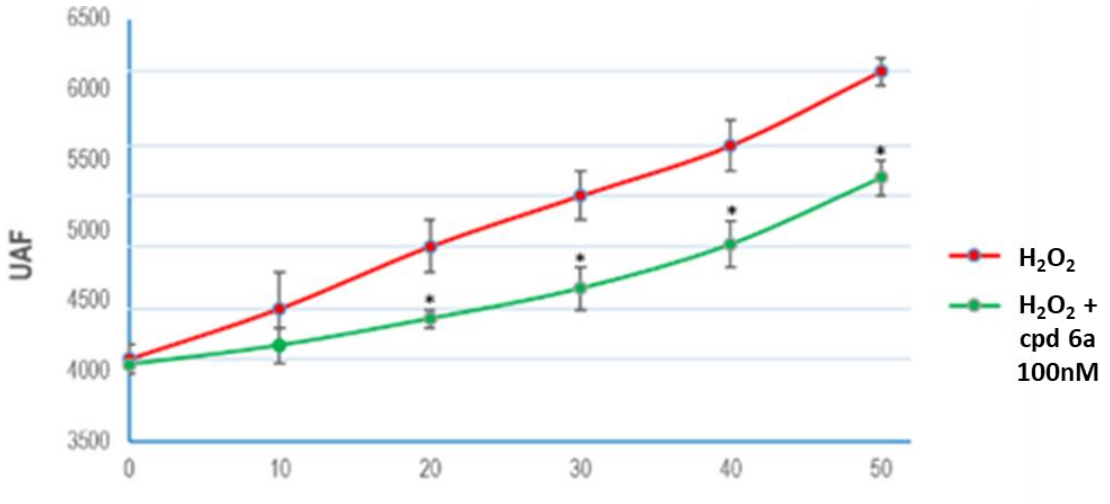

Figure 3.11. Representative example of the antioxidant capacity of compound **6a** at 100 nM; *, meaning $p < 0.05$, indicates statistically significative differences with the control, using the Newman-Keuls test.

(c) Tau aggregation inhibition

For the tau aggregation *in vitro* test, the N-acetylated and C-amidated hexapeptide AcPHF6 (MeO_2C-VQIVYK-NH_2) was used. This peptide derives from the native tau-hexapeptide sequence ^{306}VQIVYK^{311}, which is involved in fibril aggregation processes and can be used as suitable model to study tau aggregation inhibition.[111]

The styrylquinolines **6a-h** and methylene blue as a control were studied in a 0,5-20 µM range of concentrations. All tested compounds were able to inhibit the aggregation of AcPHF6 peptide in a dose dependent manner. Moreover, compounds **6c**, **6e** and **6h** were able to inhibit more than 50% of aggregation at 1 µM concentration, thus being the most active stryrylquinolines. **(Figure 3.12)**

[111] See, for instance: Mohamed, T.; Hoang, T.; Jelokhani-Niaraki, M.; Rao, P. P. N. *ACS Chem. Neurosci.* **2013**, *4*, 1559-1570.

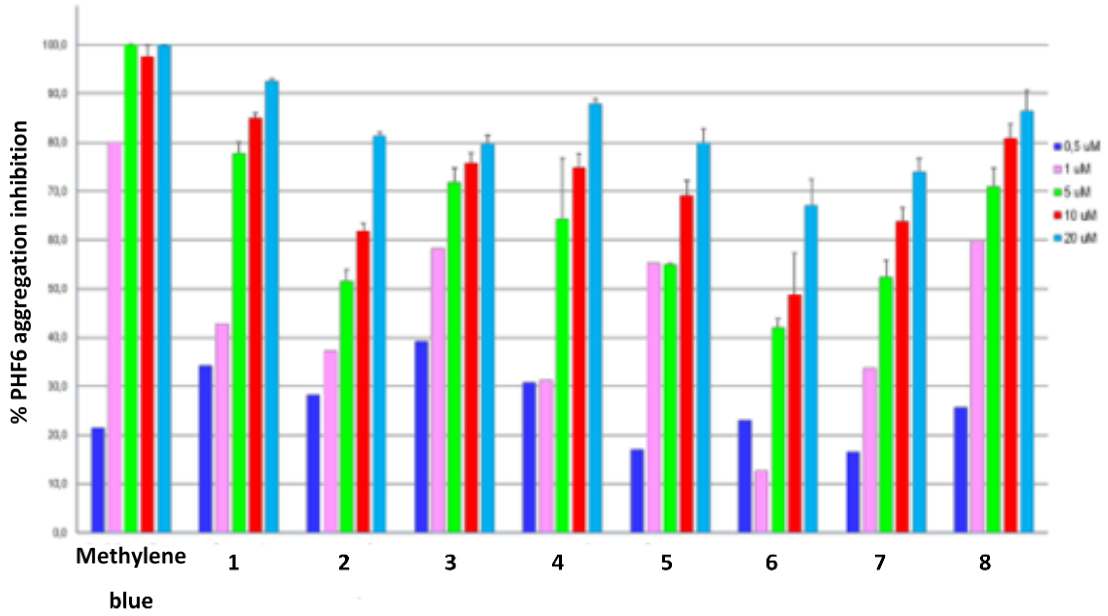

Figure 3.12. AcPHF6 peptide aggregation inhibition.

(d) Neuroprotective effect on an okadaic acid neurotoxic model.

To evaluate the neuroprotective effect of compounds **6a-h**, a neurotoxic model based on okadaic acid was set up. First the HEK293-Tau3R cells were treated with okadaic acid concentrations of from 10-50 nM during 24 h, and it was observed that above a 30 nM concentration the viability of the cells considerably decreased. To further evaluate if this decrease in viability was due to a necrosis process, the levels of dehydrogenase lactate (LDH) on the cells supernatant was evaluated. LDH is a cytoplasmatic enzyme involved in glycolysis and gluconeogenesis processes, and if it is found in the supernatant media it means that it was liberated due to a process of cellular lysis. As no significant changes on LDH levels were found, the decrease in cell viability is not cause by a necrosis process. Afterwards, to test if cell death was an apoptosis-mediated process, the levels of caspases 3, 8 and 9 were evaluated. To this end, cells were treated with okadaic acid in a range on 10-50 nM concentrations, up to a 25 nM concentration an increase in caspase 3 activity was observed. This caspase is involved in both the intrinsic and extrinsic apoptosis pathways. **(Figure 3.13)**

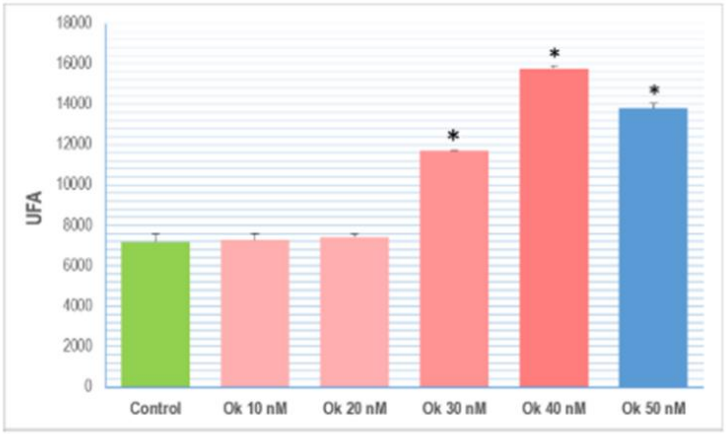

Figure 3.13. Caspase 3 activation by oxadaic acid in a HEK293-Tau3R cell line.

In the light of these results, as the cell viability was decreasing up to a 30 nM concentration, while the caspase 3 activity was increasing from a 25 nM concrentration, it was decided to expose the HEK293-Tau3R to a 25 nM concentration of okadaic acid and evaluate the neuroprotection exerted by compounds **6a-h**.

First, it was evaluated that under normal conditions compounds **6a-h** were not exhibiting any influence in the activities of caspases 3, 8 and 9. Then cells were exposed to 25 nM concentrations of okadaic acid and 10 or 100 nM concentrations of the compounds. It was observed that compounds 6b, 6d, 6e, 6g and 6h were able to considerably decrease the activity of caspase 3. **(Figure 3.14)**

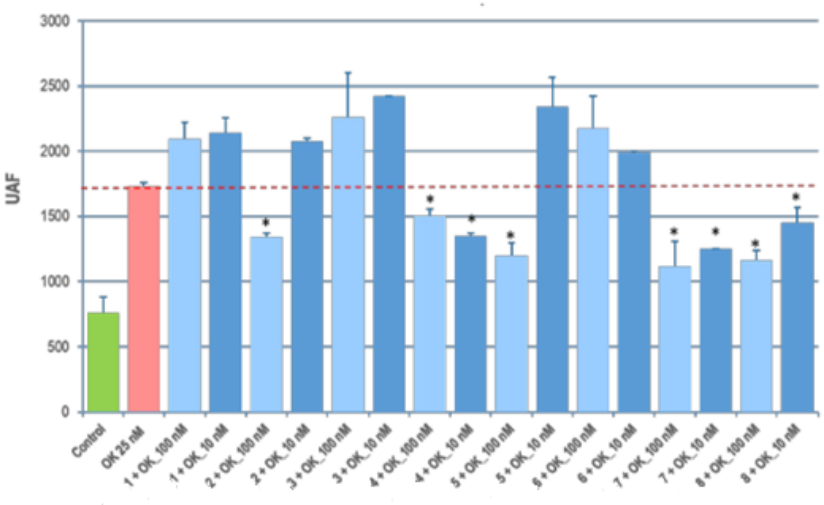

Figure 3.14. Activity of caspase 3 after co-treatment with okadaic acid and compounds **6a-h.**

To further evaluate the potential neuroprotective mechanisms of styrylquinolines **6a-h**, the activities of SOD and CAT enzymes, both involved in controlling oxidative stress processes, were measured in the neurotoxic okadaic acid model. On one hand, SOD is one of the first-line defence mechanisms against oxidative stress, as it is in charge of catalysing the transformation of the superoxide anion into hydrogen peroxide. On the other side CAT is involved in the transformation of hydrogen peroxide into water and oxygen. It has been proved that higher levels of SOD and CAT are associated with ROS control and consequently have a neuroprotective effect.[112] **(Figure 3.15)**

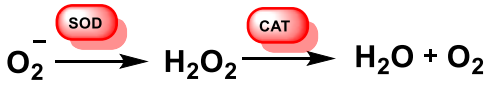

Figure 3.15.

It was observed that only compound 6a and 6b were able to increase the SOD activity after treatment with okadaic acid. **(Figure 3.15)** In the case of CAT, a decrease in its activity was observed upon okadaic acid treatment, but none of the styrylquinolines was able to recover this activity. **(Figure 3.16)**

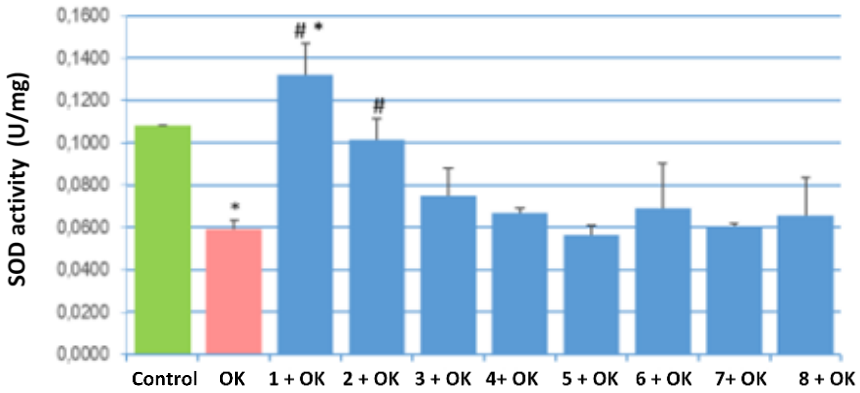

Figure 3.15. SOD activity after co-treatment with okadaic acid and compounds **6a-h**.

[112] Kim, H.; Oshikawa, J.; Urao, N.; Kaplan, N.; Razvi, N.; McKinney, R.; Poole, L.B.; Fukai, T.; Ushio-Fukai, M. *Plos One* **2010,** *5*, e10189.

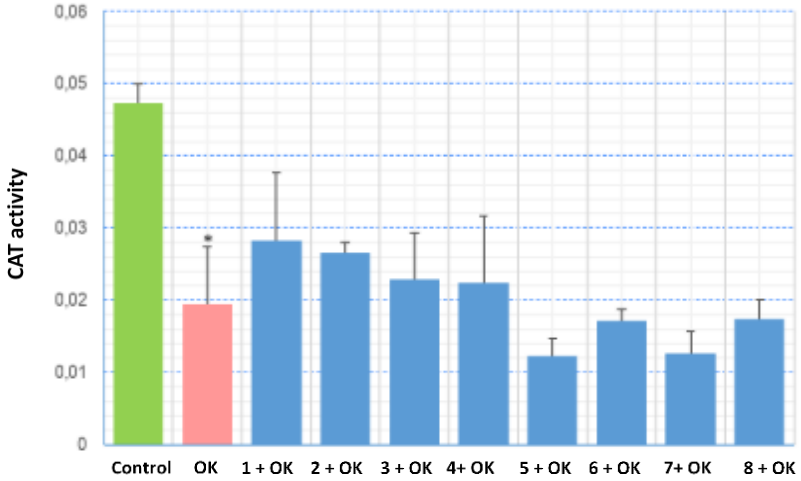

Figure 3.16. CAT activity after co-treatment with oxadaic acid and compounds **6a-h**.

3.7. Styrylquinoline imaging properties

To further evaluate the imaging properties of compounds **6a-h**, a complete characterization of their spectral porperties was carried out by Latoya Bote and Francisca Aguilar under the supervision of Drs. María Antonia Martín and Ana Isabel Olives in the Unidad Docente de Química Analítica, Facutad de Farmacia, Universidad Complutense. Further experiments of these compounds are in progress. In order to simplify the discussion, we chose **compound 6b** as a representative example, although all the experiments summarized below have been done for all the compounds of the family, which have shown a similar behaviour. The choice of **6b** was guided by its good pharmacological profile; being able to act as ROS scavenger, inhibit tau in vitro aggregation and inhibit caspase 3 activity while enhancing SOD activity after treatment with okadaic acid.

3.7.1. Spectrophotometric studies.

First, a calibration curve of all compounds was carried out in ethanol and their molar absorptivities (ε) were calculated. **(Table 3.3)**

Compound	*λ max/ nm*	*ε (M^{-1} cm^{-1})*	*Formula*	*R*
Xb	485	5926.8	Y=5926.8 x + 0.0446	0.9949
	336	3746.3	Y=3746.3 x + 0.0397	0.9982
	263	3416	Y=3416 x + 0.056	0.9899

Table 3.3. Compound **6b** calibration curve.

(α) Solvatochromism studies.

In order to evaluate how the polarity of the solvent affects to the absorption properties of the compounds their absorption spectra were measured in solvents with different properties. The chosen solvents were water, acetonitrile, dioxane, ethanol, methanol and hexane. In the case of water and hexane, due to solubility issues, 1:10 dilutions of ethanol: water or ethanol: hexane needed to be done. **(Figure 3.17)**

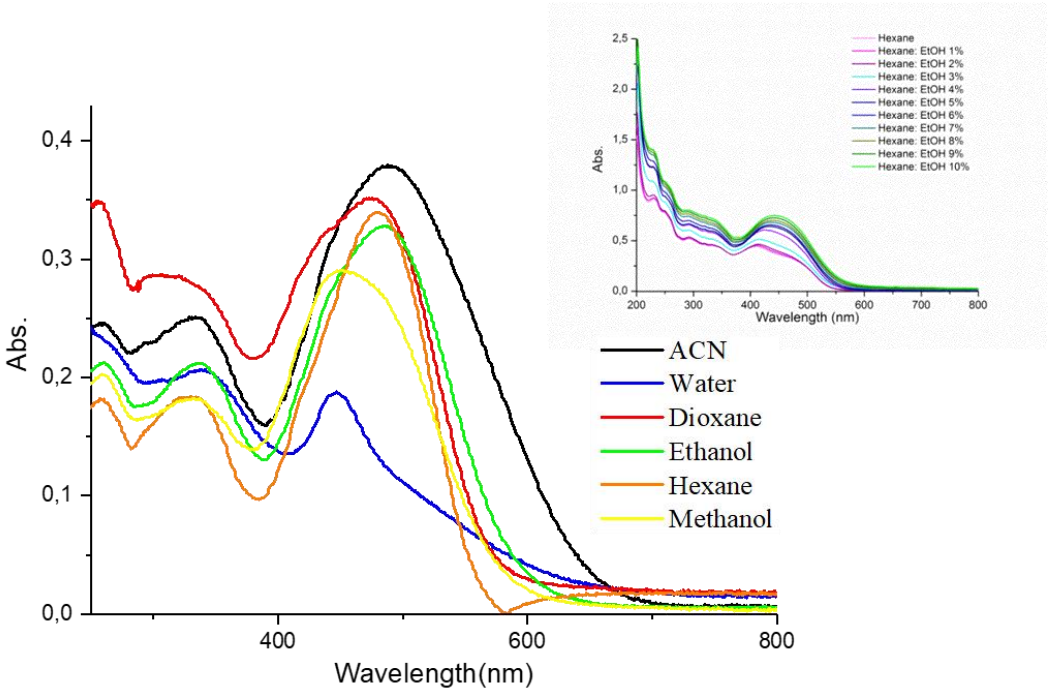

Figure 3.17. UV-Vis in polar and non-polar environments. of compound **6b** Inset: hexane: methanol titration compound **6a**.

From this study, we observed that in general in more apolar enviroments compounds tend to present a batochromic shift (towards higher wavelengths) and an increase in their absorbance, while in more polar environments the absorbance decreases with an hipsochromic shift (towards lower wavelegnths). To study this effect more directly, some compounds, such as **6a** were titrated with hexane containing increasing amounts of methanol. **(Inset Figure 3.17)**

(b) Proton transfer reaction studies.

In order to evaluate the influence of pH in the spectral behaviour of our compounds, titrations with HCl in all the different solvents were done. In **Figure 3.18**, the titration of Compound **6b** in ethanol with different HCl concentrations is shown.

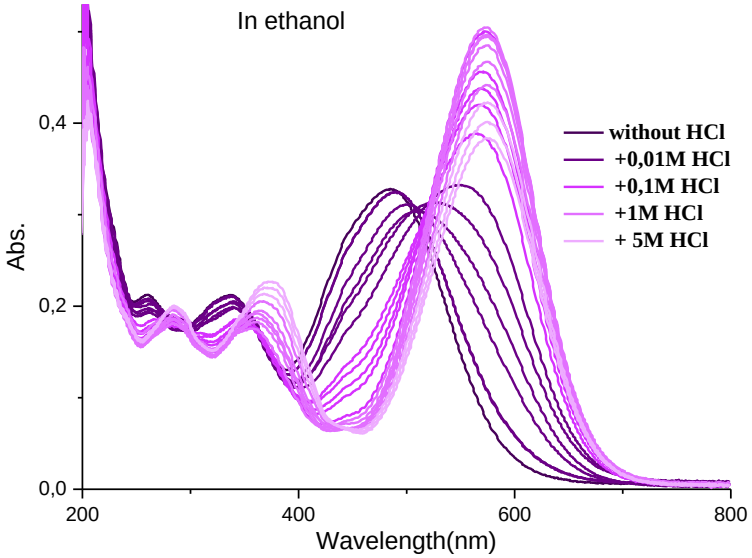

Figure 3.18. UV-Vis. HCl titration of compound **6b** in ethanol.

In all studied solvents, the addition of acid brings about the protonation of the molecule, disappearing the absorbance maximum around 450 nm, while a new maximum around 550-600 nm appears. With further increases in the concentration of HCl, this maximum tends to disappear while the intensity of the one at 375 nm increases. This behaviour is associated with the protonation of the two basic nitrogens present in the molecule, each of them associated with one of the absorption bands.

3.7.2. Spectrofluorimetry studies

(a) Solvatochromism

All compounds **6** exhibited native fluorescence. To evaluate the influence of solvent polarity in the fluorescence properties of the compounds, a soltavochromism study was carried out, this time using ethanol, hexane, water and dioxane. As in the previous case, in the case of hexane and water dilutions of the solvents with hexane needed to be done. **(Figure 3.19)**

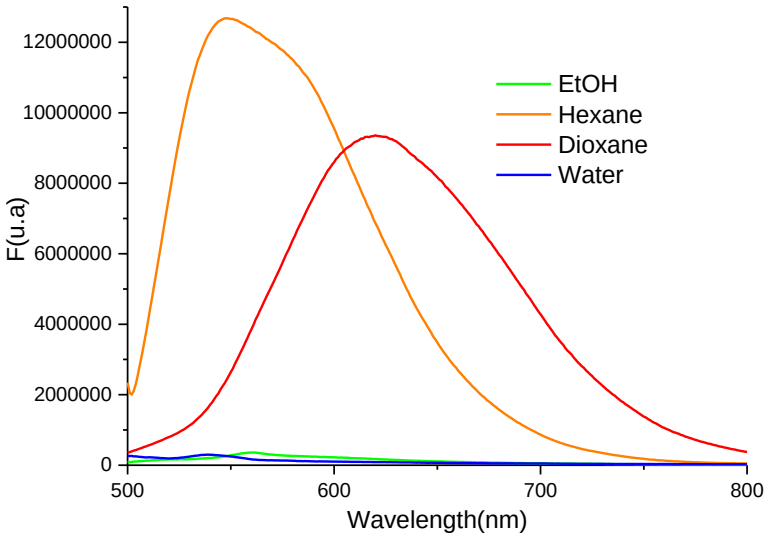

Figure 3.19. Emission spectra of **6b** in different solvents. λ_{ex}=480.

The excitation maxima selected to record the emission spectra were 330-350 nm and 438-480 nm. As shown in **Graphic 3.3**, the fluorescence intensity considerably increases in non-polar environments. Moreover, the position of the maximum is clearly polarity-dependent, being red-shifted in dioxane. This behaviour is promising in that it leads to expect very noticeable changes in compound fluorescence when it is transferred from the aqueous phase to the ordered, highly lipophilic environment found inside the fibrils.

It is also worth noting that for the lower excitation wavelength two fluorescence bands can be detected, the first one associated with the main fluorophore while the second one is associated with an energy charge transfer phenomenon.

(b) Proton transfer reaction studies.

Again, to evaluate the influence of pH on our compounds, reflected this time in their fluorescence properties, titrations with HCl in different solvents were carried out. In **Figure 3.20**, the titration of Compound **6b** in ethanol containing varying HCl concentrations is shown.

For all compounds and solvents, increasing concentrations of acid caused a decrease in fluorescence intensity of the energy charge transfer band, and at the end of the titration process only the main fluorophore band can be observed.

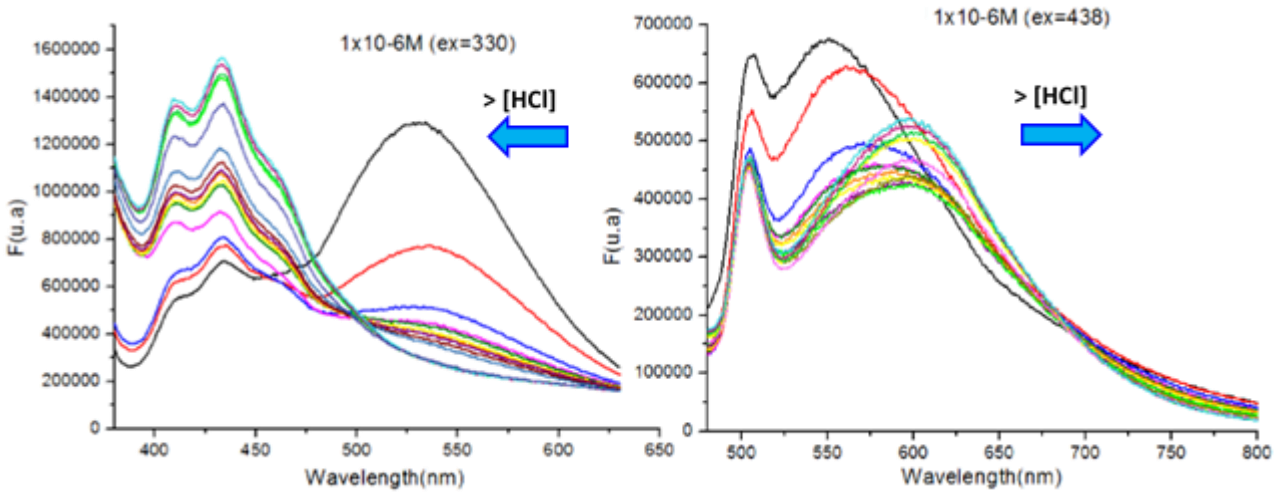

Figure 3.20. Fluorescence HCl titration of compound **6b** in ethanol.

3.7.3. Amyloidogenic protein interference studies

(a) Detection of insulin fibrils

Once the spectral properties of our compounds were determined, their ability to interact with amyloidogenic proteins was evaluated. To this end, an initial study was performed in the presence of native insulin and insulin fibrils, using thioflavin as a control. For all the studied compounds the behaviour was similar to the one described below for compound **6b**.

When native insulin was titrated with thioflavin or with our compounds, no significative changes in the emission spectra were observed. On the other hand, the titration of thioflavin and our compounds with insulin fibrils exhibited a clear increase in

fluorescence upon fibril addition, using several molar protein/sensor ratios. **(Figure 3.21 and 3.22)** The detection of insulin fibrils causes an increase in the energy charge transfer band (longer wavelengths), which is the same phenomenon observed in non-polar solvents. Thus, we can conclude that the compounds are surrounded by a non-polar environment inside the protein fibrils.

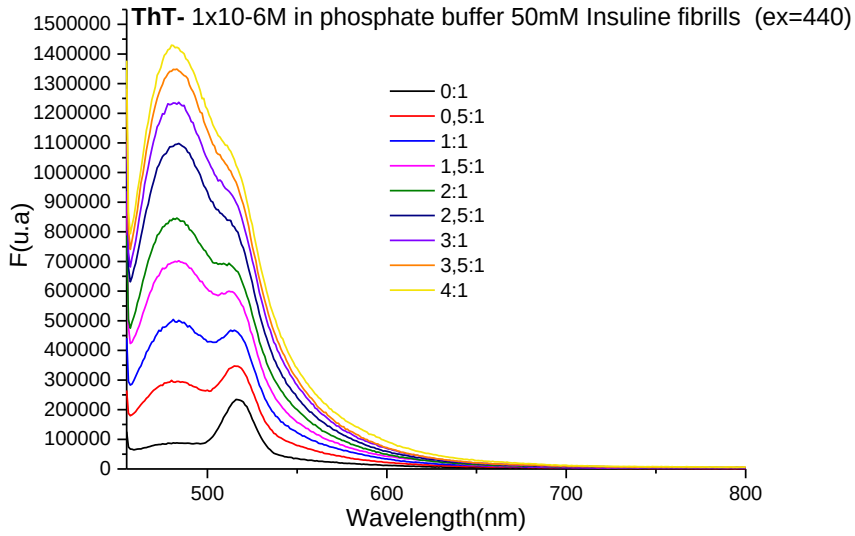

Figure 3.21. Fluorescence titration of thioflavin with insulin fibrils λex = 440 nm.

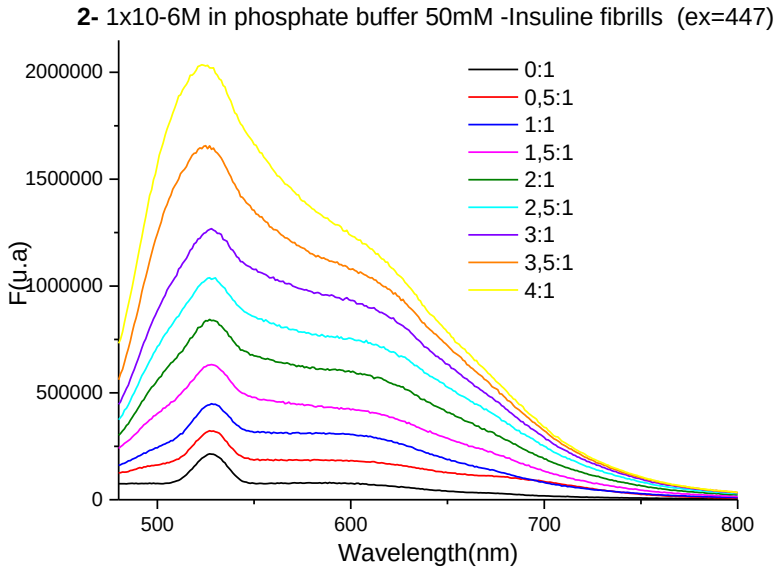

Figure 3.22. Fluorescence titration of compound **6b** with insulin fibrils λex = 447 nm.

(b) Detection of beta-amyloid fibrils.

The same experiment was then carried out, this time with fibrils generated from the $A\beta_{42}$ peptide. First, a titration of thioflavin as a positive control with the putative $A\beta_{42}$ fibrils showed a clear increase in fluorescence intensity and consequently the formation of fibrils was verified. **(Figure 3.23)**

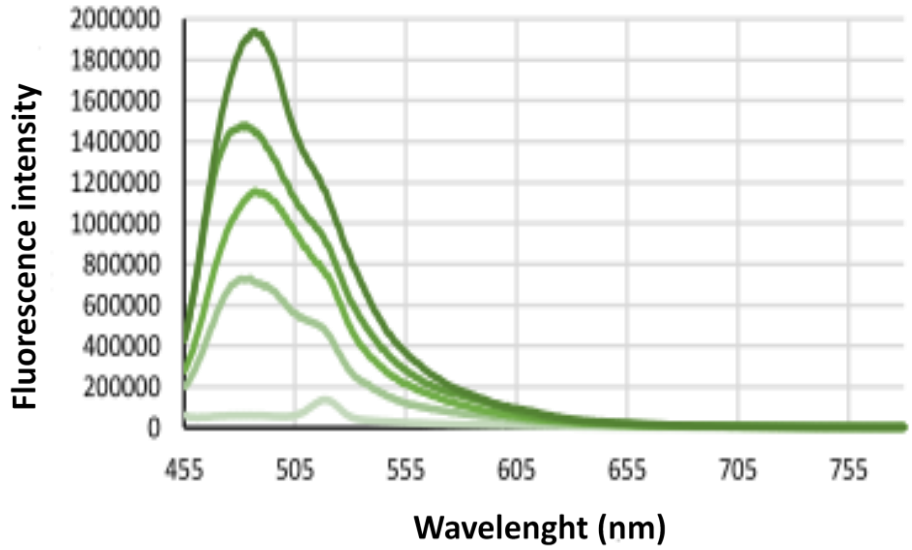

Figure 3.23. ThT - β amyloid fibrils λex = 440 nm.

Afterwards, the titriation of compounds **6a-h** with $A\beta_{42}$ fibrils was performed, showing the same behaviour as thioflavin, *i.e.* an increase in fluorescence intensity upon fibril addition in protein/sensor molar ratios studied varying from 1 to 2. **(Figure 3.24)**

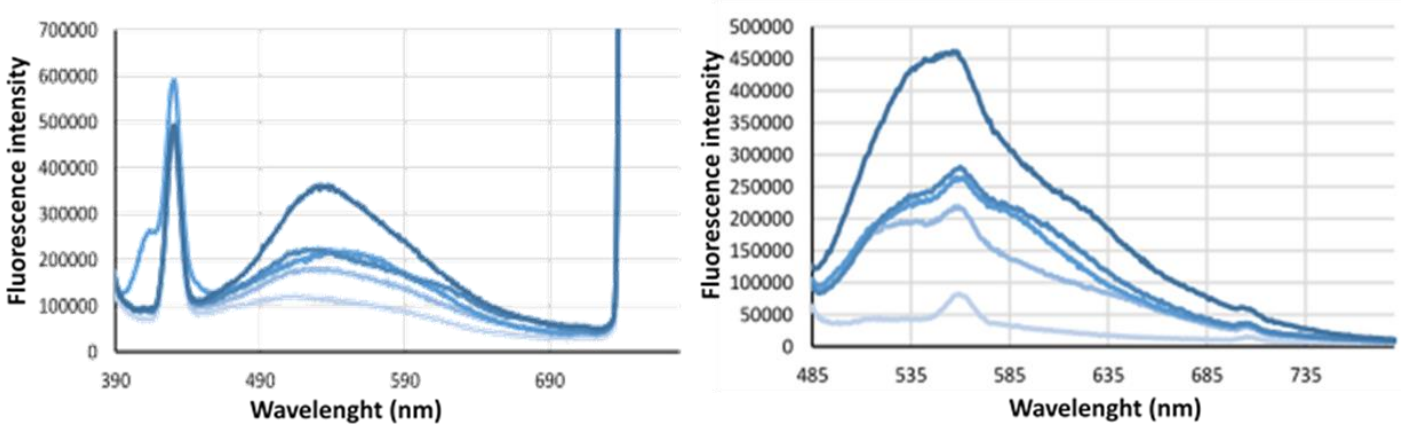

Figure 3.24. Compound **6b** - β amyloid fibrils λ_{ex} = 374 nm and λ_{ex} = 470 nm

3.7.4. Styrylquinolines ex vivo imaging.

Once the full spectroscopic characterization of the compounds was finished, we evaluated their ability to identify β amyloid plaques *ex vivo*. To this end, Dr Gonzalo León, from Departamento de Química y Bioquímica, Facultad de Farmacia, Universidad CEU San Pablo and Laboratorio Cajal de Circuitos Corticales (CTB), Universidad Politécnica de Madrid, performed the characterization of some of the compounds in several models of AD tissues.

(a) Characterization of 6b labelling in the somatosensory cortex of APP/PS1 transgenic mice.

First, compound **6b** was selected for a preliminary labelling study, in which the somatosensory cortex of APP/PS1 transgenic mice, an AD animal model that accumulates amyloid beta burden in the brain from 6 to 7 months of age, was stained.

The results showed that the compound specifically binds the β-sheet amyloid, as detected when exciting at several wavelengths. **(Figure 3.25)** The optimal signal to visualize amyloid beta plaques was obtained with an excitation wavelength of 458 nm, although the staining is also well detected at 488 and 555 nm. **(Figure 3.25 A-D)** However, no staining was observed with excitation wavelengths of 405 or 594 nm. **(Figure 3.25 E, F)**

(b) Characterization of 6b labelling in the temporal cortex of AD samples.

In the next step the ability of **6b** and **6c** to detect aggregates in human Alzheimer´s disease patients was also tested. To this end, double immunofluorescence techniques and confocal microscopy visualization were employed. Interestingly, it was found that in samples of temporal neocortex from one AD patient, the compounds specifically labelled the amyloid beta plaques, but not neurofibrillary tangles. **(Figure 3.26)** As shown in **Figure 3.26**, no colocalization was found between the structures labeled with the antibody AT8 (phosphor-tau antibody) and **6c**. This is one of the main differences compared to Thioflavin S (ThS), which has been shown to detect beta-pleated sheet

structures and phosphorylated tau in AD brain samples.[113] Moreover, as expected from the previous study in mice, the binding with beta amyloid was confirmed by the colocalization with the amyloid beta antibody. **(Figure 3.26 D-F)** It is worth nothing that **6c** binds with higher efficiency to the plaque core as shown in **Figure 3.27 D-F**.

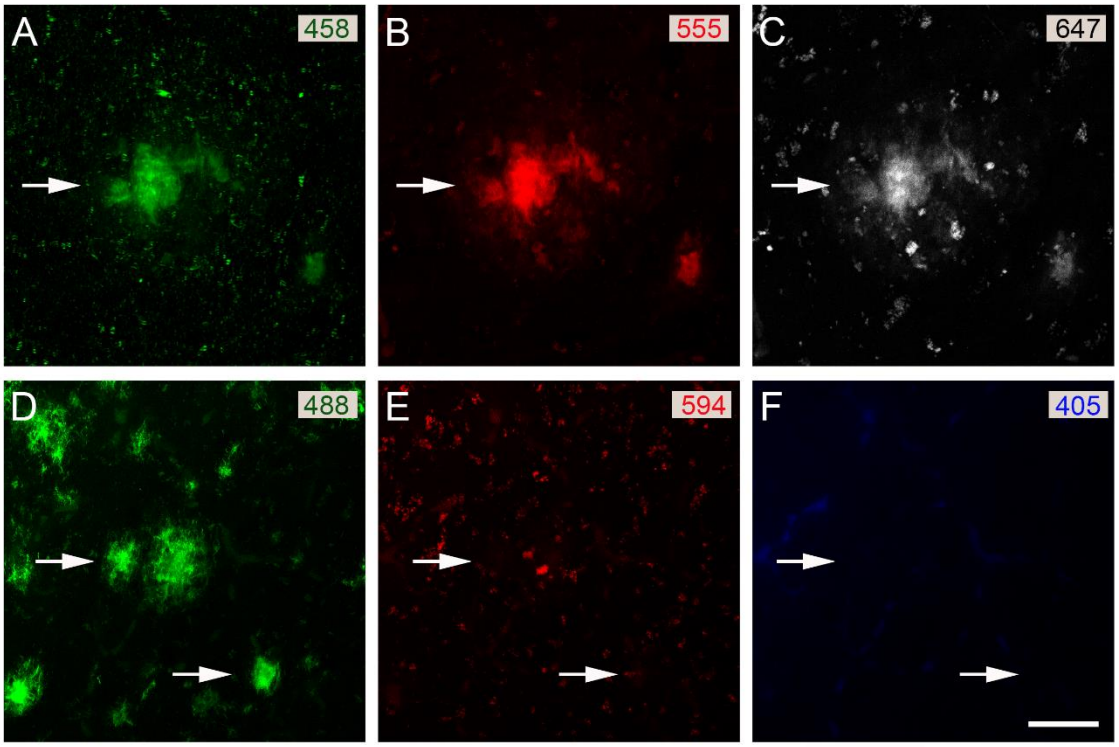

Figure 3.25. **6b** labelling in the somatosensory cortex of APP/PS1 transgenic mice. Representative Z projection photomicrographs taken from two different confocal stacks (A-C and D-F) showing amyloid beta deposits labelled with **6b**. Several excitation wavelengths are tested with positive labelling for amyloid beta plaques at 458 (A), 555 (B), 647 (C) and 488 (D). No amyloid beta deposits are detected at 594 nm (E) or 405 nm (F) wavelengths. White arrows indicate some of the amyloid beta deposits. White scale bar in F indicates 20 µm.

[113] Santa-María, I.; Pérez, M.; Hernández, F.; Avila, J.; Moreno, F.J. *J Alzheimers Dis*. **2006**, *9*, 279.

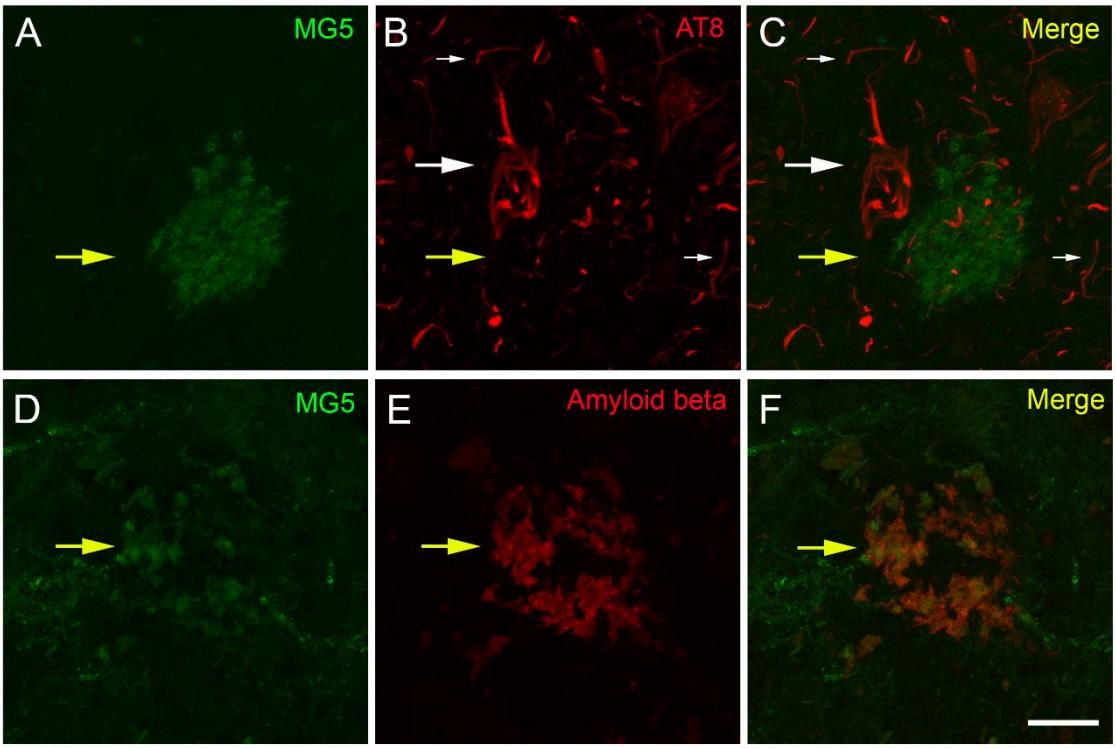

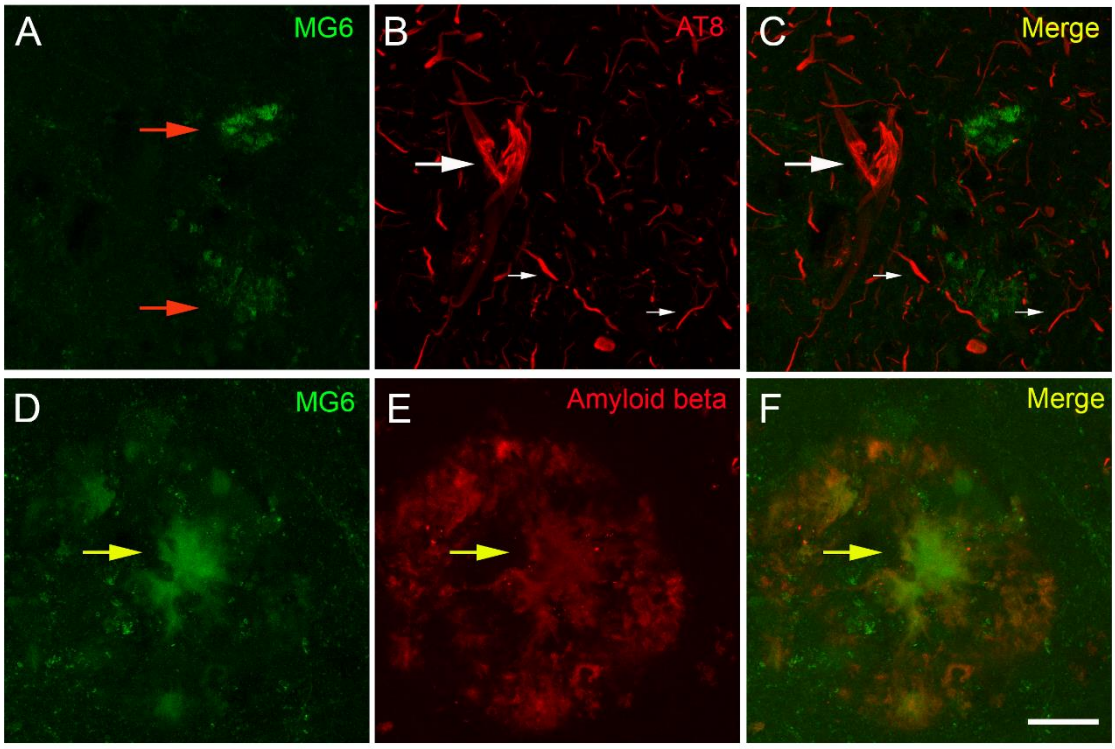

Figure 3.26 and 3.27. Characterization of **6b** and **6c** labelling in the temporal cortex of AD samples. Labelling by AT8 antibody is shown in B, whereas labelling with amyloid beta antibody is shown in E. Small white arrows indicate some of the phosphorylated tau fibrils. Big white arrows indicate the paired helical filaments and big yellow arrows indicate the core of the amyloid beta plaque. White scale bar in F indicates 20 µm

As a summary, our styrylquinolines can be considered as attractive multitarget directed ligands against oxidative stress and act as tau protein aggregation inhibitors with a safe toxicity profile. Moreover, further studies are being carried out and preliminary data showed their ability to inhibit beta amyloid aggregation.

From the imaging point of view, **styrylquinolines 6** have proved to have interesting fluorescent properties with one if their emission maximum close to the NIR region, being able to enhance their fluorescent intensity in non-polar environments, this results was correlated with their increase in fluorescence emission upon fibrils binding, with proved their ability to detect amyloid aggregates. Finally, their ability to detect amyloid plaques in samples of Alzheimer's disease brain tissue was evaluated, showing promising results and being able to selectively detect beta amyloid aggregates.

With these results, we can confirm that **styrylquinolines** 6 are an interesting starting point for developing new theranostic multitarget agents against Alzheimers diseases, being able to detect one of the main hallmarks of the disease, while delivering a therapeutic effect.

3.8. Experimental section

General experimental details.

All reagents (Aldrich, Fischer, Alpha Aesar, SDS) and solvents (Scharlau, Fischer, SDS) were of commercial quality and were used as received. Reactions under microwave irradiation were carried out in a CEM Discover SP microwave reactor. Reactions were monitored by thin layer chromatography on aluminium plates coated with silica gel and fluorescent indicator (Macherey-Nagel Xtra SIL G/UV254). Separations by flash chromatography were performed on silica gel (Scharlau 40–60 µm, 230–400 mesh ASTM) or neutral alumina (Merck S22). Melting points were determined using a Stuart Scientific apparatus, SMP3 Model, and are uncorrected. Infrared spectra were recorded with an Agilent Cary630 FTIR spectrophotometer with a diamond accessory for solid and liquid samples. NMR spectroscopic data were recorded using a Bruker Avance 250 spectrometer operating at 250 MHz for ^{1}H NMR and 63 MHz for ^{13}C NMR, maintained by the NMR facility of Universidad Complutense (CAI de Resonancia Magnética Nuclear); chemical shifts are given in ppm and coupling constants in Hertz. High-resolution mass spectra (HRMS) were recorded on a mass spectrometer fitted with an electrospray detector (ESI) by the mass spectral facility of Universidad Complutense (CAI de Espectrometría de Masas) and elemental analyses were determined by the microanalysis facility of Universidad Complutense (CAI de Microanálisis Elemental), using a Leco 932 combustion microanalyzer.

Synthesis of push-pull (*E*)-2-styrylquinolines derivatives 6a-h.

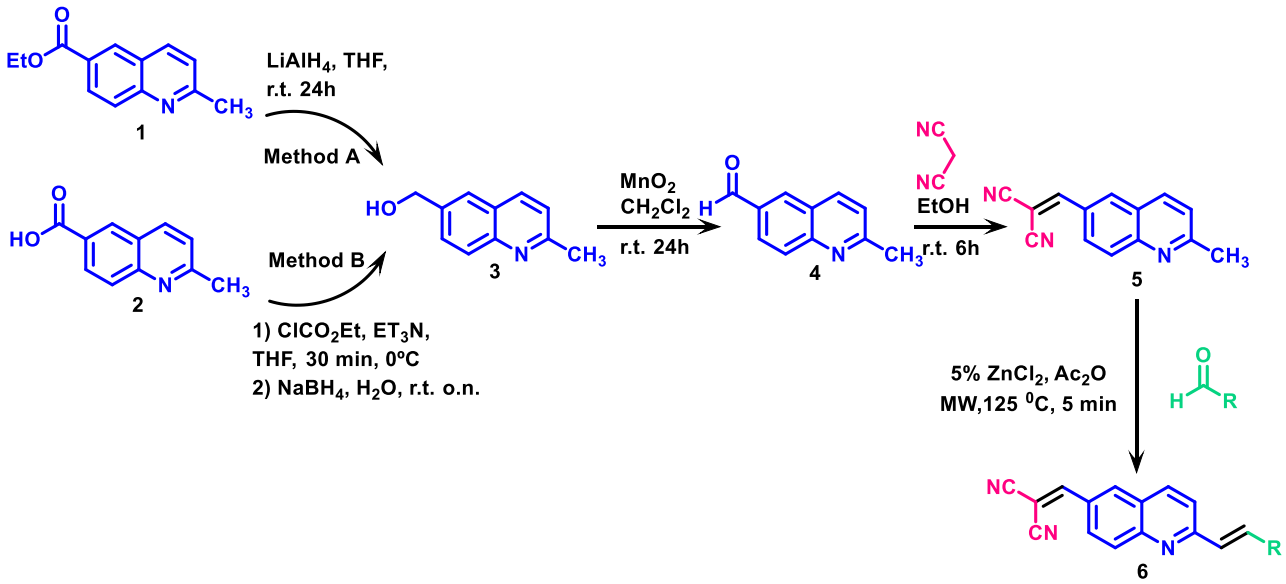

3.8.1. Synthesis of (2-methylquinolin-6-yl)methanol (3)

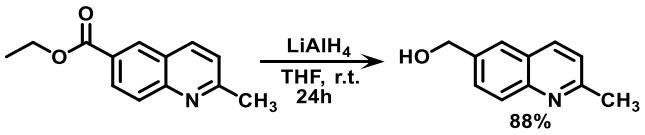

Method A: A suspension of lithium aluminium hydride (10 eq) in dry THF was prepared and cooled down to 0 °C with an ice-water bath. Then ethyl 2-methylquinoline-6-carboxylate (2 g, 9.29 mmol) was dissolved in dry THF (20 ml) under argon. This solution was slowly added to the suspension previously prepared. The mixture was stirred for 24h and then quenched by the sequential addition of ethyl acetate (30 mL) and water (2 mL). The suspension was filtered, and the filtrate was extracted with AcOEt, dried with anhydrous Na_2SO_4 and evaporated *in vacuo* to afford the title compound **3** as a yellowish solid. The compound was used in the next step without further purification. Yield: 3.52 g, 88 %.

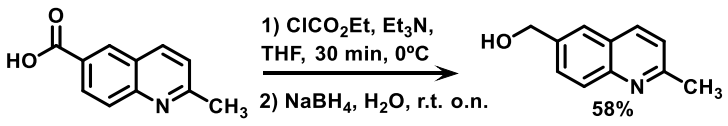

Method B: The 2-methylquinoline-6-carboxylic acid (1.5 g, 8 mmol), chloroacetyl chloride and Et_3N (1.2 eq) were dissolved in THF (45 mL) at 0 ºC and stirred for 30 min. After this time, the anhydride is formed, and $NaBH_4$ (1.210 g, 32 mmol) and H_2O (10 mL) were added and stirred over night at room temperature. Once the reaction is finished, the mixture is quenched by stirring with HCl 1 N for 1 h. Then the crude is neutralized with $NaHCO_3$, extracted with AcOEt, dried with anhydrous Na_2SO_4 and evaporated *in vacuo* to afford the title compound. Yield: 4.67 g, 58 %.

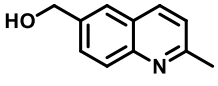

Mp 118-121 ºC.

IR (neat) 3172, 1061, 823 cm^{-1}

^{1}H NMR (250 MHz, $CDCl_3$) δ 8.05 (d, *J* = 8.4 Hz, 1H), 8.01 (d, *J* = 8.4 Hz, 1H), 7.77 (d, *J* = 1.2 Hz, 1H), 7.67 (dd, *J* = 8.4 y 1.2 Hz, 1H), 7.31 (d, *J* = 8.4 Hz, 1H), 4.90 (s, 2H), 2.76 (s, 3H) ppm.

^{13}C NMR (63 MHz, $CDCl_3$) δ 159.3, 147.7, 138.8, 136.7, 129.2, 129.1, 126.74, 125.3, 122.7, 65.3 (CH_2), 25.6 (CH_3) ppm.

Elemental analysis (%): calcd. for $C_{11}H_{11}NO$: C 76.28, H 6.40, N 8.09; found: C 76.45, H 6.35, N 7.97.

3.8.2. Synthesis of 2-methylquinoline-6-carbaldehyde (4)

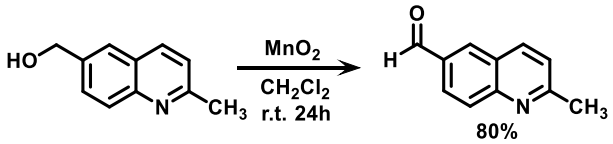

The corresponding alcohol (1.6 g, 7.43 mmol) was first dissolved in CH_2Cl_2 (40 mL) and manganese oxide (5 eq.) was added. The mixture was stirred for 24 h; the resulting suspension was filtered through a pad of Celite. The filtrate was evaporated to afford the corresponding aldehyde. The crude was purified by flash chromatography through a silica column using hexane: ethyl acetate (2:1, v/v) as the mobile phase to give compound **4** as a yellow solid. Yield: 1.27 g, 80%

Mp 103-106 ºC

IR (neat) 1684 (C=O), 823 cm^{-1}

^{1}H NMR (250 MHz, $CDCl_3$) δ 9.95 (d, *J* = 0.5 Hz, 1H), 8.08 (d, *J* = 1.6 Hz, 1H), 8.00-7.93 (m, 2H), 7.88 (dd, *J* = 8.4 y 0.5 Hz, 1H), 7.19 (d, *J* = 8.4 Hz, 1H), 2.58 (s, 3H) ppm.

^{13}C NMR (63 MHz, $CDCl_3$): δ 192.0, 162.9, 151.0, 137.8, 134.0, 133.8, 130.3, 127.3, 126.3, 123.6, 26.1 ppm.

Elemental analysis (%): calcd. for $C_{11}H_9NO$: C 77.17, H 5.30, N 8.18; found: C 77.42, H 5.42, N 8.03.

3.8.3. Synthesis of 2-((2 methylquinolin-6-yl)methylene)malononitrile (5)

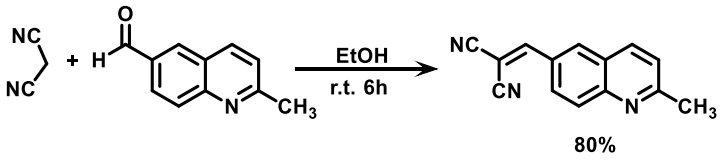

80%

The corresponding aldehyde **4** (1.2 g, 4.6 mmol) was placed in a round bottom flask and ethanol (6 ml) was added, the mixture was heated until the aldehyde was completely dissolved. The solution was cooled to room temperature and malononitrile (0.31, 4.6 mmol) was added and stirred, with immediate formation of a precipitate. The reaction was controlled by TLC; 6h later the reaction was finished, and the solvent was evaporated. The crude product was washed with a mixture of hexane and ethyl ether (10:1) and finally the product was recrystallized from acetone: methanol (5:1) yielding the desired product as a dark red solid. Yield: 0.94 g, 80%.

Mp 190-193 °C

IR (neat) 2222, 1575, 833 cm^{-1}.

^{1}H NMR (250 MHz, d_6-DMSO) δ 8.72 (s, 1H), 8.49 (d, *J* = 1.7 Hz, 1H), 8.43 (d, *J* = 8.5 Hz, 1H), 8.28 (dd, *J* = 9.0, 1.7 Hz, 1H), 8.11 (d, *J* = 9.0 Hz, 1H), 7.58 (d, *J* = 8.5 Hz, 1H), 2.72 (s, 3H) ppm.

^{13}C NMR (63 MHz, d_6-DMSO): δ 163.2, 161.1, 149.5, 137.9, 134.3, 130.0, 128.9, 128.3, 126.1, 124.1, 114.7, 113.7, 82.0 (CH_2), 25.56 (CH_3) ppm.

Elemental analysis (%): calcd. for $C_{14}H_9N_3$: C 76.70, H 4.14, N 19.17; found: C 76.89, H 4.19, N 18.86.

3.8.4. General method for the synthesis of push-pull styrylquinolines (6a-h)

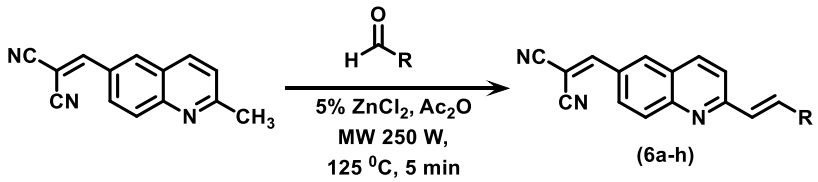

2-((2-Methylquinolin-6-yl)methylene)malononitrile (0.200 g, 0.9 mmol), the corresponding aldehyde (1.5 eq) and zinc chloride (0.006 g, 0.045 mmol) were suspended in acetic anhydride (1.5 ml) in a pressure tight microwave tube containing a stirring bar. The reaction mixture was heated under microwave irradiation for 5 min at 125 °C, with an irradiation power of 250 W. The solvent was removed under reduced pressure to give a dark purple residue which was purified by flash chromatography through a silica column using hexane: ethyl acetate (9:1, v/v) as the mobile phase to give the desired compounds **6a-h**

(*E*)-2-((2-(4-(Dimethylamino)styryl)quinolin-6-yl)methylene)malononitrile (6a)

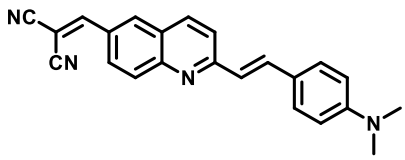

Prepared from 4-(dimethylamino)benzaldehyde (0.200 g, 1.35 mmol), as a dark red solid. Yield: 0.267 g, 85 %.

Mp 188-191 °C

IR (neat) 2224, 1568 y 1521, 1164, 818 cm^{-1}.

^{1}H NMR (250 MHz, $CDCl_3$): δ 8.33-8.03 (m, 4H), 7.87 (s, 1H), 7.73 (m, 2H), 7.58 (d, *J* = 8.4 Hz, 2H), 7.18 (d, *J* = 16.1 Hz, 1H), 6.76 (d, *J* = 8.6 Hz, 2H), 3.08 (s, 6H) ppm.

^{13}C NMR (63 MHz, $CDCl_3$): δ 160.8, 159.3, 151.6, 151.3, 138.3, 137.5, 133.6, 130.8, 129.7 (2C), 129.4, 128.2, 126.9, 124.3, 123.4, 121.4, 114.5, 113.4, 112.5 (2C), 82.1, 40.6 (2C) ppm.

Elemental analysis (%): calcd. for $C_{23}H_{18}N_4$: C 78.83, H 5.18, N 15.99; found: C 78.69, H 5.28, N 16.16.

(*E*)-2-((2-(4-(diethylamino)styryl)quinolin-6-yl)methylene)malononitrile (6b)

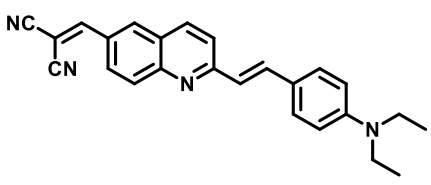

Prepared from 4-(diethylamino)benzaldehyde (0.239 g, 1.35 mmol), as a dark red solid. Yield: 0.176 g, 55 %.

Mp 197-200 °C.

IR (neat) 2221, 1564, 1518, 1177, 819 cm^{-1}.

^{1}H NMR (250 MHz, $CDCl_3$): δ 8.33-8.10 (m, 4H), 7.88 (s, 1H), 7.81-7.70 (m, 2H), 7.57 (d, *J* = 8.2 Hz, 2H), 7.19 (d, *J* = 16.4 Hz, 1H), 6.72 (d, *J* = 8.2 Hz, 2H), 3.46 (d, *J* = 6.9 Hz, 4H), 1.25 (t, *J* = 6.9 Hz, 6H) ppm.

^{13}C NMR (63 MHz, $CDCl_3$): δ 160.9, 159.2, 151.3, 149.2, 138.3, 137.3, 133.6, 130.7, 130.0 (2C), 129.4, 128.1, 126.8, 123.3, 122.8, 121.3, 114.5, 113.4, 111.8 (2C), 81.8, 44.9 (2C), 13.1 (2C) ppm.

Elemental analysis (%): calcd. for $C_{25}H_{22}N_4$: C 79.34, H 5.86, N 14.80; found: C 79.81, H 6.12, N 14.91.

(*E*)-2-((2-(4-(Piperidin-1-yl)styryl)quinolin-6-yl)methylene)malononitrile (6C)

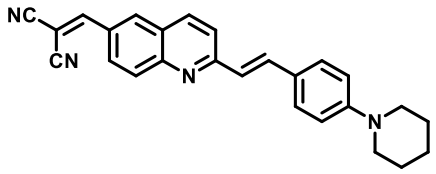

Prepared from 4-(piperidin-1-yl)benzaldehyde (0.255 g, 1.35 mmol), as a dark red solid. Yield: 0.126 g, 40 %.

Mp 180-183°C.

IR (neat) 2223, 1565,1511, 1172, 1120, 822 cm^{-1}.

^{1}H NMR (250 MHz, $CDCl_3$): δ 8.30-8.10 (m, 4H), 7.88 (s, 1H), 7.80 – 7.70 (m, 2H), 7.57 (d, *J* = 8.7 Hz, 2H), 7.22 (d, *J* = 16.1 Hz, 1H), 6.96 (d, *J* = 8.7 Hz, 2H), 3.39 – 3.28 (m, 4H), 1.78-1.64 (m, 6H) ppm.

^{13}C NMR (63 MHz, $CDCl_3$): δ 160.5, 159.2, 152.9, 151.1, 137.9, 137.5, 133.6, 130.8, 129.5 (2C), 129.4, 128.3, 126.9, 126.1, 124.2, 121.4, 115.6 (2C), 114.5, 113.4, 82.1, 49.7 (2C), 25.9 (2C), 24.7 ppm.

Elemental analysis (%): calcd for $C_{26}H_{22}N_4$: C 79.97, H 5.68, N 14.35; found: C 77.43, H 5.66, N 14.82.

(*E*)-2-((2-(4-Morpholinostyryl)quinolin-6-yl)methylene)malononitrile (6d)

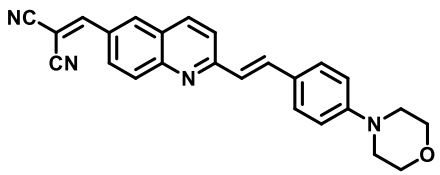

Prepared from 4-morpholinobenzaldehyde (0.257 g, 1.35 mmol), as a dark red solid. Yield: 0.129 g, 35 %.

Mp 179-182°C.

IR (neat) 2227, 1572, 924, 813 cm^{-1}.

^{1}H NMR (250 MHz, $CDCl_3$): δ 8.20-7.98 (m, 4H), 7.79 (s, 1H, H1"), 7.71-7.59 (m, 2H), 7.51 (d, *J* = 8.7 Hz, 2H), 7.15 (d, *J* = 16.2 Hz, 1H), 6.86 (d, *J* = 8.7 Hz, 2H), 3.86-3.75 (m, 4H), 3.25-3.14 (m, 4H) ppm.

^{13}C NMR (63 MHz, $CDCl_3$): δ 160.4, 159.2, 152.3, 151.1, 137.7, 137.5, 133.5, 131.0, 129.4 (3C), 128.4, 127.5, 127.0, 125.2, 121.5, 115.4 (2C), 114.4, 113.3, 82.5, 67.1 (2C), 48.7 (2C) ppm.

Elemental analysis (%): calcd. for $C_{25}H_{20}N_4O$: C 76.51, H 5.14, N 14.28; found: C 76.25, H 5.32, N 14.45.

(*E*)-((4-(2-(6-(2,2-Dicyanovinyl)quinolin-2-yl)vinyl)phenyl)azanediyl)bis(ethane-2,1-diyl) diacetate (6e)

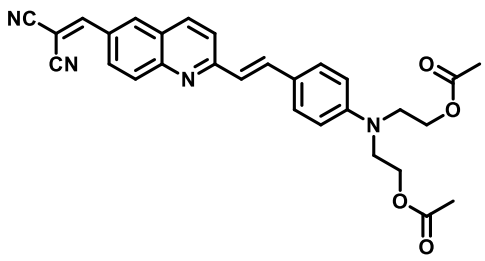

Prepared from ((4-formylphenyl)azanediyl) bis(ethane-2,1-diyl) diacetate (0.395 g, 1.35 mmol), as a dark red solid. Yield: 0.070 g, 20 %.

Mp 98-100°C.

IR (neat) 2224, 1728, 1516, 1220 cm^{-1}.

^{1}H NMR (250 MHz, $CDCl_3$): δ 8.27 (d, *J* = 1.5 Hz, 1H), 8.20 (dd, *J* = 8.9, 1.5 Hz, 1H), 8.14 (d, *J* = 8.9 Hz, 1H), 8.08 (d, *J* = 8.9 Hz, 1H), 7.85 (s, 1H), 7.72 (d, *J* = 16.2 Hz, 1H), 7.67 (d, *J* = 8.9 Hz, 1H), 7.56 (d, *J* = 8.8 Hz, 2H), 7.16 (d, *J* = 16.2 Hz, 1H), 6.81 (d, *J* = 8.8 Hz, 2H), 4.30 (t, *J* = 6.1 Hz, 4H), 3.72 (t, *J* = 6.1 Hz, 4H), 2.09 (s, 6H) ppm.

^{13}C NMR (63 MHz, $CDCl_3$): δ 171.4 (2C), 160.5, 159.2, 151.1, 148.7, 137.7, 137.6, 133.6, 130.8, 129.9, 129.4 (2C), 128.3, 126.9, 125.1, 124.0, 121.4, 114.5, 113.4, 112.4 (2C), 82.2, 61.6, 50.0 (2C), 21.3 (2C) ppm.

Elemental analysis (%): calcd. for $C_{29}H_{26}N_4O_4$: C 70.43, H 5.30, N 11.33; found: C 70.37, H 4.99, N 11.31.

(*E*)-9-(2-(6-(2,2-dicyanovinyl)quinolin-2-yl)vinyl)-2,3,6,7-tetrahydro-1H,5H-pyrido[3,2,1-ij]quinolin-8-yl acetate (6f)

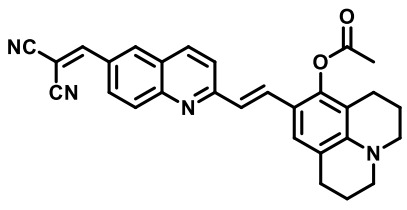

Prepared from 8-hydroxy-2,3,6,7-tetrahydro 1H,5H-pyrido[3,2,1-ij]quinoline-9-carbaldehyde (0.350 g, 1.35 mmol), as a dark red solid. Yield: 0.156g, 40%.

Mp 144-146 °C.

IR (neat) 2922, 2217, 1750, 1563, 1186 cm^{-1}.

^{1}H NMR (250 MHz, $CDCl_3$): δ 8.17 (d, *J* = 1.9 Hz, 1H), 8.10 (dd, *J* = 9.0, 1.9 Hz, 1H), 8.00 (d, *J* = 8.9 Hz, 1H), 7.96 (d, *J* = 9.0 Hz, 1H), 7.77 (s, 1H), 7.61 (d, *J* = 16.1 Hz, 1H), 7.50 (d, *J*

= 8.9 Hz, 1H), 7.23 (s, 1H), 7.01 (d, *J* = 16.1 Hz, 1H), 3.18-3.12 (m, 4H), 2.70-2.68 (m, 2H), 2.56-2.48 (m, 2H), 2.38 (s, 3H), 1.99 – 1.83 (m, 4H) ppm.

^{13}C NMR (63 MHz, $CDCl_3$): δ 169.6, 160.6, 159.2, 151.3, 146.9, 145.5, 137.3, 133.6, 131.6, 130.8, 129.3, 128.1, 126.9, 125.3, 124.2, 121.4, 119.9, 115.6, 114.5, 113.4, 113.5, 81.9, 50.3, 49.7, 30.1, 28.0, 22.0, 21.3, 21.1 ppm.

Elemental analysis (%): calcd. for $C_{29}H_{24}N_4O_2$: C 75.63, H 5.25, N 12.17; found: C 75.22, H 5.20, N 11.97.

(*E*)-2-((2-(2-(4-(Dimethylamino)naphthalen-1-yl)vinyl)quinolin-6-yl)methylene)malononitrile (6g)

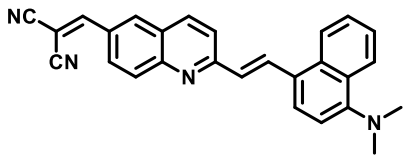

Prepared from 4-(dimethylamino)-1-naphthaldehyde (0.269 g, 1.35 mmol), as a dark red solid. Yield: 0.201 g, 56%.

Mp 95-97 °C.

IR (neat) 2930, 2105, 1568 cm^{-1}.

^{1}H NMR (250 MHz, $CDCl_3$): δ 8.63 (d, *J* = 15.9 Hz, 1H), 8.35-8.30 (m, 2H), 8.28 – 8.12 (m, 4H), 7.89 (d, *J* = 8.6 Hz, 1H), 7.83 (s, 1H), 7.78 (d, *J* = 8.6 Hz, 1H), 7.65 – 7.51 (m, 2H), 7.37 (d, *J* = 15.9 Hz, 1H), 7.13 (d, *J* = 8.0 Hz, 1H), 3,07 (s, 6H) ppm.

^{13}C NMR (63 MHz, $CDCl_3$): δ 160.1, 159.2, 153.0, 151.1, 137.8, 134.4, 133.6, 133.2, 131.1, 129.4, 128.9, 128.8, 128.6, 127.8, 127.1, 126.9, 125.7, 125.5, 125.3, 124.3, 121.8, 114.4, 114.1, 113.3, 82.6, 45.5 (2C) ppm.

Elemental analysis (%): calcd. for $C_{27}H_{20}N_4$: C 80.98, H 5.03, N 13.99; found: C 81.17, H 5.32, N 13.50.

(*E*)-2-((2-(4-(Pyrrolidin-1-yl)styryl)quinolin-6-yl)methylene)malononitrile (6h)

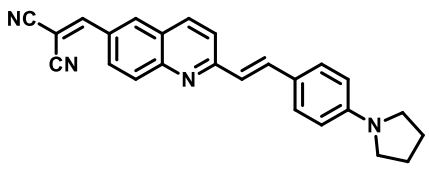

Prepared from 4-(pyrrolidin-1-yl)benzaldehyde (0.236 g, 1.35 mmol), as a dark red solid. Yield: 0.259 g, 76%.

Mp 123-125 °C.

IR (neat) 2851, 2222, 1694, 1568, 1520 cm^{-1}.

^{1}H NMR (250 MHz, $CDCl_3$): δ 8.27 (d, *J* = 1.7 Hz, 1H), 8.19 (dd, *J* = 8.9, 1.7 Hz, 1H), 8.11 (d, *J* = 9.1 Hz, 1H), 8.07 (d, *J* = 9.1 Hz, 1H), 7.85 (s, 1H), 7.76 (d, *J* = 16.1 Hz, 1H), 7.68 (d, *J*

= 8.7 Hz, 1H), 7.55 (d, *J* = 8.8 Hz, 2H), 7.15 (d, *J* = 16.1 Hz, 1H), 6.59 (d, *J* = 8.8 Hz, 2H), 3.38 (t, *J* = 6.5 Hz, 4H), 2.05 (t, *J* = 6.5 Hz, 4H) ppm.

^{13}C NMR (63 MHz, $CDCl_3$): δ 160.9, 159.2, 151.4, 149.2, 138.8, 137.4, 133.5, 130.7, 129.9 (2C), 129.4, 128.1, 126.9, 123.6, 122.7, 121.5, 113.6, 113.4, 112.2 (2C), 81.9, 48.0 (2C), 25.9 (2C) ppm.

Elemental analysis (%): calcd. for $C_{25}H_{20}N_4$: C 79.76, H 5.36, N 14.88; found: C 79.78, H 5.02, N 14.39.

Synthesis of BODIPY-styrilquinoline derivatives (11)

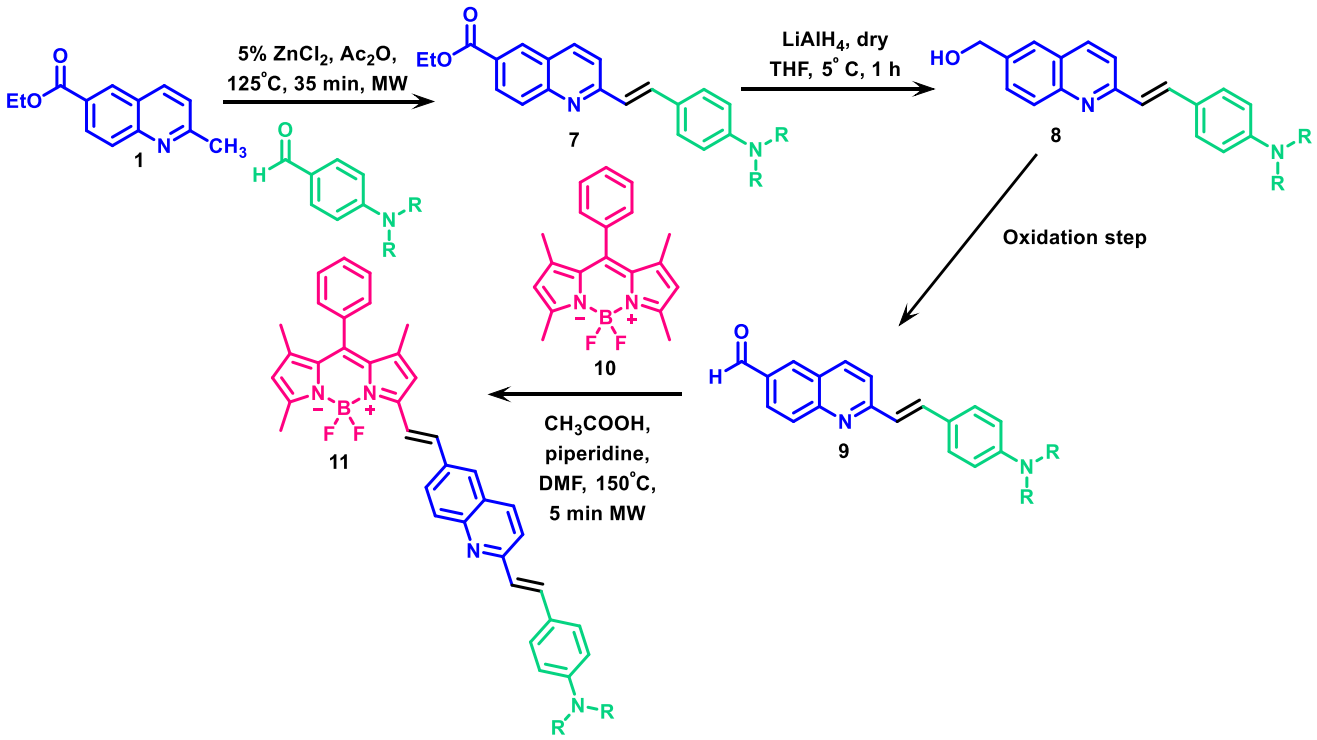

3.8.5. Condensation starting materials (7a-b)

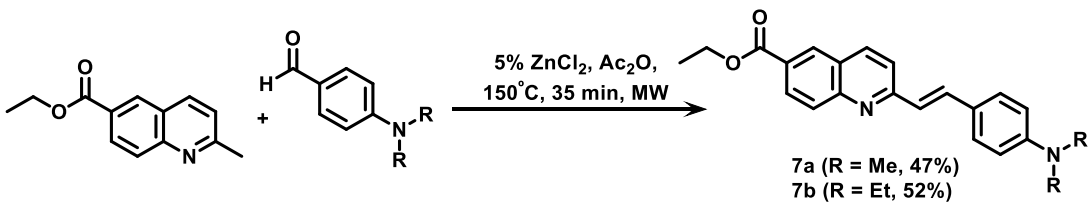

Ethyl 2-methylquinoline-6-carboxylate (1 g, 4.64 mmol), the corresponding aldehyde (1.1 eq) and zinc chloride (0.031 g, 0.232 mmol) were suspended in acetic anhydride (2 ml) in a pressure tight microwave tube containing a stirring bar. The reaction mixture was heated under microwave irradiation for 35 min at 150 °C, with an irradiation power

of 250 W. The crude product was diluted with ethyl acetate and neutralized using a $NaHCO_3$ saturated solution. The organic phase was extracted with $NaHCO_3$ (15 mL x 3), dried with anhydrous Na_2SO_4 and evaporated *in vacuo* to give a dark purple residue which was purified by flash chromatography through a silica column using hexane: ethyl acetate (7:1, v/v) as the mobile phase to give the desired compounds **7a-b**

Ethyl (*E*)-2-(4-(dimethylamino)styryl)quinoline-6-carboxylate (7a)

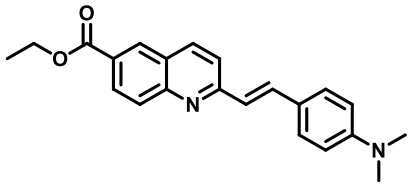

Prepared from *p*-dimethylaminobenzaldehyde (0.762 g, 5.11 mmol), brown solid. Yield: 0.75 g, 47 %.

Mp 158-160 °C.

IR (neat) 1708, 1584, 1269 cm^{-1}.

^{1}H NMR (250 MHz, $CDCl_3$): δ 8.51 (d, *J*= 1.8 Hz, 1H), 8.27 (dd, *J* = 1.8 Hz y *J* = 8.8 Hz, 1H), 8.15 (d, *J* = 8.6 Hz, 1H), 8.04 (d, *J* = 8.8 Hz, 1H), 7.69 (d, *J* = 16.2 Hz, 1H), 7.68 (d, *J* = 8.7 Hz, 1H), 7.55 (d, *J* = 8.8 Hz, 2H), 7.20 (d, *J* = 16.2 Hz, 1H), 6.73 (d, *J* = 8.7 Hz, 2H), 4.44 (c, *J* = 7.1 Hz, 2H), 3.03 (s, 6H), 1.45 (t, *J* = 7.1 Hz, 3H) ppm.

^{13}C NMR (63 MHz, $CDCl_3$): δ 166.1, 158.7, 150.7, 150.1, 136.8, 136.1, 130.3, 128.9, 128.7, 128.6 (2C), 126.8, 125.8, 123.9, 123.5, 119.6, 111.8 (2C), 60.9, 39.9 (2C), 14,2 ppm.

Elemental analysis (%): calcd. for $C_{22}H_{22}N_2O_2$: C 76.28, H 6.40, N 8.09, found: C 76.33, H 6.75, N 8.08.

Ethyl (*E*)-2-(4-(diethylamino)styryl)quinoline-6-carboxylate (7b)

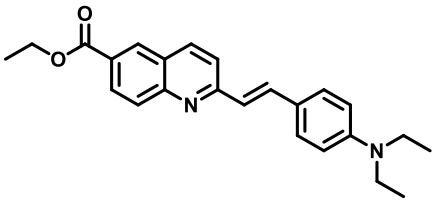

Prepared from *p*-diethylaminobenzaldehyde (0.906 g, 5.11 mmol), orange solid. Yield: 0.911 g, 52 %.

Mp 120-122 °C.

IR (neat) 1707, 1585, 1182 cm^{-1}.

^{1}H NMR (250 MHz, $CDCl_3$): δ 8.50 (d, *J* = 1.8 Hz, 1H), 8.26 (dd, *J* = 1.9 Hz y *J* = 8.8 Hz, 1H), 8.14 (d, *J* = 8.7 Hz, 1H), 8.03 (d, *J* = 8.8 Hz, 1H), 7.68 (d, *J* = 16.1 Hz, 1H), 7.67 (d, *J* = 8.7 Hz, 1H), 7.53 (d, *J* = 8.8 Hz, 2H), 7.17 (d, *J* = 16.2 Hz, 1H), 6.69 (d, *J* = 8.9 Hz, 2H), 4.44 (c, *J* = 7.1 Hz, 2H), 3.41 (c, *J* = 7.1 Hz, 4H), 1.45 (t, *J* = 7.1 Hz, 3H), 1.20 (t, *J* = 7.1 Hz, 6H) ppm.

^{13}C NMR (63 MHz, $CDCl_3$): δ 166.4, 159.1, 150.4, 148.4, 137.0, 136.4, 130.4, 129.2 (2C), 128.9 (2C), 127.0, 126.0, 123.3, 123.1, 119.9, 111.4 (2C), 61.2, 44.4 (2C), 14.4, 12.6 (2C) ppm.

Elemental analysis (%): calcd. for $C_{24}H_{26}N_2O_2$: C 76.98, H 7.00, N 7.48, found: C 76.83, H 6.75, N 7.08.

3.8.6. Reduction of styrilquinoline esters (8a-b)

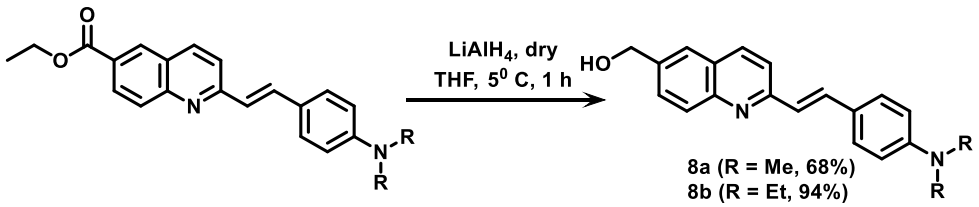

A suspension of lithium aluminium hydride (10 eq) in dry THF (10 ml) was prepared and cooled down to 0 °C with an ice-water bath. Then the suitable ester derivative (1 eq) was dissolved in dry THF (10 ml) under argon. This solution was slowly added to the suspension previously prepared. The mixture was stirred for 1h and then quenched by the sequential addition of ethyl acetate (30 mL) and water (2 mL). The suspension was filtered, and the filtrate was extracted with AcOEt, dried with anhydrous Na_2SO_4 and evaporated *in vacuo* to afford the title compounds. These compounds were directly used in the next step without purification or characterization due to solubility issues.

(*E*)-(2-(4-(Dimethylamino)styryl)quinolin-6-yl)methanol (8a)

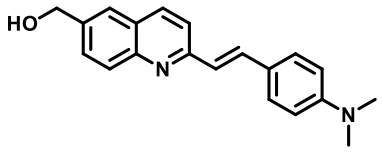

Prepared from ethyl (E)-2-(4-(dimethylamino) styryl)quinoline-6-carboxylate (0.022 g; 0,58 mmol) and $LiAlH_4$ (0.219 g, 5.8 mmol). Reddish solid. Yield: 0.120 g.

(*E*)-(2-(4-(Diethylamino)styryl)quinolin-6-yl)methanol (8b)

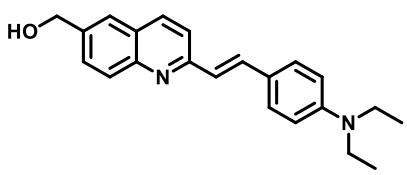

Prepared from ethyl (E)-2-(4-(diethylamino) styryl)quinoline-6-carboxylate (0.583 g; 1.55 mmol) and $LiAlH_4$ (0.591 g, 15.58 mmol). Reddish solid. Yield: 0.486 g.

3.8.7. Oxidation of styrilquinone alcohols (9a-b)

Dess Martin periodinane oxidation

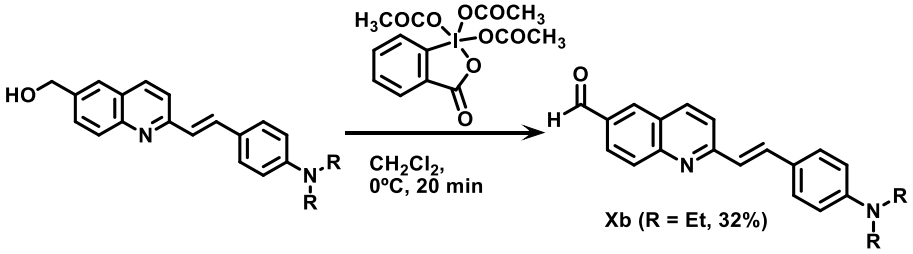

Dess Martin periodinane (0.578 g, 1.36 mmol / 0.082 g, 0.19 mmol) was added to a solution of compounds **8** (**8a** 0.277 g, 0.91 mmol / **8b** 0.043 g, 0.13 mmol) in CH_2Cl_2 (20 mL), the reaction mixture was stirred at 0 °C for 20 min. After this time, the reaction was quenched using a $Na_2S_2O_3$/$NaHCO_3$ solution (20 mL) and the mixture was stirred for 30 min at room temperature. The crude was extracted with CH_2Cl_2 (3 x 15 mL), dried with anhydrous Na_2SO_4 and evaporated *in vacuo* to give dark red crudes which were purified by flash chromatography through a silica column using hexane: ethyl acetate (7:1, v/v) as the mobile phase to give the desired compounds **9a-b.**

PCC oxidation

Pyridinium chlorochromate on alumina:

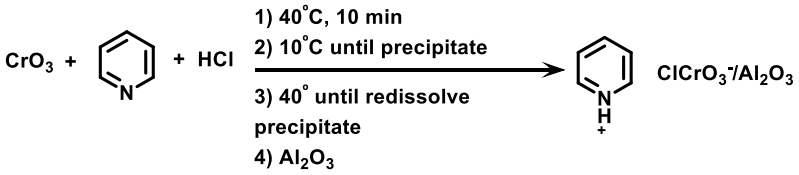

On a 250 mL round bottom flask a solution of chromium oxide (VI) 2,5 g in 5 mL of HCl (6 M) was prepared stirring and heating up to 40°C. To this solution 2,5g of pyridine were added dropwise. The solution was cooled until an orange precipitate was observed and heated up again to 40 °C until complete redissolution. At this point 20 g of Al_2O_3 were added to the stirring mixture. The solvents were evaporated under reduced pressure and dried at 100 °C under vacuum overnight. This way the load of the reagent obtained is 1 mmol/g.

PCC oxidation protocol

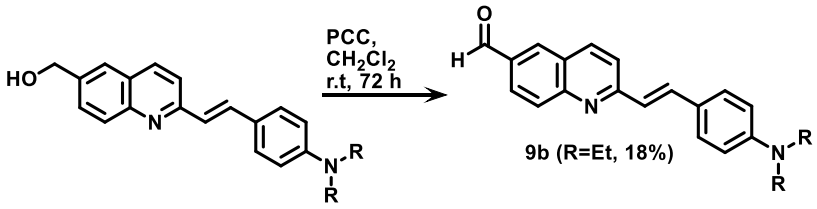

To a solution of the corresponding alcohol **8b** (0.039 g, 0.12 mmol) in dry CH_2Cl_2 (15 mL) pyridinium chlorochromate on alumina (0.120 g, 1 eq, 0.12 mmol) was added. The mixture was stirred for 72 h at room temperature. After this time, the suspension was filtered and washed with ethyl ether (5 x 10 mL). The organic solvents were dried under reduced pressure and the crude product was purified by flash chromatography through a silica column using hexane: ethyl acetate (7:1, v/v) as the mobile phase to give the compound **9b** (7 mg) as a red solid (18%).

TPAP oxidation

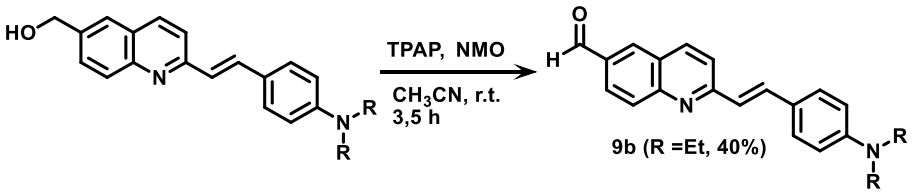

Solutions of the corresponding alcohols **8** (**8a** 0.172 g, 0.56 mmol /**8b** 0.040 g, 0.12 mmol) in dry CH_2Cl_2 (15 mL) with *N*-methylmorpholine-*N*-oxide (0.099 g, 0.85 mmol / 0.021 g, 0.18 mmol) in dry acetonitrile (4 mL) were prepared under an argon atmosphere. To these solutions, 4Å molecular sieves and tetrapropylamonium perrutenate (TPAP, 0.2 eq.) were added and the suspension was stirred at room temperature for 3.5 h. After this time, the crude was filtered through a pad of celite and washed with CH_2Cl_2 (3 x 10 mL). The filtrate was evaporated, and the crude was purified by flash chromatography through a silica gel column using hexane: ethyl acetate (7:1, v/v) as the mobile phase to give compounds **9a/9b** as reddish solids. Yield: Xa 0.025 g, 15%; Xb 0.016 g, 40%. Yield: 1.27 g, 80%. Compounds **9** were only characterized by NMR due to their instability.

(*E*)-2-(4-(Dimethylamino)styryl)quinoline-6-carbaldehyde (9a)

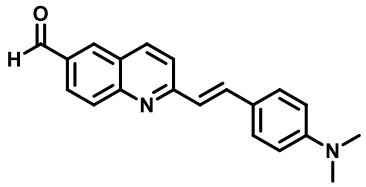

^{1}H NMR (250 MHz, $CDCl_3$): δ 10.15 (s, 1H), 8.25 (s, 1H), 8.21 – 8.11 (m, 3H), 7.74 (d, *J* = 16.2 Hz, 1H), 7.69 (d, *J* = 8.8 Hz, 1H), 7.57 (d, *J* = 8.8 Hz, 2H), 7.21 (d, *J* = 16.2 Hz, 1H), 6.74 (d, *J* = 8.8 Hz, 2H), 3.05 (s, 6H) ppm.

***(E)*-2-(4-(Diethylamino)styryl)quinoline-6-carbaldehyde (9b)**

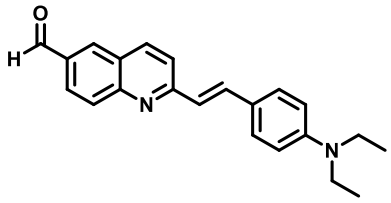

^{1}H NMR (250 MHz, $CDCl_3$): δ 10.15 (s, 1H), 8.25 (d, *J* = 1.3 Hz, 1H), 8.18 (d, *J* = 8.5 Hz, 1H), 8.13-8.07 (m, 2H), 7.69 (d, *J* = 8.6 Hz, 1H), 7.72 (d, *J* = 16.2 Hz, 1H), 7.53 (d, *J* = 8.9 Hz, 2H), 7.17 (d, *J* = 16.1 Hz, 1H), 6.69 (d, *J* = 8.9 Hz, 2H), 3.42 (c, *J* = 7.1 Hz, 4H), 1.21 (t, *J* = 7.1 Hz, 6H) ppm.

^{13}C NMR (63 MHz, $CDCl_3$): δ 191.5, 159.9, 151.4, 148.6, 137.1, 137.0, 133.2, 133.1, 129.9, 129.3 (2C), 127.1, 126.3, 123.1, 122.8, 120.3, 111.4 (2C), 44.4 (2C), 12.6 (2C) ppm.

3.8.8. Synthesis of BODIPY (10)

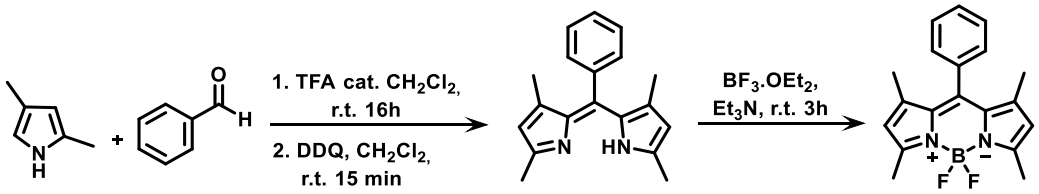

A solution of benzaldehyde (0.106 g, 1.1 mmol), 2,4-dimethyl-1H-pyrrole (0.215 g, 2.2 mmol) and a catalytic amount of trifluoroacetic acid (2-3 drops) in CH_2Cl_2 (5 mL) were stirred at room temperature for 16 h. After this time, a solution of DDQ (1 eq. in 2 ml of CH_2Cl_2) was added dropwise. The mixture was stirred for 15 minutes and after this time $BF_3O.Et$ (2 mL) and Et_3N (2 mL) were added and stirring was maintained for 3 more hours. After completion of the reaction, the crude was extracted with water (3 x 15 mL), dried with anhydrous Na_2SO_4 and evaporated *in vacuo* to give dark residue, which was purified by flash chromatography through a silica column using hexane: ethyl acetate (9:1, v/v) as the mobile phase to give the desired compound **10** as a greenish solid. Yield: 0.459 g, 29%.

Mp 155-157 °C.

IR (neat) 1502 cm^{-1}.

^{1}H NMR (250 MHz, $CDCl_3$): δ 7.40-7.37 (m, 3H), 7.19-7.15 (m, 2H), 5.89 (s, 2H), 2.47 (s, 6H), 1.28 (s, 6H) ppm.

^{13}C NMR (63 MHz, $CDCl_3$): δ 155.3 (2C), 143.1 (2C), 141.7, 134.9 (2C), 131.3, 129.1 (2C), 128.9, 127.8 (2C), 121.1 (2C), 14.5 (t, *J* = 2.1 Hz, 2C), 14.2 (2C) ppm.

^{19}F-RMN (235 MHz, $CDCl_3$, δ): -146.67 (dd, 2F, *J* = 66.0 Hz, *J* = 32.8 Hz, BF_2) ppm.

Elemental analysis (%): calcd. for $C_{19}H_{19}BF_2N_2$: C 70.40, H 5.91, N 8.64, found: C 70.58, H 5.96, N 8.24.

3.8.9. Condensation of aldehyde derivatives with the BODIPY core (11)

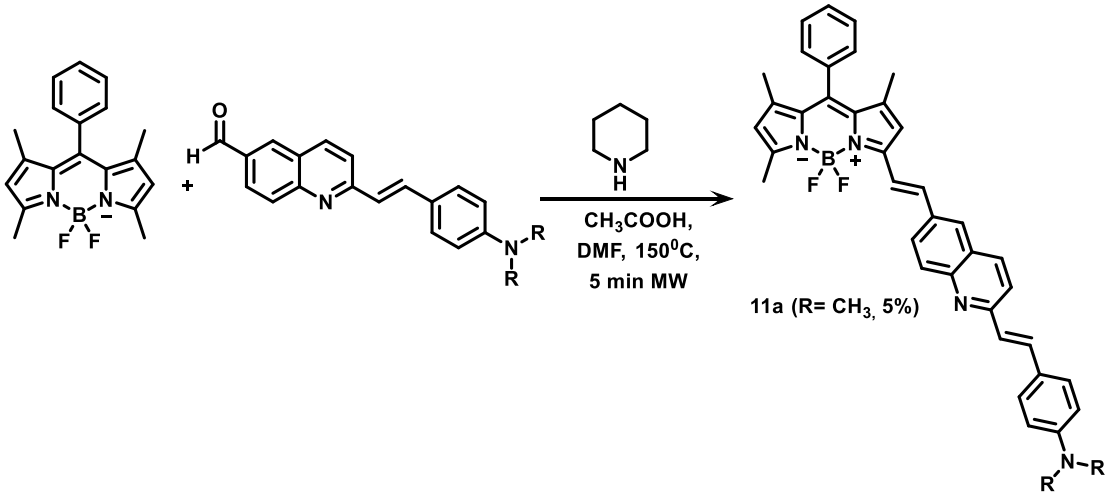

A mixture of aldehyde **9a** (0.185 g, 0.61 mmol), compound **10** (0.199 g, 0.61 mmol), acetic acid (1 drop) and piperidine (1 drop) were dissolved in DMF (1 mL) in a pressure tight microwave tube containing a stirring bar. The reaction mixture was heated under microwave irradiation for 5 min at 150 °C, with an irradiation power of 250 W. Once the reaction is finished, the crude product was diluted with ethyl acetate and washed with a LiCl saturated solution (3 x 15 mL). The organic phase was dried with anhydrous Na_2SO_4 and evaporated *in vacuo* to a crude which was purified by flash chromatography through a silica column using hexane: ethyl acetate (7:1, v/v) as the mobile phase to give the desired compound XX as a pink fluorescent solid. Yield: 0.015 g, 5%.

4-((E)-2-(6-((E)-2-(5,5-difluoro-1,7,9-trimethyl-10-phenyl-5H-4l4,5l4-dipyrrolo[1,2-c:2',1'-f][1,3,2]diazaborinin-3-yl)vinyl)quinolin-2-yl)vinyl)-N,N-dimethylaniline (11a)

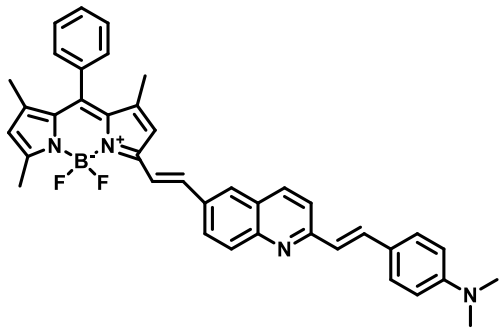

Mp 105-107 °C.

IR (neat) 2920, 1706, 1536, 1497 cm^{-1}.

^{1}H NMR (250 MHz, $CDCl_3$): δ 8.12-8.03 (m, 3H), 7.88-7.80 (m, 2H), 7.71-7.52 (m, 7H), 7.42-7.32 (m, 4H), 6.76 (d, *J* = 8.4 Hz, 2H), 6.68 (s, 1H), 6.07 (s, 1H), 3.06 (s, 6H), 2.66 (s, 3H), 1.47 (s, 3H), 1.43 (s, 3H) ppm.

^{13}C NMR (63 MHz, $CDCl_3$): δ 159.7, 156.7, 156.6, 152.3, 152.3, 143.9, 143.9, 142.7, 141.1 (2C), 137.1 (2C), 135.4, 135.2, 134.6, 129.6 (2C), 129.5 (2C), 129.2 (2C), 128.6, 128.5 (2C), 127.2, 127.1, 123.0, 122.1 (2C), 120.5 (3C), 120.5, 117.9, 25.6 (2C), 15.3, 15.00, 14.9 ppm.

^{19}F-RMN (235 MHz, $CDCl_3$) δ: -146.68 (dd, 2F, *J* = 66 Hz y *J* = 32.8 Hz, BF_2) ppm.

^{11}B NMR (160 MHz, $CDCl_3$) δ: 0.93 (t, *J* = 32.3 Hz) ppm.

HRMS found m/z 609.2942 [M+1], calculated for $C_{39}H_{35}BF_2N_4$ 608.2923.

CHAPTER 4. STYRYLQUINOLINES AS AMYLIN SENSORS

4.1. A deeper view of Type II Diabetes Mellitus etiopathology

Amylin

As previously mentioned, Type II Diabetes Mellitus (T2DM) is a multifactorial disease involving genetic and environmental factors. From a physiopathologic point of view, T2DM is mainly characterized by β-cell dysfunction, insulin resistance and chronic inflammation. All these combined failures finally provoke an increase in blood glucose levels, which leads to micro and macrovascular complications.[46]

There are several factors that contribute to β-cell failure, including ageing, genetic abnormalities, lipotoxicity, glucotoxicity, insulin resistance leading to β-cell stress hypersecretion, oxidative stress, activation of inflammatory pathways and hypersecretion of the islet amyloid polypeptide (IAPP). [46]

Islet amyloid polypeptide (IAPP), or amylin, is a 37-aminoacid peptidic pancreatic hormone found in all mammals. IAPP and insulin are co-produced, co-stored in the secretory granules and co-secreted through exocytosis with a molar ratio IAPP: insulin of 1: 100 in healthy individuals, although this ratio can increase to 1: 20 in T2DM patients. Even if the function of hIAPP remains unclear, it is known that it may be involved in glucose metabolism regulation, gastric emptying control, glucagon suppression and satiety.[114,115,116]

Monomeric hIAPP can be in numerous flexible configurations and can be classified as an intrinsically disordered protein (IDP). These are proteins that, under physiological conditions, lack a stable or fixed tertiary structure, in contrast to the traditional dogma of structural biology, in which the three-dimensional, functional structure of a protein is univocally determined by its amino acid sequence: one protein, one structure, one function. Due to their high conformational entropy, IDPs can interact with different targets or ligands, behaving as multitasking proteins. On the other hand, these proteins are prone to aggregation due to the ability of their hydrophobic amino acid side chains

[114] Caillon, L.; Hoffmann, A. R. F.; Botz, A.; Khemtemourian, L. *J. Diabetes Res.* **2016**, *2016,* ID: 5639875.
[115] Lutz, T. A.; Meyer, U. *Front. Neurosci.* **2015**, *9*, 218.
[116] Raleigh, D.; Zhang, X.; Hastoy, B.; Clark, A. *J. Mol. Endocrinol.* **2017***, 59*, 121.

to sustain intermolecular rather than intramolecular interactions, leading to their folding.[117]

It is worth nothing that only the IAPPs from humans, non-human primates and cats are able to aggregate. In contrast, the IAPPs from rodents do not form amyloid fibres and, interestingly, these animals do not develop spontaneous diabetes. Differences in the sequences of IAPP, mainly affecting the residues 20-29, have been observed. When rodent IAPP (rIAPP) and human IAPP (hIAPP) are compared, six amino acids differ in the mentioned region, being the most important the three proline residues in rIAPP at positions 25, 28 and 29. The restricted rotational freedom of proline and the disruption of hydrogen bonding and intramolecular β-sheet formation explain the lower tendency of rIAPP to aggregate and hence the lack of islet amyloid in rodent diabetes models. **(Figure 4.1)**

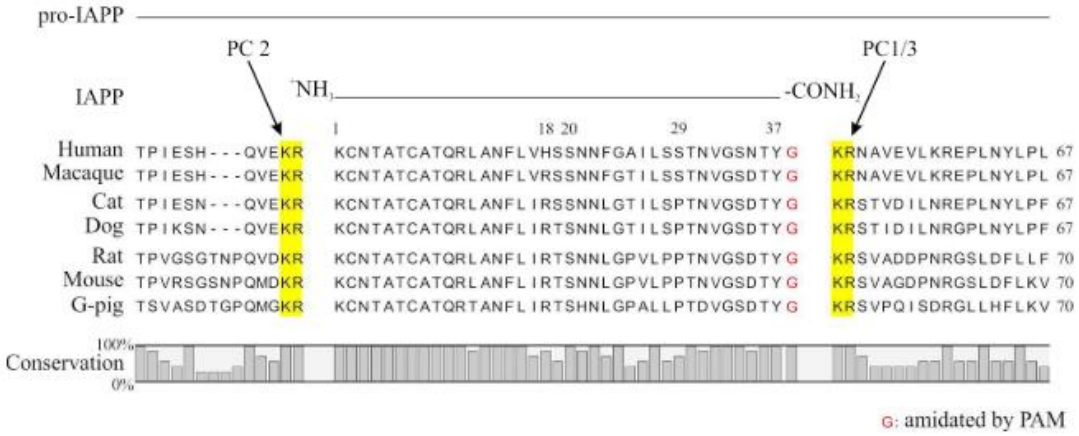

Figure 4.1

This absence of these prolines triggers the formation of β-sheet structures, which tend to aggregate creating dimers and small oligomers. These oligomers act as template structures that facilitate the quick formation of bigger oligomers, in a sigmoidal kinetics. **(Figure 4.2)**

[117] Fernández, M. S. *Cell Calcium,* **2014***, 56,* 416.

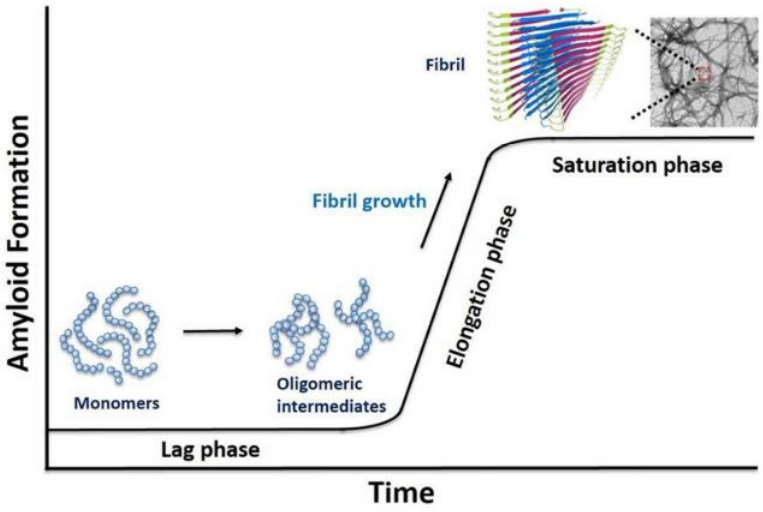

Figure 4.2.

These oligomers are thought to be the most harmful structures, due to their role as nuclear structures as well as their own potential damage capability.[118] Thus, on

one hand, it has been demonstrated that hIAPP oligomer accumulation increases oxidative stress, causes endoplasmic reticulum (ER) stress, damages mitochondrial membranes, decreases ubiquitin-proteasome functionality and impairs the autophagy recycling system. More specifically, it has been proved that pancreatic β-cell lines overexpressing hIAPP, present higher mitochondrial damage and a defective mitochondrial elimination autophagy process, called mitophagy.[119] **(Figure 4.3)**

On the other hand, larger aggregates could form fibrils that causing plasmatic membrane permeabilization and a secondary activation of the inflammatory response.[120] It is known that membranes promote hIAPP aggregation while also being the target of toxicity. It has been proved that amyloid proteins are able to induce the formation of cation-selective channels in planar lipid bilayers, causing membrane disruption.[119]

[118] *Kahn S.E. Diabetologia, **2010**, 53,* 1046.
[119] García-Hernández, M.; García-Aguilar, A.; Burillo, J.; Gómez-Oca, R.; Manca, M. A.; Novials, A.; Alcarraz-Vizan, G.; Guillén, C.; Benito, M. *Cell Death and Disease*, **2018**, *9*, 1.
[120] Mukherjee, A.; Morales-Scheihing, D.; Butler, P.C.; Soto, C. *Trends in Molecular Medicine*, **2015**, 1.

Due to this amylin overexpression and misfolding, T2DM can be classified as a protein-misfolding disease, sharing the histopathological characteristic hallmark of fibrillar amyloid deposits, in this case affecting in the pancreatic islets of Langerhans.

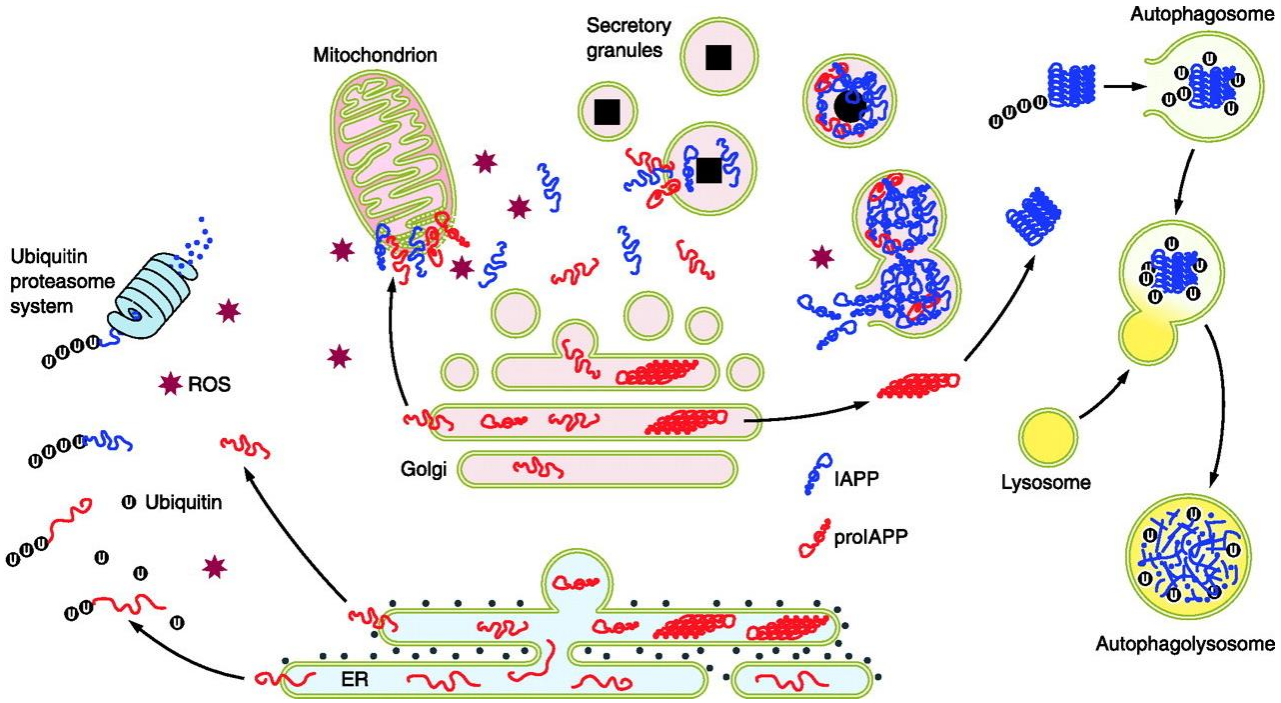

Figure 4.3. Reproduced with permission from reference [121].

4.2. hIAPP and Aβ: Partners in crime?

Both, AD and T2DM are multifactorial age-related disorders, leading to a considerable morbidity and mortality in elderly population. During the past years, several epidemiological studies demonstrated that T2DM patients present a 2 to 5 times higher risk of developing AD than the normal population. Furthermore, people with T2DM often experience a significant decline in cognitive function and around 70% of them eventually develop AD. Moreover, animal models of T2DM have been shown to develop spontaneous AD-like pathologies, exhibiting typical neuropathological characteristics

[121] Westermark, P.; Andersson, A.; Westermark, G. T. *Physiol. Rev.* **2011**, *91*, 795.

such as high APP and β-secretase levels, Aβ formation, tau hyper-phosphorylation and neuronal death.

Although both pathologies appear to share several pathophysiological pathways, the exact molecular connection between them remains unclear.[122]

One of these hypotheses is associated with hIAPP and Aβ aggregates. These two proteins have a total of 25% amino acid sequence identity and a high binding affinity to each other. Moreover, they share several biophysical and physiological properties and exert similar cytotoxic mechanisms once aggregated.

Also, hIAPP deposits have been found in cerebral samples of AD patients. Cerebral IAPP has also been found in rats overexpressing hIAPP. Additionally, IAPP has been found to precipitate with Aβ to form diffuse and dense senile plaques. **(Figure 4.4)**

It has been proved that IAPP aggregates can exert cytotoxic effects on neurons by several mechanisms. On one hand, IAPP and Aβ could interact with each other and synergistically exert their toxic effect. One possible reason is that IAPP can aggregate in the walls of cerebral blood vessels and induce failure in brain Aβ elimination.[122] On the other hand, IAPP aggregates can have a direct toxic effect on neurons, by causing damage in cellular structures, disturbing ion homeostasis (Ca^{2+}), triggering inflammatory responses, inducing oxidative stress or activating apoptotic signalling pathways.

These facts provide enough evidence to hypothesize that IAPP aggregation during T2DM development plays a key role in AD pathogenesis.

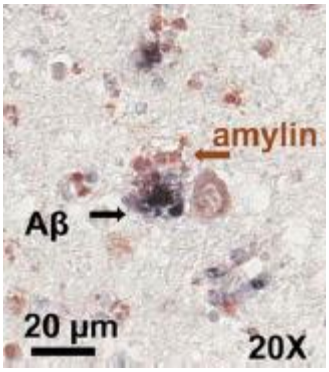

Figure 4.4. Brain parenchyma of a T2DM patient with Alzheimer´s disease

[122] Zhang, Y.; Song, W. *Prog. Neurobiol.* **2017***, 153*, 100.

The transcription levels of IAPP in brain are undetectable, and this may indicate that cerebral IAPP comes from pancreatic islet β-cells and travels through circulation to the central nervous system. This hypothesis is further corroborated by the discovery of IAPP deposits on blood vessel walls and pericapillary brain spaces. One plausible hypothesis is that that hIAPP aggregates are exported form β-cells inside exosomes and travel this way through blood vessels to reach the central nervous system.[122] **(Figure 4.5)**

To verify this hypothesis, compounds able to detect hIAPP aggregates are needed. Moreover, they could be used as diagnostic tools for advanced prediabetic stages or even early AD stages on diabetic patients.

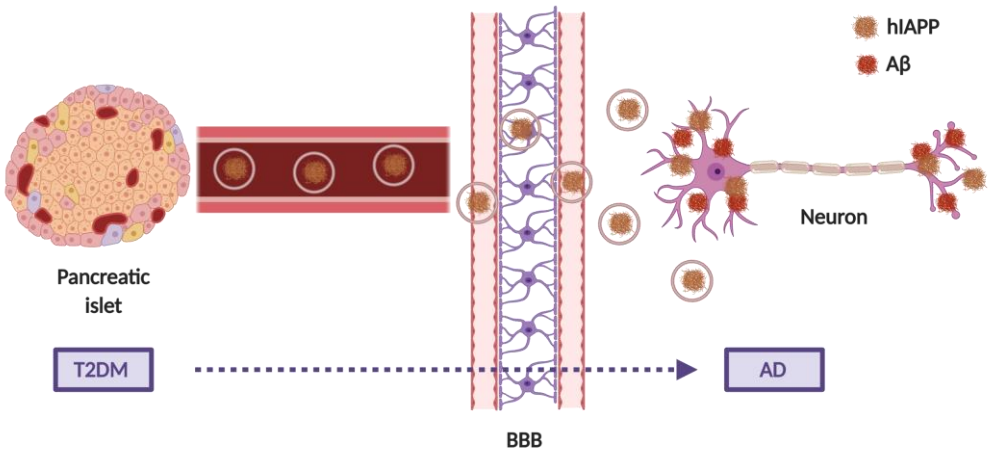

Figure 4.5.

4.4. Preliminary results

In order to test one of our styrylquinolines as an amylin sensor, preliminary experiments were carried out by Jesús Burillo, under the supervision of Drs. Carlos Guillén and Manuel Benito at the Departamento de Bioquímica y Biología Molecular, Facultad de Farmacia, Universidad Complutense de Madrid. To this end, **compound 6b** was tested in insulinoma cell lines (INS1-E) overexpressing rat amylin (non-amyloidogenic), human amylin (amyloidogenic) and wild type (WT). Due to solubility issues, DMSO was selected as solvent for preparing the stain stock solutions. First, the optimal staining concentration needed to be determined. For this purpose, different concentrations ranging from 1 to 10 µM were tested, finding that, even if staining was already observed

with the 1 µM concentration, 10 µM gave the best results, being selected for further immunofluorescence assays. Next, different staining times and labeling methods were tested in order to establish a standardized protocol, finding that, the best conditions for **6b** staining corresponded to 10 µM concentration for 20 min. **6b** staining was done on cells after fixation and antibody-labeling classic immunofluorescence protocols.

Preliminary experiments on a fluorescence microscope were initially performed. To this end, INS1-E cells were exposed to two different glucose concentrations (11 mM, "basal" concentration and 16.7 mM, secretory concentration) in order to stimulate hIAPP production and accumulation. As shown in **Figure 4.6**, only the INS1-E hIAPP cell line presents fluorescent emission, which is increased under basal glucose conditions. On the other hand, no fluorescent beyond basal "noise" is observed in INS1-E WT and INS1-e rIAPP cells, verifying that **6b** is selectively staining cell lines able to produce IAPP aggregates

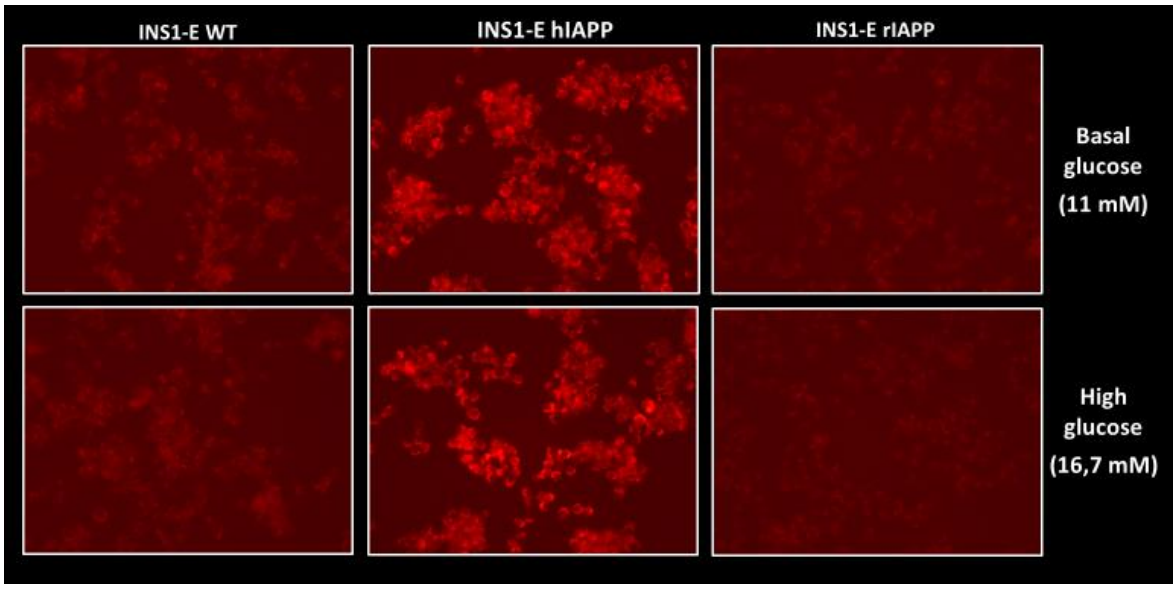

Figure 4.6.

The next experiment was performed using a confocal microscope. This time the cell lines were submitted to the same conditions and the HT-22 mouse hippocampal cell line was used as a control to confirm the specificity of **6b** for amyloid aggregates. The same staining protocol was used for **6b** and this time DAPI was used to stain the cell nuclei. As in the previous case, no fluorescent signal was observed neither in INS1-E WT, rIAPP or HT-22. However, INS1-E hIAPP showed a dot-shaped signal, pointing to a specific

labeling of hIAPP aggregates. Curiously, it seems that less dots are found in high glucose than in basal glucose conditions. **(Figure 4.7)** A tentative explanation is that hIAPP aggregates are exported inside exosomes, as a detoxifying method.

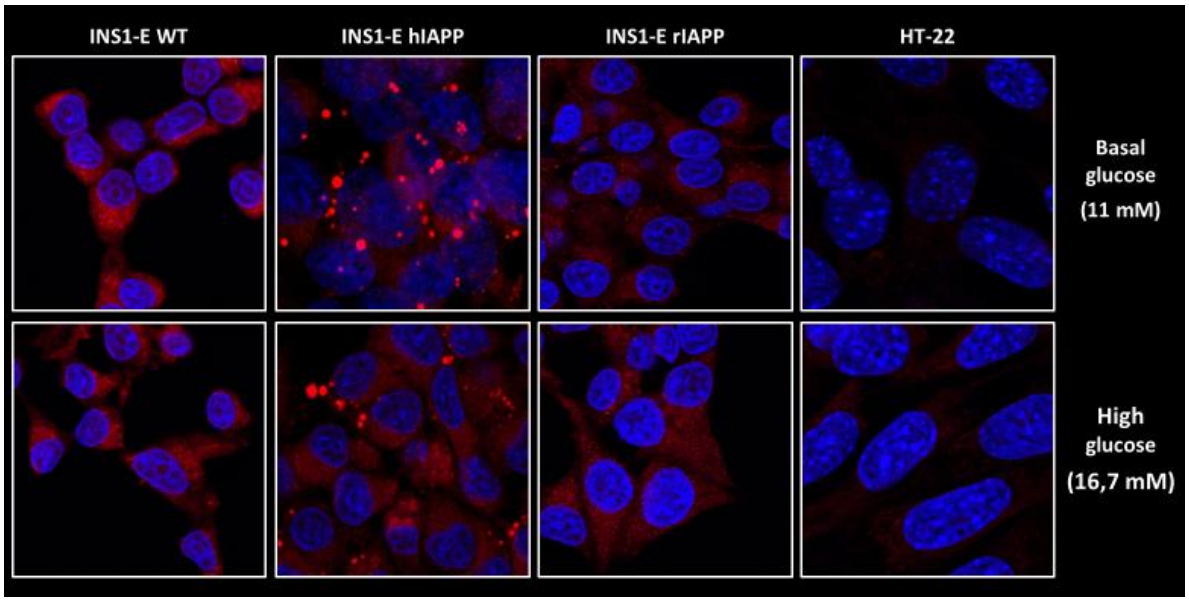

Figure 4.7.

In order to verify this possible mechanism, several experiments were performed. First, the exosomal extract was evaluated **(Figure 4.8)**, proving that the INS1E cells were able to secrete exosomes containing amylin.

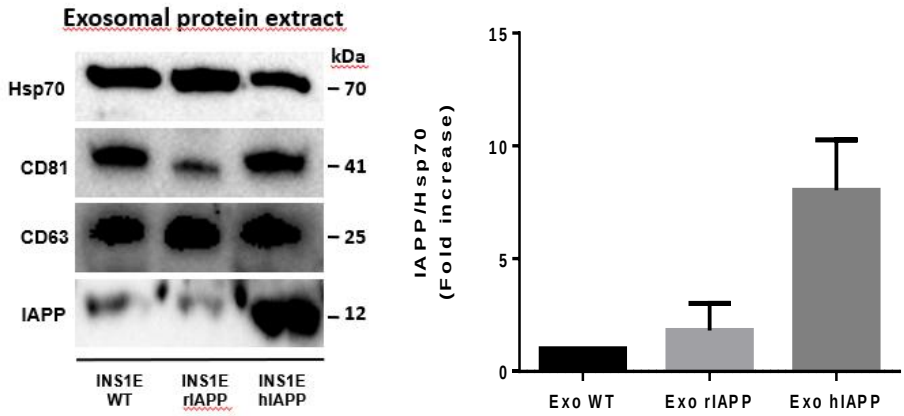

Figure 4.8. Content of amylin in exosomal protein extract.

Then cells were submitted to GW4869, an inhibitor of exosomal secretion, showing that under these conditions the amount of amylin inside cells considerably increases. **(Figures 4.9** and **4.10)**

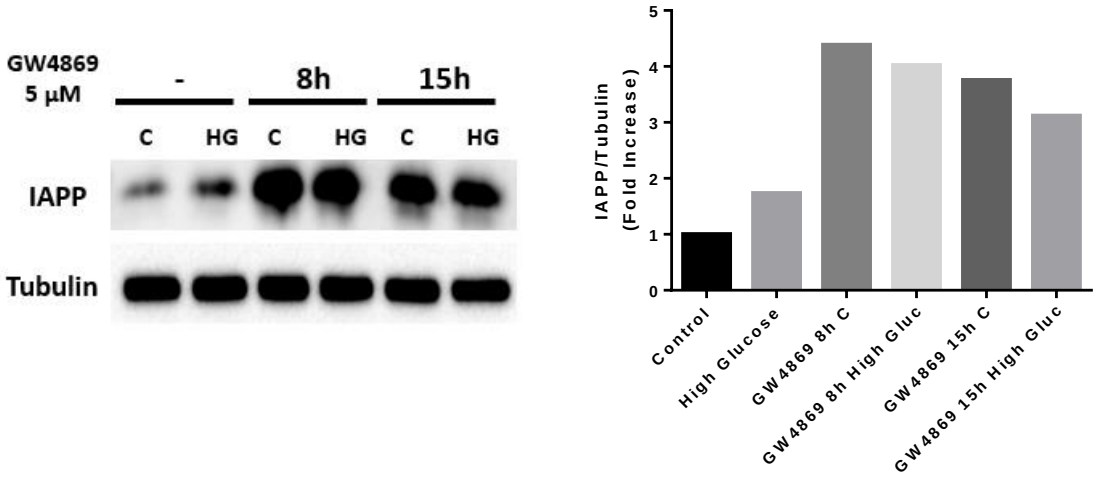

Figure 4.9. Cell protein extract after GW4869 treatment(exosomal secretion inhibitor).

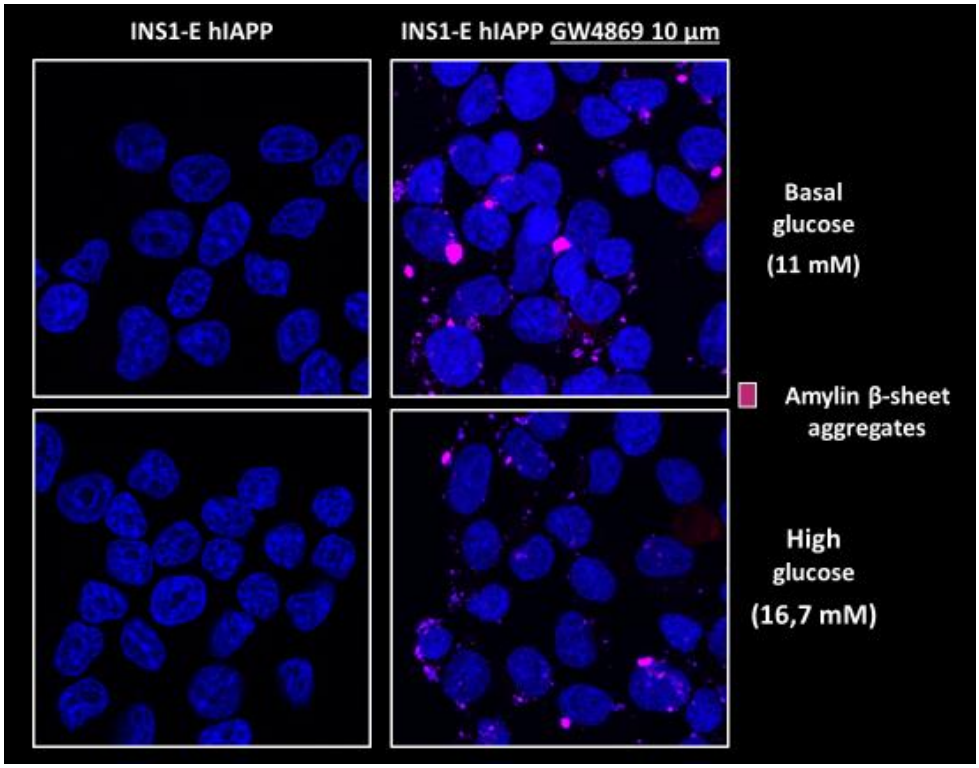

Figure 4.10.

To further verify this hypothesis, colocalization experiments were carried out. INS1-E hIAPP cells were labelled with a protein belonging to the exosome formation pathway, Tsg101, and compound **6b (Figure 4.11)**. Co-localization of **6b** signal and Tsg101 may

confirm the presence of hIAPP aggregates inside multivesicular bodies (MVB), the structures from exosomes are derived, although if positive results were found further experiments need to be done.

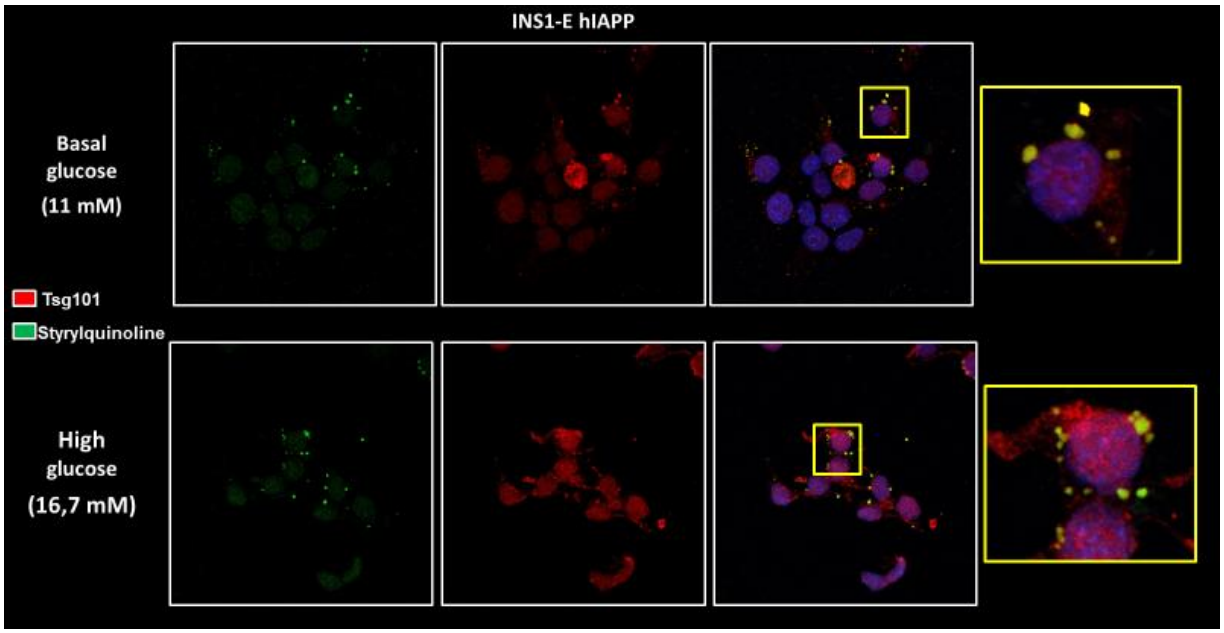

Figure 4.11.

Finally, compound **6b** and a non-aggregated hIAPP specific antibody were used in combination in order to check if **6b** acts as a β-amyloid aggregates specific dye within pancreatic β-cells. INS1-E cells were submitted to basal and high glucose conditions and labelled with the antibody and the **6b** following the standard protocol previously described. The results showed a clear different fluorescent signal of **6b** and hIAPP antibody, confirming the ability of **6b** to target specifically hIAPP aggregates. **(Figure 4.12)**

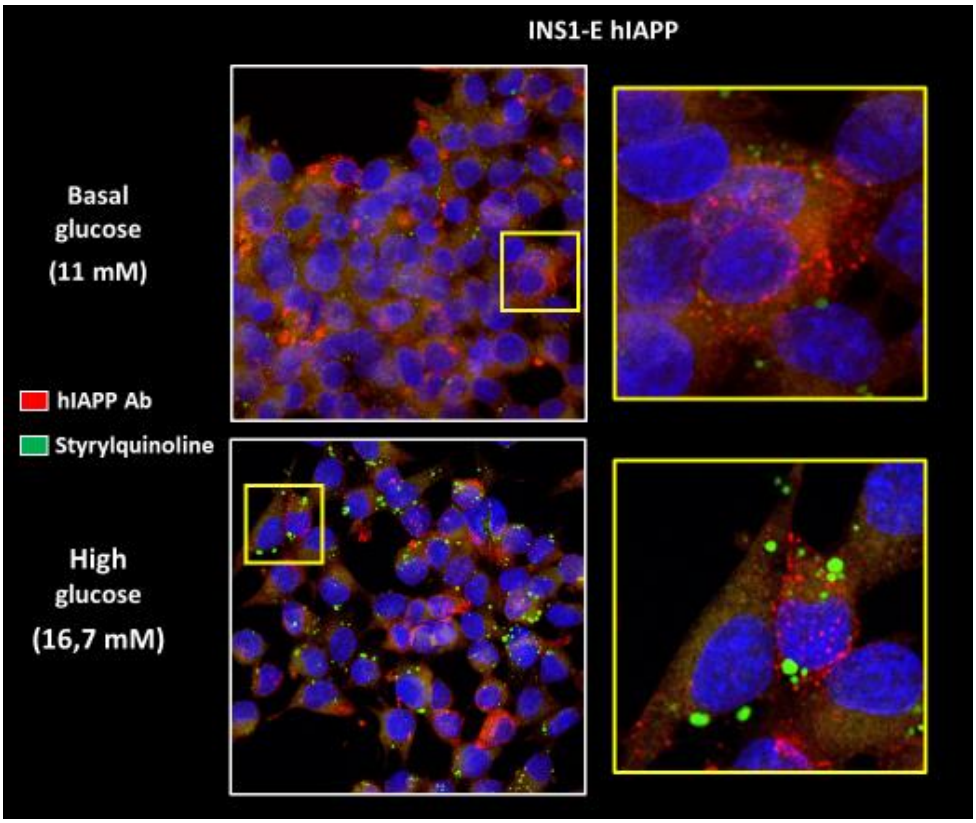

Figure 4.12.

Future experiments will be performed on a T2DM mice model, which will express human amylin within their pancreas. **6b** will be tested on sections of different tissues (pancreas, liver, kidney, etc.) in order to check the accumulation of hIAPP aggregates, focusing on the brain in order to establish a link between T2DM and neurodegenerative disorders.

CHAPTER 5. NOVEL MITOCHONDRIAL-TARGETED LEISHMANICIDAL DERIVATIVES OF THE 4-AMINOSTYRYLQUINOLINE SCAFFOLD

5.1. Why are mitochondria-targeted compounds interesting for leishmaniasis?

As mentioned in the Introduction, leishmaniasis is a protozoal tropical disease surpassed only by malaria in terms of human health impact factor. Current therapy is based in a few drugs with several drawbacks such as the need for parenteral administration with hospitalization of the patient, drug resistance and toxicity. Thus, there is still an urgent need to discover new antileishmanial drugs.[123,124]

Understanding the biology of these parasites is key for developing novel new drug targets and leishmanicidal compounds. Protozoa are interesting form a biological point of view because they possess unique organelles and cytoplasmic structures. One of the main characteristics of trypanosomatids such as *Leishmania* is that they bear a single mitochondrion, which is thus of vital importance. The structure of the trypanosomatid mitochondria is peculiar compared to multicellular organisms regarding the density of the matrix as well as the shape and number of cristae. Also, depending on the nutritional resources available, it can occupy up to 12% of the cell volume. The most unusual structure in the organelle is the kinetoplastid DNA (kDNA), which is found in the most dilated regions. [125] **(Figure 5.1)**

Moreover, about 70% of trypanosomatids energetic metabolism is based on oxidative phosphorylation. In *L. donovani* promastigotes, only 30% of ATP production is fulfilled through glycolysis, [126] and a higher mitochondrial dependence has been reported in *L. mexicana* intracellular amastigotes. [127] In addition, it was demonstrated that in tafenoquine-resistant *L. major* strains the ability of glycolysis to compensate for mitochondrial dysfunction is quite limited. [128] All these data evidence that

[123] Alvar, J.; Velez, I.D.; Bern, C.; Herrero, M.; Desjeux, P.; Cano, J.; Jannin, J.; den Boer, M. *PLoS One* **2012**, *7*, e35671.
[124] Ponte-Sucre, A.; Gamarro, F.; Dujardin, J.C.; Barrett, M.P.; Lopez-Velez, R.; García-Hernandez, R. A. Pountain, W.; Mwenechanya, R.; Papadopoulou, B. *PLoS Neglected Trop. Dis.* **2017,** *11*, e0006052.
[125] Fidalgo, L. M.; Gille, L. *Pharm. Res.* **2011***, 28,* 2758.
[126] Sen, N.; Das, B.B.; Ganguly, A.; Banerjee, B.; Sen, T.; Majumder, H.K. *Exp. Parasitol.* **2006**, *114*, 204.
[127] Saunders, E.C.; Ng, W.W.; Kloehn, J.; Chambers, J.M.; Ng, M.; McConville, M.J. *PLoS Pathog.* **2014**, *10*, e1003888.
[128] Manzano, J.I.; Carvalho, J.; Perez-Victoria, J.M.; Castanys, S.; Gamarro, F. *Antimicrob. Agents Chemother.* **2011**, *55*,1045.

mitochondrion disfunction is particularly toxic for these protozoa, in contrast to mammalian, which may contain hundreds of mitochondria in a single cell. [125]

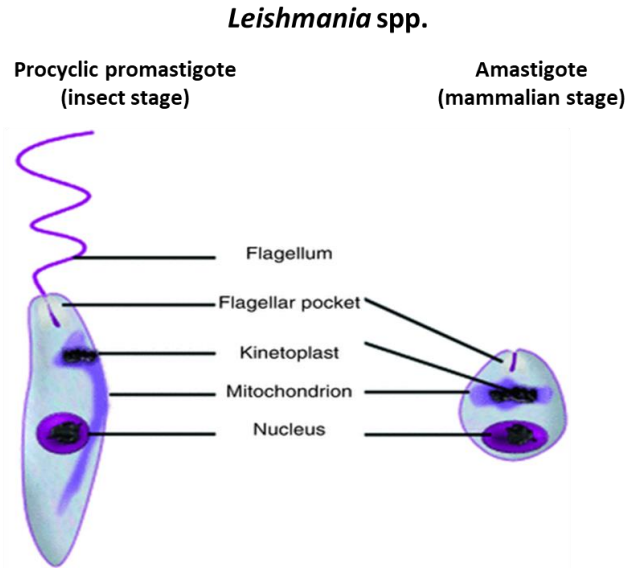

Figure 5.1

Drugs targeting the mitochondrial ATP synthesis process must hamper the bioenergetic requirements of *Leishmania*. In agreement with this idea, several studies about the mechanism of action of antiprotozoal drugs suggest that many of the drugs that show effectiveness against the parasite act on the *Leishmania* mitochondrion.[126] For example, artemisinin, a sesquiterpene lactone, is an antimalarial drug that has also shown antileishmanial activity, which is due to loss of the mitochondrial membrane potential. Moreover, amphotericin B and pentamidine induce mitochondrial membrane permeability with a rapid decrease of the mitochondrial membrane potential

Additional leishmanicidal drugs acting at mitochondria are atovaquone, a hydroxynaphthoquinone that acts as a ubiquinone competitor, inhibiting the cytochrome bc1 complex, and tafenoquine, an 8-aminoquinoline, whose antileishmanial mechanism of action involves mitochondrial dysfunction by inhibiting cytochrome C reductase (respiratory complex III), decreasing oxygen consumption and depolarizing the mitochondrial membrane potential. [125] **(Figure 5.2)**

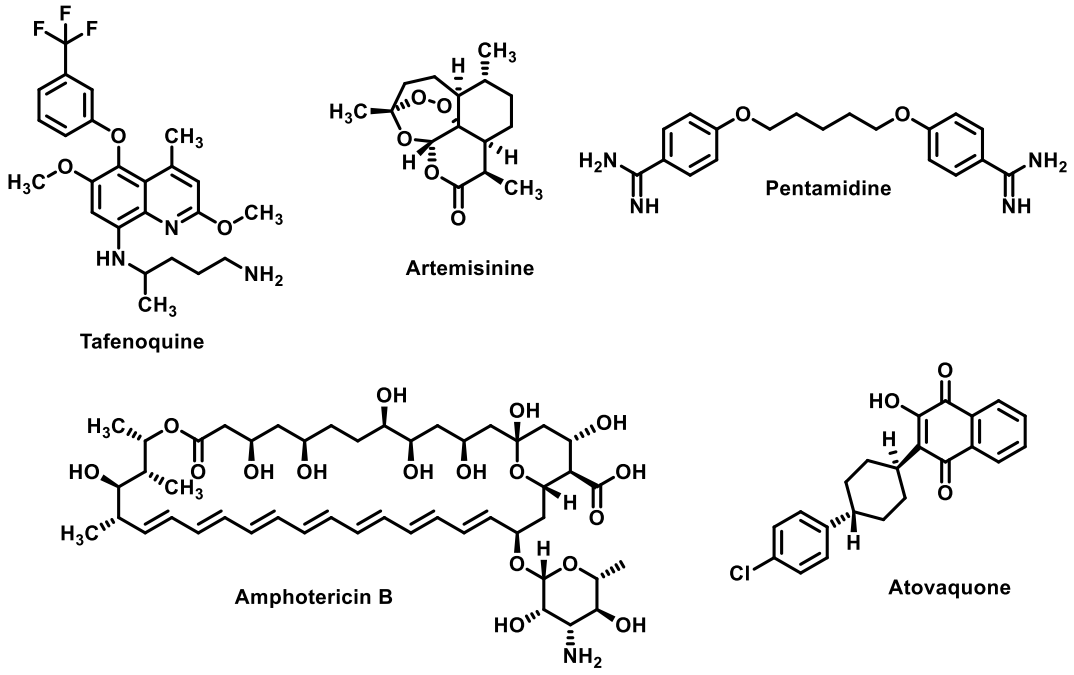

Figure 5.2

5.2. Design of antileishmanial 4-aminostyrylquinolines

Quinolines have shown a high potential to develop effective and affordable oral treatments as leishmanicidal agents.[129] For instance, the quinoline derivative **I (Figure 5.3)** showed a better antileishmanial activity than the reference drug miltefosine with a good selectivity index (SI), and it entered in the Drugs for Neglected Diseases initiative (DNDi) pipeline for *in vivo* evaluation.[130] Also, the quinaldine derivative **II (Figure 5.3)**, designed to inhibit the type-2 NADH dehydrogenase (NDH2) of *Leishmania infantum*, exhibited good activity against both promastigote and amastigote forms.[131] Moreover, as previously mentioned for the case of tafenoquine[132] **(Figure 5.3)**, it has been proved that 8-aminoquinoline polyamines inhibit the respiratory chain at the *Leishmania* mitochondrion. Among them, the most relevant example is sitamaquine **(Figure 5.3)**,

[129] K.A. Reynolds, W.A. Loughlin, D.J. Young, Quinolines as chemotherapeutic agents for leishmaniasis, *Mini Rev. Med. Chem*. **2013**, *13*, 730.
[130] Loiseau, P.M.; Gupta, S.; Verma, A.; Srivastava, S.; Puri, S.K.; Sliman, F.; Normand-Bayle, M.; Desmaele, D. *Antimicrob. Agents Chemother.* **2011**, *55*, 1777.
[131] Stevanovic, S.; Perdih, A.; Sencanski, M.; Glisic, S.; Duarte, M.; Tomas, A.M.; Sena, F.V.; Sousa, F.M.; Pereira, M.M.; Solmajer, T. *Molecules*, **2018***, 23*, 772.
[132] Carvalho, L.; Luque-Ortega, J.R.; Manzano, J.I.; Castanys, S.; Rivas, L.; Gamarro, F. *Antimicrob. Agents Chemother.* **2010**, *54*, 5344.

which reached phase IIb clinical trials, affording oral treatment for leishmaniasis by inhibiting the succinate dehydrogenase (complex II) of the respiratory chain.[133,134]

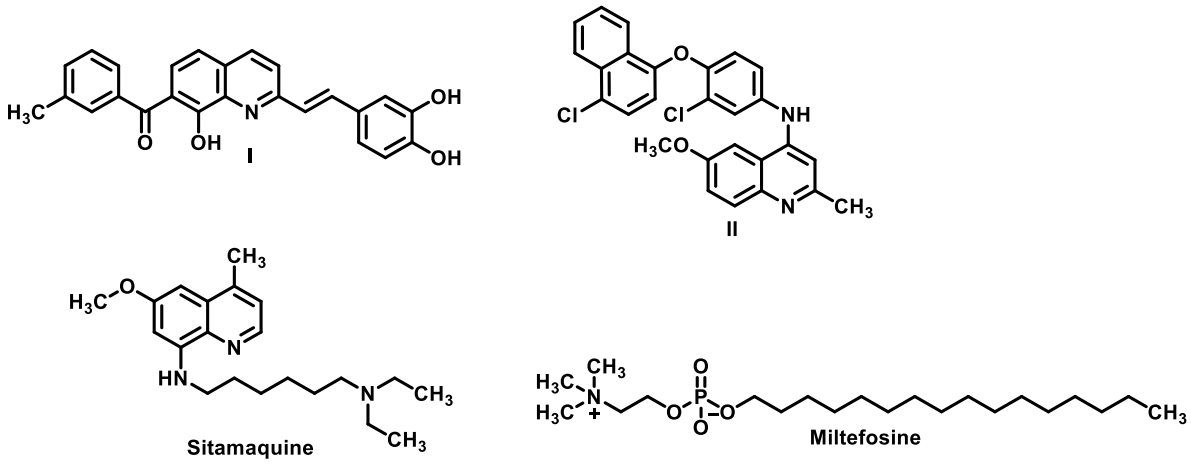

Figure 5.3

Among quinolines, 2-substituted derivatives have often shown higher activities and metabolic stabilities with lower toxicity than their non-substituted counterparts.[135] Also, the presence of conjugated double bonds seems beneficial for activity, as shown by the case of compound **I**.[136,137]

Using as a starting point the activities of 8-aminoquinoline-based polyamines, we reasoned that an increase in the positive charge of quinoline core would enable the molecules to have a preferential mitochondrial accumulation. This is because, among intracellular organelles, mitochondria present a higher electrochemical potential ($\Delta\psi_m$) that would drive the preferential accumulation.

In this context, we designed a library of 2-substituded styrylquinolines,[110] which were decorated with polyamine chains in the C-4 position of the quinoline scaffold. The 4-aminoquinoline fragment would lead to an increased basicity of the heterocyclic

[133] Loiseau, P.M.; Cojean, S.; Schrevel, J. *Parasite*, **2011**, *18*, 115.
[134] Carvalho, L.; Luque-Ortega, J.R.; Lopez-Martín, C.; Castanys, S.; Rivas, L.; Gamarro, F. *Antimicrob. Agents Chemother.* **2011**, *55*, 4204.
[135] Desrivot, J.; Herrenknecht, C.; Ponchel, G.; Garbi, N.; Prina, E.; Fournet, A.; Bories, C.; Figadere, B. Hocquemiller, R.; Loiseau, P.M. *Biomed. Pharmacother*. **2007**, *61*, 441.
[136] X. Franck, A. Fournet, E. Prina, R. Mahieux, R. Hocquemiller, B. Figadere *Bioorg. Med. Chem. Lett.* **2004**, *14*, 3635.
[137] Nakayama, H.; Desrivot, J.; Bories, C.; Franck, X.; Figadere, B.; Hocquemiller, R.; Fournet, A.; Loiseau, P.M. *Biomed. Pharmacother.* **2007**, *61*, 186.

nitrogen, and more importantly, to a delocalized positive charge by resonance across the N1=C2-C3=C4-NH fragment. This approach was expected to enhance the behaviour of the molecule as a lipophilic cation, essential for its transport across the inner mitochondrial membrane and mitochondrial accumulation.[138] Finally, the substituents at the end of the polyamine chain (represented by **Z**, **Figure 5.4**)[139] were chosen in order to modulate the basicity of the nitrogen atoms at C-4 and evaluate its influence. This may be of relevance because the presence of a second amino group in the polyamine chain would increase compound retention at the acidic pH present on the phagolysosomes, where the amastigote forms multiply.[140] Finally, the presence of the 2-styryl fragment, besides potentially increasing activity, was expected to confer fluorescence to the molecules and, ideally, allow mitochondrial imaging.

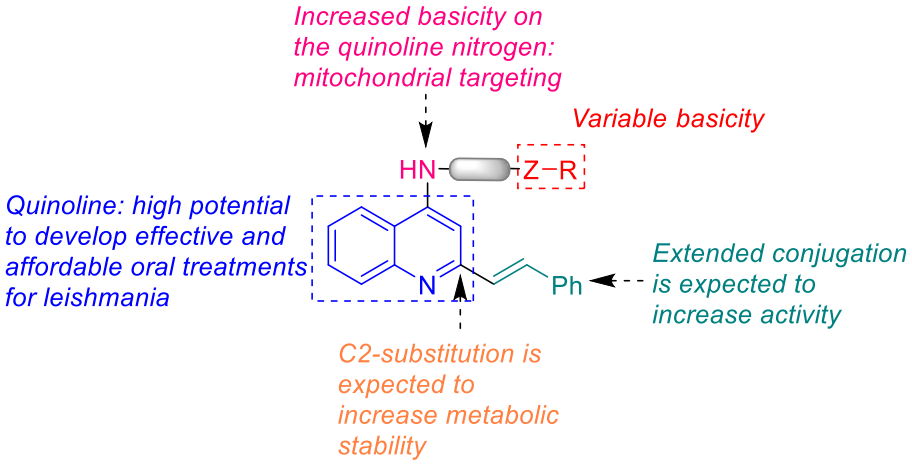

Figure 5.4

5.3. Synthesis of 4-aminostyrylquinoline derivatives

To be able tests the importance of each part of the molecules and perform some SAR studies, we synthesized and tested a library of compounds that included Boc-protected polyamine chains and deprotected ones. We also evaluated two different polyamine

[138] Murphy, M.P. *Biochim. Biophys. Acta* ***2008****, 1777, 1028.*

[139] Staderini, M.; Piquero, M.; Abengozar, M.A.; Nacher-Vazquez, M.; Romanelli, G.; Lopez-Alvarado, P.; Rivas, L.; Bolognesi, M. L.; Menendez, J.C. Eur. J. Med. Chem. **2019**, *171*, 38.

[140] Dias, M.P.; Souza, I.O.; Lima, W.P; Gameiro, J.; da Silva, A.D.; Coimbra, E.S. *Chem. Biol. Drug Des.* **2015**, *86*, 704.

chains to evaluate the importance in length of this one, and in the **Z** residue different groups such as alkylamines **(19a-h)**, arylamides **(19i-l)** or alkoxy **(20a-b)** were included.

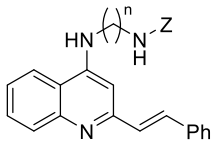

Cmpd.	n	Z
16a	2	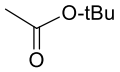
16b	4	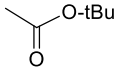
17a	2	H
17b	4	H
19a	2	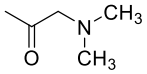
19b	2	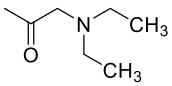
19c	2	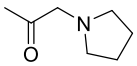
19d	2	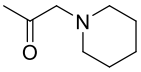
19e	2	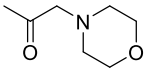
19f	2	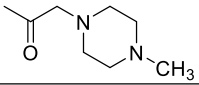

Cmpd.	n	Z
19g	2	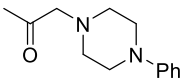
19h	4	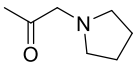
19i	2	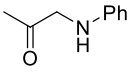
19j	4	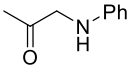
19k	2	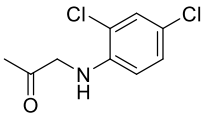
19l	4	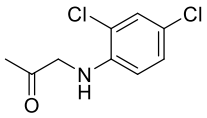
20a	2	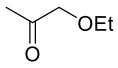
20b	4	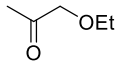

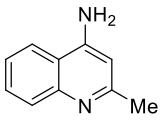

22

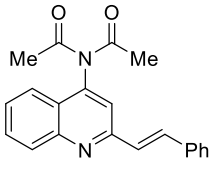

23

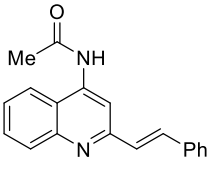

24

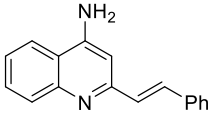

25

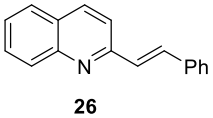

26

Table 5.1

derivatives were tested. Furthermore, compound **22** was evaluated to verify the importance of the styryl group, while compounds **25** and **26** were tested in order to evaluate the influence of the 4-amino substitution of the polyamine chain. **(Table 5.1)**

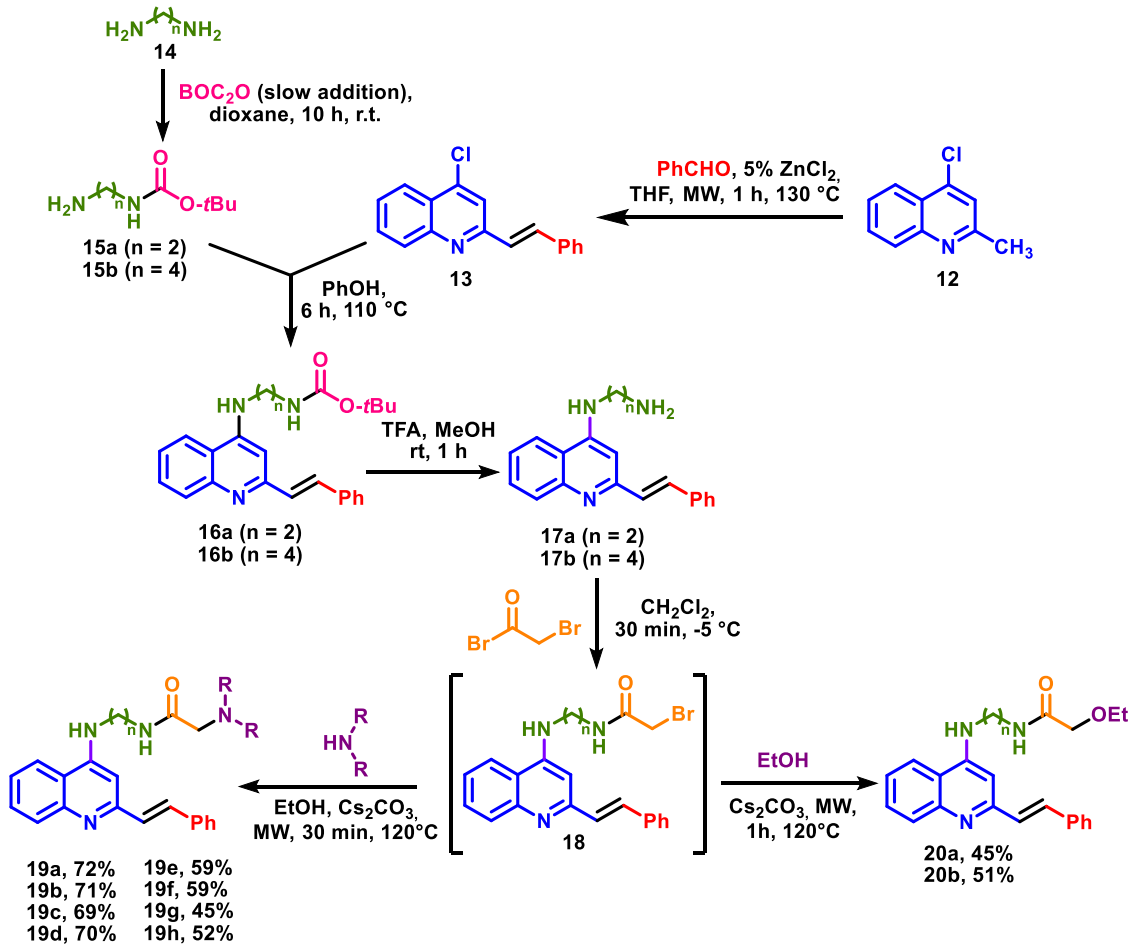

Scheme 5.1

For the preparation of our chemical library, we started with the synthesis of 4-chloro-2-styrylquinoline **13**, followed by its decoration with the selected basic chains at C-4. The commercially available 4-chloroquinaldine **12** was condensed with benzaldehyde in the presence of zinc chloride through a microwave-promoted aldol condensation. After preparation of the desired Boc-monoprotected polyamine chains (**15a** and **15b**), compound **13** and the suitable amine were heated in the presence of phenol, which acts as both the solvent and the acidic promoter of the nucleophilic aromatic substitution that yielded compounds **16a** and **16b**. **(Scheme 5.2)** These intermediates were deprotected using a solution of trifluoroacetic acid in methanol, giving **17a** and **17b**, which were directly transformed into halides **18** by treatment with bromoacetyl bromide at -5 °C for 30 minutes Finally, compounds **18** were treated with a variety of aliphatic amines under microwave irradiation in the presence of Cs_2CO_3 to yield the desired compounds **19a-h**. For the synthesis of the ethoxy intermediate **18** was treated

with ethanol under the same reaction conditions, yielding compounds **20a-b. (Scheme 5.1)**

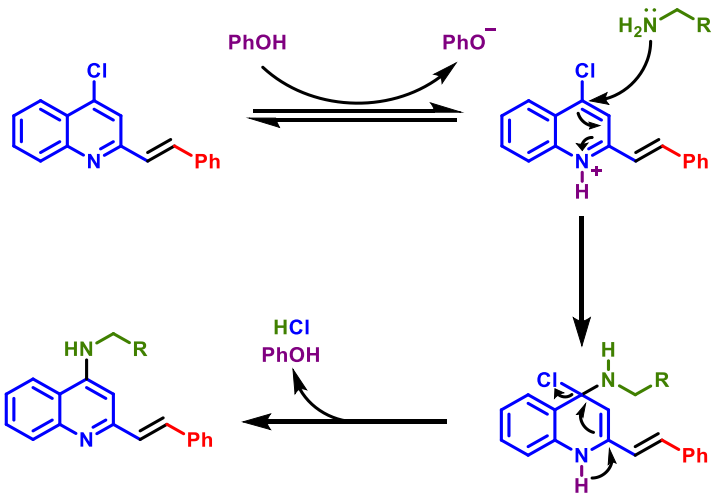

Scheme 5.1

Unfortunately, this method failed for the preparation of the aniline derivatives **19i-l**, probably due to the low nucleophilicity of the required starting amines. For this reason, alternative method was needed and to this end we prepared *N*-arylglycine derivatives by reacting the suitable commercially available anilines with ethyl bromoacetate in the presence of sodium hydride, followed by ester hydrolysis. Once compounds **21a-b** were available, the last step was the coupling with the previously mentioned primary amines **17a-b**in the presence of EDC/HOAt. **(Scheme 5.3)**

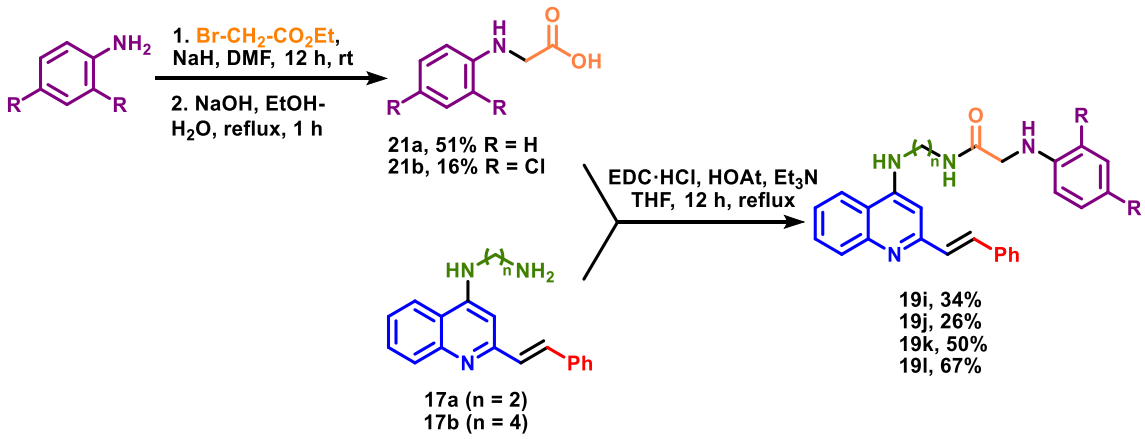

Scheme 5.3

In order to evaluate the influence of the polyaminoalkyl chain, compound **25** was required as a reference. The commercially available 4-amino-2-methylquinoline was

condensed with benzaldehyde in the presence of zinc chloride and acetic anhydride under microwave irradiation, giving a mixture of compounds **23** and **24**, with different *N*-acetylation levels. Although both compounds were purified for their biological evaluation, for synthetic purposes their mixture was hydrolysed in the presence of an hydroalcoholic solution of KOH under microwave irradiation to give the target compound **25**. **(Scheme 5.4)**

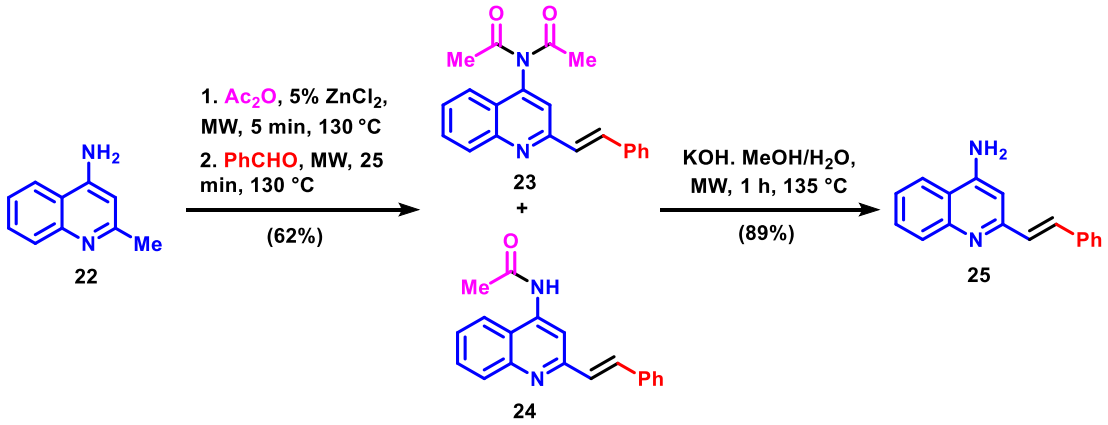

Scheme 5.4

5.4. Activity and mechanistic studies of 4-aminostyrylquinolines

5.4.1 Computational drug-likeness study

First, preliminary ADME-tox computational studies of the synthesized compounds were carried out using SwissADME. For all the compounds, a high gastrointestinal absorption, important for oral bioavailability, was predicted. Moreover, only compound **19l** showed violations Lipinski's rule of five. The details of this study are shown **Table 5.2.**

Cmpd. number	Rotable bonds	TPSA[141]	Log P $_{o/w}$[142]	Log S[143]	GI absorp.[144]	Lipinski violations[145]	PAINS alerts[146]
16a	9	63.25	4.39	-5.33	High	0	0
16b	11	63.25	4.89	-5.80	High	0	0
17a	5	50.94	3.26	-4.07	High	0	0
17b	7	50.94	3.88	-4.52	High	0	0
19a	9	57.26	3.24	-4.42	High	0	0
19b	11	57.26	3.84	-4.90	High	0	0
19c	9	57.26	3.70	-4.86	High	0	0
19d	9	57.26	3.91	-5.17	High	0	0
19e	9	66.49	3.08	-4.41	High	0	0
19f	9	60.50	3.03	-4.59	High	0	0
19g	10	60.50	4.17	-6.10	High	0	0
19h	11	57.26	4.28	-5.33	High	0	0
20a	10	63.25	3.54	-4.48	High	0	0
20b	12	63.25	4.18	-4.94	High	0	0
19i	10	66.05	4.26	-5.77	High	0	0
19j	12	66.05	4.92	-6.24	High	0	0
19k	10	66.05	5.35	-6.96	High	0	0
19l	12	66.05	6.00	-7.43	High	2	0
22	0	38.91	1.93	-2.80	High	0	0
23	5	50.27	3.56	-4.33	High	0	0
24	4	41.99	3.55	-4.21	High	0	0
25	2	38.91	3.41	-4.26	High	0	0
26	2	12.89	3.99	-4.66	High	0	0

Table 5.2: Computational drug-likeness study

5.4.2 Antileishmial activities

The biological studies were carried out in the group of Dr. Luis Rivas, at the Centro de Investigaciones Biológicas, CSIC, Madrid. First the activity of the compounds was tested against *Leishmania donovani* promastigotes (strain MHOM/SD/00/1S-2D) in a phenotypic screening. Promastigotes were chosen due to the fact that at this stage of the parasite cycle about 70 % of the ATP synthesis is accomplished through the

[141] Topological Polar Surface Area calculated from Etrl, P.; Rohde, B.; Selzer, P. *J. Med. Chem.* **2000**, *43*, 3714.
[142] Consensus Log P o/w average of 5 prediction methods.
[143] Lipinski, C. A.; Lombardo, F.; Dominy, B. W.; Feeney, P. J. *Adv. Drug Deliv. Rev.* **2001**, *46*, 3.
[144] ESOL topological method implemented from Delaney, J. S. Prediction of aqueous solubility and partition coefficient optimized by a genetic algorithm-based descriptor selection method. *J. Chem. Inf. Model.* **2004**, *44*, 1000.
[145] Saina, A.; Zoete, V. A *Chem. Med. Chem.* **2016**, *11*, 1117.
[146] Baell, J.B.; Holloway G. A. *J. Med. Chem.* **2010**, *53*, 2719.

mitochondria, and thus the study of promastigotes facilitate the identification of drugs targeting mithochondria. [126,128]

All compounds, with the exception of control **26**, inhibited the proliferation of the parasites, showing IC_{50} values in between 0.2-35.1 μM (Table 6.3). It is worth highlighting that most of our compounds present better inhibition values than the positive control miltefosine. The 2-styrylquinoline **26**, lacking the amino group at its C-4 position, was inactive (IC_{50} > 50 mM) compared to compounds **22** and **25**, verifying that this structural fragment is critical for the activity. Moreover, the lower activity of compound **22** compared to **25** proved the importance of the styryl fragment.

With these good results on our hands, the activity of our compounds against *Leishmania pifanoi* axenic amastigotes (strain MHOM-ET-67/L82) was tested **(Table 5.3)**. This model was chosen because of the extensive documentation that confirms the similarity between this axenic line and the amastigotes obtained from lesions in leishmaniasis patients.[147] Most compounds exhibited a good inhibition of amastigote proliferation, and some of them (**19b** and **19c**) showed submicromolar IC_{50} values, being only slightly less potent than miltefosine. The fact that our compounds possess similar or even higher activities against amastigotes than against promastigotes is important because both stages present remarkable differences in terms of biochemical and mitochondrial bioenergetics, and many drugs active against promastigotes tend to fail in amastigotes.[148] Finally, the mammalian cell toxicity of the compounds was evaluated on machophages, the host cells of amastigotes. For that purpose, the tumoral murine macrophage cell line J774, a model extensively used to test drug activity on intracellular amastigotes, was employed,[149] and the IC_{50} values obtained were used to calculate a selectivity index (SI). As shown in **Table 5.3**, many compounds show macrophage toxicity at leishmanicidal concentrations, with selectivity indexes below 10. However, compounds **19a**, **19c**, **19k** and **20a** present potent antileishmanial activities with acceptable or good SI values.

[147] An, A.A.; Duboise, S.M.; Eperon, S.; Rivas, L.; Hodgkinson, V.; Traub-Cseko, Y.; McMahon-Pratt, D.; J. *Eukaryot. Microbiol.* **1993*,*** *40,* 213.

[148] Peters, W.; Trotter, E.R.; Robinson, B.L.; *Ann. Trop. Med. Parasitol.* **1980***, 74,* 321.

[149] Yardley, V.; Koniordou, M. Drug assay methodology in leishmaniasis: from the microplate to image analysis, in: L. Rivas, C. Gil (Eds.), Drug Discovery for Leishmaniasis, **RSC Drug Discovery Series**, **2018**, pp. 57e76 (Chapter 4).

Regarding SAR conclusions, it is worth nothing that the two-carbon spacer always led to better results than the 4 carbon one. Moreover, while several compounds exhibit micromolar activities against amastigotes with good SI, the best one was compound **19k**. The fact that this compound presents the least basic side chain, but still carries the 4-amino substituent, suggests that while the protonation of the quinoline moiety is crucial for activity, the side chain does not need the presence of a high basic residue.

Cmpd.	*L. donovani* promastigotes, IC_{50} (μM) [a]	*L. pifanoi* amastigotes, IC_{50} (μM) [a]	J774, IC_{50} (μM) [a]	SI [b]
16a	0.45 ±0. 32	4.3 ± 1.2	6.6 ± 1.8	4.7
16b	0.56 ±0.12	4.9 ±0.8	3.7 ± 0.5	0.8
17a	2.4 ±0.3	>50	4.6 ± 0.2	<0.1
17b	0.44 ± 0.1	> 25	6.6 ± 0.6	<0.3
19a	1.6 ± 0.0	1.1 ± 0.1	15.0 ±2.7	13.6
19b	1.6 ± 0.0	0.9 ± 0.1	0.7 ± 0.1	0.8
19c	2.1 ± 0.2	0.9 ± 0.1	12.5 ±3.5	13.9
19d	2.1± 0.2	1.2 ± 0.1	4.7 ± 1.0	3.4
19e	1.3 ± 0.1	> 25	> 50	2.0
19f	3.5 ± 0.3	3.5 ± 0.3	34 ± 1.2	9.7
19g	2.1 ± 0.1	1.5 ± 0.2	4.5 ± 0.2	3.0
19h	0.2 ± 0.0	5.3 ± 0.8	7.1 ±1.0	1.4
19i	3.3 ± 0.8	4.3 ± 2.4	7.8 ± 1.2	1.8
19j	1.6 ±0.4	6.9 ± 1.5	3.3 ± 0.8	0.48
19k	8.4 ± 2.4	1.2 ± 0.8	>50	> 41.6
19l	2.1 ± 0.2	12.3 ± 3.2	7.3 ± 1.2	0.6
20a	3.4 ± 0.2	1.6 ± 0.4	22.2 ± 4.6	13.8
20b	1.06 ± 0.11	4.5 ± 1.2	7.2 ± 0.9	1.6
22	10.9 ± 2.2	> 50	> 50	-
23	35.1 ± 4.6	13.4 ±3.8	>25	>1.86
24	ND.	9.5 ±2.2	>25	>2.6
25	0.5 ±0.1	8.9 ±2.0	4.4 ± 0.2	0.5
26	>50	> 50	> 50	ND
miltefosine	4.4 ± 0.7	6.2 ± 1.6	> 50	> 8.1

Table 5.3: [a] All results are representative of two experiments performed independently.

[b] SI = IC_{50}(J774)/IC_{50} (*L. pifanoi* amastigotes).

The next step was to evaluate the leishmanicidal activity of one selected compound against macrophage cells infected with *L. pifanoi* amastigotes. Several compounds had exhibited similar activities and were suitable for the studies, but compound **20a** was selected due to its better synthetic accessibility. To this end, parasites were fluorescently labelled with carboxyfluorescein succinimidyl ester (CFSE) before the infection to facilitate their visualization inside the macrophages. As expected, treatment with compound **20a** at 10 μM concentration decreased the infection index (number of parasites/macrophage) from 5.3 ± 2.5 in untreated macrophages to 1.6 ± 0.8**. (Figure 5.5)**

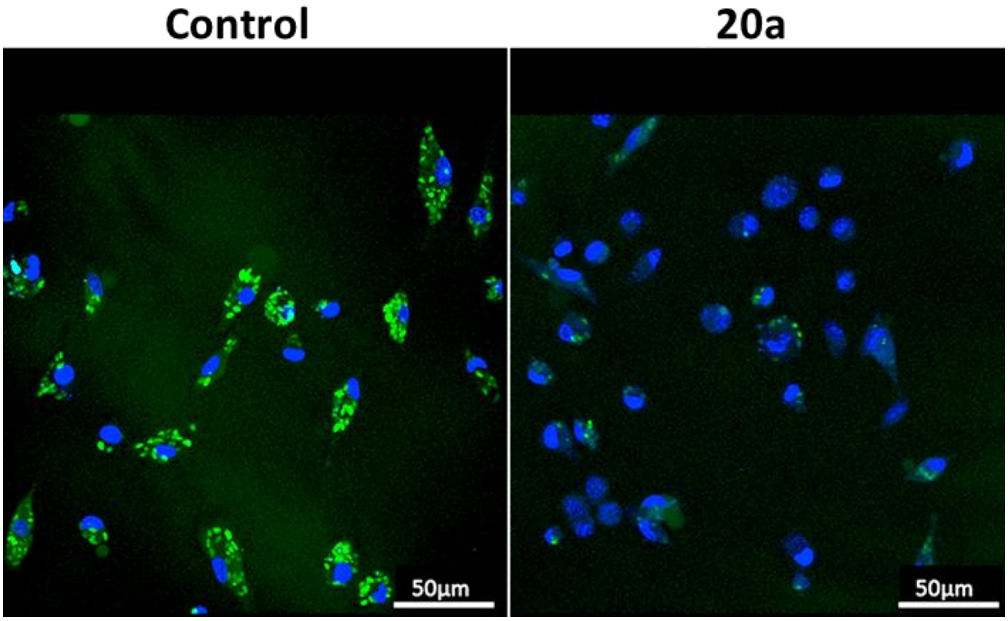

Figure 6.5: Peritoneal infected macrophages with *L. pifanoi* amastigotes were observed under a confocal microscope, after 12h incubation with 20a. Amastigotes were preloaded with CFSE (carboxyfluorescein succinimidyl ester) (green) and cell nuclei were stained with DAPI (blue). 20a reduced the infection index (number of parasites/ macrophage)

5.4.3 Mechanistic studies

In order to corroborate the mechanism of action of our compounds, some of them were selected and further experiments were carried on. First, to study whether our compounds were affecting the mitochondrion ATP synthesis of Leishmania variations in intracellular levels were monitored using *L. donovani* promastigotes from the 3-Luc

strain.[150] This strain expresses a cytoplasmic form of firefly luciferase, which upon addition of a lipophilic luciferin ester in excess that can cross the parasite's membrane, generates *in vivo* luminescence. In this reaction the free cytoplasmic ATP is the limiting substrate, this way the ATP levels can be indirectly measured. At 50 μM concentration, all studied compounds showed a fast and concentration-dependent drop in free cytoplasmatic ATP levels. **(Table 5.4)** For instance, the behaviour of compound **20a** is shown in **Figure 5.6**, which showed a threshold of 3.12 μM and reached the inhibition endpoint in less than 5 min after compound addition.

Styrylquinoline	Luminescence (% respect to control parasites)
19a	62.7±2.3
19b	43.2±2.5
19c	49.9±5.7
19d	46.4±1.4
19e	79.8±0.0
19f	78.5±2.0
19h	23.3±0.7
20a	16.7±0.1

Table 5.4: Percentage of luminescence relative to untreated 3-Luc *L. donovani* promastigotes after 10 min incubation with 50 μM of the respective styrylquinoline. Results were expressed as mean of triplicate ± SD.

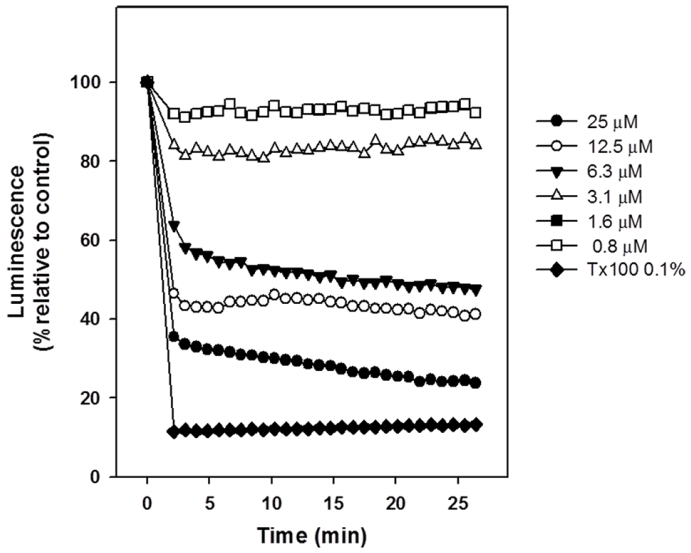

Figure 5.6. Real time variation of luminescence of living 3-Luc *L. donovani* promastigotes caused by styrylquinoline 20a.

[150] Luque-Ortega, J.R.; Rivero-Lezcano, O.M.; Croft, S.L.; Rivas L. *Antimicrob. Agents Chemother.* **2001**, *45,* 1121.

This dramatic drop in ATP levels can be attributed to permeabilization of the cell membrane or to mitochondrial dysfunction. To check which of these two possible mechanisms was responsible for this ATP drop, further experiments were done. First the ability of the compounds to induce plasma membrane permeabilization was tested. To this end, cells were treated with the corresponding styrylquinolines and then the entry of the vital dye SYTOX Green, included in the incubation medium, was monitored by examining the increase in, fluorescence due to its binding to intracellular nucleic acids. As a positive control, fully permeabilized cells were obtained by addition of 0.1% Triton X-100. It was concluded that none of the compounds was able to alter the membrane permeability. **(Figure 5.7)**

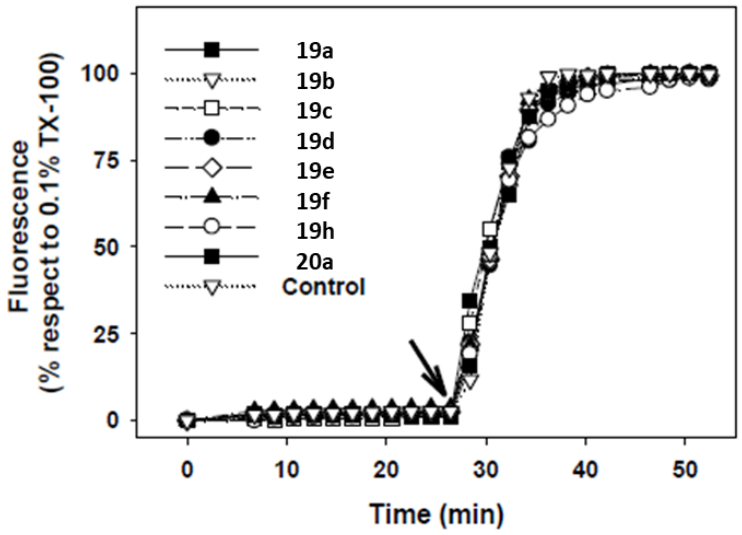

Figure 5.7: Plasma membrane permeabilization of *L. donovani* promastigotes by styrylquinolines

.

As membrane permeabilization was discarded, the ability of compounds to produce loss of mitochondrial functionality was tested. To this end, after addition of the selected compounds, variations in the mitochondrial electrochemical potential ($\Delta\psi_m$), essential for ATP synthesis, were monitored. Under physiological conditions rhodamine 123 is accumulated in mitochondrion driven by $\Delta\psi_m$, and can be measured by flow cytometry. Compounds **19d**, **19h**, and **20a** showed the highest inhibition and were selected for a concentration dependency study. The selected styrylquinolines markedly decreased rhodamine 123 levels at a 25 μM concentration, corresponding to the decrease induced by KCN 20mM, employed as a control for full mitochondrial depolarization. **(Figure 5.8)**

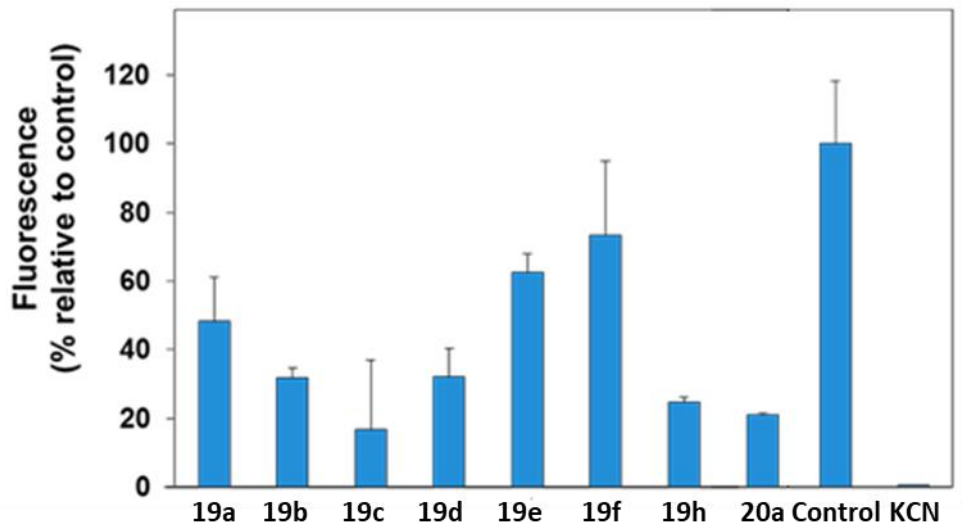

Figure 5.8. Variation of the intracellular accumulation of rhodamine 123 in *L. donovani* promastigotes induced by selected styrylquinolines.

In the light of these results, we assume that exposure to our compounds induces mitochondrial dysfunction. To further corroborate this hypothesis, the localization of compound **20a** inside Leishmania was determined on axenic amastigotes by confocal microscopy. First, at 20 mM, compound **20a** appeared as a punctuated fluorescence pattern. **(Figure 5.9, panel A)** Upon addition of 1mM KCN, concentration able to depolarize mitochondrion while preserving parasite viability, fluorescence was considerably inhibited. This experiment verified the importance of the $\Delta\psi_m$ in the compound accumulation. Furthermore, a double-labelling experiment was performed. Compound **20a** and MitoTracker Red (MTR), a mitochondrial probe, were incubated together, showing a high degree of overlapping. **(Figure 5.9, panel B)**

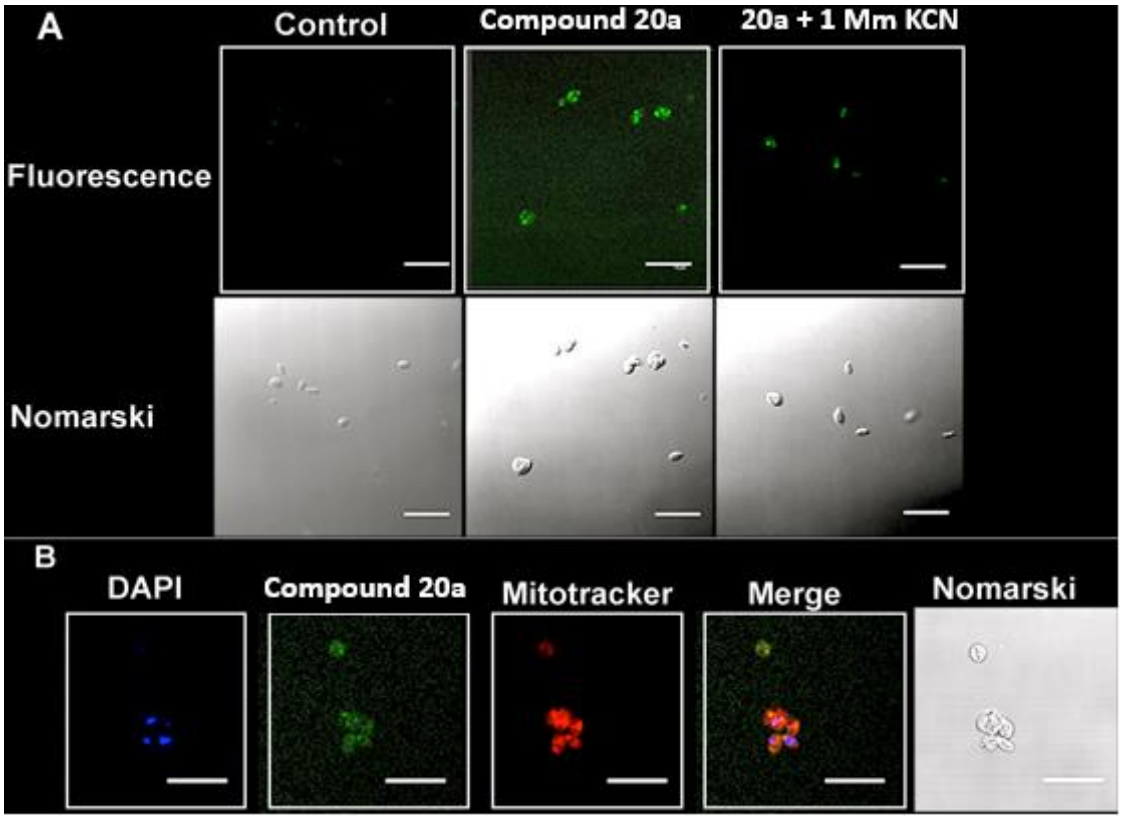

Figure 5.9. Confocal microscopy of L. pifanoi axenic amastigotes incubated with compound 20a.

Due to the key role that mitochondria play in apoptosis,[151] the possibility that the *Leishmania* toxicity involved programmed cell death processes was also explored. Cells at the late stage of apoptosis, characterized by a fragmented chromatin, can be identified by a lower degree of staining with propidium iodide (subG1 population). The experiments summarized in **Figure 5.10**, which used miltefosine (HePc) as a control, discard this possibility.

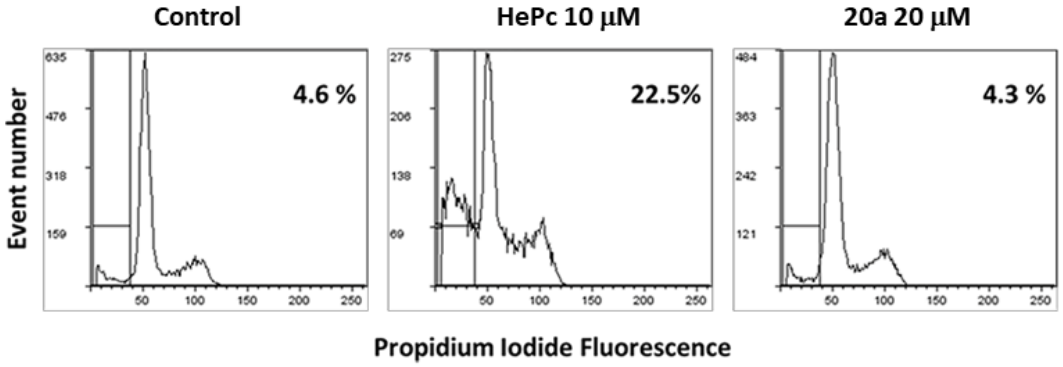

Figure 5.10. Induction of subG$_1$ population in *L. donovani* promastigotes by compound 20a.

[151]Wang, C.; Youle, R. J. *Annu. Rev. Genet*. **2009**, *43*, 95.

Finally, morphological studies of the treated *L. donovani* promastigotes were assessed by transmission electron microscopy. Parasites treated with compound **20a** showed a swollen mitochondrion, strong vacuolization of the cytoplasm and the appearance of expanded acidocalcisomes. **(Figure 5.11)**

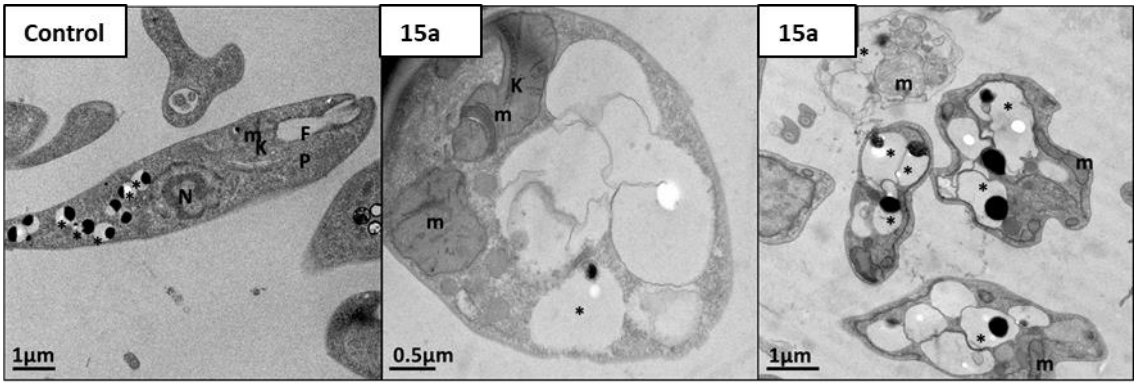

Figure 5.11. Transmission electron microscopy of *L. donovani* promastigotes treated with 20a (5 mM). Legend: (K) kinetoplast, (M) mitochondrion, (N) nucleus, (FP) flagellar pocket, (*) acidocalcisome.

To summarize, all these results suggested that the 4-aminostyrylquinoline derivatives owe their leishmanicidal activity to an alteration of the mitochondrial activity of the parasite, which leads to ATP depletion and bioenergetic collapse.

5.5. Experimental section

General experimental details

All reagents (Aldrich, Fischer, Alpha Aesar, SDS) and solvents (Scharlau, Fischer, SDS) were of commercial quality and were used as received. Reactions under microwave irradiation were carried out in a CEM Discover SP microwave reactor. Reactions were monitored by thin layer chromatography on aluminium plates coated with silica gel and fluorescent indicator (Macherey-Nagel Xtra SIL G/UV254). Separations by flash chromatography were performed on silica gel (Scharlau 40–60 µm, 230–400 mesh ASTM) or neutral alumina (Merck S22). Melting points were determined using a Stuart Scientific apparatus, SMP3 Model, and are uncorrected. Infrared spectra were recorded with an Agilent Cary630 FTIR spectrophotometer with a diamond accessory for solid and liquid samples. NMR spectroscopic data were recorded using a Bruker Avance 250 spectrometer operating at 250 MHz for 1H NMR and 63 MHz for 13C NMR, maintained by the NMR facility of Universidad Complutense (CAI de Resonancia Magnética Nuclear); chemical shifts are given in ppm and coupling constants in Hertz. High-resolution mass spectra (HRMS) were recorded on a mass spectrometer fitted with an electrospray detector (ESI) by the mass spectral facility of Universidad Complutense (CAI de Espectrometría de Masas) and elemental analyses were determined by the microanalysis facility of Universidad Complutense (CAI de Microanálisis Elemental), using a Leco 932 combustion microanalyzer.

5.5.1. Preparation of (E)-4-Amino-2-styrylquinolines

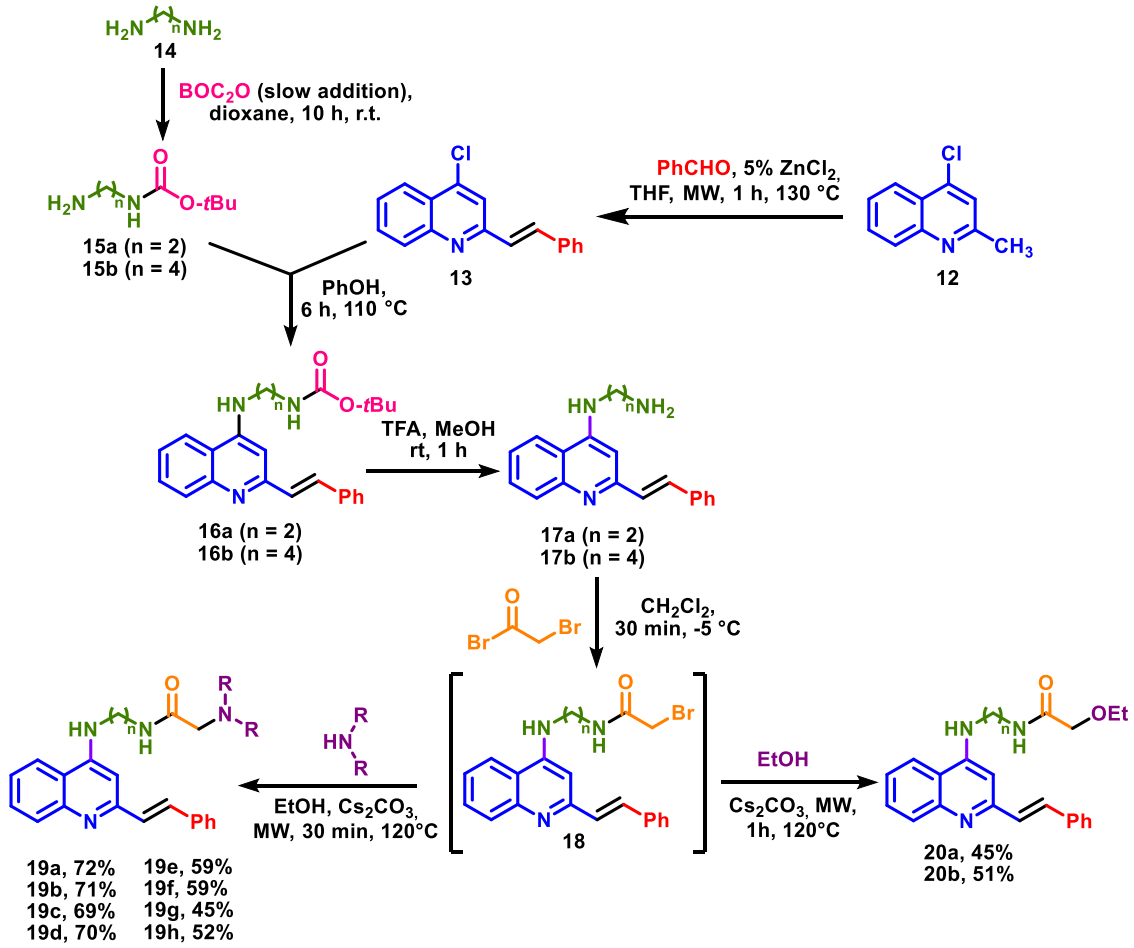

5.5.2. Synthesis of (E)-4-Chloro-2-styrylquinoline (13)

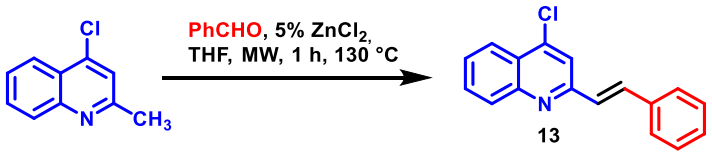

4-Chloroquinaldine (1.500 g, 8.44 mmol), benzaldehyde (1.343 g, 12.66 mmol) and $ZnCl_2$ (0.057 g, 0.422 mmol) were suspended in THF (3 ml) in a pressure tight microwave tube containing a stirring bar. The reaction mixture was heated under microwave irradiation for 1 hour at 130 ºC, with an irradiation power of 250 W. The reaction mixture was extracted with CH_2Cl_2, dried with anhydrous Na_2SO_4 and evaporated *in vacuo*. The dark residue was purified by flash chromatography through a silica gel column eluting with

hexane: ethyl acetate (98:2, v/v) as the mobile phase to give compound **13** as a yellow solid. Yield: 1.188 g, 53%.

Mp 113- 115 °C.

IR (neat) 3048, 2100, 1573, 1488, 968, 752, 695 cm^{-1}.

^{1}H NMR (250 MHz, $CDCl_3$): δ 8.21 (dd, *J*= 8.4, 1.3 Hz, 1H), 8.11 (dd, *J*= 8.4, 1.3 Hz, 1H), 7.82 – 7.57 (m, 6H), 7.49 – 7.28 (m, 4H) ppm.

^{13}C NMR (63 MHz, $CDCl_3$): δ 156.0, 149.1, 142.8, 136.2, 135.4, 130.8, 129.6, 129.1, 128.9 (2C), 128.0, 127.5 (2C), 127.2, 125.5, 124.1, 119.4 ppm. These spectral data were identical to those found in the literature.[152]

5.5.3. Synthesis of monoprotected diamines (15a-b)

A solution of di-tert-butyl dicarbonate (14 mmol, 1 eq) in 1,4-dioxane (50 ml) was slowly added (4 h), using a syringe pump, to the suitable diamine (56 mmol, 4 eq.) dissolved in 1,4-dioxane (30 ml). The reaction mixture was stirred at room temperature overnight, the solvent was evaporated under vacuum and water (20 ml) was added. The precipitate obtained was filtered to eliminate the diprotected amine and the aqueous phase was extracted with dichlorometane (3 x 20 ml), dried with anhydrous Na2SO4 and evaporated in vacuo, to give the desired products.

tert-Butyl _N_-(2-aminoethyl)carbamate (15a)

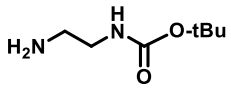

Prepared from 1,2-diaminoethane (3.365 g, 56 mmol) and di-tert-butyl dicarbonate (3.055 g, 14 mmol); whitish oil. Yield: 1.288 g, 57%.

IR (neat) 3354, 2973, 2484, 2114, 1683, 1518, 1247, 1163 cm^{-1}.

^{1}H NMR (250 MHz, *d_4*-methanol): δ 3.11 (t, *J* = 6.2 Hz, 2H), 2.69 (t, *J* = 6.2 Hz, 2H), 1.44 (s, 9H) ppm.

^{13}C NMR (63 MHz, *d4-methano*): δ 158.5, 79.9, 43.7, 42.3, 28.8 (3C) ppm. These data are in good agreement with the literature.[153]

[152] Gong, L.; Xing, L.-J.; Xu, T.; Zhu, X.-P.; Zhou, W.; Kang, N.; Wang, B. *Org. Biomol. Chem.* **2014**, *12*, 6557.
[153] Holland, J. P.; Fisher, V.; Hickin, J. A.; Peach, J. M. *Eur. J. Inorg. Chem*. **2010**, 48.

***tert*-Butyl *N*-(4-aminobutyl)carbamate (15b)**

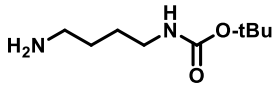

Prepared from 1,4-diaminobutane (4.936 g, 56 mmol) and di-tert-butyl dicarbonate (3.055 g, 14 mmol); whitish oil, Yield: 1.950 g, 74 %.

IR (neat) 3363, 2930, 2864, 2116, 1680, 1520, 1474, 1164 cm^{-1}.

^{1}H NMR (250 MHz, *d4-methano*): δ 3.06 (d, *J* = 6.4 Hz, 2H), 2.69 (m, 2H), 1.57 – 1.46 (m, 4H), 1.43 (s, 9H) ppm.

^{13}C NMR (63 MHz, *d4-methano*): δ 158.5 79.8, 41.8, 41.0, 30.0, 28.8 (3C), 28.2 ppm. These data are in good agreement with the literature.[154]

5.5.4. General procedure for the synthesis of protected polyamino styrylquinolines (16a-b)

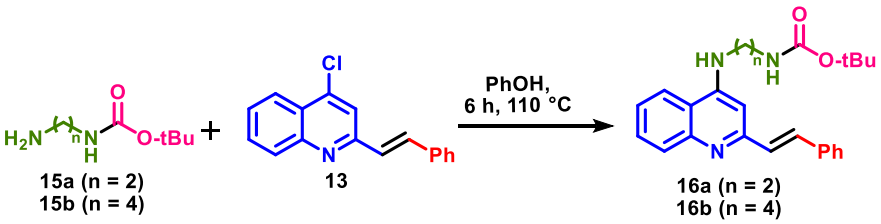

(E)-4-Chloro-2-styrylquinoline **13** (1 eq), the corresponding monoprotected diamine **15** (1.5 eq) and phenol (6 eq) were placed in a round bottom flask and stirred at 110 °C for 6 h. The reaction mixture was basified with an aqueous solution of NaOH (5M) and extracted with ethyl acetate (3 × 10 ml). The combined organic phases were dried with anhydrous Na_2SO_4 and evaporated. The resulting crude was purified by flash chromatography through a silica gel column eluting with hexane: ethyl acetate (2:1, v/v) as the mobile phase to give the desired products.

***tert*-Butyl (*E*)-(2-((2-styrylquinolin-4-yl)amino)ethyl) carbamate (16a).**

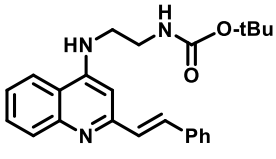

Prepared from *(E)*-4-chloro-2-styrylquinoline **13** (0.654 g, 2.46 mmol), *tert*-butyl (2-aminoethyl)carbamate **15a** (0.591 g, 3.69 mmol) and phenol (2.1 g, 22.3 mmol); brown solid. Yield: 0.678 g, 71%.

Mp 71-73 °C.

[154] Vonlanthen, M.; Finney, N. S. *J. Org. Chem*. **2013**, *78*, 3980.

IR (neat) 3346, 2925, 1682, 1585, 1534, 1161 cm^{-1}.

^{1}H NMR (250 MHz, *d4-methano*): δ 8.00 (d, *J* = 8.3 Hz, 1H), 7.82 (d, *J* = 8.3 Hz, 1H), 7.77 – 7.59 (m, 4H), 7.44 – 7.32 (m, 4H), 7.25 (d, *J* = 16.5 Hz, 1H), 7.03 (s, 1H), 3.53 (t, *J* = 5.8 Hz, 2H), 3.42 (t, *J* = 5.8 Hz, 2H), 1.44 (s, 9H) ppm.

^{13}C NMR (63 MHz, *d4-methano*): δ 159.6, 157.6, 153.6, 148.3, 138.3, 136.7, 131.6, 130.3 (3 C), 129.0, 128.7 (2 C), 128.1, 126.1, 122.6, 119.9, 96.6, 80.7, 45.1, 40.4, 29.2 (3C) ppm.

Elemental analysis (%): calcd. for $C_{24}H_{27}N_3O_2$: C 74.01, H 6.99, N 10.79; found: C 73.85, H 6.84, N 10.46.

***tert*-Butyl (*E*)-(4-((2-styrylquinolin-4-yl)amino)butyl) carbamate (16b).**

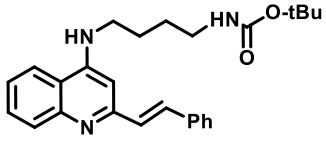

Prepared from *(E)*-4-chloro-2-styrylquinoline **13**(0.6 g, 2.25 mmol), *tert*-butyl (4-aminobutyl) carbamate **15b** (0.637 g, 3.38 mmol) and phenol (1.91 g, 20.3 mmol); orange solid. Yield: 0.627 g, 74%.

Mp 93- 95 °C.

IR (neat) 3338, 2923, 1681, 1586, 1535, 1162 cm^{-1}.

^{1}H NMR (250 MHz, d_4-methanol): δ 8.07 (d, *J* = 8.4 Hz, 1H), 7.84 (d, *J* = 8.4 Hz, 1H), 7.69 – 7.57 (m, 4H), 7.45 – 7.24 (m, 5H), 6.84 (s, 1H), 3.48 (t, *J* = 6.7 Hz, 2H), 3.14 (t, *J* = 6.7 Hz, 2H), 1.87 – 1.74 (m, 2H), 1.72 – 1.59 (m, 2H), 1.41 (s, 9H)ppm.

^{13}C NMR (63 MHz, d_4-methanol): δ 159.1, 158.2, 153.1, 149.6, 138.5, 135.5, 131.1, 130.3, 130.3 (2 C), 130.0, 129.0, 128.6 (2C), 125.7, 122.5, 120.2, 96.9, 80.3, 44.1, 41.5, 29.2 (3C), 27.2(2C) ppm.

Elemental analysis (%): calcd. for $C_{26}H_{31}N_3O_2$: C 74.79, H 7.48, N 10.06; found: C 74.54, H 7.51, N 9.70.

5.5.5. General procedure for the synthesis of polyamino styrylquinolines (17a-b)

The suitable styrylquinoline **16** was dissolved in a mixture of methanol: trifluoroacetic acid (2:1, v/v) and stirred at room temperature for 1h. Once the reaction was finished, the reaction mixture was basified with aqueous NaOH (5 M) and extracted with a mixture of CH_2Cl_2: MeOH (10:1, v/v), which was dried with anhydrous Na_2SO_4 and evaporated *in vacuo* to give the pure product.

(*E*)-*N*^{1}-(2-Styrylquinolin-4-yl)ethane-1,2-diamine (17a).

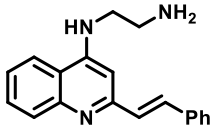

Prepared from compound **16a** (0.578 g, 1.49 mmol); yellow solid. Yield: 0.374 g, 87%.

Mp 85- 86 °C.

IR (neat) 3250, 2921, 1583, 1531, 753 cm^{-1}.

^{1}H NMR (250 MHz *d*$_4$-methanol): δ 8.06 (d, *J* = 8.3 Hz, 1H), 7.84 (d, *J* = 8.3 Hz, 1H), 7.68 – 7.55 (m, 4H), 7.43 – 7.22 (m, 5H), 6.87 (s, 1H), 3.51 (t, *J* = 6.3 Hz, 2H), 3.01 (t, *J* = 6.3 Hz, 2H) ppm.

^{13}C NMR (63 MHz, *d*$_4$-methanol): δ 158.2, 153.1, 149.5, 138.5, 135.6, 131.2, 130.3 (3 C), 130.1, 129.1, 128.6 (2 C), 125.9, 122.5, 120.3, 96.9, 46.7, 41.5 ppm.

Elemental analysis (%): calcd. for $C_{19}H_{19}N_3$: C 78.86, H 6.62, N 14.52; found: C 78.56, H 6.72, N 14.32.

(*E*)-*N*^{1}-(2-Styrylquinolin-4-yl)butane-1,4-diamine (17b).

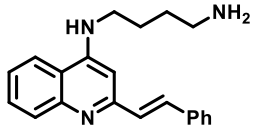

Prepared from compound **16b** (0.150 g, 0.359 mmol); yellow solid. Yield: 0.100 g, 88%.

Mp 68-69 °C.

IR (neat) 3261, 2918, 2850, 1580, 1531, 752 cm^{-1}.

^{1}H NMR (250 MHz, *d*$_4$-methanol): δ 8.05 (d, *J* = 8.3 Hz, 1H), 7.83 (d, *J* = 8.3 Hz, 1H), 7.68 – 7.53 (m, 4H), 7.44 – 7.22 (m, 5H), 6.78 (s, 1H), 3.41 (t, *J* = 6.7 Hz, 2H), 2.70 (t, *J* = 6.7 Hz, 2H), 1.78 (dd, *J* = 13.8, 6.9 Hz, 2H), 1.64 (dd, *J* = 13.8, 6.9 Hz, 2H) ppm.

^{13}C NMR (63 MHz, *d*$_4$-methanol): δ 158.2, 153.1, 149.6, 138.5, 135.5, 131.1, 130.4, 130.3 (2 C), 130.0, 129.1, 128.6 (2C), 125.8, 122.5, 120.2, 96.9, 44.2, 42.6, 31.5, 27.4ppm.

Elemental analysis (%): calcd. for $C_{21}H_{23}N_3$: C 79.46, H 7.30, N 13.24; found: C, 79.12; H, 6.93; N, 13.13.

5.5.6. Synthesis of intermediates 18a and 18b.

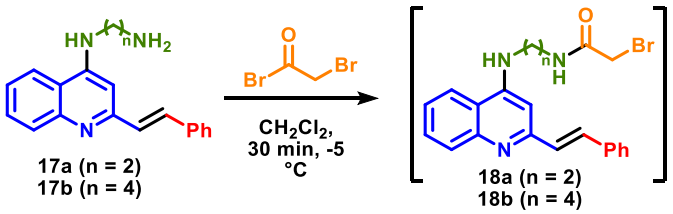

A solution of 2-bromoacetyl bromide (1 eq, 0.53 mmol) in CH_2Cl_2 (20 ml) was slowly added (30 min) using a syringe pump to a solution of compound **17a** or **17b** (1 eq) in dichlorometane (20 ml). Once the addition was finished, the reaction mixture was stirred at -5 °C for an additional 30 min period. Then, the resulting crude was basified with an aqueous solution of NaOH (1M) and extracted with a mixture of CH_2Cl_2: MeOH (10:1, v/v), dried with anhydrous Na_2SO_4 and evaporated *in vacuo,* to give the desired product, which was used in the next step without further purification.

5.5.7. General procedure for the synthesis of 4-aminostyrylquinolines (19a-l) and (20a-b)

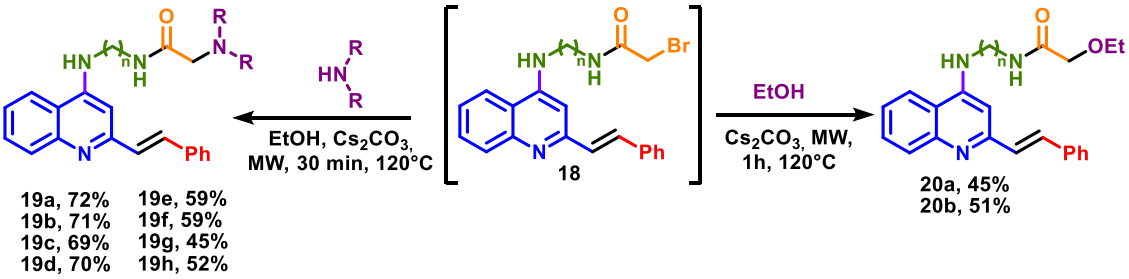

5.5.8. Aliphatic amine derivatives (19a-h)

Compound **18** (80 mg, 0.195 mmol), the suitable amine (1 eq) and Cs_2CO_3 (0.127 g, 0.39 mmol, 2 eq) were suspended in EtOH (1 ml) in a pressure-tight microwave tube containing a stirring bar. The mixture was heated under microwave irradiation for 30 minutes at 120 °C, with an irradiation power of 200 W, using a focused microwave reactor. Thereafter, the cooled reaction mixture was dissolved in CH_2Cl_2 and washed with water, which was re-extracted with CH_2Cl_2. The combined organic layers were dried with anhydrous Na_2SO_4 and evaporated *in vacuo.* The resulting crude products were subsequently crystallized from MeOH-hexane mixtures or purified *via* a neutral alumina column.

(*E*)-2-(Dimethylamino)-*N*-[2-(2-styrylquinolin-4-ylamino)ethyl]acetamide (19a)[110]

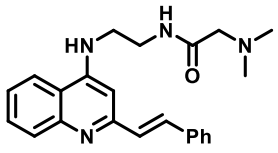

Prepared from **18a** (80 mg, 0.195 mmol) and dimethylamine (0.02 ml, 0.195 mmol); the compound was crystallized from a MeOH-hexane mixture to give **19a** as an orange powder. Yield: 0.052 g, 72%

IR (neat) 3346, 2923, 2850, 2780, 1660, 1588, 1365, 1044 cm^{-1}.

^{1}H NMR (250 MHz, $CDCl_3$): δ 7.99 (d, *J* = 8.4 Hz, 1H), 7.85 (d, *J* = 8.4 Hz, 1H), 7.76 (t, *J* = 6.7 Hz, 1H), 7.71 – 7.60 (m, 4H), 7.47-7.32 (m, 5H), 6.62 (s, 1H), 6.55 (br s, 1H), 3.86-3.75 (m, 2H), 3.60 – 3.47 (m, 2H), 3.03 (s, 2H), 2.30 (s, 6H) ppm.

^{13}C NMR (63 MHz, $CDCl_3$): δ 174.0, 156.7, 150.7, 137.3, 133.7, 133.5, 130.5, 129.8 (2C), 129.1 (2C), 128.7, 127.6 (2C), 125.0, 120.6, 118.7, 96.3, 63.3, 46.5 (2C), 46.2, 38.9 ppm.

Elemental analysis (%): calcd. for $C_{23}H_{26}N_4O$: C 73.77, H 7.00, N 14.96; found: C 73.61, H 7.16, N 14.40.

(*E*)-2-(Diethylamino)-*N*-[2-(2-styrylquinolin-4-ylamino)ethyl]acetamide (19b)[110]

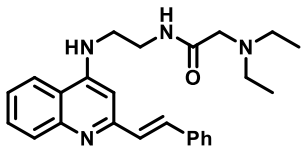

Prepared from **18a** (80 mg, 0.195 mmol) and diethylamine (14 mg, 0.195 mmol); the compound was crystallized from a MeOH-hexane mixture to give **19b** as an orange powder. Yield: 0.056 g, 71 %.

Mp 54- 57 °C.

IR (neat) 3341, 2959, 2905, 2850, 1658, 1588, 1430, 1367, 756 cm^{-1}.

^{1}H NMR (250 MHz, $CDCl_3$): δ 7.99 (d, *J* = 8.4 Hz, 1H), 7.86 (d, *J* = 7.6 Hz, 1H), 7.71-7.59 (m, 4H), 7.49 – 7.30 (m, 5H), 6.62 (s, 1H), 3.85 – 3.75 (m, 2H), 3.60 – 3.46 (m, 2H), 3.12 (s, 2H), 2.56 (q, *J* = 7.1 Hz, 4H), 1.04 – 0.93 (t, *J* = 7.1 Hz, 6H) ppm.

^{13}C NMR (63 MHz, $CDCl_3$): δ 175.6, 156.6, 150.8, 137.2, 133.6, 130.3, 130.3, 129.8, 129.6, 129.1 (2C), 128.7, 127.6 (2C), 125.1, 120.6, 118.7, 96.2, 57.8, 49.2 (2C), 46.2, 38.9, 12.7 (2C) ppm.

Elemental analysis (%): calcd. for $C_{25}H_{30}N_4O$: C 74.59, H 7.51, N 13.92; found: C 74.52, H 7.10, N 13.50.

(*E*)-2-(Pyrrolidin-1-yl)-*N*-(2-(2-styrylquinolin-4-ylamino)ethyl)acetamide (19c)

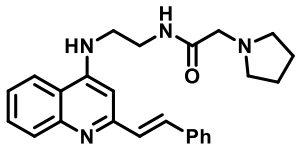

Prepared from **18a** (80 mg, 0.195 mmol) and pyrrolidine (14 mg, 0.195 mmol); the compound was crystallized from a MeOH-hexane mixture to give **19c** as a red solid. Yield: 0.054 g, 69 %.

Mp 68- 71 °C.

IR (neat) 3346, 2918, 2848, 2809, 1655, 1588, 1539, 1365 cm^{-1}.

^{1}H NMR (250 MHz, $CDCl_3$): δ 7.98 (d, *J* = 7.7 Hz, 1H), 7.85 (d, *J* = 8.1 Hz, 1H), 7.70 – 7.60 (m, 4H), 7.48-7.32 (m, 5H), 6.62 (s, 1H), 6.59 (br s, 1H), 3.85-3-78 (m, 2H), 3.60 – 3.46 (m, 2H), 3.26 (s, 2H), 2.67-2.53 (m, 4H), 1.85-1.75 (m, 4H) ppm.

^{13}C NMR (63 MHz, $CDCl_3$): δ 174.4, 156.7, 150.7, 148.9, 137.3, 133.5, 130.5, 129.8 (2C), 129.1 (2C), 128.7, 127.6 (2C), 125.0, 120.6, 118.7, 96.3, 59.4, 55.1 (2C), 46.2, 38.9, 24.4 (2C) ppm.

Elemental analysis (%): calcd. for $C_{25}H_{28}N_4O$: C 74.97, H 7.05, N 13.99; found: C 74.04, H 6.98, N 13.83.

(*E*)-2-(Piperidin-1-yl)-*N*-(2-(2-styrylquinolin-4-ylamino)ethyl)acetamide (19d)[110]

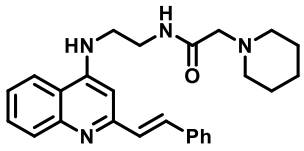

Prepared from **18a** (80 mg, 0.195 mmol) and piperidine (17 mg, 0.195 mmol); the compound was crystallized from a MeOH-hexane mixture to give **19d** as a yellow solid. Yield: 0.057 g, 70%.

Mp 71- 74°C.

IR (neat) 3348, 2936, 2851, 1659, 1563, 1538, 1366, 1129 cm^{-1}.

^{1}H NMR (250 MHz, $CDCl_3$): δ 8.10 (d, *J* = 8.2 Hz, 1H), 7.97 (d, *J* = 8.2 Hz, 1H), 7.8-7.72 (m, 4H), 7.6-7.4 (m, 5H), 6.74 (s, 1H), 3.99 – 3.84 (m, 2H), 3.72-3.58 (m, 2H), 3.14 (s, 2H), 2.62-2.48 (m, 4H), 1.70 – 1.67 (m, 4H), 1.57 – 1.55 (m, 2H) ppm.

^{13}C NMR (63 MHz, $CDCl_3$): δ 174.2, 156.6, 150.8, 137.2, 133.6, 130.3 (2C), 129.8, 129.7, 129.1 (2C), 128.7, 127.6 (2C), 125.1, 120.6, 118.7, 96.2, 62.6, 55.4 (2C), 46.2, 38.9, 26.6 (2C), 24.0 ppm.

Elemental analysis (%): calcd. for $C_{26}H_{30}N_4O$: C 75.33, H 7.29, N 13.52; found: C 75.66, H 7.05, N 13.70.

(*E*)-2-Morpholino-*N*-[2-(2-styrylquinolin-4-ylamino)ethyl]acetamide (19e)[110]

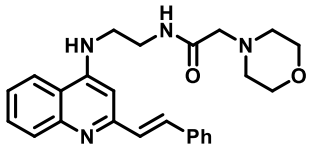

Prepared from **18a** (80 mg, 0.195 mmol) and morpholine (17 mg, 0.195 mmol); the compound was crystallized from a MeOH-hexane mixture to give **19e** as an orange powder. Yield: 0.048 g, 59%.

Mp 67- 70 °C.

IR (neat) 3297, 2918, 2850, 1656, 1599, 1560, 1538, 1464 cm^{-1}.

^{1}H NMR (250 MHz, $CDCl_3$): δ 8.03 (d, *J* = 8.0 Hz, 1H), 7.88 (d, *J* = 8.5 Hz, 1H), 7.79 (br s, 1H), 7.72 -7.57 (m, 4H), 7.48 – 7.31 (m, 5H), 6.59 (s, 1H), 3.88 3.77 (m, 2H), 3.77 – 3.65 (m, 4H), 3.62 – 3.45 (m, 2H), 3.10 (s, 2H), 2.60 – 2.49 (m, 4H)ppm.

^{13}C NMR (63 MHz, $CDCl_3$): δ 173.2, 153.1, 151.5, 147.6, 136.8, 131.4, 130.4, 129.6, 129.2 (2C), 129.1, 128,4, 127.8 (2C), 125.4, 120.9, 118.3, 95.8, 67.3 (2C), 62.2, 54.3 (2C), 45.9, 38.8ppm.

Elemental analysis (%): calcd. for $C_{25}H_{28}N_4O_2$: C 72.09, H 6.78, N 13.45; found: C 71.73, H 6.81, N 13.24.

(*E*)-2-(4-Methylpiperazin-1-yl)-*N*-[2-(2-styrylquinolin-4-ylamino)ethyl] acetamide (19f)[110]

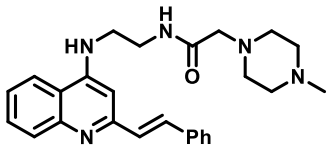

Prepared from **18a** (80 mg, 0.195 mmol) and 1-methylpiperazine (20 mg, 0.195 mmol); the compound was crystallized from a MeOH-hexane mixture to give **19f** as an orange powder. Yield: 0.049 g, 59 %.

Mp 64- 67 °C.

IR (neat) 3348, 2923, 2850, 1666, 1588, 1537, 1373, 756 cm^{-1}.

^{1}H NMR (250 MHz, $CDCl_3$): δ 7.99 (d, *J* = 8.5 Hz, 1H), 7.83 (d, *J* = 8.1 Hz, 1H), 7.61 – 7.50 (m, 4H), 7.38 – 7.20 (m, 5H), 6.52 (s, 1H), 6.05 (br s, 1H), 3.75 – 3.64 (m, 2H), 3.48 – 3.38 (m, 2H), 3.11 (s, 2H), 2.52 –.2.41 (m, 4H), 2.37 – 2.25 (m, 4H), 2.28 (s, 3H) ppm.

^{13}C NMR (63 MHz, $CDCl_3$): δ 173.5, 156.7, 150.7, 148.9, 137.2, 133.5, 130.4, 129.8 (2C), 129.3 (2C), 128.7, 127.6 (2C), 125.1, 120.5, 118.7, 96.3, 61.6, 55.5 (2C), 53.9 (2C), 46.4, 46.0, 38.9 ppm.

Elemental analysis (%): calcd. for $C_{26}H_{31}N_5O$: C 72.70, H 7.27, N 16.30; found: C 71.87, H 7.86, N 15.39.

(*E*)-2-(4-Phenylpiperazin-1-yl)-*N*-[2-(2-styrylquinolin-4-ylamino)ethyl]acetamide (19g)[110]

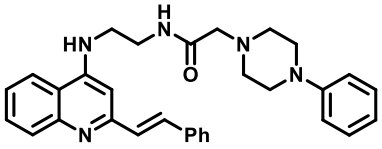

Prepared from **18a** (80 mg, 0.195 mmol) and 1-phenylpiperazine (32 mg, 0.195 mmol); the compound was purified by chromatography through a neutral alumina column using CH_2Cl_2-MeOH (95:5, v/v) as mobile phase to give **19g** as an orange solid. Yield: 0.043 g, 45 %.

Mp 92- 95 °C.

IR (neat) 3352, 2940, 2825, 1661, 1588, 1538, 1435, 969, 757 cm^{-1}.

^{1}H NMR (250 MHz, d_4-methanol) δ 8.04 (dd, *J* = 8.4, 0.8 Hz, 1H), 7.88 (dd, *J* = 8.4, 0.8 Hz, 1H), 7.76 – 7.61 (m, 4H), 7.47 – 7.31 (m, 5H), 7.23 – 7.15 (m, 2H), 7.03 (s, 1H), 6.86 – 6.78 (m, 3H), 3.68 (s, 2H), 3.35 – 3.31 (m, 4H), 3.03 – 2.97 (m, 4H), 2.59 – 2.52 (m, 4H) ppm.

^{13}C NMR (63 MHz, d_4-methanol): δ 174.2, 158.3, 153.2, 153.0, 149.6, 138.5, 135.9, 131.3, 130.4 (2C), 130.3 (2C), 130.2, 130.1, 129.2, 128.7 (2C), 126.0, 122.4, 121.5, 120.1, 117.9 (2C), 96.8, 62.7, 54.8 (2C), 50.9 (2C), 43.9, 39 ppm.

Elemental analysis (%): calcd. for $C_{31}H_{33}N_5O$: C 75.73, H 6.77, N 14.25; found: C 75.01, H 6.44, N 13.92.

(*E*)-2-(Pyrrolidin-1-yl)-*N*-[4-((2-styrylquinolin-4-yl)amino)butyl]acetamide (19h)

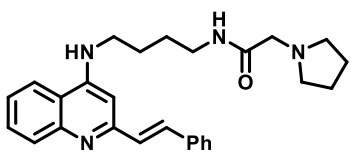

Prepared from **18b** (80 mg, 0.18 mmol) and pyrrolidine; the crude product was purified by flash chromatography through a silica gel column using hexane: ethyl acetate (3:7, v/v) as the mobile phase to give **19h** as a red solid. Yield: 0.04 g, 52%.

Mp 72-73 °C.

IR (neat) 3313, 2922, 2853, 1654, 1582, 1530, 965,754 cm^{-1}.

^{1}H NMR (250 MHz, *d_4*-methanol): δ 8.07 (d, *J* = 8.4 Hz, 1H), 7.85 (d, *J* = 8.4 Hz, 1H), 7.71 – 7.57 (m, 4H), 7.46 – 7.24 (m, 5H), 6.82 (s, 1H), 3.48 (t, *J* = 6.6 Hz, 2H), 3.39 – 3.29 (m, 2H), 3.12 (s, 2H), 2.54 (m, 4H), 1.90 – 1.64 (m, 8H) ppm.

^{13}C NMR (63 MHz, *d_4*-methanol) δ 173.2, 157.5, 152.7, 148.8, 138.0, 135.3, 130.8, 129.9 (2 C), 129.7, 128.4, 128.2 (2 C), 125.4, 122.1, 119.8, 96.5, 59.9, 55.2 (2C), 43.5, 39.7, 28.3, 26.7, 24.6 (2C) ppm.

Elemental analysis (%): calcd. for $C_{27}H_{32}N_4O$: C 75.67, H 7.53, N 13.07; found: C 74.91, H 7.79, N 12.77.

5.5.9. Ethoxy derivatives (20a-b)

The suitable halide **18** (1 eq) and Cs_2CO_3 (2 eq) were suspended in EtOH (1 ml) in a pressure-tight microwave tube containing a stirring bar. The mixture was heated under microwave irradiation for 30 minutes at 120 °C, with an irradiation power of 200 W, using a focused microwave reactor. Thereafter, the reaction mixture was dissolved in CH_2Cl_2 and washed with water. The combined organic layers were dried with anhydrous Na_2SO_4 and evaporated *in vacuo.* The crude product was directly purified by flash chromatography through a silica gel column using hexane: ethyl acetate (1:1, v/v) as the mobile phase to give the desired product.

(*E*)-2-Ethoxy-*N*-(2-((2-styrylquinolin-4-yl)amino)ethyl)acetamide (20a)

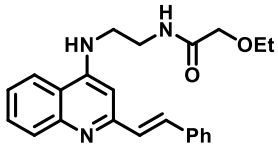

Prepared from **18a** (0.124 g, 0.3 mmol), and Cs_2CO_3 (0.195 g, 0.6 mmol, 2 eq); yellow solid. Yield: 0.051 g, 45 %

Mp 59- 61 °C.

IR (neat) 3329, 2865, 2108, 1654, 1583, 1528, 1111,753 cm^{-1}.

^{1}H NMR (250 MHz, *d_4*-methanol) δ 7.86 (dd, *J* = 8.4, 0.8 Hz, 1H), 7.73 (dd, *J* = 8.4, 0.8 Hz, 1H), 7.61 – 7.47 (m, 4H), 7.34 – 7.12 (m, 5H), 6.86 (s, 1H), 3.83 (s, 2H), 3.45 (m, 6H), 1.06 (t, *J* = 7.0 Hz, 3H) ppm.

^{13}C NMR (63 MHz, *d_4*-methanol) δ 173.9, 157.8, 152.6, 149.0, 138.0, 135.5, 130.8, 129.8 (2C), 129.7, 129.6, 129.6, 128.2 (2C), 125.5, 121.9, 119.7, 96.3, 70.7, 68.1, 43.28, 38.9, 15.3 ppm.

Elemental analysis (%): calcd for $C_{23}H_{25}N_3O_2$: C 73.57, H 6.71, N 11.19; found: C 73.16, H 6.84, N 10.95.

(*E*)-2-Ethoxy-*N*-(4-((2-styrylquinolin-4-yl)amino)butyl)acetamide (20b)

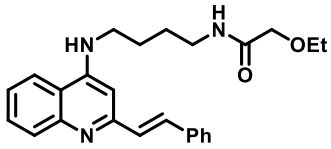

Prepared from **18b** (0.089 g, 0.2 mmol), and Cs_2CO_3 (0.132 g, 0.40 mmol, 2 eq); yellow solid. Yield: 0.044 g, 51%.

Mp 52- 54 °C.

IR (neat) 3313, 2925, 2358, 1662, 1585, 1535 cm^{-1}.

^{1}H NMR (250 MHz, d_4-methanol) δ 8.09 (dd, *J* = 8.4, 0.9 Hz, 1H), 7.86 (dd, *J* = 8.4, 0.9 Hz, 1H), 7.71 – 7.58 (m, 4H), 7.46 – 7.27 (m, 5H), 6.85 (s, 1H), 3.91 (s, 2H), 3.60 – 3.45 (m, 4H), 3.39 – 3.35 (m, 2H), 1.92 – 1.62 (m, 4H), 1.20 (t, *J* = 7.0 Hz, 3H) ppm.

^{13}C NMR (63 MHz, $CDCl_3$): δ $CDCl_3$) δ 170.6, 156.8, 150.4, 148.9, 137.2, 133.7, 130.3, 130.1, 129.7, 129.1 (2C), 128.7, 127.6 (2C), 124.8, 119.8, 118.7, 97.3, 70.3, 67.5, 43.5, 38.7, 28.2, 26.3, 15.5 ppm.

Elemental analysis (%): calcd for $C_{25}H_{29}N_3O_2$: C 74.41, H 7.24, N 10.41; found: C 73.98, H 7.05, N 10.06.

5.5.10. General procedure for the synthesis of glycine derivatives (21a-b)

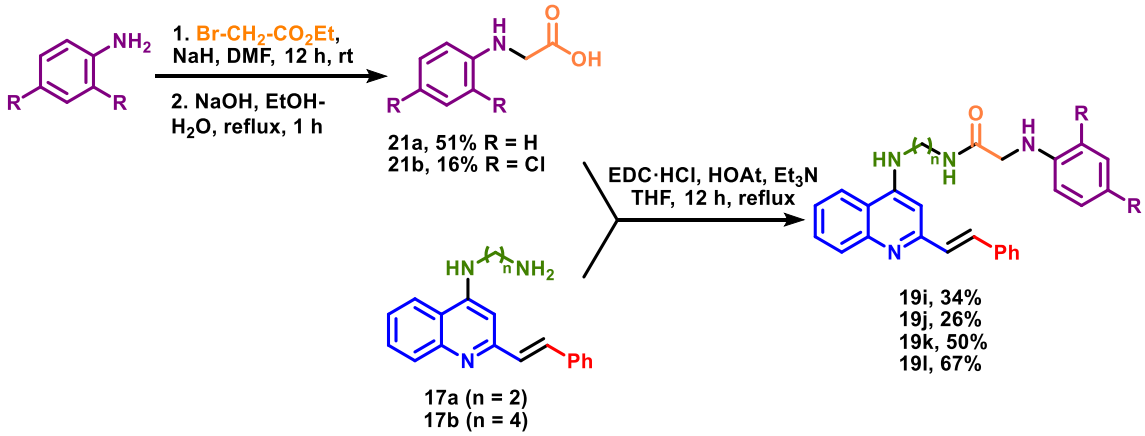

The suitable aniline (1 eq, 20 mmol) and ethyl 2-bromoacetate (1 eq) were dissolved in dry DMF (100 ml) under argon atmosphere. To this mixture was added NaH (1 eq) portionwise and the reaction was stirred at room temperature for 18 h. Upon completion of the reaction, the solvent was removed under reduced pressure and the

residue was suspended in a LiCl aqueous saturated solution (100 ml) and extracted with ethyl acetate (3 x 100 ml) to eliminate the DMF. The combined organic layers were dried with anhydrous Na_2SO_4 and evaporated *in vacuo.* The crude ester thus obtained was hydrolysed using a 5 M aqueous solution of NaOH (2.5 eq) in EtOH (5 ml) at reflux for 1 h. The cooled reaction mixture was extracted with ethyl acetate. The aqueous phase was acidified and extracted again with ethyl acetate, the organic phase was dried with anhydrous Na_2SO_4 and evaporated *in vacuo* to obtain the desired product, which was finally purified by flash chromatography through a silica column using hexane: ethyl acetate as the mobile phase.

_N_-Phenylglycine (21a)

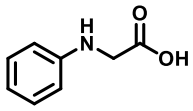

Prepared from aniline (1.862 g, 20 mmol), and ethyl 2-bromoacetate (3.36 ml, 20 mmol); pale brown solid. Yield: 1.529 g; 51 %.

Mp 118-120°C.

IR (neat) 3019, 2944, 1556, 1489, 1378, 1314, 692 cm^{-1}.

^{1}H NMR (250 MHz, d_4-methanol): δ 7.18 – 7.08 (m, 2H), 6.73 – 6.59 (m, 3H), 3.88 (s, 2H) ppm.

^{13}C NMR (63 MHz, d_4-methanol): δ 174.1, 148.3, 129.1 (2C), 117.7, 113.1 (2C), 45.4 ppm. These data are in good agreement with the literature.[155]

_N_-(2,4-Dichlorophenyl)glycine (21b)

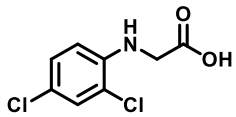

Prepared from 2,4-dichloroaniline (3.220 g, 20 mmol), and ethyl 2-bromoacetate (3.36 ml, 20 mmol); brown solid. Yield: 0.704 g;16 %.

Mp 147- 150 °C (Lit,[156] 148-151 °C).

IR (neat) 3405, 2875, 2082, 1717, 1593, 1494, 1236, 861, 796 cm^{-1}.

^{1}H NMR (250 MHz, d_4-methanol): δ 7.28 (d, J = 2.4 Hz, 1H), 7.13 (dd, J = 8.7, 2.4 Hz, 1H), 6.57 (d, J = 8.7 Hz, 1H), 3.97 (s, 2H) ppm.

^{13}C NMR (63 MHz, d_4-methanol): δ 174.4, 144.4, 130.0, 129.2, 122.8, 120.9, 113.6, 46.1 ppm.

[155] Zhikuan, L.; Twieg, R. J. *Tetrahedron Lett*. **2005**, *46*, 2997.

[156] Arct, J.; *Przemysl Chemiczny* **1964**, *43*, 332.

Elemental analysis (%): calcd. for $C_8H_7Cl_2NO_2$: C 43.67, H 3.21, N 6.37; found: C 43.58, H 3.43, N 6.26.

5.5.11. General procedure for the synthesis of arylamino derivatives (21i-l)

To a solution of the suitable glycine derivative, 1-ethyl-3-(3-dimethylaminopropyl)carbodiimide hydrochloride (EDC·HCl, 1 eq), and the suitable 2-styrylquinoline derivative **17** (1 eq) in dry THF, Et_3N (2 eq) was added, followed by the addition of 1-hydroxy-7-azabenzotriazole (HOAt, 0.6M solution in DMF, 1 eq). The reaction mixture was refluxed for 12 hours. Then, the solvent was removed under reduced pressure and the residue was suspended in a LiCl saturated aqueous solution (5 ml) and extracted with ethyl acetate (3 × 5 ml). The combined organic layers were dried with anhydrous Na_2SO_4 and evaporated *in vacuo.* The product was purified by flash chromatography through a silica column using hexane: ethyl acetate (1:1, v/v) as the mobile phase to give the desired products.

(*E*)-2-(Phenylamino)-*N*-(2-((2-styrylquinolin-4-yl)amino)ethyl)acetamide (19i)

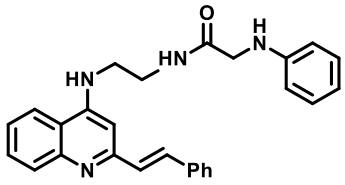

Prepared from phenylglycine **21a** (0.037 g, 0.127 mmol), and **17a** (0.024 g, 0.127 mmol); yellow solid. Yield: 0.018 g; 34 %.

Mp 174- 176 °C.

IR (neat) 3362, 2922, 2430, 1657, 1586, 1306, 963, 749, 689 cm^{-1}.

^{1}H NMR (250 MHz, d_4-methanol) δ 7.95 – 7.82 (m, 2H), 7.75 – 7.62 (m, 4H), 7.47 – 7.26 (m, 5H), 7.06 – 6.94 (m, 3H), 6.64 – 6.50 (m, 3H), 3.78 (s, 2H), 3.61 (m, 4H) ppm.

^{13}C NMR (63 MHz, d_4-methanol) δ 175.9, 158.1, 153.2, 149.8, 149.1, 138.5, 136.1, 131.3, 130.5 (2 C), 130.3 (2C), 130.1, 129.8, 128.7, 128.7 (2C), 126.1, 122.4, 120.0, 119.4, 114.2 (2C), 96.7, 49.7, 44.3, 39.5 ppm.

HRMS found m/z 422.2155 [M^+], calculated for $C_{27}H_{26}N_4O$ 422.2107.

(*E*)-2-(Phenylamino)-*N*-(4-((2-styrylquinolin-4-yl)amino)butyl)acetamide (19j)

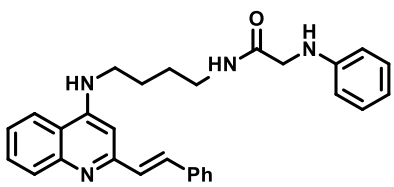

Prepared from phenylglycine **21a** (0.042 g, 0.22 mmol), and **17b** (0.070, 0.22 mmol); yellow solid. Yield: 0.026 g; 26 %.

Mp 82- 85 °C.

IR (neat) 3315, 2929, 1654, 1582, 964, 749, 691 cm^{-1}.

^{1}H NMR (250 MHz, *d_4*-methanol) δ 8.07 (d, *J* = 7.8 Hz, 1H), 7.87 (d, *J* = 7.8 Hz, 1H), 7.72 – 7.62 (m, 4H), 7.46 – 7.27 (m, 5H), 7.14 – 7.02 (m, 2H), 6.84 (s, 1H), 6.66 – 6.52 (m, 3H), 3.74 (s, 2H), 3.47 (t, *J* = 6.7 Hz, 2H), 3.37 (m, 2H), 1.82 – 1.61 (m, 4H) ppm.

^{13}C NMR (63 MHz, *d_4*-methanol) δ 174.7, 158.2, 153.1, 149.7, 149.5, 138.5, 135.6, 131.1, 130.5 (2C), 130.3 (3C), 130.1, 129.0, 128.6 (2C), 125.8, 122.5, 120.2, 119.5, 114.3 (2C), 96.9, 49.5, 43.9, 40.2, 28.6, 27.1 ppm.

HRMS found m/z 451.2497 [M+1], calculated for $C_{29}H_{31}N_4O$ 451.2498.

(*E*)-2-((2,4-Dichlorophenyl)amino)-*N*-(2-((2-styrylquinolin-4-yl)amino)ethyl)acetamide (19k)

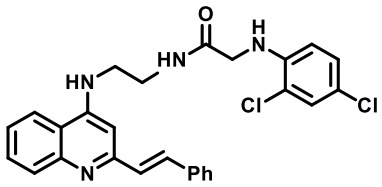

Prepared from (2,4-dichlorophenyl)glycine **21b** (0.101 g, 0.46 mmol), and **17a** (0.134 g, 0.46 mmol); yellow solid. Yield: 0.111 g, 50 %.

Mp 99- 102 °C.

IR (neat) 3332, 2922, 1657, 1585, 1500, 754 cm^{-1}.

^{1}H NMR (250 MHz, , *d_4*-methanol): δ 7.90 (d, *J* = 8.4 Hz, 1H), 7.85 (d, *J* = 8.4 Hz, 1H), 7.73 – 7.60 (m, 4H), 7.45 – 7.19 (m, 6H), 6.96 (s, 1H), 6.80 (dd, *J* = 8.8, 2.4 Hz, 1H), 6.36 (d, *J* = 8.8 Hz, 1H), 3.85 (s, 2H), 3.66 – 3.50 (m, 4H) ppm.

^{13}C NMR (63 MHz, *d_4*-methanol): δ 173.9, 157.4, 152.9, 148.2, 143.9, 137.9, 136.0, 131.1, 129.9 (2C), 129.8, 129.7, 128.9, 128.7, 128.3 (2C), 128.0, 125.7, 122.9, 122.0, 120.7, 119.5, 113.0, 96.2, 48.2, 43.8, 39.2 ppm.

HRMS found m/z 491.1410 [M+1], calculated for $C_{27}H_{25}Cl_2N_4O$ 491.1405.

(*E*)-2-((2,4-Dichlorophenyl)amino)-*N*-(4-((2-styrylquinolin-4-yl)amino)butyl)acetamide (19l)

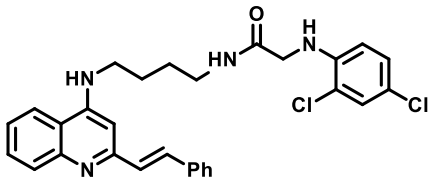

Prepared from (2,4-dichlorophenyl)glycine **21b** (0.138 g, 0.63 mmol), and **17b** (0.200 g, 0.63 mmol); yellow solid. Yield: 0.220 g, 67 %.

Mp 74- 76 °C.

IR (neat) 2929, 2493, 1654, 1581, 1491, 1438, 755 cm^{-1}.

^{1}H NMR (250 MHz, *d*$_4$-methanol): δ 8.04 (d, *J* = 8.4 Hz, 1H), 7.83 (d, *J* = 8.4 Hz, 1H), 7.66 – 7.57 (m, 4H), 7.43 – 7.21 (m, 6H), 7.00 (dd, *J* = 8.7, 2.4 Hz, 1H), 6.80 (s, 1H), 6.44 (d, *J* = 8.7 Hz, 1H), 3.80 (s, 2H), 3.45-3.40 (m, 2H), 3.33-3.29 (m, 2H), 1.75 – 1.67 (m, 4H) ppm.

^{13}C NMR (63 MHz, *d*$_4$-methanol): δ 173.2, 158.2, 153.1, 149.6, 144.5, 138.5, 135.6, 131.1, 130.3, 130.3 (2C), 130.1, 130.0, 129.2, 129.0, 128.6 (2C), 125.8, 123.3, 122.5, 121.2, 120.2, 113.5, 96.9, 48.6, 43.90, 40.4, 28.6, 27.2 ppm.

HRMS found m/z 519.1713 [M+1], calculated for $C_{29}H_{29}Cl_2N_4O$ 519.1718.

5.5.12. Synthesis of compound 25.

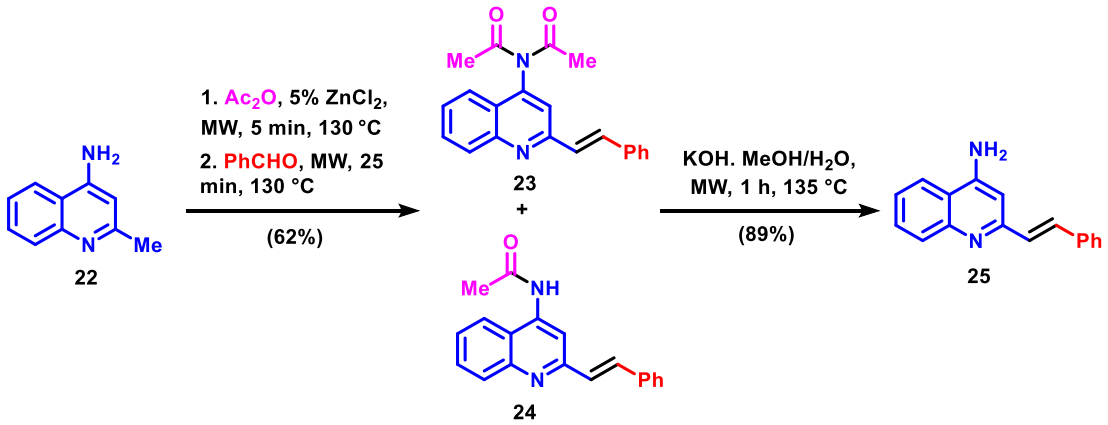

Compound **22** (0.500 g, 3.1 mmol) and $ZnCl_2$ (0.021 g, 0.15 mmol) were suspended in acetic anhydride (3 ml) in a pressure-tight microwave tube containing a stirring bar. The reaction mixture was heated under microwave irradiation for 5 min at 130 °C, with an irradiation power of 250 W, using a CEM Discover SP microwave reactor. Then, benzaldehyde (0.498 g, 4.7 mmol) was added and the mixture was again heated under microwave irradiation for 25 min at 130 °C. The reaction mixture was basified with an aqueous solution of NaOH (5M) and extracted with CH_2Cl_2, dried with anhydrous Na_2SO_4 and evaporated *in vacuo*. The dark purple residue was purified by flash chromatography through a silica column using hexane: ethyl acetate (4:1, v/v) as the mobile phase to give 0.335 g (33%) of compound **18** as a yellow solid and 0.265 g (30%) of compound **19** as a white solid.

(*E*)-*N*-Acetyl-*N*-(2-styrylquinolin-4-yl)acetamide (23)

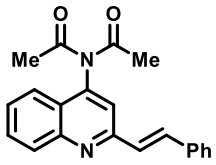

Mp 130-133 °C.

IR (neat) 2652, 2321, 2112, 1718, 1699, 1362, 1217, 754 cm^{-1}.

^{1}H NMR (250 MHz, $CDCl_3$): δ 8.20 (d, *J* = 8.4 Hz, 1H), 7.86 – 7.55 (m, 7H), 7.49 – 7.36 (m, 4H), 2.39 (s, 6H) ppm.

^{13}C NMR (63 MHz, $CDCl_3$): δ 172.8 (2C), 157.3, 150.2, 145.2, 136.5, 136.0, 131.1, 130.5, 129.5, 129.3 (2C), 128.4, 128.3, 127.8 (2C), 125.0, 121.8, 120.1, 27.05 (2C) ppm.

Elemental analysis (%): calcd. for $C_{21}H_{18}N_2O_2$: C 76.34, H 5.49, N 8.48; found: C 75.83, H 5.47, N 8.25.

(*E*)-*N*-(2-Styrylquinolin-4-yl)acetamide (24)

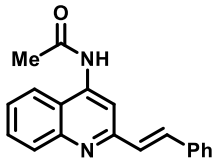

Mp 198- 200 °C.

IR (neat) 3258, 2322, 1737, 1657, 1523, 1371, 954, 755 cm^{-1}.

^{1}H NMR (250 MHz, $CDCl_3$): δ 8.31 (s, 1H), 7.86 (d, *J* = 8.4 Hz, 2H), 7.56 (d, *J* = 8.4 Hz, 1H), 7.51 – 7.37 (m, 4H), 7.30 – 7.05 (m, 5H), 2.14 (s, 3H) ppm.

^{13}C NMR (63 MHz, $CDCl_3$): δ 169.3, 156.9, 148.9, 140.5, 136.5, 134.9, 130.3, 129.8, 129.0, 128.9 (2C), 128.8, 127.4 (2C), 126.1, 119.3, 119.1, 109.5, 25.2 ppm.

Elemental analysis (%): calcd. for $C_{19}H_{16}N_2O$: C 79.14, H 5.59, N 9.72; found: C 78.74, H 5.47, N 9.37.

(*E*)-2-Styrylquinolin-4-amine (25)

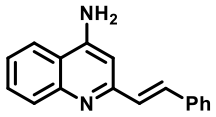

Compound **23** (0.150 g, 0.454 mmol) and KOH (5M) (10 eq) were dissolved in MeOH (3 ml) in a pressure tight microwave tube containing a stirring bar. The reaction mixture was heated under microwave irradiation for 1 hour at 135 °C, with an irradiation power of 200 W, using a CEM Discover SP microwave reactor. Thereafter, the reaction mixture was extracted with ethyl acetate, dried with anhydrous Na_2SO_4 and evaporated *in vacuo,* to give compound **25** (0.100 g, 89% yield) as a yellow solid.

Mp 103-106 °C.

IR (neat) 3446, 3296, 3047, 2920, 1640, 1578, 1511, 967, 752 cm^{-1}.

^{1}H NMR (250 MHz, $CDCl_3$): δ 8.03 (dd, *J* = 8.5, 0.6 Hz, 1H), 7.75 (d, *J* = 8.5 Hz, 1H), 7.72 – 7.58 (m, 4H), 7.47 – 7.26 (m, 5H), 6.91 (s, 1H), 4.79 (s, 2H) ppm.

^{13}C NMR (63 MHz, $CDCl_3$): δ 156.3, 149.9, 149.0, 136.8, 133.7, 129.9, 129.7, 129.4, 128.9 (2C), 128.5, 127.3 (2C), 124.7, 120.2, 118.4, 101.7ppm.

Elemental analysis (%): calcd for $C_{17}H_{14}N_2$: C 82.90, H 5.73, N 11.37; found: C 81.92, H 5.92, N 11.08.

When applied to **24** (0.200 g, 0.69 mmol), the same procedure furnished 0.150 g of compound **25** (88% yield).

CHAPTER 6. NEW ONE-POT MECHANOCHEMICAL METHODOLOGIES FOR THE SYNTHESIS OF BIS-INDOLYLQUINONES

6.1. Bis-indolyl quinones: interesting natural scaffolds

6.1.1. Origin of bis-indolyl quinones or Asterriquinones

In the 80s, some bis-indolyl quinones were isolated from *Aspergillus terreus* by Yamamoto *et al.*, receiving the name of asterriquinones. They are secondary metabolites produced by several fungal species, like *Chaetomium sp*. *Aspergillus terreus* or *Pseudomassaria sp*.[157] Asterriquinones are based on two indolyl groups, bearing different substituents, attached through position 3 to a central benzoquinone core, which usually possess hydroxy or methoxy groups. **(Figure 6.1**)

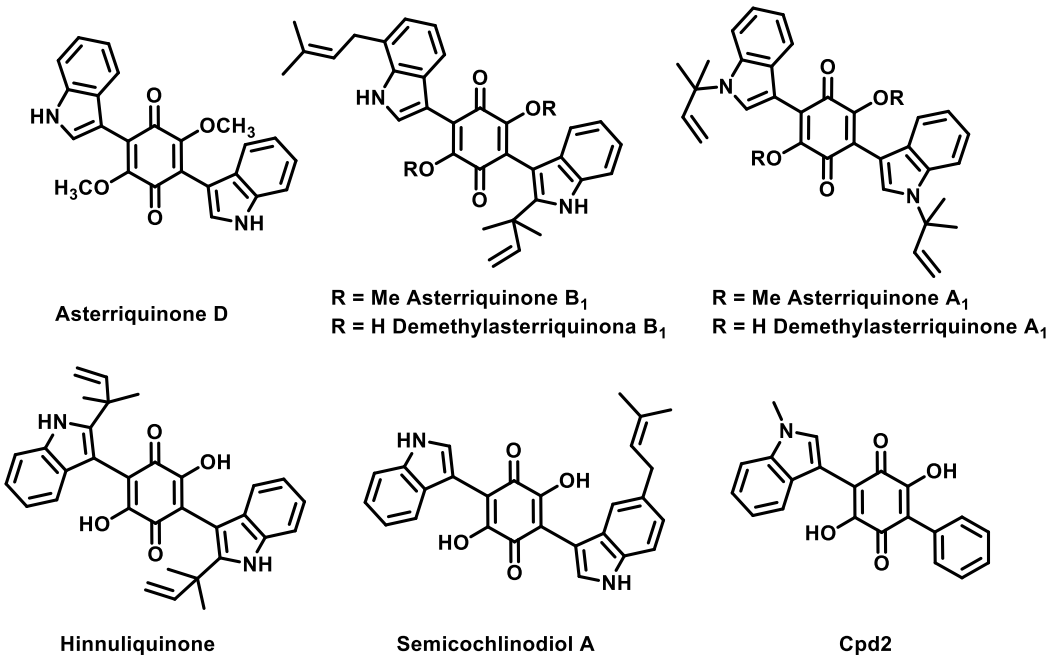

Figure 6.1.

6.1.2. Pharmacological properties of bis-indolyl quinones

The main interest on indolylquinones lies on their potential as pharmacophores due to their wide range of biological activities among different pathologies. Some of them have shown activity against different enzymes involved in human immunodeficiency virus (HIV). For instance, semicochlinodiol A inhibits the HIV protease by forming hydrogen

[157] a) Arai, K.; Yamamoto, Y. Chem. *Pharm. Bull.* **1990**, *38*, 2929. b) Kaji, A.; Saito, R.; Nomura, M.; Miyamoto, K.; Kiriyama, N. *Biol. Pharm. Bull.* **1998**, *21*, 945. c) Brewer, D.; Jerram, W.; Taylor, A. Can. *J. Microbiol.* **1968**, *14*, 861. d) Sekita, S. Chem. *Pharm. Bull.* **1983**, *31*, 2998. e) Kaji, A.; Saito, R.; Hata, Y.; Kiriyama, N. *Chem. Pharm. Bull*. **1999**, *47*,77.

bonds with the aspartic acid and isoleucine residues present in the active site of the enzyme.[158] On the other hand, demethylasterriquinone A is able to inhibit the viral reverse transcriptase.[159]

Some analogues of natural asterriquinones have shown antitumoral properties due to direct DNA interaction,[160] while some others show the same response by inhibiting the union of Grb-2 grown factor to the tyrosine kinase receptor EGF-R. In human cancers, Grb2 is viewed as an attractive therapeutic target because it mediates the activation of receptor tyrosine kinase and adapters to the $p21^{ras}$ signal transduction pathway.[161]

Moreover, a potent oral antidiabetic activity was found for demethylasterriquinone B_1 (DMAQ-B_1), which attracted a great deal of interest due to being the first small organic molecule being able to act as an insulin mimetic while showing a very good oral bioability. This compound was discovered by a virtual screening process designed to find new compounds able to activate the tyrosine kinase activity of the insulin human receptor. DMAQ-B1 showed selectivity against insulin receptor among other tyrosine kinase receptors, and it was orally active in two diabetes mice models, reducing glycaemia levels considerably. These findings promoted the development of simpler, non-natural analogues such as Cpd2, a compound developed by Merck.[162] **(Figure 6.1)**

The nerve growth factor (NGF) belongs to a family of neurotrophin proteins that support the growth and survival of many populations of neurons. NGF binds TrkA, a neurotrophin receptor able to protect neuronal cells from apoptosis and stimulate neuronal regeneration in model systems. Some preclinical and clinical findings suggest that neurotrophins could be a promising therapy for neurodegenerative diseases. However, the main disadvantage of using neurotrophins as drug candidates is their poor pharmacokinetic properties, including the inability to cross the blood-brain barrier. For these reasons, a great effort has been done to find non-peptidic small molecules able to

---

[158] Fredenhagen, A.; Petersen, F.¸Tintelnot-Blomley, M.; Rosel, J.; Mett, H.; Hug, P. *J. Antibiot*. **1996**, 395.
[159] Ono, K.; Nakane, H.; Shimizu, S.; Koshimura, S. *Biochem. Biophys. Res. Commun*. **1991**, *174*, 56.
[160] a) Shimizu, S.; Yamamoto, Y.; Koshimura, S. *Chem. Pharm. Bull.* **1982**, *30*, 1896. b) Kaji, A.; Saito, R.; Nomura, M.; Miyamoto, K.I.; Kiriyama, N. *Biol. Pharm. Bull.* **1998**,*21*, 945.
c) Kaji, A.; Iwata, T.; Kiriyama, N.; Nomura, M.; Miyamoto, K.I. *J. Antibiot*. **1998**, *51*, 235.
[161] Alvi, K.A.; Pu, H.; Luche, M.; Rice, A.; App, H.; McMahon, G.; Dare, H.; Margolis, B. *J. Antibiot.* **1999**, *52*, 215.
[162] a) Wood, H. B.; Black, R.; Salituro, G.; Szalkowski, D.; Li, Z., Zhang, Y.; Moller, D.E.; Zhang, B.; Jones, A. B.; *Bioorg. Med. Chem. Lett.* **2000**, *10*, 1189. (b) Liu, K.; Xu, L.; Szalkowski, D.; Li, Z.; Ding, V.; Kwei, G.; Huskey, S.; Moller, D. E.; Heck, J. V.; Zhang, B. B.; Jones, A. B. *J. Med. Chem.* **2000**, *43*, 3487. (c) Tsai, H. J.; Chou, S. Y. *J. Biomed. Sci*. **2009**, *16*, 68.

activate TrkA receptors. In this context, it has been proved that certain asterriquinones are with good oral bioavailability are able to activate Trk receptors and cross the BBB. Thus, Lin and co-workers screened a chemical library of mono- and bis-indolylquinones, in order to detect hit compounds able to activate TrkA receptor while not exhibiting cytotoxic activity due to the activation of other Trk receptors. In this study, compounds 1H5 and 5E5 were the ones exhibiting the best profile. **(Figure 6.2)** In this context, it is interesting to note that some functionalized quinones, such as a tryptophan-naphthoquinone hybrid[163] and memoquin,[164] have shown very interesting multi-target profiles of relevance in the treatment of Alzheimer's disease.

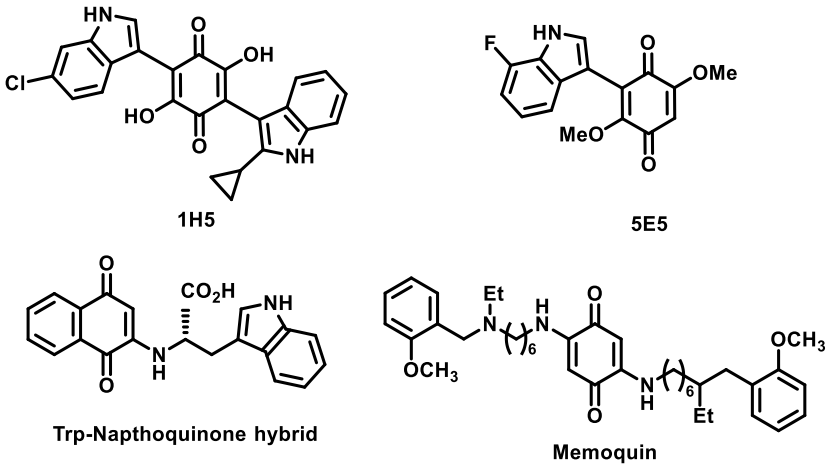

Figure 6.2.

6.1.3. Bis-indolyl quinones as potential MSOT theranostic agents

As mentioned in the introduction, MSOT is appealing as an alternative imaging technique, but its main problem relies on the difficulty of developing adequate MSOT probes. These probes should possess low toxicity, biocompatibility, suitable lipophilicity to cross membranes and good clearance values, while exhibiting absorbance maxima (λ_{abs}) in the NIR range with a low fluorescence quantum yield. To achieve this goal, conjugated structures bearing aromatic systems with push-pull architectures and fluorescence quenchers are the best alternative.

[163] Scherzer-Attali, R; Pellarin, R.; Convertino, M.; Frydman-Marom, A.; Egoz-Matia, N.; Peled, S.; Levy-Sakin, M.; Shalev, D. E.; Caflisch, A.; Gazir, E., Segal, D. *PLoS One* **2010**, *5*: e11101.
[164] Bolognesi, M. L.; Cavalli, A.; Melchiorre, C. *Neurotherapeutics* **2009**, *6*, 152.

In this context, we envisioned that bis-indolylquinones could be a good starting point for developing MSOT theranostic agents. On one hand, they have exhibited interesting therapeutic effects that can be modulated depending on the chosen substituents. Moreover, many of them present good oral bioavailability and capacity to cross the blood-brain barrier.

To this end, we designed a chemical library of compounds based on a bis-indolylquinone core. First, the highly conjugated non-planar nature of this kind of structures would endow them with high absorbance maxima in or close to the NIR region and low fluorescence quantum yields. Moreover, the introduction of halogen groups such as bromine and chlorine would quench their fluorescence due to a heavy-atom effect.[165] In order to displace absorption into the NIR region, we considered introducing different electron donor groups into the indole core, as well as acceptor groups different from carbonyl, like cyanimines or dicyanomethylene, onto the quinone core, thus building a double push-pull system. **(Figure 6.3)**

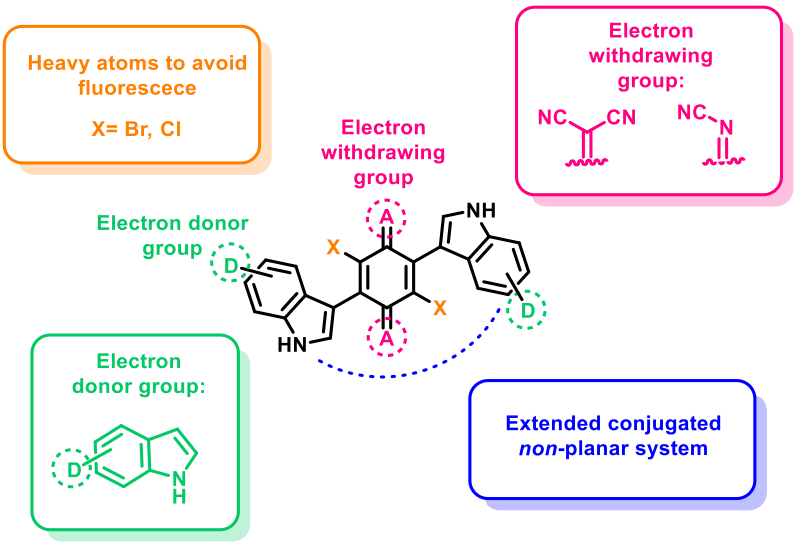

Figure 6.3.

6.2. Precedent for the synthesis of bis-indolylquinones

Even though several methodologies for the synthesis of indolylquinones have been described, many of them are based on cross-coupling reactions. In order to do a review

[165] Berberán-Santos, M. N. *Phys. Chem. Comm.* **2000**, *3,* 18.

on previously described synthesis procedures, we will focus only on the ones using direct Michael additions due to their similarity to our planned route.

Pirrung and co-workers described the synthesis of di-chlorinated indolylquinones by a direct Michael addition of indole derivatives into dichloro benzoquinones. In this methodology, different Brønsted acids (hydrochloric acid, sulphuric acid or acetic acid) were used as catalysts and DDQ was added in order to oxidize the formed hydroquinone. Long reactions times (8-24 h) were usually needed.[166] **(Scheme 6.1)** Yadav and co-workers demonstrated afterwards that these Michael additions, followed by oxidations, can also take place by using Lewis acids such as bismuth triflate [167] or indium tribromide.[168]

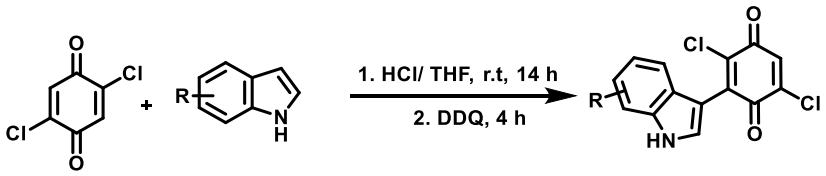

Scheme 6.1.

Harris and co-workers reported a faster methodology to obtain this kind of compounds, using tetrabromobenzoquinone as the starting material. This reaction has the advantage of not needing an oxidation step, but it gives 1:1 mixture of regioisomers.[169] (**Scheme 6.2)**

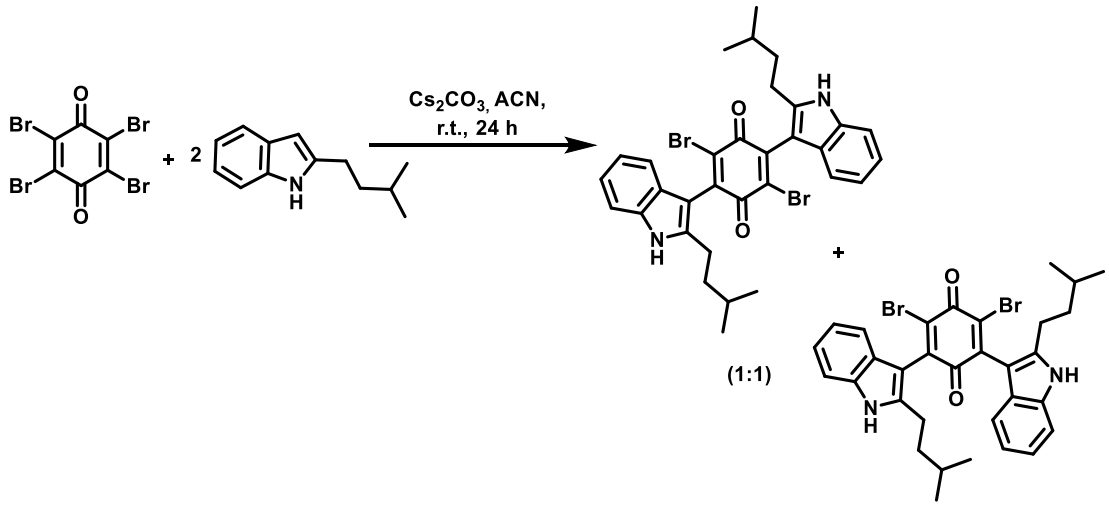

Scheme 6.2.

[166] a) Pirrung, M. C.; Park, K.; Li, Z. *Org. Lett.*, **2001**, *3*, 365. b) Pirrung, M. C.; Deng, L.; Li, Z.; Park, K. *J. Org. Chem.* **2002**, *67*, 8374.
[167] Yadav, J. S.; Reddy, B. V. S.; Swamy, T. *Tetrahedron Lett*. **2003**, *44*, 9121.
[168] Yadav, J. S.; Reddy, B. V. S.; Swamy, T. *Synthesis* **2004**, *1*, 106.
[169] Harris, G. D.; Nguyen, A.; App, H.; Hirth, P.; McMahon, G.; Tang, C. *Org. Lett*. **1999**, *1*, 431.

Some examples of single Michael additions of indoles to quinones, followed by oxidation of the obtained hydroquinone, have been reported, three of which will be discussed below. The first example is based on the use of molecular iodine as a catalyst under ultrasound irradiation at room temperature.[170] **(Scheme 6.3)**

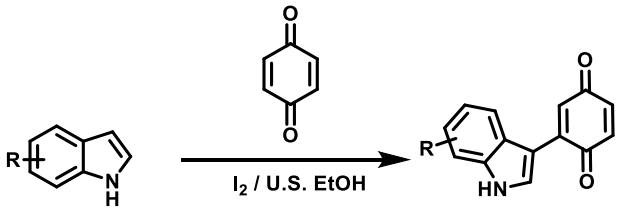

Scheme 6.3.

In the second example, Kamble and co-workers developed a heterogeneously catalysed domino synthesis of 3-indolylquinones, starting from either quinones or hidroquinones as starting materials. The addition reaction was catalysed by ferrite (Fe_3O_4)/povidone−phosphotungstic acid (PVP−PWA), while the oxidation step took place thanks to the presence of Ag_2O and H_2O_2. The main advantages of this methodology are the shorter times needed (2-5 h) and the possibility of recover and reuse the catalytic system. [171] **(Scheme 6.4)**

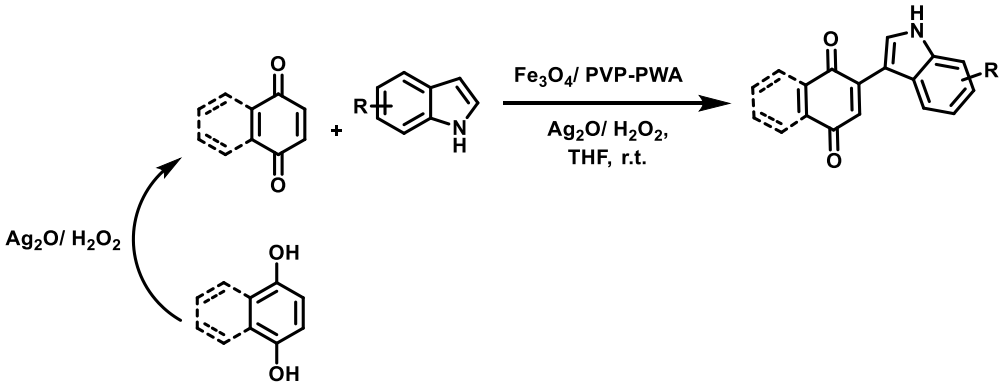

Scheme 6.4.

Finally, the third example comes from Escobedo-González *et al.*, who compared the synthesis of four natural indolylquinone derivatives **(Scheme 6.5)** under different conditions in order to compare typical synthetic procedures with uncommon activating modes such as microwave irradiation, IR irradiation and mechanochemical procedures.

[170] Liu, B.; Ji, S.J.; Su, X.M.; Wang S. Y. *Synth. Commun*., **2008**, *38*, 1279.

[171] Kamble, S. B.; Vyas, P. P.; Jayaram, R. V.; Rode, C. V. *ACS Omega*, **2017**, *2,* 2238.

To this end, different quinones and naphthoquinones were reacted with indole under different conditions, as summarized in **Table 6.1**.[172]

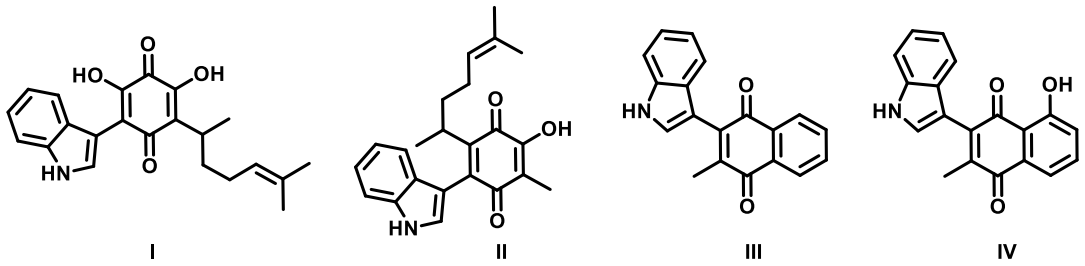

Scheme 6.5.

Product	Yields %			
	MH	MW	IR	HSBM
I	24	79	62	24
II	12	35	31	18
III	46	42	51	30
IV	25	41	64	35

Table 6.1. MH: mantle heating, 95 °C, 60 min; MW: microwave, 250 W, 100 °C, 10 min; IR, 121 °C, 10 min; HSBM: High speed ball milling, 500 rpm, 60 min.

The introduction of a second indole ring is much more difficult, usually needing the isolation of the mono addition intermediates. Thus, Pirrung and co-workers reported a second indole addition to the mono-indolyl-2,5-dichlorobenzoquinones previously mentioned by using different Brønsted or Lewis acids. [173] **(Scheme 6.6)** The reported methodology requires an inert atmosphere, long reaction times (12 to 48 h), reflux and 1 to 4 equivalents of the acid promoter. Moreover, an additional long (14h) oxidation step was needed.

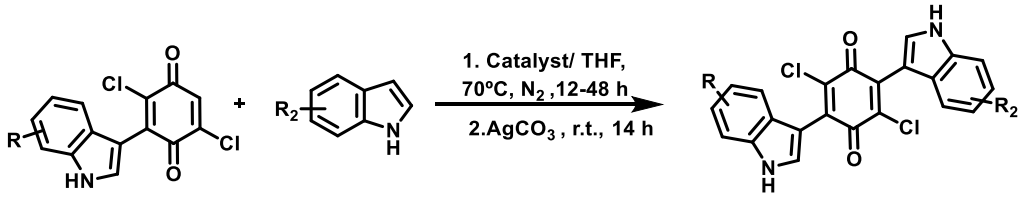

Scheme 6.6.

[172] Escobedo-González, R. G.; Pérez-Martínez, H.; Nicolás-Vázquez, M.; Martínez, J. Gómez, G.; Serrano, J. N.; Carranza-Téllez, V. Vargas-Requena, C. L.; Miranda-Ruvalcaba, R. *J. Chem.* **2016**, ID 3870529.
[173] Pirrung, M. C.; Liu, Y.; Deng, L.; Halstead, D. K.; Li, Z.; May, J. F.; Wedel, M.; Austin, D. A.; Webster N. J. G. *J. Am. Chem. Soc.* **2005**, *127*, 4609.

Finally, a last methodology for the synthesis of indolylquinones is based on a solvent-free photochemical reaction between 1,4-naphtoquinone and indole, giving the desired compound **A** and a second product **B**, which comes from the Diels-Alder reaction between **A** and a second molecule of the starting quinone, followed by a final oxidation step. **(Scheme 6.7)**[174]

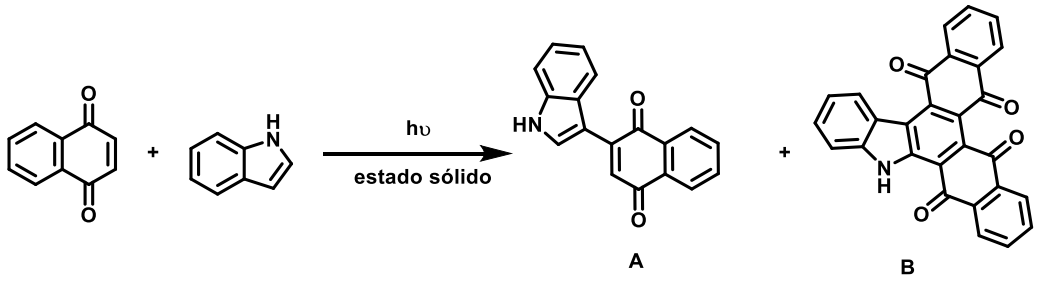

Scheme 6.7.

6.3. Multiple bond-forming synthetic methodologies under mechanochemical conditions.

Typical synthetic methodologies generate large amounts of residues, mainly coming from organic solvents. They are typically considered essential, as most reactions take place in solution to facilitate thorough mixing and thermal energy transfer. Nevertheless, with the beginning of the green chemistry era the interest in developing solvent-free synthetic methodologies has considerably increased. In this context, mechanochemical activation techniques such as manual grinding or ball-milling appear as attractive approaches to solvent-free synthesis.[175]

Wilhelm Ostwald, a Russian-German chemist who received the Nobel Prize in Chemistry in 1909, defined for the first time ¨mechanochemistry¨ in 1919 as ¨a branch of chemistry which is concerned with chemical and physicochemical changes of substances of all states of aggregation due to the influence of mechanical energy¨.[176] Similarly, in its *Compendium of chemical terminology*, also known as the "Gold book", IUPAC defines

[174] Wang, Y. M., Wen, Z., Chen, X. M., Du, D. M*., J. Heterocycl. Chem*. **1998**, *36*, 313.
[175] Achar, T. K.; Bose, A.; Mal, P. *Beilstein J. Org. Chem.* **2017***, 13*, 1907.
[176] Stauch, T.; Dreuw, A. *Chem. Rev.* **2016**, *116*, 14137.

mechanochemical reactions as those that are induced by the absorption of mechanical energy,[177] which comes from grinding or milling processes.

During the grinding of two solids, complex transformations are generated. Mechanical energy can break the order of crystalline structures and produce novel surfaces, where at the collision points, solids can be deformed and even melt, generating the so called ¨hot spots¨ where molecules can achieve high vibrational energies that lead to bond breaking. Moreover, under solvent-free conditions, solvation phenomenon are not relevant, potentially leading to accelerated reactions. This factor, associated with the fact that reactions are performed at very high concentrations, can lead to alterations in product selectivity and therefore to new chemistry.[178]

The first mechanochemical reactions took place by grinding reactants with a mortar and a pestle. This technique does no need any specialized equipment and is easy to perform, but relies on the strength of the operator and is not feasible for long reaction times. **(Figure 6.4)** Therefore, specifically designed milling equipment is preferred.[179] nowadays. With these instruments energy input can be controlled by adjusting the milling frequency, making the work more reproducible. Also, as the reactions take place in closed vessels, the operator is not exposed to the reactants, enabling safer reaction conditions. Two main types of such equipment are available **(Figure 6.4)**:

1. ***Mixer (shaker) mills:*** Reagents are loaded into a jar with one or more balls. The jars are then fit horizontally and shaken at the desired frequency. In this case the main mechanical energy is impact force. This kind of milling is usually described as high-speed vibration milling (HSVM) or high-speed ball milling (HSBM).
2. ***Planetary mills:*** Reagents are loaded in the same way, but the movement is different. In this case the jars are mounted on to a spinning disc called the ¨sun wheel¨, and the jars orbit around it while spinning in the opposite direction.

[177] https://goldbook.iupac.org/terms/view/MT07141.
[178] Hernández, J. C.; C. Bolm, *J. Org. Chem.*, **2017**, *82*, 4007.
[179] Howard, J. L.; Cao, Q.; Browne, D. L. *Chem. Sci.* **2018**, *9*, 3080.

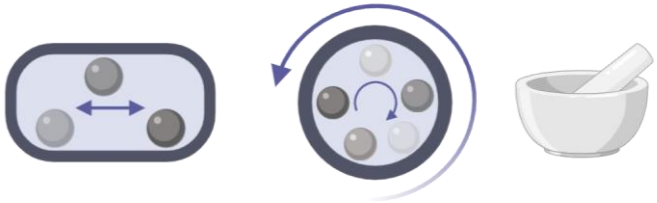

Figure 6.4: Types of grinding.

In both cases, the reaction time, milling frequency, material or jar size and balls can be varied. Sometimes inert milling auxiliaries, such as NaCl, Al_2O_3 or SiO_2, can be used in order to increase the friction, especially when liquid reagents are employed.[180]

On the other hand, the interest on reactions able to generate several bonds in one single step (multiple bond-forming transformations, MBFTs) is considerably increasing.[181] This is mainly due to their high synthetic efficiency, which is a goal in itself and also allows the reduction of isolation and purification steps and consequently the use of lower amounts of organic solvents.

Among MBFTs, reactions can be classified into domino, consecutive or multicomponent. Tietze and Beifuss[182] defined a domino reaction as "a transformation of two or more bond-forming reactions under identical reaction conditions, in which the latter transformations take place at the functionalities obtained in the former bond forming reactions". These domino reactions can be inter-, intramolecular, or combine both modalities.[183] Consecutive (or sequential) reactions, unlike domino, require some change in reaction conditions to complete the bond forming sequence. Examples of such changes are an increase in temperature or a successive addition of reagents.

Multicomponent reactions (MCR) are defined as convergent process in which three or more starting materials are combined, by mixing all of them simultaneously or by sequential addition in a single reaction vessel, to form a product that contains significant fragments of all the reactants. MCRs are characterized by the creation of a high molecular complexity and diversity by using simple and accessible building blocks.

[180] Leonardi, M.; Villacampa, M.; Menéndez, J. C. *Chem. Sci.* **2018**, *9*, 2042.
[181] Bonne, D.; Constantieux, T.; Coquerel, Y.; Rodriguez, J. *Chem. Eur. J.* **2013**, *19*, 2218.
[182] Tietze, L. F.; Beifuss, U.; *Angew. Chem*. **1993**, *32*, 131.
[183] Green, N. J.; Sherburn, M. S. *Aust. J. Chem.* **2013**, *66*, 267.

Moreover, the experimental simplicity and the possibility of automatization make MCRs a promising green chemistry methodology.[184,185]

Compared to conventional methods in which the diversity is introduced step by step MBFTs, due to their highly convergent character, allow obtaining of high number of diverse compounds with a minimal number of steps. **(Figure 6.5)**

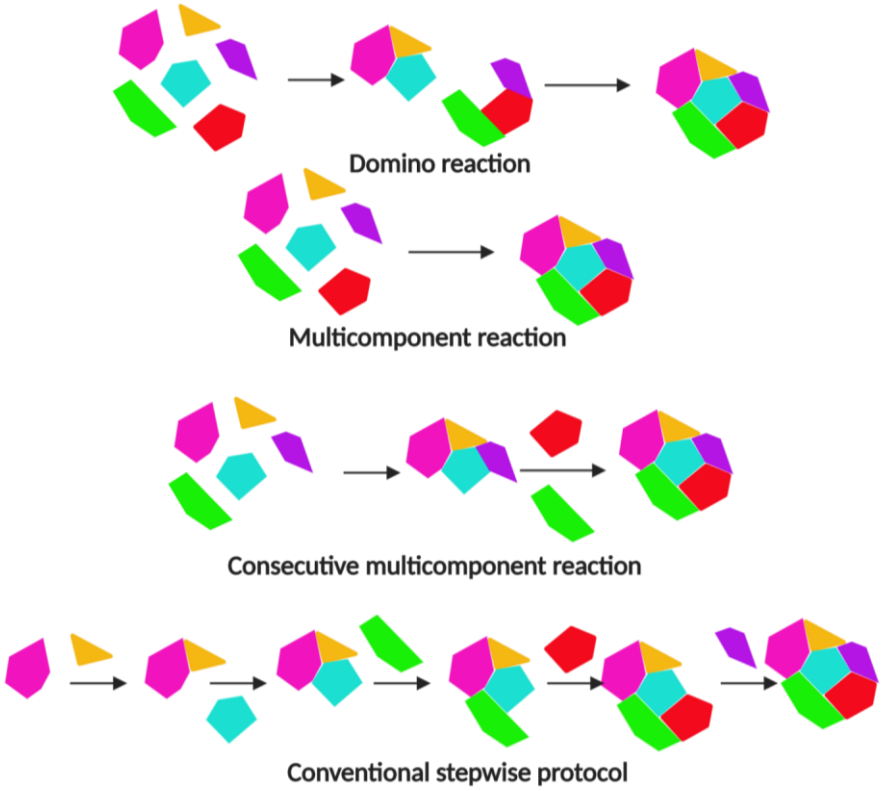

Figure 6.5: MBFTs vs. conventional steps reactions

As previously mentioned, with MBFT reactions the number of isolation and purification steps is reduced, decreasing the amount of solvents employed, and the residues generated. For these reasons, the combination of mechanochemical methodologies with MBFTs appears as an interesting approach to the synthesis of new bioactive compounds using green chemistry methodologies.

[184] Dömling, A.; Ugi, I. *Angew. Chem. Int. Ed. Engl.* **2000**, *39*, 3168.

[185] Zhu, J.; Bienayme, H. (*eds.*), Multicomponent Reactions. Wiley-VCH, **2005**.

6.4. Synthesis of indolylquinones

Most of the previously reported methodologies for the synthesis of indolylquinones present several disadvantages associated to the poor solubility and difficult purification of quinone derivatives. As one of the interests in our group is the development of novel mechanochemical synthetic methodologies, we reasoned that mechanochemistry was a perfect choice to overcome these problems. In this context, we set as our goal the development of a general mechanochemical method to obtain mono- indolylquinones or symmetric or non-symmetric bis-indolylquinones, using indoles and dihalogenated quinones as starting materials.

To obtain these derivatives, two Michael additions followed by oxidation steps are needed. Position 3 of the indole core may attack to one of the available positions of the quinone, forming intermediate **I**, which will tautomerize into the corresponding hydroquinone **II**. After oxidation, this intermediate will give the desired mono-substituted indolylquinone **III**, which can suffer a second nucleophilic attack from another molecule of indole, that after keto-enol tautomerization will give hydroquinone **V**. A final oxidation step will provide the desired compound **VI**. **(Scheme 6.8)**

According to literature precedent, [166,173] the Michael addition of the indole takes place selectively on the position adjacent to the halogen group. This can be explained by the Spartan-calculated Mulliken charges, which show that this position is more electrophilic than the one directly attached to the bromine group. **(Figure 6.6)**

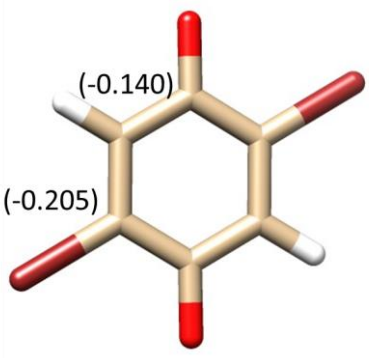

Figure 6.6.

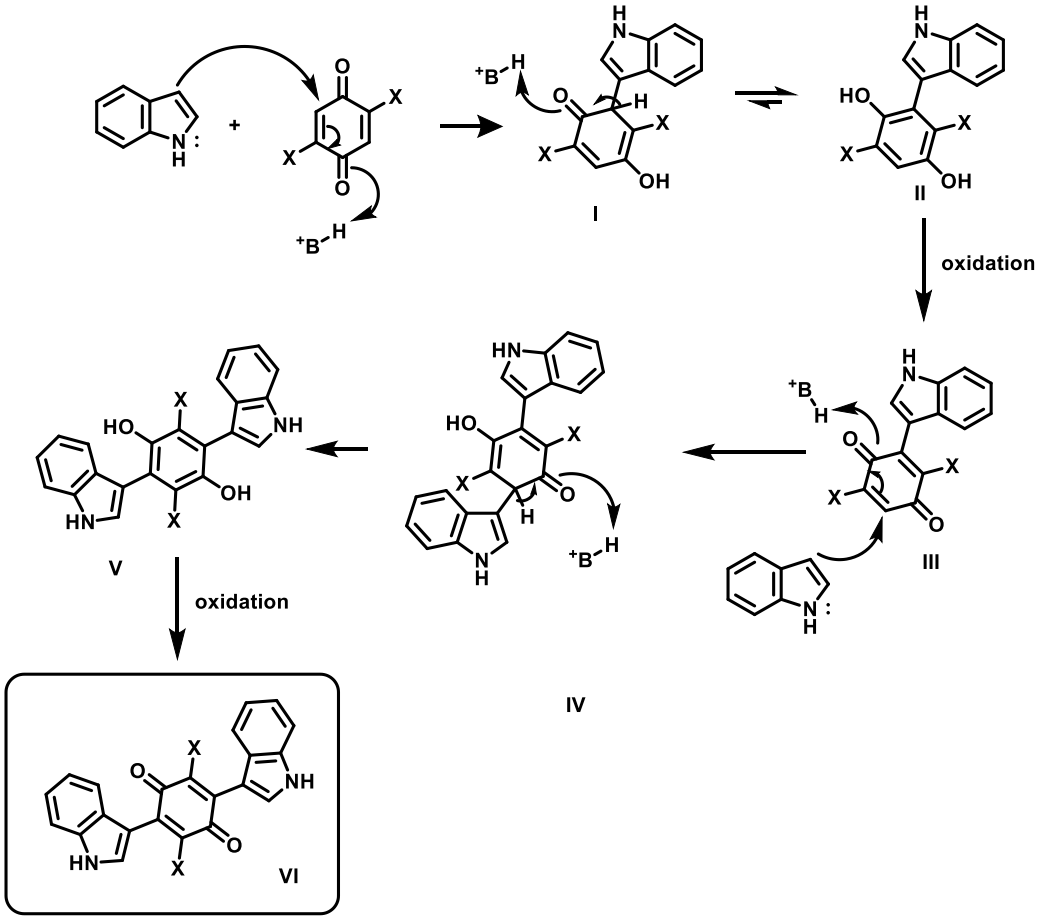

Scheme 6.8.

6.4.1 Synthesis of mono-indolylquinones

In order to start with the synthesis of our library of indolyl-quinone derivatives, we first needed to optimize the preparation of mono-indolyl derivatives. To this end, in a first attempt 1 equivalent of indole and 1 equivalent of 2,5-dibromoquinone were placed in a 20 mL ball mill vessel, along with a zirconium oxide ball. The vessel was fitted to one of the horizontal vibratory arms of the ball mill, while the other arm was occupied with an empty vessel, and the mill was set to vibrate at a frequency of 20 s^{-1} for 60 min at room temperature. Under these conditions, the desired product was obtained in a 20% yield, along with starting materials, hydroquinone and the desired compound in its hydroquinone form. Many of the previously reported methodologies for the synthesis of this kind of derivatives used an excess of the starting quinone in order to act as the oxidizing agent, but the main problem of such a protocol lies on the difficult separation of the mixture obtained. To avoid these problems, we decided to add an external

oxidizing agent. As we were performing mechanochemical reactions, solid reagents were preferable; moreover, in order to avoid a purification step, we wanted to be able to remove the oxidant by simple filtration in the workup. This way, different reagents were studied. **(Scheme 6.9 and Table 6.2)** Many of the tested oxidizers, such as cerium amonium nitrate (CAN), molecular iodine (I_2), ferric chloride ($FeCl_3$) and percarbamide (urea-hydrogen peroxide adduct) resulted in indole degradation. On the other hand, with manganesum oxide (MnO_2) or magnesium monoperoxyphthalate (MMPP) no reaction was observed. The best results were obtained with the use of Fetizon´s reagent (Ag_2CO_3 on celite), which has been used in some cases for the oxidation of hydroquinones. [166,173]

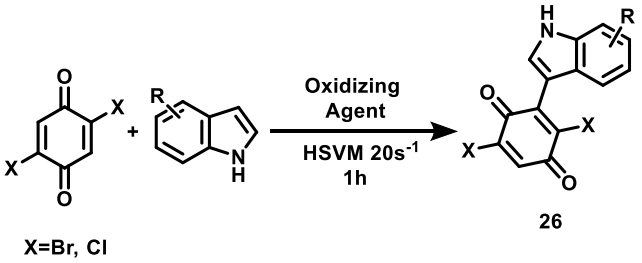

Oxidizing agent	Auxiliar	Eq.	Time (min)	Conversion*	Other products
-	-	-	60	20%	Q + I+ HQ + reduced **26**
CAN	-	2	60	-	Indole decomposition
I_2	-	2	60	-	Indole decomposition
$FeCl_3$	-	2	60	-	Indole decomposition
Percarbamide	-	2	60	-	Q + I + HQ
Percarbamide	**ethanol**	2	60	-	Indole decomposition
Percarbamide	-	4	60	-	Indole decomposition
Percarbamide	**celite**	2	60	-	Indole decomposition
MnO_2	-	2	60	-	Q + I
MMPP		2	60	-	Q + I
Ag_2CO_3 celite	-	1	30	65%	Q + I+ reduced **26**
Ag_2CO_3 celite	-	1	60	88%	Q + I + reduced **26**
Ag_2CO_3 celite	-	2	60	97%	Q
Ag_2CO_3 celite	-	2	30	88%	Q + I
Ag_2CO_3 celite	-	3	60	100%	-

Scheme 6.9. and Table 6.2. *Crude ^{1}H-RMN calculated conversions. Q: 2,5-dibromoquinone; HQ: 2,5-dibromohydroquinone; I: indole

Once Fetizons´s reagent was selected as the best alternative, different conditions were tried for the reaction. When just one equivalent of the oxidizing agent was employed, complex mixtures of the starting materials, hydroquinone, the desired compound and its reduced form were found. Only with 2 equivalents of the Fetizon´s reagent the

reduced species disappeared. It is worth highlighting that other authors using different oxidizing agents as DDQ also reported the need for at least 2 equivalents of oxidizer.[166,173]

This way, we decided to establish our standard protocol with 1 equivalent of the suitable indole derivative and quinone, 2 equivalents of Fetizon´s reagent, for 1 hour under high-speed vibration milling at a frequency of 20 s^{-1}.

Once we started exploring the scope of the method, we observed that, not unexpectedly, the reactivity changed depending on the nature of the substituents found in the indole nucleophile, and when electron acceptor groups were introduced, the reactivity decreased considerably. Another problem came from compound purification, which was accompanied by considerable loss of material when performed by chromatography. Thus, when using conventional silica gel column chromatography, most of the compound decomposes. The same behaviour was observed when using alumina, both in its activated commercial form or de-activated by addition of controlled amounts of water. When silica gel was previously deactivated with oxalic acid, better results were observed, but still a high amount of compound was lost. Finally, it was observed that most of the compounds precipitate in hexane/dichloromethane mixtures, giving the best purification method. However, precipitation was only possible when the crude compounds were almost pure.

For these reasons, we considered that the efficiency of the method needed to be improved. For this purpose, one equivalent of *para*-toluensulphonic acid (*p*-TsOH) was added, which was hoped to enhance the quinone reactivity by acting as a Brønsted acid. After some preliminary assays, this was regarded as the optimal method and was used to establish the scope of our reaction **(Scheme 6.10).** As can be observed in **Table 6.3**, a broad scope of indole derivatives were employed, generally giving good to excellent isolated yields. Regarding the quinone component, no significant changes were observed between 2,5-dibromoquinone and 2,5-diclhoroquinone.

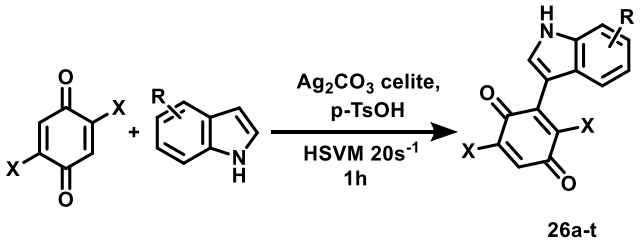

26a-t

Cpd.	R	X	Yield (%)
26a	H	Br	80
26b	H	Cl	96
26c	H	Quinone **I**	Complex mixture
26d	H	Quinone **II**	45
26e	H	Quinone **III**	Complex mixture
26f	5-NO_2	Br	69
26g	5-NO_2	Cl	15
26h	*N*-Methyl	Br	42
26i	2- Methyl	Br	53
26j	7- Methyl	Br	72
26k	5-Br	Br	81
26l	4-Br	Br	79
26m	4-Br	Cl	67
26n	5-Methoxy	Br	75
26o	5-Methoxy	Cl	95
26p	5-Methoxy-2-methyl	Br	98
26q	5-Methylcarboxylate	Br	64
26r	5-NH_2	Br	Unstable
26s	5-NH_2	Cl	Unstable
26t	5-Methoxy-*N*-methyl	Br	75

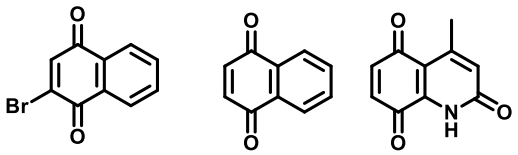

I II III

Scheme 6.10 and Table 6.3.

Although not related to asterriquinones, some more complex quinones were also briefly examined in order to establish the scope of the method. In the case of 2-bromonaphtoquinone (**I**), the reaction took place, but product purification was not possible because of compound instability. When other quinones, with both positions free, as 1,4-naftoquinone (**II**) or 4-methylquinoline-2,5,8(1*H*)-trione (**III**) were used, complex insoluble mixtures were obtained. It is possible that in such cases the desired reaction is not the only one taking place, after the indolylquinone formation, and that

second Diels Alder reaction between the formed product and a molecule of the starting quinone takes place.[174,186]

6.4.2. Synthesis of symetric bis-indolylquinones

Once the methodology to obtained mono-indolylquinones was optimized, we decided to extend the method to the preparation of bis-indolylquinones. In a first attempt, after following the standard protocol for the obtention of mono-indolylquinones, a second equivalent of indole and 2 equivalents of Fetizon´s reagent were added to the same milling vessel, which was then submitted to one additional hour at the same vibration frequency. Under these conditions, no reaction was observed. However, in a second attempt, when the same conditions were tried in the presence of a second equivalent of the Brønsted acid catalyst, the desired double substitution product was isolated in an 60% yield. **(Scheme 6.11)**

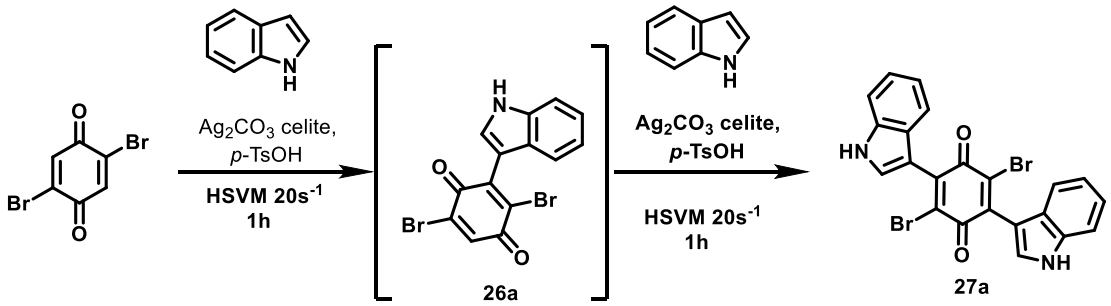

Scheme 6.11.

As in the case of the monoindolylquinones, the methodology needed to be improved to avoid the presence of intermediate species of the domino mechanism so that chromatographic purification could be avoided. For this purpose, the combination of *p*-TsOH with CAN as a Lewis acid catalyst was assayed at different reaction times and substrate/Brønsted acid ratios. **(Scheme 6.12)**

[186] a) López-Alvarado P.; Alonso M. A.; Avendaño C.; Menéndez J. C. *Tetrahedron Lett.* **2001**, *42,* 7971. b) Alonso M.A.; López-Alvarado P.; Avendaño C.; Menéndez J.C. *Tetrahedron* **2003**, *59*, 2821.

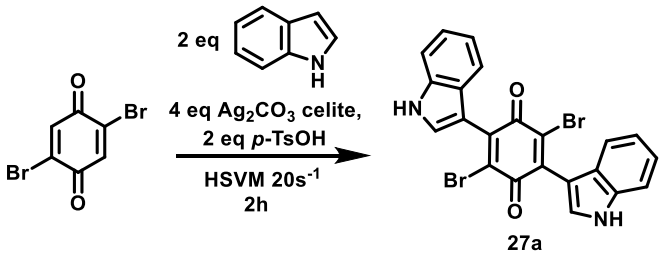

Scheme 6.12.

At this point we decided to start synthesizing derivatives; but when different substituents were introduced, the obtained yields were not as good as expected. This was mainly due to the difficult purification of the compounds, as soon as a mixture of mono- and bis-indolylquinone was obtained, column chromatography was needed, decomposing a considerable amount of product. Thus, we decided that the methodology needed to be improved in order to avoid purification. For this purpose, different times and equivalents of *p*-TsOH were tried in the presence of a 10 % of CAN as a Lewis catalyst. **(Table 6.4)**

Entry	Indole eq	*p*-TsOH eq	CAN (%)	Time (min)	Mono- (%)	Indole (%)	Bis- (%)
1	2	2	--	120	30	10	60
2	2	1	10	60	65	35	--
3	2	1	10	120	40	30	30
4	2	2	10	60	16	18	66
5	2	2	10	120	8	22	70

Table 6.4. *Crude ^{1}H-RMN calculated conversions.

Since the improvements were not sufficient, we decided to try a different milling technique. Thus, the same reaction was performed in a planetary ball mill. To first evaluate the adequate milling settings, the previous conditions of 1 equivalent of the corresponding quinone, 4 equivalents of Fetizon´s reagent, 2 equivalents of *p*-TsOH and 10% of CAN were submitted to different times and milling settings. **(Scheme 6.13 and Table 6.5)**

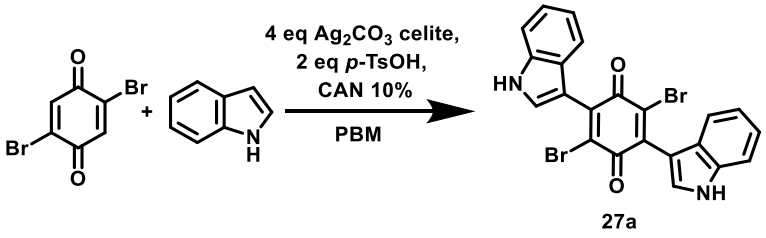

Scheme 6.13.

After trying different settings and indole equivalents, the best conditions found were 2.1 equiv. of indole, at a rotation speed of 650 rpm, changing the direction every 2 min for a reaction time of 90 min and without a pause between these changes in rotation direction.

Entry	Indole eq	Milling	Time (min)	Mono- (%)*	Indole (%)*	Bis- (%)*
4	2	500 rpm, 2 min↔, 10 s pause	60	56	39	5
5	2	500 rpm, 2 min↔, 10 s pause	75	45	36	19
6	2	500 rpm, 2 min ↔, 10 s pause	90	24	40	36
7	2	600 rpm, 2 min ↔, 5 s pause	120	50	--	50
8	2	650 rpm, 2 min ↔	90	44	--	56
9	2,1	650 rpm, 2 min ↔	120	30	--	70
10	2,2	650 rpm, 2 min ↔	90	--	44	56
11	2,2	650 rpm, 2 min ↔	120	16	27	57
12	2,1	650 rpm, 2 min ↔	90	27	--	72

Table 6.5. *Crude ^{1}H-RMN calculated conversions.

Once the milling conditions were selected the influence of different Lewis acids was studied. As it is shown in **Table 6.6** Ferric chloride ($FeCl_3$) gave the best results. To further evaluate the best conditions in the presence of $FeCl_3$, shorter reaction times were tested, but lower yields were obtained (63 %).

Lewis acid (10%)	Mono- (%)	Bis- (%)
CAN	27	72
$InCl_3$	49	49
$BF_3{\cdot}Et_2O$	51	50
$ScTfO_3$	37	63
$FeCl_3$	5	95
$ZnCl_2$	33	67

Table 6.6. *Crude ^{1}H-RMN calculated conversions.

Afterwards, the same reaction times but with lower amounts of the catalyst were evaluated. It was found that the use of 1 % catalyst decreased considerably the yield to

a 64 %, while 5 % was enough to maintain a 92 % yield, being chosen as our optimal conditions.

Once this protocol was established, indoles bearing different substitution patterns were used **(Scheme 6.14 and Table 6.7).** As expected, the heterocycles bearing electron-acceptor substituents afford considerably lower yields, with the reaction involving 5-nitroindole affording only the mono-substituted product in a 92 % yield.

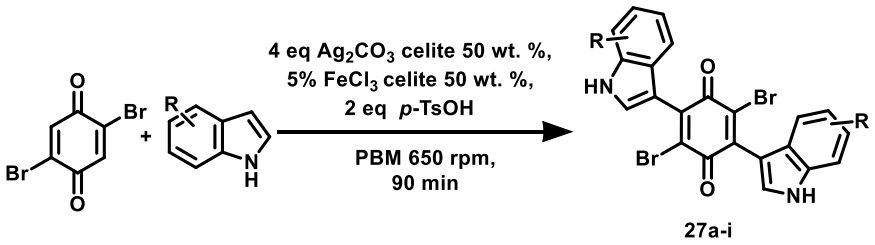

Cpd.	R	Yield (%)
27a	H	92
27b	5-Methoxy	77
27c	5-Br	21
27d	4-Br	26
27e	*N*-Methyl	50
27f	2-Methyl	80
27g	5-Methoxy-2-methyl	94

Scheme 6.14. and Table 6.7.

As it can be shown in **Table 6.6**, indoles bearing different substitution patterns were used. On one side, as it can be expected the heterocycles bearing electron acceptor substituents afford considerably lower yields. Moreover, the addition of a second 5-nitroindole did not took place, affording just the mono-substituted in a 92% yield.

6.4.3. Synthesis of non-symmetric bis-indolylquinones

Finally, in order to obtained *non*-symmetric bis-indolylquinones, we assayed a two-steps, one-pot protocol introducing two different indoles, which allowed us to obtain compounds **28a**-**g (Scheme 6.15 and Table 6.8)**

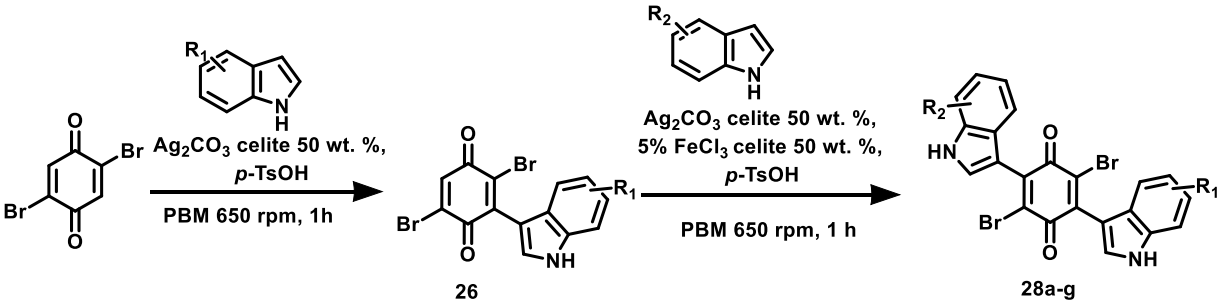

Scheme 6.15.

Cpd.	R_1	R_2	Yield (%)
28a	5-NO2	2-Methyl	70
28b	H	5-Br	40
28c	H	2-Methyl	83
28d	H	5-Methoxy	80
28e	5-Methoxy	5-Methoxy-2-methyl	55
28f	5-Methoxy	2-Methyl	71
28g	5-Methoxy	5-Br	65

Table 6.8.

Some preliminary studies regarding the UV absorption maxima of representative indolylbenzoquinones (**26a**, **26h**, **26n** and **27b**) showed that compounds present a maximum of absorption between 500 and 650 nm. As expected, indoles bearing electron donor groups present a red-shift in their maximum of absorption. Moreover, compound **26h** showed a clear solvatochromic effect in polar environments, displacing its maximum towards red region. **(Table 6.9)**

Compound	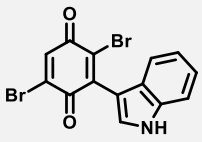 **26a**	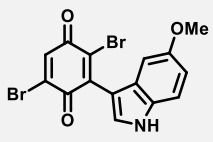 **26n**	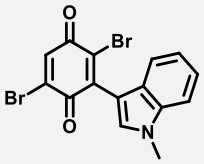 **26h**	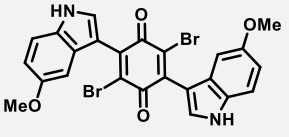 **27b**
MeOH	532	573	570	529
H_2O	550	575	607	543

Table 6.9.

In order to advance towards our goal of developing MSOT probes, a further displacement of these absorption maxima towards the IR region was considered relevant. With this goal, some preliminary experiments to substitute the carbonyls with more electron-withdrawing groups were performed **(Scheme 6.15)**. Unfortunately, none of them afford positive results, and further studies will be needed.

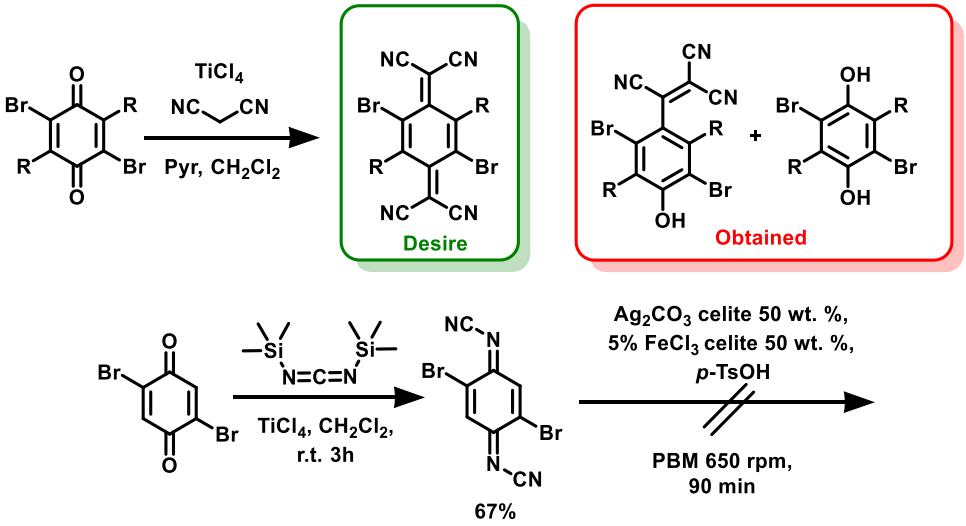
TiCl4
Pyr, CH2Cl2
Desire
Obtained
Ag2CO3 celite 50 wt. %,
5% FeCl3 celite 50 wt. %,
p-TsOH
TiCl4, CH2Cl2,
r.t. 3h
67%
PBM 650 rpm,
90 min

Scheme 6.15.

6.5. Experimental section

General experimental details.

All reagents (Aldrich, Fischer, Alpha Aesar, SDS) and solvents (Scharlau, Fischer, SDS) were of commercial quality and were used as received. Mechanochemical reactions were carried out in a vibratory mixer mill (Retsch MM 200) at a frequency of 20 Hz using a 25 mL zirconium oxide grinding jar and a single zirconium oxide ball 20 mm in diameter or in a planetary ball mill (Retsch PM 100) at 650 rpm using a 12 mL stainless steel grinding jar and 30 steel balls 5 mm in diameter. Reactions were monitored by thin layer chromatography on aluminium plates coated with silica gel and fluorescent indicator (Macherey-Nagel Xtra SIL G/UV254). Compounds were purified by precipitation in different solvent mixtures or by separation by flash chromatography with oxalic acid precoated silica gel (Scharlau 40–60 μm, 230–400 mesh ASTM), Melting points were determined using a Stuart Scientific apparatus, SMP3 Model, and are uncorrected. Infrared spectra were recorded with an Agilent Cary630 FTIR spectrophotometer working by attenuated total reflection (ATR), with a diamond accessory for solid and liquid samples. NMR spectroscopic data were recorded using a Bruker Avance 250 spectrometer operating at 250 MHz for ^{1}H NMR and 63 MHz for ^{13}C NMR maintained by the NMR facility of Universidad Complutense (CAI de Resonancia Magnética Nuclear); chemical shifts are given in ppm and coupling constants in Hertz. High-resolution mass spectra (HRMS) were recorded on a mass spectrometer fitted with an electrospray detector (ESI) by the mass spectral facility of Universidad Complutense (CAI de Espectrometría de Masas) and elemental analyses were determined by the microanalysis facility of Universidad Complutense (CAI de Microanálisis Elemental), using a Leco 932 combustion microanalyzer.

6.5.1 Preparation of non-commercial reactives

Synthesis of Fetizon's reagent

17 g of $AgNO_3$ were dissolved in 100 ml of distilled water, the resulting solution was stirred and 15 g of Celite were added. A solution of 5.299 g of Na_2CO_3 in 150 ml of distilled water was added to the previous suspension. The resulting mixture was stirred for 1h and after this time the yellowish-green precipitate was filtered and washed with water until its neutralization. The resulting precipitate was dried in an oven overnight.[187]

Oxalic acid-precoated silica gel

Silica gel was added over a 0.1N solution of oxalic acid and the mixture was stirred over night at room temperature. After this time, the excess of oxalic acid was eliminated with water (3 x 250 mL), the resulting precoated silica was dried overnight under 110°C in an oven.[188]

2,5-Dibromobenzoquinone [189]

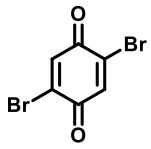

To a solution of 1,4-dimethoxybenzene (10 g, 72.5 mmol) in acetic acid (20 mL) was dropwise added Br_2 (23.15 g, 145 mmol) in acetic acid (7 mL), at room temperature. After stirring for 2 h, the solution was cooled and the white precipitate (16.2 g) of 2,5-dibromo-1,4-dimethoxybenzene was filtered. The filtrate was diluted with water (15 mL) and extracted with $CHCl_3$, which was washed with 10% aqueous $NaHCO_3$, dried over anhydrous sodium sulphate and evaporated, yielding an additional amount (3.1 g) of 2,5-dibromo-1,4-dimethoxybenzene. A part of the 2,5-dibromo-1,4-dimethoxybenzene obtained (15 g, 50.7 mmol) was dissolved in CH_3CN (150 mL) in an oil bath at 100 ºC. A solution of cerium ammonium nitrate (75.0 g, 136.8 mmol) in water (300 mL) was added to the boiling CH_3CN solution. After completion of the addition, the reacting mixture was left to cool to room temperature while stirred over 30 min. The precipitate that formed was filtered and washed with water (50 mL), yielding 11.5 g (87% overall) of 2,5-dibromobenzoquinone, as a yellow solid.[190]

^{1}H NMR (250 MHz, *d_6*-DMSO) δ: 7.77 (s, 2H) ppm.
^{13}C NMR (63 MHz, *d_6*-DMSO) δ: 178.37 (2C), 138.09 (2C), 137.48 (2C) ppm.

[187] Fieser, M.; Fieser, L. *Reagents for Organic Synthesis*, *Vol. 2*, p. 363.
[188] Yamamoto, Y.; Nishimura, K.; Kiriyama, N.; *Chem. Pharm. Bull*. **1976**, *24*, 1853-1859.
[189] López-Alvarado P., Avendaño C., Menéndez J. C. *Synth. Commun.* **2002,** *20*, 3233-3239**.**
[190] These spectral data were identical to those found in literature [189]

2,5-Dichlorobenzoquinone [189]

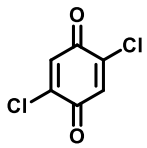

Neat SO_2Cl_2 (15.17 mL,188.17 mmol, 2.6 eq.) was slowly added at room temperature to 1,4-dimethoxybenzene (10 g, 72.37 mmol). The mixture was warmed at 40 ºC and stirred for 3.5 h. Excess SO_2Cl_2 was removed by attaching the flask to a water pump for 1 h. The residue was triturated with Et_2O (10 mL), filtered and washed with Et_2O (10 mL), yielding 10.27 g of 2,5-dichloro-1,4-dimethoxybenzene as a white solid. A further amount of 2,5-dichloro-1,4-dimethoxybenzene (4.44 g) precipitated from the ether solution. An aliquot of 0.5 g (2.4 mmol) of the 2,5-dichloro-1,4-dimethoxybenzene obtained was dissolved in CH_3CN (7 mL) at 50 ºC. A solution of cerium ammonium nitrate (7.28 g, 12.0 mmol) in water (7 mL) was added, and the reacting mixture was stirred at room temperature for 1 h. The yellow precipitate was filtered and washed with water (1 mL), yielding 0.417 g (97% overall) of 2,5-dichlorobenzoquinone as a yellow solid.[191]

^{1}H NMR (250 MHz, *d_6*-acetone): δ 7.35 (s) ppm.

^{13}C NMR (63 MHz, *d_6*-acetone): δ 178.4 (2C), 144.6 (2C), 134.2 (2C) ppm.

5-Methoxy-1-methyl-1*H*-indole

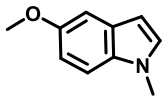

To a stirring solution at 0 ºC of 5-methoxyindole (2 g, 13.60 mml) in dry DMF (60 mL) NaH 60% dispersion in mineral oil (0.54 g, 20.40 mmol) was added. After stirring for 15 min at this temperature methyl iodide (2,54 mL, 40.80 mmol) was added. The mixture was stirred for 1 h at room temperature, after this time, water (200 mL) was added to quench the reaction and the white solid obtained is filtered, washed with water and dried, yielding the desired product. Yield: 1.753 mg, 80%.[192]

Mp 97-99 °C.

^{1}H NMR (250 MHz, *d_4*-methanol): 7.23 (d, *J* = 8.8 Hz, 1H), 7.08 (d, *J* = 3.0 Hz, 1H), 7.04 (d, *J* = 2.4 Hz, 1H), 6.80 (dd, *J* = 8.8, 2.4 Hz, 1H), 6.32 (dd, *J* = 3.0, 0.7 Hz, 1H), 3.80 (s, 3H), 3.75 (s, 3H) ppm.

[191] These spectral data were identical to those found in the literature [189]

[192] These spectral data were identical to those found in literature: Qinqin X.; Xiaodong B.; Chuchu S.; Di W.; Xiaona R.; Zhiguo L.; Yugui G.; Jianmin Z.; Guang L. *Eur. J. Med. Chem*. **2018**, *160*,120-132.

^{13}C NMR (63 MHz, d_4-methanol): δ 155.3, 133.7, 130.4, 130.4, 112.5, 110.8, 103.4, 101.2, 56.6, 56.2, 32.9 ppm.

6.5.1. Synthesis of mono indolylquinones (26a-s)

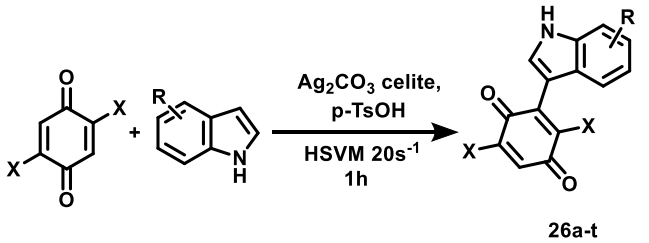

The suitable quinone (1 eq), the corresponding indole (1 eq), *p*-toluensulphonic acid (PTSA, 1 eq) and silver carbonate on Celite 50 wt. % (2 eq) were added to a 12 mL ball mill vessel, along with a zirconium oxide ball. The vessel was fitted to one of the horizontal vibratory arms of the mall mill, while the other arm was occupied with an empty vessel. The ball mill was set to vibrate at a frequency of 20 s^{-1} for 60 min at room temperature. Then, the reaction vessel was cleansed with ethyl acetate and the suspension obtained was filtered to remove the silver carbonate. The organic layer was washed with water (6 mL), dried over anhydrous sodium sulphate and the solvent was removed under reduced pressure. The compounds were purified by column chromatography, using oxalic acid precoated silica gel silica gel as stationary phase and eluting with a mixture hexane-ethyl acetate or by precipitation in different solvent mixtures.

2,5-Dibromo-3-(1*H*-indol-3-yl)cyclohexa-2,5-diene-1,4-dione (26a)

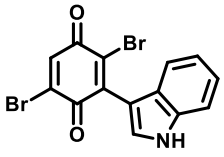

Prepared from 2,5-dibromobenzoquinone (0.250 g, 0,94 mmol), indole (110 mg, 0.94 mmol); the compound was purified by precipitation in a CH_2Cl_2/hexane mixture to give the desired product as a purple solid. Yield: 0.284 g, 80%

Mp 83– 85°C.

IR (neat) 3346 (NH), 1666 (C=O), 741 (C-Br) cm^{-1}.

^{1}H NMR (250 MHz, d_4-methanol): δ 7.66 (s, 1H), 7.61 (s, 1H), 7.47 (dd, *J* = 7.2, 0.8 Hz, 1H), 7.38 (dd, *J* = 7.2, 0.8 Hz, 1H), 7.24 – 7.17 (m, 1H), 7.15 – 7.08 (m, 1H) ppm.

^{13}C NMR (63 MHz, *d*$_4$-methanol): δ 179.7, 178.6, 145.1, 139.0, 138.8, 138.3, 132.2, 131.5, 126.4, 123.5, 122.9, 121.5, 113.3, 110.1 ppm.

Elemental analysis (%): calcd. for $C_{14}H_7Br_2NO_2$: C 44.13 H 1.85, N 3.68; found: C 44.45, H 1.54, N 3.33.

2,5-Dichloro-3-(1*H*-indol-3-yl)cyclohexa-2,5-diene-1,4-dione (26b)

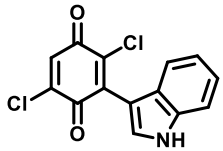

Prepared from 2,5-dichlorobenzoquinone (0.250 g, 1.42 mmol) 1*H*-indole, (0.230 g, 1.42 mmol); the compound was purified by precipitation in a mixture of hexane: ethyl eter to give the desired product as a purple solid. Yield: 0.395 g, 96 %.

Mp 153-155 °C.

IR (neat) 3293 (NH), 1646 (C=O) cm^{-1}.

^{1}H NMR (250 MHz, *d*$_4$-methanol) δ: 7.60 (s, 1H), 7.45 (d, *J* = 8.0 Hz, 1H), 7.35 (d, *J* = 8 Hz, 1H), 7.28 (d, *J* = 1.0 Hz, 1H), 7.21 – 7.14 (m, 1H), 7.12-7.06 (m, 1H) ppm.

^{13}C NMR (63 MHz, *d*$_4$-methanol) δ: 179.7, 179.3, 145.4, 140.7, 138.10 137.7, 134.8, 132.0, 127.3, 123.6, 122.9, 121.6, 113.3, 107.9 ppm.

Elemental analysis (%): calcd. for $C_{14}H_7Cl_2NO_2$: C 57.56, H 2.42, N 4.80; found: C 57.91, H 2.70, N 4.70.

2-Bromo-3-(1*H*-indol-3-y)naphthalene-1,4-dione (26d)

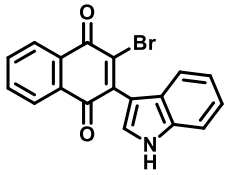

Prepared from 2-bromo-1,4-naftoquinone (0.250 g, 1.06 mmol), 1*H*-indole (0.171 g, 1.06 mmol); the compound was purified by flash chromatography using oxalic acid precoated silica gel[188] as stationary phase and hexane: ethyl acetate (3:1, v/v) as the mobile phase. The compound was unstable, so no further characterization could be done. Brown solid, yield: 0.167 g, 45 %.

^{1}H NMR (250 MHz, *d*$_6$-acetone) δ: 8.21 – 8.17 (m, 1H), 8.16 – 8.12 (m, 1H), 7.91 (d, *J* = 3.2 Hz, 1H), 7.89 (d, *J* = 3.3 Hz, 1H), 7.78 (d, *J* = 2.8 Hz, 1H), 7.53 (d, *J* = 7.8 Hz, 1H), 7.48 (d, *J* = 7.8 Hz, 1H), 7.27 (dd, *J* = 6.1, 3.2 Hz, 1H), 7.22 – 7.15 (m, 1H), 7.15 – 7.06 (m, 1H) ppm.

2,5-Dibromo-3-(5-nitro-1*H*-indol-3-yl)cyclohexa-2,5-diene-1,4-dione (26f)

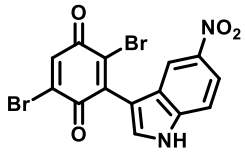

Prepared from 2,5-dibromobenzoquinone (0.250 g, 0,94 mmol), 5-nitro-1*H*-indole (0.152 g, 0,94 mmol); the compound was purified by precipitation in hexane to give the desired product as a purple solid. Yield: 0.275 g, 69%.

Mp 129 – 131°C.

IR (neat) 3346 (NH), 1669 (C=O), 1570 (NO_2) 735 (C-Br) cm^{-1}.

^{1}H NMR (250 MHz, d_6-DMSO) δ: 8.49 (d, *J* = 2.2 Hz, 1H), 8.07 (dd, *J* = 9.0, 2.2 Hz, 1H), 7.87 (s, 1H), 7.86 (s, 1H), 7.67 (d, *J* = 9.0 Hz, 1H) ppm

^{13}C NMR (63 MHz, d_6-DMSO) δ: 178.4, 176.6, 141.5, 141.4, 139.4, 137.4, 137.3, 134.3, 133.0, 125.1, 118.5, 117.3, 113.1, 110.8 ppm.

Elemental analysis (%): calcd. for $C_{14}H_6Br_2N_2O_4$: C 39.47, H 1.42, N 6.58; found: C 39.04, H 1.76, N 6.51.

2,5-Dibromo-3-(*N*-methyl-1*H*-indol-3-yl)cyclohexa-2,5-diene-1,4-dione (26h)

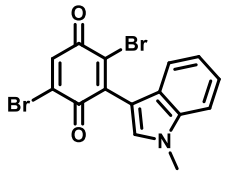

Prepared from 2,5-dibromobenzoquinone (0.250 g, 0,94 mmol), *N*-methylindole (0.123 g, 0,94 mmol); the compound was purified by precipitation in hexane to give the desired product as a purple solid. Yield: 0.156 g, 42%

Mp 98 – 100°C.

IR (neat) 3458 (NH), 1666 (C=O), 738 (C-Br) cm^{-1}.

^{1}H NMR (250 MHz, $CDCl_3$) δ: 7.57 (s, 1H), 7.49 (s, 1H), 7.45 (t, *J* = 1.3 Hz, 1H), 7.42 (t, *J* = 1.3 Hz, 1H), 7.32 (m, 1H), 7.24 (m, 1H), 3.92 (s, 3H) ppm.

^{13}C NMR (63 MHz, $CDCl_3$) δ: 178.3, 177.6, 142.0, 137.9, 137.4, 137.2, 134.4, 131.6, 125.9, 123.0, 122.6, 121.2, 110.6, 107.8, 34.0 ppm.

Elemental analysis (%): calcd. for $C_{15}H_9Br_2NO_2$: C 45.61, H 2.30, N 3.55; found: C 45.75, H 2.37, N 3.71.

2,5-Dibromo-3-(2-methyl-1*H*-indol-3-yl)cyclohexa-2,5-diene-1,4-dione (26i)

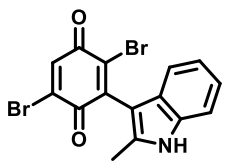

Prepared from 2,5-dibromobenzoquinone (0.250 g, 0,94 mmol) 2-methyl-1*H*-indole (0.124 g, 0,94 mmol); the compound was purified by precipitation in hexane to give the desired product as a purple solid. Yield: 0.197 g, 53%.

Mp 82-84 °C.

IR (neat) 3375 (NH), 1667 (C=O) cm^{-1}.

^{1}H NMR (250 MHz, d_6-acetone) δ: 10.59 (s, 1H), 7.70 (s, 1H), 7.37 (d, *J* = 7.9 Hz, 1H), 7.25 (d, *J* = 7.9 Hz, 1H), 7.13 – 7.05 (m, 1H), 7.05 – 6.97 (m, 1H), 2.36 (s, 3H) ppm.

^{13}C NMR (63 MHz, d_6-acetone) δ: 178.8, 177.0, 144.0, 138.2, 137.9, 137.4, 136.6, 136.3, 127.9, 122.0, 120.5, 120.4, 111.7, 108.1, 13.5 ppm.

Elemental analysis (%): calcd. for $C_{15}H_9Br_2NO_2$: C 45.61, H 2.30, N 3.55; found: C 45.29, H 2.06, N 3.68.

2,5-Dibromo-3-(7-methyl-1*H*-indol-3-yl)cyclohexa-2,5-diene-1,4-dione (26j)

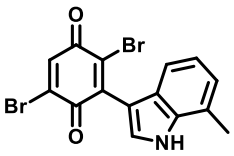

Prepared from 2,5-dibromobenzoquinone (100 mg, 0.376 mmol), 7-methyl-1*H*-indole (0.049 g, 0,376 mmol); the compound was purified by precipitation in hexane to give the desired product as a purple solid. Yield: 0.105mg, 72%.

Mp 132 – 134°C.

IR (neat) 3398 (NH), 1646 (C=O), 745 (C-Br) cm^{-1}.

^{1}H NMR (250 MHz, $CDCl_3$) δ: 8.66 (s, 1H), 7.39 (s, 1H), 7.35 (d, *J* = 2.1 Hz, 1H), 7.10 (d, *J* = 7.8 Hz, 1H), 6.96 (t, *J* = 7.8 Hz, 1H), 6.90 (d, *J* = 7.8 Hz, 1H), 2.35 (s, 3H) ppm.

^{13}C NMR (63 MHz, $CDCl_3$) δ: 178.3, 177.4, 142.4, 137.8, 137.6, 137.4, 135.6, 132.9, 129.4, 124.8, 123.9, 121.5, 119.9, 109.8, 17.0 ppm.

Elemental analysis (%): calcd. for $C_{15}H_9Br_2NO_2$: C 45.61, H 2.30, N 3.55; found: C 45.32, H 2.21, N 3.29.

2,5-Dibromo-3-(5-bromo-1*H*-indol-3-yl)cyclohexa-2,5-diene-1,4-dione (26k)

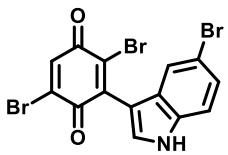

Prepared from 2,5-dibromobenzoquinone (0.100g, 0,376 mmol), 5-bromo-1*H*-indol (0.073 g, 0.376 mmol); the compound was purified by precipitation in hexane to give the desired product as a purple solid. Yield: 0.139 g, 81 %.

Mp 106 – 108 °C.

IR (neat) 3347 (NH), 1646 (C=O), 796 (Br), 736 (C-Br) cm^{-1}.

^{1}H NMR (250 MHz, d_4-methanol) δ: 7.66 (s, 1H), 7.63 (s, 1H), 7.55 (d, *J* = 1.8 Hz, 1H), 7.40 (d, *J* = 8.6 Hz, 1H), 7.30 (dd, *J* = 8.6, 1.8 Hz, 1H) ppm.

^{13}C NMR (63 MHz, *d*$_6$-acetone) δ: 179.1, 177.9, 143.2, 138.6, 138.2, 136.2, 134.4, 132.1, 128.7, 126.0, 125.0, 115.2, 114.2, 109.7 ppm.

Elemental analysis (%): calcd. for $C_{14}H_6Br_3NO_2$: C 36.56, H 1.32, N 3.05; found: C 36.29, H 1.13, N 3.13.

2,5-Dibromo-3-(4-bromo-1*H*-indol-3-yl)cyclohexa-2,5-diene-1,4-dione (26l)

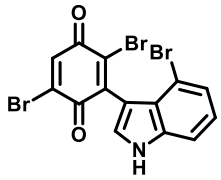

Prepared from 2,5-dibromobenzoquinone (0.250 g, 0,94 mmol), 4-bromo-1*H*-indole (0.184 g, 0,94 mmol); the compound was purified by precipitation in a mixture of hexane: ethyl acetate to give the desired product as a purple solid. Yield: 0.337 g, 79 %.

Mp 103 - 107 °C.

IR (neat) 3330 (NH), 1648 (C=O), 771 (C-Br), 736 (C-Br) cm^{-1}.

^{1}H NMR (250 MHz, *d*$_4$-methanol) δ: 7.77 (s, 1H), 7.65 (d, *J* = 2.8 Hz, 1H), 7.60 – 7.56 (dd, *J* = 2.8, 0.8 Hz, 1H), 7.29 (dd, *J* = 7.6, 0.8 Hz, 1H), 7.13 (t, *J* = 7.6 Hz, 1H) ppm.

^{13}C NMR (63 MHz, *d*$_6$-acetone) δ: 179.1, 178.0, 145.5, 138.8, 138.7, 138.3, 136.9, 129.1, 126.9, 125.3, 124.6, 114.2, 113.0, 111.1 ppm.

Elemental analysis (%): calcd. for $C_{14}H_6Br_3NO_2$: C 36.56, H 1.32, N 3.05; found: C 36.34, H 1.70, N 3.03

2,5-Dichloro-3-(4-bromo-1*H*-indol-3-yl)cyclohexa-2,5-diene-1,4-dione (26m)

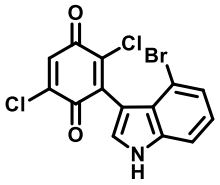

Prepared from 2,5-dichlorobenzoquinone (0.250 g, 1.42 mmol) 4-bromo-1*H*-indole, (0.279 g, 1.42 mmol); the compound was purified by precipitation in a hexane: ethyl acetate mixture to give the desired product as a purple solid. Yield: 0.353 g, 67%.

Mp 228-230 °C.

IR (neat) 3336 (NH), 1652 (C=O) cm^{-1}.

^{1}H NMR (250 MHz, *d*$_6$-acetone) δ: 11.11 (s, 1H), 7.63 (d, *J* = 2.3 Hz, 1H), 7.57 (d, *J* = 8 Hz, 1H), 7.45 (s, 1H), 7.28 (d, *J* = 7.5 Hz, 1H), 7.14 (d, *J* = 8 Hz, 1H) ppm.

^{13}C NMR (63 MHz, *d*$_6$-acetone) δ: 178.6, 178.3, 144.8, 141.7, 141.2, 138.4, 134.3, 128.9, 126.6, 124.9, 124.2, 113.8, 112.6, 107.9 ppm.

Elemental analysis (%): calcd. for $C_{14}H_6BrCl_2NO_2$: C 45.32, H 1.63, N 3.78; found: C 45.53, H 2.02, N 3.90.

2,5-Dibromo-3-(5-methoxy-1*H*-indol-3-yl)cyclohexa-2,5-diene-1,4-dione (26n)

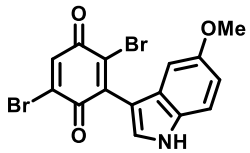

Prepared from 2,5-dibromobenzoquinone (0.250 g, 0,94 mmol), 5-methoxy-1*H*-indole (0.138 g, 0,94 mmol); the compound was purified by precipitation in a mixture of hexane: CH_2Cl_2 to give the desired product as a purple solid. Yield: 0.290 g, 75%

Mp 112 – 115 °C.

IR (neat) 3325 (NH), 1650 (C=O), 1211 (OCH_3), 792 (C-Br) cm^{-1}.

^{1}H NMR (250 MHz, d_6-acetone): δ 10.91 (s, 1H), 7.71 (s, 1H), 7.67 (s, 1H), 7.43 (d, *J* = 8.8 Hz, 1H), 6.94 (d, *J* = 2.4 Hz, 1H), 6.86 (dd, *J* = 8.8, 2.4 Hz, 1H), 3.79 (s, 3H) ppm.

^{13}C NMR (63 MHz, d_6-acetone): δ 179.1, 178.2, 155.8, 138.6, 138.2, 138.0, 132.7, 132.5, 131.7, 127.4, 113.9, 113.5, 109.9, 104.9, 56.2 ppm.

Elemental analysis (%): calcd. for $C_{15}H_9Br_2NO_3$: C 43.83, H 2.21, N 3.41; found: C 43.98, H 2.45, N 3.81

2,5-Dichloro-3-(5-methoxy-1*H*-indol-3-yl)cyclohexa-2,5-diene-1,4-dione (26o)

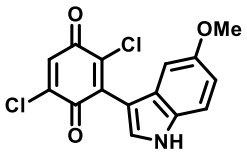

Prepared from 2,5-dichlorobenzoquinone (0.250 g, 1.42 mmol) 5-methoxy-1*H*-indole, (0.209 g, 1.42 mmol); the compound was purified by precipitation in a mixture of hexane: methanol to give the desired product as a purple solid. Yield: 0.435 g, 95%.

Mp 174-176 °C.

IR (neat) 3306 (NH), 1672 (C=O) cm^{-1}.

^{1}H NMR (250 MHz, d_6-acetone) δ: 10.93 (s, 1H), 7.68 (d, *J* = 3.0 Hz, 1H), 7.42 (d, *J* = 8.8 Hz, 1H), 7.36 (s, 1H), 6.91 (d, *J* = 2.3 Hz, 1H), 6.85 (dd, *J* = 8.8, 2.3 Hz, 1H), 3.77 (s, 3H) ppm.

^{13}C NMR (63 MHz, d_6-acetone) δ: 178.7, 178.4, 155.5, 144.4, 139.8, 136.8, 134.1, 132.1, 131.7, 127.2, 113.5, 113.1, 107.3, 104.4, 55.8 ppm.

Elemental analysis (%): calcd. for $C_{15}H_9Cl_2NO_3$: C 55.93, H 2.82, N 4.35; found: C 56.16, H 3.23, N 4.39.

2,5-Dibromo-6-(5-methoxy-2-methyl-1*H*-indol-3-yl)cyclohexa-2,5-diene-1,4-dione (26p)

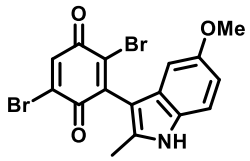

Prepared from 2,5-dibromobenzoquinone (0.250 g, 0,94 mmol) 5-methoxy-2-methyl-1*H*-indole (0.151 g, 0,94 mmol); the compound was purified by precipitation in a mixture of hexane: CH_2Cl_2 to give the desired product as a purple solid. Yield: 0.391 g, 98%.

Mp 108 - 111°C.

IR (neat) 3362 (NH), 1658 (C=O), 686 (C-Br) cm^{-1}.

^{1}H NMR (250 MHz, d_6-acetone) δ: 10.50 (s, 1H), 7.72 (s, 1H), 7.27 (d, *J* = 8.7 Hz, 1H), 6.82 (d, *J* = 2.5 Hz, 1H), 6.75 (dd, *J* = 8.7, 2.5 Hz, 1H), 3.73 (s, 3H), 2.35 (s, 3H) ppm.

^{13}C NMR (63 MHz, d_6-acetone) δ: 179.3, 177.5, 155.7, 144.5, 138.6, 138.5, 138.4, 136.4, 132.0, 128.9, 112.7, 112.2, 108.5, 103.5, 56.3, 14.0 ppm.

Elemental analysis (%): calcd. for $C_{16}H_{11}Br_2NO_3$: C 45.21, H 2.61, N 3.30; found: C 45.15, H 2.44, N 3.36.

Methyl 3-(2,5-dibromo-3,6-dioxocyclohexa-1,4-dien-1-yl)-1*H*-indole-5-carboxylate (26q)

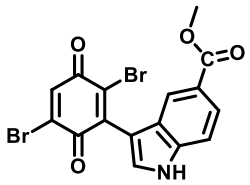

Prepared from 2,5-dibromobenzoquinone (0.250 g, 0,94 mmol), methyl 1*H*-indole-5-carboxylate (0.164 g, 0,94 mmol); the compound was purified by precipitation in a mixture of hexane: ethyl acetate mixture to give the desired product as a purple solid. Yield: 0.264 g, 64%.

Mp 132 - 135°C.

IR (neat) 3319 (NH), 1696 (C=O), 771 (C-Br) cm^{-1}.

^{1}H NMR (250 MHz, d_6-acetone) δ: 11.27 (s, 1H), 8.21 (s, 1H), 7.89 (dd, *J* = 8.4, 1.7 Hz, 1H), 7.81 (d, *J* = 1.7 Hz, 1H), 7.75 (s, 1H), 7.62 (d, *J* = 8.4 Hz, 1H), 3.88 (s, 3H) ppm.

^{13}C NMR (63 MHz, d_6-acetone) δ: 179.1, 177.9, 168.4, 143.3, 140.1, 138.7, 138.2, 134.8, 132.2, 126.5, 125.2, 124.4, 123.5, 113.2, 111.2, 52.4 ppm.

Elemental analysis (%): calcd. for $C_{16}H_9Br_2NO_4$: C 43.77, H 2.07, N 3.19; found: C 43.66, H 2.36, N 3.16.

2,5-Dibromo-3-(5-methoxy-1-methyl-1*H*-indol-3-yl)cyclohexa-2,5-diene-1,4-dione (26t)

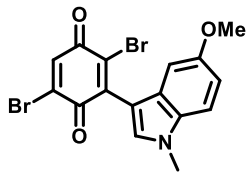

Prepared from 2,5-dibromobenzoquinone (0.250 g, 0,94 mmol) 5-methoxy-1-methyl-1*H*-indole (0.124 g, 0,94 mmol); the compound was purified by precipitation in hexane to give the desired product as a purple solid. Yield: 0.299 g, 75%.

Mp 92-94 °C.

IR (neat) 3040 (NH), 1667 (C=O),1643 (C=O) cm^{-1}.

^{1}H NMR (250 MHz, d_6-acetone) δ: 7.67 (s, 1H), 7.57 (s, 1H), 7.44 – 7.35 (m, 1H), 6.91 – 6.86 (m, 2H), 3.93 (s, 3H), 3.77 (s, 3H) ppm.

^{13}C NMR (63 MHz, d_6-acetone) δ: 178.6, 177.8, 155.6, 142.9, 138.2, 137.5, 135.1, 132.9, 131.6, 127.3, 112.9, 111.8, 108.1, 104.9, 55.8, 33.6 ppm.

Elemental analysis (%): calcd. for $C_{16}H_{11}Br_2NO_3$: C 45.21, H 2.61, N 3.30; found: C 45.48, H 3.02, N 3.29.

6.5.2. Synthesis of symmetric bis-indolylquinones (27a-i)

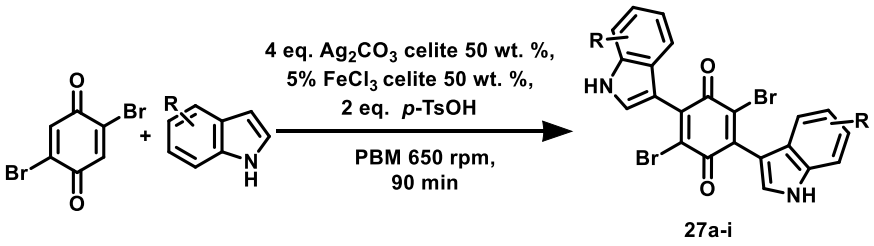

The suitable quinone (1 eq), the corresponding indole (2.1 eq), *p*-toluensulphonic acid (*p*-TsOH, 2 eq), silver carbonate on Celite 50 wt. % (4 eq) and $FeCl_3$ on Celite 50 wt. % (0.05 eq)[193] were added to a 12 mL stainless steel grinding jar with 30 steel balls of 5 mm in diameter. In the case of methoxy derivatives the use of $FeCl_3$ produces decomposition of the corresponding indole, so cerium ammonium nitrate (0.05 eq.) was used. The vessel was fitted into the planetary mill and it was set at a frequency of 650 rpm for 90 min at room temperature. Then, the reaction vessel was cleansed with ethyl acetate and the suspension obtained was filtered to remove the silver carbonate. The organic layer

was washed with water (6 mL), dried over anhydrous sodium sulphate and the solvent was removed under reduced pressure. The compounds were purified by column chromatography, using oxalic acid precoated silica gel silica gel as stationary phase and eluting with a mixture of hexane-ethyl acetate or by precipitation in different solvent mixtures.

2,5-Dibromo-3,6-di(1*H*-indol-3-yl)cyclohexa-2,5-diene-1,4-dione (27a)

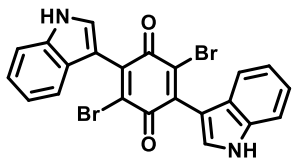

Prepared from 2,5-dibromobenzoquinone (0.05 g, 0.19 mmol) 1*H*-indole (0.046 g, 0.399 mmol), the compound was purified by precipitation in hexane to give the desired product as a purple solid. Yield: 0.102 g, 92 %.

Mp 104 – 107 °C.

IR (neat) 3364 (NH), 1651 (C=O), 742 (C-Br) cm^{-1}.

^{1}H NMR (250 MHz, d_6-DMSO): δ 11.87 (s, 2H), 7.73 (d, *J* = 2.7 Hz, 2H), 7.50 (d, *J* = 7.8 Hz, 2H), 7.44 (d, *J* = 7.8 Hz, 2H), 7.19 (t, *J* = 6.9 Hz, 2H), 7.11 (t, *J* = 6.9 Hz, 2H) ppm.

^{13}C NMR (63 MHz, d_6-DMSO): δ 177.6 (2C), 142.2(2C), 136.2 (2C), 132.2 (2C), 130.5 (2C), 125.7 (2C), 122.0 (2C), 121.7 (2C), 120.0 (2C), 112.5 (2C), 108.6 (2C) ppm.

Elemental analysis (%): calcd. for $C_{22}H_{12}Br_2N_2O_2$: C 53.26, H 2.44, N 5.65; found: C 53.40, H 2.60, N 5.72.

2,5-Dibromo-3,6-bis(5-methoxy-1*H*-indol-3-yl)cyclohexa-2,5-diene-1,4-dione (27b)

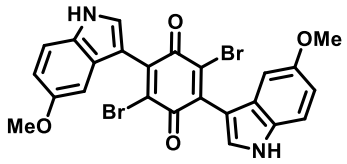

Prepared from 2,5-dibromobenzoquinone (0.05 g, 0.19 mmol) 5-methoxy-1*H*-indole (0.058 g, 0.399 mmol) and cerium ammonium nitrate (0.05 eq) instead of $FeCl_3$ on Celite 50 wt. %. The compound was purified by precipitation in hexane to give the desired product as a purple solid. Yield: 0.081 g, 77 %.

Mp 138 - 139°C.

IR (neat) 3352 (NH), 1653 (C=O), 743 (C-Br) cm^{-1}.

^{1}H NMR (300 MHz, d_6-DMSO): δ 11.71 (s, 2H), 7.65 (d, *J* = 2.8 Hz, 2H), 7.39 (d, *J* = 8.8 Hz, 2H), 6.91 (d, *J* = 2.3 Hz, 2H), 6.83 (dd, *J* = 8.8, 2.3 Hz, 2H), 3.75 (s, 6H) ppm.

^{13}C NMR (75 MHz, d_6-DMSO): δ 177.9 (2C), 154.3 (2C), 142.3 (2C), 132.1 (2C), 131.3 (2C), 131.1 (2C), 126.1 (2C), 112.8 (2C), 111.8 (2C), 108.6 (2C), 104.4 (2C), 55.2 (2C) ppm.

Elemental analysis (%): calcd. for $C_{24}H_{16}Br_2N_2O_4$: C 51.83, H 2.90, N 5.04; found: C 51.70, H 3.03, N 4.71.

2,5-Dibromo-3,6-bis(5-bromo-1*H*-indol-3-yl)cyclohexa-2,5-diene-1,4-dione (27c)

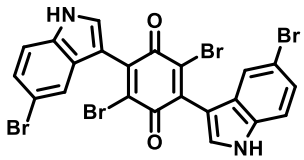

Prepared from 2,5-dibromobenzoquinone (0.05 g, 0.19 mmol) 5-bromo-1*H*-indole (0.078 g, 0.399 mmol), the compound was purified by flash chromatography to give the desired product as a purple solid. Yield: 0.026 g, 21%.

Mp 98 – 100°C.

IR (neat) 3373 (NH), 1652 (C=O), 748 (C-Br) cm^{-1}.

^{1}H NMR (300 MHz, d_6-acetone): δ 11.02 (s, 2H), 7.70 (d, *J* = 1.8 Hz, 2H), 7.59 (d, *J* = 1.8 Hz, 2H), 7.42 (d, *J* = 8.6 Hz, 2H), 7.22 (dd, ,*J* = 8.6, 1.8 Hz, 2H) ppm.

^{13}C NMR (75 MHz, d_6-acetone): δ 177.2 (2C), 141.8 (2C), 135.0 (2C), 133.3 (2C), 130.7 (2C), 127.6 (2C), 124.7 (2C), 123.8 (2C), 113.8 (2C), 112.9 (2C), 108.7 (2C) ppm.

Elemental analysis (%): calcd. for $C_{22}H_{10}Br_4N_2O_2$: C 40.41, H 1.54, N 4.28; found: C 40.65, H 1.27, N 4.26.

2,5-Dibromo-3,6-bis(4-bromo-1*H*-indol-3-yl)cyclohexa-2,5-diene-1,4-dione (27d)

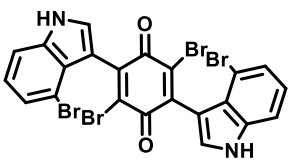

Prepared from 2,5-dibromobenzoquinone (0.05 g, 0.19 mmol) 4-bromo-1*H*-indole (0.078 g, 0.399 mmol), the compound was purified by flash chromatography to give the desired product as a purple solid. Yield: 0.032, 26 %.

The NMR spectra show a mixture of rotamers A and B in a 1:3 relation.

Mp 95 – 99 °C.

IR (neat) 3317 (NH), 1660 (C=O), 734 (C-Br), 678 (C-Br) cm^{-1}.

^{1}H NMR (250 MHz, d_6-acetone): δ 11.12 (s, 2H), 7.75 (d, *J* = 2.7 Hz, 0.5H, B), 7.71 (d, *J* = 2.7 Hz, 1.5H, A), 7.61 (dd, *J* = 8.0, 0.8 Hz, 2H), 7.31 (dd, *J* = 8.0, 0.8 Hz, 2H), 7.15 (t, *J* = 8.0 Hz, 2H) ppm.

^{1}H NMR (300 MHz, d_6-DMSO): δ 11.98 (s, 2H), 7.77 (d, *J* = 2.6 Hz, 0.5H, B), 7.66 (d, *J* = 2.6 Hz, 1.5H, A), 7.54 (d, *J* = 7.8 Hz, 1.5H, A), 7.53 (d, *J* = 7.8 Hz, 0.5H, B), 7.25 (d, *J* = 7.8 Hz, 2H), 7.11 (t, *J* = 7.8 Hz, 2H) ppm.

^{13}C NMR (63 MHz, d_6-acetone): δ 178.8 (2C), 145.4 (2C), 138.7 (2C), 136.7 (2C), 128.9 (2C), 127.1 (2C), 125.3 (2C), 124.6 (2C), 114.2 (2C), 113.0 (2C), 111.3 (2C) ppm.

Elemental analysis (%): calcd. for $C_{22}H_{10}Br_4N_2O_2$: C 40.41, H 1.54, N 4.28; found: C 40.19, H 1.92, N 4.33.

2,5-Dibromo-3,6-bis(1-methyl-1*H*-indol-3-yl)cyclohexa-2,5-diene-1,4-dione (27e)

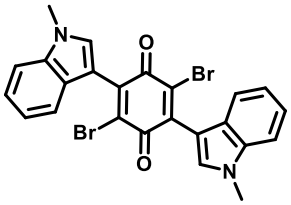

Prepared from 2,5-dibromobenzoquinone (0.05 g, 0.19 mmol) 1-methyl-1*H*-indole (0.052g, 0.399 mmol), the compound was purified by precipitation in hexane to give the desired product as a purple solid. Yield: 0.049 g, 50%.

Mp 98 – 101 °C.

IR (neat) 3456 (NH), 1643 (C=O), 739 (C-Br) cm^{-1}.

^{1}H NMR (250 MHz, d_6-acetone): δ 7.65 (s, 2H), 7.52 (d, *J* = 8.1 Hz, 2H), 7.44 (d, *J* = 8.1 Hz, 2H), 7.27 (t, *J* = 7.3 Hz, 2H), 7.16 (t, *J* = 7.3 Hz, 2H), 3.99 (s, 6H) ppm.

^{13}C NMR (63 MHz, d_6-acetone): δ 179.1 (2C), 138.7 (2C), 138.2 (2C), 137.9 (2C), 135.0 (2C), 132.8 (2C), 127.3 (2C), 123.3 (2C), 123.1 (2C), 121.3 (2C), 111.5 (2C), 33.9 (2C) ppm.

Elemental analysis (%): calcd. for $C_{24}H_{16}Br_2N_2O_2$: C 54.99, H 3.08, N 5.34; found: C 53.97, H 3.00, N 5.22.

2,5-Dibromo-3,6-bis(2-methyl-1*H*-indol-3-yl)cyclohexa-2,5-diene-1,4-dione (27f)

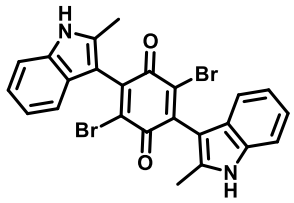

Prepared from 2,5-dibromobenzoquinone (0.05 g, 0.19 mmol) 2-methyl-1*H*-indole (0.052g, 0.399 mmol), the compound was purified by precipitation in hexane to give the desired product as a purple solid. Yield: 0.079 g, 80%.

Mp 147 – 149 °C.

IR (neat) 3369 (NH), 1658 (C=O), 731 (C-Br) cm^{-1}.

^{1}H NMR (250 MHz, d_6-acetone): δ 10.65 (s, 2H), 7.41 (d, *J* = 6.8 Hz, 2H), 7.38 – 7.28 (m, 2H), 7.16 – 7.09 (m, 2H), 7.09 – 7.00 (m, 2H), 2.44 (d, *J* = 4.9 Hz, 6H) ppm.

^{13}C NMR (63 MHz, d_6-acetone): δ 177.4 (2C), 143.5 (2C), 136.8 (2C), 136.3 (2C), 127.7 (2C), 121.5 (2C), 120.3 (2C), 120.2 (2C), 119.9 (2C), 111.3 (2C), 108.0 (2C), 13.2 (2C) ppm.

Elemental analysis (%): calcd. for $C_{24}H_{16}Br_2N_2O_2$: C 54.99, H 3.08, N 5.34; found: C 54.59, H 3.02, N 5.24.

2,5-Dibromo-3,6-bis(5-methoxy-2-methyl-1*H*-indol-3-yl)cyclohexa-2,5-diene-1,4-dione (27g)

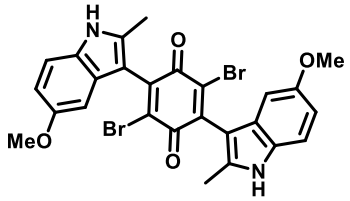

Prepared from 2,5-dibromobenzoquinone (0.05 g, 0.19 mmol) 5-methoxy-2-methyl-1*H*-indole (0.064g, 0.399 mmol), the compound was purified by precipitation in hexane to give the desired product as a purple solid. Yield: 0.105 g, 94 %

Mp 131 - 135 °C.

IR (neat) 3356 (NH), 1658 (C=O), 730 (Br) cm^{-1}.

^{1}H NMR (250 MHz, d_6-DMSO): δ 11.36 (s, 2H), 7.24 (d, *J* = 8.7 Hz, 2H), 6.84 (dd, *J* = 8.3, 2.3 Hz, 2H), 6.73 (dd, *J* = 8.7, 1.4 Hz, 2H), 3.73 (d, *J* = 0.9 Hz, 6H), 2.32 (d, *J* = 4.8 Hz, 6H) ppm.

^{13}C NMR (63 MHz, d_6-DMSO): δ 177.4 (2C), 154.0 (2C), 142.9 (2C), 137.9 (2C), 135.6 (2C), 130.9 (2C), 127.7 (2C), 111.8 (2C), 110.7 (2C), 107.3 (2C), 103.4 (2C), 56.0 (2C), 14.0 (2C) ppm.

Elemental analysis (%): calcd. for $C_{26}H_{20}Br_2N_2O_4$: C 53.45, H 3.45, N 4.79; found: C 52.68, H 4.11, N 4.73.

6.5.3. Synthesis of asymmetric bis-indolylquinones (28a-g)

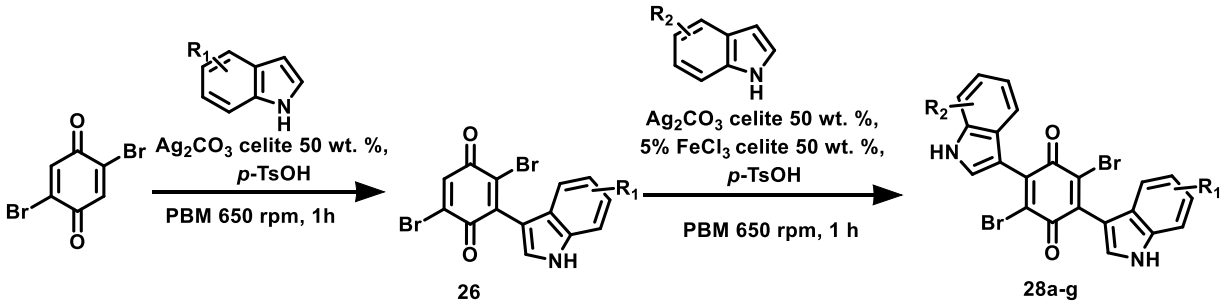

The suitable quinone (1 eq.), the corresponding indole (1 eq.), *p*-toluensulphonic acid (PTSA, 1 eq.) and silver carbonate on Celite 50 wt. % (2 eq.) were added to a 12 mL stainless steel grinding jar with 30 steel balls of 5 mm in diameter. The vessel was fitted into the planetary mill and it was set at a frequency of 650 rpm for 1 h at room temperature. Once this time was finished and the first addition was completed, the second indole (1 eq.), *p*-toluensulphonic acid (PTSA, 1 eq.), silver carbonate on Celite 50 wt. % (2 eq.) and $FeCl_3$ on Celite 50 wt. % (0.05 eq.) [In the case of methoxy derivatives

the use of $FeCl_3$ produces decomposition of the corresponding indole, so Cerium ammonium nitrate (0.05 eq.) was used.] were added to the same grinding jar. Once again, the vessel was fitted into the planetary mill and it was set at a frequency of 650 rpm for 1 more hour. Then, the reaction vessel was cleansed with ethyl acetate and the suspension obtained was filtered to remove the silver carbonate. The organic layer was washed with water (6 mL), dried over anhydrous sodium sulphate and the solvent was removed under reduced pressure. The compounds were purified by column chromatography, using oxalic acid precoated silica gel silica gel as stationary phase and eluting with a petroleum ether-ethyl acetate mixture or by precipitation in different solvent mixtures.

2,5-Dibromo-3-(2-methyl-1H-indol-3-yl)-6-(5-nitro-1H-indol-3-yl) cyclohexa-2,5-diene-1,4-dione (28a)

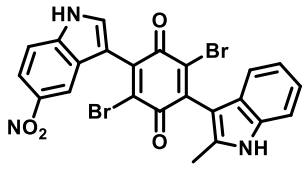

Prepared from 2,5-dibromobenzoquinone (0.060 g, 0.23), 5-nitro-1*H*-indole (0.037 g, 0.23 mmol) and 2-methyl-1*H*-indole (0.030 g, 0.23 mmol); the compound was purified by flash chromatography through a silica gel column using hexane: ethyl acetate as the mobile phase to give the desired product as a purple solid. Yield: 0.089 g,70 %

Mp 136-138 °C.

IR (neat) 3374 (NH), 1664 (C=O), 741 (Br) cm^{-1}.

^{1}H NMR (250 MHz, d_6-acetone): δ 11.53 (s, 1H), 10.62 (s, 1H), 8.53 (d, *J* = 2.2 Hz, 1H), 8.13 (dd, *J* = 9.0, 2.2 Hz, 1H), 7.98 (d, *J* = 1.7 Hz, 1H), 7.75 (d, *J* = 9.0 Hz, 1H), 7.39 (d, *J* = 7.3 Hz, 1H), 7.32 (d, *J* = 7.3Hz, 1H), 7.10 (td, *J* = 7.5, 1.5 Hz, 1H), 7.03 (td, *J* = 7.5, 1.5 Hz, 1H) ppm.

^{13}C NMR (63 MHz, d_6-acetone): δ 178.5, 178.1, 144.5, 143.3, 142.4, 140.6, 137.8, 137.2, 136.9, 133.7, 128.5, 126.6, 122.4, 121.05, 120.8, 119.5, 118.5, 113.8, 112.6, 112.1, 108.9, 14.1 ppm.

Elemental analysis (%): calcd. for $C_{23}H_{13}Br_2N_3O_4$: C 49.76, H 2.36, N 7.57; found: C 49.46, H 3.18, N 6.92

2,5-Dibromo-3-(5-bromo-1H-indol-3-yl)-6-(1H-indol-3-yl) cyclohexa-2,5-diene-1,4-dione (28b)

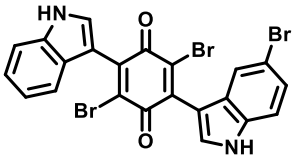

Prepared from 2,5-dibromobenzoquinone (0.060 g, 0.23 mmol),1*H*-indole (0.027 g, 0.23 mmol) and 5-bromo-1*H*-indole (0.045 g, 0.23 mmol); the compound was purified by flash chromatography through a silica gel column using hexane: ethyl acetate as the mobile phase to give the desired product as a purple solid. Yield: 0.053 g, 40 %

Mp >250 °C.

IR (neat) 3384 (NH), 1661 (C=O), 746 (Br) cm^{-1}.

^{1}H NMR (250 MHz, d_6-acetone): δ 11.21 (s, 1H), 11.06 (s, 1H), 7.80 (d, *J* = 2.8 Hz, 1H), 7.77 (d, *J* = 2.8 Hz, 1H), 7.70 (d, *J* = 1.9 Hz, 1H), 7.56 – 7.45 (m, 3H), 7.32 (dd, *J* = 8.6, 1.9 Hz, 1H), 7.24 – 7.17 (m, 1H), 7.16 – 7.09 (m, 1H) ppm.

^{13}C NMR (63 MHz, d_6-acetone): δ 178.2, 178.1, 143.2, 142.6, 137.2, 135.8, 134.1, 133.1, 131.7, 130.6, 128.4, 126.6, 125.5, 124.7, 122.8, 122.5, 120.7, 114.7, 113.7, 112.8, 109.8, 109.5 ppm.

Elemental analysis (%): calcd. for $C_{22}H_{11}Br_3N_2O_2$: C 45.95, H 1.93, N 4.87; found: C 45.25, H 1.42, N 4.54.

2,5-Dibromo-3-(1H-indol-3-yl)-6-(2-methyl-1H-indol-3-yl) cyclohexa-2,5-diene-1,4-dione (28c)

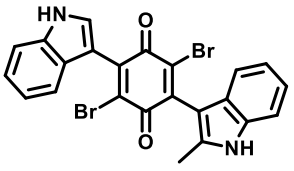

Prepared from 2,5-dibromobenzoquinone (0.060 g, 0.23 mmol),1*H*-indole (0.027 g, 0.23 mmol) and 2-methyl-1*H*-indole (0.030 g, 0.23 mmol); the compound was purified by precipitation in hexane to give the desired product as a purple solid. Yield: 0.097 g, 83 %

Mp 117-119 °C.

IR (neat) 3366 (NH), 1658 (C=O), 731 (Br) cm^{-1}.

^{1}H NMR (250 MHz, d_6-acetone): δ 11.02 (s, 1H), 10.64 (s, 1H), 7.76 (s, 1H), 7.52 (app. t, *J* = 8.0 Hz, 2H), 7.42 – 7.32 (m, 2H), 7.17 (m, 2H), 7.10 – 6.99 (m, 2H), 2.41 (s, 3H) ppm.

^{13}C NMR (63 MHz, d_6-acetone): δ 178.3, 177.7, 143.8, 143.1, 137.3, 137.1, 136.6, 136.3, 133.4, 130.6, 128.1, 126.5, 122.7, 122.4, 121.9, 120.7, 120.6, 120.3, 112.8, 111.7, 109.7, 108.4, 13.7 ppm.

Elemental analysis (%): calcd. for $C_{23}H_{14}Br_2N_2O_2$: C 54.15, H 2.77, N 5.49; found: C 54.10, H 2.62, N 5.41.

2,5-Dibromo-3-(1H-indol-3-yl)-6-(5-methoxy-1H-indol-3-yl) cyclohexa-2,5-diene-1,4-dione (28d)

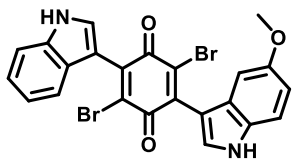

Prepared from 2,5-dibromobenzoquinone (0.060 g, 0.23 mmol),1*H*-indole (0.027 g, 0.23 mmol), 5-methoxy-1*H*-indole (0.034 g, 0.23 mmol) and cerium ammonium nitrate (0.05 eq) instead of $FeCl_3$ on Celite 50 wt. %.; the compound was purified by flash chromatography through a silica gel column using hexane: ethyl acetate as the mobile phase to give the desired product as a purple solid. Yield: 0.097 g, 80 %

Mp 225-227 °C.

IR (neat) 3317 (NH), 1652 (C=O), 741 (Br) cm^{-1}.

^{1}H NMR (250 MHz, d_6-DMSO): δ 11.85 (s, 1H), 11.73 (s, 1H), 7.71 (d, *J* = 2.7 Hz, 1H), 7.65 (d, *J* = 2.7 Hz, 1H), 7.49 (d, *J* = 8.0 Hz, 1H), 7.42 (d, *J* = 8 Hz, 1H), 7.38 (d, *J* = 8.8 Hz, 1H), 7.17 (t, *J* = 7.0 Hz, 1H), 7.09 (t, *J* = 7.0 Hz, 1H), 6.91 (d, *J* = 2.2 Hz, 1H), 6.82 (dd, *J* = 8.8, 2.4 Hz, 1H), 3.74 (s, 3H) ppm.

^{13}C NMR (63 MHz, d_6-DMSO): δ 177.4, 177.3, 153.7, 141.8, 135.9, 131.9, 131.3, 130.8, 130.7, 130.13, 125.8, 125.3, 121.7, 121.4, 119.7, 112.7, 112.1, 111.7, 108.3, 108.1, 103.6, 79.2, 55.4, 30.7 ppm.

Elemental analysis (%): calcd. for $C_{23}H_{14}Br_2N_2O_3$: C 52.50, H 2.68, N 5.32; found: C 52.40, H 2.39, N 4.82

2,5-Dibromo-3-(5-methoxy-1H-indol-3-yl)-6-(5-methoxy-2-methyl-1H-indol-3-yl)cyclohexa-2,5-diene-1,4-dione (28e)

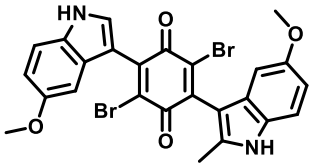

Prepared from 2,5-dibromobenzoquinone (0.060 g, 0.23 mmol), 5-methoxy-1*H*-indole (0.034 g, 0.23 mmol),2-methyl-5-methoxy-1*H*-indole (0.037 g, 0.23 mmol) and cerium ammonium nitrate (0.05 eq) instead of $FeCl_3$ on Celite 50 wt. %.; the compound was purified by flash chromatography through a silica gel column using hexane: ethyl acetate as the mobile phase to give the desired product as a purple solid. Yield: 0.072 g, 55 %

Mp 250 °C.

IR (neat) 3360 (NH), 1659 (C=O), 745 (Br) cm^{-1}.

^{1}H NMR (250 MHz, *d_6*-acetone): δ 10.92 (s, 1H), 10.50 (s, 1H), 7.71 (d, *J* = 2.9 Hz, 1 H), 7.43 (d, *J* = 8.8 Hz, 2H), 7.27 (d, *J* = 8.8 Hz, 1H), 6.97 (d, *J* = 2.4 Hz, 1H), 6.85 (m, 2H), 6.75 (dd, *J* = 8.8, 2.4 Hz, 2H), 3.78 (s, 3H), 3.73 (s, 3H), 2.38 (s, 3H) ppm.

^{13}C NMR (63 MHz, *d_6*-acetone): δ 206.3, 178.5, 155.4, 155.2, 143.9, 143.1, 137.9, 136.0, 132.8, 132.1, 131.6, 131.3, 128.6, 127.0, 113.4, 112.9, 112.3, 111.6, 109.6, 108.4, 104.7, 103.3, 55.9, 55.9, 13.7 ppm.

Elemental analysis (%): calcd. for $C_{25}H_{18}Br_2N_2O_4$: C 52.66, H 3.18, N 4.91; found: C 53.85, H 3.95, N 5.05

2,5-Dibromo-3-(5-methoxy-1H-indol-3-yl)-6-(2-methyl-1H-indol-3-yl) cyclohexa-2,5-diene-1,4-dione (28f)

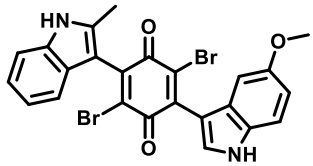

Prepared from 2,5-dibromobenzoquinone (0.060 g, 0.23 mmol), 2-methyl-1*H*-indole (0.030 g, 0.23 mmol), 5-methoxy-1*H*-indole (0.034 g, 0.23 mmol) and cerium ammonium nitrate (0.05 eq.) instead of $FeCl_3$ on Celite 50 wt. %.; the compound was purified by precipitation in hexane to give the desired product as a purple solid. Yield: 0.088 g, 71 %

Mp 168-170 °C.

IR (neat) 3362 (NH), 1656 (C=O), 730 (Br) cm^{-1}.

^{1}H NMR (250 MHz, *d_6*-acetone): δ 10.90 (s, 1H), 10.62 (s, 1H), 7.71 (d, *J* = 2.9 Hz, 1H), 7.43 (d, *J* = 8.8 Hz, 1H), 7.38 (dd, *J* = 7.2, 12 Hz, 2H), 7.31 (d, *J* = 7.1 Hz, 1H), 7.12 – 7.07 (m, 1H), 7.04 (dd, *J* = 7.6, 1.2 Hz, 2H), 6.99 (d, *J* = 2.4 Hz, 2H), 6.86 (dd, *J* = 8.8, 2.4 Hz, 1H), 3.78 (s, 3H), 2.41 (s, 3H) ppm.

^{13}C NMR (63 MHz, *d_6*-acetone): δ 178.5, 177.7, 15546, 143.9, 143.1, 137.3, 136.7, 136.4, 132.83, 132.1, 131.2, 128.1, 127.1, 121.9, 120.6, 120.4, 113.4, 112.9, 111.7, 109.6, 108.5, 104.68, 55.8, 13.7 ppm.

Elemental analysis (%): calcd for $C_{24}H_{16}Br_2N_2O_3$: C 53.36, H 2.99, N 5.19; found: C 52.46, H 3.55, N 5.36

2,5-Dibromo-3-(5-bromo-1H-indol-3-yl)-6-(5-methoxy-1H-indol-3-yl) cyclohexa-2,5-diene-1,4-dione (28g)

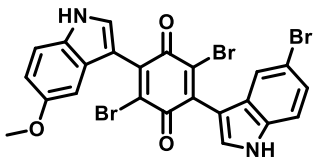

Prepared from 2,5-dibromobenzoquinone (0.060 g, 0.23 mmol), 5-bromo-1*H*-indole (0.045 g, 0.23 mmol), 5-

methoxy-1*H*-indole (0.034 g, 0.23 mmol) and cerium ammonium nitrate (0.05 eq) instead of $FeCl_3$ on Celite 50 wt. %.; the compound was purified by flash chromatography through a silica gel column using hexane: ethyl acetate as the mobile phase to give the desired product as a purple solid. Yield: 0.090 g, 65%

Mp >250 °C.

IR (neat) 3338 (NH), 1649 (C=O), 745 (Br) cm^{-1}.

^{1}H NMR (250 MHz, d_6-acetone): δ 11.17 (s, 1H), 10.91 (s, 1H), 7.80 (d, *J* = 2.8 Hz, 1H), 7.72 (d, *J* = 2.8 Hz, 1H), 7.69 (d, *J* = 1.8 Hz, 1H), 7.52 (d, *J* = 8.7 Hz, 1H), 7.43 (d, *J* = 8.7 Hz, 1H), 7.31 (dd, *J* = 8.7, 1.9 Hz, 1H), 6.98 (d, *J* = 2.4 Hz, 1H), 6.85 (dd, *J* = 8.7, 2.4 Hz, 1H), 3.78 (s, 3H) ppm.

^{13}C NMR (63 MHz, d_6-acetone): δ 178.4, 178.0, 155.4, 143.2, 142.5, 135.8, 134.1, 132.4, 132.1, 131.7, 131.2, 128.4, 127.1, 125.5, 124.7, 114.7, 113.7, 113.5, 113., 109.63, 109.5, 104.6, 55.8 ppm.

Elemental analysis (%): calcd for $C_{23}H_{13}Br_3N_2O_3$: C 45.66, H 2.17, N 4.63; found: C 46.57, H 2.77, N 4.49.

CHAPTER 7. MULTITARGET ANTI-TUBERCULOSIS AGENTS BEARING PYRROLE-ISONIAZID FRAGMENTS

7.1. Drug combinations *vs.* Multitarget Directed Ligands in Tuberculosis

As previously mentioned, the current pharmacological treatments of tuberculosis are based on combinations of the available drugs. Tuberculosis treatment started in 1944 with the discovery of streptomycin (SM) and para-aminosalicylic acid (PAS). It was in 1950 when the first clinical trial comparing their efficacy as monotherapy or combination demonstrated that combined therapies were more effective and resulted in the first multidrug antitubercular treatment. Isoniazid (INH) appeared in 1952, and it was soon added to this previous combination, shortening the duration of treatments, but still 18 to 24 months of administration were needed. In the '60s, ethambutol (EMB) replaced PAS, shortening the treatment to 18 months, while in the '70s the addition of rifampicin (RIF) allowed the physicians to shorten the treatment to just 9 months. Finally, in 1980, the introduction of pyrazinamide (PZA) reduced the treatments to six months. **(Figure 7.1)** There are three main reasons that explain why combination therapies are more effective than monotherapies in TB. The first one is that treatment of TB with just one drug results in the selection of drug-resistant bacilli and fails to eliminate the disease. The second one is that different populations of bacilli, with different drug susceptibilities may coexist in the same patient, and the third one is that by inhibiting different biochemical pathways of the bacteria a synergic effect can be elicited. Although during the last decades of the twentieth century important improvements in the treatment of TB were achieved, it is worth nothing that for the last 40 years no antitubercular drug with a novel mechanism of action has been approved.

Moreover, soon after soon after the introduction of the first antimycobacterial drugs, drug resistant strains started to emerge. During the first decades the launch of combination therapies and more effective drugs seemed to control the disease, and indeed it was thought that TB could be eradicated by the end of the 20th century. However, in the '80s tuberculosis re-emerged and the rate of appearance of MDR-TB and XDR-TB increased, showing that the currently available treatments are not enough to control the disease.[194]

[194] Almeida de Silva, P.; Ainsa, J. A. *Tuberculosis 2007. From basic science to patient care*, first edition, **2007.**

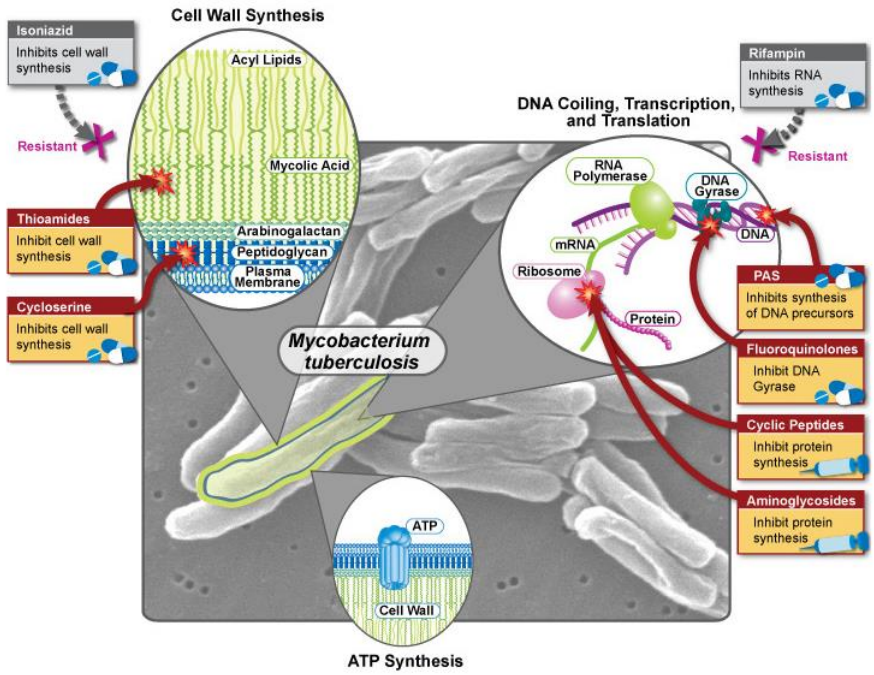

Figure 7.1: Mechanism of action of the currently available antitubercular treatments.

As mentioned in the Introduction, the current therapies present several drawbacks including the long treatments, which compromise the adherence to the therapy of the patients, the toxicities associated to this long term drug exposition, the frequently found drug-drug interactions and the increasing appearance of MDR and XDR strains. [53]

To fight against these drawbacks, an ideal new antitubercular agent should possess:[195]

- Adequate ADME properties and good pharmacokinetics so it can be orally administered.
- Long half-life, so the frequency can be reduced to a single dose per day preferentially.
- Novel mechanism of action, to ensure effectiveness against resistant strains.
- Availability at relatively low cost in order to be accessible to patients in low-income countries.
- Admit co-administration with other therapies such as anti-HIV.
- Lower toxicities.

[195] Koul, A.; Arnoult, E.; Lounis, N.; Guillemont, J.; Andries, K. *Nature* **2011**,*469*, 483.

- Ability to shorten treatment, with strong bactericidal activity to kill the active TB and good activity on latent populations

In this context, it seems that a good approach to achieve all these goals is the design of multitarget-directed ligands (MTDLs) as antitubercular agents.[64] With MTDLs several targets can be inhibited at the same time, obtaining a synergic effect. Moreover, as tubercular drug resistance is chromosomally encoded, agents directed against several targets are likely to be effective against drug-resistant strains. Thus, if two different pharmacophores are combined in a single molecule, one of them based on a well-known antitubercular drug while the other inhibits a new target, the new drug would be potentially active against sensible and resistant strains, hence solving the problem of having different strains in one patient.

Although several formulations which contain some of the drug combinations needed in one single dose are commercially available, facilitating patient's adherence to treatment and supervision of therapy. Nevertheless, the possibility of having one single chemical entity able to perform several activities would avoid drug-drug interactions, simplify the formulation processes, the pharmacokinetic profiles, the clinical trials and of course the patient's adherence.

During the past years several authors have disclosed some examples of hybrid structures as antitubercular agents, showing promising results.[196, 197, 198, 199, 200, 201, 202, 203] Even though most of these examples showed encouraging results, few of them were conceived through a rational design, and moreover most of their mechanism of actions remain still unknow.

[196] Bijev, A. *Arzneimittelforschung* **2009**, *59*, 34.
[197] Shaveta, S. M.; Singh. S. *Eur. J. Med. Chem.* **2016**, *124,* 500.
[198] Yan, M.; Xu, L.; Wang, Y.; Wan, J.; Liu, T.; Liu, W.; Wan, Y.; Zhang, B.; Wang, R.; Li, Q. *Drug Dev. Res.* **2020**, doi: 10.1002/ddr.21638.
[199] Hu, Y. Q.; Zhang, S.; Zhao, F.; Gao, C.; Feng, L.; Lv, Z.; Xu, Z.; Wu, X.*Eur. J. Med. Chem.* **2017***, 133,* 255.
[200] Stewart, G. R., Robertson, B. D.; Young, D. B. *Nat. Rev. Microbiol.* **2003,** *1*, 97.
[201] Sirim, M. M.; Krishna, V. S.; Sriram, D.; Unsal Tan, O. *Eur. J. Med. Chem.* **2020***, 188,* 112010.
[202] Gao, F.; Ye, L.; Wang, Y.; Kong, F.; Zhao, S.; Xiao, J.; Huang, G. *Eur. J. Med. Chem.* **2019***, 183,* 111678.
[203] Shah, S. R.; Katariya, K. D. *J. Heterocycl. Chem.* **2020**, doi:10.1002/jhet.3893.

7.2. MmpL3 (*Mycobacterium* membrane protein Large 3) as an anti-TB target

During the past years several efforts have been done in order to identify new targets for TB. To achieve this goal, libraries of compounds have been phenotypically screened in whole cells. Once the initial hits were obtained, efforts were made to find their targets by mutant generation coupled to whole genome sequencing. As the whole genome of *Mycobacterium tuberculosis* is known, it is assumed that by comparing the genomes of hit-resistant strains to the wild type the mutations found would correspond to their main target. This way, several targets as AtpE, DprE1 or MmpL3, have been identified.[204]

MmpL3 is a membrane protein belonging to the MDR RND family (resistance nodulation division). This superfamily is a group of transmembrane proteins that mediate the transport of several compounds, which include positively charged, negatively charged and neutral compounds, including drugs, fatty acids or salts. This activity is driven by the proton motive force (PMF).[205]

Mycobacteria contain 13 RND proteins known as Mycobacterial membrane protein large (MmpL), which usually possess 12 transmembrane domains and two extra cytoplasmic loops. MmpL3, 4, 5, 7, 8, 10, and 11 have been reported to participate in the biosynthesis of the complex cell envelope of mycobacteria, while MmpL5 and MmpL7 can actively efflux anti-tubercular drugs. MmpL3 is the only protein of this family essential for Mtb viability and replication. Indeed, downregulation of MmpL3 expression prevents cell division and leads to rapid cell death.[206,207]

Two essential activities have been so far attributed to MmpL3. On one hand, it has been proved that MmpL3 is involved in the *Mycobacterium* cell wall formation. Mycolic acids are key components of the mycobacterial outer membrane. Mycolic acids are synthetized inside cells from fatty acids, and then they are conjugated with a trehalose molecule in order to form trehalose monomycolate (TMM). In this form, they are

[204] Goldman, R. C. *Tuberculosis*, **2013**, 93, 569.
[205] Székely, R.; Cole, T. Molecular Microbiology, **2016**, *99*, 831.
[206] Domenech, P.; Reed, M.B.; Barry, C.E. *Infect. Immun*. **2005***, 73,* 3492.
[207] Degiacomi, G.; Benjak, A.; Madacki, J.; Boldrin, F.; Provvedi, R.; Palu, G.; Kor- dulakova, J.; Cole, S.T.; Manganelli, R. *Sci. Rep*. **2017***, 7,* 43495.

transported through the inner membrane thanks to MmpL3. Once in the periplasmic space, micolyltransferases transfer the TMM chain onto a molecule of arabinogalactan, yielding wall-bound mycolates, or to another TMM molecule forming a trehalose dimycolate (TDM). These molecules give the bacterial envelope its characteristic thick, waxy, and difficult-to-permeate consistence. [208] **(Figure 7.2)**

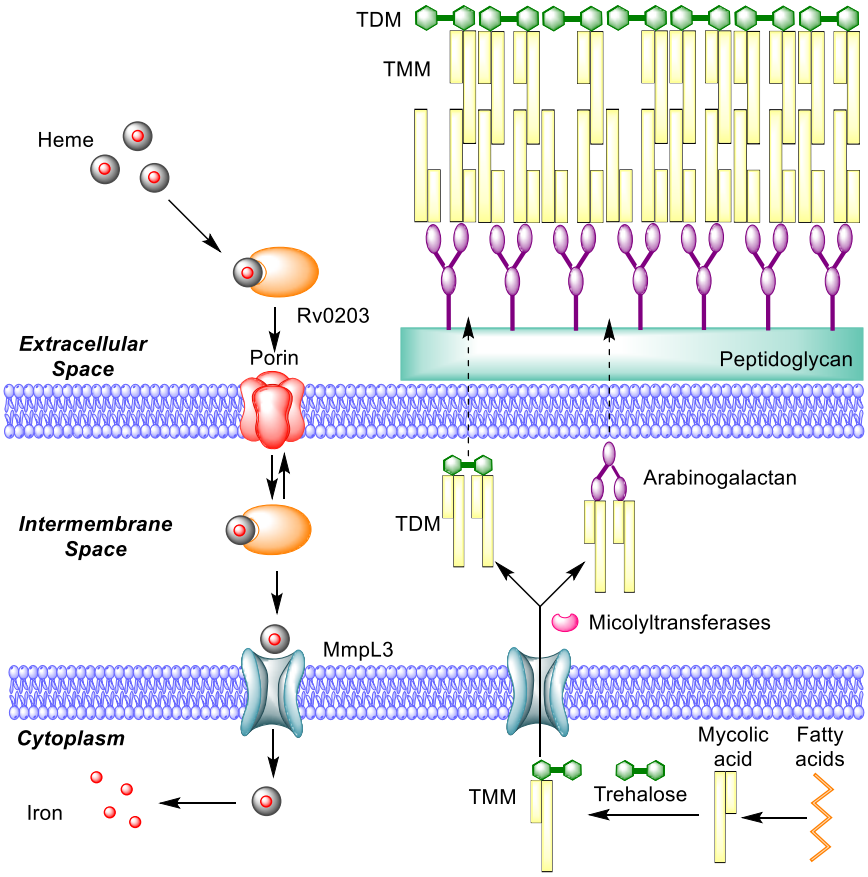

Figure 7.2: MmpL3 functions.

On the other hand, *Mycobacteria*, like most organisms, require iron for many vital functions. During infection, iron acquisition is challenging for pathogenic bacteria, because usually iron cations are bound to host iron-binding proteins in charge of its storage or transport; thus, in vertebrates two thirds of iron is incorporated into the heme group. For this reason, bacteria need to develop heme acquisition systems. Mtb secretes some hemophore proteins such as Rv0203, which is able to acquire heme from haemoglobin, allowing its transport through the inner membrane mediated by MmpL11

[208] Zhang, B.; Li, J.; Yang, X.; Guddat, L. W.; Yang, H.; Rao, Z. *Cell* **2019**, *176*, 636.

or MmpL3. Once inside the bacteria, heme can be degraded to release iron or be used whole for the synthesis of heme-containing proteins.[209] **(Figure 7.2)**

During the last years several compounds with apparently very different structures, haven been identified as MmpL3 inhibitors. These inhibitors include 1,2-ethylenediamine, [210] the 1,5-diarylpyrrole derivative BM212 [211] and its analogues, including the repurposed inverse agonist for the cannabinoid receptor CB_1 rimonabant, derivatives of the tetrahydropyrazolo[1,5-*a*]pyrimidine-3-carboxamide framework (THPPs), [212 , 213] indole-2-carboxamides (e.g. NITD-304 and NITD-349) [214 , 215] and adamantyl ureas (AUs), such as SQ109 and AU1235.[216] **(Figure 7.3)**

Understanding the mechanism of action of MmpL3 inhibitors is critical for their optimization process. Due to the diversity of the chemical scaffolds and differences in their activities, several authors wondered how all these widely heterogeneous compounds were all able to inhibit MmpL3. In answer to this question, several theories have been proposed.

---

[209] Fang, Z.; Leigh Sampson, S.; Warren. R. M. *Tuberculosis* **2015**, *95*, 123.

[210] Protopopova, M.; Hanrahan, C.; Nikonenko, B.; Samala, R.; Chen, P.; Gearhart, J.; Einck, L.; Nacy, C.A. *J. Antimicrob. Chemother.* **2005,** *56,* 968.

[211] La Rosa, V.; Poce, G.; Canseco, J. O.; Buroni, S.; Pasca, MR.; Biava, M.; Raju, RM.; Porretta, GC.; Alfonso, S.; Battilocchio, C.; Javid, B.; Sorrentino, F.; Ioerger, T.R.; Sacchettini, J.C.; Manetti, F.; Botta, M.; De Logu, A.; Rubin, E.J.; De Rossi, E. *Antimicrob. Agents Chemother.* **2012**, *56*, 324.

[212] Remuiñán, M. J.; Pérez-Herrán, E.; Rullás, J.; Alemparte, C.; Martínez-Hoyos, M.; Dow, D.J.; Afari, J.; Mehta, N.; Esquivias, J.; Jiménez, E.; Ortega-Muro, F.; Fraile-Gabaldón, MT.; Spivey, V. L.; Loman, N. J.; Pallen, M. J.; Constantinidou, C.; Minick, D. J.; Cacho, M.; Rebollo-López, M. J.; González, C.; Sousa, V.; Angulo-Barturen, I.; Mendoza-Losana, A.; Barros, D.; Besra, G. S.; Ballell, L.; Cammack, N. *PLoS One,* **2013**, *8*, e60933.

[213] Ioerger, T.R.; O'Malley, T.; Liao, R.; Guinn, K.M.; Hickey, M.J.; Mohaideen, N.; Murphy, K C.; Boshoff. H.I.; Mizrahi, V.; Rubin, E.J.; Sassetti, C.M.; Barry, C.E.; Sherman, D.R.; Parish, T.; Sacchettini, C. *PLoS One*. **2013**, *8*, e75245.

[214] Onajole, O.K.; Pieroni, M.; Tipparaju, SK.; Lun, S.; Stec, J.; Chen, G.; Gunose-Woyo, H.; Guo, H.; Ammerman, N.C.; Bishai, W.R.; Kozikowski, A.P. *J. Med. Chem.* **2013***, 56,* 4093.

[215] Rao SP.; Lakshminarayana SB.; Kondreddi RR.; Herve M.; Camacho LR.; Bifani P.; Kalapala SK.; Jiricek J.; Ma, N.L.; Tan, B.H.; Ng, S.H.; Nanjundappa, M.; Ravindran, S.; Seah, P.G.; Thayalan, P.; Lim, S.H.; Lee, B.H.; Goh, A.; Barnes, W.S.; Chen, Z.; Gagaring, K.; Chatterjee, A.K.; Pethe, K.; Kuhen, K.; Walker, J.; Feng, G.; Babu, S.; Zhang, L.; Blasco, F.; Beer, D.; Weaver, M.; Dartois, V.; Glynne, R.; Dick, T.; Smith, P.W.; Diagana, T,T.; Manjunatha, U.H. *Sci. Transl. Med.* **2013**, *5,* 214.

[216] Grzegorzewicz, A.E.; Pham, H.; Gundi, V.A.; Scherman, M.S.; North, E.J.; Hess T.; Jones, V.; Gruppo, V.; Born, S.E.; Korduláková, J.; Chavadi, S.S.; Morisseau, C.; Lenaerts, A.J.;Lee, R.E.; McNeil, M.R.; Jackson, M.; *Nat. Chem. Biol.* **2012**, *8*, 334.

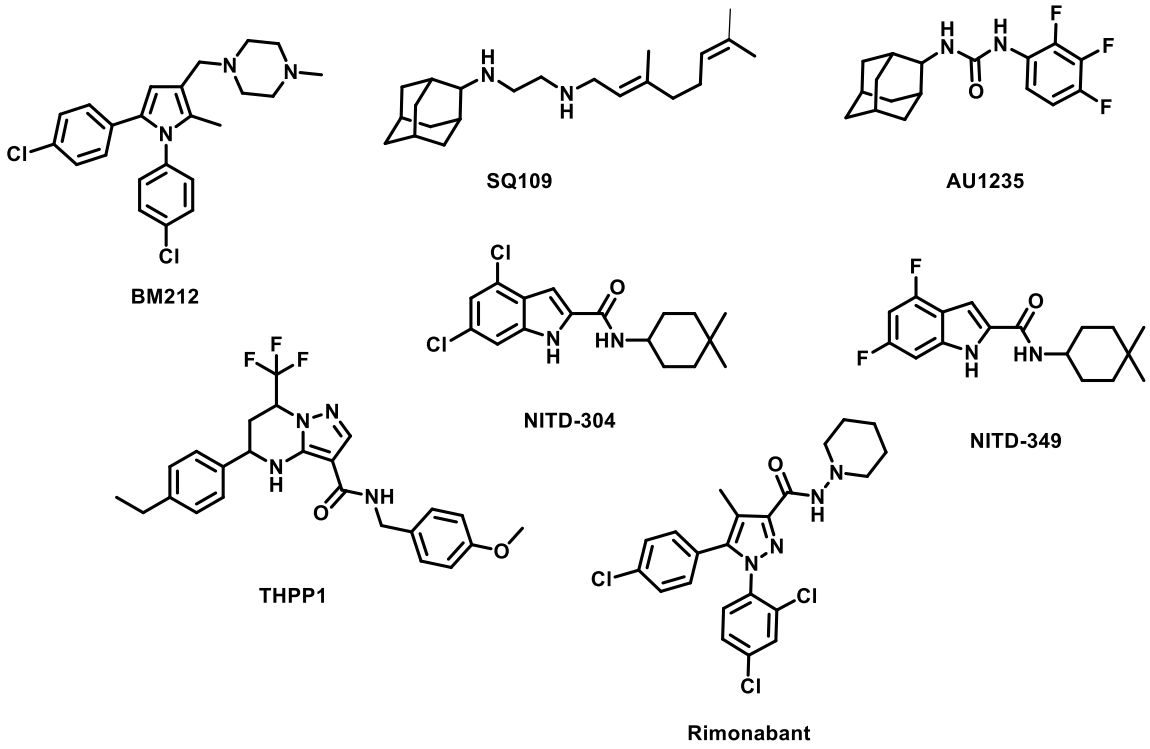

Figure 7.3.

Some studies revealed that SQ109 inhibits enzymes involved in menaquinone synthesis, respiration, and, consequently ATP synthesis; moreover, this compound acts as an uncoupler of the proton gradient that is established during the normal activity of electron carriers in the electron transport chain, collapsing the proton motive force (PMF), arising from the Δψ and ΔpH contributions, where Δψ is the membrane potential and ΔpH is the pH gradient.[217] Later, Wei Li and coworkers proved that BM212, indolecarboxamides, AUs, and THPPs, also abolish PMF-driven translocation processes through the dissipation of the transmembrane electrochemical proton gradient (ΔpH) or membrane potential (Δψ) or both components of the PMF.[218] While these authors propose an indirect inhibition mechanism, some others have proved MmpL3 direct inhibition.

[217] Li, K.; Schurig-Briccio, L.A.; Feng, X.; Upadhyay, A.; Pujari, V.; Lechartier, B.; Fontes, F.; Yang ,H.; Rao, G.; Zhu, W.; Gulati, A.; No, J.H.; Cintra, G.; Bogue, S.; Liu, Y.L.; Molohon, K.; Orlean, P.; Mitchell, D.A.; Freitas-Junior, L.; Ren, F.; Sun, H.; Jiang T.; Li, Y.; Guo, R.T.; Cole, S T.; Gennis, R.B.; Crick, D.C.; Oldfield, E. *J. Med. Chem.* **2014,** *57*, 3126.

[218] Li, W.; Upadhyay, A.; Fontes, F. L.; North, E. J.; Wang, Y.; Crans, D. C.; Grzegorzewicz, A. E; Jones, V.; Franzblau, S. G; Lee, R. E; Crick, D. C *Antimicrob. Agents Chemother.* **2014***, 58,* 6413.

In 2017, Zhujun Xu and co-workers proved that [^{14}C]-labelled BM212 bound directly to the purified MmpL3 protein from *Mycobacterium smegmatis*.[219] After this finding, Wei Li and co-workers reported in 2019 an *in vitro* whole cell method for the identification of direct MmpL3 inhibitors, moreover, they were able to prove that most of the described compounds inhibit MmpL3 by targeting the protein in a direct manner, even if its also true that some of them also exert an indirect inhibition by altering the PMF. Furthermore, they found that the expression of Mtb MmpL3 conditional knock-down, leads to a dramatic increase in $\Delta\psi$, suggesting that the alteration in $\Delta\psi$ can be either a cause or a consequence of MmpL3 inhibition.[220] Finally, also in 2019, Bing Zhang and colleagues determined the crystal structure *of Mycobacterium smegmatis* MmpL3, in the presence and absences of four different inhibitors, validating the direct binding mode of different families of inhibitors in the same site within the proton translocation channel of the transporter and providing a structural vision of MmpL3 inhibition.[221] Moreover, their crystal structure provides some basis about the TMM export molecular mechanism. MmpL3 is a transmembrane protein, whose periplasmic domain is composed of two subdomains, PN and PC. **(Figure 7.4.A)** These domains interact creating a central cavity, with three openings, GT (top), GF (front) and GB (back). **(Figure 7.4.A)** The transmembrane region of MmpL3 contains 12 transmembrane α helices (TMHs) and two extra α helices attached to the cytoplasmic membrane. The central core of the transmembrane domain is formed by TMH IV and TMH X, where two pairs of hydrophilic residues (Asp256-Tyr646 and Asp645-Tyr257) are located. These residues link the two helices by hydrogen bonds formed between their side chains. **(Figure 7.4.B)** These Asp-Tyr pairs are highly conserved residues among the MmpL family of transporters. Furthermore, their location is quite similar to the one found in other families of transporter, in which they are known to be involved in a proton-relay pathway. In addition, it has been proved that mutations in MmpL3 Asp-Tyr pairs compromise the growth of mycobacterial cultures, in agreement with them playing an important role in proton translocation.[221,221]

[219] Xu, Z.; Meshcheryakov, V. A.; Poce, G.; Chang, S. S. *Proc. Natl. Acad. Sci.* **2017,** *114*, 7993.
[220] Li, W.; Stevens, Casey, M.; Pandya, A. N.; Darzynkiewicz, Z.; Bhattarai, P.; Tong, W.; Gonzalez-Juarrero, M.; Weiwei, T.; North, E. J.; Zgurskaya, H. I.; Jackson, M. *ACS Infect. Dis.* **2019**, *5*, 1001.
[221] Zhang, B.; Li, Jun;Yang, X.; Guddat, L. W.; Yang, H.; Rao, Z. *Cell* **2019**, *176*, 636.

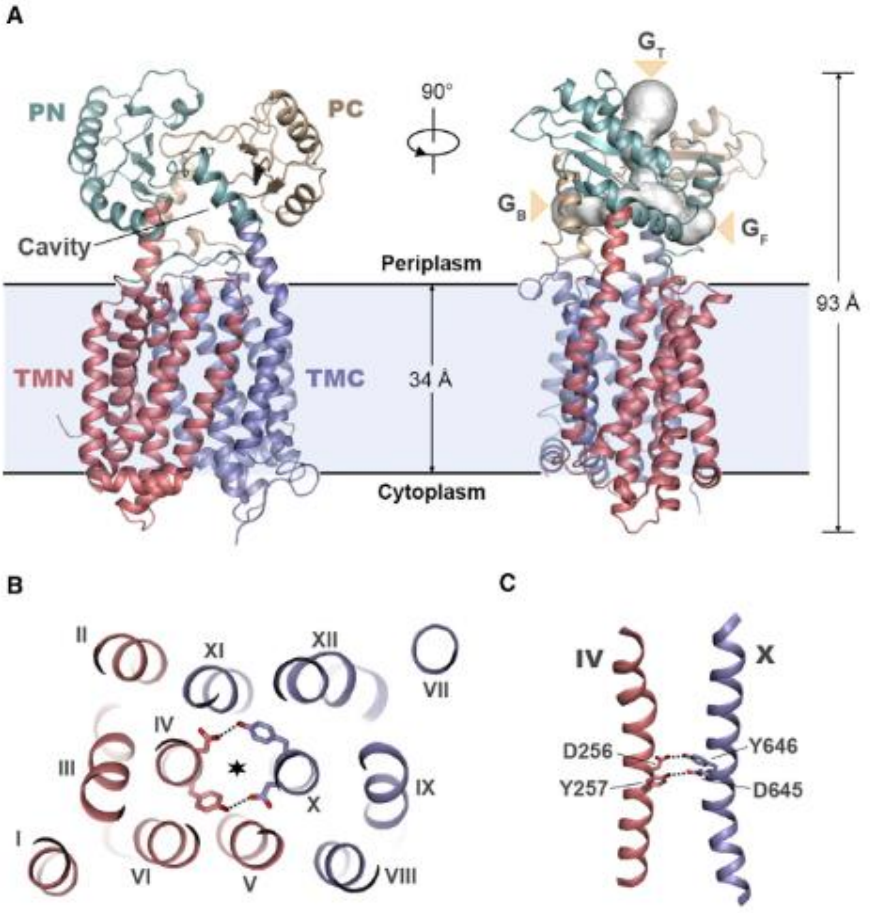

Figure 7.4. Reproduced with permission of reference[221].

Regarding the MmpL3 mechanism, the authors proposed two plausible pathways for substrate entry into the transporter. **(Figure 7.5)** They suggest that substrates located in the inner side of the membrane could be transported across the membrane through the transmembrane channel at the periphery of transmembrane domain. Alternatively, TMM located in the outer side of the membrane could be transport through the GF that opens into the periplasm. GT is proposed as the TMM exit, since it does not appear to form strong interactions with the trehalose, making it convenient for substrate release. It is unknown whether this flipping and release mechanism is coupled or not and it seems clear that these events are driven by the PMF, in which the Asp-Tyr pairs play a key role.

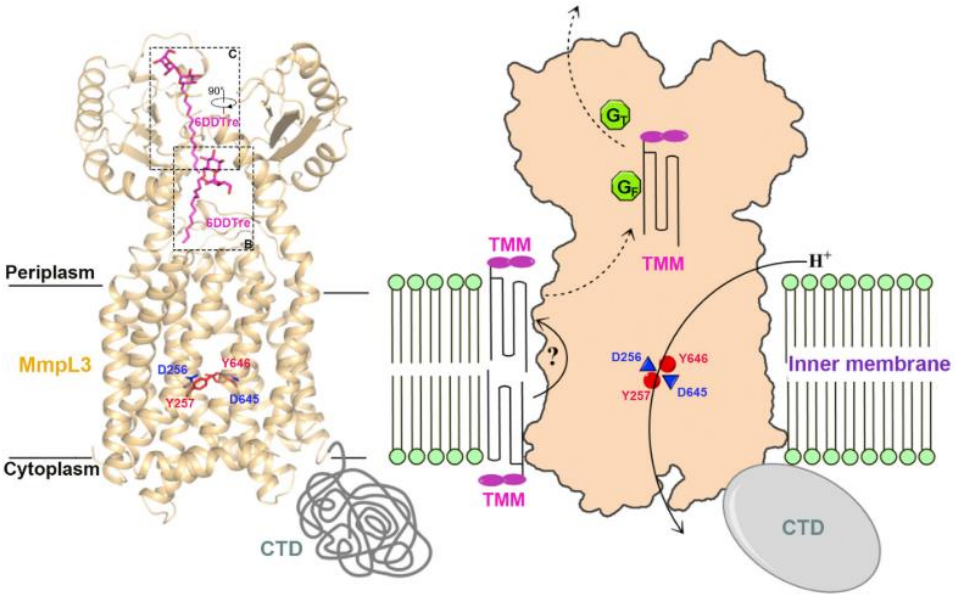

Figure 7.5. Reproduced with permission of reference[221].

In this context, MmpL3 has emerged as an attractive therapeutic target to develop new antitubercular agents, owing to its essentiality to Mtb. In the past few years the scientific community has done a big effort in order to elucidate its biological implication in mycobacterial physiology. Finally, the inhibition mechanism of the most importer inhibitors reported has been elucidated. In addition, many of the reported inhibitors have demonstrated efficacy in animal models, and the most advanced one, SQ109, has shown promising results in Phase 2b-3 clinical studies[222] as an anti-TB agent, with excellent activity against all forms of Mtb, including drug-resistant clinical strains.

7.3. Isoniazid (INH)

Since its approval as an antitubercular agent, isoniazid has been used as first-line treatment for both active and latent tuberculosis. After it was launched, an extensive research on its mode of action started, but it took about 50 years to establish a general consensus. Still nowadays there are several hypotheses, even though the main mechanism is clear.

[222] World Health Organization. Global Tuberculosis Report 2018 (WHO)

This principal mode of action proposes that IHN acts as a prodrug that needs to be activated. This activation process involves an enzymatic oxidation by katG, a catalase-peroxidase expressed in Mtb. The isonicotinoyl radical formed by the action of this enzyme reacts with nicotinamide adenine dinucleotide, forming the so-called INH-NAD adduct. **(Figure 7.6)** [223,224] Due to its structural analogy with the NADH cofactor, this adduct acts as a potent inhibitor of enoyl acyl-carrier-protein reductase (InhA), an enzyme essential for mycobacteria due to its key role in the reduction of fatty acids, a step of the biosynthesis of essential components of Mtb cell wall, the mycolic acids. **(Figure 7.7)**

Some authors also propose that the isonicotinoyl radical can similarly react with NADP forming an INH-NADP adduct that inhibits dfrA-encoded dihydrofolate reductase[225] and MabA (3-oxoacyl-ACP reductase).[226]

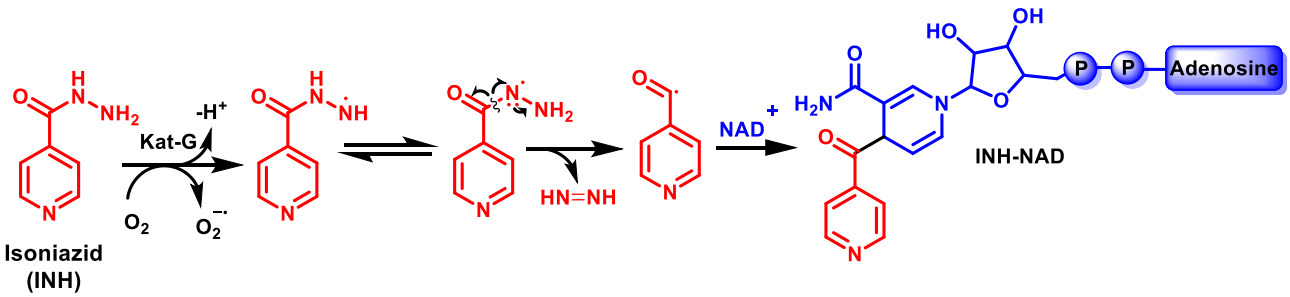

Figure 7.6: Bioactivation of isoniazid.

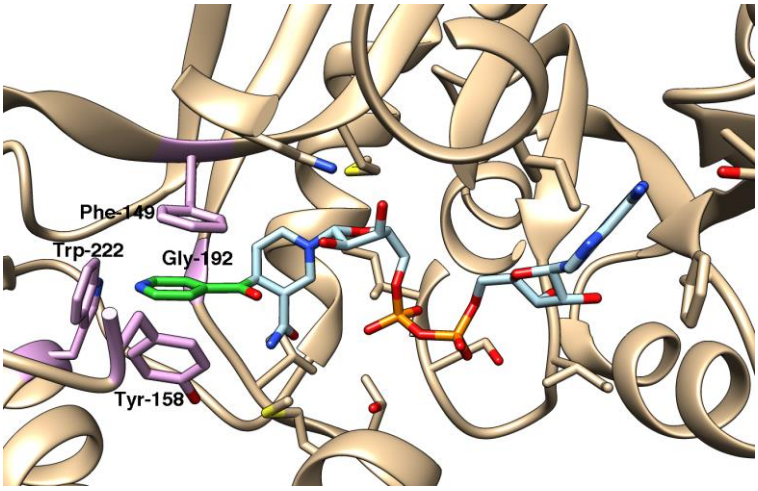

Figure 7.7: Interaction between InhA and the INH-NAD adduct, generated from 1ZID.

[223] Unissa, A. N.; Subbian, S.; Hanna, L. E.; Selvakumar, N. *Infect. Genet. Evol.* **2016**, *45,* 474.
[224] Jena, L.; Nayak, T.; Deshmukh, S.; Wankhade, G.; Waghmare, P.; Harinath, B. C. *J. Infect. Dis. Ther.* **2016**, *4,* 1000297.
[225] Argyrou, A.; Jin, L.; Siconilfi-Baez, L.; Angeletti, R.H.; Blanchard, J.S.; *Biochemistry,* **2006**, *45*, 13947.
[226] Timmins, G. S.; Deretic, V. *Mol. Microbiol.* **2006**, *62*, 1220.

Even if these are the most accepted mechanisms of action of isoniazid, during the past years some concerns have been expressed. The main one is the observation that isoniazid is active on latent Tb, a stage where Mtb does not possess a cell wall. These observations make it clear that INH must possess one or more additional mechanisms of action that remain to be identified. The main hypotheses proposed in this regard are:[227]

1. As mentioned above, INH requires a one-electron enzymatic oxidation step to be activated. Inside Mtb, katG promotes this activation, however, there are several human enzymes able to perform this kind of reactions. One of them is myeloperoxidase (MPO), which is mainly present in neutrophils, monocytes and macrophages and has been shown to activate INH. This may explain how INH is able to kill Mtb without penetrating the granuloma, since neutrophils may be able to activate and deliver the active form of INH directly in latent TB.
2. The second mechanism proposes a protective role of INH against oxidative stress-induced necrosis. During Mtb infection, the host phagocytes induce the formation of reactive species to kill bacteria; however, Mtb has efficient strategies to defend itself against these species, particularly reactive oxygen species (ROS). This way the generated ROS, not able to kill the bacteria, promote phagocytic necrosis, the main cause of granuloma degradation. This way, the INH cytoprotective effect, may strengthen the host immune defence.
3. On a third study the authors reveal the capacity of INH to induce monocytic differentiation. It is known that monocytes play a key role in killing active and latent TB. The capacity of INH to induce differentiation is quite weak, taking several weeks to increase the circulating monocytes population, and this could be a possible explanation of the long treatment times needed for INH.
4. Finally, some authors have proposed that INH acts as a nitric oxygen (NO) generator through the peroxidation cycle of katG. However, even if this mechanism may contribute to isoniazid activity, it is probably not enough to explain the activity on the latent form.

[227] Khan, S. R.; Manialawy, Y.; Siraki, A. G. *Br. J. Pharmacol.* **2019***, 176,* 4599.

7.4. Design of pyrrole-isoniazid derivatives

Several years ago, our group reported a one pot multicomponent reaction related to the Hantzsch pyrrole synthesis, which takes place under solvent-free mechanochemical conditions, using the High-Speed Vibration Milling (HSVM) technique.[228, 229] This technique allowed the efficient synthesis of pyrroles with different substitution patterns. With this capacity in our hands, and bearing in mind the analogy of the compounds accessible by this method the above-mentioned MmpL3 inhibitor BM-212,[211] we decided to explore the antitubercular activities of our pyrrole derivatives.

On the other hand, since its approval isoniazid remains as one of the first-line treatments against tuberculosis. One of the main problems associated with INH is its ability to generate resistance. Serum concentrations of INH are influenced by several factors, one of the most important of which is enzymatic acetylation by human N-acetyltransferase (NAT). During long-term treatments with INH, acetylation leads to a lower bioavailability and consequent generates INH resistance. Furthermore, polymorphisms in NAT are a source of large variability in the individual response to isoniazid, with a clear ethnic component. One strategy that can be followed is blocking acetylation by chemical modifications of the hydrazine. Moreover, increasing the lipophilicity of INH can increase its permeation into bacterial cells. Consequently, INH derivatives with greater lipophilicity and higher metabolic stability can lead into more potent anti-TB compounds.

In the last years, the concept of combining two pharmacophores to give one single molecule with several activities has been one of the hottest topics in medicinal chemistry. When it comes to TB, it seems that the development of MTDL is a perfect approach to overcome the increasing resistance problem. Sudoterb (LL-3858), an INH-pyrrole hybrid that reached phase II clinical trials, is a good example of the efficacy of this strategy. **(Figure 7.8)**[230,231]

[228] V. Estévez, M. Villacampa, J. C. Menéndez, *Chem. Commun*. **2013**, *49*, 591.
[229] V. Estévez, V. Sridharan, S. Sabaté, M. Villacampa, J.C. Menéndez, *Asian J. Org. Chem.* **2016**, *5*,652.
[230] Beena, D.K.; Khare, G.; Kidwai, S.; Tyagi, A.K.; Singh, R.; Rawat, D.S.; *Eur. J. Med. Chem.* **2014**, *81,* 301.
[231] Martins, F.; Santos, S.; Ventura, C.; Elvas-Leitao, R.; Santos, L.; Vitorino, S.; Reis, M.; Miranda, V.; Correia, H.F.; Aires-de-Sousa, J.; Kovalishyn, V.; Latino, D.A.R.S.; Ramos, J.; Viveiros, M.; *Eur. J. Med. Chem.* **2014**, *81*, 119.

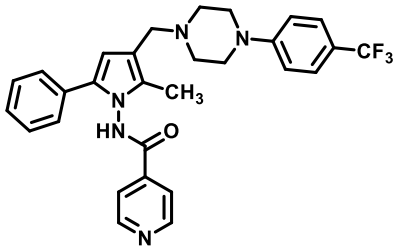

Figure 7.8

With these ideas in mind, we undertook the design, synthesis and pharmacological and SAR studies of a family of hybrid compounds bearing pyrrole and isoniazid frameworks. These compounds may act as MTDLs against tuberculosis, by inhibiting Iron acquisition pathways and cell wall formation through two different mechanism, involving InhA and MmpL3 inhibition. At the same time, as they are more lipophilic than isoniazid and their acetylation is not possible, they may be more metabolically stable INH derivatives, enhancing this way their activity against sensitive and resistant tuberculosis strains. **(Figure 7.9)**

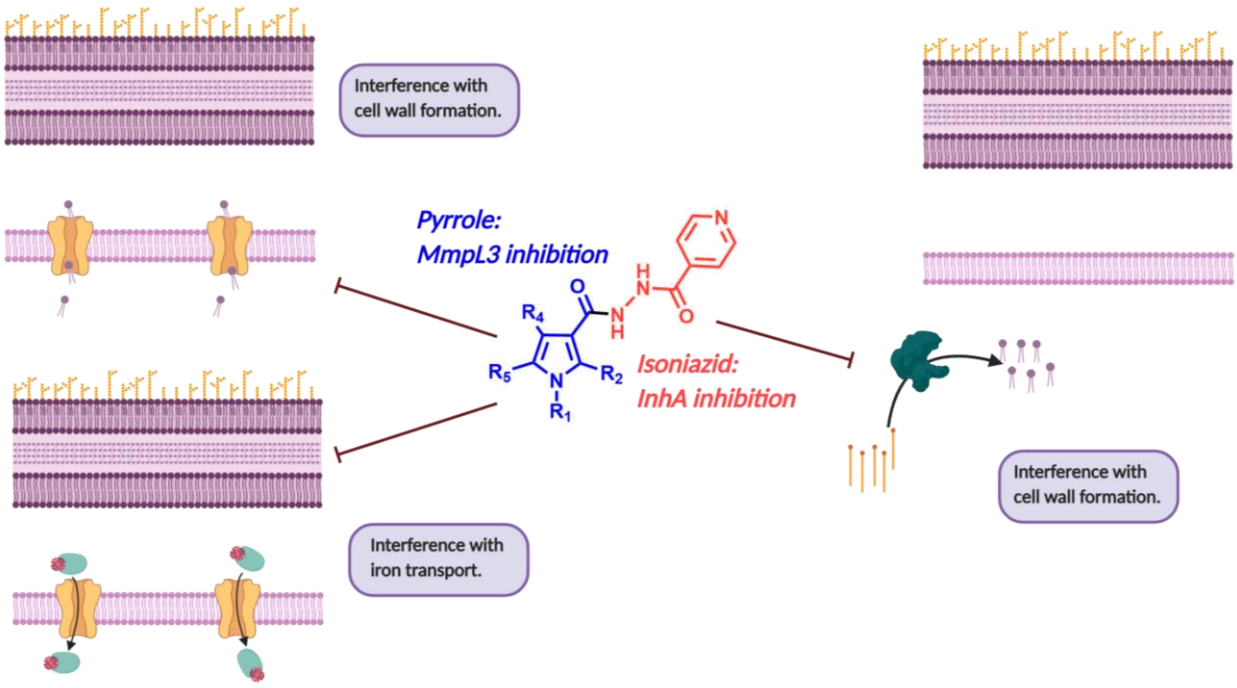

Figure 7.9.

7.5. Synthesis of pyrrole-isoniazid derivatives

To achieve our goal, we synthesized a chemical library of pyrrole derivatives bearing a wide variety of substituents in all positions to evaluate their activities and try to elucidate some Structure Activity Relationships (SAR). **(Figure 7.10)**

- In position 1 on the pyrrole core, hydrogen, alkyl, aminoalkyl or phenyl groups were introduced.
- In position 2, due to synthetic accessibility issues, only methyl or propyl groups were tested.
- In position 3, carboxylic acids, ethyl esters, amides or isoniazid hybrids were synthesized.
- Position 4 was most commonly free, but methyl, phenyl or fused structures were also evaluated.
- Finally, in position 5, alkyl, aryl or heteroaryl substituted rings were obtained.

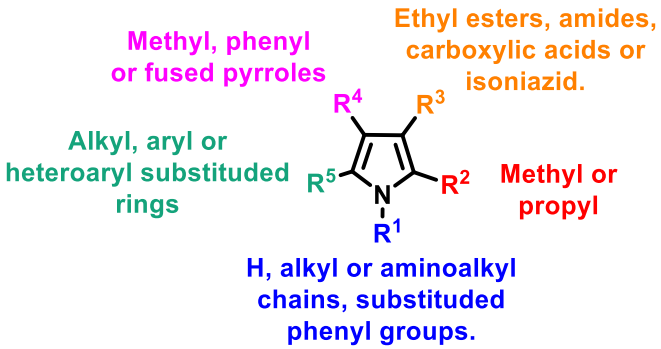

Figure 7.10.

As mentioned above, some years ago our group published a one pot multicomponent reaction related to the Hanztsch pyrrole synthesis. This reaction takes place under solvent-free mechanochemical conditions, starting from primary amines, α-iodoketones and β-dicarbonyl compounds in the presence of cerium ammonium nitrate (CAN) as a catalyst.[228,229]

Thus, to obtain the desired pyrroles, the suitable α-iodoketones need to be prepared first. To this end, two different methodologies were employed depending on the stability of the starting materials. The ones containing electron-rich heterocycles were

too reactive under HSVM conditions and were prepared through **Method A**, using molecular Iodide and Copper (II) oxide in refluxing methanol. **(Scheme 7.1)**

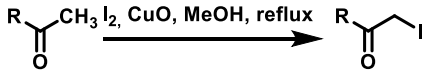

Scheme 7.1: Method A.

For the rest of the derivatives, we were able to perform the iodation step directly using the high-speed vibration milling technique, **Method B**, so that the pyrrole formation could be performed as a single sequential process. In this case, the iodation of the starting ketones was performed under HSVM conditions by using *N*-iodosuccinimide (NIS) and *p*-toluensulphonic acid (PTSA), which acts as Brønsted acid, favouring the enolic form of the ketone necessary for the iodation process. **(Scheme 7.2)**

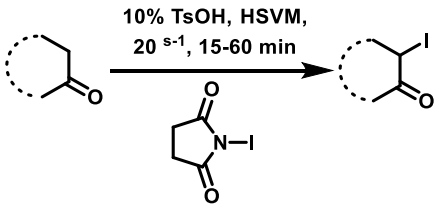

Scheme 7.2: Method B.

Once the iodo derivatives were obtained, a mixture of the suitable β-dicarbonyl compound, amine and CAN, previously stirred together at room temperature for 30 min to yield the corresponding enaminone, together with silver nitrate, were added to the reaction vessel. For R^1 = H, the enaminone was commercially available. **(Scheme 7.4)**

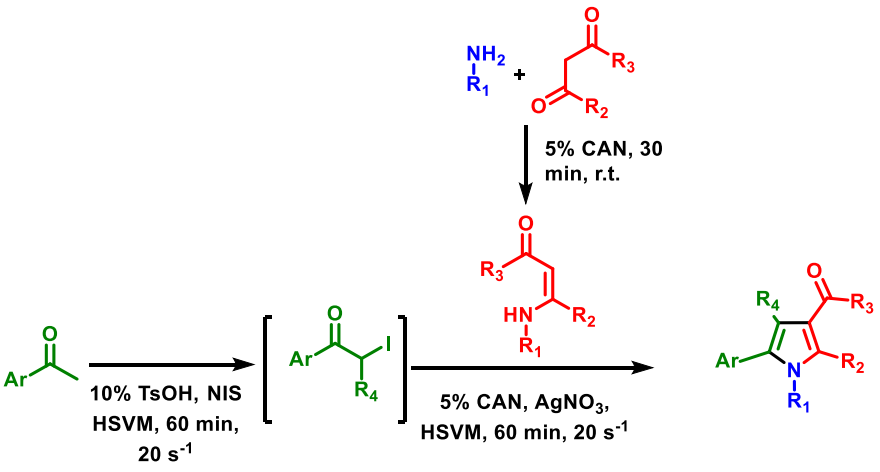

Scheme 7.4: Pyrrole formation.

The hydrogen iodide generated in the first step of the reaction can promote a reductive dehalogenation of the starting α-iodoketone. For this reason, the silver nitrate, able to precipitate the generated free iodine was added to the reaction, avoiding this way the dehalogenation process. **(Scheme 7.5)**

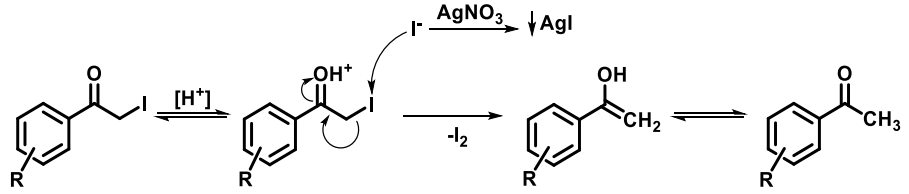

Scheme 7.5: Silver nitrate mechanism.

Once the starting pyrroles were synthetized, in order to obtain the desired isoniazid hybrids, the ester group was hydrolysed with ethanolic NaOH, yielding the corresponding carboxylic acids. **(Scheme 7.6)** Finally, the carboxylic acids were coupled to the isoniazid moiety through peptide synthesis methodologies, using 1-ethyl-3-(3-dimethylaminopropyl)carbodiimide hydrochloride (EDC.HCl) and 1-hydroxy-7-azabenzotriazole (HOAt) as activating agents. **(Scheme 7.6)**

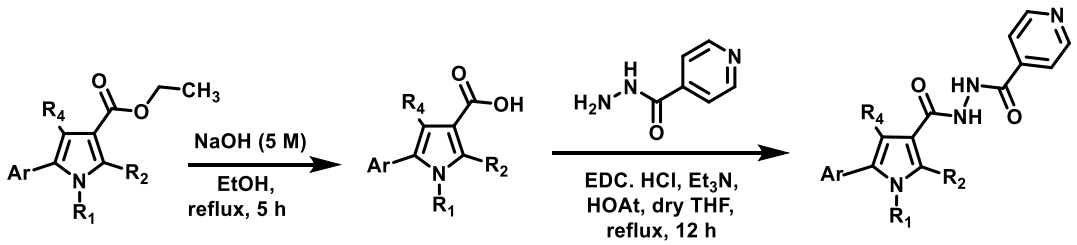

Scheme 7.6: Hydrolysis of the ester derivatives and coupling with isoniazid.

The structures of all compounds studied for antitubercular activity can be found in **Figures 7.11-7.14**. Some of them, marked with *, were described in a previous PhD thesis.[232]

[232] Verónica Estévez. PhD thesis, Universidad Complutense, 2013.

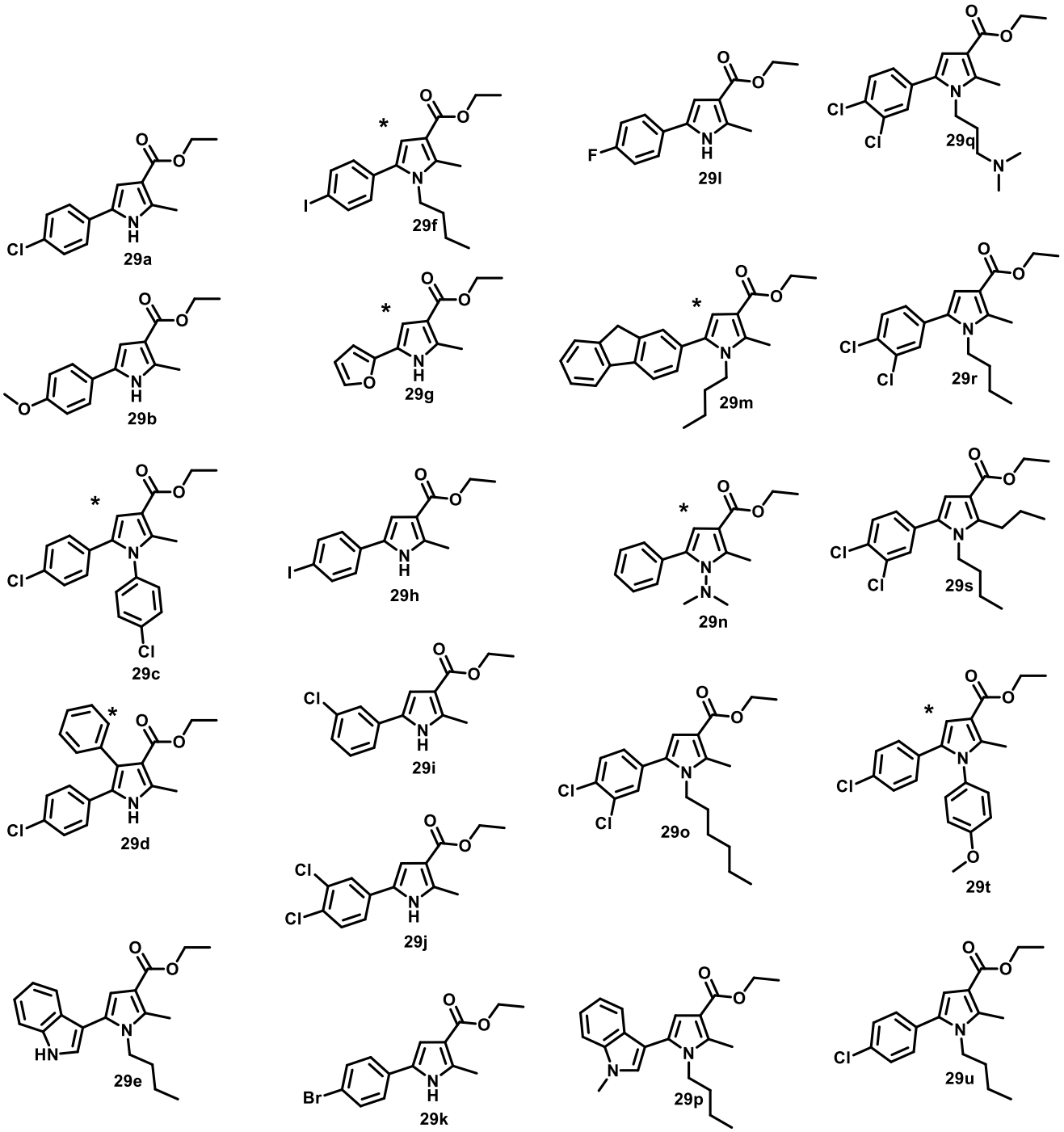

Figure 7.11: Ethyl ester pyrrole derivatives.

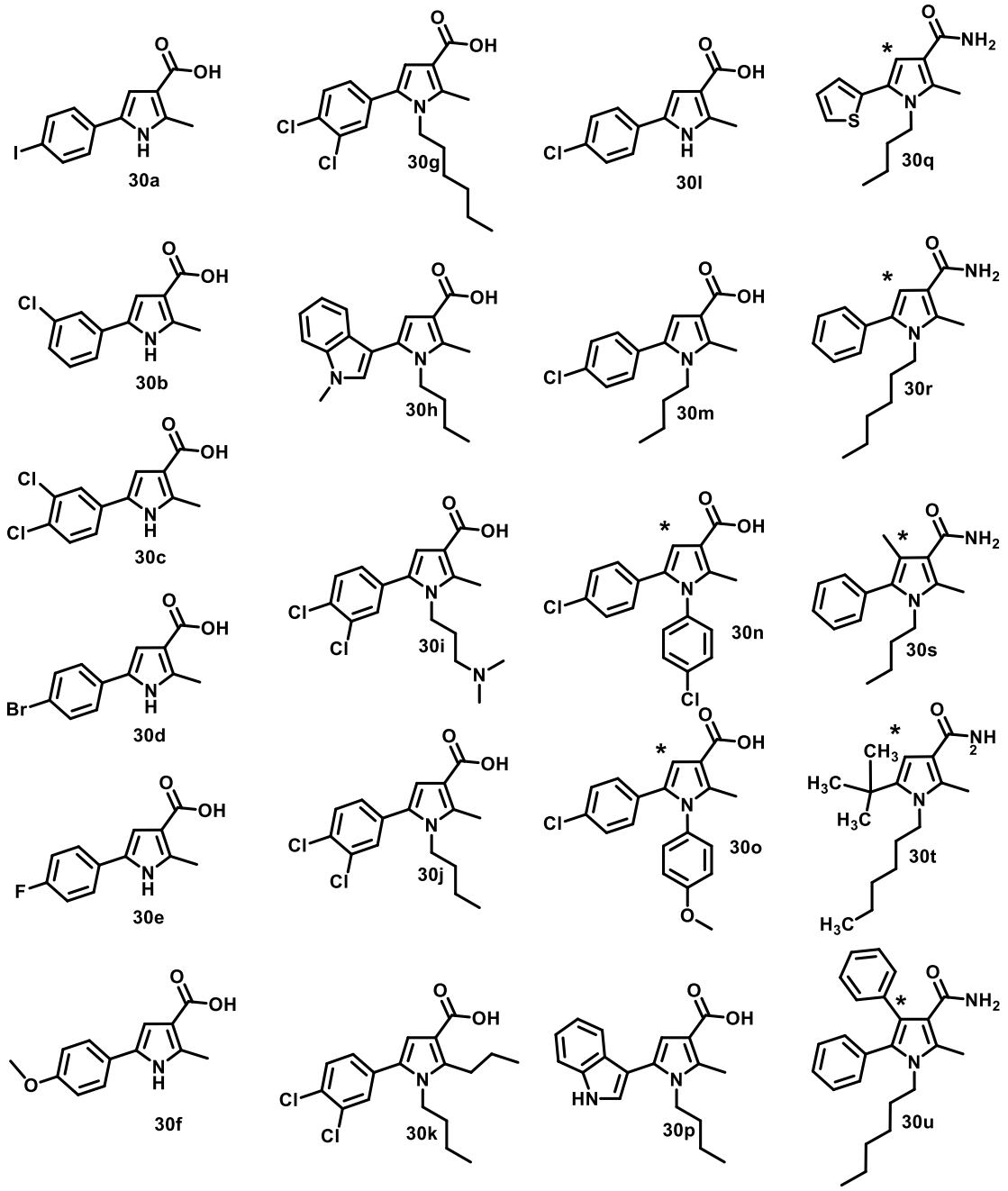

Figure 7.12: Carboxylic acids and amide pyrrole derivatives.

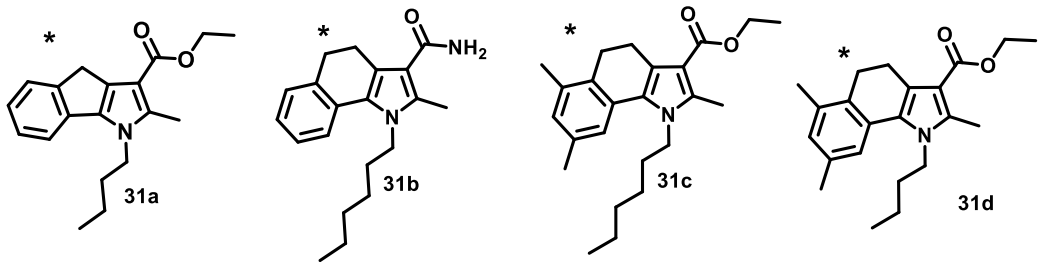

Figure 7.13: Fused pyrrole derivatives.

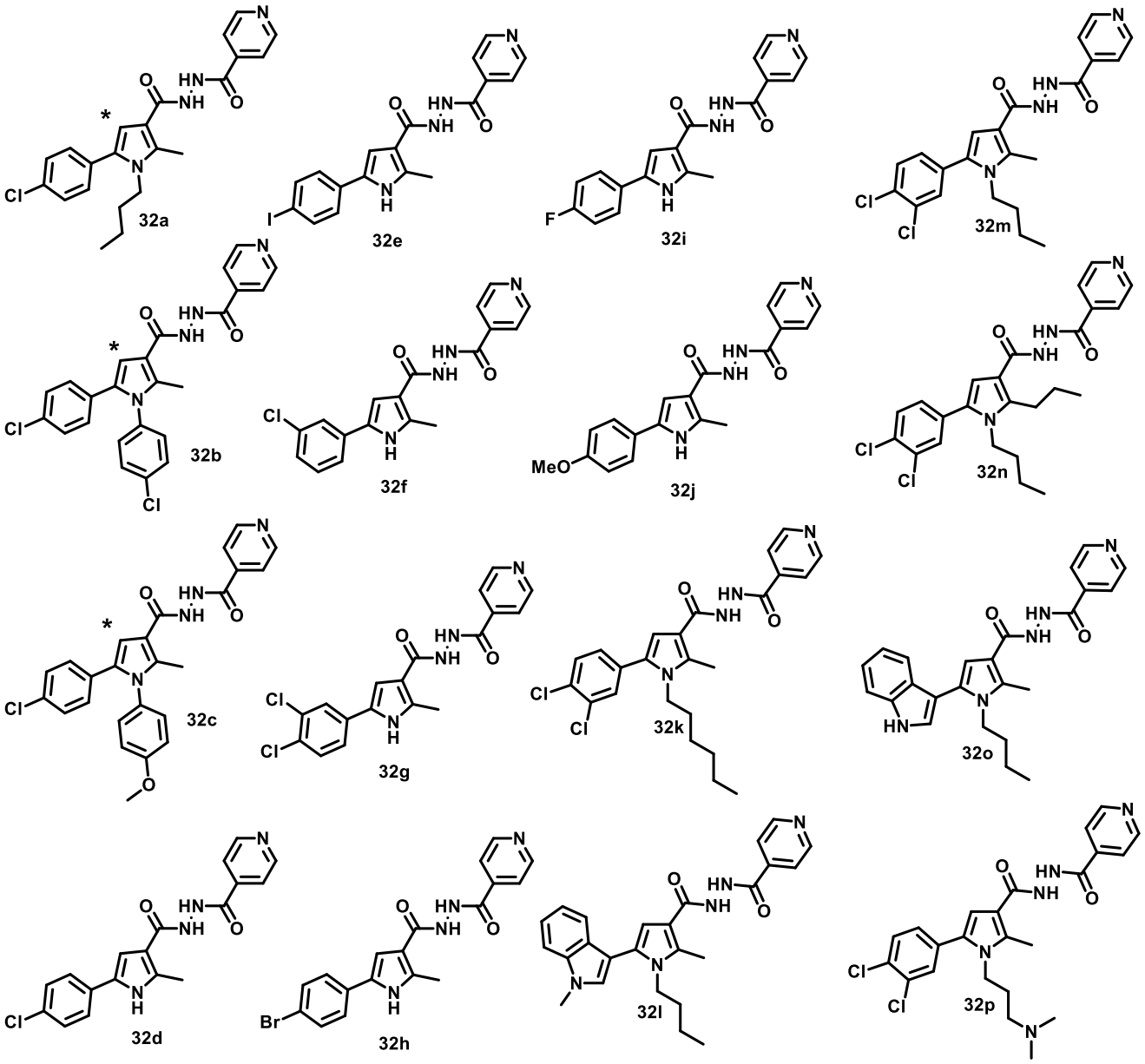

Figure 7.14: Pyrrole-isoniazid hybrids.

7.6. Activity and mechanistic studies of pyrrole-isoniazid derivatives

7.6.1 Computational drug-likeness study

First, to evaluate the drug-like properties of the compounds ADME-tox computational studies of the synthesized derivatives were carried out using SwissADME and are summarized in **Tables 7.1**, **7.2** and **7.3**.

Cmpd. number	Rotable bonds	TPSA[141]	Log P $_{o/w}$[142]	Log S[143]	GI absorp.[144]	Lipinski violations[145]	PAINS alerts[145]
29a	4	42.09	3.51	-3.94	High	0	0
29b	5	51.32	2.98	-3.41	High	0	0
29c	5	31.23	5.26	-6.03	High	1	1
29d	5	42.09	4.83	-5.45	High	0	0
29e	7	47.02	4.10	-4.50	High	0	0
29f	7	31.23	4.65	-5.31	High	0	0
29g	4	55.23	2.27	-2.71	High	0	0
29h	4	42.09	3.64	-4.52	High	0	0
29i	4	42.09	3.51	-3.94	High	0	0
29j	4	42.09	4.03	-4.53	High	0	0
29k	4	42.09	3.60	-4.26	High	0	0
29l	4	42.09	3.29	-3.51	High	0	0
29m	7	31.23	5.45	-5.77	High	1	0
29n	5	34.47	3.03	-3.81	High	0	0
29o	9	31.23	5.75	-6.02	High	1	0
29p	7	36.16	4.14	-4.54	High	0	0
29q	8	34.47	4.45	-4.87	High	0	0
29r	6	31.23	4.70	-5.09	High	0	0
29s	7	31.23	5.02	-5.36	High	1	0
29t	6	40.46	4.73	-5.50	High	0	1
29u	7	31.23	4.54	-4.73	High	0	0

Table 7.1: Properties of ethyl ester pyrrole derivatives.

Cmpd. number	Rotable bonds	TPSA[141]	Log P o/w[142]	Log S[143]	GI absorp.[144]	Lipinski violations[145]	PAINS alerts[145]
30a	4	53.09	2.92	-4.10	High	0	0
30b	5	53.09	2.79	-3.52	High	0	0
30c	5	53.09	3.31	-4.10	High	0	1
30d	5	53.09	2.88	-3.84	High	0	0
30e	7	53.09	2.56	-3.09	High	0	0
30f	7	42.23	4.97	-5.56	High	1	0
30g	4	47.16	3.27	-4.10	High	0	0
30h	4	45.47	3.20	-2.98	High	0	0
30i	4	42.23	4.32	-4.87	High	0	0
30j	2	42.23	4.94	-5.38	High	1	0
30k	2	53.09	2.79	-3.52	High	0	0
30l	2	42.23	3.80	-4.28	High	0	0
30m	2	42.23	4.51	-5.59	High	1	0
30n	2	51.46	3.98	-5.06	High	0	0
30o	7	76.26	2.86	-3.12	High	0	0
30p	5	48.02	3.60	-3.97	High	0	0
30q	6	48.02	3.20	-3.58	High	0	0
30r	5	48.02	3.40	-3.68	High	0	0
30s	7	48.02	4.94	-5.48	High	0	0
30t	7	48.02	4.87	-5.57	High	0	0
31a	6	48.02	3.92	-4.26	High	0	0
31b	8	31.23	5.65	-4.34	High	0	0
31c	6	31.23	4.93	-5.82	High	1	0
31d	6	31.23	4.93	-5.12	High	0	0

Table 7.2: Properties of carboxylic acid pyrrole derivatives and fused pyrroles.

Cmpd. number	Rotable bonds	TPSA[141]	Log P o/w[142]	Log S[143]	GI absorp.[144]	Lipinski violations[145]	PAINS alerts[145]
32a	9	76.02	3.78	-4.69	High	0	0
32b	7	76.02	4.48	-5.95	High	0	1
32c	8	85.25	3.86	-5.43	High	0	1
32d	6	86.88	2.68	-3.90	High	0	0
32e	6	86.88	2.82	-4.48	High	0	0
32f	6	86.88	2.73	-3.90	High	0	0

Cmpd. number	Rotable bonds	TPSA[141]	Log P $_{o/w}$[142]	Log S[143]	GI absorp.[144]	Lipinski violations[145]	PAINS alerts[145]
32g	6	86.88	3.17	-4.48	High	0	0
32h	6	86.88	2.74	-4.21	High	0	0
32i	6	86.88	2.43	-3.46	High	0	0
32j	7	96.11	2.23	-3.37	High	0	0
32k	11	76.02	4.94	-5.98	High	0	0
32l	9	80.95	3.39	-4.49	High	0	0
32m	9	76.02	4.18	-5.29	High	0	0
32n	11	76.02	4.82	-5.80	High	0	0
32o	9	91.81	3.25	-4.45	High	0	0
32p	10	79.26	3.63	-4.83	High	0	0
Isoniazid	2	68.01	-0.35	-0.56	High	0	0

Table 7.3: Properties of pyrrole-isoniazid hybrids.

For all compounds, the TPSA value was under 140, important for been able to permeate cells. Moreover, a high gastrointestinal absorption, important for oral bioavailability, was predicted. Furthermore, only compounds 6 compounds showed a PAINS alert. And finally, the few violations of Lipinski's rule of five were always due to a high lipophilicity, which is usually considered a positive feature in antitubercular agents, which need to penetrate the granuloma and cross the very lipophilic cover of mycobacteria. It is also worth noting that all isoniazid derivatives exhibit high LogP values.

7.6.2 Antitubercular activity

The synthetitized compounds were then analysed *in vitro* against *Mycobacterium tuberculosis* H_{37}Rv (Mtb H_{37}Rv) in a high-throughput screen by Professor Ashraf Ali Mohamed in the University Sains Malaysia, Penang. Selected compounds were also tested against clinically isolated MDR-TB strains, obtained from the Tuberculosis Research Centre (Chennai, India). These strains were resistant to isoniazid, rifampicin and ethambutol. The toxicity of the compounds was evaluated in mammalian Vero cell line at concentrations of 6.25 mg/L. After 72 h of exposure, viability was assessed, and none the tested compounds showed toxicity.

The results obtained can be found in **Tables 7.4**, **7.5** and **7.6**.

Cmpd.	H37Rv IC_{50} (µM)	H37Rv MIC (µM)	MDR-TB MIC (µM)	Cytotoxicity µg/ml
29a	7.87	25	---	>6.25
29b	22.87	50	---	>6.25
29c	44.95	100	---	>6.25
29d	37	100	---	>6.25
29e	2.87	6.25	10.17	>6.25
29f	25.87	100	---	>6.25
29g	44.95	100	---	>6.25
29h	---	1.170	1.970	>6.25
29i	18.57	50	---	>6.25
29j	08.28	50	---	>6.25
29k	12.87	50	---	>6.25
29l	25.87	100	---	>6.25
29m	---	Inactive	---	>6.25
29n	---	Inactive	---	>6.25
29o	---	1.000	1.200	>6.25
29p	---	2.270	2.527	>6.25
29q	---	0.100	0.170	>6.25
29r	---	8.0000	8.200	>6.25
29s	---	22.27	22.527	>6.25
Rifamycin	---	0.200	4.120	>6.25
Ethambutol	32.79	5.790	92.500	>6.25
Isoniazid	0.29	0.390	11.740	>6.25

Table 7.4: Antitubercular activity of ethyl ester pyrrole derivatives.

Cmpd.	IC_{50} (µM)	H37Rv MIC (µM)	MDR-TB MIC (µM)	Cytotoxicity µg/ml
30a	7.87	50.00	---	>6.25
30b	25.87	50.00	---	>6.25
30c	44.95	25.00	---	>6.25
30d	37	50.00	---	>6.25
30e	2.87	50.00	---	>6.25
30f	25.87	50.00	---	>6.25
30g	44.95	1.470	1.970	>6.25
30h	---	1.420	3.200	>6.25
30i	18.57	0.600	0.750	>6.25
30j	08.28	6.470	6.970	>6.25
30k	12.87	11.420	13.20	>6.25
30p	25.87	10.600	10.75	>6.25
30q	---	Inactive	---	>6.25
30r	---	Inactive	---	>6.25
30s	---	Inactive	---	>6.25
30t	---	Inactive	---	>6.25
30u	---	Inactive	---	>6.25

Cmpd.	IC_{50} (μM)	H37Rv MIC (μM)	MDR-TB MIC (μM)	Cytotoxicity μg/ml
31a	---	Inactive	---	>6.25
31b	---	Inactive	---	>6.25
31c	---	Inactive	---	>6.25
31d	---	Inactive	---	>6.25
Rifamycin	---	0.200	4.120	>6.25
Ethambutol	32.79	5.790	92.500	>6.25
Isoniazid	0.29	0.390	11.740	>6.25

Table 7.5: Antitubercular activity of carboxylic acid pyrrole derivatives and fused pyrroles.

Cmpd.	IC_{50} (μM)	H37Rv MIC (μM)	MDR-TB MIC (μM)	Cytotoxicity μg/ml
32a	3.28	15	---	>6.25
32b	6.38	25	---	>6.25
32c	2.81	15	---	>6.25
32d	4.28	15	---	>6.25
32e	47.20	1.320	2.320	>6.25
32f	1.87	25.00	---	>6.25
32g	0.90	6.25	---	>6.25
32h	5.81	25.00	---	>6.25
32i	2.20	25.00	---	>6.25
32j	47.20	100.00	---	>6.25
32k	---	0.100	0.320	>6.25
32l	---	0.230	0.250	>6.25
32m	---	9.320	9.320	>6.25
32n	---	15.230	20.25	>6.25
32o	---	12.000	13.200	>6.25
Rifamycin		0.200	4.120	>6.25
Ethambutol	32.79	5.790	92.500	>6.25
Isoniazid	0.29	0.390	11.740	>6.25

Table 7.6: Antitubercular activity of pyrrole-isoniazid hybrids.

Aanalysing these data, we were able to obtain some structure activity relationship (SAR) conclusions. **(Figure 7.15)**

- In position 1 of the pyrrole ring the best results were obtained with H, hexyl, butyl or dimethylaminopropyl groups. The latter residue seems to be the most promising one, and the corresponding isoniazid hybrid is now under study.
- In position 2, a methyl group gave considerably better results than a propyl group.
- As expected, the hybrid derivatives exhibited considerably better activities than the corresponding esters or carboxylic acids. On the other hand, all the amide derivatives were inactive.

- In position 4 of the pyrrole, it seems that aryl substituents are not favourable for the activity, although the number of examples available is not high. The option of smaller substituents remains unexplored.
- More complex and rigid systems containing an additional ring fused at the 4 and 5 positions were inactive.
- In position 5, clearly indole rings, 3-4-dichlorophenyl or p-iodophenyl groups exhibited the best activities.

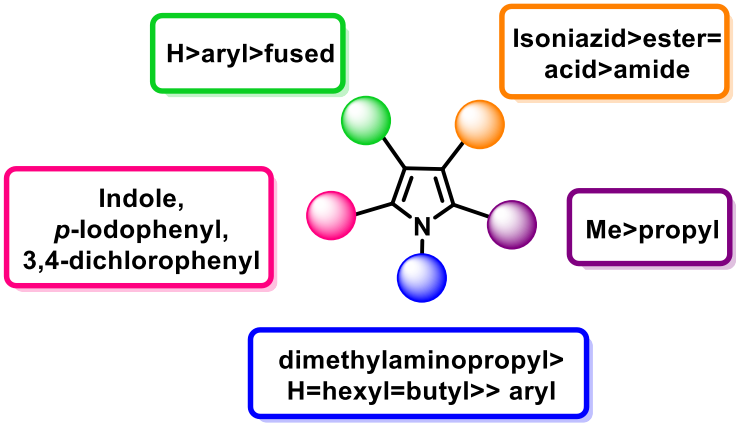

Figure 7.15. Preliminary SAR study of pyrrole-isoniazid hybrids.

Remarkably, many of the active compounds with the higher activities were also active against multidrug-resistant strains, which can be viewed as a proof of concept of the alternative mechanisms of the hybrids and confirms that using MTDL against TB is a promising approach. None of these hit compounds exhibited any PAINS alerts.

7.6.3 Mechanistic studies

Once the activities of our compounds were tested, we wanted to prove if our compounds were acted on the desired targets. For that purpose, mechanistic studies were carried out by Dr. Katherine Abrahams in the group of Professor Gurdyal S. Besra from the School of Biosciences, University of Birmingham.

7.6.3.1. KatG activation and InhA *inhibition*

First, to evaluate if our compounds could be activated by katG, INH resistant mutants were generated to sequence katG and InhA. A mutant which had a frameshift in katG,

making the gene non-functional, was selected. Also, it was verified that InhA had no mutations so that the resistance to INH was due to the inability of the cells to make katG. Three of the hybrid compounds (**32g**, **32i** and **32j**) and INH as control, were tested against these strains, and it was observed that the katG mutant was resistant to them, meaning that the compounds are katG substrates. **(Figure 7.16)**

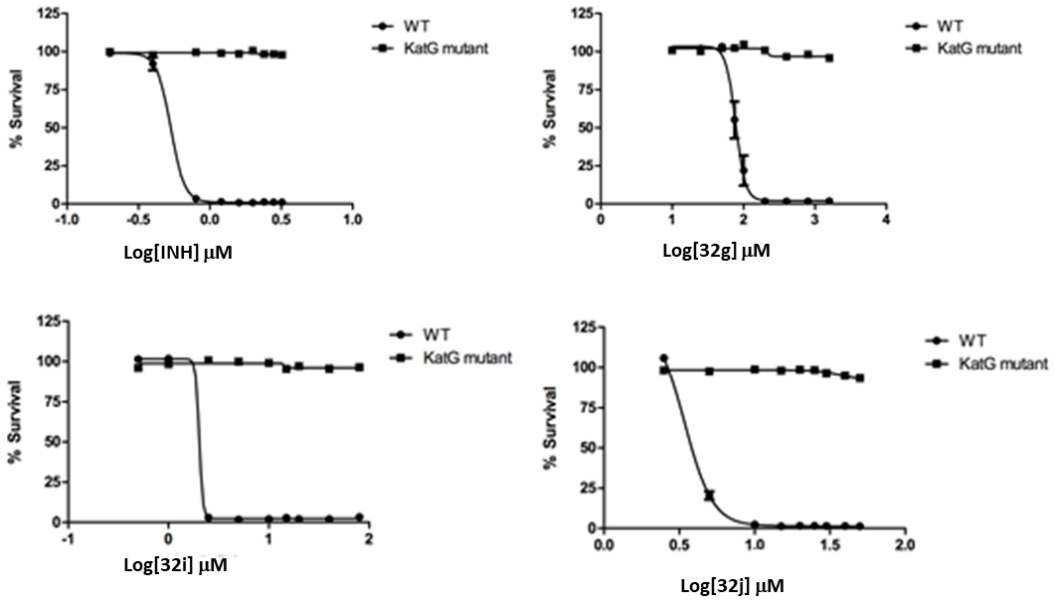

Figure 7.16: Resistance of the katG mutant strain on compounds INH, 32g, 32i and 32j. The katG (INH resistant) mutant survived at all concentrations of compound tested.

To further evaluate if our compounds were able to inhibit InhA, strains overexpressing InhA were cultured, and again compounds **32g**, **32i** and **32j** and INH as control, were tested against these strains. Once again, the hybrid compounds exhibit the same behaviour as INH, causing the death of the wild type strains while the InhA over-expressing strains survived, proving that our compounds target InhA. **(Figure 7.17)**

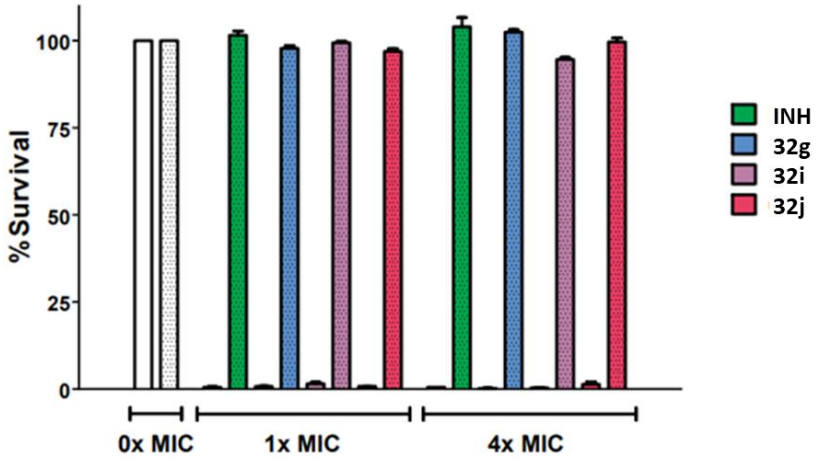

Figure 7.17: Impact of InhA over-expression on resistance to INH, 32g, 32i and 32j. Unshaded and shaded bars represent pMV261 empty vector and InhA over-expressor strains respectively. Bars are the mean of duplicate data with error bars showing the SEM.

In the aggregate, these results verified that the hybrid compound are able acts as isoniazid prodrugs that are activated by katG and further inhibit InhA.

On the other hand, due to their design and as the antitubercular activities showed we were intrigued by the observation that no antibacterial activity could be detected on the katG mutants or InhA over-expressors. Moreover, some of the pyrrole derivatives not bearing the isoniazid moiety showed excellent antimycobacterial activities, demonstrating that they should inhibit and alternative target. To clarify these doubts, the compounds **30p** and **30e**, not presenting the isoniazid fragment, were tested against the katG mutants and InhA over-expressor.

This time, as expected, the compound exhibited the same behaviour against the wild type cells and the mutants, while again INH presented no effect against any of the mutants. **(Figure 7.18)** This experiment verified the existence of an additional mechanism due to the pyrrole core.

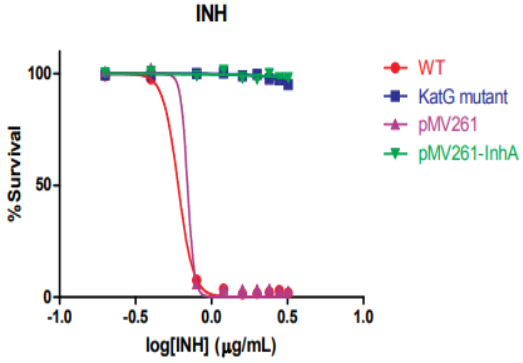

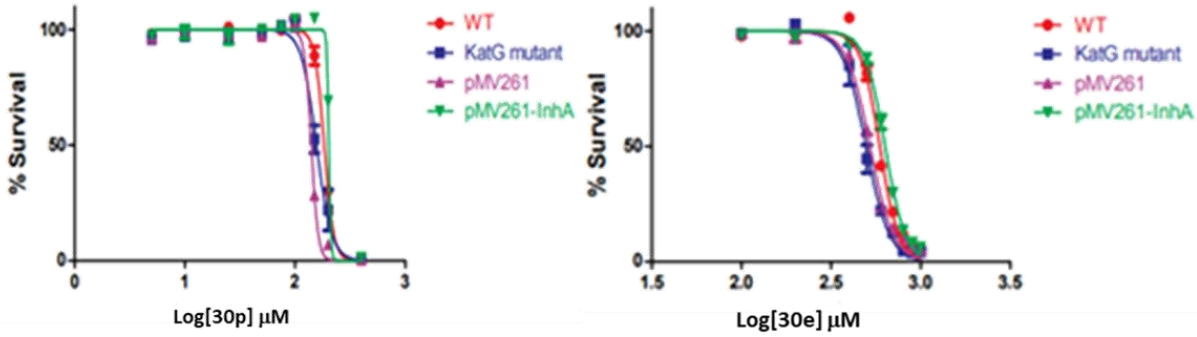

Figure 7.18. Impact of InhA over-expression and katG mutant on INH, 30p and 30e.

7.6.3.2. MmpL3 target

Spontaneous resistant mutants against **32g**, **32i** and **32j** in *M. bovis* BCG were generated, 8 of them were cultured, and their genomic DNA was extracted. The *mmpL3* gene was amplified via PCR and sequenced. It was observed that every mutant contained two mutations responsible of the loss of activity, phenylalanine 384 changed into isoleucine and aspartic acid 466 into a glutamic acid. This result can be interpreted as indirect proof of an interaction of our compounds with MmpL3. When we mapped our mutations into the MmpL3, structure we found they are located in opposite sides of the protein structure. Nevertheless, it has to be borne in mind that 80% of mutations found lie inside or within 10 Å of the known binding pocket, altering in a direct way the mechanism of action of inhibitors. The remaining 20% are located in different domains, probably altering in an indirect way the binding of inhibitors.[221] **(Figure 7.19)**

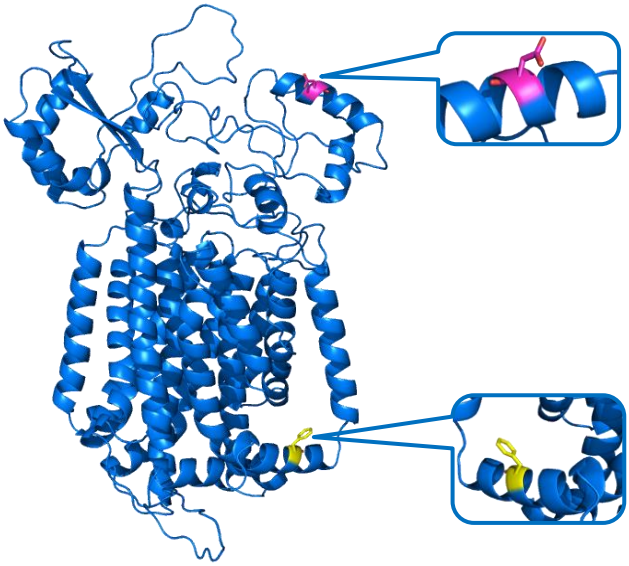

Figure 7.19. Homology model obtained from the Mmpl3 sequence (P9WJV5) using Phyre2.

7.6.3.3. MmpL3 docking studies

As mentioned above, in 2019 Zhang and colleagues reported the crystal structure of *Mycobacterium smegmatis* MmpL3, in the presence and absence of several inhibitors. Moreover, docking studies of other reported inhibitors were performed.

Analysing the structures of the four crystalized ligands, the authors verified that all of them bind to the proton-translocation channel, even if their ways of interacting differ slightly. The binding pocket was divided into four subsites (S1-S5). While S1, S2, S3, and S5 are hydrophobic pockets, the key components of S4 are two hydrophilic Asp-Tyr pairs S1 and S2 are smaller compared to S3 and S5, which can accommodate bulky hydrophobic groups to enhance binding. As the superposition image of the four structures shows **(Figure 7.20)**, the four drug candidates so far crystallized with the protein occupy 3-5 subsites in the proton-translocation channel. While rimonabant (yellow sticks) occupies S1, S2 and S4, SQ109 (magenta sticks), AU1235 (green sticks) and ICA38 (orange sticks) are located at the S3, S4 and S5 subsites. All of them disrupt the two Asp-Tyr pairs, consequently blocking the proton motive force, essential for substrate translocation.[221]

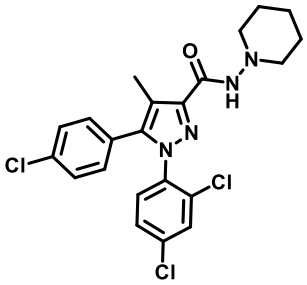

Rimonabant

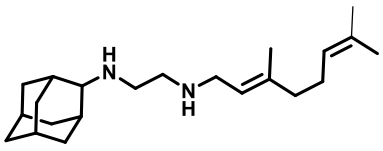

SQ109

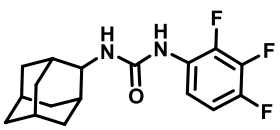

AU1235

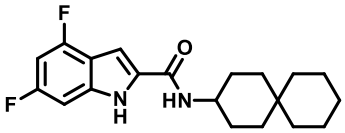

ICA38

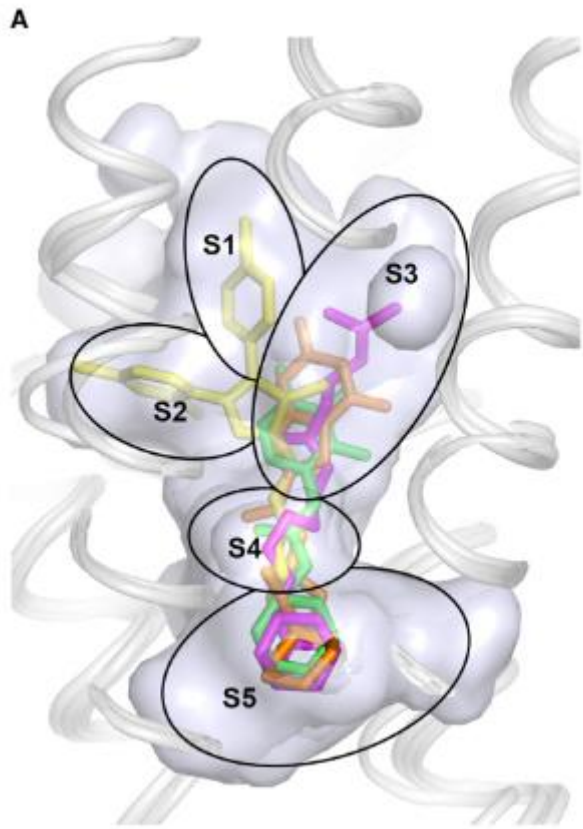

Figure 7.20. Reproduced with permission from reference [221].

Whit this information in hand, preliminary docking studies of some of our inhibitors were performed by Dr. Ángel Cores from our group. To this end, the crystal structure of *Mycobacterium smegmatis* MmpL3 in the presence of rimonabant (PDB 6AJI) was chosen due to the structural analogy between rimonabant and our compounds.

First, the docking was performed with the rimonabant structure and compare to the reported crystal structure, in order to validate the docking method. The arm of rimonabant bearing the 2, 4-dichlorophenyl ring occupies S2 (green), a hydrophobic pocket surrounded by five aliphatic amino acid. The 4-chlorophenyl ring goes into the nearby hydrophobic S1 pocket (yellow), while the pyrazole ring core is inserted into the centre of the TMH package, perpendicular to the membrane at the S4 pocket (purple). Finally, the polar piperidinyl-1-carbamoyl residue is the one inserted into the Asp-Tyr pairs at the S4 pocket (red), breaking the hydrogen bonds by forming polar interactions with them. S3 (blue) and S5 (red) remain empty. **(Figure 7.21)**

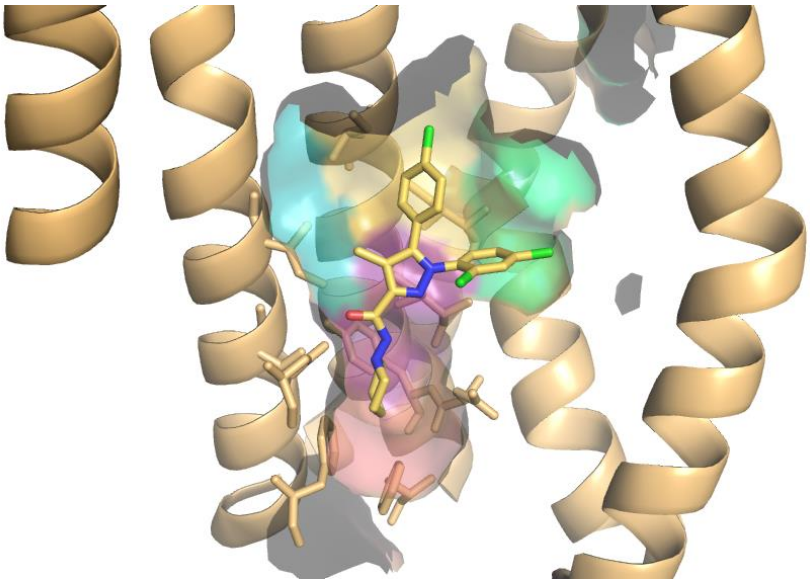

Figure 7.21.

We chose our derivatives **32k** and **29o** as representative examples for docking studies. As it is shown in **Figure 7.22**, comparing the poses of **32k** (grey) and rimonabant (yellow), both compounds share a similar pose. While the central pyrrole core shares the same position as the pyrazole ring in the middle of the TMH package, the 2, 4-dichlorophenyl ring occupies S1. In contrast with rimonabant, the hexyl chain appears located inside S2, while S3 remains empty. Moreover, the two amide functions of our compounds are able to interact with S4, were the Asp-Tyr pairs are located. The pyridine ring is able to occupy S5 in a very efficient way by establishing π–π interactions with adjacent tyrosine and phenylalanine residues.

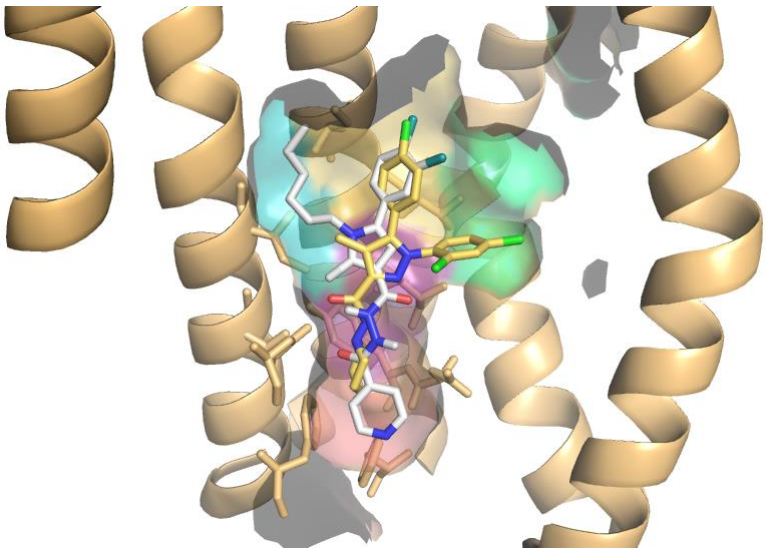

Figure 7.22.

When we examined the docking of **29o**, the compound could be located in the same pocket, even if it seems that its size is too small to interact with it in an efficient way. This suggests that the isoniazid fragment is important for an efficient MmpL3 inhibition. **(Figure 7.23)**

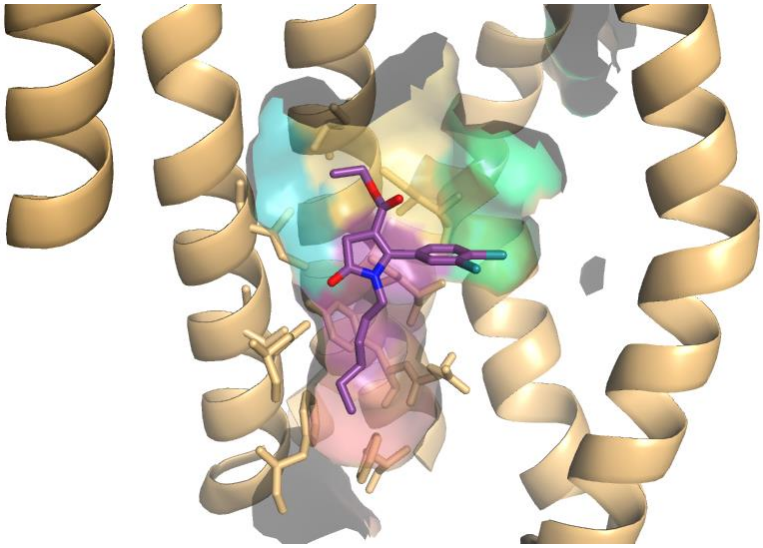

Figure 7.23.

From these results, it seems that the introduction of a phenyl ring at C-4 position, directly or with a flexible linker between both rings, would considerably improve binding, as shown by the docking of the non-synthesized derivative **32z (Figure 7.24)**. The antitubercular activity results seemed to show that bulky substituents in position 4 of the pyrrole core were not beneficial for activity, but it has to be borne in mind that all of them bear an amide function, which always has led to inactive compounds, probably due to their physicochemical characteristics rather than structural factors.

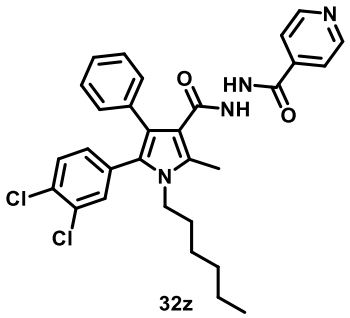

32z

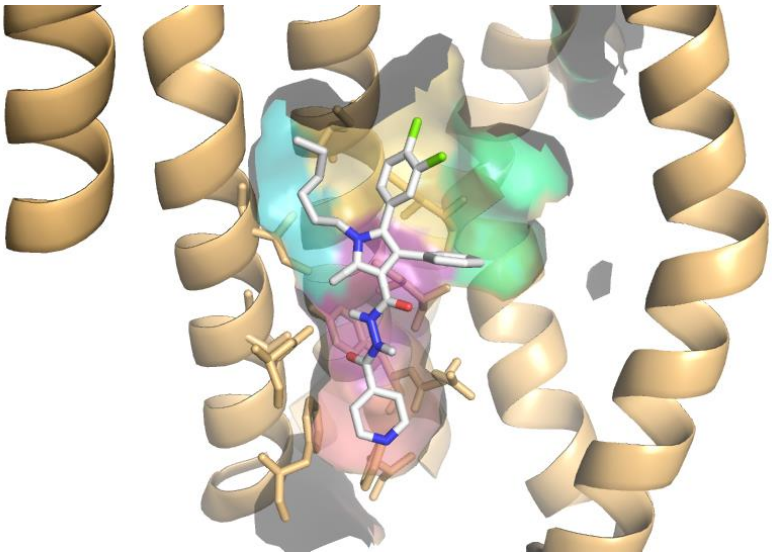

Figure 7.24.

7.6.4 Proposed mechanism of action for the pyrrole-isoniazid hybrids

We can conclude that the pyrrole-isoniazid hybrids are able to exert their antibacterial activity through two different mechanisms. On one hand, there are able to inhibit Mmpl3 by direct interaction with the protein, probably by occupy the S3 to S5 subsites in the proton-translocating channel of MmpL3, and consequently disrupting the proton motive force necessary for substrate translocation.[221] On the other hand, it was proved that our compounds act as prodrugs, which need to be activated by katG and furnish a metabolite that finally inhibits InhA. This mechanism involves the synergistic effects of a compound and its active metabolite, which is an emerging type of multitarget strategy described as metabolism-activated multitargeting (MAMUT).[62] Thus, it can proposed that, when the hybrids get in contact with MmpL3 they directly interact with the protein and by inhibiting the PMF, they inhibit mycolic acid translocation and heme internalization. On the other hand, considering the possible metabolism of the hybrid compounds according to literature data for isoniazid[233], once katG activates the hybrid compounds, isonicotinoyl radical exert its action by inhibiting InhA, and the resulting acyldiazenepyrrole derivative is formed. **(Figure 7.25)**

[233] Laborde, J.; Deraeve, C.; Lecoq, L.; Sournia-Saquet, A.; Stigliani, J. L.; Orena, B. S.; Mori, G.; Pratviel, G.; Bernardes-Génisson, V. *ChemistrySelect* **2016***, 1,* 172.

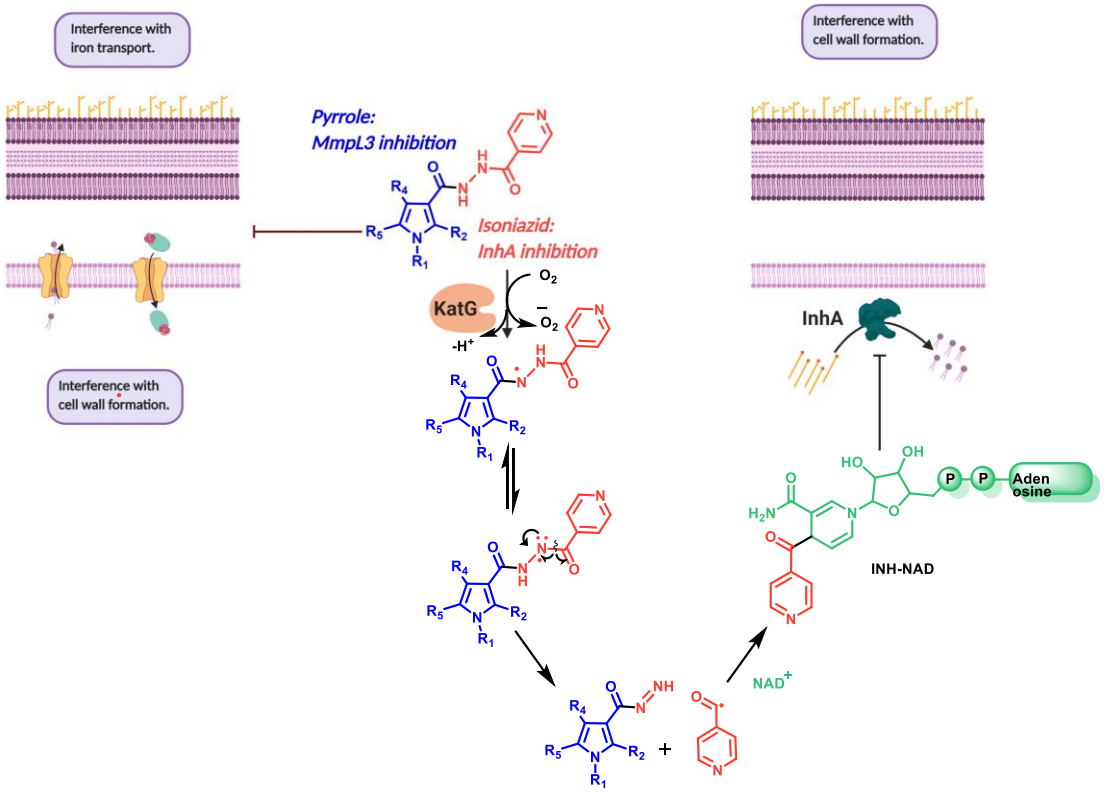

Figure 7.25: Proposed mechanism of pyrrole-isoniazid hybrids

Even though the participation of both mechanisms seems unequivocal, some details remain still unclear. When it comes to the hybrid activity against InhA over-expressors and katG mutants, it is not clear why no bactericidal activity was observed. This could be due to the fact that antitubercular activities were assessed in *M. tuberculosis* strains while the mechanistic studies were performed in *M. bovis.* Furthermore, high doses required to observe antibacterial activity of the pyrrole derivatives against mutant strains. As consequence, it is possible that in the case of the hybrids higher concentrations needed to be achieve in order to see the bactericidal effect corresponding to the pyrrole fragment.

7.7. Experimental section

General experimental details.

All reagents (Aldrich, Fischer, Alpha Aesar, SDS) and solvents (Scharlau, Fischer, SDS) were of commercial quality and were used as received. Mechanochemical reactions were carried out in a vibratory mixer mill at a frequency of 20 Hz using a 25 mL zirconium oxide grinding jar and a single zirconium oxide ball 20 mm in diameter. Reactions were monitored by thin layer chromatography on aluminium plates coated with silica gel and fluorescent indicator (Macherey-Nagel Xtra SIL G/UV254). Separations by flash chromatography were performed on silica gel (Scharlau 40–60 µm, 230–400 mesh ASTM) or neutral alumina (Merck S22). Melting points were determined using a Stuart Scientific apparatus, SMP3 Model, and are uncorrected. Infrared spectra were recorded with an Agilent Cary630 FTIR spectrophotometer working by attenuated total reflection (ATR), with a diamond accessory for solid and liquid samples. NMR spectroscopic data were recorded using a Bruker Avance 250 spectrometer operating at 250 MHz for ^{1}H NMR and 63 MHz for ^{13}C NMR maintained by the NMR facility of Universidad Complutense (CAI de Resonancia Magnética Nuclear); chemical shifts are given in ppm and coupling constants in Hertz. High-resolution mass spectra (HRMS) were recorded on a mass spectrometer fitted with an electrospray detector (ESI) by the mass spectral facility of Universidad Complutense (CAI de Espectrometría de Masas) and elemental analyses were determined by the microanalysis facility of Universidad Complutense (CAI de Microanálisis Elemental), using a Leco 932 combustion microanalyzer.

7.7.1. Preparation of α-iodocarbonyl derivatives

Method A:

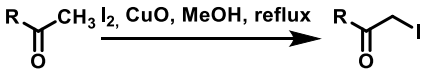

To a solution of the suitable ketone (1 eq) in anhydrous methanol, iodine (1 eq) and copper (II) oxide (1 eq) were added. The mixture was stirred at room temperature for 5 min and, then, refluxed until no starting material was detected by TLC. The reaction was cooled, filtered and the solvent was removed. The residue was dissolved in ethyl acetate (10 mL) and washed with a 10% solution of $Na_2S_2O_3$ (20 mL). The aqueous phase was extracted with ethyl acetate (2 x 20 mL) and the combined organic layers were dried over anhydrous sodium sulphate and the solvent was evaporated. The α-iodoketones thus obtained were used in the next reaction without further purification.

Method B:

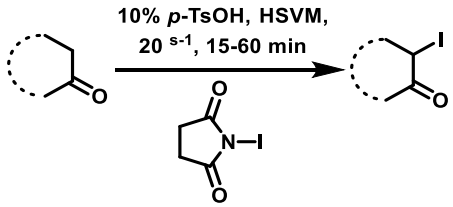

The corresponding ketone (1 mmol), *N*-iodosuccinimide (NIS, 225 mg, 1 mmol) and *p*-toluenesulphonic acid (18 mg, 10% mmol) were added to a ball mill vessel, along with a zirconium oxide ball. The vessel was fitted to one of the horizontal vibratory arms of the ball mill, while the other arm was occupied with an empty vessel. The ball mill was set to vibrate at a frequency of 20 s^{-1} for 15-60 min at room temperature. Then, the reaction vessel was cleansed with ethyl acetate. The organic layer was washed with water (2 mL), dried over anhydrous sodium sulphate and the solvent was evaporated under reduced pressure.

1-(3-Indolyl)-2-iodoethanone

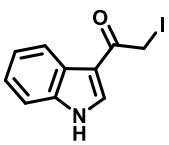

Method A. Prepared from 1-(3-indolyl)ethanone (0.395 g, 2.5 mmol); reaction time: 3 h. Yellowish solid. Yield: 0.620 g, 87%

Mp 87-89 °C.

IR (neat) 3222.7 (N-H), 1635.7 (C=O) cm^{-1}.

^{1}H NMR (250 MHz, *d*$_4$-methanol): δ 8.30 (s, 1H); 8.24-8.19 (m, 1H); 7.51-7.45 (m, 1H); 7.28-7.25 (m, 2H); 4.94 (s, 2H) ppm.

^{13}C NMR (63 MHz, *d*$_4$-methanol): δ 191.8, 138.9, 136.2, 127.5, 124.9, 123.8, 123.2, 115.0, 113.3, 3.5 ppm.

Elemantal analysis (%): calcd. for $C_{10}H_8NOI$: C 42.13, H 2.83, N 4.91; found: C 41.42, H 2.85, N 5.10.

2-Iodo-1-(2-furyl)ethenone[232]

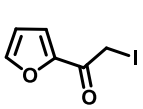

Method B. Prepared from 1-(2-furyl) ethanone (0.550 g, 5 mmol). Reddish oil. Yield: 1.1 g, 93%

IR (neat) 1665.7 (C=O), 766.8 (C-I) cm^{-1}.

^{1}H NMR (250 MHz, CDCl3): δ 7.65 (dd, *J* = 1.7, 0.7 Hz, 1H); 7.34 (dd, *J* = 3.6, 0.7 Hz, 1H); 6.61 (dd, *J* = 3.6, 1.7 Hz, 1H); 4.27 (s, 2H) ppm.

^{13}C NMR (63 MHz, CDCl3): δ 182.1, 149.8, 147.0, 118.9, 112.9, 0.51 ppm.

1-(*9H*-Fluoren-2-yl)-2-iodoethanone[232]

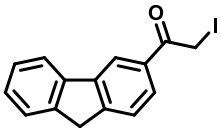

Method A. Prepared from 1-(9*H*-fluoren-2-yl)ethanone (0.624 g, 3 mmol); reaction time: 2 h.

White solid. Yield: 0.972 g, 97%

Mp: 162-164 °C.

IR (neat) 1658.8 (C=O) cm^{-1}.

^{1}H NMR (250 MHz, $CDCl_3$): δ 8.21 (d, *J* = 0.8 Hz, 1H); 8.07 (d, *J* = 8.1 Hz,1H); 7.89 (d, *J* = 7.5 Hz, 2H); 7.65-7.62 (m, 1H); 7.49-7.39 (m, 2H); 4.45 (s, 2H), 4.02 (s, 2H) ppm.

^{13}C NMR (63 MHz, $CDCl_3$): δ 192.7, 147.2, 144.6, 143.5, 140.3, 131.8, 128.5, 128.3, 127.1, 125.7, 125.3, 121.0, 119.9, 36.9, 2.0 ppm.

Elemental analysis (%): calcd. for $C_{15}H_{11}IO$: C 53.92, H 3.32; found: C 53.94, H 3.26.

1-(1-methyl-1*H*-indol-3-yl)ethan-1-one

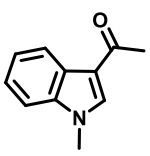

A mixture of 1-(3-indolyl)ethanone (2.5 g, 15.8 mmol), potassium hydroxide (1.7 g, 31.61 mmol) and methyl iodide (1.96 mL, 31.61 mmol) in DMF (3 mL) were stirred at room temperature for 4 h. Upon completion of the reaction, a saturated solution of amonium chloride (5 mL) was added. This solution was extracted with ethyl acetate (3 x 10 mL), dried over anhydrous sodium sulphate and

the organic solvents were evaporated under reduced pressure, to give the desired product.

Beige solid. Yield: 2.4 g, 99%

Mp: 106-107 °C

IR (neat) 1634.8 (C=O), 1096.3 (N-C) cm^{-1}.

^{1}H NMR (250 MHz, $CDCl_3$): δ 8.30 – 8.14 (m, 1H), 7.55 (s, 1H), 7.20 – 7.10 (m, 3H), 3.69 (s, 3H), 2.37 (s, 3H) ppm.

^{13}C NMR (63 MHz, $CDCl_3$): δ 193.4, 137.8, 136.2, 126.6, 123.7, 122.9, 122.9, 117.2, 110.0, 33.9, 28.0 ppm.

Elemental analysis (%): calcd. for $C_{11}H_{11}NO$: C 76.28 H 6.48 N 8.09; found: C 76.23 H 6.45 N 7.99.

2-Iodo-1-(1-methyl-1*H*-indol-3-yl)ethan-1-one

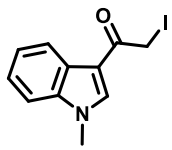

Method A. Prepared from 1-(1-methyl-1*H*-indol-3-yl)ethan-1-one (2.4 g, 13.54 mmol); reaction time: 5 h. Orange solid. Yield: 0.890 g, 36%

Mp 106-108 °C.

IR (neat) 1624.3 (C=O), 1125.2 (N-C) cm^{-1}.

^{1}H NMR (250 MHz, $CDCl_3$): δ 8.41 – 8.34 (m, 1H), 7.83 (s, 1H), 7.39 (t, *J* = 2.7 Hz, 3H), 4.27 (s, 2H), 3.89 (s, 3H) ppm.

^{13}C NMR (63 MHz, $CDCl_3$): δ 188.1, 138.01, 136.7, 126.8, 124.2, 123.3, 123.1, , 113.1, 110.2, 34.1, 4.1 ppm.

Elemantal analysis (%): calcd. for $C_{11}H_{10}INO$: C 44.17, H 3.37, N 4.68; found: C 44.14, H 3.35, N 4.64.

2-Iodo-1-(2-thienyl)ethanone[232]

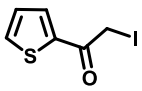

Method A. Prepared from 1-(2-thienyl)ethanone (0.315 g, 2.5 mmol); reaction time: 1 h. Yellow solid. Yield: 0.559 g, 89%

Mp: 130-134 °C.

IR (neat) 1705.6 (C=O) cm^{-1}.

^{1}H NMR (250 MHz, $CDCl_3$): δ 7.81 (dd, *J* = 3.9 Hz, 1.1 Hz, 1H); 7.71 (dd, *J* = 7.3, 2.4 Hz, 1H,); 7.17 (dd, *J* = 7.3, 2.4 Hz, 1H); 4.32 (s, 2H) ppm.

^{13}C NMR (63 MHz, $CDCl_3$): δ 186.0, 140.2, 135.1, 133.4, 128.3, 1.4 ppm.

7.7.2. Pyrrole synthesis

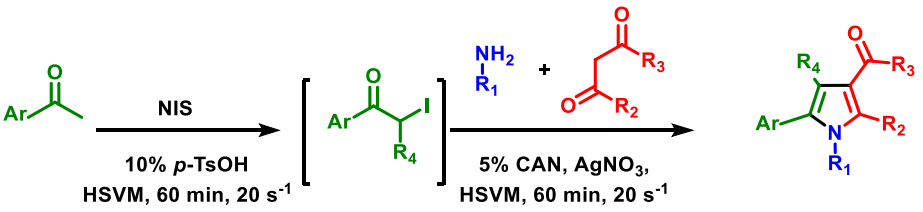

The suitable ketone (1 mmol), *N*-iodosuccinimide (NIS, 1 mmol) and *p*-toluensulphonic acid (PTSA, 10% mmol) were added to a ball mill vessel, along with a zirconium oxide ball. The vessel was fitted to one of the horizontal vibratory arms of the mall mill, while the other arm was occupied with an empty vessel. The ball mill was set to vibrate at a frequency of 20 s^{-1} for 60 min at room temperature. Then, a mixture of the corresponding amine (1.95 mmol), the suitable β-dicarbonyl compound (1.5 mmol) and cerium (IV) ammonium nitrate (CAN, 5% mmol), previously stirred at room temperature during 30 min, and silver nitrate (1 mmol) were added to the vessel. The reaction was subjected to the vibratory movement at the same frequency for 60 min. Then, the reaction vessel was cleansed with ethyl acetate and the suspension was filtered to remove the silver iodide precipitate. The organic layer was washed with water (2 mL), dried over anhydrous sodium sulphate and the solvent was removed under reduced pressure. Purification by column chromatography on silica gel eluting with a hexane-ethyl acetate mixture afforded the desired compounds **29a-u**.

Ethyl 5-(4-chlorophenyl) -2-methyl-1*H*-pyrrole-3-carboxylate) (29a)

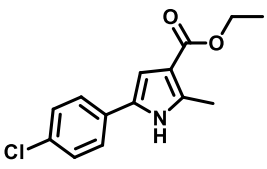

Prepared from 2-(*p*-chlorophenyl)ethanone (0.464 g, 3 mmol) and comercially available ethyl 3-amino-2-butenoate (0.580 mg, 4.5 mmol); the compound was purified by flash chromatography through a silica gel column using hexane: ethyl acetate as the mobile phase to give the desired product as a white solid. Yield: 0.475 g, 60%.

Mp 155-157 °C

IR (neat) 3321.8 (N-H), 1672.1 (C=O), 1235.2 (C-O) cm^{-1}

^{1}H RMN (250 MHz, $CDCl_3$): δ 8.69 (s, 1H); 7.43-7.33 (m, 4H); 6.85 (d, *J* = 2.9 Hz, 1H); 4.32 (q, *J* = 7.1Hz, 2H); 2.61 (s, 3H); 1.39 (t, *J* = 7.1 Hz, 3H) ppm.

^{13}C RMN (63 MHz, $CDCl_3$): δ 165.5, 136.6, 132.1, 130.3, 129.1 (2C), 128.9, 124.8 (2C), 113.5, 107.8, 59.7, 14.5, 13.4 ppm.

Elemental analysis (%): calcd. for $C_{14}H_{14}ClNO_2$: C 63.76, H 5.35, N 5.31; found: C 63.69, H 5.30, N 5.30.

Ethyl 5-(4-methoxyphenyl)-2-methyl-1H-pyrrole-3-carboxylate (29b)

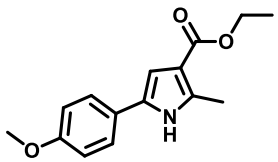

Prepared from 2-(*p*-methoxyphenyl)ethanone (0.450 g, 3 mmol) and comercially available ethyl 3-amino-2-butenoate (0.580 mg, 4.5 mmol); the compound was purified by flash chromatography through a silica gel column using hexane: ethyl acetate as the mobile phase to give the desired product as a grey solid. Yield: 0.210 g, 27%.

Mp 141-145 °C

IR (neat) 3308.5 (N-H), 1669.9 (C=O), 1250.6 y 1234.9 (C-O) cm^{-1}.

^{1}H RMN (250 MHz, $CDCl_3$): δ 8.58 (s, 1H); 7.41 (d, *J* = 8.7 Hz, 2H); 6.92 (d, *J* = 8.7 Hz, 2H); 6.74 (d, *J* = 2.7Hz, 1H); 4.32 (q, *J* = 7.1Hz, 2H); 3.84 (s, 3H) 2.59 (s, 3H); 1.38 (t, *J* = 7.1Hz, 3H) ppm.

^{13}C RMN (63 MHz, $CDCl_3$): δ 165.7, 158.4, 135.6, 130.0, 125.1 (2C), 124.8, 114.3 (2C), 113.1, 106.1, 59.4, 55.3, 14.5, 13.3 ppm.

Elemental analysis (%): calcd. for $C_{15}H_{17}NO_3$: C 69.48, H 6.61, N 5.40; found: C 69.45, H 6.60, N 5.36.

Ethyl 1,5-bis(*p*-chlorophenyl)-2-methyl-1*H*-pyrrole-3-carboxylate (29c)[232]

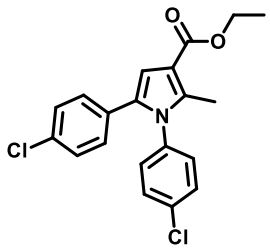

Prepared from 2-(*p*-chlorophenyl)ethanone (0.154 g, 1 mmol), *p*-chloroaniline (0.191 g, 1.5 mmol) and ethyl acetoacetate (0.195 g, 1.5 mmol); the compound was purified by flash chromatography through a silica gel column using hexane: ethyl acetate as the mobile phase to give the desired product as a yellow solid. Yield: 0.296 g, 79%.

Mp 123-127 °C.

IR (neat) 1701.7 (C=O), 1229.5 (C-O), 1088.7 and 1073.7 (C-Cl) cm^{-1}.

^{1}H RMN (250 MHz, $CDCl_3$): δ 7.41 (d, *J* = 8.6 Hz, 2H); 7.16 (d, *J* = 8.6 Hz, 2H); 7.09 (d, *J* = 8.6 Hz, 2H); 6.99 (d, *J* = 8.6 Hz, 2H); 6.81 (s, 1H); 4.35 (q, *J* = 7.1 Hz, 2H); 2.42 (s, 3H); 1.40 (t, *J* = 7.1 Hz, 3H) ppm.

^{13}C RMN (63 MHz, $CDCl_3$): δ 165.3, 138.2, 136.3, 134.4, 132.6, 132.6, 130.5, 129.6 (2C).129.6 (2C), 129.2 (2C), 128.4 (2C), 113.3, 110.6, 59.7, 14.5, 12.5 ppm.

Elemental analysis (%): calcd. for $C_{20}H_{17}Cl_2NO_2$: C 64.18, H 4.58, N 3.74; found: C 64.00, H 4.50, N 3.68.

Ethyl 5-(*p*-chlorophenyl)-2-methyl-4-phenyl-*1H*-pyrrole-3-carboxylate (29d)[232]

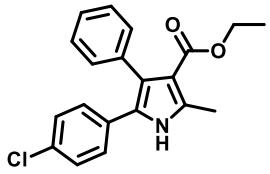

Prepared from 1-(*p*-chlorophenyl)-2-iodo-2-phenylethanone (0.355 g, 1 mmol), ethyl 3-amino-2-butenoate (0.194 g, 1.5 mmol); the compound was purified by flash chromatography through a silica gel column using hexane: ethyl acetate as the mobile phase to give the desired product as a yellowish solid. Yield: 0.173 g, 51 %.

Mp 232-234 °C.

IR (neat) 3292.9 (N-H), 1672.4 (C=O), 1093.9 (C-Cl) cm^{-1}.

^{1}H RMN (250 MHz, $CDCl_3$): δ 8.39 (br s, 1H), 7.33-7.22 (m, 5H), 7.18 (d, *J*=8.7 Hz, 2H), 7.04 (d, *J*=8.7 Hz, 2H), 4.10 (q, *J*=7.1 Hz, 2H), 2.63 (s, 3H), 1.06 (t, *J*=7.1 Hz, 3H) ppm.

^{13}C NMR (63 MHz, $CDCl_3$): δ 165.5, 135.7, 135.0, 132.1, 131.4, 131.2 (2C), 130.6 (2C), 128.0 (2C), 127.4 (2C), 126.7, 126.5, 123.8, 112.7, 59.3, 13.9, 13.8 ppm.

Elemental analysis (%): calcd. for $C_{20}H_{18}ClNO_2$: C 70.69, H 5.34, N 4.12; found: C 70.59, H 5.30, N 4,00.

Ethyl 1-butyl-5-(3-indolyl)-2-methyl-1*H*-pyrrole-3-carboxylate (29e)

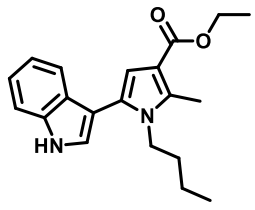

Prepared from 1-(3-indolyl)-2-iodoethanone (0.285 g, 1 mmol), butylamine (0.142 g, 1.95 mmol) and ethyl acetoacetate (0.195 g, 1.5 mmol); the compound was purified by flash chromatography through a silica gel column using hexane: ethyl acetate as the mobile phase to give the desired product as a yellowish solid. Yield: 0.243 g, 75%.

Mp 87-91°C.

IR (neat) 3318.6 (N-H), 1672.9 (C=O), 1244.9 (C-O) cm^{-1}.

^{1}H RMN (250 MHz, $CDCl_3$): δ 8.33 (br s, 1H); 7.59 (d, *J* = 7.8 Hz, 1H); 7.46 (d, *J* = 8.0 Hz, 1H); 7.27 (t, *J* = 7.1 Hz, 1H); 7.24 (d, *J* = 2.6 Hz, 1H); 7.18 (t, *J* = 7.1 Hz, 1H); 6.65 (s, 1H);

4.32 (q, *J* = 7.1 Hz, 2H); 3.91-3.85 (m, 2H); 2.67 (s, 3H); 1.58-1.46 (m, 2H); 1.38 (t, *J* =7.1 Hz, 3H); 1.15 (sext, *J* = 7.3 Hz, 2H); 0.76 (t, *J* = 7.3, 3H) ppm.

^{13}C RMN (63 MHz, $CDCl_3$): δ 165.8, 135.9, 135.7, 127.7, 125.6, 123.7, 122.5, 120.3, 119.8, 111.7, 111.2, 110.4, 108.9, 59.2, 44.0, 32.9, 19.7, 14.6, 13.5, 11.7 ppm.

Elemental analysis (%): calcd. for $C_{20}H_{24}N_2O_2$: C 74.04, H 7.46, N 8.63; found: C 73.99, H 7.39, N 8.59.

Ethyl 1-butyl-5-(*p*-iodophenyl)-2-methyl-*1H*-pyrrole-3-carboxylate (29f)[232]

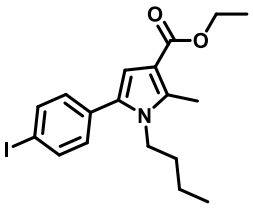

Prepared from 1-(*p*-iodophenyl)ethanone (0,492 g, 2 mmol), butylamine (0,284 g, 3.9 mmol), ethyl acetoacetate (0,390 g, 3 mmol); the compound was purified by flash chromatography through a silica gel column using hexane: ethyl acetate as the mobile phase to give the desired product as a white solid. Yield: 0,632 g, 77%.

Mp 65-68 °C.

IR (neat) 1685.2 (C=O), 1235.6 (C-O) cm^{-1}.

^{1}H NMR (250 MHz, $CDCl_3$): δ 7.75 (d, *J* = 8.3 Hz, 2H); 7.11 (d, *J* = 8.3 Hz, 2H); 6.56 (s, 1H); 4.30 (q, *J* = 7.1 Hz, 2H); 3.90-3.84 (m, 2H); 2.63 (s, 3H); 1.58-1.46 (m); 1.26-1.11 (m, 2H); 1.37 (t, *J* = 7.1 Hz, 3H); 0.83 (t, *J* = 7.2 Hz, 3H) ppm.

^{13}C NMR (63 MHz, $CDCl_3$): δ 165.5, 136.8, 132.6, 132.2, 137.5 (2C), 130.9 (2C), 112.1, 110.1, 93.0, 59.3, 43.9, 32.7, 19.7, 14.5, 13.5, 11.6 ppm.

Elemental analysis (%): calcd. for $C_{18}H_{22}INO_2$: C 52.57, H 5.39, N 3.41; found: C 52.49, H 5.30, N 3.37.

Ethyl 5-(2-furyl) -2-methyl-1*H*-pyrrole-3-carboxylate (29g)[232]

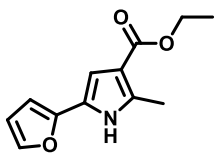

Prepared from 2-iodo-1-(2-furyl)ethanone (0.236 m, 1 mmol), ethyl aminocrotonate (0.194 g, 1.5 mmol); the compound was purified by flash chromatography through a silica gel column using hexane: ethyl acetate as the mobile phase to give the desired product as a white solid. Yield: 0,164 g, 75%.

Mp 133-135 °C.

IR (neat) 3298.1 (N-H), 1674.5 (C=O), 1242.3 (C-O) $cm^{-1.}$

^{1}H RMN (250 MHz, $CDCl_3$): δ 8.62 (br s, 1H, NH); 7.36 (dd, *J* =1.8, 0.7 Hz, 1H); 6.76 (d, *J* = 2.9 Hz, 1H); 6.45 (dd, *J* = 3.4, 1.8 Hz, 1H); 6.38 (dd, *J* = 3.4, 0.7 Hz, 1H); 4.31 (q, *J* = 7.1 Hz, 2H); 2.59 (s, 3H); 1.38 (t, *J* = 7.1 Hz, 3H) ppm.

^{13}C RMN (63 MHz, $CDCl_3$): δ 165.4, 147.2, 140.5, 135.5, 121.8, 113.0, 111.5, 106.5, 102.8, 59.2, 14.5, 13.2 ppm.

Elemental analysis (%): calcd for $C_{12}H_{13}NO_3$: C 65.74, H 5.98, N 6.39; found: C 65.63, H 5.91, N 6.32.

Ethyl 5-(4-iodophenyl)-2-methyl-1*H*-pyrrole-3-carboxylate (29h)

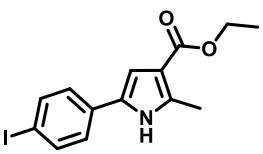

Prepared from 1-(*p*-iodophenyl)ethanone (0.738 g, 3 mmol), ethyl 3-amino-2-butenoate (0.580 g, 4.5 mmol); the compound was purified by flash chromatography through a silica gel column using hexane: ethyl acetate as the mobile phase to give the desired product as a grey solid. Yield: 0,362 g, 34%.

Mp 153-155 °C.

IR (neat) 3330.3 (N-H), 1657.5 (C=O), 1239.94 (C-O) cm^{-1}.

^{1}H NMR (250 MHz, $CDCl_3$): δ 8.29 (s, 1H), 7.62 – 7.54 (m, 2H), 7.14 – 7.06 (m, 2H), 6.75 (d, *J* = 3.0 Hz, 1H), 4.20 (q, *J* = 7.1 Hz, 2H), 2.50 (s, 3H), 1.27 (t, *J* = 7.1 Hz, 3H) ppm.

^{13}C NMR (63 MHz, $CDCl_3$): δ 165.7, 138.4 (2C), 136.9, 131.7, 129.2, 125.7 (2C), 114.1, 108.4, 91.6, 60.0, 14.9, 13.8 ppm.

Elemental analysis (%): calcd. for $C_{14}H_{14}INO_2$: C 47.34, H 3.97, N 3.94; found: C 47.15, H 3.90, N 3.92.

Ethyl 5-(3-chlorophenyl)-2-methyl-1*H*-pyrrole-3-carboxylate (29i)

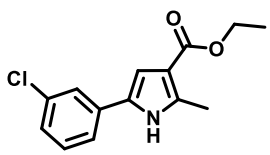

Prepared from 2-(*m*-chlorophenyl)ethanone (0.464 g, 3 mmol), ethyl 3-amino-2-butenoate (0.580 g, 4.5 mmol); the compound was purified by flash chromatography through a silica gel column using hexane: ethyl acetate as the mobile phase to give the desired product as a grey solid. Yield: 0.403 g, 51%.

Mp 139-141 °C.

IR (neat) 3279.4 (N-H), 1662.2 (C=O), 760.0 (C-Cl) cm^{-1}.

^{1}H NMR (250 MHz, $CDCl_3$): δ 8.35 (s, 1H), 7.30 – 6.93 (m, 4H), 6.67 (d, *J* = 3.0 Hz, 1H), 4.11 (q, *J* = 7.1 Hz, 2H), 2.40 (s, 3H), 1.18 (t, *J* = 7.1 Hz, 3H) ppm.

^{13}C NMR (63 MHz, $CDCl_3$): 165.8, 137.1, 135.3, 133.9, 130.6, 128.9, 126.8, 124.0, 122.1, 114.1, 108.8, 60.1, 14.9, 13.8 ppm.

Elemental analysis (%): calcd. for $C_{14}H_{14}ClNO_2$: C 63.76, H 5.35, N 5.31; C 62.84, H 5.39, N 5.22.

Ethyl 5-(3,4-dichlorophenyl)-2-methyl-1*H*-pyrrole-3-carboxylate (29j)

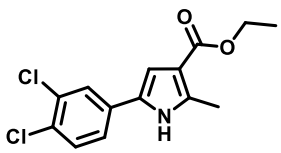

Prepared from 2-(3,4-dichlorophenyl)ethanone (0.576 g, 3 mmol), ethyl 3-amino-2-butenoate (0.580 g, 4.5 mmol); the compound was purified by flash chromatography through a silica gel column using hexane: ethyl acetate as the mobile phase to give the desired product as a yellowish solid. Yield: 0.420 g, 47 %.

Mp 178-180 °C.

IR (neat) 3287.2 (N-H), 1661.72 (C=O), 768.3 (C-Cl) cm^{-1}.

^{1}H NMR (250 MHz, $CDCl_3$): δ 8.44 (s, 1H), 7.53 (d, *J* = 2.1 Hz, 1H), 7.44 (d, *J* = 8.4 Hz, 1H), 7.32 – 7.26 (m, 1H), 6.87 (d, *J* = 3.0 Hz, 1H), 4.31 (q, *J* = 7.1 Hz, 2H), 2.61 (s, 3H), 1.38 (t, *J* = 7.1 Hz, 3H) ppm.

^{13}C NMR (63 MHz, $CDCl_3$): δ 163.1, 134.8, 131.0, 129.7, 128.7, 127.9, 125.4, 123.1, 120.7, 111.7, 106.6, 57.6, 12.4, 11.3 ppm.

Elemental analysis (%): calcd. for $C_{14}H_{13}Cl_2NO_2$: C 56.39, H 4.39, N 4.70; found: C 56.06, H 4.35, N 4.64.

Ethyl 5-(4-bromophenyl)-2-methyl-1*H*-pyrrole-3-carboxylate (29k)

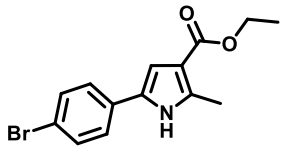

Prepared from 2-(*p*-bromophenyl)ethanone (597 mg, 3 mmol), ethyl 3-amino-2-butenoate (0.580 g, 4.5 mmol); the compound was purified by flash chromatography through a silica gel column using hexane: ethyl acetate as the mobile phase to give the desired product as a beige solid. Yield: 0.517 g, 56 %.

Mp 169-171°C.

IR (neat) 3332.4 (N-H), 1658.9 (C=O), 775.3 (C-Br) cm^{-1}.

^{1}H NMR (250 MHz, $CDCl_3$): δ 8.48 (s, 1H), 7.43 – 7.37 (m, 2H), 7.28 – 7.21 (m, 2H), 6.76 (d, *J* = 3.0 Hz, 1H), 4.22 (q, *J* = 7.1 Hz, 2H), 2.51 (s, 3H), 1.29 (t, *J* = 7.1 Hz, 3H) ppm.

^{13}C NMR (63 MHz, $CDCl_3$): δ 165.8, 136.9, 132.4 (2C), 131.1, 129.2, 125.5 (2C), 120.5, 114.0, 108.3, 60.1, 14.9, 13.8 ppm.

Elemental analysis (%): calcd. for $C_{14}H_{14}BrNO_2$: C 54.56, H 4.58, N 4.55; found: C 54.58, H 4.69, N 4.50.

Ethyl 5-(4-fluorophenyl)-2-methyl-1*H*-pyrrole-3-carboxylate (29l)

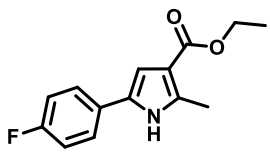

Prepared from 2-(*p*-fluorophenyl)ethanone (0.414 g, 3 mmol), ethyl 3-amino-2-butenoate (0.580 mg, 4.5 mmol); the compound was purified by flash chromatography through a silica gel column using hexane: ethyl acetate as the mobile phase to give the desired product as a violet solid. Yield: 0.526 g, 71%.

Mp 137-139°C.

IR (neat) 3282.9 (N-H), 1656.0 (C-OH),1226.7 (C-F) cm^{-1}.

^{1}H NMR (250 MHz, $CDCl_3$): δ 8.49 (s, 1H), 7.41 – 7.25 (m, 2H), 6.97 (ddd, *J* = 10.6, 6.0, 2.6 Hz, 2H), 6.67 (d, *J* = 2.8 Hz, 1H), 4.21 (q, *J* = 7.1 Hz, 2H), 2.49 (s, 3H), 1.27 (t, *J* = 7.1 Hz, 3H) ppm.

^{13}C NMR (63 MHz, $CDCl_3$): δ 166.0, 162.1 (d, *J* = 246.2 Hz), 136.6, 129.6, 128.6 (d, *J* = 2.9 Hz, 2C), 125.8 (d, *J* = 8.0 Hz, 2C), 116.3 (d, *J* = 21.8 Hz), 113.8, 107.6, 60.02, 14.9, 13.7 ppm.

Elemental analysis (%): calcd. for $C_{14}H_{14}FNO_2$:C 68.00, H 5.71, N 5.66; found: C 67.80, H 5.35, N 5.55.

Ethyl 1-butyl-5-(9*H*-fluoren-2-yl)-2-methyl-1*H*-pyrrole-3-carboxylate (29m)[232]

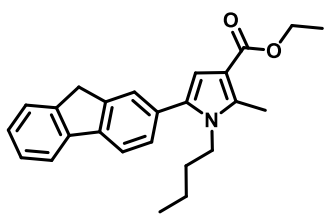

Prepared from 1-(9*H*-fluoren-2-yl)ethanone (0.208 g, 1 mmol), butylamine (0.142 g, 1.95 mmol) and ethyl acetoacetate (0.195 g, 1.5 mmol); the compound was purified by flash chromatography through a silica gel column using hexane: ethyl acetate as the mobile phase to give the desired product as a white solid. Yield: 0.362 g, 97%.

Mp 68-70 °C.

IR (neat) 1697.7 (C=O), 1229.3 (C-O) cm^{-1}.

^{1}H NMR (250 MHz, $CDCl_3$): δ 7.84 (d, *J* = 7.8 Hz, 2H); 7.60 (d, *J* = 7.3 Hz, 1H); 7.55 (s, 1H); 7.46-7.32 (m, 3H); 6.62 (s, 1H); 4.32 (q, *J* = 7.1 Hz, 2H); 3.97 (s, 2H); 3.97-3.91 (m, 2H); 2.66 (s, 3H); 1.56 (q, *J* = 7.3 Hz, 2H); 1.38 (t, *J* = 7.1 Hz, 3H); 1.20 (sext, *J* = 7.3 Hz, 2H); 0.82 (t, *J* = 7.3 Hz, 3H) ppm.

^{13}C NMR (63 MHz, $CDCl_3$): δ 165.7, 143.4, 143.3, 141.2, 141.0, 136.4, 133.8, 131.6, 128.0, 126.8 (2C), 126.0, 125.1, 119.9, 119.7, 111.9, 109.7, 59.3, 43.9 , 36.9, 32.7, 19.7, 14.5, 13.5, 11.6 ppm.

Elemental analysis (%) calcd. for $C_{25}H_{27}NO_2$: C 80.40, H 7.29, N 3.75; found: C 80.26, H 7.25, N 3.76.

Ethyl 1-dimethylamino-2-methyl-5-phenyl-*1H*-pyrrole-3-carboxylate (29n)[232]

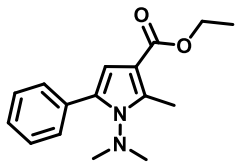

Prepared from acetophenone (0.120g, 1mmol), *N,N*-dimethylhydrazine (0.90 g, 1.5 mmol) and ethyl acetoacetate (0.195 g, 1.5 mmol); the compound was purified by flash chromatography through a silica gel column using hexane: ethyl acetate as the mobile phase to give the desired product as a reddish oil Yield: 0.163 g, 60%.

IR (neat) 1695.8 (C=O), 1241.8 (C-O) cm^{-1}.

^{1}H NMR (250 MHz, $CDCl_3$): δ 7.52 (dd, *J* = 8.3, 1.8 Hz, 2H); 7.43-7.32 (m, 3H); 6.53 (s, 1H); 4.30 (q, *J* = 7.1 Hz, 2H); 2.95 (s, 6H); 2.71 (s, 3H); 1.37 (t, *J* = 7.1 Hz, 3H) ppm.

^{13}C NMR (63 MHz, $CDCl_3$): δ 165.3, 137.3, 132.7, 132.7, 129.0, 127.8, 127.0, 110.3, 107.4, 59.3, 45.2, 14.5, 12.1 ppm.

Elemental analysis (%) calcd. for $C_{16}H_{20}N_2O_2$: C 70.56, H 7.40, N 10.29; found: C 70.48, H 7.35, N 10.19.

Ethyl 5-(3,4-dichlorophenyl)-1-hexyl-2-methyl-1*H*-pyrrole-3-carboxylate (29o)

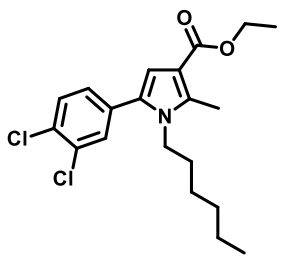

Prepared from 2-(3,4-dichlorophenyl)ethanone (2.84 g, 15 mmol), hexylamine (2.964 g, 29.3 mmol) and ethyl acetoacetate (2.928 g, 22.5 mmol); the compound was purified by flash chromatography through a silica gel column using hexane: ethyl acetate as the mobile phase to give the desired product as a yellow oil. Yield: 1.70 g, 30%.

IR (neat) 1185.1 (N-C), 1695.7 (C=O), 1185.1 (C-O) cm^{-1}.

^{1}H NMR (250 MHz, $CDCl_3$): δ 7.35 – 7.29 (m, 2H), 7.04 (dd, *J* = 8.2, 2.1 Hz, 1H), 6.42 (s, 1H), 4.13 (q, *J* = 7.1 Hz, 2H), 3.66 (t, *J* = 7.6 Hz, 2H), 2.46 (s, 3H), 1.33 (m, 2H), 1.16 (t, *J* = 7.1 Hz, 3H), 0.97 (m, 6H), 0.67 (t, *J* = 7.1 Hz, 3H) ppm.

^{13}C NMR (63 MHz, $CDCl_3$): δ 166.1, 137.9, 133.9, 133.2, 132.2, 131.5 (2C), 131.1, 128.9, 112.9, 111.4, 60.1, 44.9, 31.8, 31.3, 26.8, 23.1, 15.2, 14.6, 12.3 ppm.

Elemental analysis (%): calcd. for $C_{20}H_{25}Cl_2NO_2$: C 62.83, H 6.59, N 3.66; found: C 62.74, H 6.60, N 3.61.

Ethyl 1-butyl-2-methyl-5-(1-methyl-1*H*-indol-3-yl)-1*H*-pyrrole-3-carboxylate (29p)

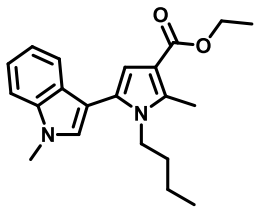

Prepared from 2-iodo-1-(1-methyl-1*H*-indol-3-yl)ethan-1-one (0.7 g, 2.67 mmol), butylamine (0.380 g, 5.206 mmol) and ethyl acetoacetate (0.521 g; 4 mmol); the compound was purified by flash chromatography through a silica gel column using hexane: ethyl acetate as the mobile phase to give the desired product as an orange solid. Yield: 0.398 g, 35 %.

Mp 122-123 °C.

IR (neat) 1189.7 (N-C), 1690.7 (C=O), 1227.5 (C-O) cm^{-1}.

^{1}H NMR (250 MHz, $CDCl_3$): δ 7.40 – 7.34 (m, 1H), 7.21 – 7.15 (m, 1H), 7.13 – 7.06 (m, 1H), 6.96 (ddd, *J* = 8.0, 6.9, 1.2 Hz, 1H), 6.86 (s, 1H), 6.41 (s, 1H), 4.11 (q, *J* = 7.1 Hz, 2H), 3.65 (d, *J* = 4.5 Hz, 5H), 2.46 (s, 3H), 1.35 – 1.25 (m, 2H), 1.17 (t, *J* = 7.1 Hz, 3H), 0.95 (dd, *J* = 15.0, 7.4 Hz, 2H), 0.56 (t, *J* = 7.3 Hz, 3H) ppm.

^{13}C NMR (63 MHz, $CDCl_3$): δ 166.3, 137.8, 136.3, 128.6 (2C), 122.5, 120.4, 120.2, 112.1, 110.7, 109.7, 107.6, 59.6, 44.4, 33.3, 33.2, 20.1, 15.0, 14.0, 12.1ppm.

Elemental analysis %): calcd. for $C_{21}H_{26}N_2O_2$: C 74.53, H 7.74, N 8.28; found: C 74.50, H 7.69, N 8.20.

Ethyl 5-(3,4-dichlorophenyl)-1-(3-(dimethylamino)propyl)-2-methyl-1*H*-pyrrole-3-carboxylate (29q)

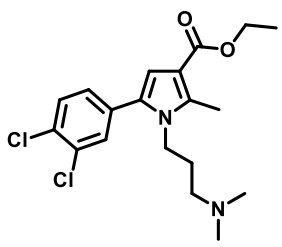

Prepared from 2-(3,4-dichlorophenyl)ethanone (3.15 g 10 mmol), N^1,N^1-dimethylpropane-1,3-diamine (1.999 g, 19.57 mmol) and ethyl and acetoacetate (1.957 g; 15.05 mmol); the compound was purified by flash chromatography through a silica gel column using hexane: ethyl acetate as the mobile phase to give the desired product as an orange oil Yield: 0.905 g, 24 %.

IR (neat) 1197.7 (N-C), 1690.5 (C=O), 1064.8 (C-O) cm^{-1})

^{1}H NMR (250 MHz, $CDCl_3$): δ 7.40 (dd, *J* = 8.0, 5.1 Hz, 2H), 7.15 – 7.09 (m, 1H), 6.50 (s, 1H), 4.20 (q, *J* = 7.1 Hz, 2H), 3.95 – 3.85 (m, 2H), 2.53 (s, 3H), 2.24 (d, *J* = 8.3 Hz, 8H), 1.75 – 1.63 (m, 2H), 1.27 (t, *J* = 7.1 Hz, 3H) ppm.

^{13}C NMR (63 MHz, $CDCl_3$): δ 165.7, 137.67, 133.2, 133.1, 132.1, 131.1, 131.0, 131.02, 128.6, 112.9, 111.6, 59.9, 56.1, 44.7 (2C), 42.3, 27.9, 14.9, 11.9 ppm.

Elemental analysis (%): calcd. for $C_{19}H_{24}Cl_2N_2O_2$: C 59.54, H 6.31, N 7.31; found: C 59.46, H 6.29, N 7.25.

Ethyl 1-butyl-5-(3,4-dichlorophenyl)-2-methyl-1*H*-pyrrole-3-carboxylate (29r)

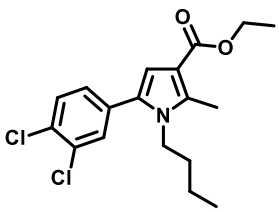

Prepared from 2-(3,4-dichlorophenyl)ethanone (0.567 g, 3 mmol), butylamine (0.402 g, 5.5 mmol) and ethyl and acetoacetate (0.523 g, 4.25 mmol); the compound was purified by flash chromatography through a silica gel column using hexane: ethyl acetate as the mobile phase to give the desired product as a yellow oil. Yield: 0.438 g, 41 %.

IR (neat) 1695 (C=O), 773 (C-Cl) cm^{-1}.

^{1}H NMR (250 MHz, d_6-acetone): δ 7.65 (d, *J* = 8.3 Hz, 1H), 7.61 (d, *J* = 2.1 Hz, 1H), 7.41 (dd, *J* = 8.3, 2.1 Hz, 1H), 6.56 (s, 1H), 4.23 (q, *J* = 7.1 Hz, 2H), 4.06 – 3.97 (m, 2H), 2.62 (s, 3H), 1.63 – 1.48 (m, 2H), 1.32 (t, *J* = 7.1 Hz, 3H), 1.21 (dd, *J* = 14.9, 7.4 Hz, 2H), 0.82 (t, *J* = 7.3 Hz, 3H) ppm.

^{13}C NMR (63 MHz, d_6-acetone): δ 165.8; 138.5; 135.1; 133.2; 132.0 (2C); 131.9; 130.1 (2C); 113.5; 112.1; 60.0; 45.0; 33.8; 20.7; 15.3; 14.2; 12.0 ppm.

Elemental analysis (%): calcd. for $C_{18}H_{21}Cl_2NO_2$: C 61.03, H 5.98, N 3.95; found: C 60.79, H 5.82, N 4.24.

Ethyl 1-butyl-5-(3,4-dichlorophenyl)-2-propyl-1*H*-pyrrole-3-carboxylate (29s)

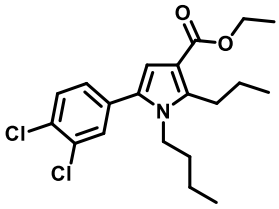

Prepared from 2-(3,4-dichlorophenyl)ethanone (0.567 g, 3 mmol), butylamine (0.657 g, 9 mmol) and ethyl 3-oxohexanoate (0.950 g, 6 mmol); the compound was purified by flash chromatography through a silica gel column using hexane: ethyl acetate as the mobile phase to give the desired product as a yellow oil. Yield: 0.411 g, 36 %.

IR (neat) 1697 (C=O), 775 (C-Cl) cm^{-1}.

^{1}H NMR (250 MHz, d_6-acetone): δ 7.44 (d, *J* = 5.6 Hz, 1H), 7.41 (s, 1H), 7.21 (dd, *J* = 8.4, 2.0 Hz, 1H), 6.34 (s, 1H), 4.00 (q, *J* = 7.1 Hz, 2H), 3.89 – 3.78 (m, 2H), 2.85 – 2.76 (m, 2H),

1.43 (dq, *J* = 14.9, 7.4 Hz, 2H), 1.28 (dt, *J* = 21.4, 7.5 Hz, 2H), 1.09 (t, *J* = 7.1 Hz, 3H), 0.97 (dd, *J* = 14.9, 7.4 Hz, 2H), 0.79 (t, *J* = 7.4 Hz, 3H), 0.57 (t, *J* = 7.3 Hz, 3H) ppm.

^{13}C NMR (63 MHz, d_6-acetone): δ 165.5; 143.1; 135.3; 133.3; 132.0 (2 C); 131.9; 131.8; 130.1; 113.3; 112.5; 60.0; 45.0; 34.4; 28.4; 24.6; 20.7; 15.3; 14.8; 14.2 ppm.

Elemental analysis (%) calcd. for $C_{20}H_{25}Cl_2NO_2$: C 62.83, H 6.59, N 3.66; found: C 62.70, H 6.53, N 3.90.

Ethyl 5-(*p*-chlorophenyl)-1-(*p*-methoxyphenyl)-2-methyl-*1H*-pyrrole-3-carboxylate (29t)[232]

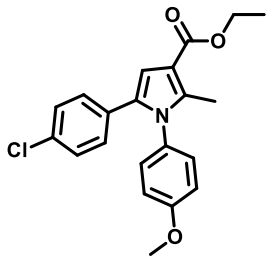

Prepared from *p*-anisidine (0.185 g, 1.5 mmol), 2-(*p*-chlorophenyl)ethanone (0.154 g, 1 mmol) and ethyl acetoacetate (0.195 g, 1.5 mmol); the compound was purified by flash chromatography through a silica gel column using hexane: ethyl acetate as the mobile phase to give the desired product as a white solid. Yield: 0.229 g, 62 %.

Mp 108-111°C

IR (neat) 1699.3 (C=O), 1227.4 (C-O), 1076.3 (C-Cl) cm^{-1}.

^{1}H NMR (250 MHz, $CDCl_3$): δ 7.15 (d, *J* = 8.7 Hz, 2H); 7.07 (d, *J* = 9.0 Hz, 2H); 7.00 (d, *J* = 8.7 Hz, 2H); 6.93 (d, *J* = 9.0 Hz, 2H); 6.80 (s, 1H); 4.35 (q, *J* = 7.1 Hz, 2H); 3.87 (s, 3H); 2.41 (s, 3H); 1.40 (t, *J* = 7.1 Hz, 3H) ppm.

^{13}C NMR (63 MHz, $CDCl_3$): δ 165.4, 159.3, 138.7, 132.7, 132.3, 130.9, 130.5, 129.4 (2C), 129.2 (2C), 128.3 (2C), 114.4 (2C), 112.7 (C), 110.0 (C_4), 59.5, 55.4, 14.5, 12.4 ppm.

Elemental analysis (%): calcd. for $C_{21}H_{20}ClNO_3$: C 68.20, H 5.45, N 3.79; found: C 68.00, H 5.36, N 3.70.

Ethyl 1-butyl-5-(*p*-chlorophenyl)-2-methyl-1*H*-pyrrole-3-carboxylate (29u)

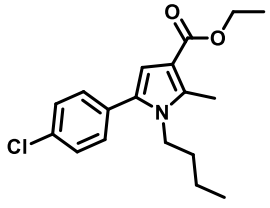

Prepared from *p*-chloroacetophenone (0.154 g, 1 mmol), butylamine (0.142 g, 1.95 mmol) and ethyl acetoacetate (0.195 g, 1.5 mmol); the compound was purified by flash chromatography through a silica gel column using hexane: ethyl acetate as the mobile phase to give the desired product as a yellowish viscous liquid. Yield: 0.252 g, 79 %.

IR (neat) 1698.2 (C=O), 1246.2 (C-O) cm^{-1}.

^{1}H NMR (250 MHz, $CDCl_3$): δ 7.43-7.28 (m, 4H); 6.56 (s, 1H); 4.31 (q, *J* = 7,1 Hz, 2H); 3.91-3.84 (m, 2H); 2.64 (s, 3H); 1.55-1.48 (m, 2H); 1.37 (t, *J* = 7.1 Hz, 3H); 1.19 (sext, *J* = 7.3 Hz, 2H); 0.83 (t, *J* = 7.3 Hz, 3H) ppm.

^{13}C NMR (63 MHz, $CDCl_3$): δ 165.4, 136.6, 133.4, 132.0, 131.6, 130.5 (2C), 128,6 (2C), 112.0, 110.1, 59.3, 43.9, 32.7, 19.7, 14.5, 13.5, 11.5 ppm.

Elemental analysis (%): calcd. for $C_{18}H_{22}ClNO_2$: C 67.60, H 6.93, N 4.38; found: C 67.56, H 6.84, N 4.22.

7.7.3. Preparation pyrrole-3-carboxylic acid derivatives 30a-p

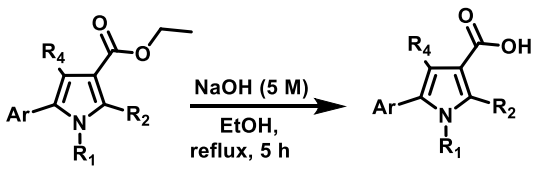

The suitable pyrrole derivative (1 mmol) was dissolved in ethanol (3 mL) and a solution of 5M NaOH was added (10 eq). Then, the mixture was refluxed for 5h. After completion of the reaction, the resulting suspension was neutralized with 2N HCl and extracted with ethyl acetate (5 mL) and. The organic layer was washed with water (3 mL) and dried over anhydrous sodium sulphate. Removal of the solvent gave the desired pyrrole-3-carboxylic acid derivatives.

5-(4-Iodophenyl)-2-methyl-1*H*-pyrrole-3-carboxylic acid (30a)

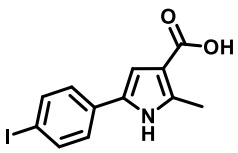

Prepared from pyrrole **29h** (0.300 g, 0.85 mmol). Beige solid. Yield: 0.255 g, 92%.

Mp 200-202 °C.

IR (neat) 3410.6 (N-H), 1648.2 (C=O) cm^{-1}.

^{1}H RMN (250 MHz, d_4-methanol): δ 7.57 (d, *J* = 8.5 Hz, 2H), 7.24 (d, *J* = 8.6 Hz, 2H), 6.71 (s, 1H), 2.42 (s, 3H) ppm.

^{13}C RMN (63 MHz, d_4-methanol): δ 169.9, 139.4, 139.3 (2C), 133.7, 130.9, 127.1 (2C), 114.5, 109.5, 91.1, 13.7 ppm.

Elemental analysis (%): calcd. for $C_{12}H_{10}INO_2$: C 44.06, H 3.08, N 4.28; found: C 44.03, H 3.01, N 3.96.

5-(3-Chlorophenyl)-2-methyl-1*H*-pyrrole-3-carboxylic acid (30b)

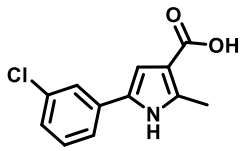

Prepared from pyrrole **29i** (0.304 g, 1.15 mmol). Brown solid. Yield: 0.203 g, 75%.

Mp 177-179 °C.

IR (neat) 3426.1 (N-H), 1599.21 (C=O), 763.44 (C-Cl) cm^{-1}.

^{1}H RMN (250 MHz, d_4-methanol): δ 7.44 (t, *J* = 1.8 Hz, 1H), 7.38 – 7.31 (m, 1H), 7.17 (t, *J* = 7.9 Hz, 1H), 7.05 – 6.99 (m, 1H), 6.69 (s, 1H), 2.39 (s, 3H) ppm.

^{13}C RMN (63 MHz, d_4-methanol): δ 169.7, 139.4, 136.2, 136.1, 131.7, 130.5, 127.2, 124.8, 123.3, 114.3, 109.7, 13.5 ppm.

Elemental analysis (%): calcd. for $C_{12}H_{10}ClNO_2$: C 61.16, H 4.28, N 5.94; found: C 60.90, H 4.28, N 5.94.

5-(3,4-Dichlorophenyl)-2-methyl-1*H*-pyrrole-3-carboxylic acid (30c)

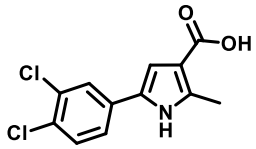

Prepared from pyrrole **29j** (0.298 g, 2.41 mmol). Brown solid. Yield: 0.546 g, 84 %.

Mp 194-196 °C.

IR (neat) 3349.0 (N-H), 1624.9 (C=O), 767.52 (C-Cl) cm^{-1}.

^{1}H NMR (250 MHz, d_4-methanol): δ 7.62 (d, *J* = 1.1 Hz, 1H), 7.37 (d, *J* = 1.7 Hz, 2H), 6.75 (s, 1H), 2.43 (s, 3H) ppm.

^{13}C RMN (63 MHz, d_4-methanol): δ 169.6, 139.7, 134.5, 134.1, 132.2, 130.6, 129.5, 126.5, 124.7, 114.6, 110.2, 13.5 ppm.

Elemental analysis (%): calcd. for $C_{12}H_9Cl_2NO_2$: C 53.36, H 3.36, N 5.19; found: C 52.98, H 3.29, N 5.02.

5-(4-Bromophenyl)-2-methyl-1*H*-pyrrole-3-carboxylic acid (30d)

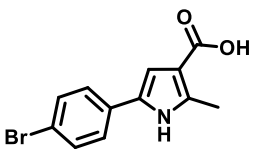

Prepared from pyrrole **29k** (0.300 mg, 0.97 mmol). Reddish solid. Yield: 0.236 g, 87 %.

Mp 152-154 °C.

IR (neat) 3224.5 (N-H), 1627.3 (C=O), 781.7 (C - Br) cm^{-1}.

^{1}H RMN (250 MHz, d_6-acetone): δ 10.68 (br s, 1H), 7.43 (q, *J* = 8.6 Hz, 4H), 6.75 (d, *J* = 2.6 Hz, 1H), 2.41 (s, 3H) ppm.

^{13}C RMN (63 MHz, *d_4*-methanol): δ 199.8, 169.8, 139.2, 133.2 (2C), 130.8, 126.7(2C), 120.8, 114.3, 109.2, 13.4 ppm.

Elemental analysis (%): calcd. for $C_{12}H_{10}BrNO_2$: C 51.45, H 3.60, N 5.00; found: C 51.20, H 3.60, N 4.63.

5-(4-Fluorophenyl)-2-methyl-1H-pyrrole-3-carboxylic acid (30e)

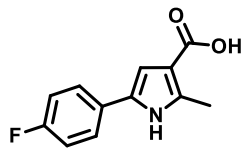

Prepared from pyrrole **29l** (0.381 g, 1.54 mmol). Reddish solid. Yield: 0.330 g, 98%.

Mp 148-150 °C.

IR (neat) 3282.9 (N-H), 1656.0 (C=O), 1226.7 (C-F) cm^{-1}.

^{1}H RMN (250 MHz, *d_4*-methanol): δ 11.12 (br s, 1H), 7.58 (dd, *J* = 8.3, 5.6 Hz, 2H), 7.10 (t, *J* = 8.8 Hz, 2H), 6.74 (s, 1H), 2.55 (s, 3H) ppm.

^{13}C RMN (63 MHz, *d_4*-methanol): δ 169.9, 163.2 (d, *J* = 243.8 Hz), 138.7, 131.18, 130.72 (d, *J* = 3.3 Hz), 126.9 (d, *J* = 7.8 Hz, 2C), 116.9 (d, *J* = 21.9 Hz, 2C), 114.0, 108.5, 13.4 ppm.

Elemental analysis (%): calcd. for $C_{12}H_{10}FNO_2$: C 65.75, H 4.60, N 6.39; found: C 65.61, H 4.63, N 6.41.

5-(4-Methoxyphenyl)-2-methyl-1*H*-pyrrole-3-carboxylic acid (30f)

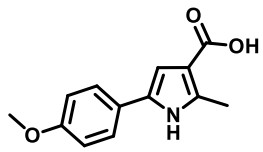

Prepared from pyrrole **29b** (0.105 g, 0.4 mmol). Red solid. Yield: 0.067 g, 73%.

Mp 179-181°C.

IR (neat) 3414.8 (N-H), 1654.5 (C=O), 1250.4 y 1231.7 (C-O) cm^{-1}.

^{1}H RMN (250 MHz, *d_6*-acetone): δ 10.47 (br s, 1H), 7.42 (d, *J* = 8.9 Hz, 2H), 6.81 (d, *J* = 8.9 Hz, 2H), 6. 56 (s, 1H), 3.67 (s, 3H), 2.39 (s, 3H) ppm.

^{13}C RMN (63 MHz, *d_6*-acetone): δ 167.3, 159.9, 137.2, 130.9, 126.6, 126.2 (2C), 116.1 (2C), 114.1, 107.2, 55.8, 13.8 ppm.

Elemental analysis (%): calcd. for $C_{13}H_{13}NO_3$: C 67.52, H 5.67, N 6.06; found: C 67.84, H 5.58, N 5.87.

5-(3,4-Dichlorophenyl)-1-hexyl-2-methyl-1*H*-pyrrole-3-carboxylic acid (30g)

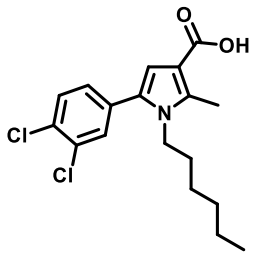

Prepared from pyrrole **29o** (1 g, 2.65 mmol). White solid. Yield: 0.580 g, 62%.

Mp 103-105 °C

IR (neat) 1640.4 (C=O), 1268.7 (C-O) cm^{-1}

^{1}H RMN (250 MHz, d_6-acetone): δ 7.51 (dd, *J* = 8.9, 5.2 Hz, 2H), 7.29 (dd, *J* = 8.3, 2.1 Hz, 1H), 6.43 (s, 1H), 3.87 (d, *J* = 7.7 Hz, 2H), 2.48 (s, 3H), 1.47 – 1.35 (m, 2H), 1.06 (d, *J* = 9.1 Hz, 6H), 0.68 (t, *J* = 6.6 Hz, 3H) ppm

^{13}C RMN (63 MHz, d_6-acetone): δ 206.6, 166.8, 138.7, 135.2, 133.2, 131.9, 131.8, 130.2, 113.3, 112.4, 45.1, 32.2, 31.5, 31.0, 27.1, 23.5, 14.6, 11.9 ppm

Elemental analysis (%): calcd. for $C_{18}H_{21}Cl_2NO_2$: C 61.03, H 5.98, N 3.95; found: C 61.01, H 5.92, N 3.92.

1-Butyl-2-methyl-5-(1-methyl-1*H*-indol-3-yl)-1*H*-pyrrole-3-carboxylic acid (30h)

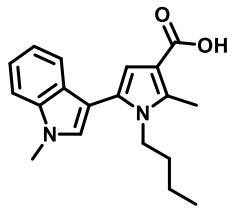

Prepared from pyrrole **29p** (0.300 g, 0.886 mmol). Grey solid. Yield: 0.195 g, 71%.

Mp 160-161 °C

IR (neat) 1654.7 (C=O), 1254.8 (C-O) cm^{-1}

^{1}H NMR (500 MHz, d_4-methanol): δ 7.43 (t, *J* = 8.2 Hz, 2H), 7.26 – 7.20 (m, 2H), 7.10 (t, *J* = 7.5 Hz, 1H), 6.50 (s, 1H), 3.94 – 3.89 (m, 2H), 3.86 (s, 3H), 2.62 (s, 3H), 1.48 – 1.43 (m, 2H), 1.11 (dt, *J* = 14.7, 7.4 Hz, 2H), 0.71 (t, *J* = 7.4 Hz, 3H) ppm.

^{13}C NMR (63 MHz, d_6-acetone): δ 169.7, 138.3, 137.3, 129.7, 129.6, 127.6, 123.0, 120.7, 120.4, 112.5, 111.8, 110.5, 108.1, 44.9, 33.9, 32.9, 20.6, 13.8, 11.9 ppm

Elemental analysis (%): calcd. for $C_{19}H_{22}N_2O_2$: C 73.52, H 7.14, N 9.03; found: C 73.51, H 7.07, N 9.39.

5-(3,4-dichlorophenyl)-1-(3-(dimethylamino)propyl)-2-methyl-1*H*-pyrrole-3-carboxylic acid (30i)

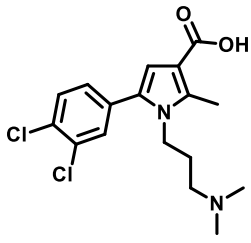

Prepared from pyrrole **29q** (0.150 g, 0.392 mmol). Orange solid. Yield: 0.098 g, 65%.

Mp 112-114 °C

IR (neat) 1672.6 (C=O), 1237.8 (C-O) cm^{-1}.

^{1}H NMR (500 MHz, *d*$_4$-methanol): δ 7.60 (t, *J* = 5.4 Hz, 2H), 7.36 (dd, *J* = 8.3, 1.9 Hz, 1H), 6.56 (s, 1H), 4.10 (s, 2H), 2.78 (d, *J* = 7.8 Hz, 2H), 2.74 (s, 3H), 2.65 (1, 6H), 1.93 – 1.84 (m, 2H) ppm.

^{13}C NMR (126 MHz, *d*$_4$-methanol): δ 169.0, 137.4, 133.7, 132.6, 131.6, 130.9, 130.8, 128.9, 114.1, 111.9, 55.9, 48.5 (2C), 42.3, 27.3, 11.8 ppm.

Elemental analysis (%): calcd. for $C_{17}H_{20}Cl_2N_2O_2$: C 57.48, H 5.67, N 7.89; found: C 57.43, H 5.68, N 7.86.

1-Butyl-5-(3,4-dichlorophenyl)-2-methyl-1*H*-pyrrole-3-carboxylic acid (30j)

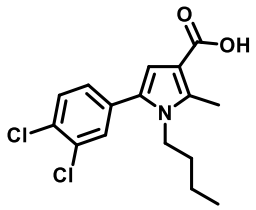

Prepared from pyrrole **29r** (0.320 g, 0.91 mmol). Yellow solid. Yield: 0.238 g, 81 %.

Mp 150-152 °C.

IR (neat) 3427.3 (O-H), 1651.7 (C=O), 819.5 (C-Cl) cm^{-1}.

^{1}H-RMN (250 MHz, *d*$_6$-acetone): δ 7.53 – 7.50 (m, 1H), 7.48 (d, *J* = 2.0 Hz, 1H), 7.28 (dd, *J* = 8.3, 2.1 Hz, 1H), 6.43 (s, 1H), 4.03 – 3.69 (m, 2H), 2.48 (s, 3H), 1.41 (ddd, *J* = 12.5, 8.4, 6.7 Hz, 2H), 1.18 – 0.88 (m, 2H), 0.67 (t, *J* = 7.3 Hz, 3H) ppm.

^{13}C-RMN (250 MHz, *d*$_6$-acetone): δ 167.0, 138.9, 135.2, 133.2, 132.0 (2C), 131.9 (2C), 130.2, 113.3, 112.5, 45.0, 33.7, 20.7, 14.2, 12.0 ppm.

Elemental analysis (%): calcd. for $C_{16}H_{17}Cl_2NO_2$: C 58.91, H 5.25, N 4.29; found: C 58.58, H 5.68, N 3.95.

1-Butyl-5-(3,4-dichlorophenyl)-2-propyl-1*H*-pyrrole-3-carboxylic acid (30k)

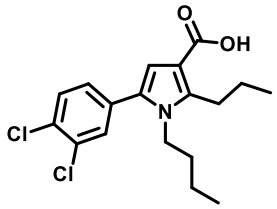

Prepared from pyrrole **29s** (0.300 g, 0.79 mmol). Yellow solid. Yield: 0.189 g, 68 %.

Mp 110-112 °C

IR (neat) 3462.4 (O-H), 1637.7 (C=O), 769.5 (C-Cl) cm^{-1}.

^{1}H-RMN (250 MHz, *d*$_6$-acetone): δ 7.52 (d, *J* = 4.4 Hz, 1H), 7.50 (d, *J* = 1.7 Hz, 1H), 6.44 (s, 1H), 3.89 (dd, *J* = 22.1, 14.3 Hz, 2H), 2.95 – 2.84 (m, 2H), 1.52 (dq, *J* = 14.9, 7.4 Hz, 2H), 1.43 – 1.29 (m, 2H), 1.11 - 1.02 (m, 2H), 0.86 (t, *J* = 7.4 Hz, 3H), 0.65 (t, *J* = 7.3 Hz, 3H) ppm.

^{13}C-RMN (250 MHz, *d*$_6$-acetone): δ 166.8, 143.4, 135.3, 133.2, 132.0 (2C), 131.9, 131.7, 130.1, 113.1, 112.9, 45.0, 34.4, 28.3, 24.6, 20.7, 14.7, 14.2 ppm.

Elemental analysis (%): calcd for $C_{18}H_{21}Cl_2NO_2$: C 61.03, H 5.98, N 3.95; found: C 60.83, H 5.59, N 3.66.

5-(4-Chlorophenyl)-2-methyl-1*H*-pyrrole-3-carboxylic acid (30l)

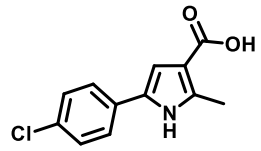

Prepared from pyrrole **29a** (0. 380 g, 1.44 mmol). Brown solid. Yield: 0.237 g, 70%.

^{1}H RMN (250 MHz, d_6-DMSO): δ 7.91 (d, *J* = 8.4 Hz, 2H), 7.80 (d, *J* = 8.5 Hz, 2H), 7.01 (s, 1H), 1.91 (s, 3H) ppm.

^{13}C RMN (63 MHz, d_6-DMSO): δ 173.70, 168.63, 138.51, 132.56, 131.49, 129.65 (2C), 129.50, 129.13 (2C), 128.86, 21.25 ppm.

Elemental analysis (%): calcd for $C_{12}H_{10}ClNO_2$: C 61.16, H 4.28, N 5.94; found: C 61.11, H 4.81, N 5.31.

1-Butyl-5-(*p*-chlorophenyl)-2-methyl-1*H*-pyrrole-3-carboxylic acid (30m)

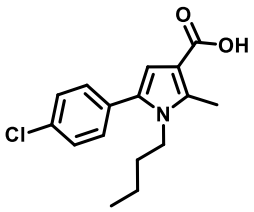

Prepared from pyrrole **29u** (0.315 g, 1 mmol). White solid. Yield: 0.270 g, 93%.

Mp 179-181°C.

IR (neat) 1660.6 (C=O), 1091.7 (C-Cl) cm^{-1}.

^{1}H NMR (250 MHz, $CDCl_3$): δ 7.42 (d, *J* = 8.6 Hz, 2H), 7.31 (d, 2H, *J* = 8.6), 6.62 (s, 1H), 3.92-3.85 (m, 2H), 2.65 (s, 3H), 1.57-1.46 (m, 2H), 1.28-1.12 (m, 2H), 0.84 (t, *J* = 7.2 Hz, 3H) ppm.

^{13}C NMR (63 MHz, $CDCl_3$): δ 170.7, 138.0, 133.6, 132.4, 131.4, 130.6, 128.7, 111.1 110.7, 44.0, 32.7, 19.7, 13.5, 11.7 ppm.

Elemental analysis (%): calcd. for $C_{16}H_{18}ClNO_2$: C 65.86, H 6.22, N 4.80; found: C 65.80, H 6.15, N 4.77.

1,5-Bis(*p*-chlorophenyl)-2-methyl-*1H*-pyrrole-3-carboxylic acid (30n)232

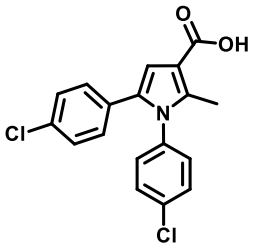

Prepared from pyrrole **29c** (0.374 g, 1 mmol). Yellow oil. Yield: 0.280 g, 81%.

IR (neat) 1662.8 (C=O), 1081.9 (C-Cl) cm^{-1}.

^{1}H NMR (250 MHz, $CDCl_3$): δ 7.42 (d, *J* = 8.6 Hz, 2H), 7.20 (d, *J* = 8.5 Hz, 2H), 7.12 (d, *J* = 8.6 Hz, 2H), 6.99 (d, *J* = 8.5 Hz, 2H), 6.87 (s, 1H), 2.45 (s, 3H) ppm.

^{13}C NMR (63 MHz, $CDCl_3$): δ 167.6, 136.2, 136.0, 134.6, 133.1, 132.9, 130.3, 129.7 (2C), 129.6 (2C), 129.3 (2C), 128.5 (2C), 111.1, 108.8, 12.7 ppm.

Elemental analysis (%): calcd. for $C_{18}H_{13}Cl_2NO_2$: C 62.45, H 3.79, N 4.05; found: C 62.37, H 3.75, N 4.04.

5-(*p*-Chlorophenyl)-1-(*p*-methoxyphenyl)-2-methyl-*1H*-pyrrole-3-carboxylic acid (30o)[232]

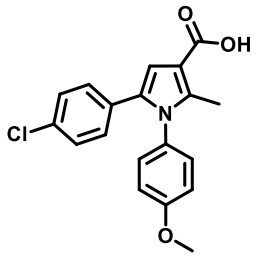

Prepared from pyrrole **29t** (0.369 g, 1 mmol). White solid. Yield: 0.283 g, 83%.

Mp 186-188 °C.

IR (neat) 1667.4 (C=O), 1248.8 (C-O), 1090.3 (C-Cl) cm^{-1}.

^{1}H NMR (250 MHz, $CDCl_3$): δ 7.16 (d, *J* = 8.7 Hz, 2H), 7.09 (d, *J* = 9.0 Hz, 2H), 7.01 (d, *J* = 8.7 Hz, 2H), 6.97 (d, *J* = 9.0 Hz, 2H), 6.86 (s, 1H), 3.87 (s, 3H), 2.43 (s, 3H) ppm.

^{13}C NMR (63 MHz, $CDCl_3$): δ 170.5, 159.4, 140.1, 133.2, 132.5, 130.7 (2C), 130.4 (2C) ,129.4 (2C), 129.2 (2C), 114.5 (2C), 111.8, 110.6, 55.5, 12.6 ppm.

Elemental analysis (%): calcd. for $C_{19}H_{16}ClNO_3$: C 66.77, H 4.72, N 4.10; found: C 66.71, H 4.66, N 4.02.

1-Butyl-5-(1H-indol-3-yl)-2-methyl-1H-pyrrole-3-carboxylic acid (30p)

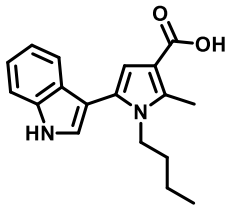

Prepared from pyrrole **29e** (0.200 g, 0.62 mmol). Brown solid. Yield: 0.189 g, 87 %.

Mp 112-114 °C

IR (neat) 3386.5 (O-H), 3053.9 (N-H), 1649.2 (C=O) cm^{-1}.

^{1}H-RMN (250 MHz, d_6-acetone): δ 7.41 (d, *J* = 8.1 Hz, 2H), 7.25 (s, 1H), 7.15 (m, 1H), 7.04 (m, 1H), 6.51 (s, 1H), 3.98 – 3.89 (m, 2H), 2.63 (s, 3H), 1.54 – 1.45 (m, 2H), 1.14 (m, 2H), 0.72 (t, *J* = 7.3 Hz, 3H) ppm.

^{13}C-RMN (250 MHz, d_4-methanol): δ 166.9, 141.2, 137.8, 137.3, 128.1, 125.6, 122.9, 120.7, 120.1, 112.5, 112.4, 111.7, 108.8, 44.9, 34.0, 20.7, 13.9, 12.0 ppm.

Elemental analysis (%): calcd. for a $C_{18}H_{20}N_2O_2$: C 72.95, H 6.80, N 9.45; found: C 73.23, H 6.66, N 9.53.

7.7.4. Preparation of the pyrrole-isoniazid derivatives 32a-p.

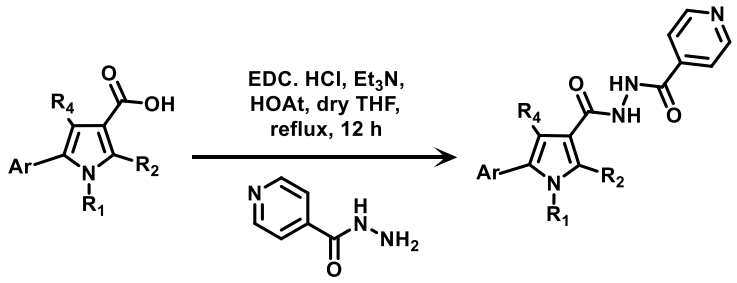

To a solution of the suitable pyrrole derivative (0.5 mmol), 1-ethyl-3-(3-dimethylaminopropyl)carbodiimide hydrochloride (EDCI·HCl, 1 eq), and isoniazid (1 eq) in dry THF (3 mL), was added Et_3N (0.02 mL, 2 eq), followed by the addition of 1-hydroxy-7-azabenzotriazole (HOAt, in 0.6M DMF, 0.16 mL, 1 eq). The reaction mixture was refluxed for 12 hours. Then, the solvent was removed under reduced pressure and chloroform (3 mL) was added. The obtained precipitate was recrystalized in ethanol, providing the expected hydrazides (**32a-p**)**.**

If after the addition no precipitate was observed, the solvent was eliminated under reduced pressure and the residue was purified by flash chromatography through a silica gel column using ethyl acetate: methanol (5:1) as the mobile phase. Finally, the desired compounds were recrystalized in ethanol.

***N*'-[1-Butyl-5-(*p*-chlorophenyl)-2-methyl-1*H*-pyrrole-3-carbonyl]-isonicotinohydrazide (32a)**[232]

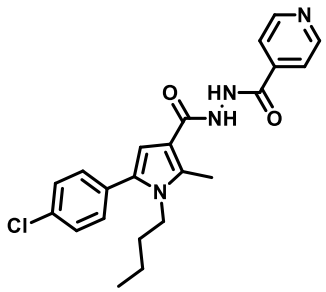

Prepared from pyrrole **30m** (0.158 g, 0.5 mmol). Yellow solid. Yield: 0.150 g, 73%.

Mp 154-157 °C.

IR (neat) 3226.3 (N-H),1636.0 (C=O) cm^{-1}.

^{1}H NMR (250 MHz, d_4-methanol): δ 8.73 (dd, *J* = 4.7, 1.4 Hz, 2H), 7.87 (dd, 2H, *J* = 4.7, 1.4 Hz), 7.48-7.37 (m, 4H), 6.57 (s, 1H), 4.00- 3.94 (m, 2H), 2.61 (s, 3H), 1.55-1.43 (m, 2H), 1.24- 1.09 (m, 2H), 0.80 (t, *J* = 7.3 Hz, 3H) ppm.

^{13}C NMR (63 MHz, d_4-methanol): δ 167.6 (2C), 151.3 (2C), 142.6, 137.7, 134.9, 134.0, 133.6, 132.2 (2C), 130.1 (2C), 123.5 (2C), 113.7, 109.0, 45.0, 34.1, 20.9, 14.1, 12.0 ppm.

Elemental analysis (%): calcd. for $C_{22}H_{23}ClN_4O_2$: C 64.31, H 5.64, N 13.64; found: C 64.20, H 5.62, N 13.61.

***N*'-[1,5-Bis(*p*-chlorophenyl)-2-methyl-1*H*-pyrrole-3-carbonyl] isonicotinohydrazide (32b)[232]**

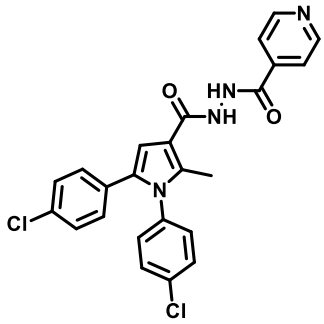

Prepared from pyrrole **30n** (0.172 g, 0.5 mmol). White solid. Yield: 0.141 g, 61%.

Mp 182-184 °C.

IR (neat) 3200.7 (N-H), 1633.2 (C=O), 1266.9 (C-N) cm^{-1}.

^{1}H NMR (250 MHz, d_4-methanol): δ 8.78 (dd, *J* = 4.7, 1.5 Hz, 2H), 7.93 (dd, *J* = 4.7, 1.5 Hz, 2H), 7.52 (d, *J* = 8.6 Hz,2H), 7.25 (d, *J* = 8.7 Hz, 4H), 7.11 (d, *J* = 8.5 Hz, 2H), 6.89 (s, 1H), 2.43 (s, 3H) ppm.

^{13}C NMR (63 MHz, d_4-methanol): δ 167.7, 167.6, 151.4 (2C), 142.5, 139.0, 138.1, 136.0, 134.6, 134.2, 132.6, 131.7 (2C), 131.1 (2C), 131.0 (2C), 129.7 (2C), 123.5 (2C), 114.9, 109.5, 12.9 ppm.

Elemental analysis (%): calcd. for $C_{24}H_{18}Cl_2N_4O_2$: C 61.95, H 3.90, N 12.04; found: C 61.88, H 3.87, N 11.98.

***N*'-[5-(*p*-Chlorophenyl)-1-(*p*-methoxyphenyl)-2-methyl-1*H*-pyrrole-3-carbonyl] isonicotinohydrazide (32c)[232]**

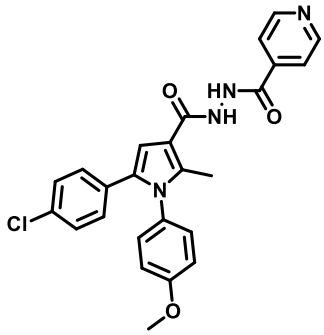

Prepared from pyrrole **30o** (0.171 g, 0.5 mmol). White solid. Yield: 0.179 g, 78%.

Mp 172-173 °C.

IR (neat) 3216.4 (N-H), 1630.4 (C=O), 1247.4 (C-N), 1090.3 (C-Cl) cm^{-1}.

^{1}H NMR (250 MHz, d_4-methanol): δ 8.78 (dd, *J* = 4.5, 1.6 Hz, 2H), 7.93 (dd, *J* = 4.5, 1.6 Hz, 2H); 7.22 (d, *J* = 8.7 Hz, 2H); 7.18-7.10 (m, 4H); 7.04 (d, *J* = 9.0 Hz, 2H), 6.87 (s, 1H); 3.87 (s, 3H); 2.41 (s, 3H) ppm.

^{13}C NMR (63 MHz, d_4-methanol): δ 167.6, 167.4, 161.2, 151.1 (2C), 142.3, 139.1, 134.4, 133.6, 132.6, 131.7, 130.8 (2C), 130.6 (2C), 129.2 (2C), 123.2 (2C), 115.6 (2C), 114.0, 108.6, 56.0, 12.6 ppm.

Elemental analysis (%): calcd for $C_{25}H_{21}ClN_4O_2$: C 65.15, H 4.59, N 12.16; found: C 65.35, H 4.65, N 11.97.

_N'_-(5-(4-Chlorophenyl)-2-methyl-1_H_-pyrrole-3-carbonyl) isonicotinohydrazide (32d)

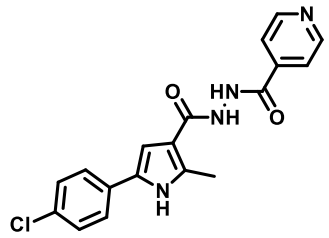

Prepared from pyrrole **30l** (0.250 g, 1.06 mmol). Yellow solid.

Yield: 0.131 g, 35 %.

Mp 152-154 °C.

IR (neat) 3281.3 (N-H), 1624.8 (C=O), 1275.8 (C-N), 751.16 (C-Cl) cm^{-1}.

^{1}H RMN (250 MHz, d_6-acetone): δ 10.69 (s, 1H), 9.72 (s, 1H), 8.99 (s, 1H), 8.63 (d, *J* = 5.8 Hz, 2H), 7.70 (d, *J* = 6.0 Hz, 2H), 7.49 (d, *J* = 8.6 Hz, 2H), 7.26 (d, *J* = 8.6 Hz, 2H), 6.94 (d, *J* = 2.6 Hz, 1H), 2.42 (s, 3H) ppm.

^{13}C RMN (63 MHz, d_4-methanol): δ 168.1, 167.7, 151.4 (2C), 142.7, 138.2, 133.1, 132.9, 131.1, 130.3 (2C), 126.5 (2C), 123.6 (2C), 114.4, 106.3, 13.3 ppm.

Elemental analysis (%) calcd for $C_{18}H_{15}ClN_4O_2$: C 60.94, H 4.26, N 15.79; found: C 60.73, H 4.50, N 15.44.

_N'_-(5-(4-Iodophenyl)-2-methyl-1_H_-pyrrole-3-carbonyl) isonicotinohydrazide (32e)

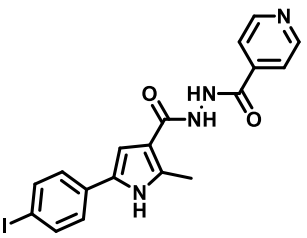

Prepared from pyrrole **30a** (0.196 g, 0.60 mmol). Yellow solid.

Yield: 0.104 g, 39 %.

Mp >250 °C

IR (neat) 3331.2 (N-H), 1637.4 (C=O), 1271.1 (C-N) cm^{-1}.

^{1}H RMN (250 MHz, d_4-methanol): δ 8.62 (s, 2H), 7.76 (d, *J* = 6.0 Hz, 2H), 7.57 (d, *J* = 8.4 Hz, 2H), 7.25 (d, *J* = 8.4 Hz, 2H), 6.79 (s, 1H), 2.43 (s, 3H) ppm.

^{13}C RMN (63 MHz, d_4-methanol): δ 168.1, 167.7, 151.8 (2C), 142.9 (2C), 139.7, 138.1, 133.7, 131.4, 127.0 (2C), 123.8 (2C), 114.5, 106.3, 91.7, 13.4 ppm.

Elemental analysis (%): calcd. for $C_{18}H_{15}IN_4O_2$: C 48.45, H 3.39, N 12.56; found: C 48.37, H 3.70, N 12.85.

_N'_-(5-(3-Chlorophenyl)-2-methyl-1_H_-pyrrole-3-carbonyl) isonicotinohydrazide (32f)

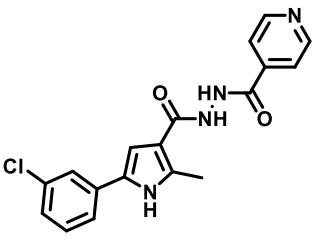

Prepared from pyrrole **30b** (0.308 g, 1.31 mmol). Yellow solid.

Yield: 0.178 g, 42%.

Mp >250 °C

IR (neat) 3197.1 (N-H), 1594.4 (C=O), 1408.2 (C-N), 791.81 (C-Cl) cm^{-1}.

^{1}H RMN (250 MHz, d_4-methanol): δ 8.62 (d, *J* = 4.7 Hz, 2H), 7.77 (dd, *J* = 4.6, 1.5 Hz, 2H), 7.50 (t, *J* = 1.7 Hz, 1H), 7.40 (d, *J* = 7.9 Hz, 1H), 7.22 (t, *J* = 7.9 Hz, 1H), 7.09 – 7.03 (m, 1H), 6.82 (s, 1H), 2.45 (s, 3H) ppm.

^{13}C RMN (63 MHz, d_4-methanol): δ 168.0, 167.7, 151.4 (2C), 142.6, 138.51, 136.2, 136.1, 131.8, 130.7, 127.3, 124.9, 123.6 (2C), 123.4, 114.5, 106.7, 13.3 ppm.

Elemental analysis (%): calcd. for $C_{18}H_{15}ClN_4O_2$: C 60.94, H 4.26, N 15.79; found: C 61.07, H 4.47, N 15.72.

***N'*-(5-(3,4-Dichlorophenyl)-2-methyl-1*H*-pyrrole-3-carbonyl) isonicotinohydrazide (32g)**

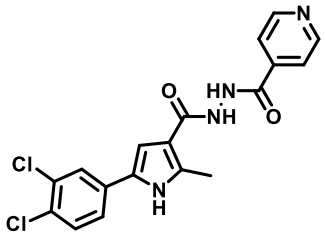

Prepared from pyrrole **30c** (0.452 g, 1.67 mmol). White solid. Yield: 0.266 g, 41%.

Mp >250 °C

IR (neat) 3218.3 (N-H), 1637.2 (C=O), 1257.0 (C-N), 807.5 (C-Cl) cm^{-1}.

^{1}H RMN (250 MHz, d_6-DMSO): δ 10.64 (s, 1H), 9.83 (s, 1H), 8.80 (d, *J* = 5.8 Hz, 2H), 7.88 – 7.79 (m, 3H), 7.67 (d, *J* = 8.5 Hz, 1H), 7.55 (dd, *J* = 8.5, 2.0 Hz, 1H), 7.15 (d, *J* = 2.2 Hz, 1H), 2.58 – 2.44 (m, 3H) ppm.

^{13}C RMN (63 MHz, d_6-DMSO): δ 164.8, 164.3, 150.8 (2C), 140.1, 136.6, 133.1, 132.0, 131.5, 128.0, 127.0, 124.8, 123.6 (2C), 121.7, 113.9, 106.7, 13.0 ppm.

Elemental analysis (%) calcd. for $C_{18}H_{14}Cl_2N_4O_2$: C 55.54, H 3.63, N 14.39; found: C 55.12, H 3.80, N 14.05.

***N'*-(5-(4-Bromophenyl)-2-methyl-*1H*-pyrrole-3-carbonyl) isonicotinohydrazide (32h)**

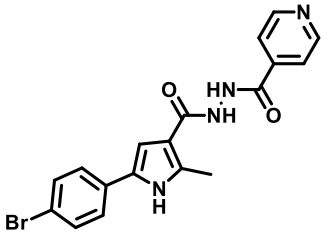

Prepared from pyrrole **30d** (0.140 g, 0.49 mmol). Yellow solid. Yield: 0.059 g, 30 %.

Mp 210-212 °C

IR (neat) 3272.9 (N-H), 1640.7 (C=O), 1418.6 (C-N), 754.2 (C-Br) cm^{-1}.

^{1}H RMN (250 MHz, d_4-methanol): δ 8.77 (s, 2H), 7.91 (d, *J* = 6.0 Hz, 2H), 7.53 (s, 4H), 6.93 (s, 1H), 2.58 (s, 3H) ppm.

^{13}C RMN (63 MHz, d_4-methanol): δ 194.2, 167.7, 151.4 (2C), 142.7, 138.3, 133.3 (2C), 131.0, 126.8 (2C), 123.6 (2C), 120.8, 114.4, 106.3, 88.0, 13.3 ppm.

Elemental analysis (%): calcd. for $C_{18}H_{15}BrN_4O_2$: C 54.15, H 3.79, N 14.03; found: C 52.45, H 4.30, N 13.25.

***N'*-(5-(4-Fluorophenyl)-2-methyl-1*H*-pyrrole-3-carbonyl) isonicotinohydrazide (32i)**

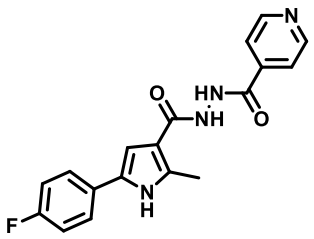

Prepared from pyrrole **30e** (0.149 g, 0.68 mmol). Yellow solid. Yield: 0.085 g, 37 %.

Mp 148-150 °C

IR (neat) 3262.7 (N-H), 1659.1 (C=O), 1259.5 (C-N), 1232.1 (C-F) cm^{-1}.

^{1}H RMN (250 MHz, d_4-methanol): δ 8.51 (br s, 2H), 7.67 (dd, *J* = 7.0, 2.4 Hz, 2H), 7.43 – 7.30 (m, 2H), 6.88 (t, *J* = 8.8 Hz, 2H), 6.61 (s, 1H), 2.34 (s, 3H) ppm.

^{13}C RMN (63 MHz, d_4-methanol): δ 168.2, 167.7, 166.7 (d, *J* = 188.8 Hz), 151.4 (2C), 142.7, 137.8, 131.8 , 130.7 (d, *J* = 3.2 Hz), 127.0 (d, *J* = 7.8 Hz, 2C), 123.6 (2C), 116.9 (d, *J* = 21.9 Hz, 2C), 114.2 , 105.5 , 13.3 ppm.

Elemental analysis (%): calcd. for $C_{18}H_{15}FN_4O_2$: C 63.90, H 4.47, N 16.56; found: C 64.27, H 4.34, N 16.51.

***N'*-(5-(4-Methoxyphenyl)-2-methyl-1H-pyrrole-3-carbonyl) isonicotinohydrazide (32j)**

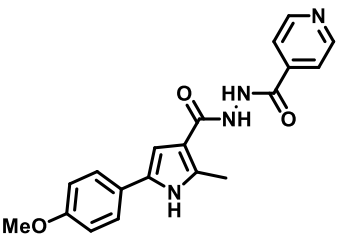

Prepared from pyrrole **30f** (0.047 g, 0.47 mmol). Yellow solid. Yield: 0.047 g, 29 %.

Mp 200-204 °C

IR (neat) 3319.9 (N-H), 1651.0 (C=O), 1250.2 (C-O) cm^1.

^{1}H RMN (250 MHz, d_4-methanol): δ 8.61 (dd, *J* = 4.5, 1.6 Hz, 2H), 7.76 (dd, *J* = 4.5, 1.6 Hz, 2H), 7.39 (d, *J* = 8.8 Hz, 2H), 6.80 (d, *J* = 8.9 Hz, 2H), 6.62 (s, 1H), 3.68 (s, 3H), 2.42 (s, 3H) ppm

^{13}C RMN (63 MHz, d_4-methanol): δ 168.4, 167.7, 160.2, 151.4 (2C), 142.8, 137.2, 132.3, 127.1, 126.5 (2C), 123.6 (2C), 115.6 (2C), 113.9, 104.3, 56.1, 13.3 ppm

Elemental analysis (%): calcd. for $C_{19}H_{18}N_4O_3$: C 65.13, H 5.18, N 15.99; found: C 65.21, H 5.41, N 16.30.

***N*'-(5-(3,4-Dichlorophenyl)-1-hexyl-2-methyl-1*H*-pyrrole-3-carbonyl) isonicotinohydrazide (32k)**

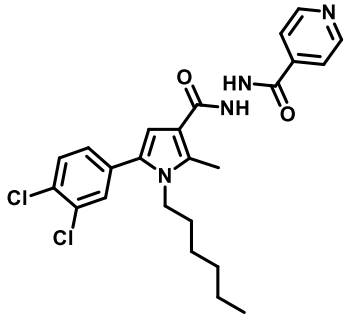

Prepared from pyrrole **30g** (0.350 g, 0.99 mmol). White solid. Yield: 0.078 g, 15 %.

Mp 203-205 °C

IR (neat) 3218.8 (NH), 1632.4 (C=O) cm^{-1}

^{1}H NMR (250 MHz, *d*$_4$-methanol): δ 8.57 (d, *J* = 4.5 Hz, 2H), 7.72 (d, *J* = 5.4 Hz, 2H), 7.44 (t, *J* = 4.8 Hz, 2H), 7.19 (dd, *J* = 8.3, 2.0 Hz, 1H), 6.46 (s, 1H), 3.81 (d, *J* = 7.6 Hz, 2H), 2.45 (s, 3H), 1.35 (s, 2H), 0.99 (s, 6H), 0.67 (s, 3H) ppm.

^{13}C NMR (63 MHz, *d*$_4$-methanol): δ 167.9, 167.7, 151.4 (2C), 142.6, 138.3, 135.4, 133.9, 132.9, 132.8, 132.3, 132.1, 130.4, 123.6 (2C), 114.0, 109.7, 45.2, 32.6, 31.8, 27.4, 23.9, 14.7, 12.14 ppm.

Elemental analysis (%): calcd. for $C_{24}H_{26}Cl_2N_4O_2$: C 60.89, H 5.54, N 11.84; found: C 60.99, H 5.80, N 11.53.

***N*'-(1-Butyl-2-methyl-5-(1-methyl-1*H*-indol-3-yl)-1*H*-pyrrole-3-carbonyl) isonicotinohydrazide (32l)**

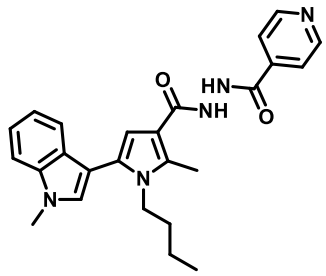

Prepared from pyrrole **30h** (0.100 g, 0.322 mmol). White solid. Yield: 0.022 g, 17 %.

Mp 250 °C

IR (neat) 3265.23 (NH), 1631.45 (C=O) cm^{-1}

^{1}H NMR (300 MHz, *d*$_4$-methanol) δ: 8.75 (br s, 2H), 7.89 (d, *J* = 6.0 Hz, 2H), 7.50 (d, *J* = 7.8 Hz, 1H), 7.44 (d, *J* = 7.8 Hz, 1H), 7.28 – 7.19 (m, 2H), 7.11 (s, 1H), 6.59 (s, 1H), 4.01 – 3.91 (m, 2H), 3.88 (s, 3H), 2.64 (s, 3H), 1.51-1.46 (m, 2H), 1.17-1.09 (m, 2H), 0.72 (t, *J* = 7.3 Hz, 3H) ppm.

^{13}C NMR (63 MHz, *d*$_4$-methanol): δ 169.9, 169.9, 150.0 (2C), 137.5, 135.4, 128.7, 128.6, 126.7, 122.2 (2C), 122.2, 122.0, 121.8, 119.7, 119.5, 111.9, 109.5, 107.8, 107.1, 32.9, 31.9, 19.6, 12.8, 10.8 ppm.

Elemental analysis (%): calcd. for $C_{25}H_{27}N_5O_2$: C 69.91, H 6.34, N 16.31; found: C 69.64, H 6.39, N 16.29.

_N'_-(1-Butyl-5-(3,4-dichlorophenyl)-2-methyl-1_H_-pyrrole-3-carbonyl) isonicotinohydrazide (32m)

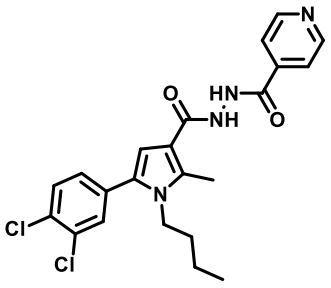

Prepared from pyrrole **30k** (0.200 g, 0.57mmol). White solid. Yield: 0.103 g, 38 %.

Mp 180-182 °C

IR (neat) 3194 (N-H), 3046 (N-H), 1674 (C=O), 1632 (C=O), 750 (C-Cl) cm^{-1}.

^{1}H-RMN (250 MHz, d_4-methanol): δ 8.73 (d, *J* = 5 Hz, 1H), 7.88 (d, *J* = 5 Hz, 1H), 7.60 (d, *J* = 8.4 Hz, 1H), 7.58 (d, *J* = 2.1 Hz, 1H) , 7.35 (dd, *J* = 8.3, 2.1 Hz, 1H), 6.62 (s, 1H), 4.08 – 3.93 (m, 2H), 2.61 (s, 3H), 1.58 – 1.41 (m, 2H), 1.22-1.14 (m, 2H), 0.81 (t, *J* = 7.3 Hz, 2H) ppm.

^{13}C-RMN (250 MHz, d_4-methanol): δ 168.0, 167.7, 151.6 (2C), 142.7, 138.4, 135.4, 133.9 (2C), 132.8, 132.3, 132.2, 130.4, 123.6 (2C), 114.0, 109.8, 45.2, 34.2, 21.1,14.3, 12.1 ppm.

Elemental analysis (%): calcd for $C_{22}H_{22}Cl_2N_4O_2$: C 59.33, H 4.98, N 12.58. found: C 59.65, H 4.84, N 12.71.

_N'_-(1-Butyl-5-(3,4-dichlorophenyl)-2-propyl-1_H_-pyrrole-3-carbonyl) isonicotinohydrazide (32n)

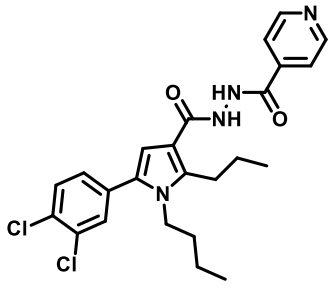

Prepared from pyrrole **30k** (0.200 g, 0.62 mmol). White solid. Yield: 0.139 mg, 51 %.

Mp >250 °C

IR (neat) 3223 (N-H), 3050 (N-H), 1693 (C=O), 1621 (C=O), 750 (C-Cl) cm^{-1}

^{1}H-RMN (250 MHz, d_4-methanol) δ 8.73 (d, *J* = 5.8 Hz, 1H), 7.88 (d, *J* = 5.8 Hz, 1H), 7.60 (d, *J* = 8.2 Hz, 1H), 7.58 (d, *J* = 2 Hz, 1H), 7.37 (dd, *J* = 8.2, 2.0 Hz, 1H), 6.63 (s, 1H), 4.06 – 3.95 (m, 2H), 3.06 – 2.98 (m, 2H), 1.71-1.62 (m, 2H), 1.53 – 1.39 (m, 2H), 1.22-1.13 (m, 2H), 1.02 (t, *J* = 7.3 Hz, 3H), 0.80 (t, *J* = 7.3 Hz, 3H) ppm.

^{13}C-RMN (250 MHz, d_6-acetone): δ 166.4, 151.8, 142.4 (2C), 141.4, 135.3, 133.3 (2C), 132.0, 131.9, 131.8, 131.7, 130.0, 122.5, 113.9, 109.9, 44.9, 34.5, 28.2, 24.7, 20.8, 14.8, 14.3, 14.2 ppm.

Elemental analysis (%): calcd. for $C_{24}H_{26}Cl_2N_4O_2$: C 60.89, H 5.54, N 11.84. found: C 60.60, H 5.51, N 11.95.

_N'_-(1-butyl-5-(1_H_-indol-3-yl)-2-methyl-1_H_-pyrrole-3-carbonyl) isonicotinohydrazide (32o)

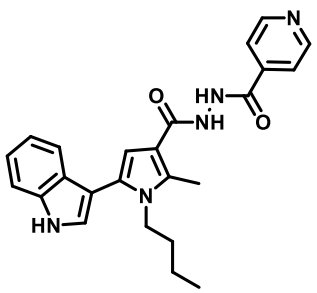

Prepared from pyrrole **30p** (0.100 g, 0.34 mmol). White solid. Yield: 0.078 g, 55 %.

Mp 188-190 °C

IR (neat) 3464 (N-H), 3327 (N-H), 3202 (N-H), 1666 (C=O), 1625 (C=O) cm^{-1}

^{1}H-RMN (250 MHz, d_4-methanol): δ 8.73 (dd, *J* = 4.5, 1.6 Hz, 2H), 7.89 (dd, *J* = 4.5, 1.6 Hz, 2H), 7.48 (d, *J* = 7.8 Hz, 1H), 7.43 (d, *J* = 7.8 Hz, 1H), 7.29 (s, 1H), 7.19- 7.13 (m, 1H), 7.09-7.03 (m, 1H), 6.59 (s, 1H), 3.94 (q, *J* = 7.3 Hz, 2H), 1.56 – 1.39 (m, 2H), 1.13 (m, 2H), 0.71 (t, *J* = 7.3 Hz, 3H) ppm.

^{13}C-RMN (250 MHz, d_4-methanol): δ 167.8, 151.4, 142.9, 138.1, 136.6, 129.5, 128.6, 125.9 (2C), 123.7 (2C), 123.3, 121.1, 113.2, 112.9, 109.2 (2C), 109.0 (2C), 45.2, 34.4, 21.1, 14.2, 12.3 ppm.

Elemental analysis (%): calcd. for $C_{24}H_{25}N_5O_2$: C 69.38, H 6.07, N 16.86. found: C 68.71, H 5.93, N 16.57.

_N'_-(5-(3,4-Dichlorophenyl)-1-(3-(dimethylamino)propyl)-2-methyl-1_H_-pyrrole-3-carbonyl) isonicotinohydrazide (32p)

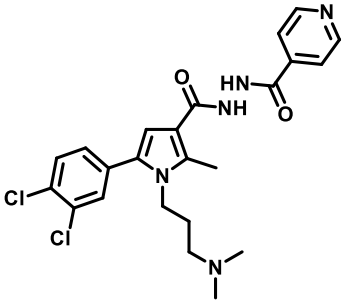

Prepared from pyrrole **30i** (0.130 g, 0.36 mmol). White solid. Yield: 0.050 g, 30 %.

Mp 155-157 °C

IR(neat)) 3197 (N-H), 2946 (N-H), 1631 (C=O)cm^{-1}

^{1}H NMR (250 MHz, d_4-methanol): δ 8.73 (d, *J* = 6.0 Hz, 2H), 7.88 (d, *J* = 6.0 Hz, 2H), 7.63 (d, *J* = 1.8 Hz, 1H), 7.61 (d, *J* = 8.3 Hz, 1H), 7.37 (dd, *J* = 8.3, 1.8 Hz, 1H), 6.64 (s, 1H), 4.15 – 3.88 (m, 2H), 2.63 (s, 3H), 2.35 – 2.09 (m, 8H), 1.75 – 1.53 (m, 2H) ppm.

^{13}C NMR (63 MHz, d_4-methanol): δ 167.8, 167.7, 151.5 (2C), 142.8, 138.4, 135.2, 134.0, 133.1, 132.7, 132.4, 132.3, 130.4, 123.6 (2C), 114.2, 110.1, 57.5, 45.5 (2C), 43.4, 29.5, 12.1 ppm.

Elemental analysis (%): calcd for $C_{23}H_{25}Cl_2N_5O_2$: C 58.23, H 5.31, N 14.76 found: C 58.15, H 5.29, N 13.50.

CHAPTER 8. CONCLUSIONS

1. A family of theranostic styrylquinoles bearing a push pull architecture has been designed and synthesized *via* a good-yielding four-step procedure. Their pharmacological profiles were studied, showing their ability to inhibit tau aggregation and neuroprotective effects in okadaic acid models. Their full spectroscopic characterization has been carried out, showing thet the compounds have native fluorescence in the NIR region.
2. The ability of the styrylquinolines to act as amyloid sensors has been verified with different amyloidogenic proteins. First, they were used for *ex-vivo* imaging, showing the capacity to selectively detect □-amyloid plaques in the somatosensory cortex of APP/PS1 transgenic mice and in the temporal cortex of human Alzheimer's disease samples. Due to the ability to interact with amyloidogenic proteins, styrylquinolines were also used to detect amylin, a pancreatic protein overexpressed in type II Diabetes mellitus that may be involved in the development of Alzheimer's disease.
3. As quinolines have shown potential to develop effective and affordable oral treatments for leishmaniasis, a family of 2-substituded styrylquinolines, with polyamine chains in the C-4 position of the quinoline scaffold has been synthesized. Their leishmanicidal activities were tested, showing good activities and selectivity indexes for the best compounds. Further mechanistical studies were carried out pointing out their ability cause mitochondrial disruption.
4. In order to achieve our goal of developing novel push-pull multi-spectral optoacoustic tomography (MSOT) probes, a new one-pot mechanochemical methodology to obtain dihalo-bis-indolylquinones as starting scaffolds has been developed.
5. Finally, a novel family of pyrrole-isoniazid hybrid compounds have been synthesised. Their antitubercular activities have been studied, showing interesting activities against *Mycobacterium tuberculosis*, including multidrug-resistant tuberculosis. Further, their ability to inhibit MmpL3 and InhA was verified, proving that they could act through a metabolism-activated multitargeting (MAMUT) mechanism.

REPRESENTATIVE ^{1}H-NMR AND ^{13}C-NMR

SPECTRA

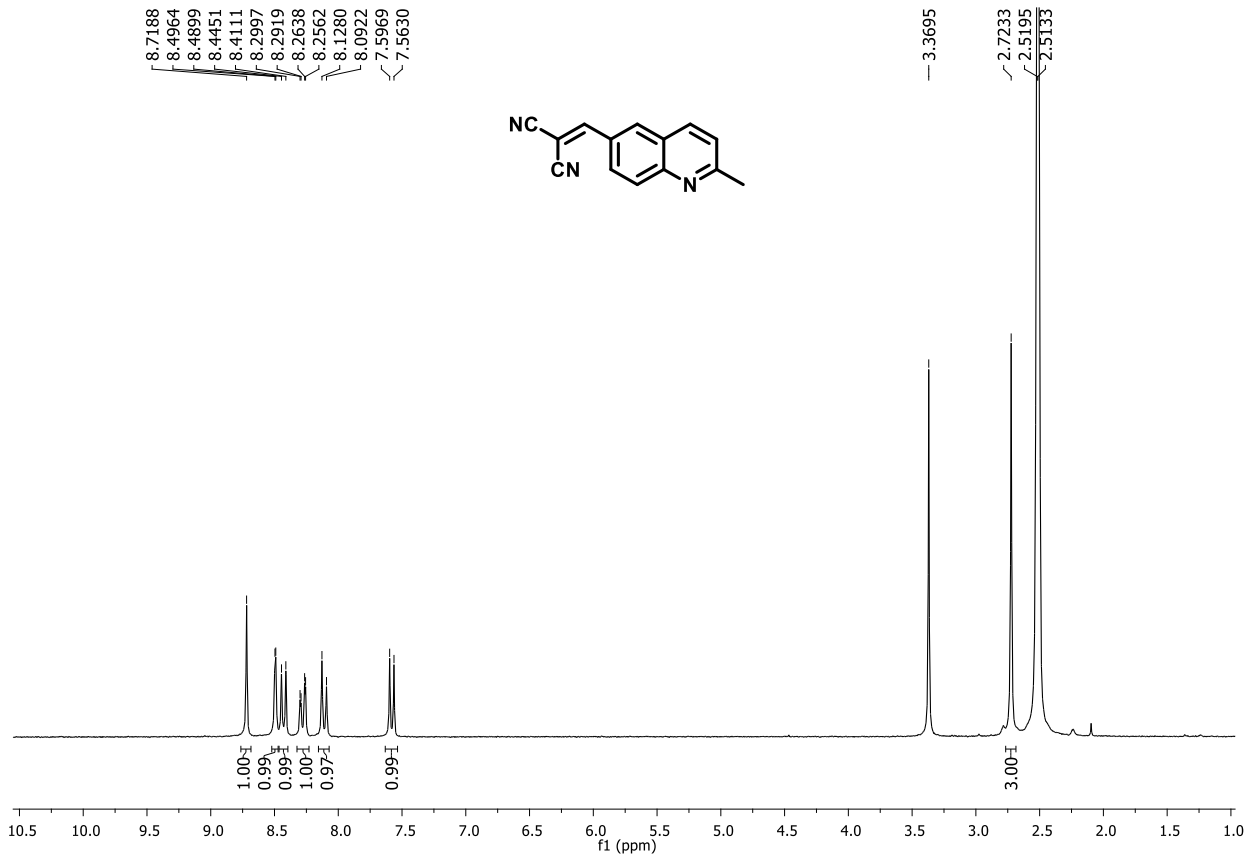
8.7188
8.4964
8.4899
8.4451
8.4111
8.2997
8.2919
8.2638
8.2562
8.1280
8.0922
7.5969
7.5630
3.3695
2.7233
2.5195
2.5133
NC
CN
N
1.00
0.99
0.99
1.00
0.97
0.99
3.00
f1 (ppm)

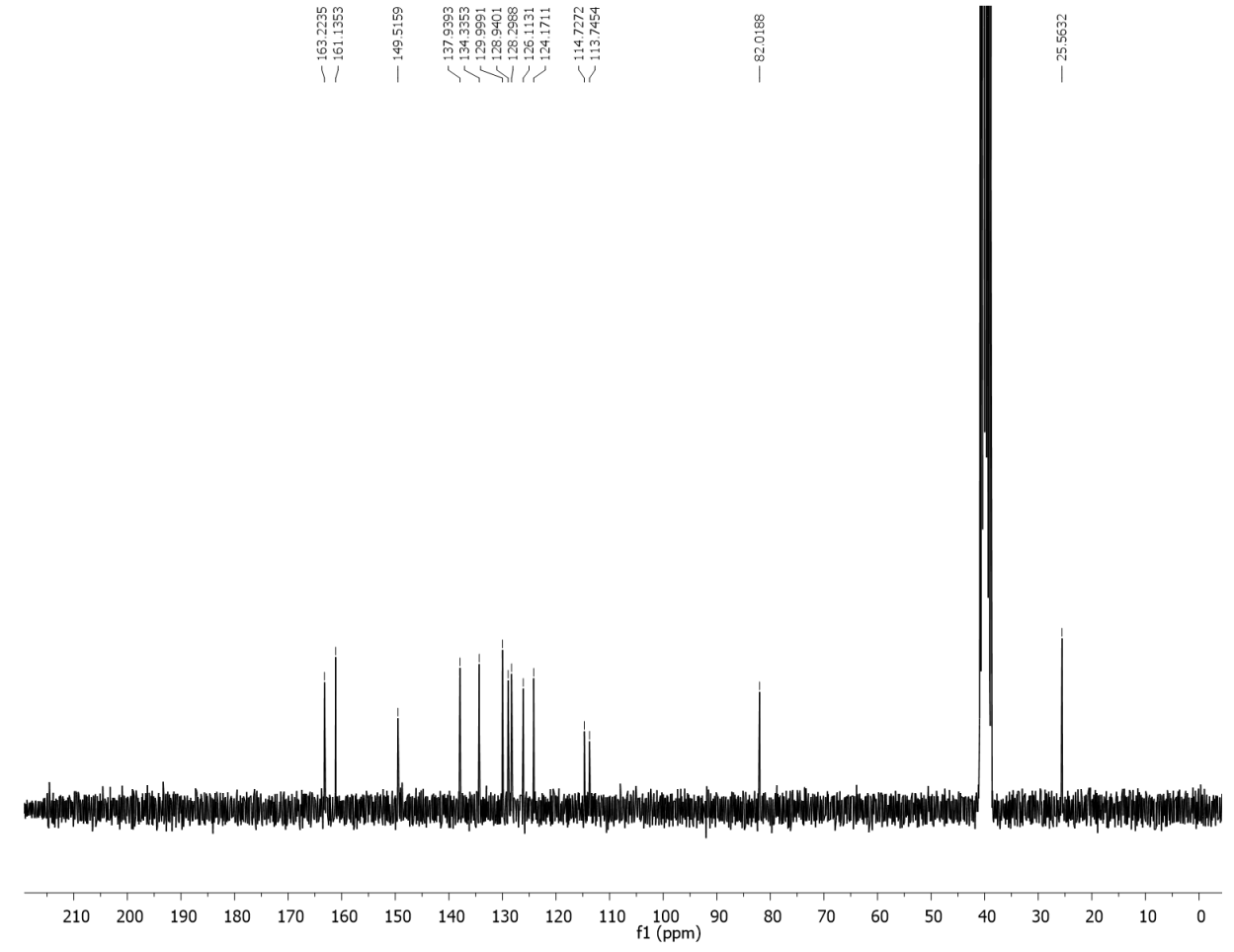
163.2235
161.1353
149.5159
137.9393
134.3353
129.9991
128.9401
128.2988
126.1131
124.1711
114.7272
113.7454
82.0188
25.5632
f1 (ppm)

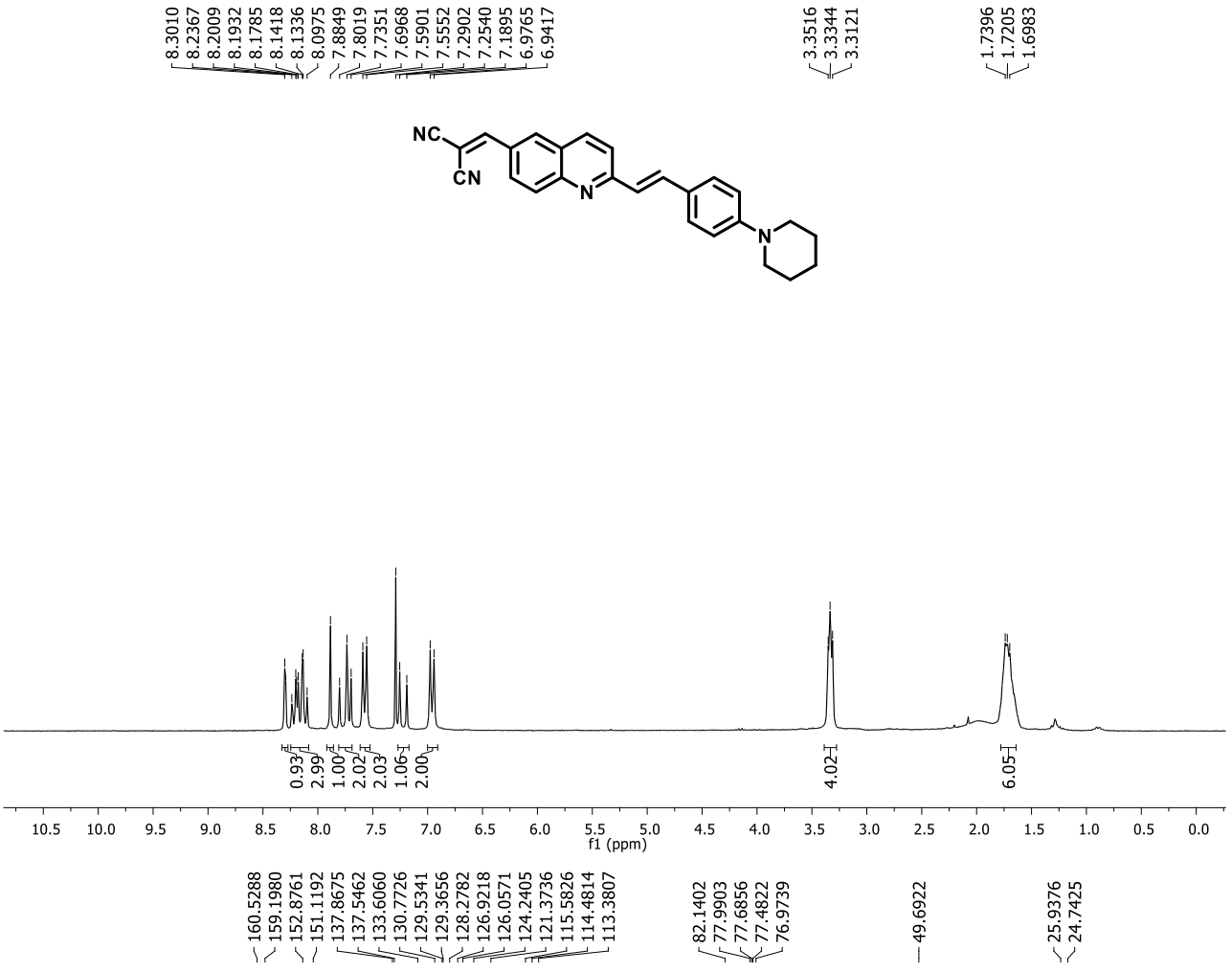
8.3010
8.2367
8.2009
8.1932
8.1785
8.1418
8.1336
8.0975
7.8849
7.8019
7.7351
7.6968
7.5901
7.5552
7.2902
7.2540
7.1895
6.9765
6.9417
3.3516
3.3344
3.3121
1.7396
1.7205
1.6983
NC
CN
N
N
0.93
2.99
1.00
2.02
2.03
1.06
2.00
4.02
6.05
10.5 10.0 9.5 9.0 8.5 8.0 7.5 7.0 6.5 6.0 5.5 5.0 4.5 4.0 3.5 3.0 2.5 2.0 1.5 1.0 0.5 0.0
f1 (ppm)

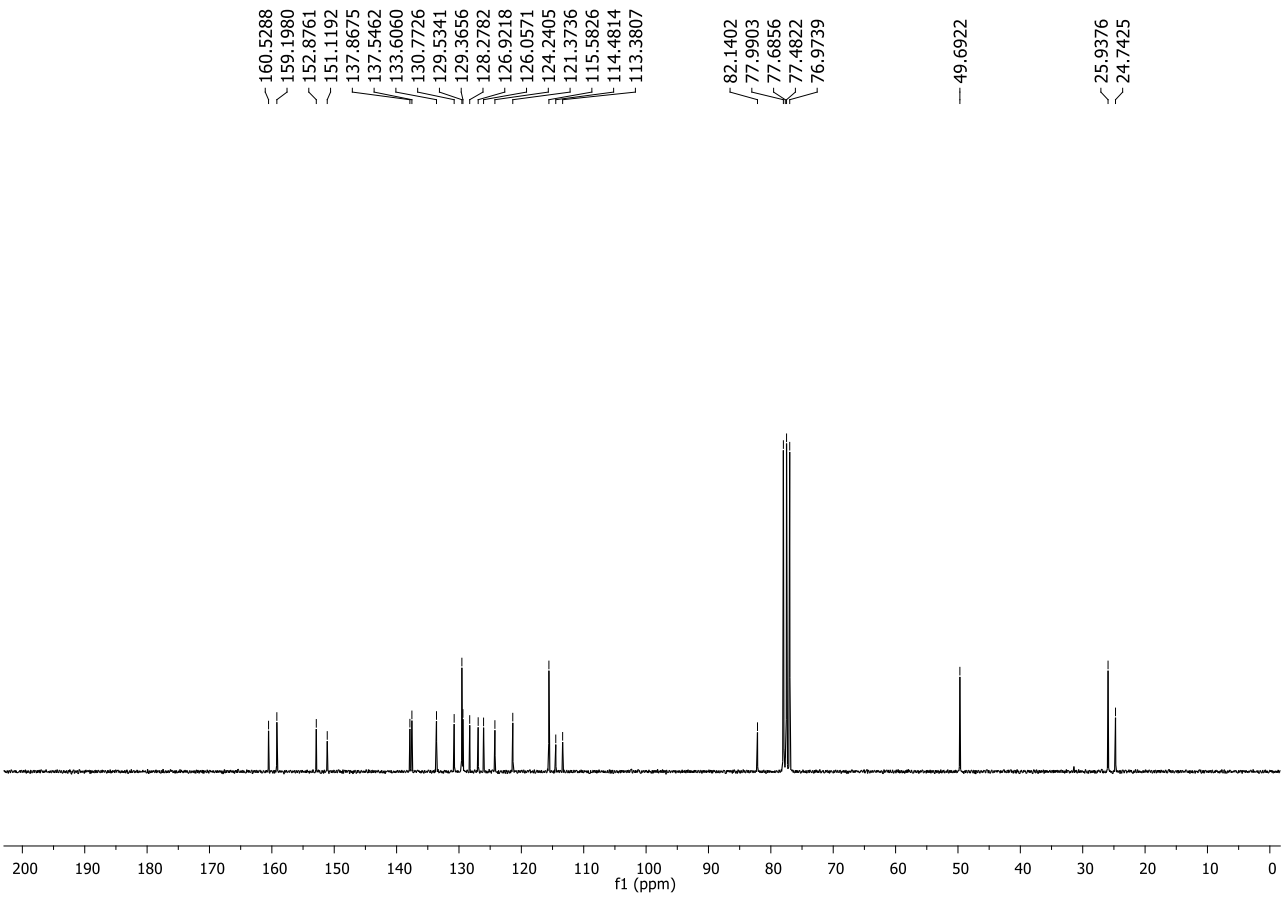
160.5288
159.1980
152.8761
151.1192
137.8675
137.5462
133.6060
130.7726
129.5341
129.3656
128.2782
126.9218
126.0571
124.2405
121.3736
115.5826
114.4814
113.3807
82.1402
77.9903
77.6856
77.4822
76.9739
49.6922
25.9376
24.7425
200 190 180 170 160 150 140 130 120 110 100 90 80 70 60 50 40 30 20 10 0
f1 (ppm)

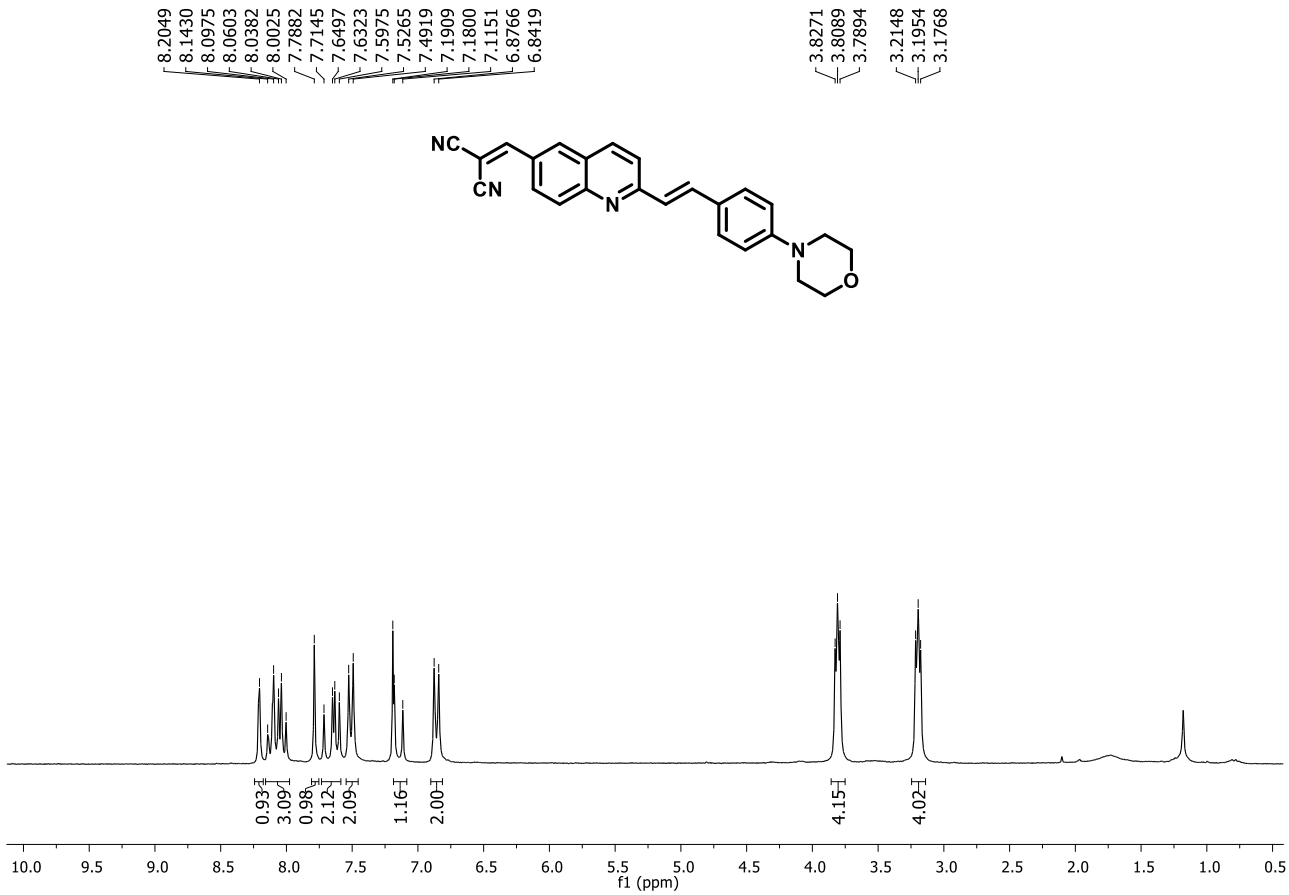
8.2049
8.1430
8.0975
8.0603
8.0382
8.0025
7.7882
7.7145
7.6497
7.6323
7.5975
7.5265
7.4919
7.1909
7.1800
7.1151
6.8766
6.8419
3.8271
3.8089
3.7894
3.2148
3.1954
3.1768
NC
CN
N
N
O
0.93
3.09
0.98
2.12
2.09
1.16
2.00
4.15
4.02
f1 (ppm)
160.3869
159.2141
152.3352
151.1449
137.6691
137.5178
133.5079
130.9682
129.4421
128.4391
127.5350
127.0361
125.2258
121.5140
115.3778
114.3950
113.3051
82.5153
77.9520
77.6492
77.4438
76.9358
67.1353
48.6778
f1 (ppm)

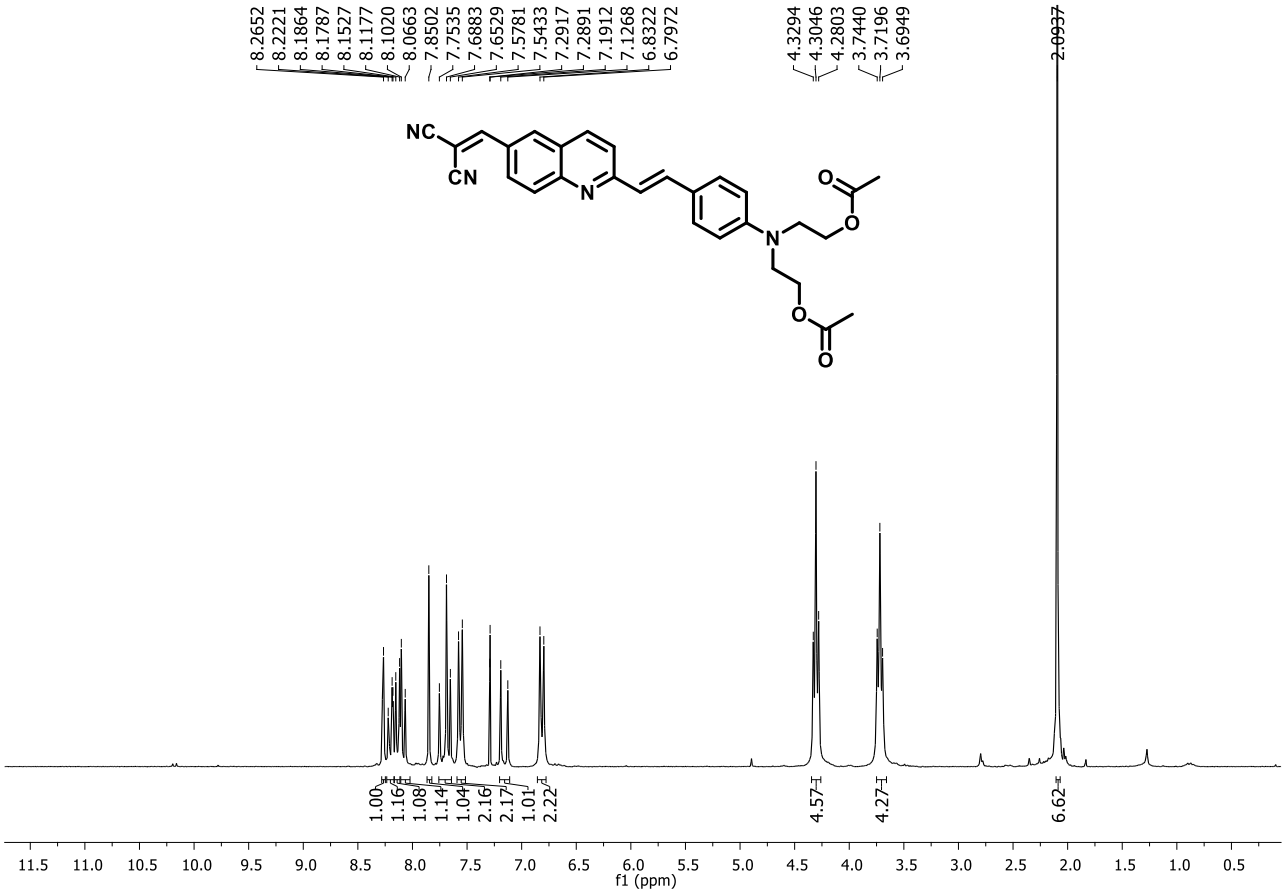
8.2652
8.2221
8.1864
8.1787
8.1527
8.1177
8.1020
8.0663
7.8502
7.7535
7.6883
7.6529
7.5781
7.5433
7.2917
7.2891
7.1912
7.1268
6.8322
6.7972
4.3294
4.3046
4.2803
3.7440
3.7196
3.6949
2.0937
NC
CN
N
O
O
N
O
O
1.00
1.16
1.08
1.14
1.04
2.16
2.17
1.01
2.22
4.57
4.27
6.62
11.5 11.0 10.5 10.0 9.5 9.0 8.5 8.0 7.5 7.0 6.5 6.0 5.5 5.0 4.5 4.0 3.5 3.0 2.5 2.0 1.5 1.0 0.5
f1 (ppm)

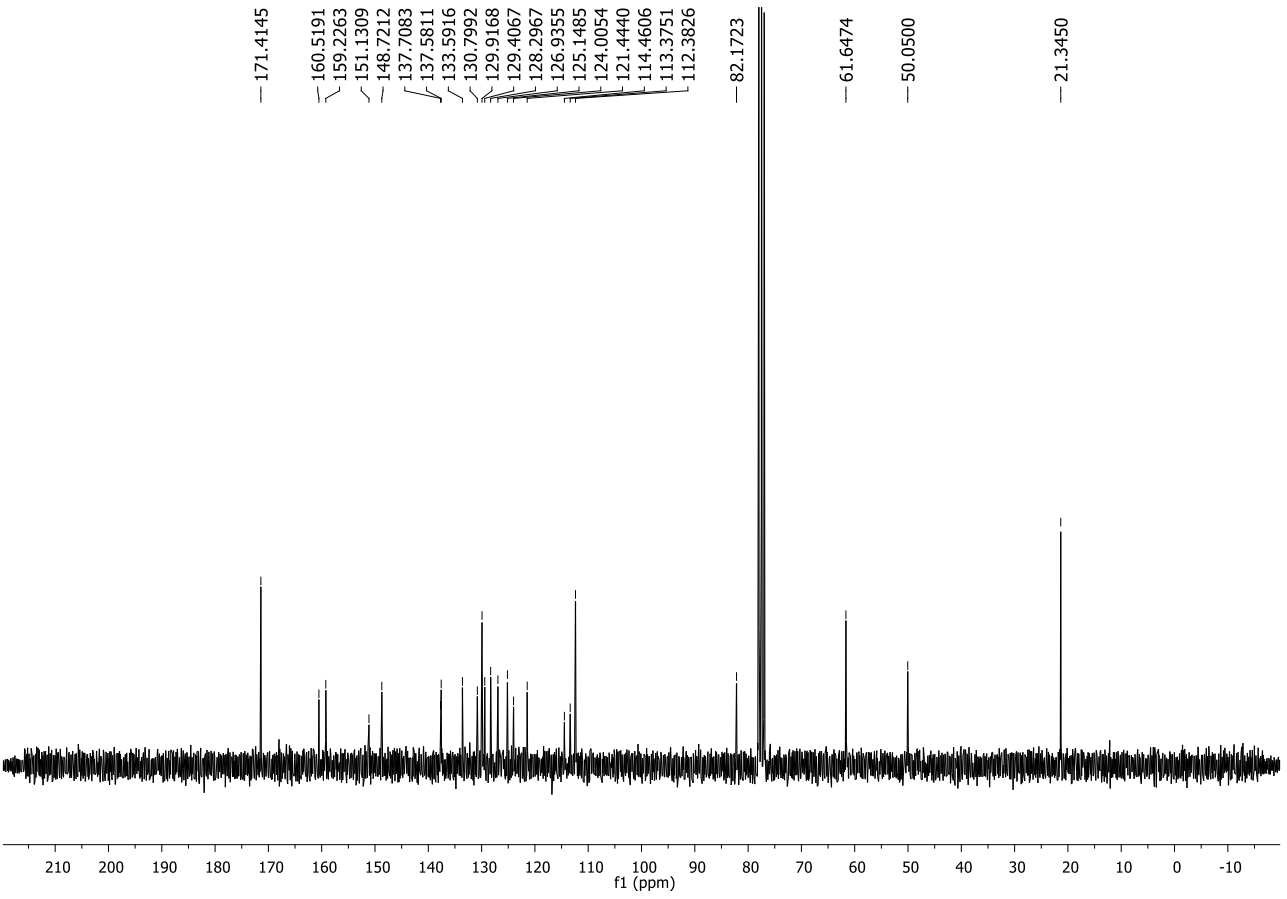
171.4145
160.5191
159.2263
151.1309
148.7212
137.7083
137.5811
133.5916
130.7992
129.9168
129.4067
128.2967
126.9355
125.1485
124.0054
121.4440
114.4606
113.3751
112.3826
82.1723
61.6474
50.0500
21.3450
210 200 190 180 170 160 150 140 130 120 110 100 90 80 70 60 50 40 30 20 10 0 -10
f1 (ppm)

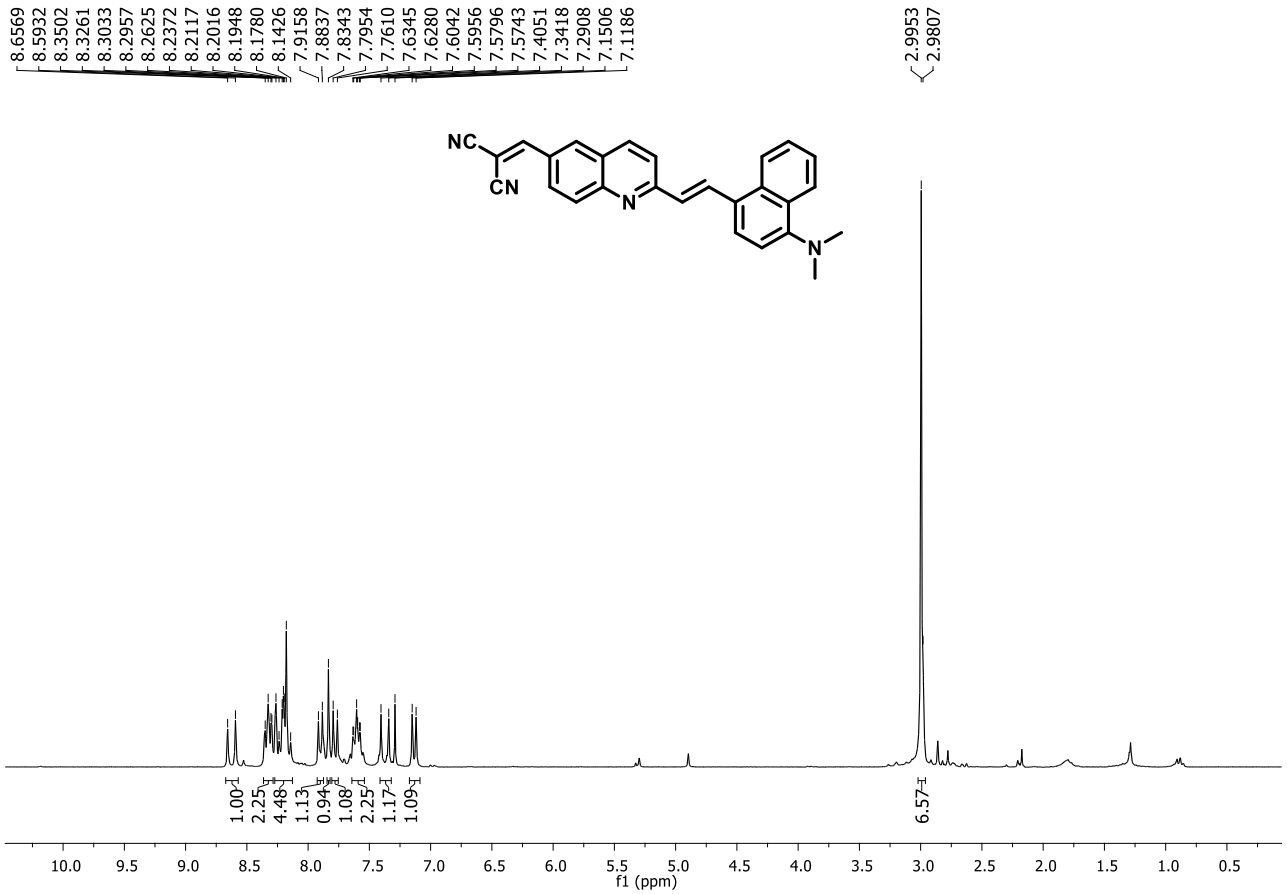
8.6569
8.5932
8.3502
8.3261
8.3033
8.2957
8.2625
8.2372
8.2117
8.2016
8.1948
8.1780
8.1426
7.9158
7.8837
7.8343
7.7954
7.7610
7.6345
7.6280
7.6042
7.5956
7.5796
7.5743
7.4051
7.3418
7.2908
7.1506
7.1186
2.9953
2.9807
NC
CN
N
N
1.00
2.25
4.48
1.13
0.94
1.08
2.25
1.17
1.09
6.57
10.0 9.5 9.0 8.5 8.0 7.5 7.0 6.5 6.0 5.5 5.0 4.5 4.0 3.5 3.0 2.5 2.0 1.5 1.0 0.5
f1 (ppm)

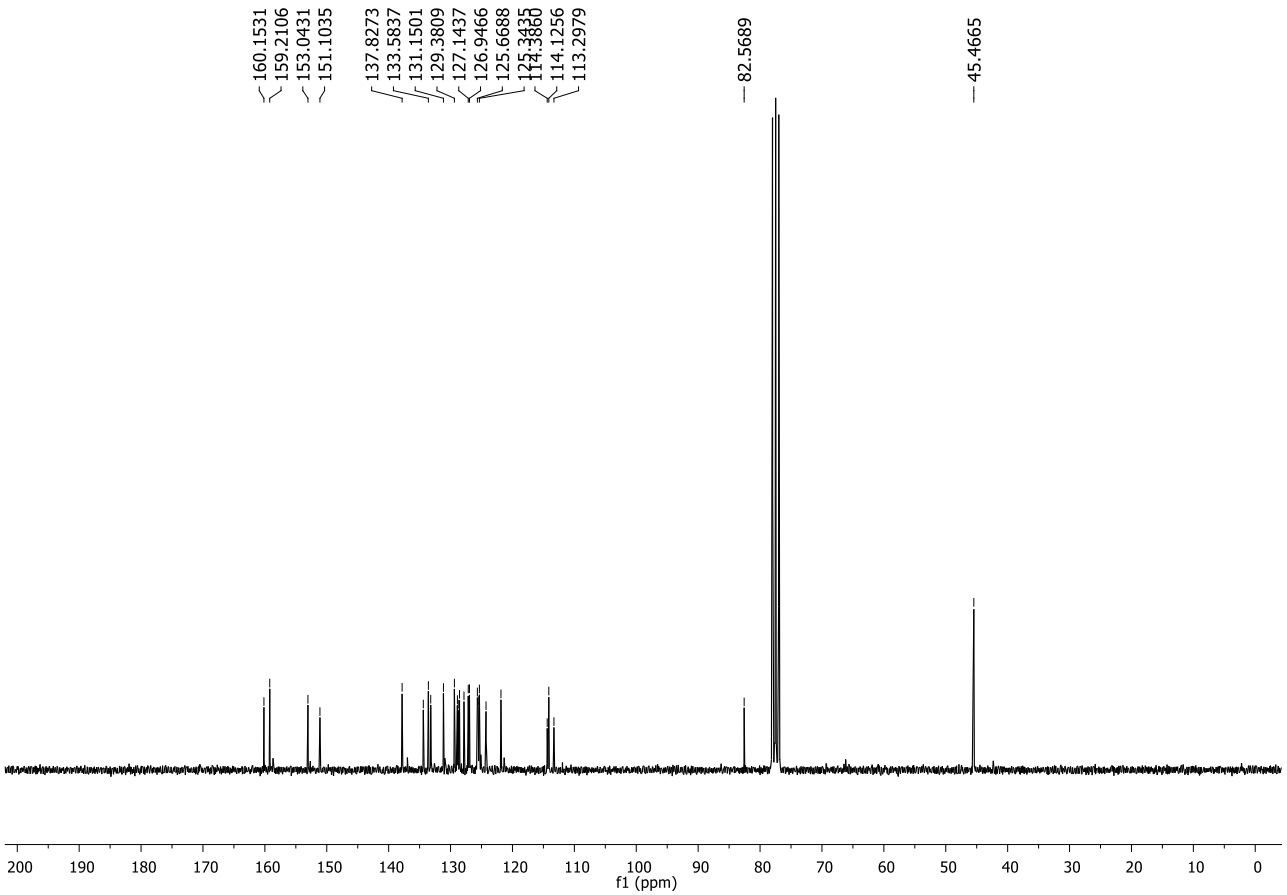
160.1531
159.2106
153.0431
151.1035
137.8273
133.5837
131.1501
129.3809
127.1437
126.9466
125.6688
114.1256
113.2979
82.5689
45.4665
200 190 180 170 160 150 140 130 120 110 100 90 80 70 60 50 40 30 20 10 0
f1 (ppm)

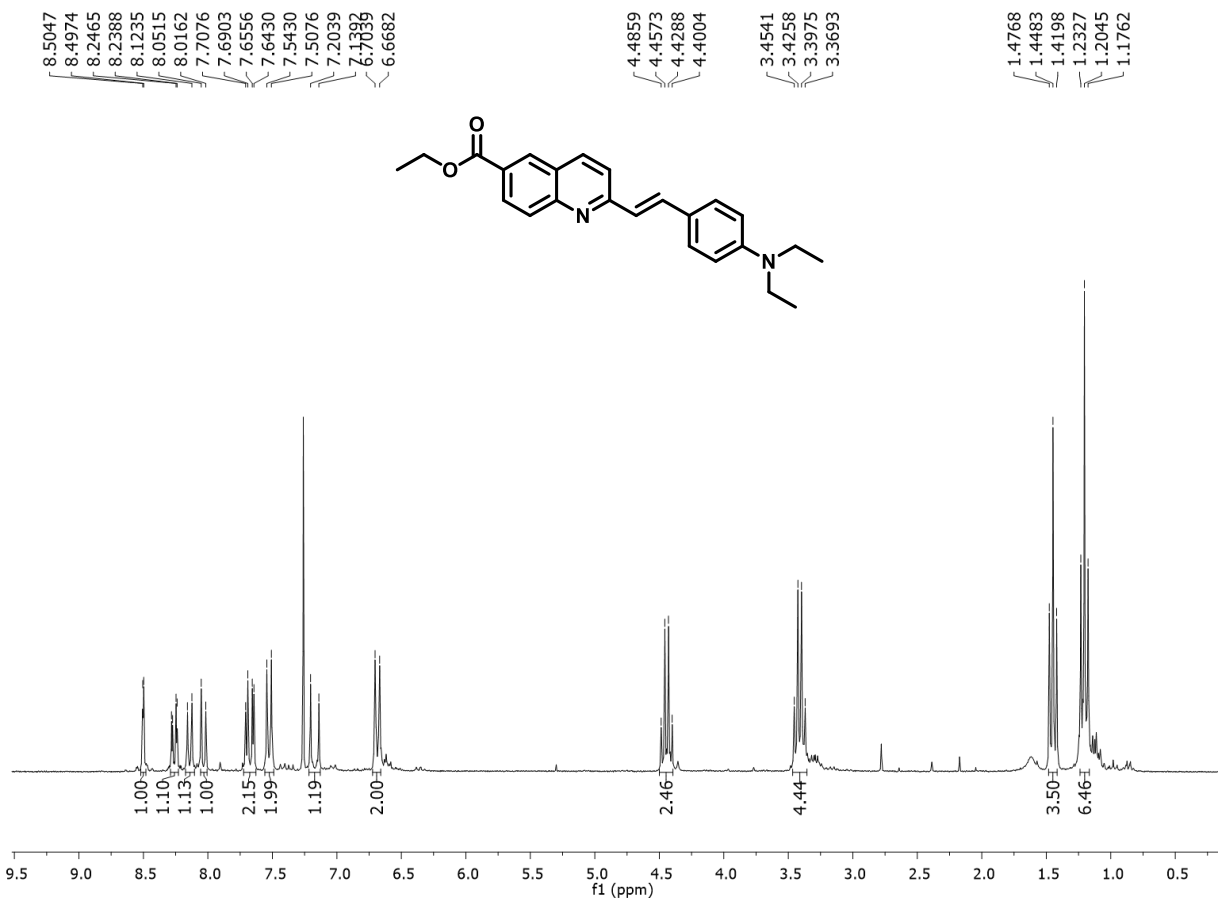
8.5047
8.4974
8.2465
8.2388
8.1235
8.0515
8.0162
7.7076
7.6903
7.6556
7.6430
7.5430
7.5076
7.2039
7.1392
7.1039
6.6682
4.4859
4.4573
4.4288
4.4004
3.4541
3.4258
3.3975
3.3693
1.4768
1.4483
1.4198
1.2327
1.2045
1.1762
O
O
N
N
1.00
1.10
1.13
1.00
2.15
1.99
1.19
2.00
2.46
4.44
3.50
6.46
9.5 9.0 8.5 8.0 7.5 7.0 6.5 6.0 5.5 5.0 4.5 4.0 3.5 3.0 2.5 2.0 1.5 1.0 0.5
f1 (ppm)

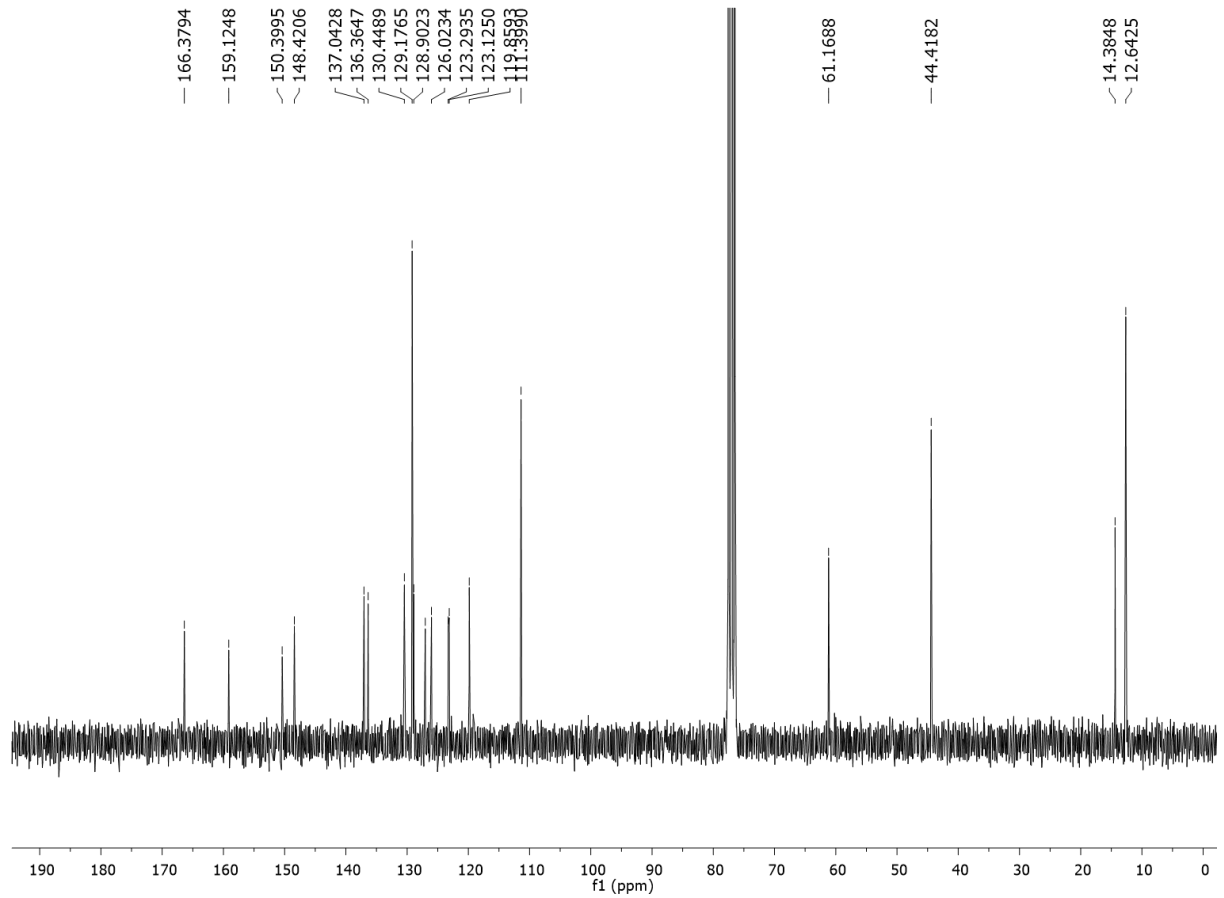
166.3794
159.1248
150.3995
148.4206
137.0428
136.3647
130.4489
129.1765
128.9023
126.0234
123.2935
123.1250
119.8593
111.3990
61.1688
44.4182
14.3848
12.6425
190 180 170 160 150 140 130 120 110 100 90 80 70 60 50 40 30 20 10 0
f1 (ppm)

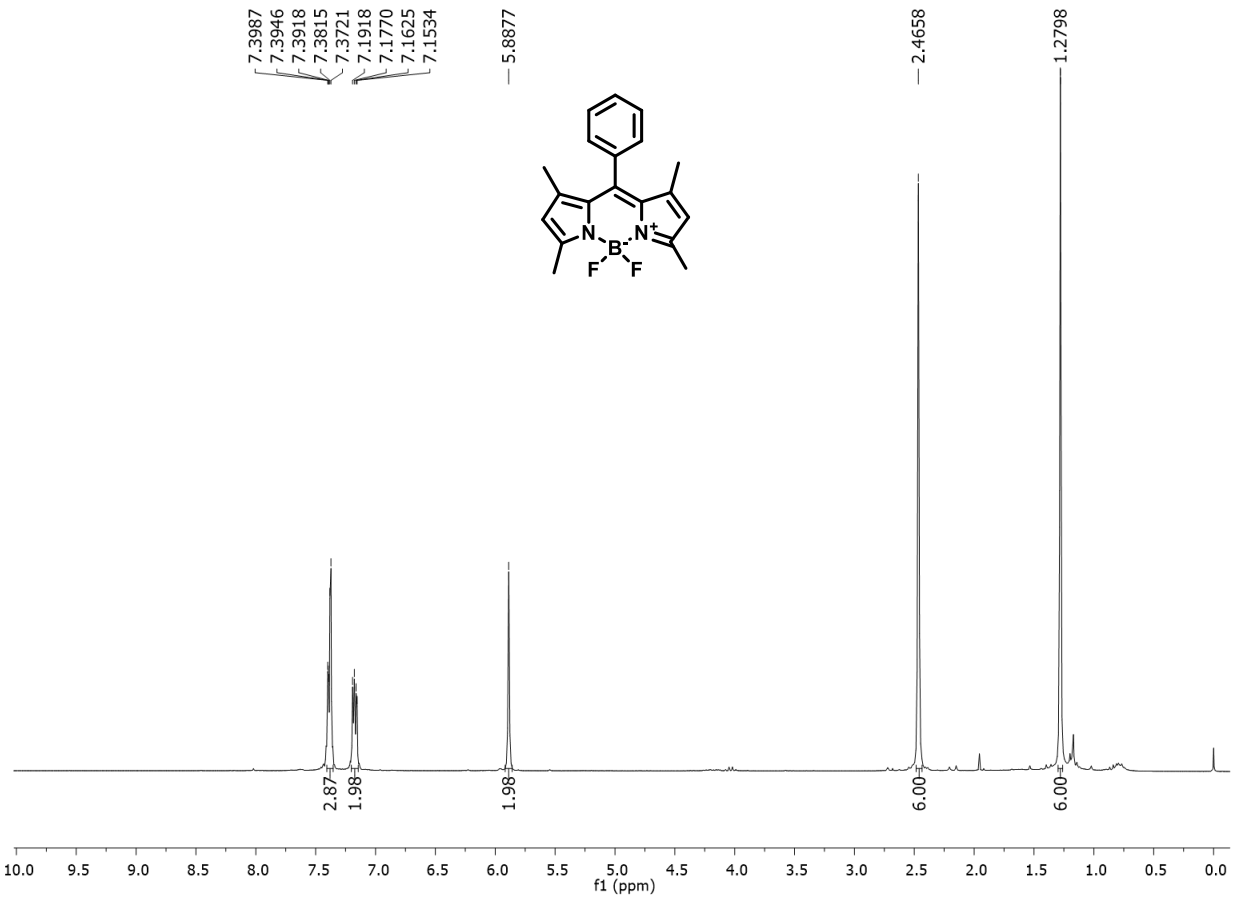
7.3987
7.3946
7.3918
7.3815
7.3721
7.1918
7.1770
7.1625
7.1534
5.8877
2.4658
1.2798
N
B
N+
F
F
2.87
1.98
1.98
6.00
6.00
f1 (ppm)

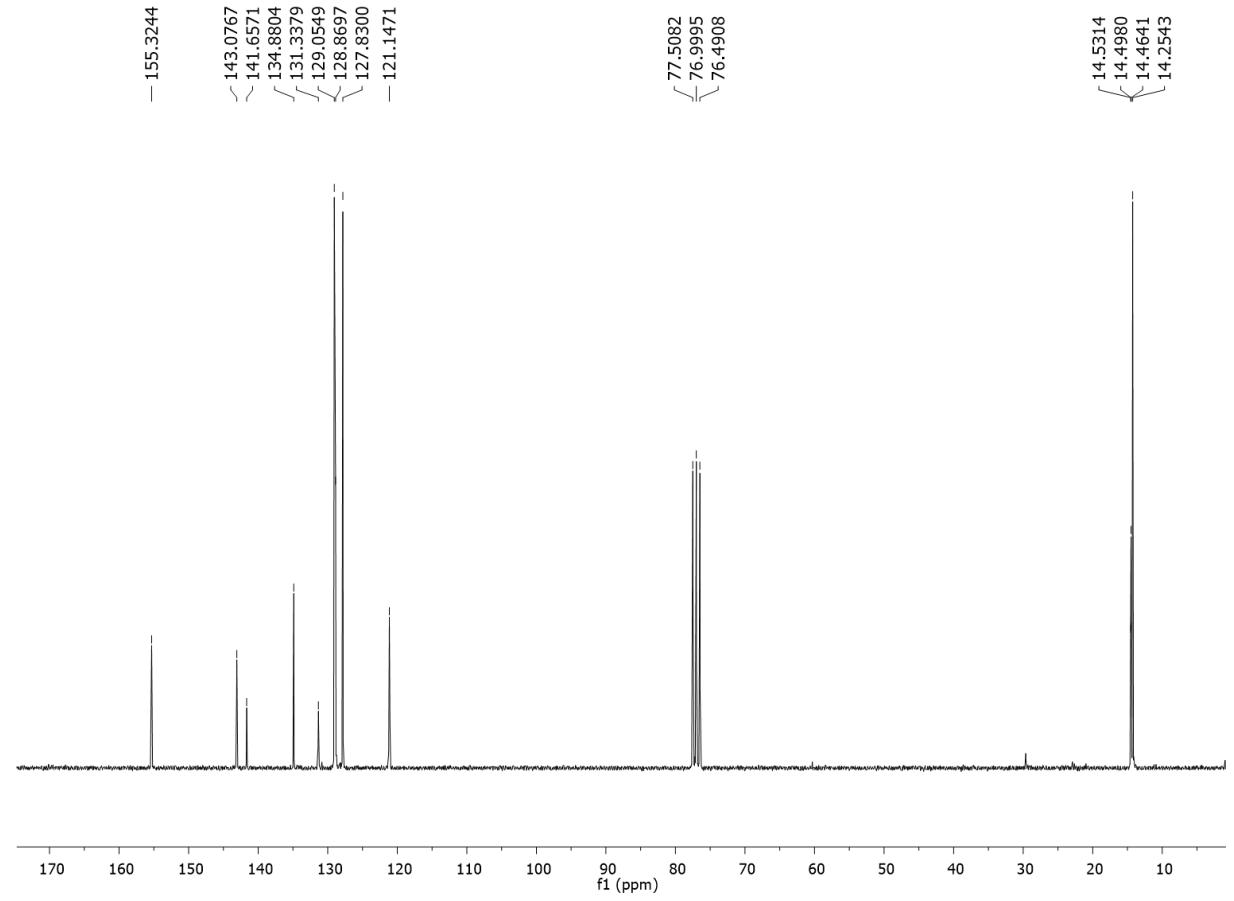
155.3244
143.0767
141.6571
134.8804
131.3379
129.0549
128.8697
127.8300
121.1471
77.5082
76.9995
76.4908
14.5314
14.4980
14.4641
14.2543
f1 (ppm)

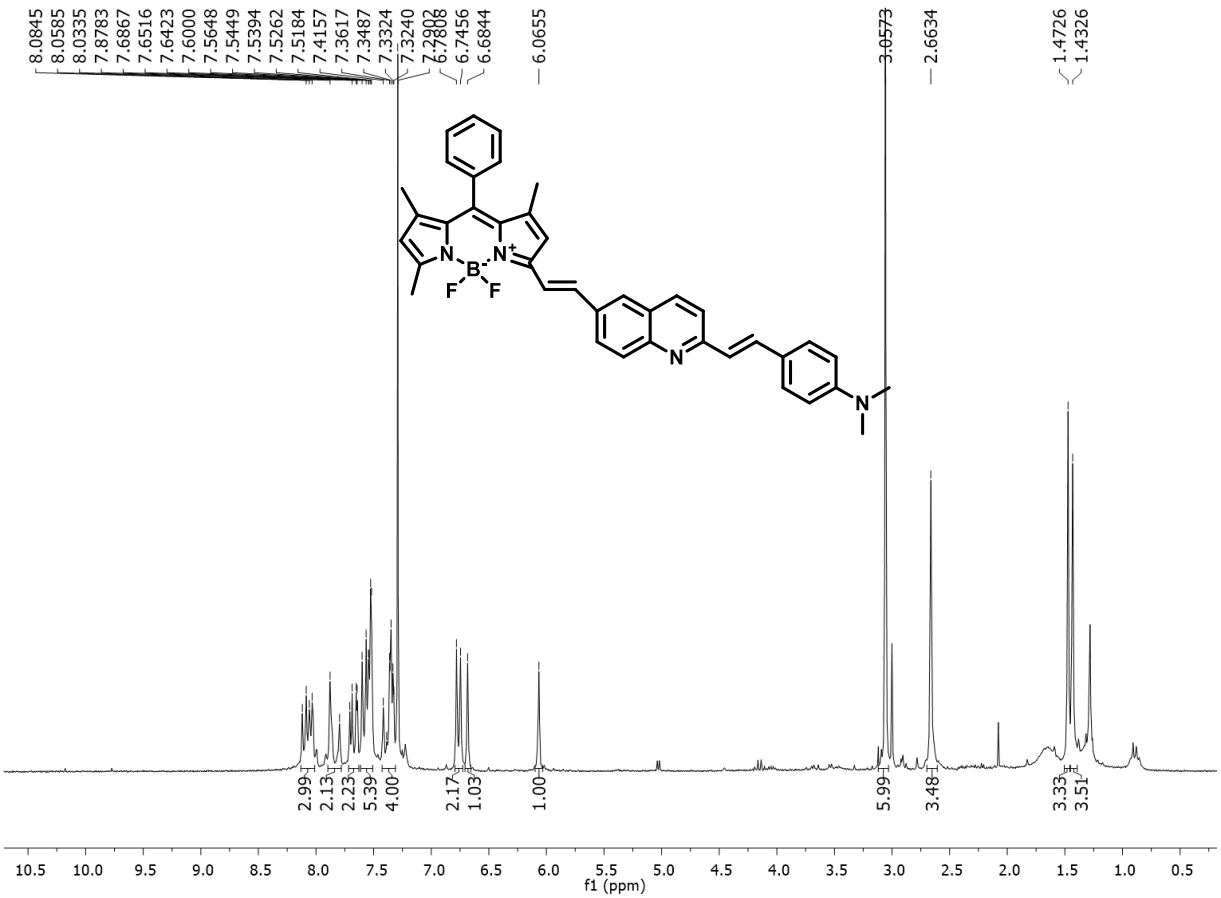
8.0845
8.0585
8.0335
7.8783
7.6867
7.6516
7.6423
7.6000
7.5648
7.5449
7.5394
7.5262
7.5184
7.4157
7.3617
7.3487
7.3324
7.3240
7.2902
6.7808
6.7456
6.6844
6.0655
3.0573
2.6634
1.4726
1.4326
2.99
2.13
2.23
5.39
4.00
2.17
1.03
1.00
5.99
3.48
3.33
3.51
10.5 10.0 9.5 9.0 8.5 8.0 7.5 7.0 6.5 6.0 5.5 5.0 4.5 4.0 3.5 3.0 2.5 2.0 1.5 1.0 0.5
f1 (ppm)

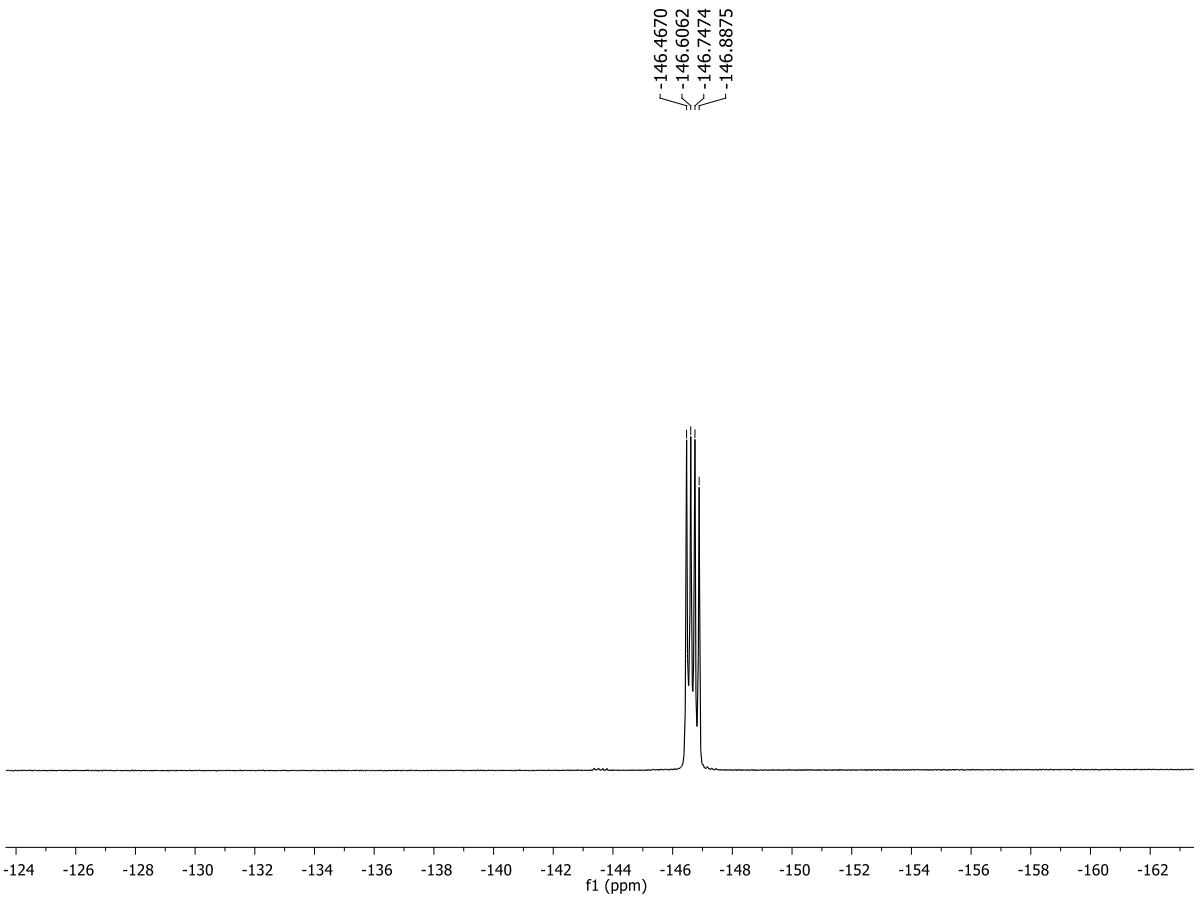
-146.4670
-146.6062
-146.7474
-146.8875
-124 -126 -128 -130 -132 -134 -136 -138 -140 -142 -144 -146 -148 -150 -152 -154 -156 -158 -160 -162
f1 (ppm)

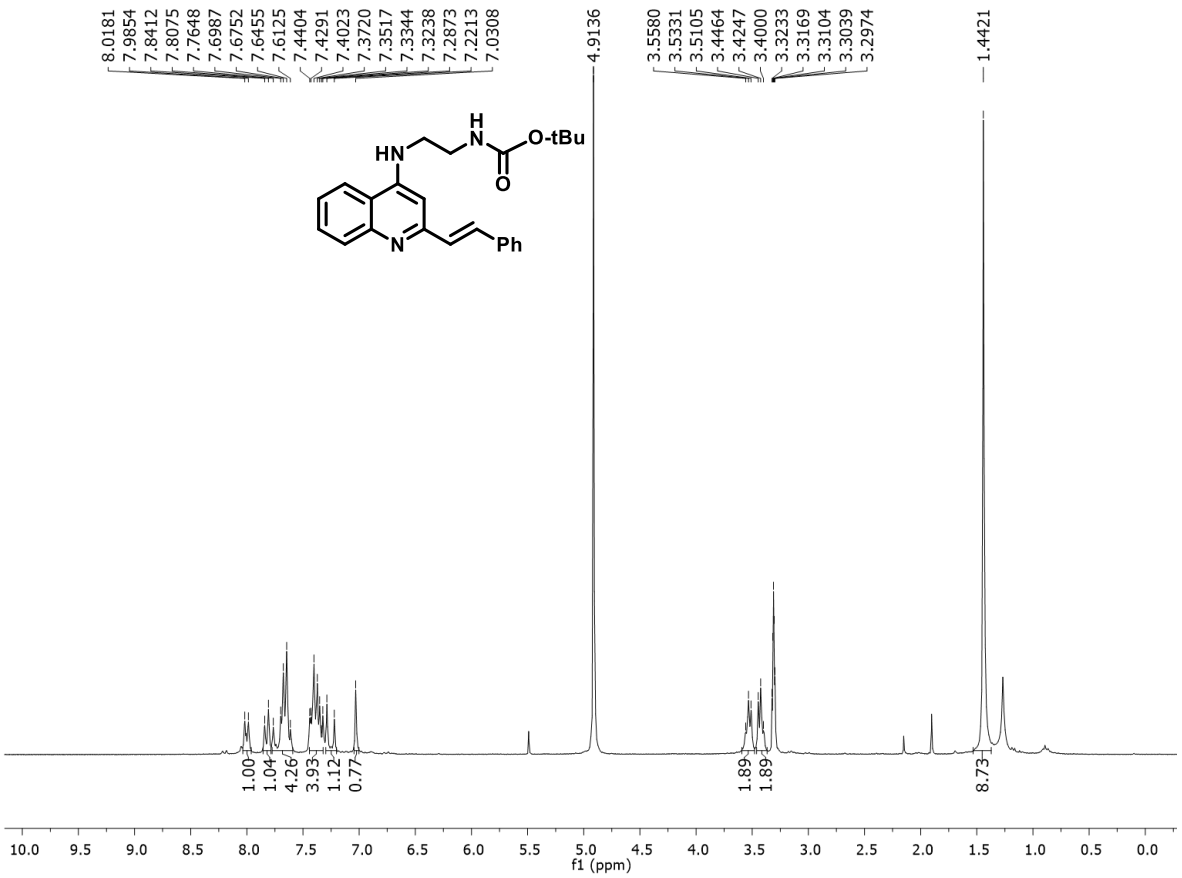
8.0181
7.9854
7.8412
7.8075
7.7648
7.6987
7.6752
7.6455
7.6125
7.4404
7.4291
7.4023
7.3720
7.3517
7.3344
7.3238
7.2873
7.2213
7.0308
4.9136
3.5580
3.5331
3.5105
3.4464
3.4247
3.4000
3.3233
3.3169
3.3104
3.3039
3.2974
1.4421
HN
H
N
O-tBu
O
N
Ph
1.00
1.04
4.26
3.93
1.12
0.77
1.89
1.89
8.73
f1 (ppm)

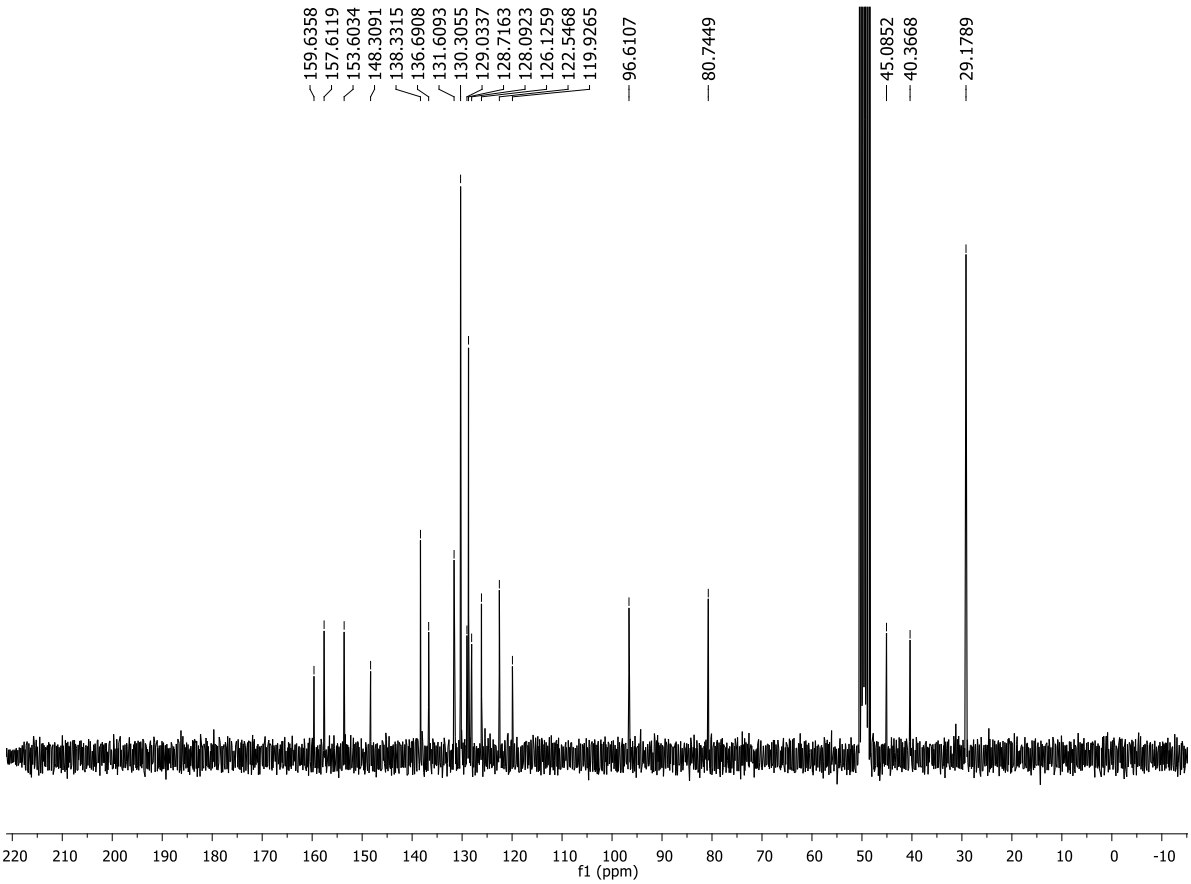
159.6358
157.6119
153.6034
148.3091
138.3315
136.6908
131.6093
130.3055
129.0337
128.7163
128.0923
126.1259
122.5468
119.9265
96.6107
80.7449
45.0852
40.3668
29.1789
f1 (ppm)

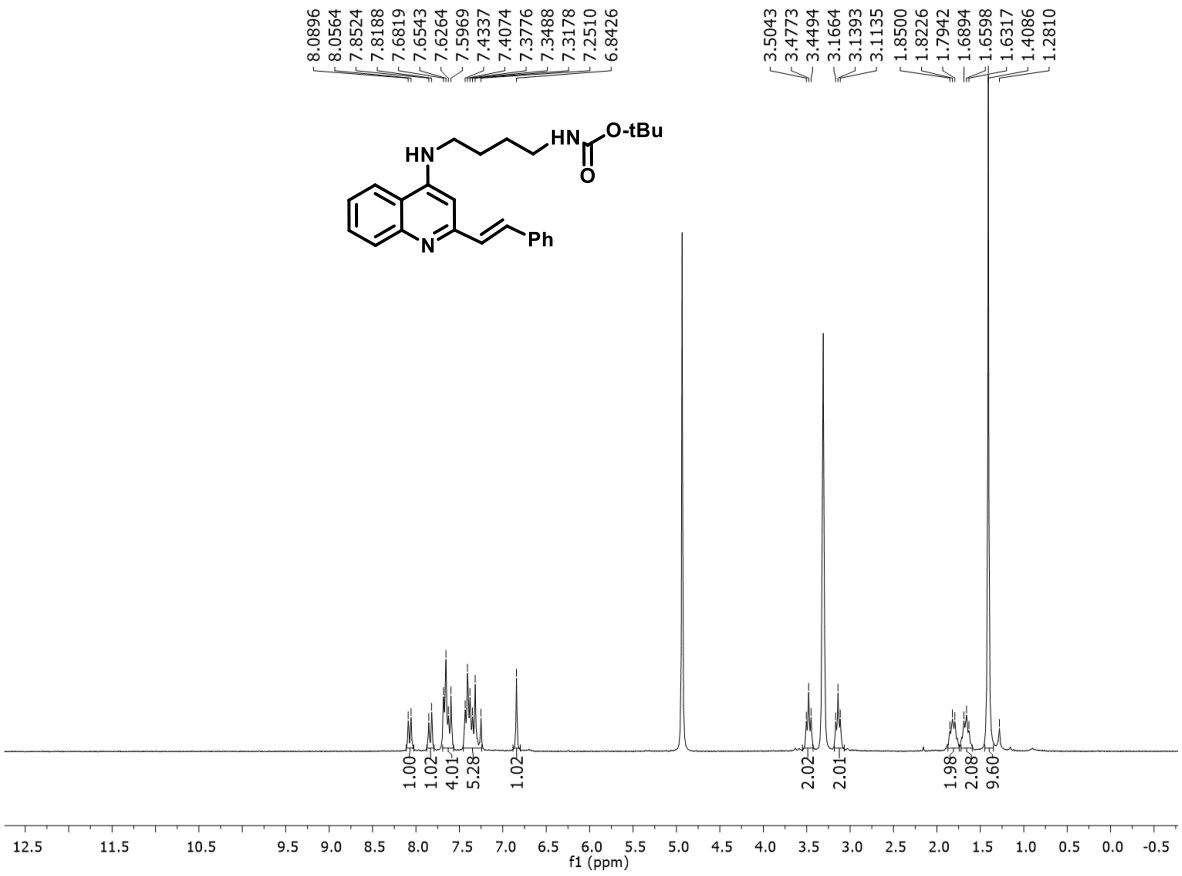
8.0896
8.0564
7.8524
7.8188
7.6819
7.6543
7.6264
7.5969
7.4337
7.4074
7.3776
7.3488
7.3178
7.2510
6.8426
3.5043
3.4773
3.4494
3.1664
3.1393
3.1135
1.8500
1.8226
1.7942
1.6894
1.6598
1.6317
1.4086
1.2810
HN
HN
O-tBu
O
N
Ph
1.00
1.02
4.01
5.28
1.02
2.02
2.01
1.98
2.08
9.60
f1 (ppm)

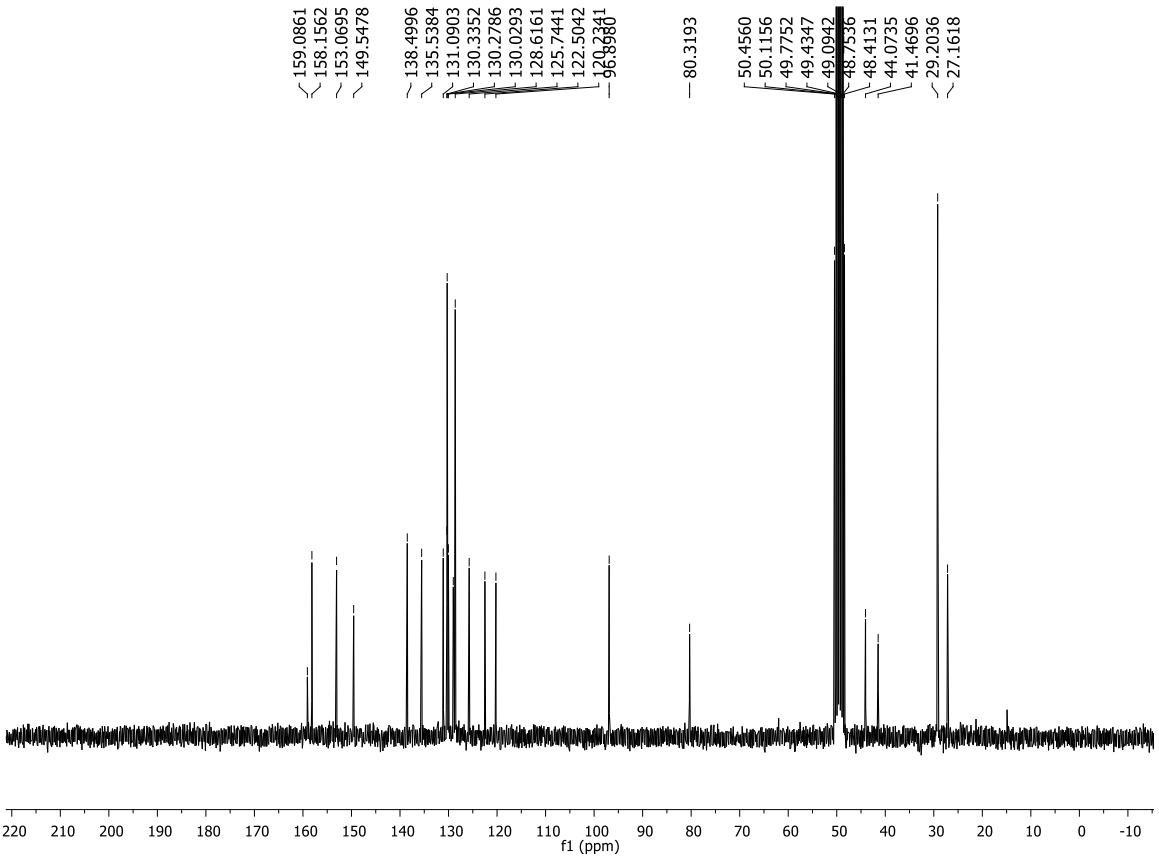
159.0861
158.1562
153.0695
149.5478
138.4996
135.5384
131.0903
130.3352
130.2786
130.0293
128.6161
125.7441
122.5042
96.8980
80.3193
50.4560
50.1156
49.7752
49.4347
49.0942
48.7536
48.4131
44.0735
41.4696
29.2036
27.1618
f1 (ppm)

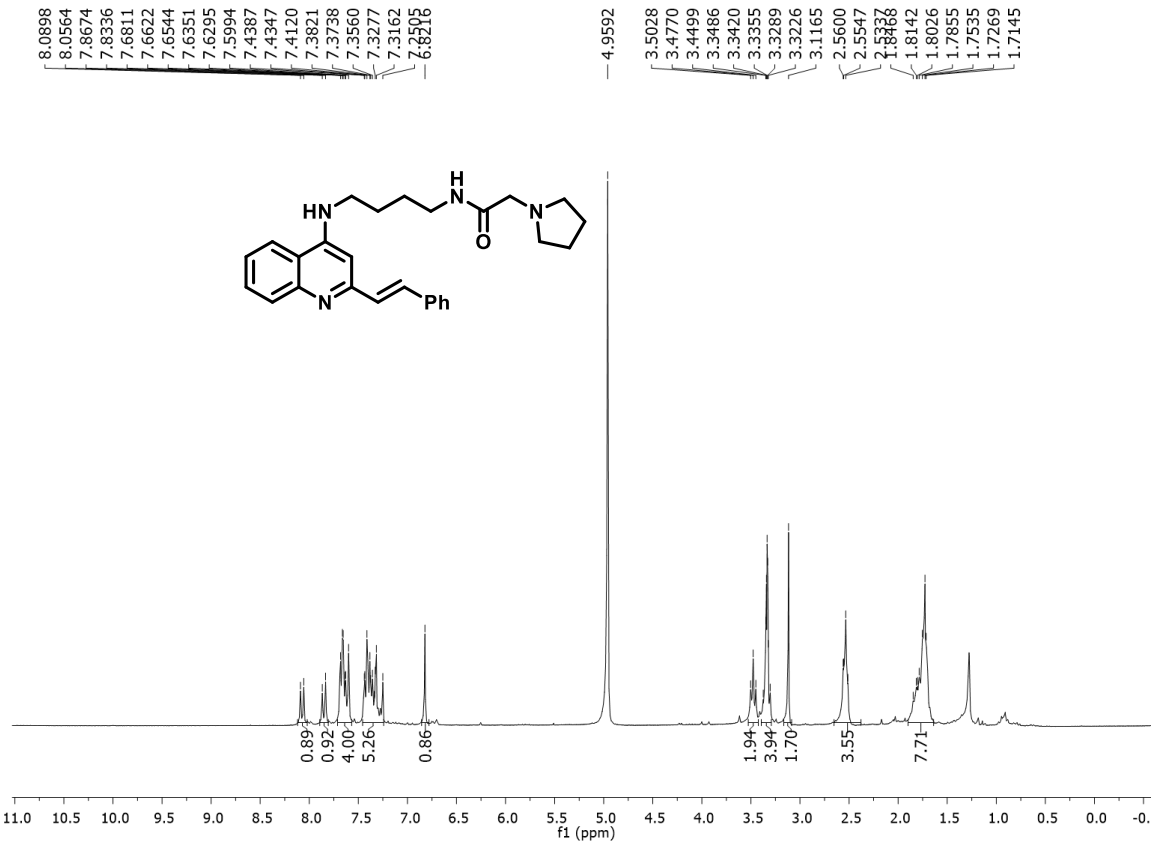
8.0898
8.0564
7.8674
7.8336
7.6811
7.6622
7.6544
7.6351
7.6295
7.5994
7.4387
7.4347
7.4120
7.3821
7.3738
7.3560
7.3277
7.3162
7.2505
6.8216
4.9592
3.5028
3.4770
3.4499
3.3486
3.3420
3.3355
3.3289
3.3226
3.1165
2.5600
2.5547
2.5337
1.8468
1.8142
1.8026
1.7855
1.7535
1.7269
1.7145
HN
H
N
O
N
N
Ph
0.89
0.92
4.00
5.26
0.86
1.94
3.94
1.70
3.55
7.71
f1 (ppm)

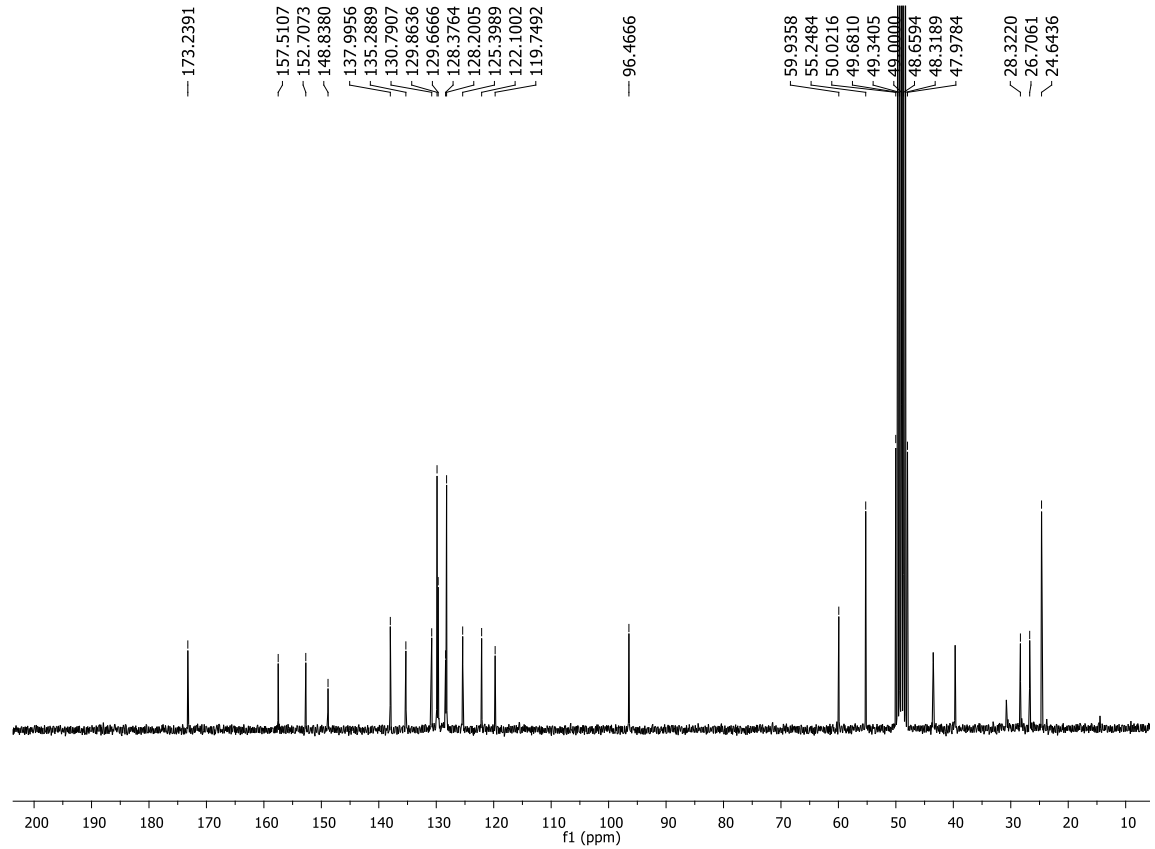
173.2391
157.5107
152.7073
148.8380
137.9956
135.2889
130.7907
129.8636
129.6666
128.3764
128.2005
125.3989
122.1002
119.7492
96.4666
59.9358
55.2484
50.0216
49.6810
49.3405
49.0000
48.6594
48.3189
47.9784
28.3220
26.7061
24.6436
f1 (ppm)

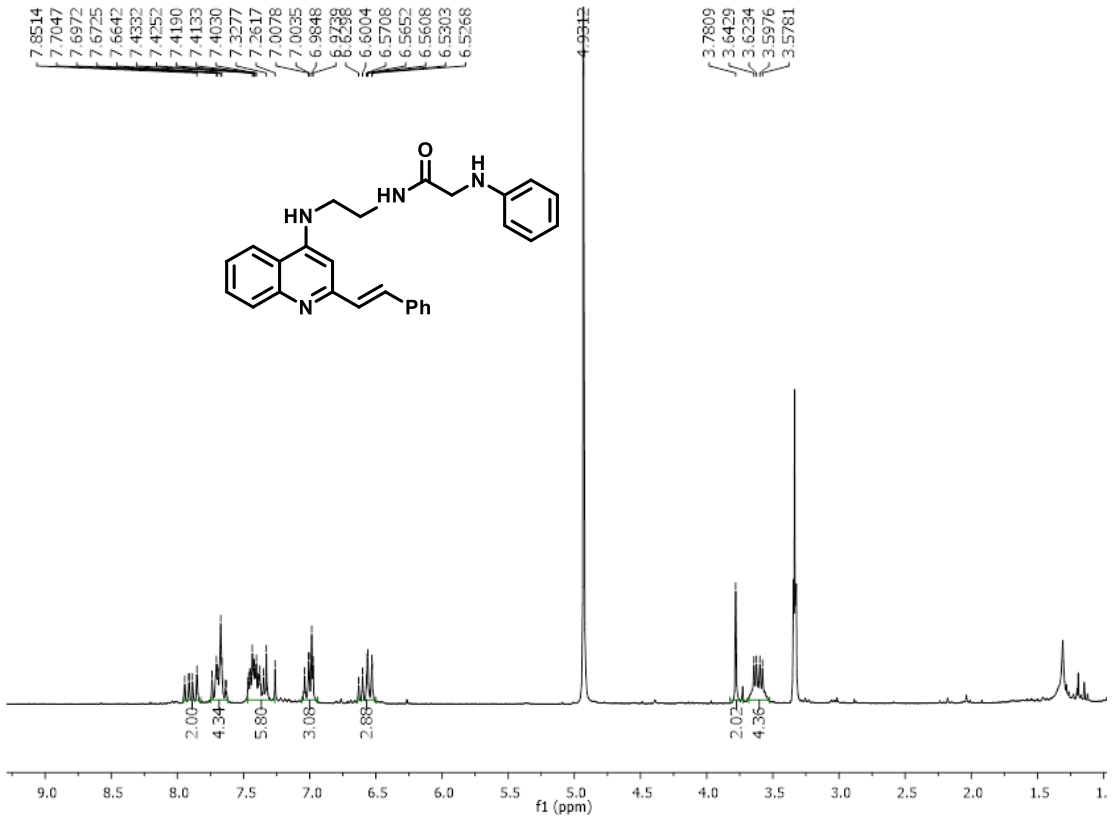
7.8514
7.7047
7.6972
7.6725
7.6642
7.4332
7.4252
7.4190
7.4133
7.4030
7.3277
7.2617
7.0078
7.0035
6.9848
6.6004
6.5708
6.5652
6.5608
6.5303
6.5268
4.9312
3.7809
3.6429
3.6234
3.5976
3.5781
O
H
N
HN
HN
N
Ph
2.00
4.34
5.80
3.08
2.88
2.02
4.36
f1 (ppm)

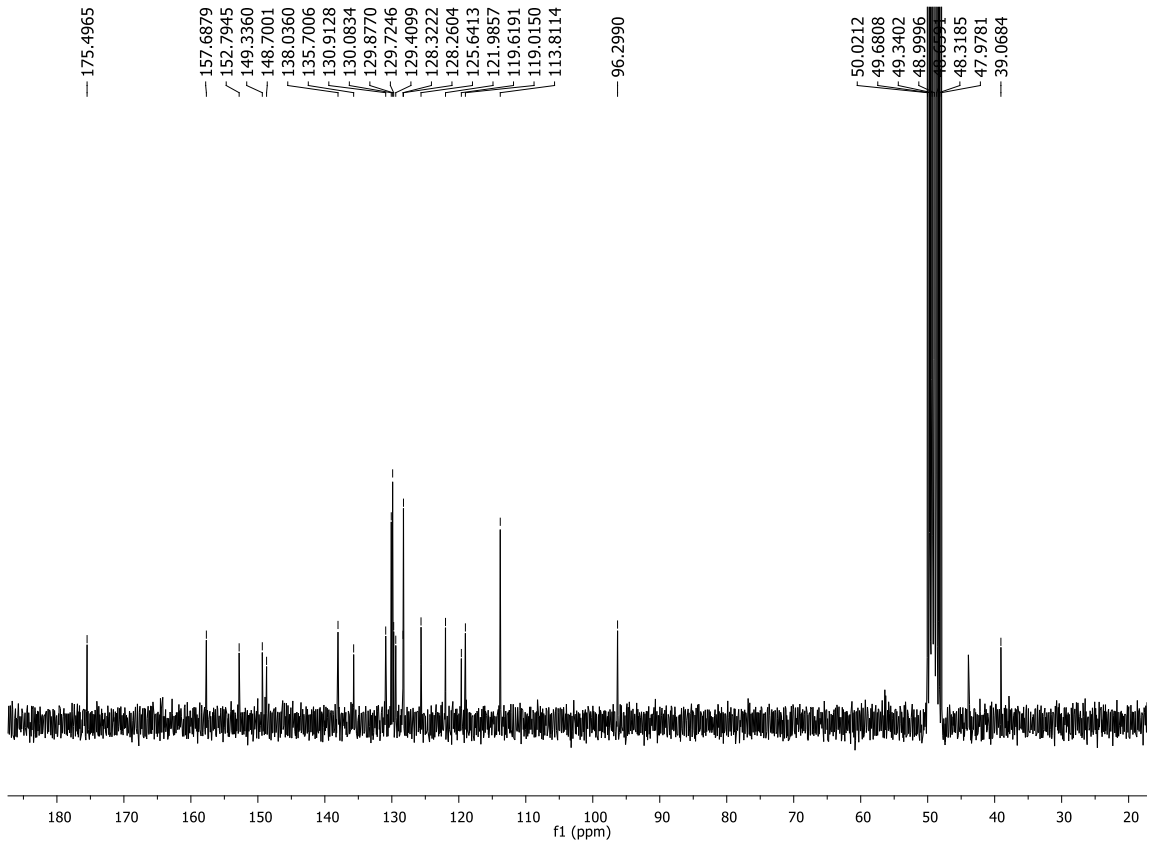
175.4965
157.6879
152.7945
149.3360
148.7001
138.0360
135.7006
130.9128
130.0834
129.8770
129.7246
129.4099
128.3222
128.2604
125.6413
121.9857
119.6191
119.0150
113.8114
96.2990
50.0212
49.6808
49.3402
48.9996
48.3185
47.9781
39.0684
f1 (ppm)

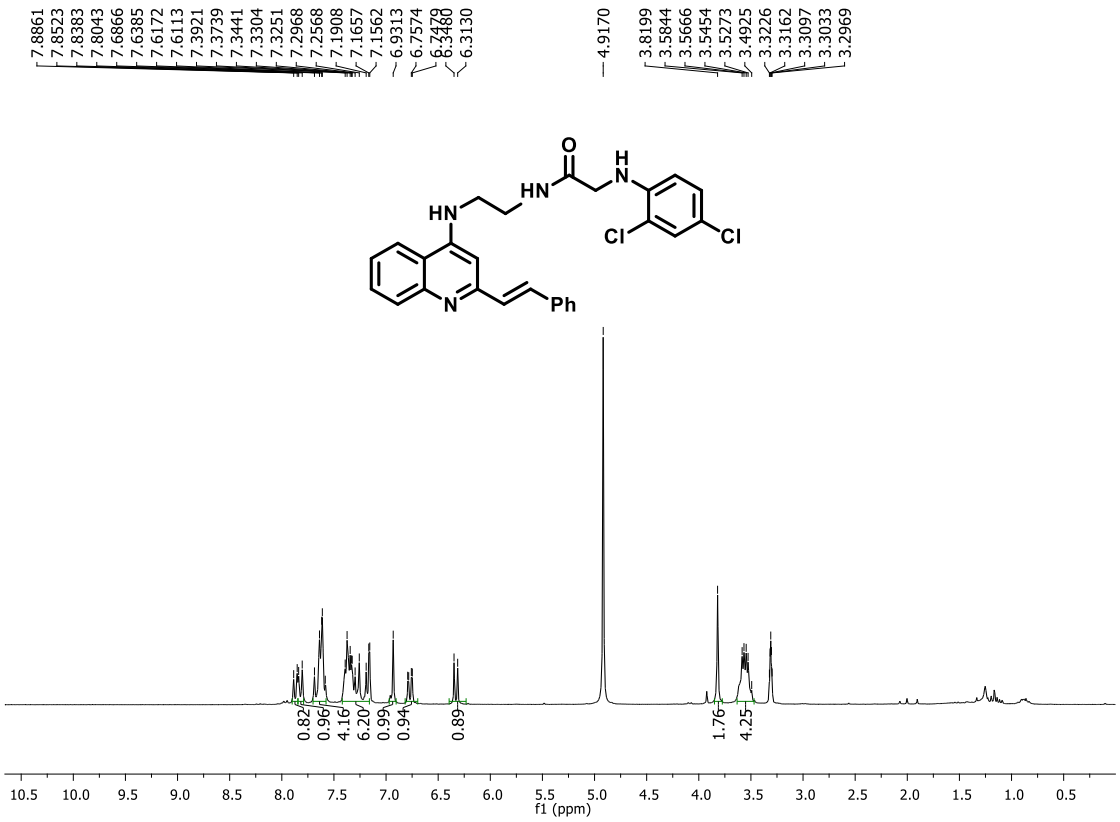
7.8861
7.8523
7.8383
7.8043
7.6866
7.6385
7.6172
7.6113
7.3921
7.3739
7.3441
7.3304
7.3251
7.2968
7.2568
7.1908
7.1657
7.1562
6.9313
6.7574
6.3480
6.3130
4.9170
3.8199
3.5844
3.5666
3.5454
3.5273
3.4925
3.3226
3.3162
3.3097
3.3033
3.2969
HN
HN
O
H
N
Cl
Cl
N
Ph
0.82
0.96
4.16
6.20
0.99
0.94
0.89
1.76
4.25
f1 (ppm)

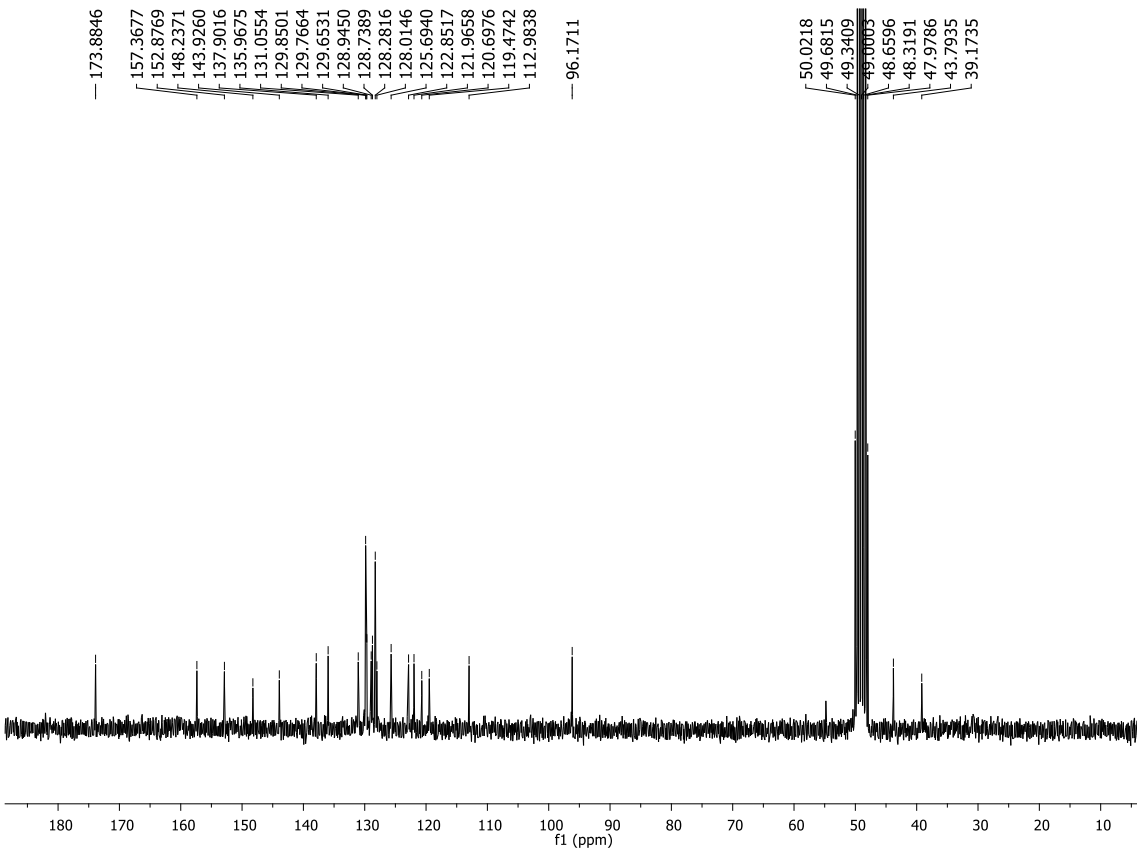
173.8846
157.3677
152.8769
148.2371
143.9260
137.9016
135.9675
131.0554
129.8501
129.7664
129.6531
128.9450
128.7389
128.2816
128.0146
125.6940
122.8517
121.9658
120.6976
119.4742
112.9838
96.1711
50.0218
49.6815
49.3409
49.0003
48.6596
48.3191
47.9786
43.7935
39.1735
f1 (ppm)

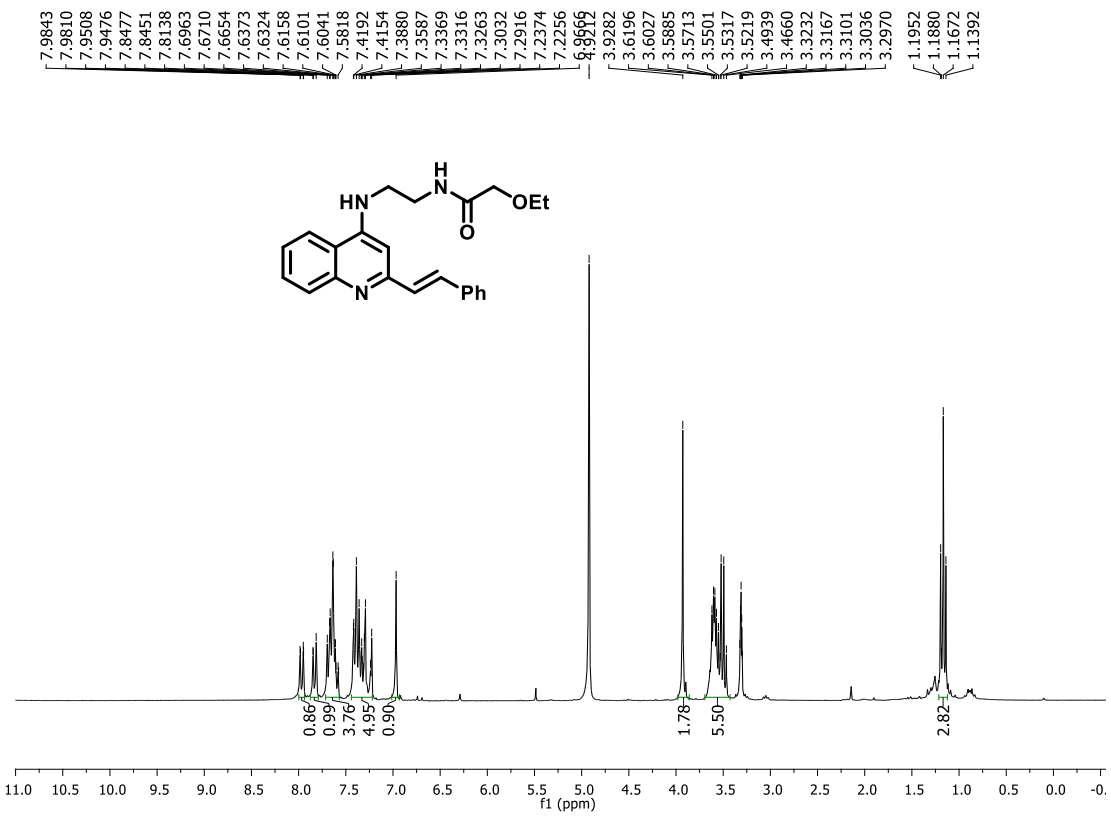
7.9843
7.9810
7.9508
7.9476
7.8477
7.8451
7.8138
7.6963
7.6710
7.6654
7.6373
7.6324
7.6158
7.6101
7.6041
7.5818
7.4192
7.4154
7.3880
7.3587
7.3369
7.3316
7.3263
7.3032
7.2916
7.2374
7.2256
6.9666
4.9212
3.9282
3.6196
3.6027
3.5885
3.5713
3.5501
3.5317
3.5219
3.4939
3.4660
3.3232
3.3167
3.3101
3.3036
3.2970
1.1952
1.1880
1.1672
1.1392
HN
H
N
OEt
O
N
Ph
0.86
0.99
3.76
4.95
0.90
1.78
5.50
2.82
f1 (ppm)

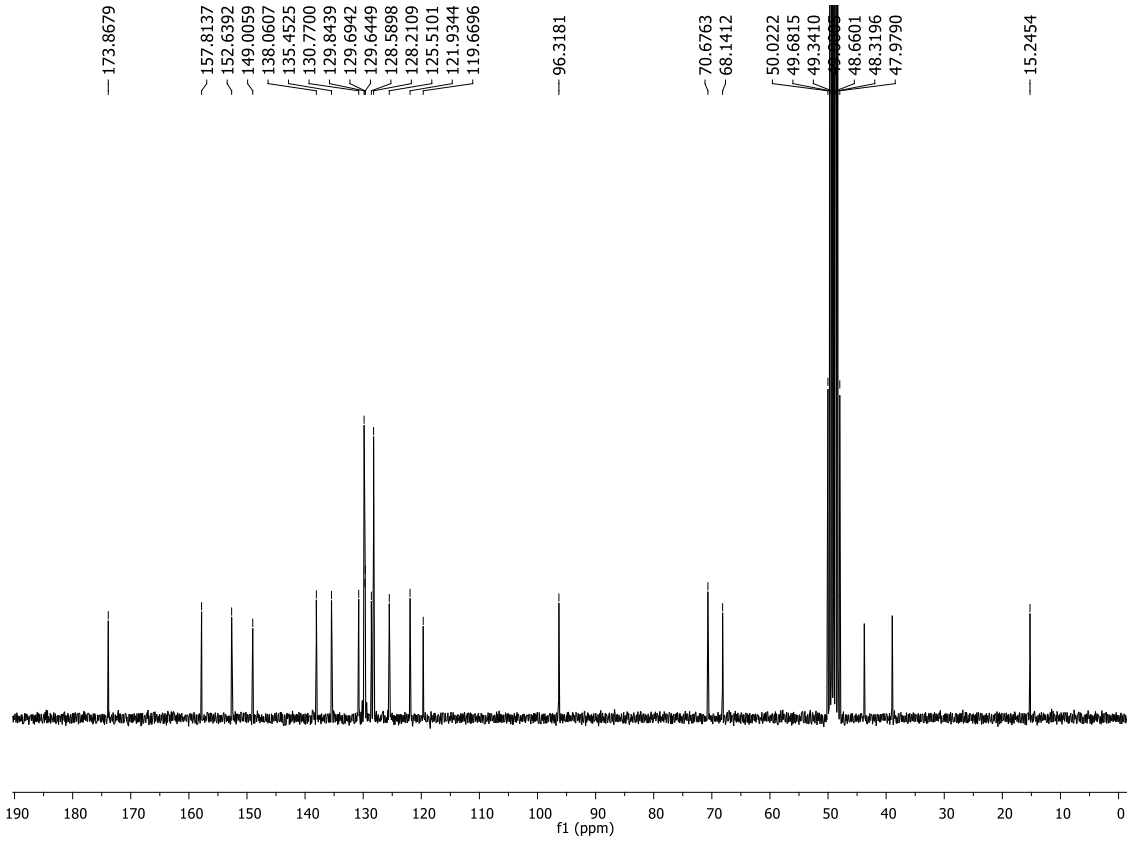
173.8679
157.8137
152.6392
149.0059
138.0607
135.4525
130.7700
129.8439
129.6942
129.6449
128.5898
128.2109
125.5101
121.9344
119.6696
96.3181
70.6763
68.1412
50.0222
49.6815
49.3410
48.6601
48.3196
47.9790
15.2454
f1 (ppm)

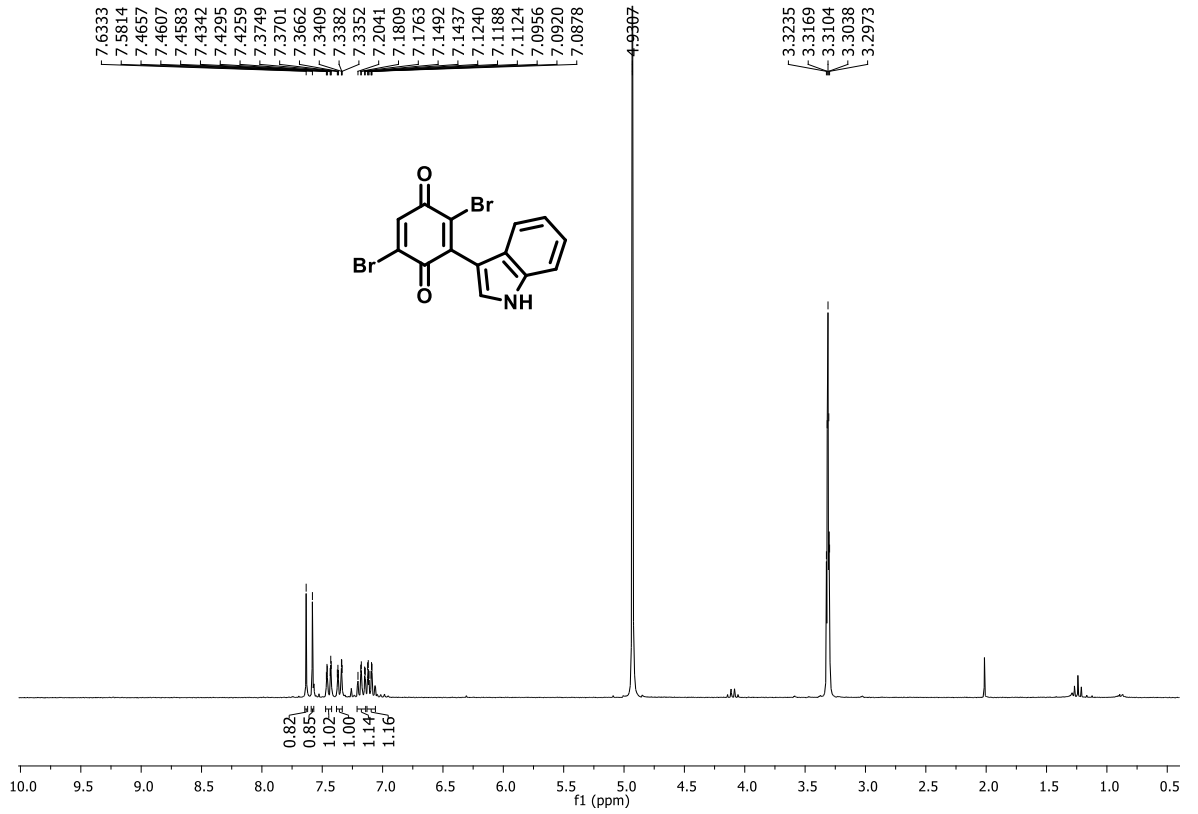
7.6333
7.5814
7.4657
7.4607
7.4583
7.4342
7.4295
7.4259
7.3749
7.3701
7.3662
7.3409
7.3382
7.3352
7.2041
7.1809
7.1763
7.1492
7.1437
7.1240
7.1188
7.1124
7.0956
7.0920
7.0878
4.9307
3.3235
3.3169
3.3104
3.3038
3.2973
O
Br
Br
O
NH
0.82
0.85
1.02
1.00
1.14
1.16
f1 (ppm)

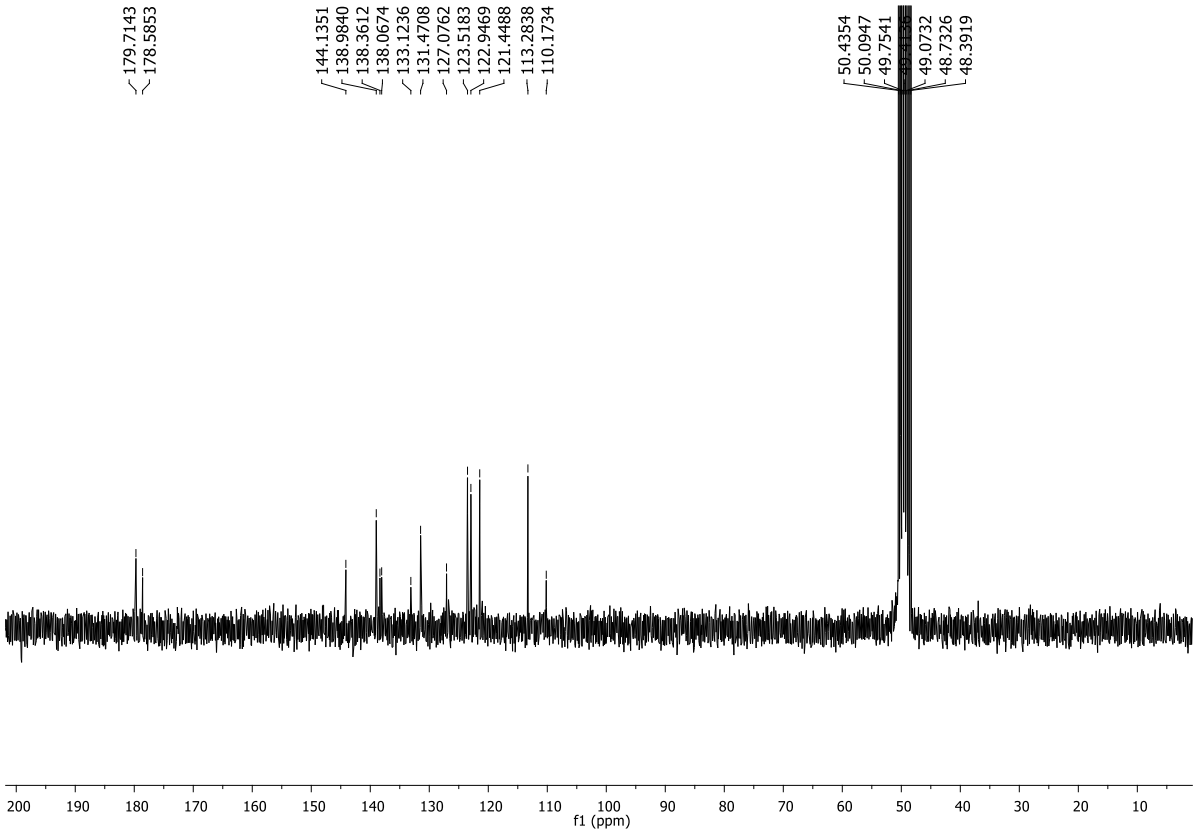
179.7143
178.5853
144.1351
138.9840
138.3612
138.0674
133.1236
131.4708
127.0762
123.5183
122.9469
121.4488
113.2838
110.1734
50.4354
50.0947
49.7541
49.0732
48.7326
48.3919
f1 (ppm)

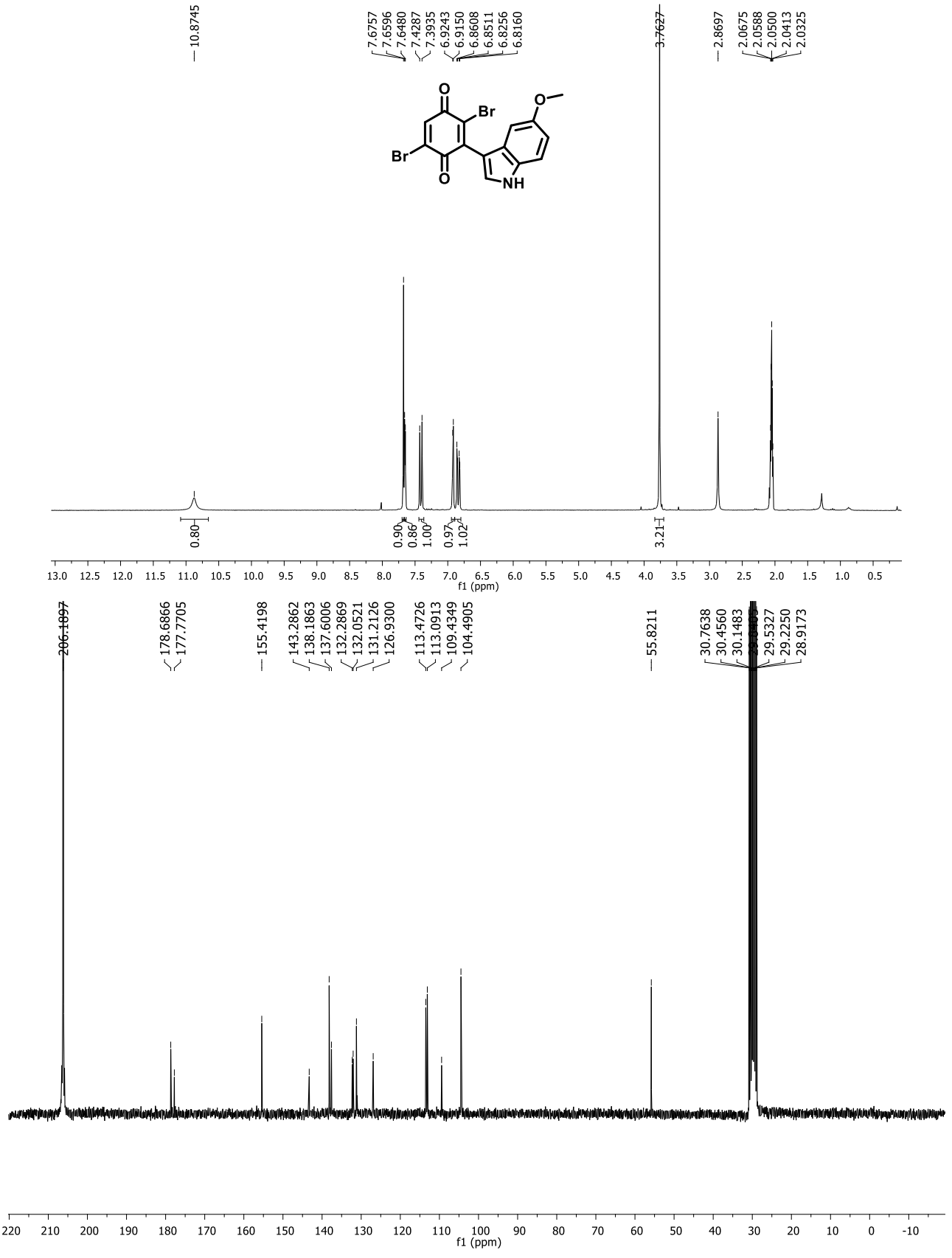
10.8745
7.6757
7.6596
7.6480
7.4287
7.3935
6.9243
6.9150
6.8608
6.8511
6.8256
6.8160
3.7627
2.8697
2.0675
2.0588
2.0500
2.0413
2.0325
O
Br
O
Br
O
NH
0.80
0.90
0.86
1.00
0.97
1.02
3.21
f1 (ppm)
206.1897
178.6866
177.7705
155.4198
143.2862
138.1863
137.6006
132.2869
132.0521
131.2126
126.9300
113.4726
113.0913
109.4349
104.4905
55.8211
30.7638
30.4560
30.1483
29.5327
29.2250
28.9173
f1 (ppm)

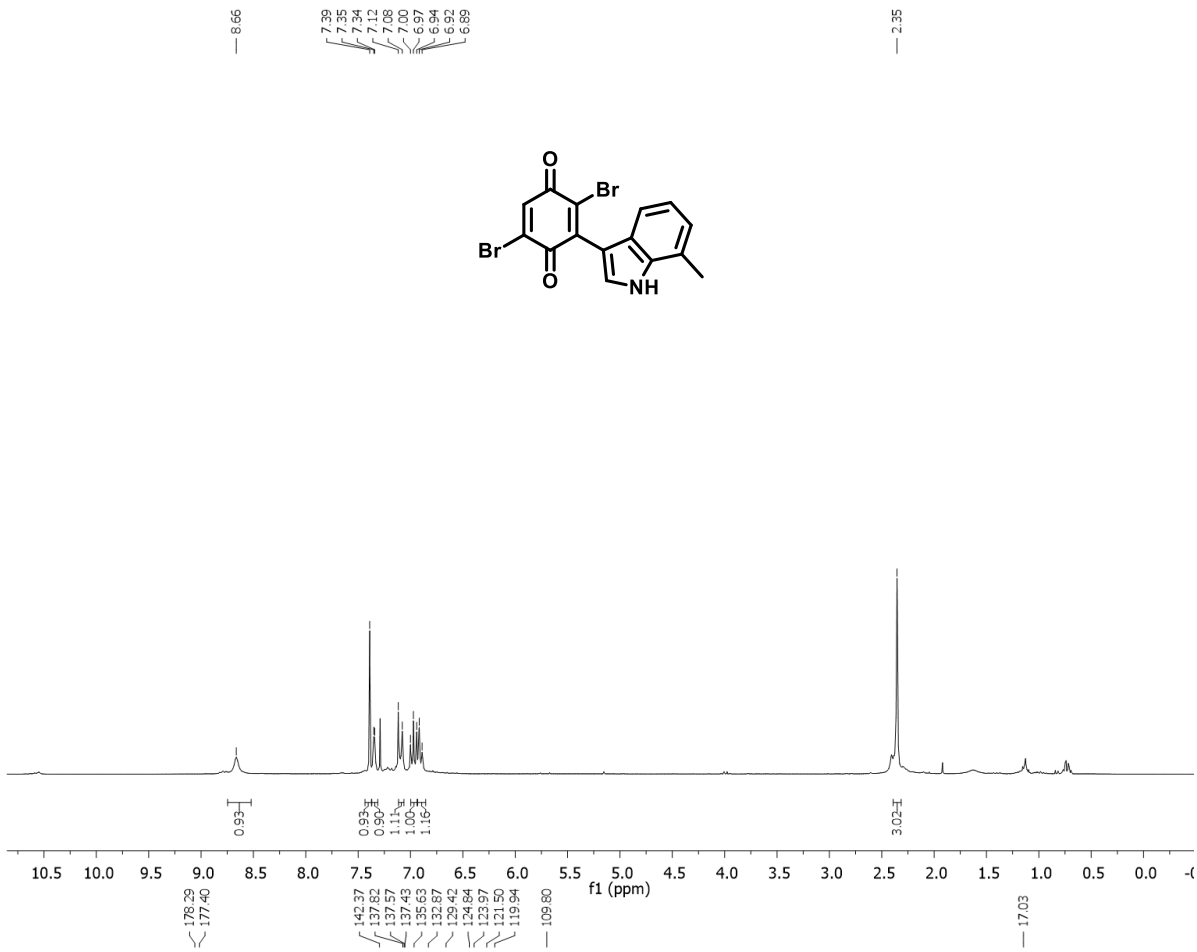
8.66
7.39
7.35
7.34
7.12
7.08
7.00
6.97
6.94
6.92
6.89
2.35
O
Br
Br
O
NH
0.93
0.93
0.90
1.11
1.00
1.16
3.02
f1 (ppm)
178.29
177.40
142.37
137.82
137.57
137.43
135.63
132.87
129.42
124.84
123.97
121.50
119.94
109.80
17.03
f1 (ppm)

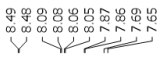
8.49
8.48
8.09
8.08
8.06
8.05
7.87
7.86
7.69
7.65

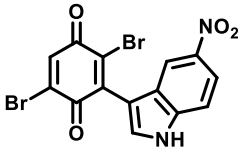
O
Br
NO2
Br
O
NH

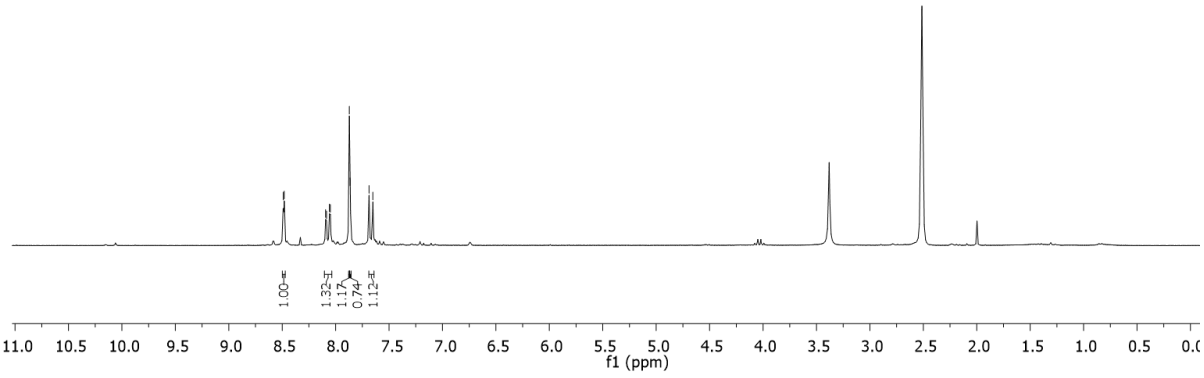
1.00
1.32
1.17
0.74
1.12
11.0 10.5 10.0 9.5 9.0 8.5 8.0 7.5 7.0 6.5 6.0 5.5 5.0 4.5 4.0 3.5 3.0 2.5 2.0 1.5 1.0 0.5 0.0
f1 (ppm)

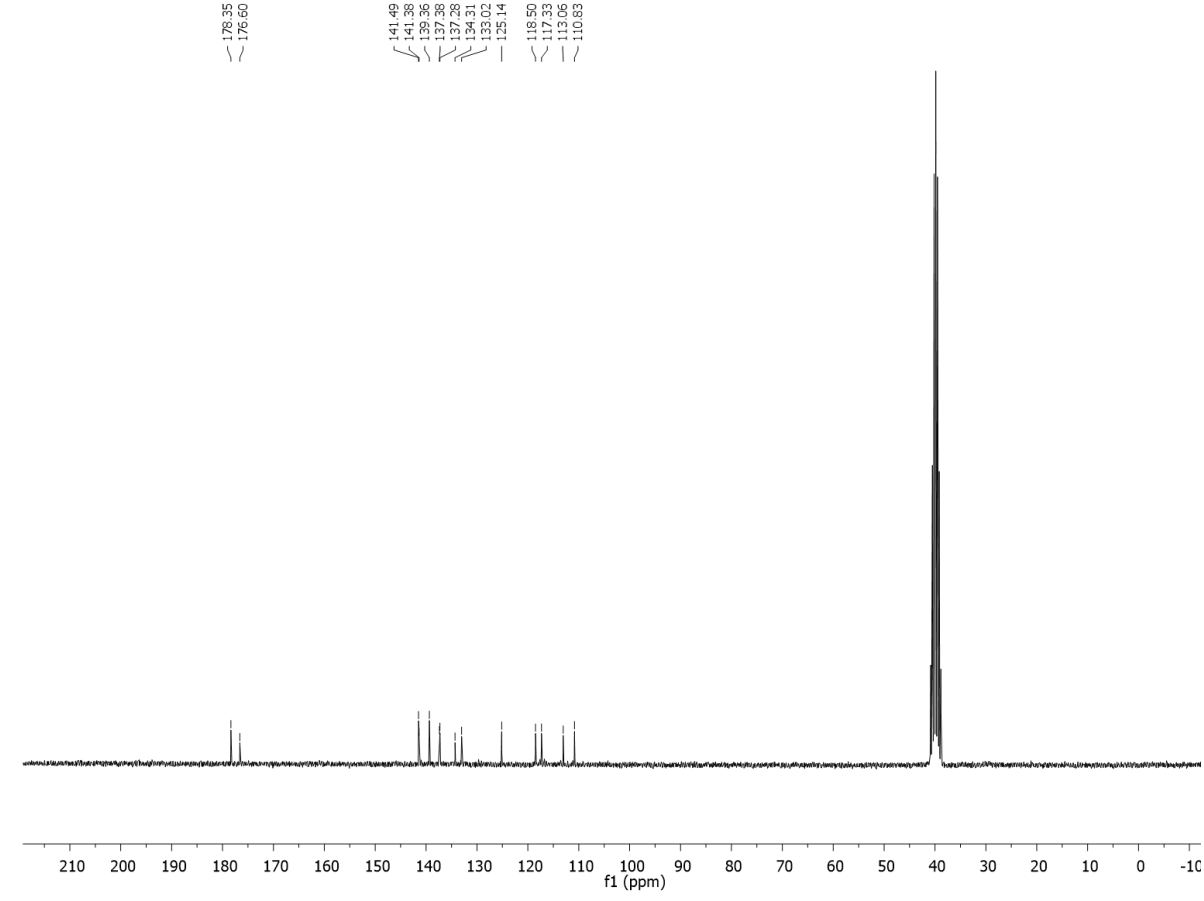
178.35
176.60
141.49
141.38
139.36
137.38
137.28
134.31
133.02
125.14
118.50
117.33
113.06
110.83
210 200 190 180 170 160 150 140 130 120 110 100 90 80 70 60 50 40 30 20 10 0 -10
f1 (ppm)

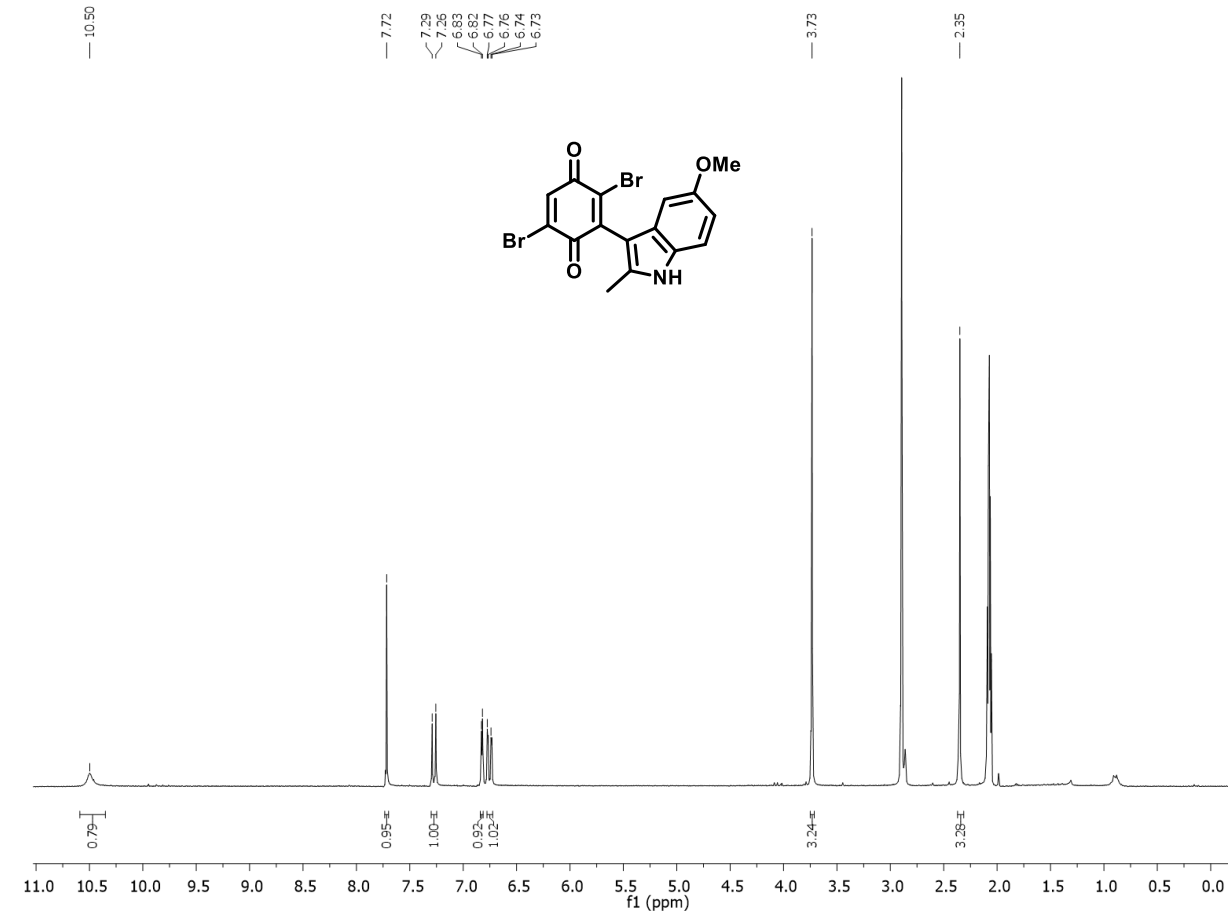
10.50
7.72
7.29
7.26
6.83
6.82
6.77
6.76
6.74
6.73
3.73
2.35
O
Br
OMe
Br
O
NH
0.79
0.95
1.00
0.92
1.02
3.24
3.28
f1 (ppm)

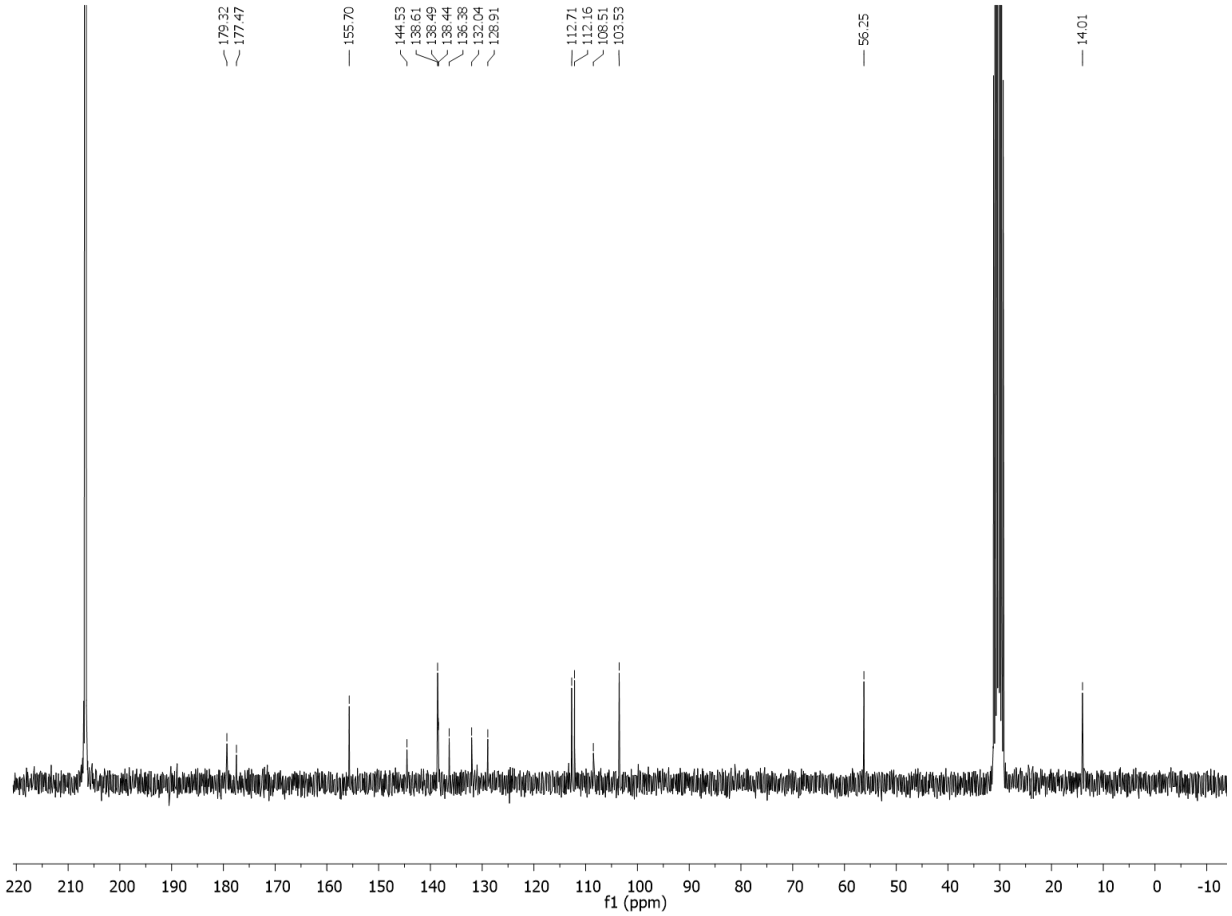
179.32
177.47
155.70
144.53
138.61
138.49
138.44
136.38
132.04
128.91
112.71
112.16
108.51
103.53
56.25
14.01
f1 (ppm)

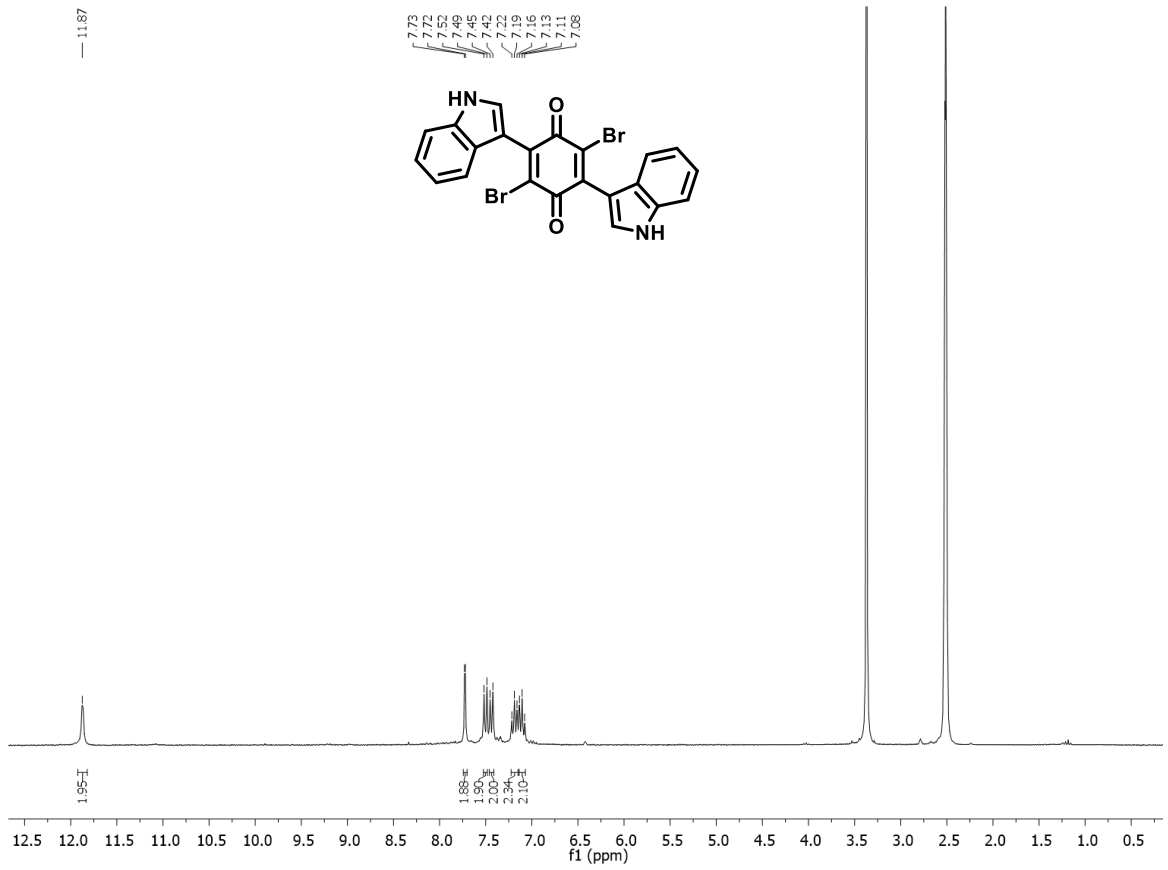
11.87
7.73
7.72
7.52
7.49
7.45
7.42
7.22
7.19
7.16
7.13
7.11
7.08
HN
O
Br
Br
O
NH
1.95
1.88
1.90
2.00
2.34
2.10
12.5 12.0 11.5 11.0 10.5 10.0 9.5 9.0 8.5 8.0 7.5 7.0 6.5 6.0 5.5 5.0 4.5 4.0 3.5 3.0 2.5 2.0 1.5 1.0 0.5
f1 (ppm)

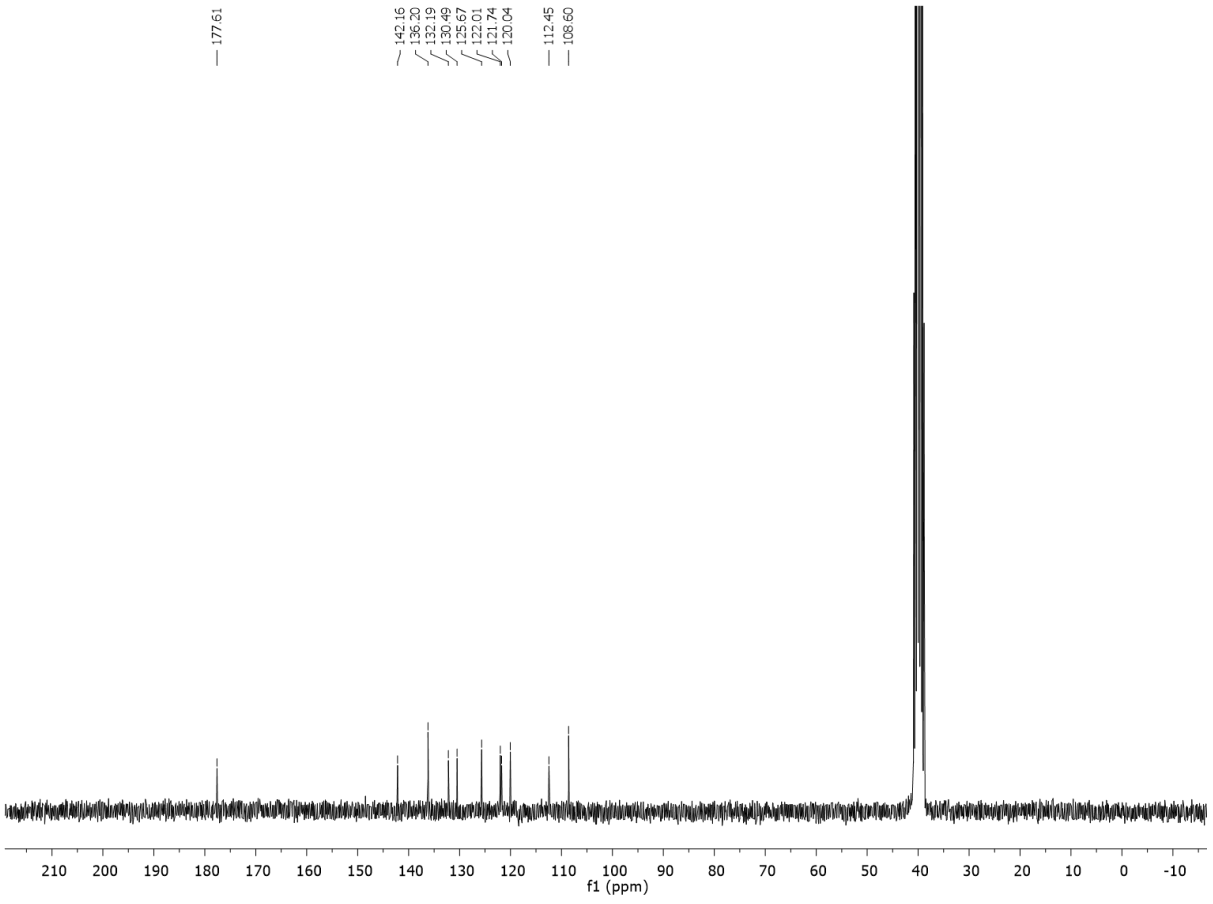
177.61
142.16
136.20
132.19
130.49
125.67
122.01
121.74
120.04
112.45
108.60
210 200 190 180 170 160 150 140 130 120 110 100 90 80 70 60 50 40 30 20 10 0 -10
f1 (ppm)

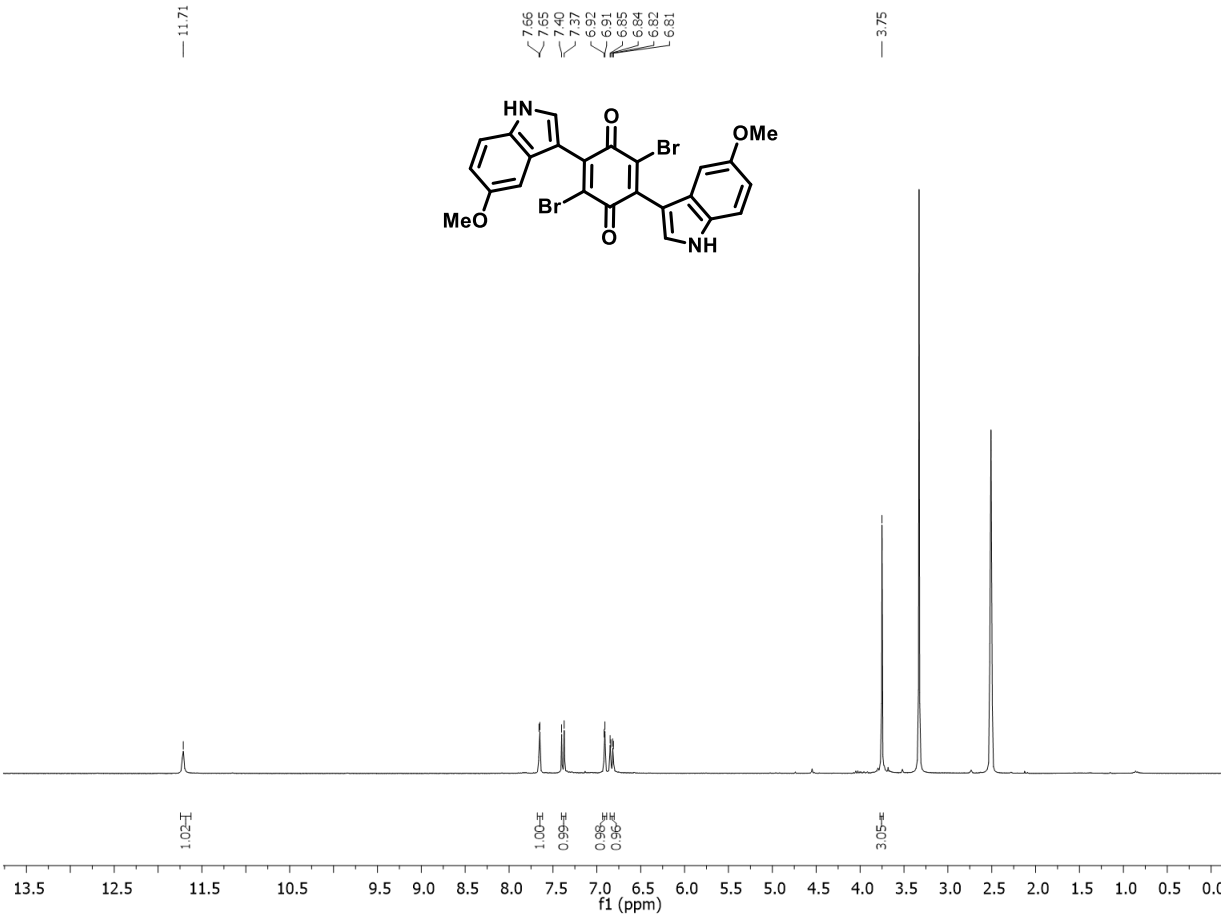
11.71
7.66
7.65
7.40
7.37
6.92
6.91
6.85
6.84
6.82
6.81
3.75
HN
O
Br
OMe
Br
MeO
O
NH
1.02
1.00
0.99
0.98
0.96
3.05
f1 (ppm)

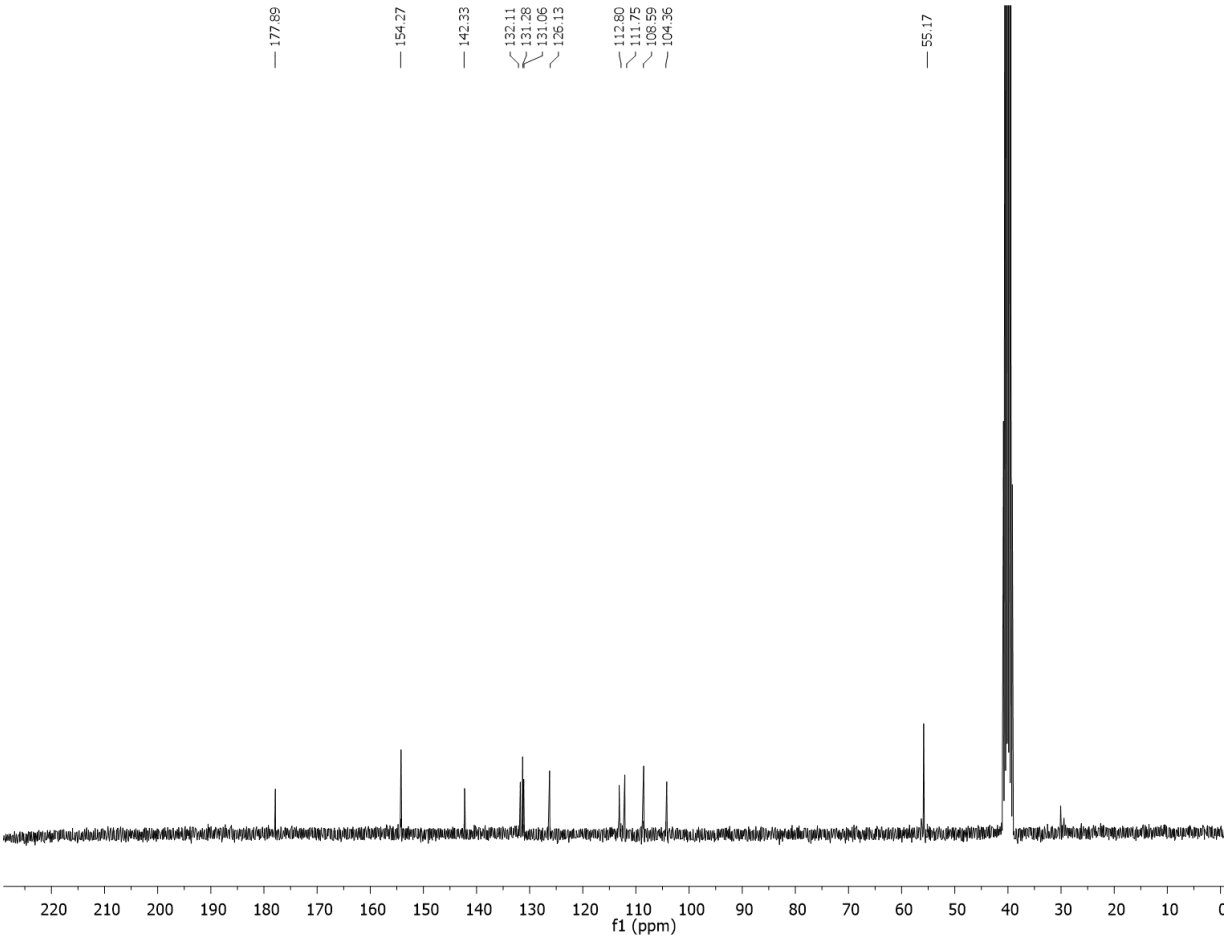
177.89
154.27
142.33
132.11
131.28
131.06
126.13
112.80
111.75
108.59
104.36
55.17
f1 (ppm)


11.2148
11.0619
7.8082
7.7969
7.7740
7.7626
7.7071
7.6996
7.5580
7.5551
7.5524
7.5338
7.5323
7.5271
7.5227
7.5186
7.4994
7.4745
7.4722
7.3364
7.3288
7.3018
7.2943
7.2290
7.2061
7.2011
7.1751
7.1687
7.1602
7.1545
7.1286
7.1240
7.1005
2.9174
2.0678
2.0591
2.0503
2.0415
2.0328

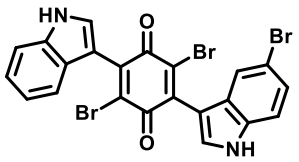
HN
O
Br
Br
Br
O
NH

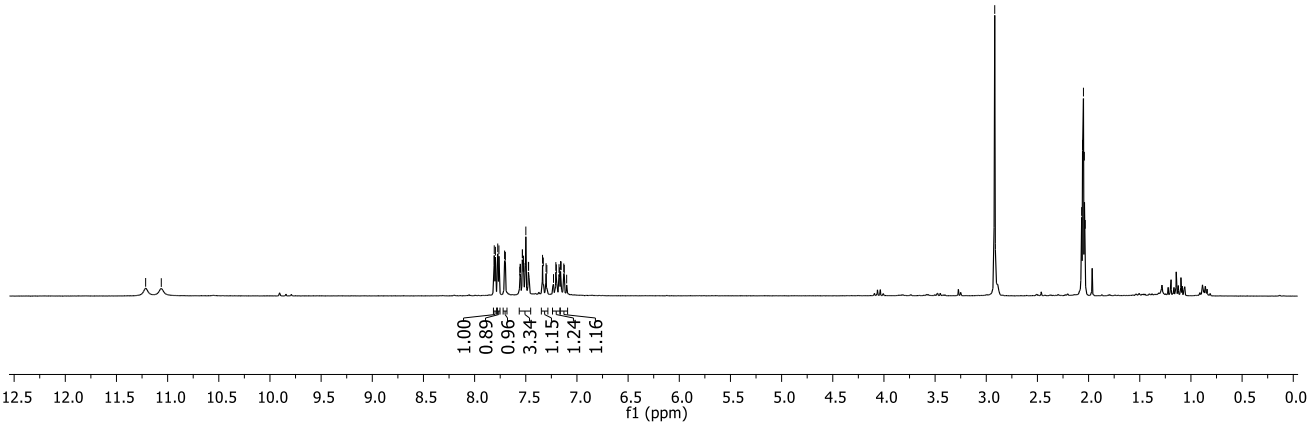
1.00
0.89
0.96
3.34
1.15
1.24
1.16
12.5 12.0 11.5 11.0 10.5 10.0 9.5 9.0 8.5 8.0 7.5 7.0 6.5 6.0 5.5 5.0 4.5 4.0 3.5 3.0 2.5 2.0 1.5 1.0 0.5 0.0
f1 (ppm)

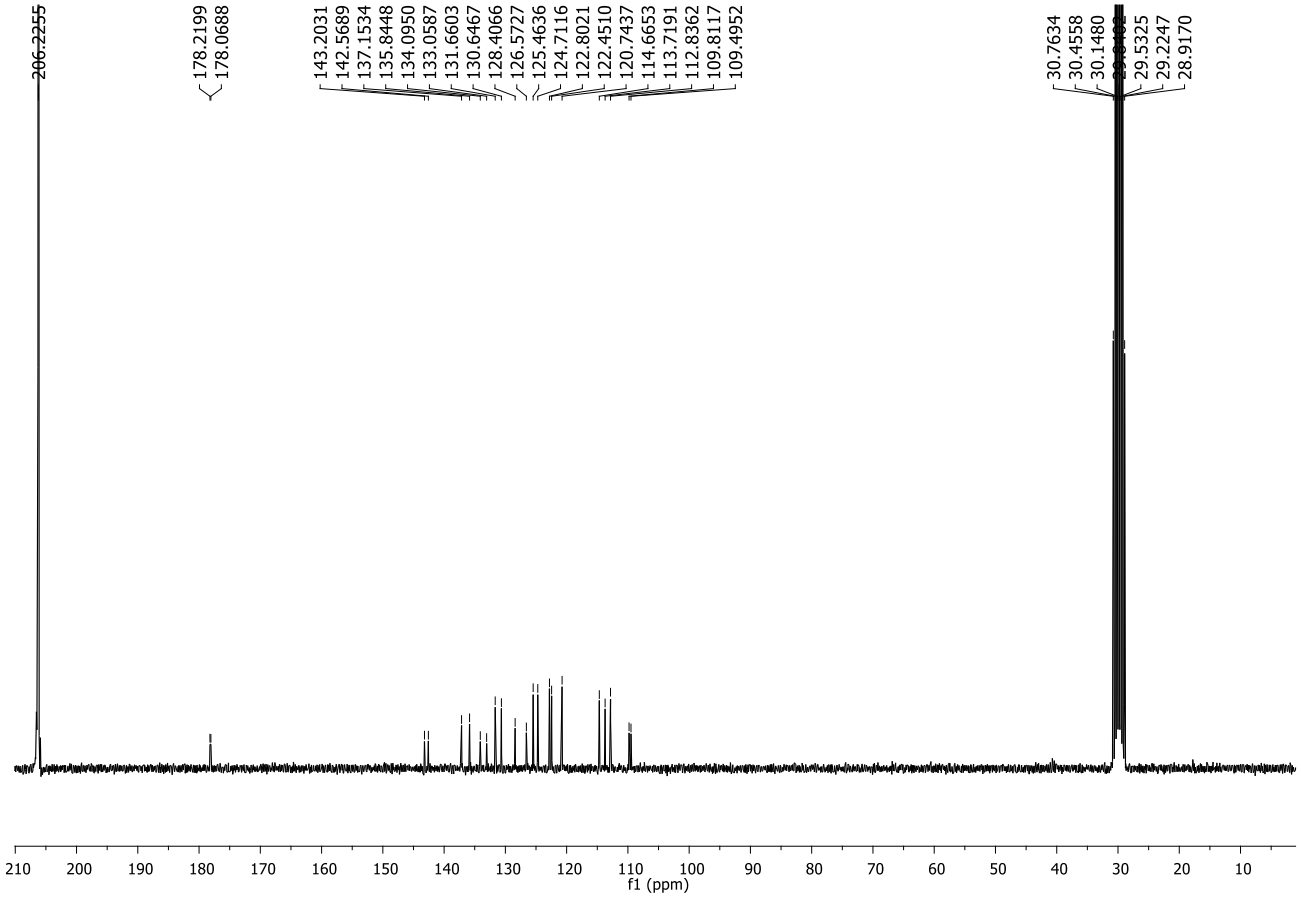
206.2255
178.2199
178.0688
143.2031
142.5689
137.1534
135.8448
134.0950
133.0587
131.6603
130.6467
128.4066
126.5727
125.4636
124.7116
122.8021
122.4510
120.7437
114.6653
113.7191
112.8362
109.8117
109.4952
30.7634
30.4558
30.1480
29.5325
29.2247
28.9170
210 200 190 180 170 160 150 140 130 120 110 100 90 80 70 60 50 40 30 20 10
f1 (ppm)

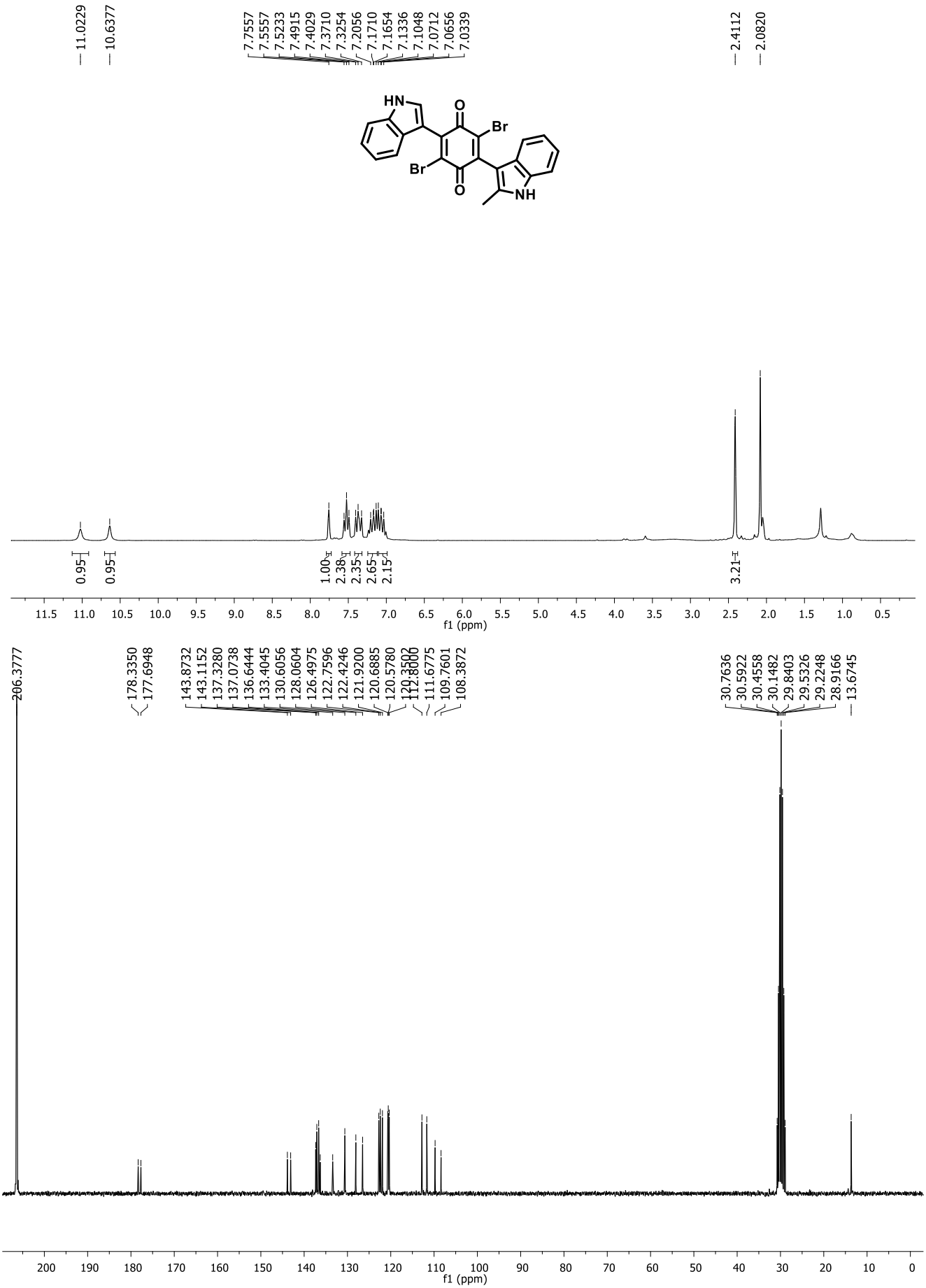
11.0229
10.6377
7.7557
7.5557
7.5233
7.4915
7.4029
7.3710
7.3254
7.2056
7.1710
7.1654
7.1336
7.1048
7.0712
7.0656
7.0339
2.4112
2.0820
HN
O
Br
Br
O
NH
0.95
0.95
1.00
2.38
2.35
2.65
2.15
3.21
f1 (ppm)
206.3777
178.3350
177.6948
143.8732
143.1152
137.3280
137.0738
136.6444
133.4045
130.6056
128.0604
126.4975
122.7596
122.4246
121.9200
120.6885
120.5780
120.3502
112.3800
111.6775
109.7601
108.3872
30.7636
30.5922
30.4558
30.1482
29.8403
29.5326
29.2248
28.9166
13.6745
f1 (ppm)

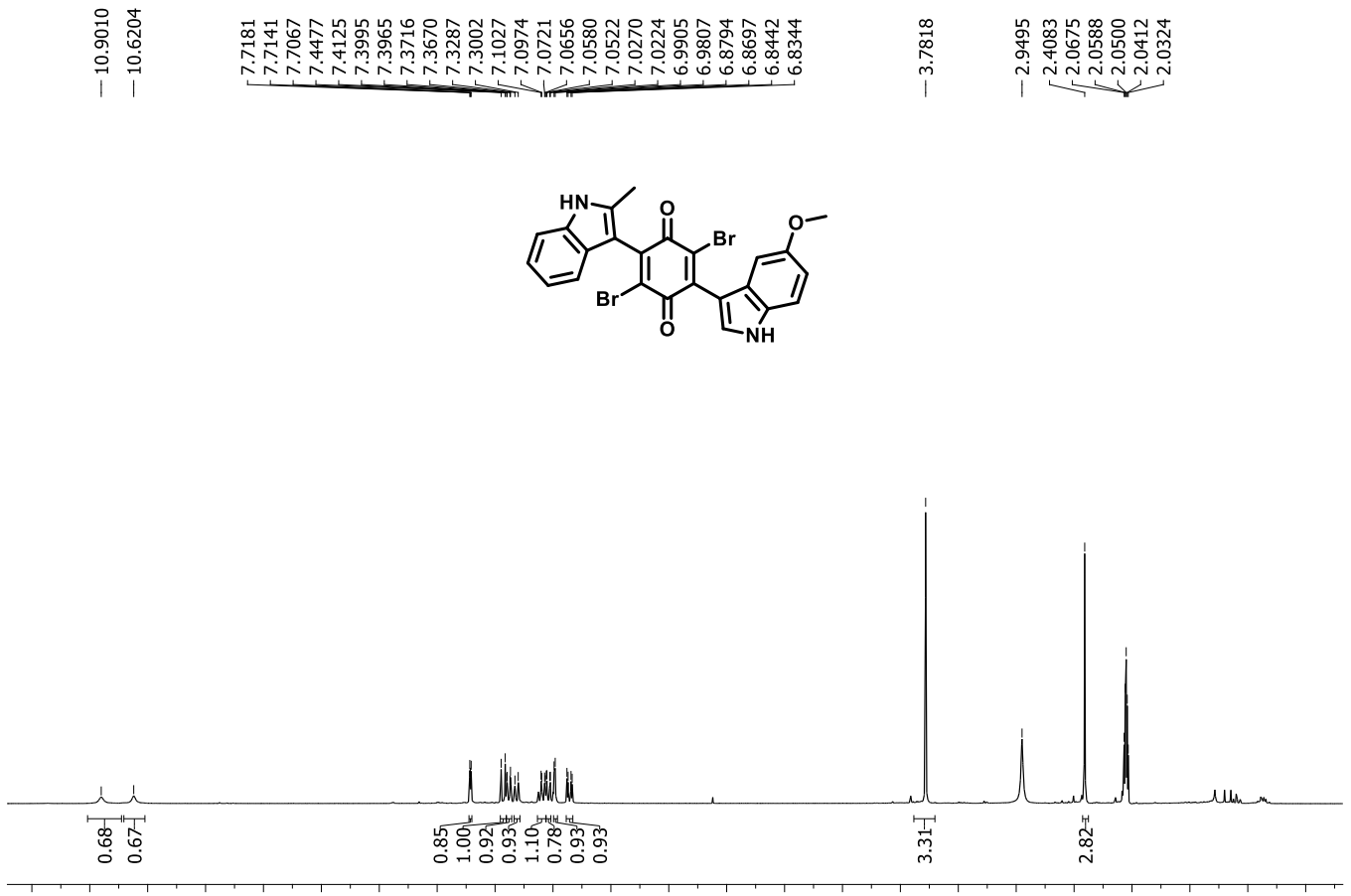
10.9010
10.6204
7.7181
7.7141
7.7067
7.4477
7.4125
7.3995
7.3965
7.3716
7.3670
7.3287
7.3002
7.1027
7.0974
7.0721
7.0656
7.0580
7.0522
7.0270
7.0224
6.9905
6.9807
6.8794
6.8697
6.8442
6.8344
3.7818
2.9495
2.4083
2.0675
2.0588
2.0500
2.0412
2.0324
HN
O
Br
O
Br
O
NH
0.68
0.67
0.85
1.00
0.92
0.93
1.10
0.78
0.93
0.93
3.31
2.82
f1 (ppm)

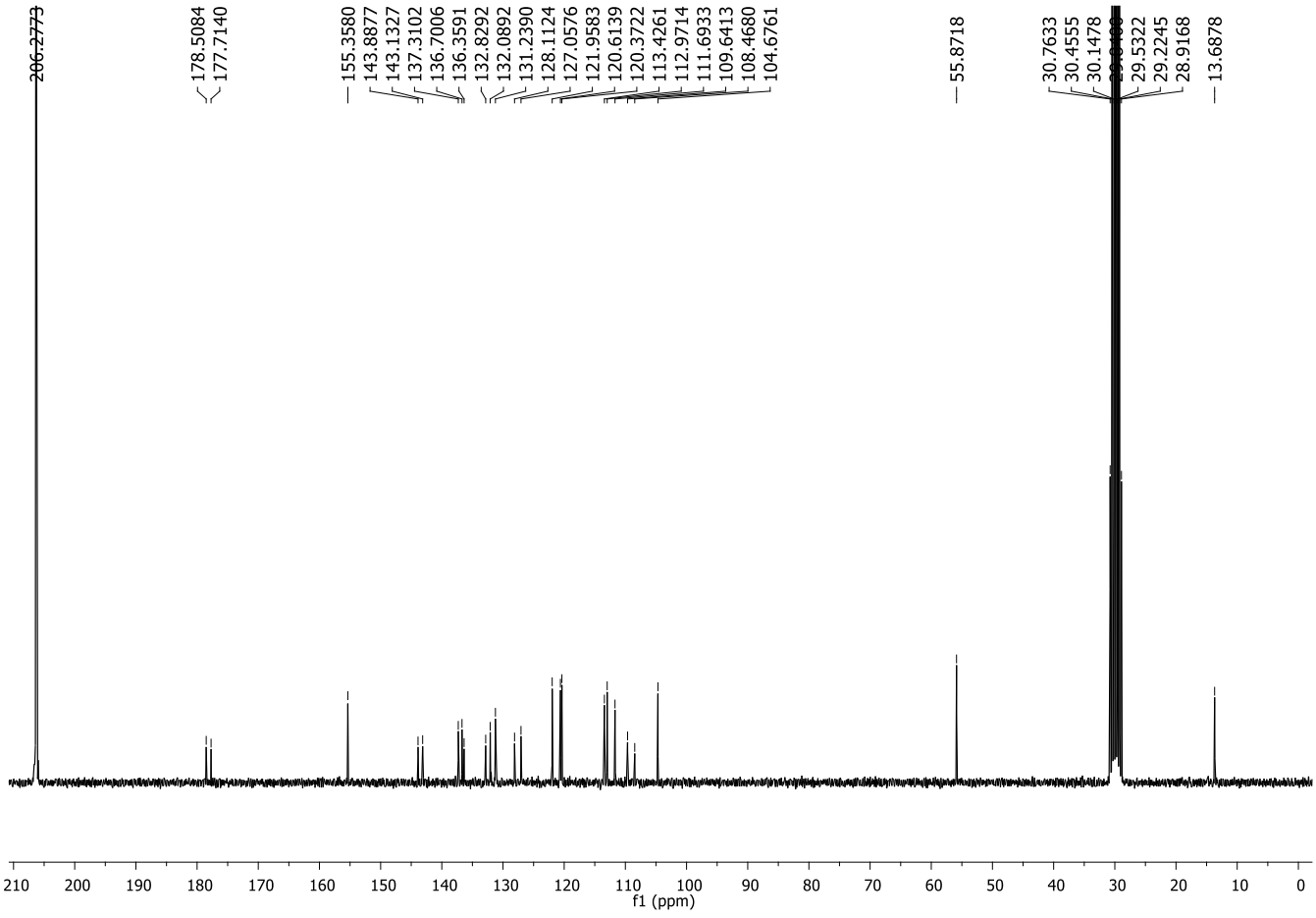
206.2773
178.5084
177.7140
155.3580
143.8877
143.1327
137.3102
136.7006
136.3591
132.8292
132.0892
131.2390
128.1124
127.0576
121.9583
120.6139
120.3722
113.4261
112.9714
111.6933
109.6413
108.4680
104.6761
55.8718
30.7633
30.4555
30.1478
29.5322
29.2245
28.9168
13.6878
f1 (ppm)

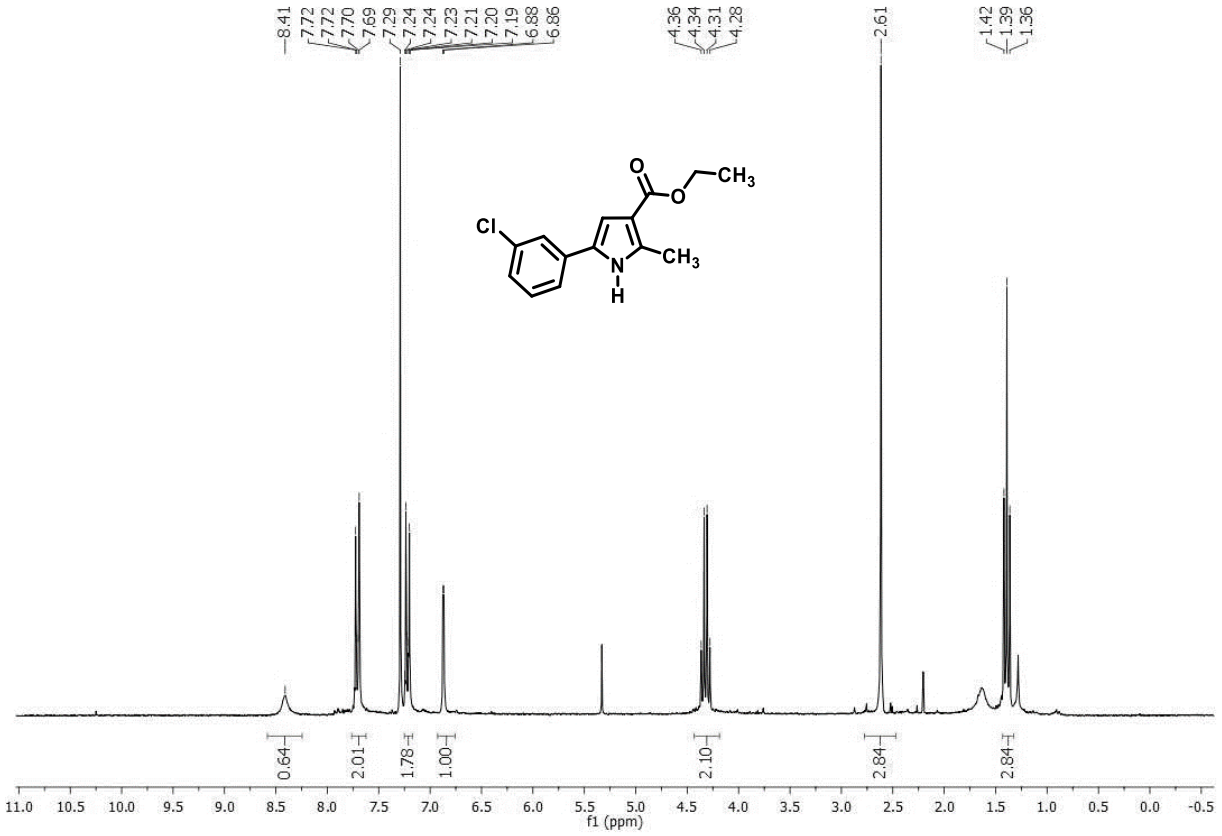
8.41
7.72
7.72
7.70
7.69
7.29
7.24
7.24
7.23
7.21
7.20
7.19
6.88
6.86
4.36
4.34
4.31
4.28
2.61
1.42
1.39
1.36
Cl
O
O
CH3
CH3
N
H
0.64
2.01
1.78
1.00
2.10
2.84
2.84
f1 (ppm)

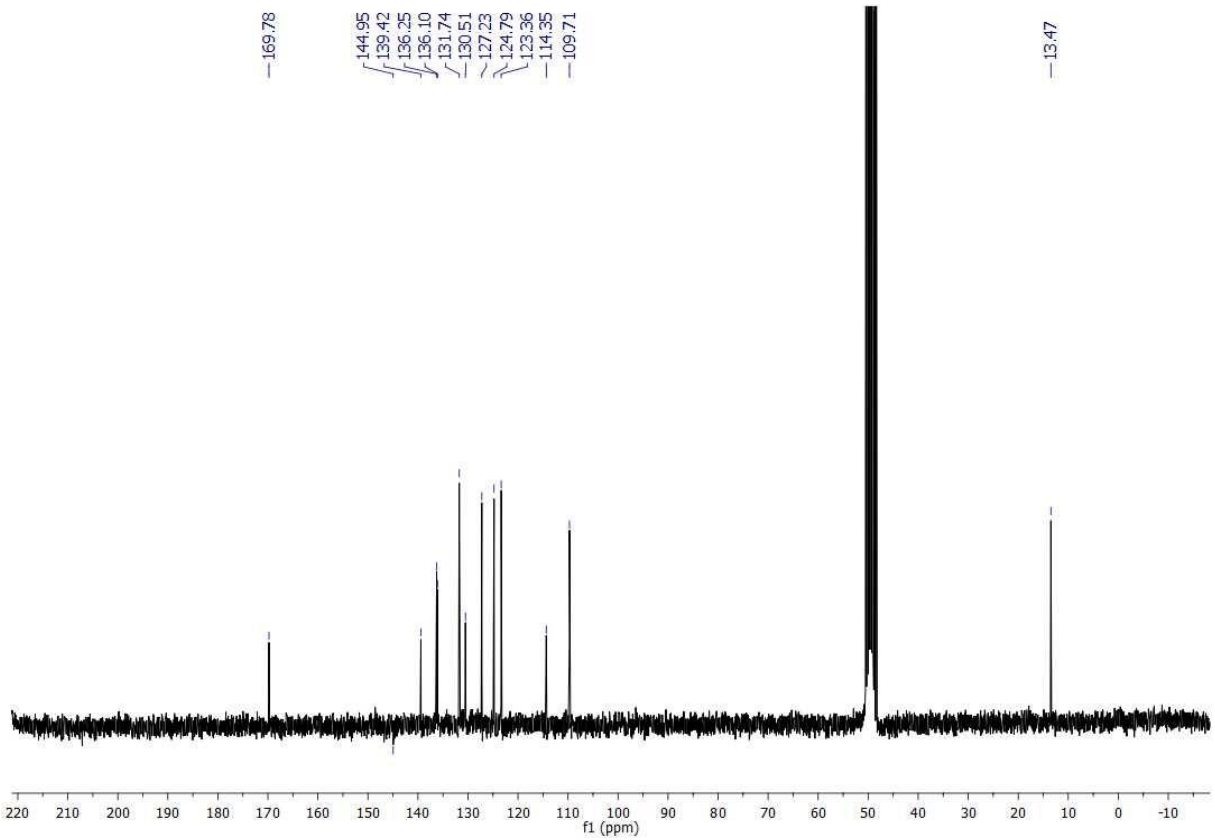
169.78
144.95
139.42
136.25
136.10
131.74
130.51
127.23
124.79
123.36
114.35
109.71
13.47
f1 (ppm)

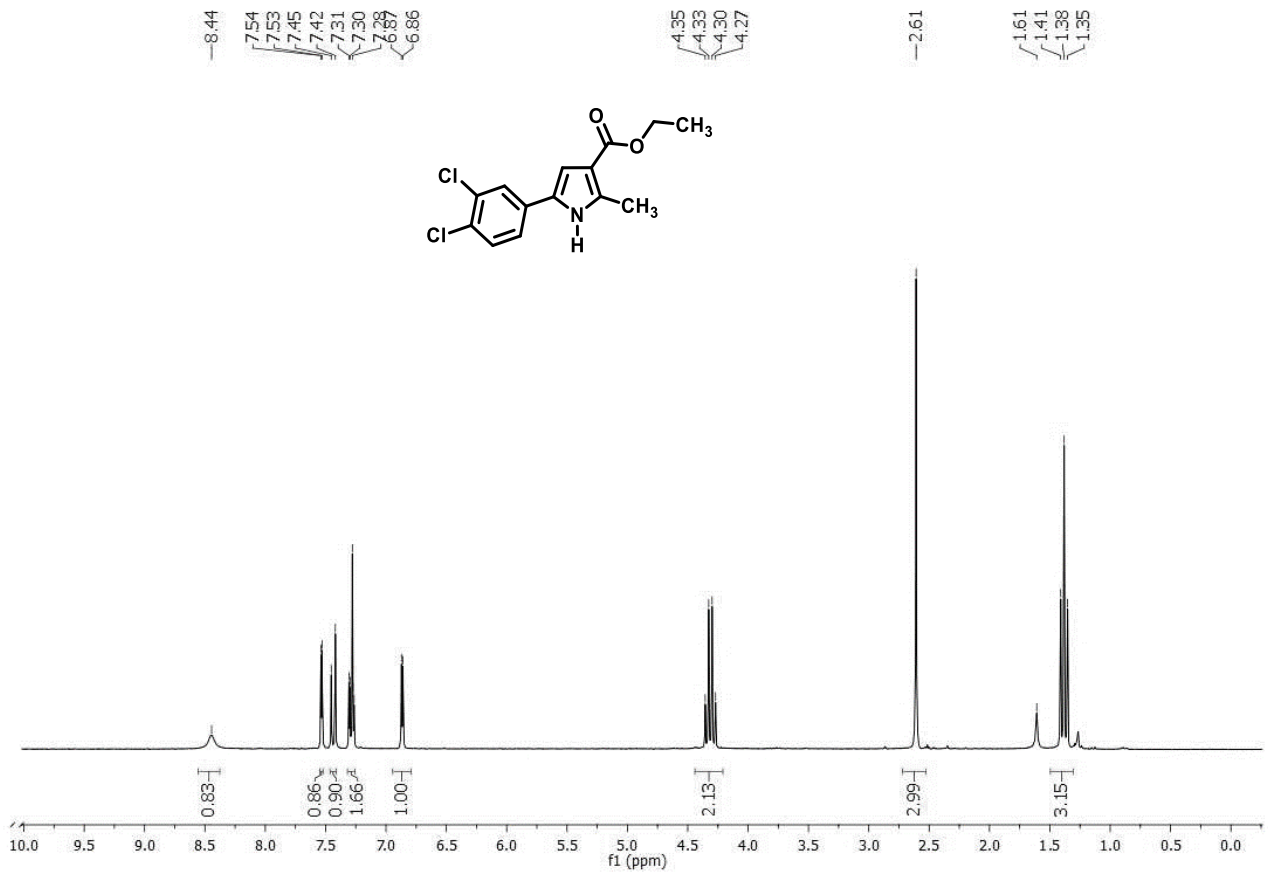
8.44
7.54
7.53
7.45
7.42
7.31
7.30
7.28
6.87
6.86
4.35
4.33
4.30
4.27
2.61
1.61
1.41
1.38
1.35
Cl
Cl
N
H
O
O
CH3
CH3
0.83
0.86
0.90
1.66
1.00
2.13
2.99
3.15
f1 (ppm)

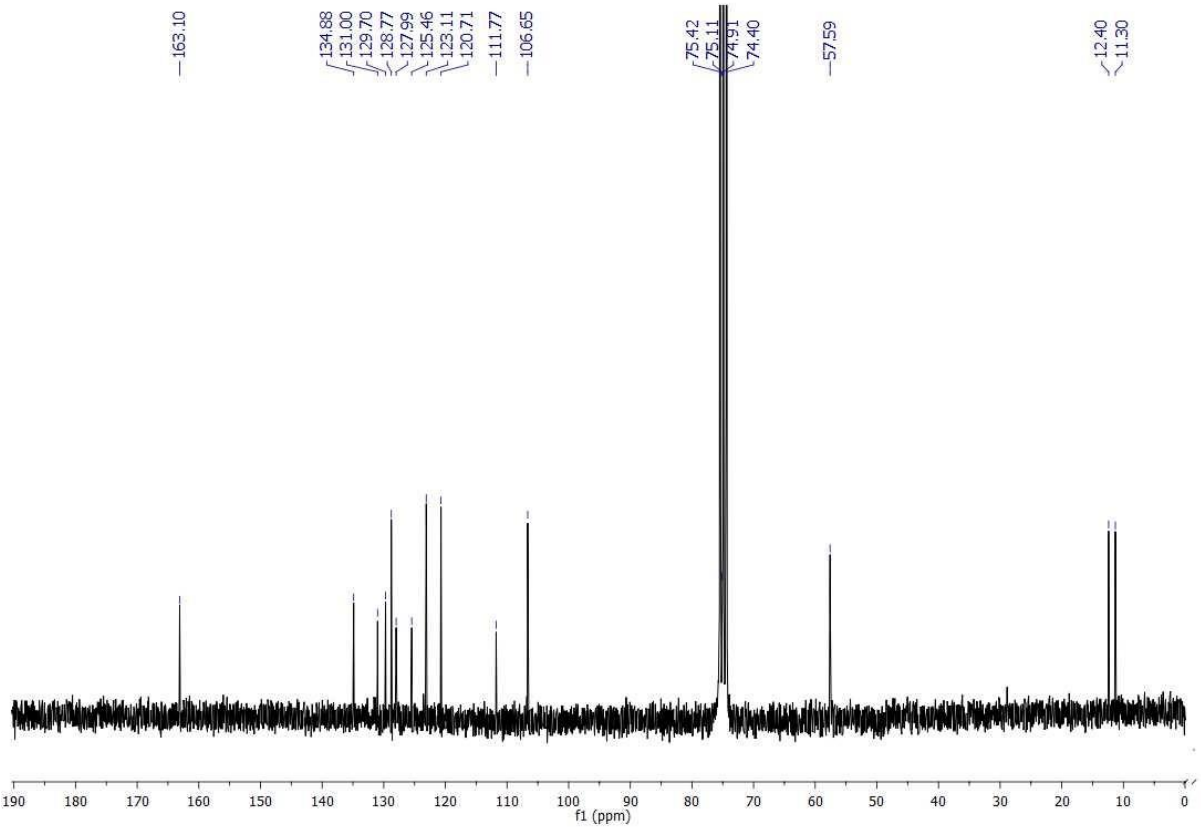
163.10
134.88
131.00
129.70
128.77
127.99
125.46
123.11
120.71
111.77
106.65
75.42
75.11
74.91
74.40
57.59
12.40
11.30
f1 (ppm)

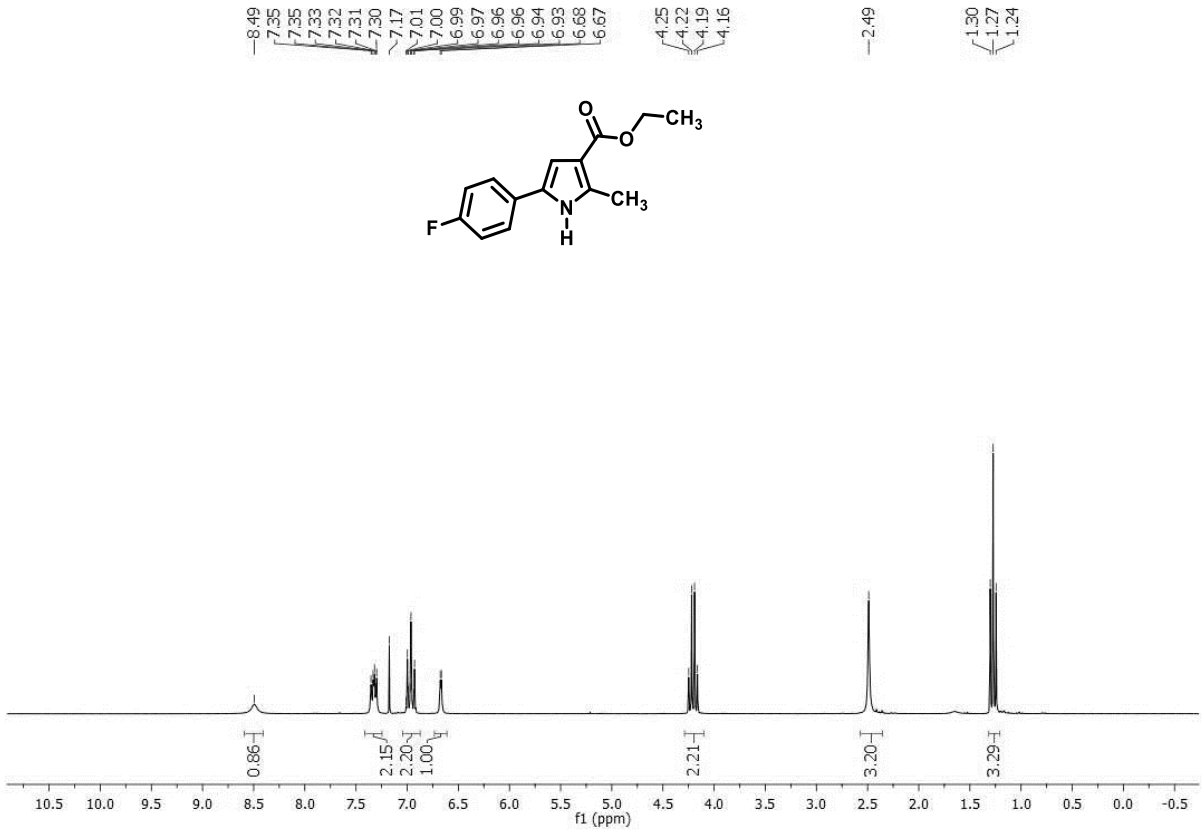
8.49
7.35
7.35
7.33
7.32
7.31
7.30
7.17
7.01
7.00
6.99
6.97
6.96
6.96
6.94
6.93
6.68
6.67
4.25
4.22
4.19
4.16
2.49
1.30
1.27
1.24
O
O
CH3
CH3
N
H
F
0.86
2.15
2.20
1.00
2.21
3.20
3.29
f1 (ppm)

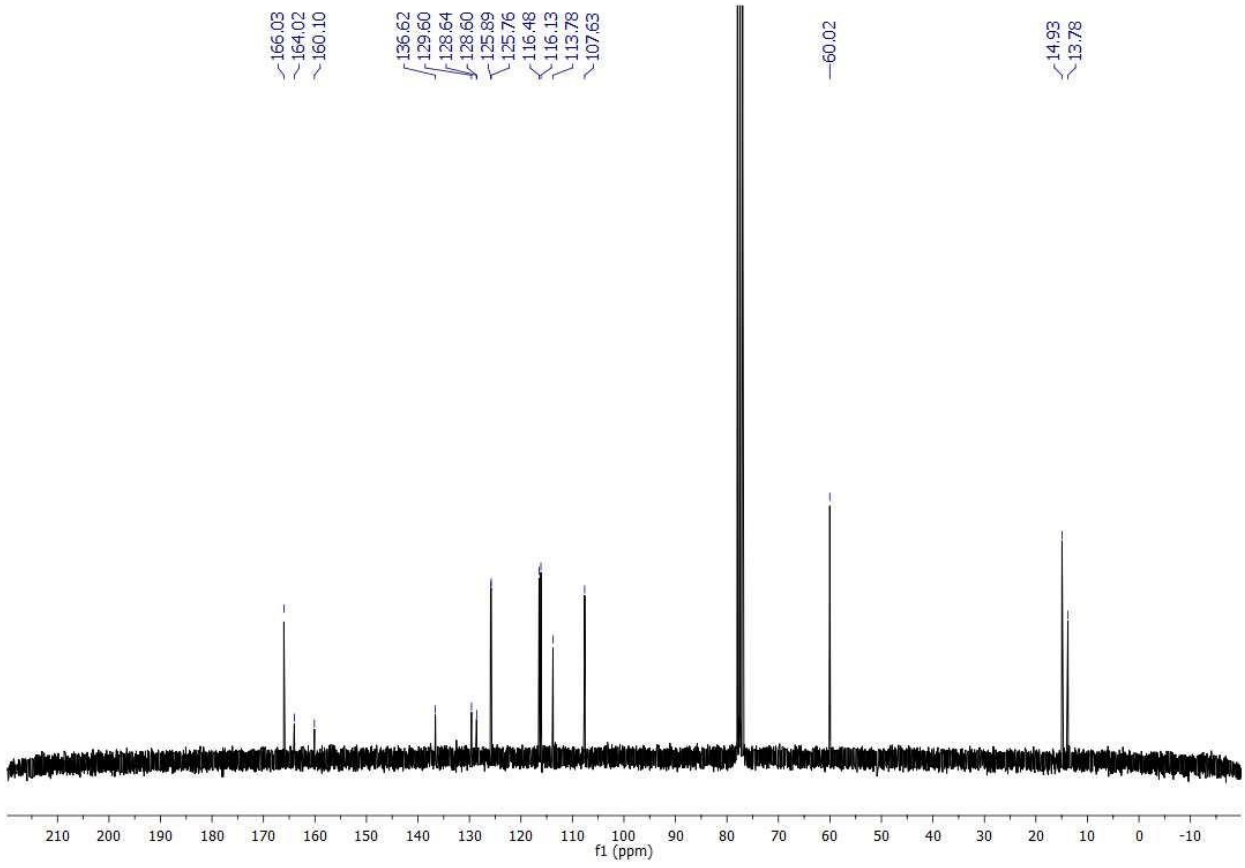
166.03
164.02
160.10
136.62
129.60
128.64
128.60
125.89
125.76
116.48
116.13
113.78
107.63
60.02
14.93
13.78
f1 (ppm)

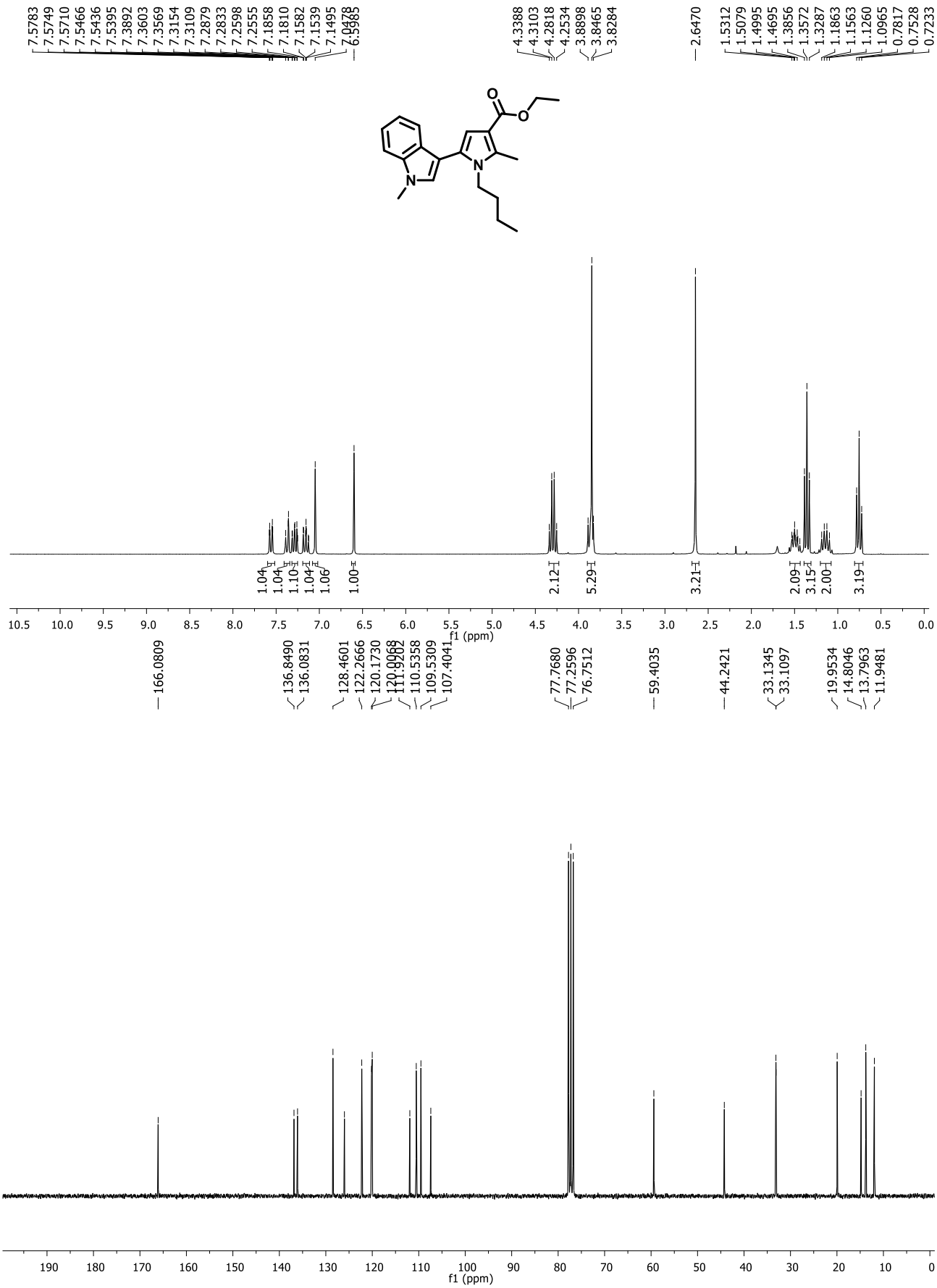
7.5783
7.5749
7.5710
7.5466
7.5436
7.5395
7.3892
7.3603
7.3569
7.3154
7.3109
7.2879
7.2833
7.2598
7.2555
7.1858
7.1810
7.1582
7.1539
7.1495
7.0478
6.5985
4.3388
4.3103
4.2818
4.2534
3.8898
3.8465
3.8284
2.6470
1.5312
1.5079
1.4995
1.4695
1.3856
1.3572
1.3287
1.1863
1.1563
1.1260
1.0965
0.7817
0.7528
0.7233
O
O
N
N
1.04
1.04
1.10
1.04
1.06
1.00
2.12
5.29
3.21
2.09
3.15
2.00
3.19
10.5 10.0 9.5 9.0 8.5 8.0 7.5 7.0 6.5 6.0 5.5 5.0 4.5 4.0 3.5 3.0 2.5 2.0 1.5 1.0 0.5 0.0
f1 (ppm)
166.0809
136.8490
136.0831
128.4601
122.2666
120.1730
120.0068
111.9202
110.5358
109.5309
107.4041
77.7680
77.2596
76.7512
59.4035
44.2421
33.1345
33.1097
19.9534
14.8046
13.7963
11.9481
190 180 170 160 150 140 130 120 110 100 90 80 70 60 50 40 30 20 10 0
f1 (ppm)

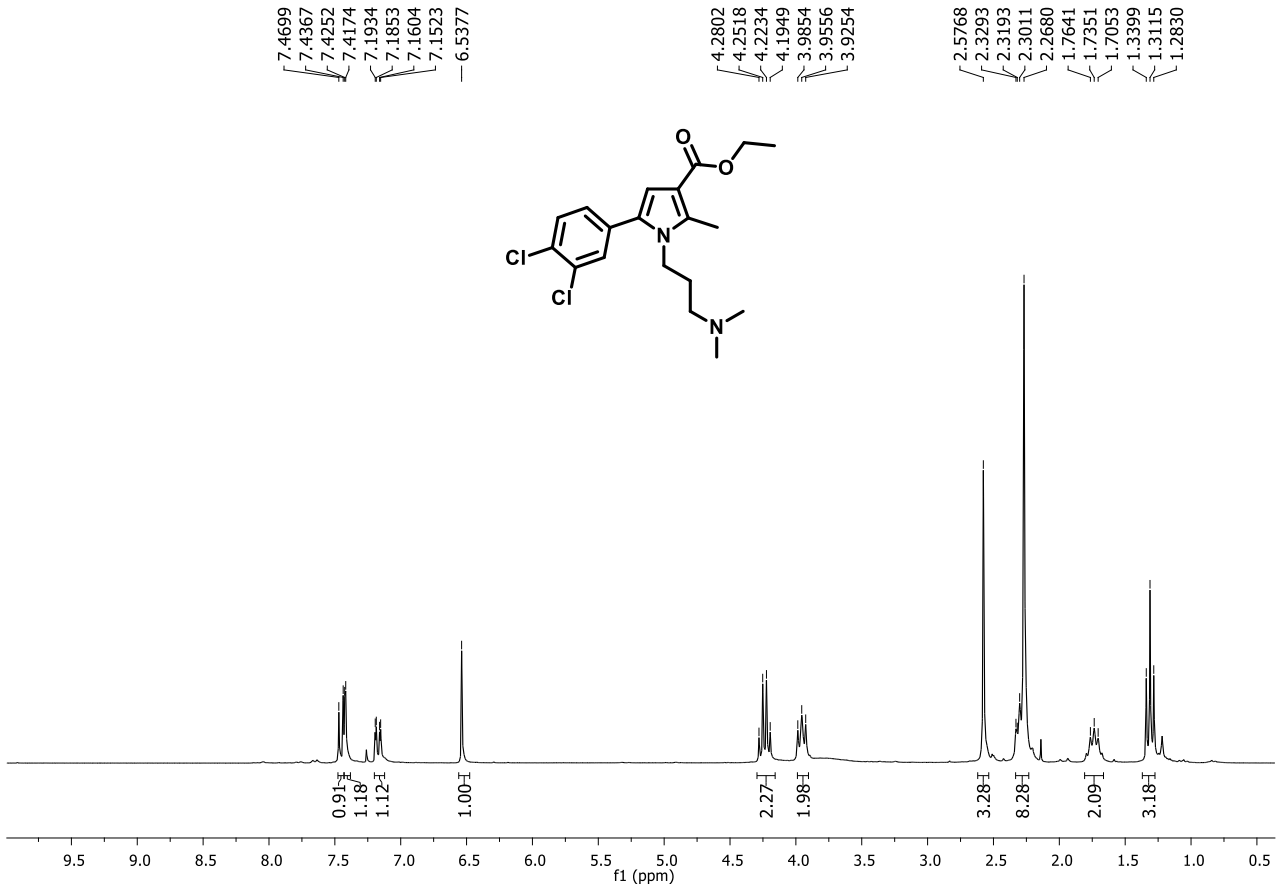
7.4699
7.4367
7.4252
7.4174
7.1934
7.1853
7.1604
7.1523
6.5377
4.2802
4.2518
4.2234
4.1949
3.9854
3.9556
3.9254
2.5768
2.3293
2.3193
2.3011
2.2680
1.7641
1.7351
1.7053
1.3399
1.3115
1.2830
O
O
N
Cl
Cl
N
0.91
1.18
1.12
1.00
2.27
1.98
3.28
8.28
2.09
3.18
f1 (ppm)

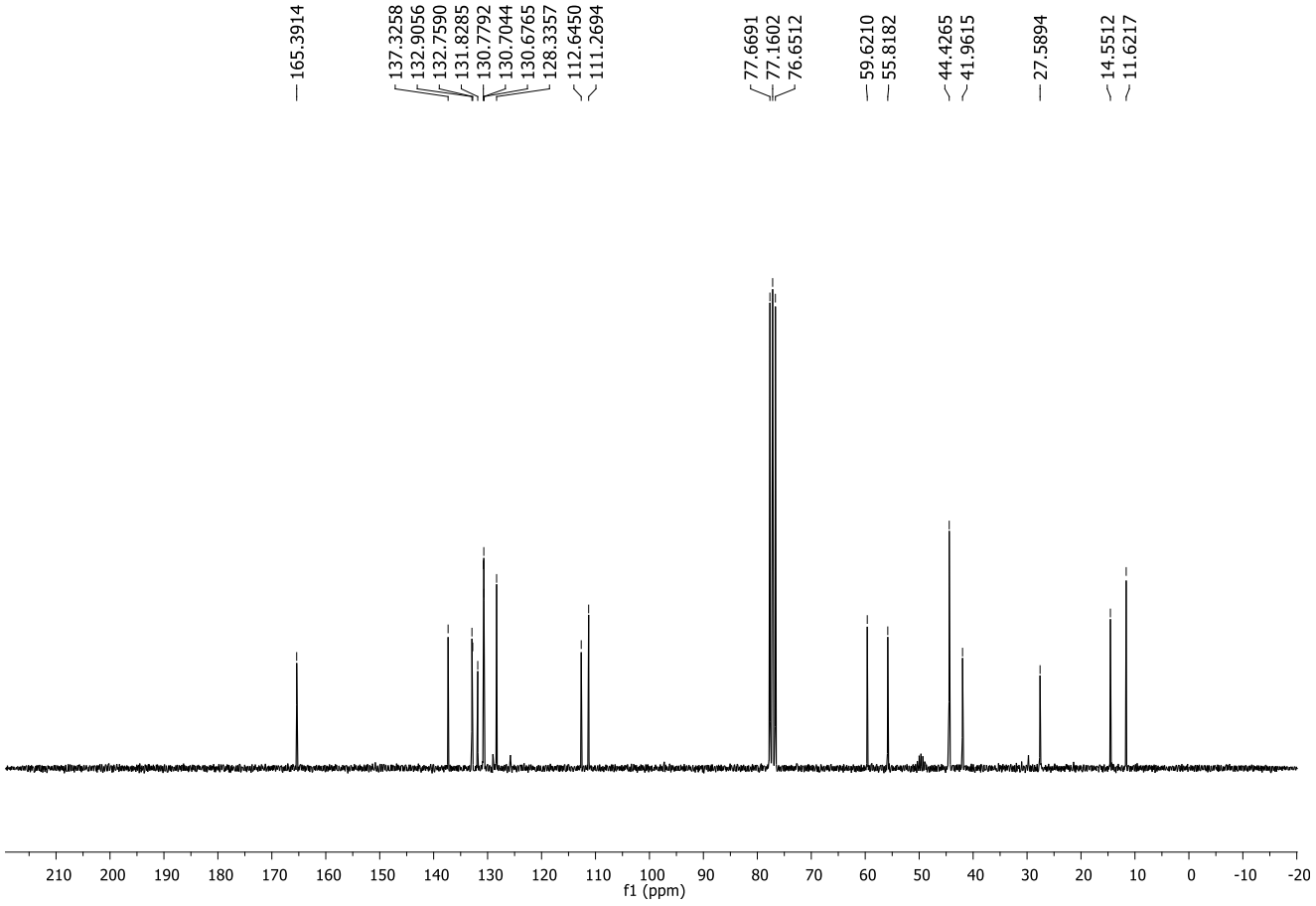
165.3914
137.3258
132.9056
132.7590
131.8285
130.7792
130.7044
130.6765
128.3357
112.6450
111.2694
77.6691
77.1602
76.6512
59.6210
55.8182
44.4265
41.9615
27.5894
14.5512
11.6217
f1 (ppm)

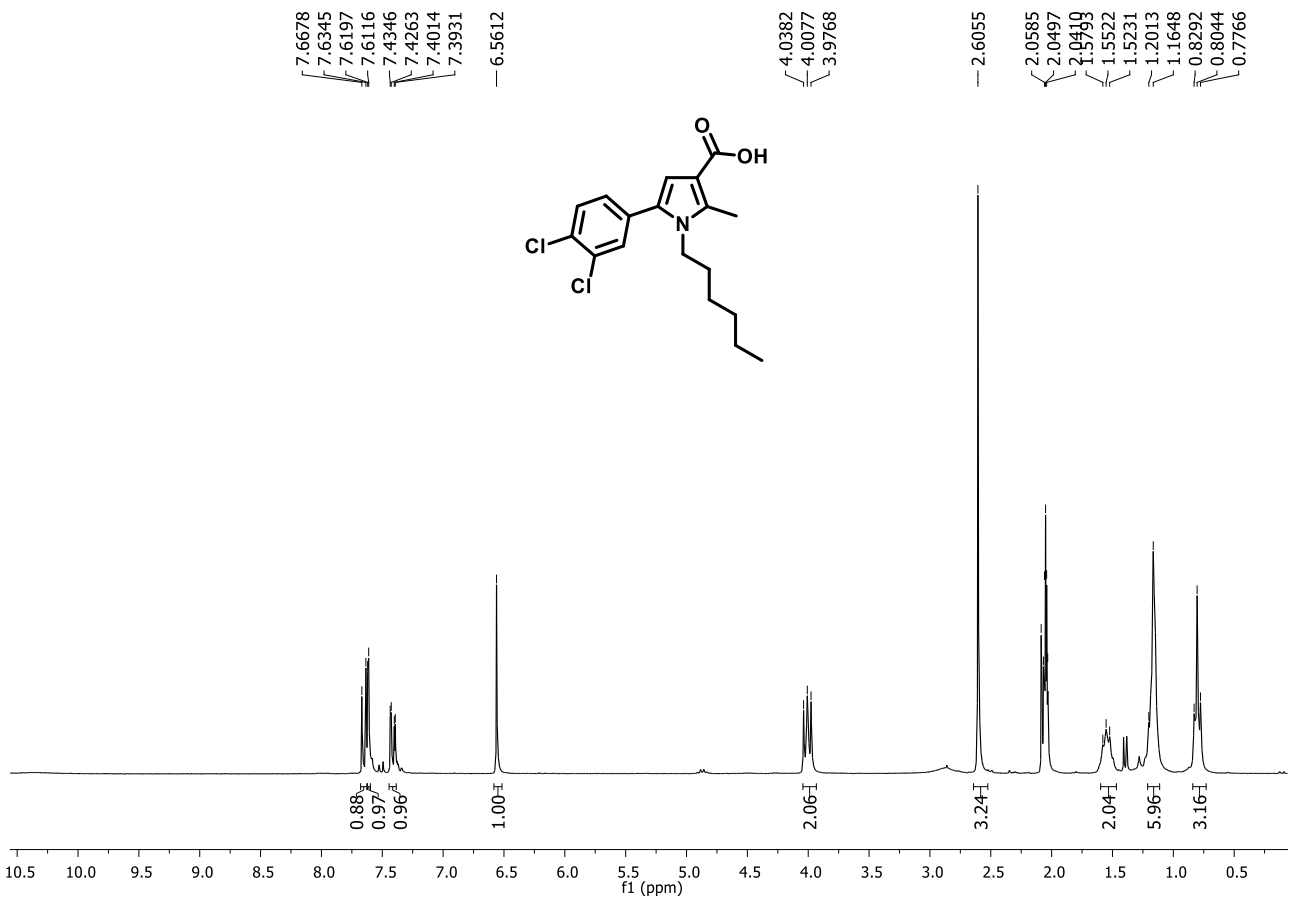
7.6678
7.6345
7.6197
7.6116
7.4346
7.4263
7.4014
7.3931
6.5612
4.0382
4.0077
3.9768
2.6055
2.0585
2.0497
1.5793
1.5522
1.5231
1.2013
1.1648
0.8292
0.8044
0.7766
O
OH
N
Cl
Cl
0.88
0.97
0.96
1.00
2.06
3.24
2.04
5.96
3.16
f1 (ppm)

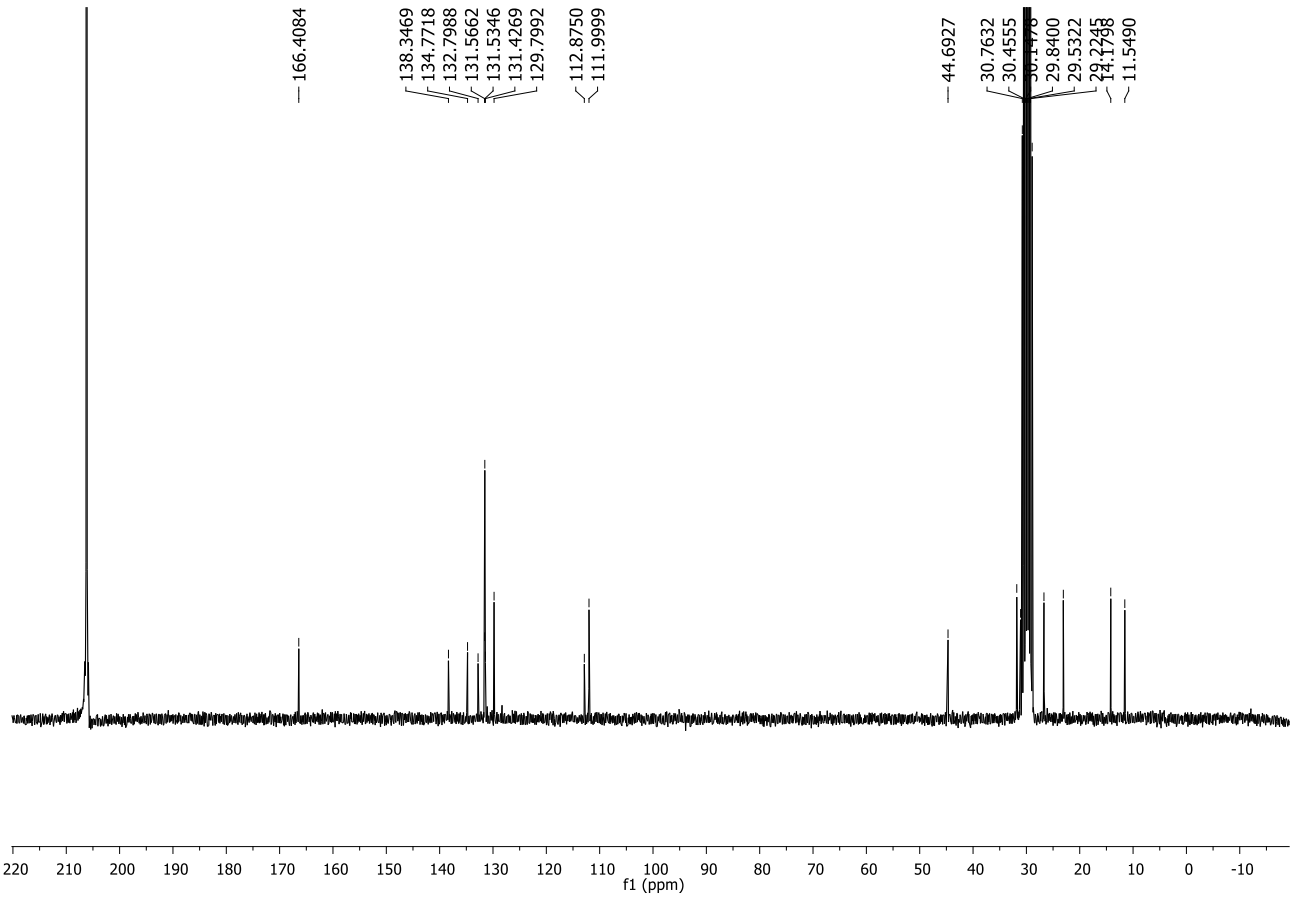
166.4084
138.3469
134.7718
132.7988
131.5662
131.5346
131.4269
129.7992
112.8750
111.9999
44.6927
30.7632
30.4555
29.8400
29.5322
11.5490
f1 (ppm)

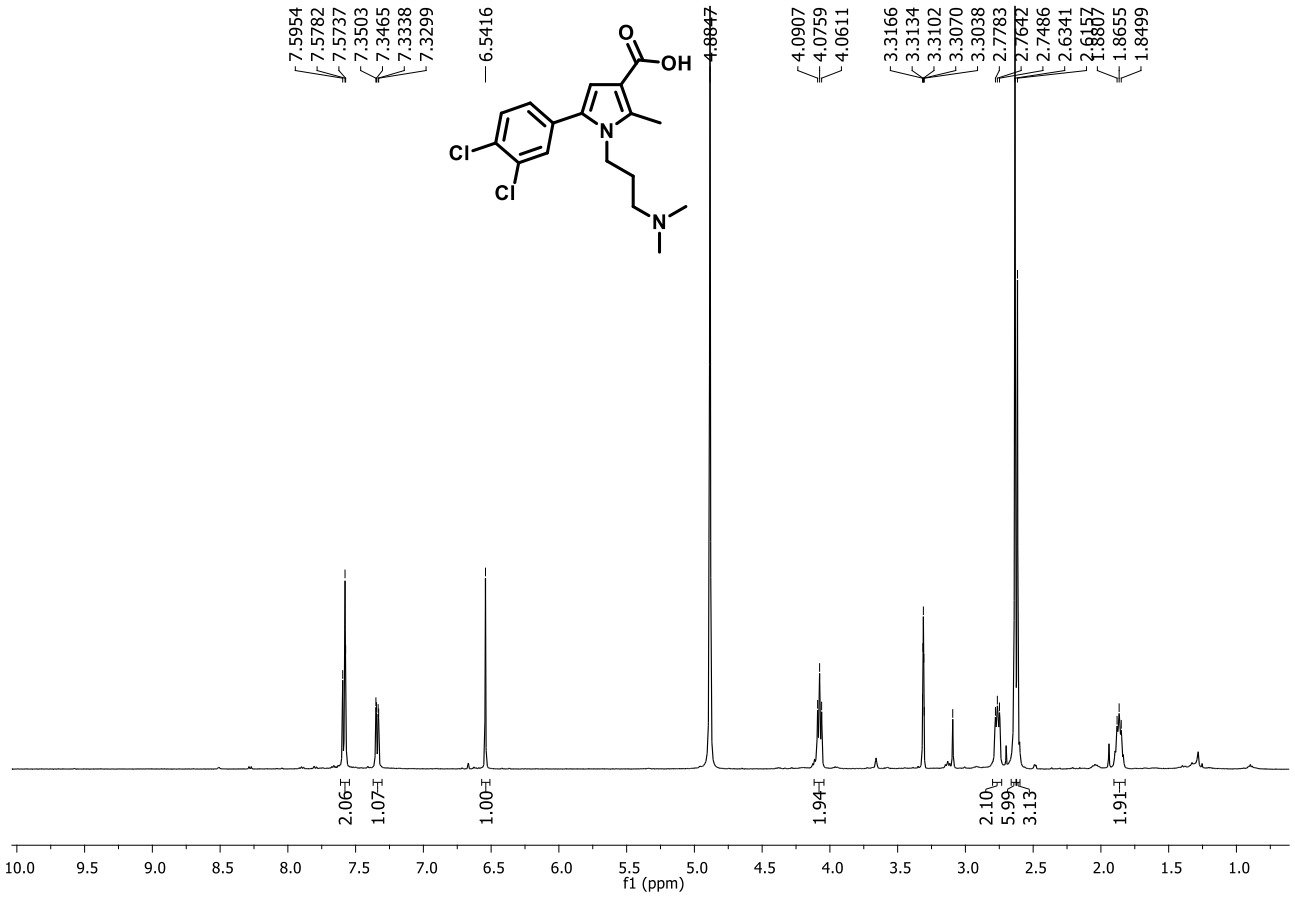
7.5954
7.5782
7.5737
7.3503
7.3465
7.3338
7.3299
6.5416
4.8847
4.0907
4.0759
4.0611
3.3166
3.3134
3.3102
3.3070
3.3038
2.7783
2.7642
2.7486
2.6341
2.6157
1.8807
1.8655
1.8499
O
OH
N
Cl
Cl
N
2.06
1.07
1.00
1.94
2.10
5.99
3.13
1.91
f1 (ppm)

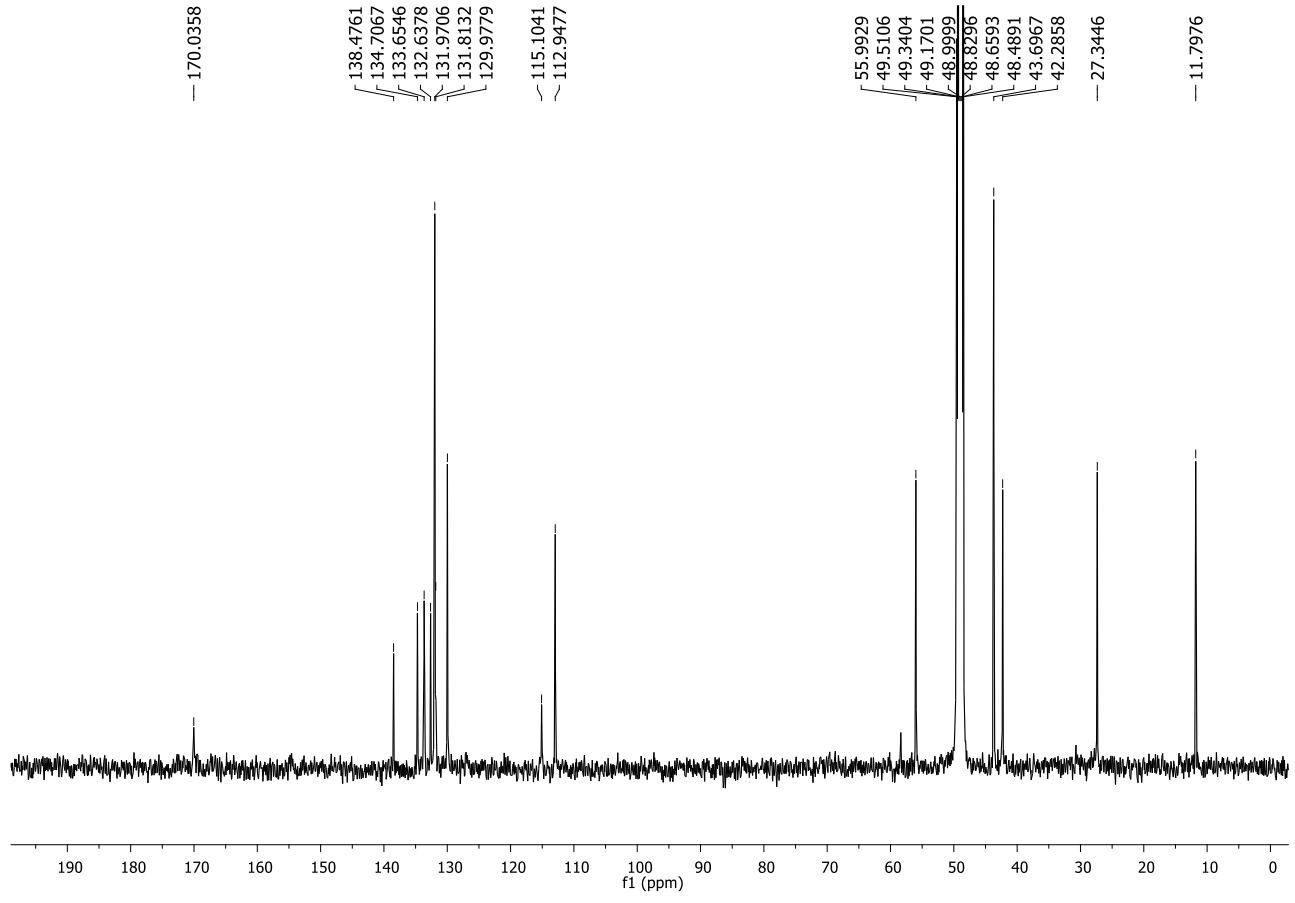
170.0358
138.4761
134.7067
133.6546
132.6378
131.9706
131.8132
129.9779
115.1041
112.9477
55.9929
49.5106
49.3404
49.1701
48.9999
48.8296
48.6593
48.4891
43.6967
42.2858
27.3446
11.7976
f1 (ppm)

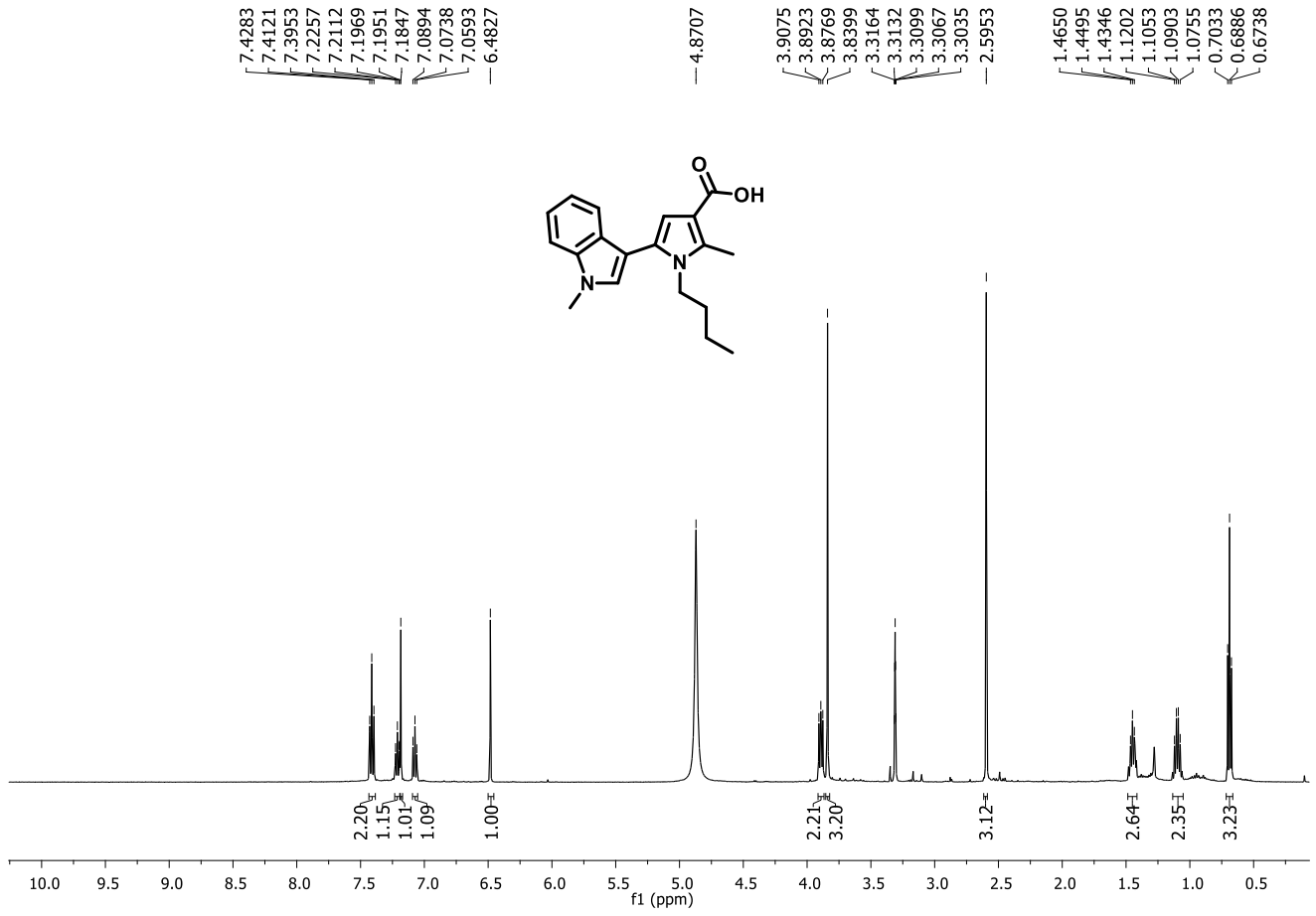
7.4283
7.4121
7.3953
7.2257
7.2112
7.1969
7.1951
7.1847
7.0894
7.0738
7.0593
6.4827
4.8707
3.9075
3.8923
3.8769
3.8399
3.3164
3.3132
3.3099
3.3067
3.3035
2.5953
1.4650
1.4495
1.4346
1.1202
1.1053
1.0903
1.0755
0.7033
0.6886
0.6738
O
OH
N
N
2.20
1.15
1.01
1.09
1.00
2.21
3.20
3.12
2.64
2.35
3.23
f1 (ppm)

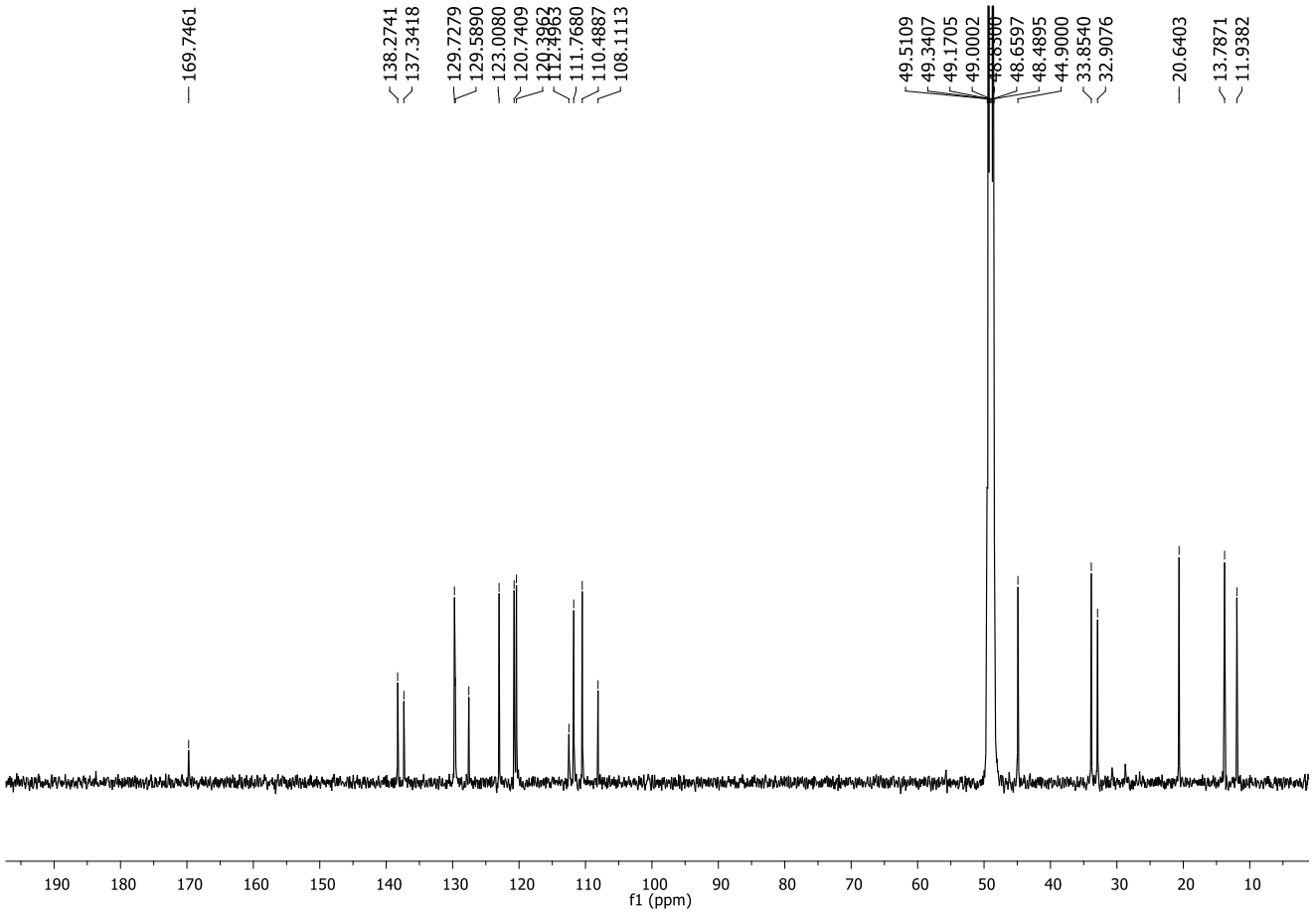
169.7461
138.2741
137.3418
129.7279
129.5890
123.0080
120.7409
111.7680
110.4887
108.1113
49.5109
49.3407
49.1705
49.0002
48.8300
48.6597
48.4895
44.9000
33.8540
32.9076
20.6403
13.7871
11.9382
f1 (ppm)

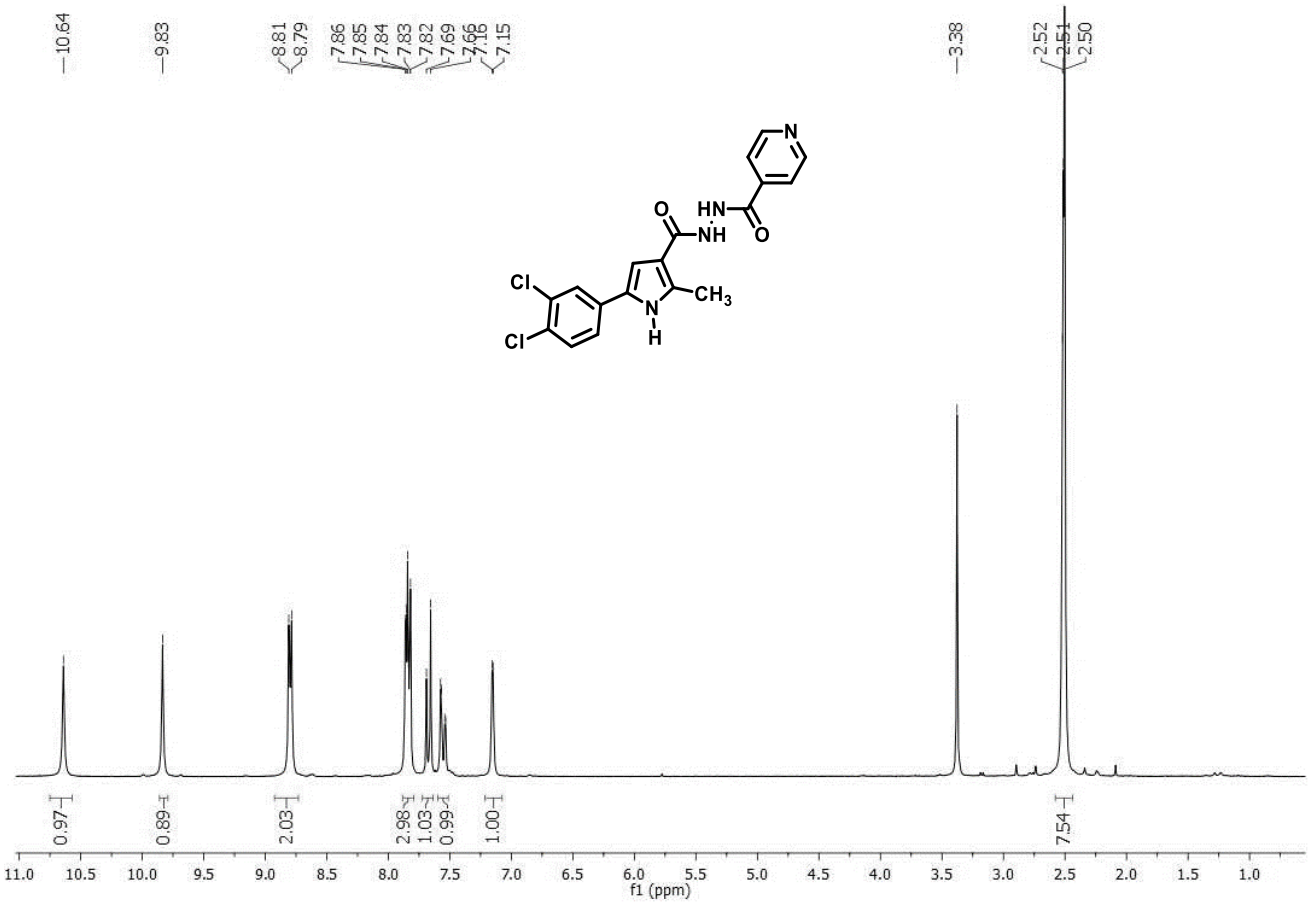
10.64
9.83
8.81
8.79
7.86
7.85
7.84
7.83
7.82
7.69
7.66
7.16
7.15
3.38
2.52
2.51
2.50
0.97
0.89
2.03
2.98
1.03
0.99
1.00
7.54
f1 (ppm)

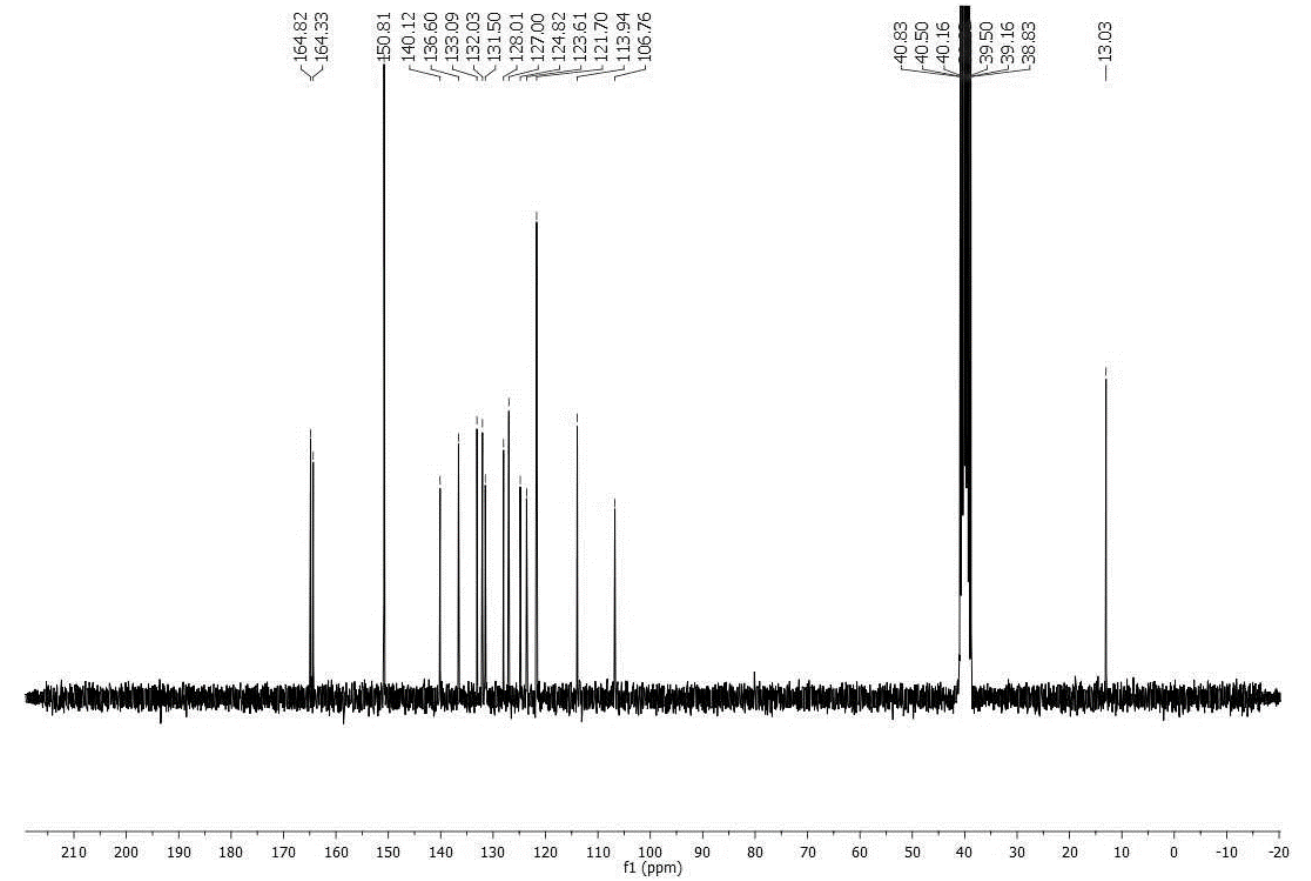
164.82
164.33
150.81
140.12
136.60
133.09
132.03
131.50
128.01
127.00
124.82
123.61
121.70
113.94
106.76
40.83
40.50
40.16
39.50
39.16
38.83
13.03
f1 (ppm)

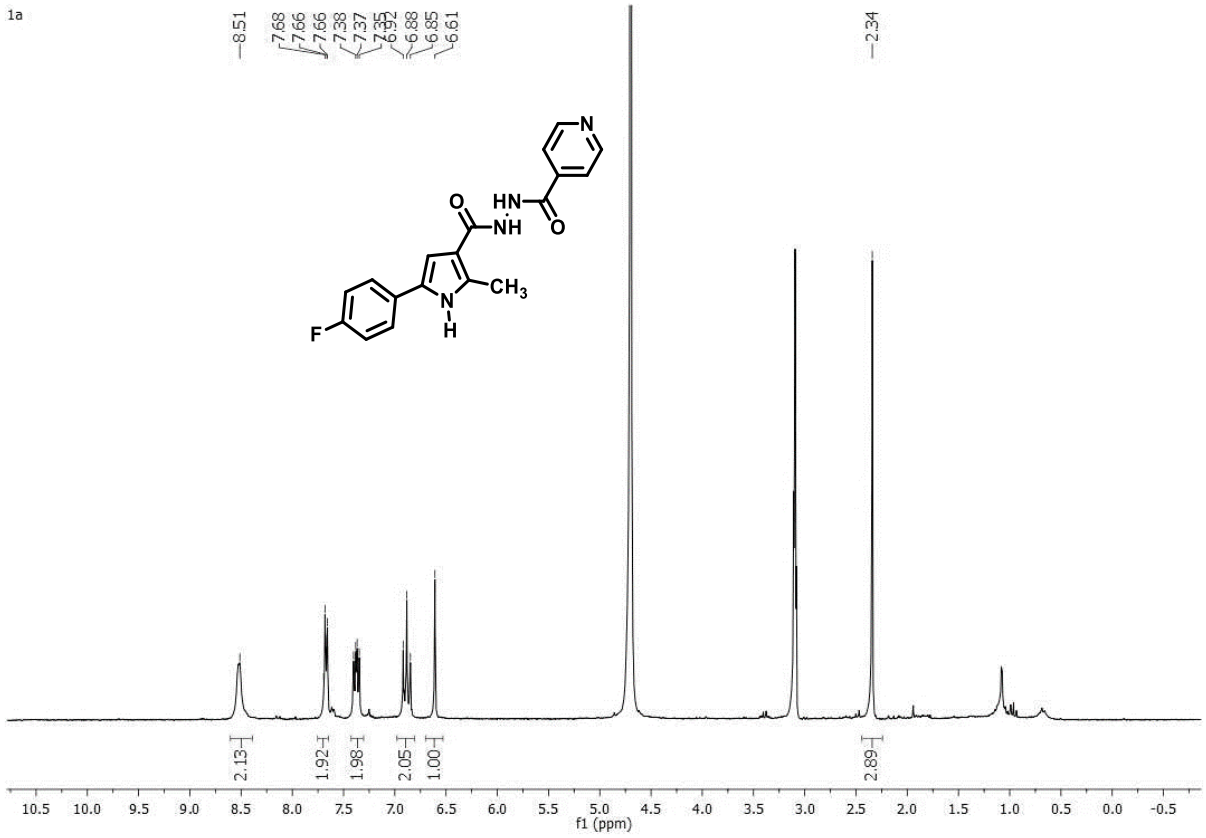
1a
8.51
7.68
7.66
7.66
7.38
7.37
7.35
6.92
6.88
6.85
6.61
2.34
2.13
1.92
1.98
2.05
1.00
2.89
f1 (ppm)

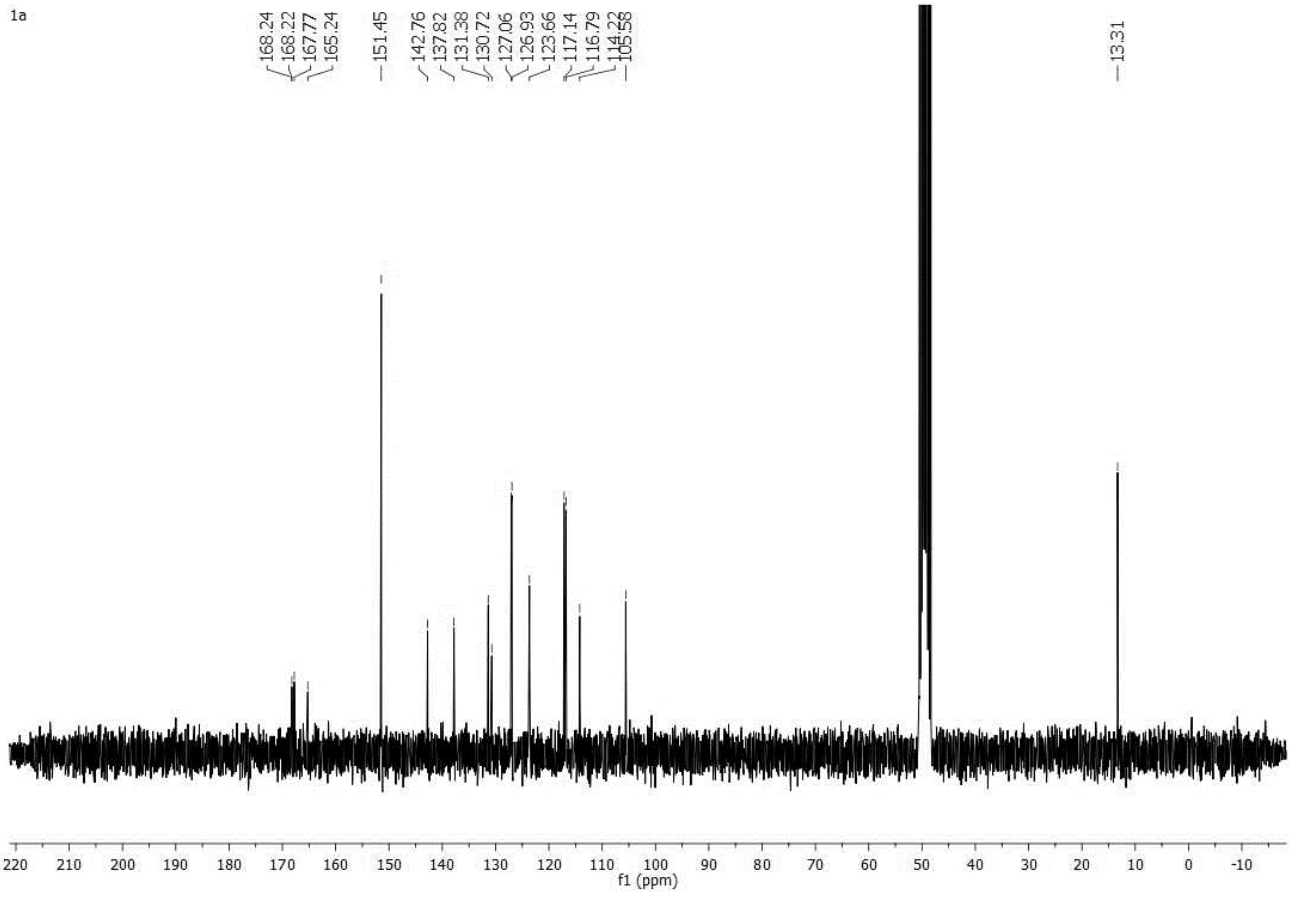
1a
168.24
168.22
167.77
165.24
151.45
142.76
137.82
131.38
130.72
127.06
126.93
123.66
117.14
116.79
114.22
105.58
13.31
f1 (ppm)

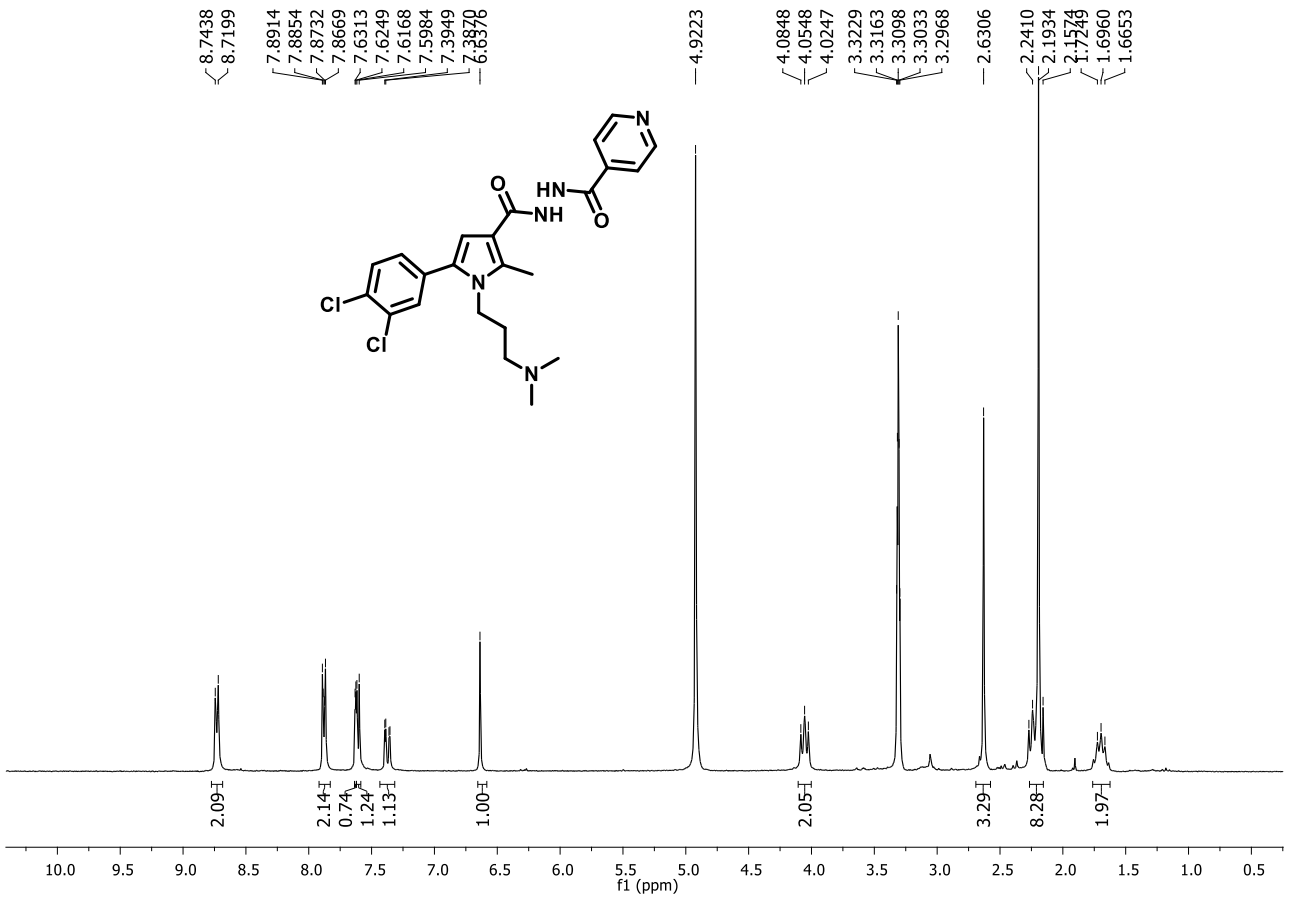
8.7438
8.7199
7.8914
7.8854
7.8732
7.8669
7.6313
7.6249
7.6168
7.5984
7.3949
6.8376
4.9223
4.0848
4.0548
4.0247
3.3229
3.3163
3.3098
3.3033
3.2968
2.6306
2.2410
2.1934
1.6960
1.6653
HN
NH
O
O
N
Cl
Cl
N
2.09
2.14
0.74
1.24
1.13
1.00
2.05
3.29
8.28
1.97
f1 (ppm)

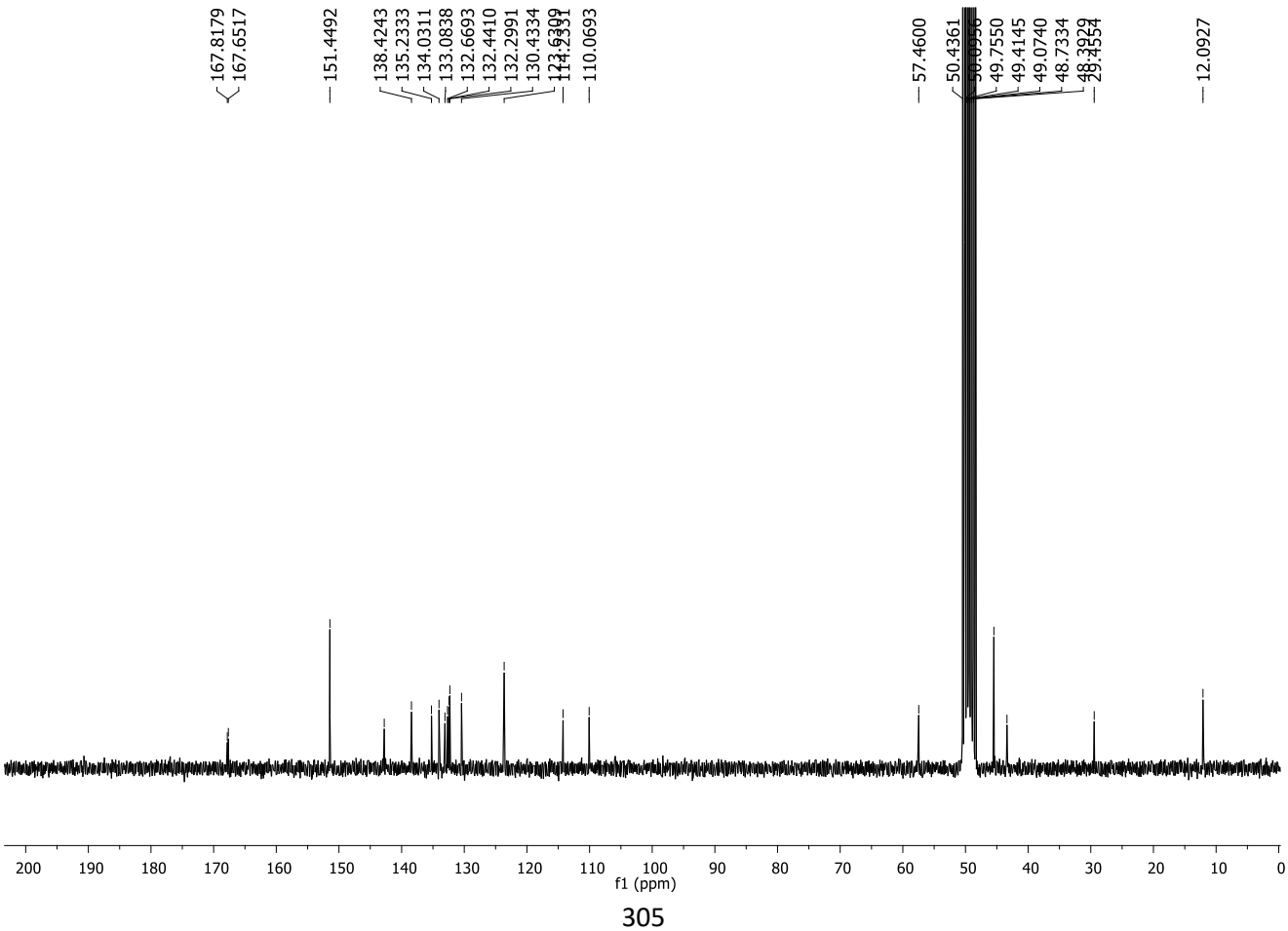
167.8179
167.6517
151.4492
138.4243
135.2333
134.0311
133.0838
132.6693
132.4410
132.2991
130.4334
110.0693
57.4600
50.4361
49.7550
49.4145
49.0740
48.7334
12.0927
f1 (ppm)

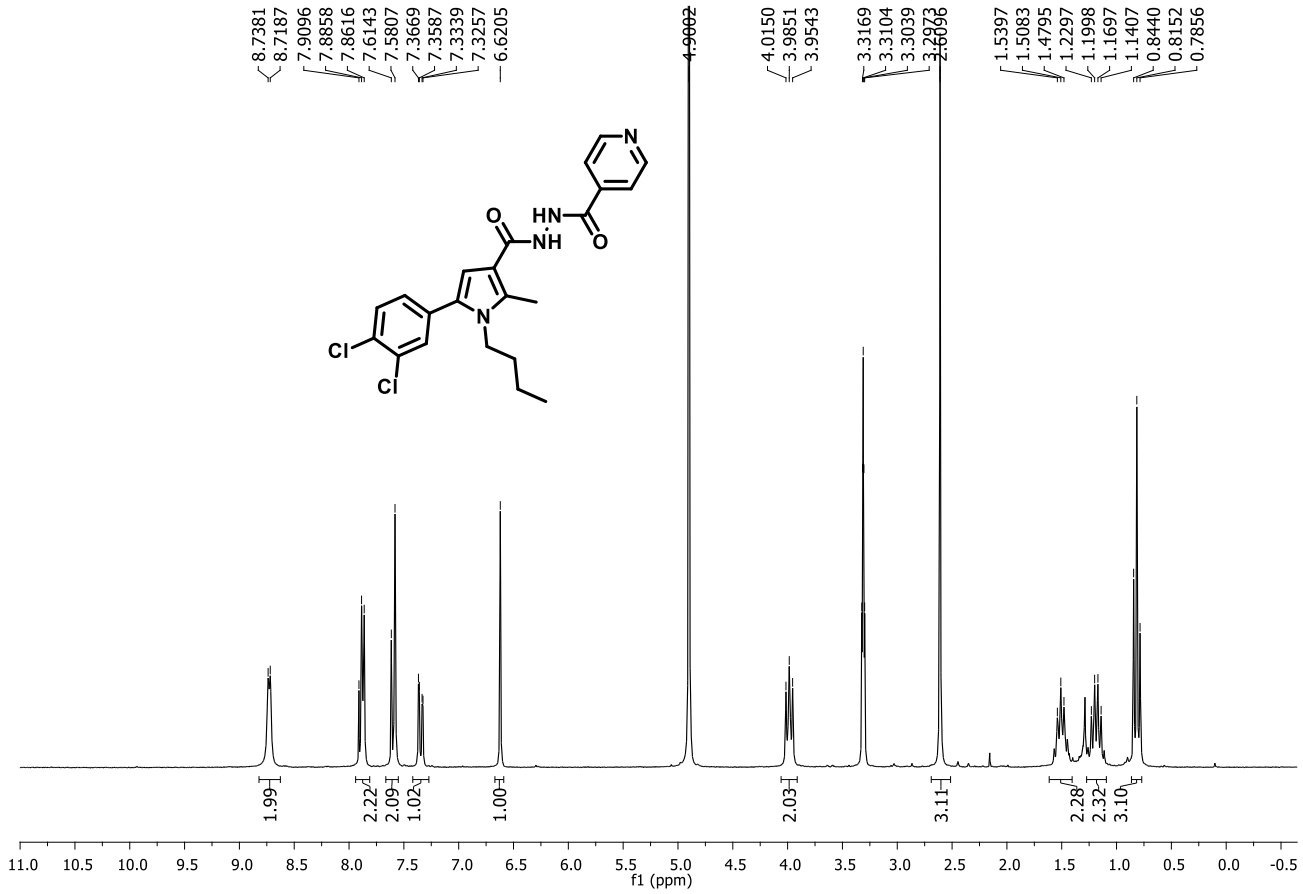
8.7381
8.7187
7.9096
7.8858
7.8616
7.6143
7.5807
7.3669
7.3587
7.3339
7.3257
6.6205
4.0002
4.0150
3.9851
3.9543
3.3169
3.3104
3.3039
3.2973
2.6036
1.5397
1.5083
1.4795
1.2297
1.1998
1.1697
1.1407
0.8440
0.8152
0.7856
1.99
2.22
2.09
1.02
1.00
2.03
3.11
2.28
2.32
3.10
f1 (ppm)

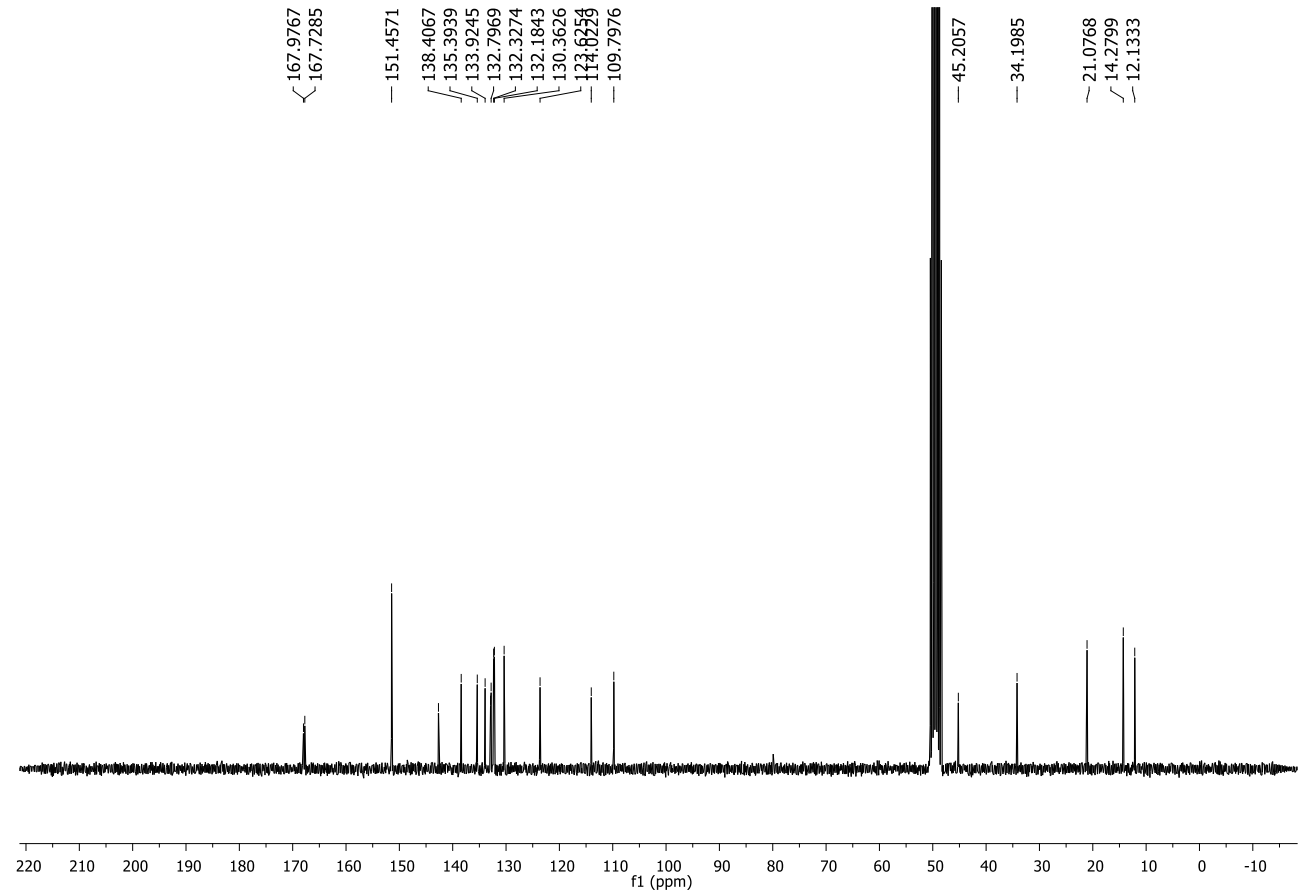
167.9767
167.7285
151.4571
138.4067
135.3939
133.9245
132.7969
132.3274
132.1843
130.3626
109.7976
45.2057
34.1985
21.0768
14.2799
12.1333
f1 (ppm)

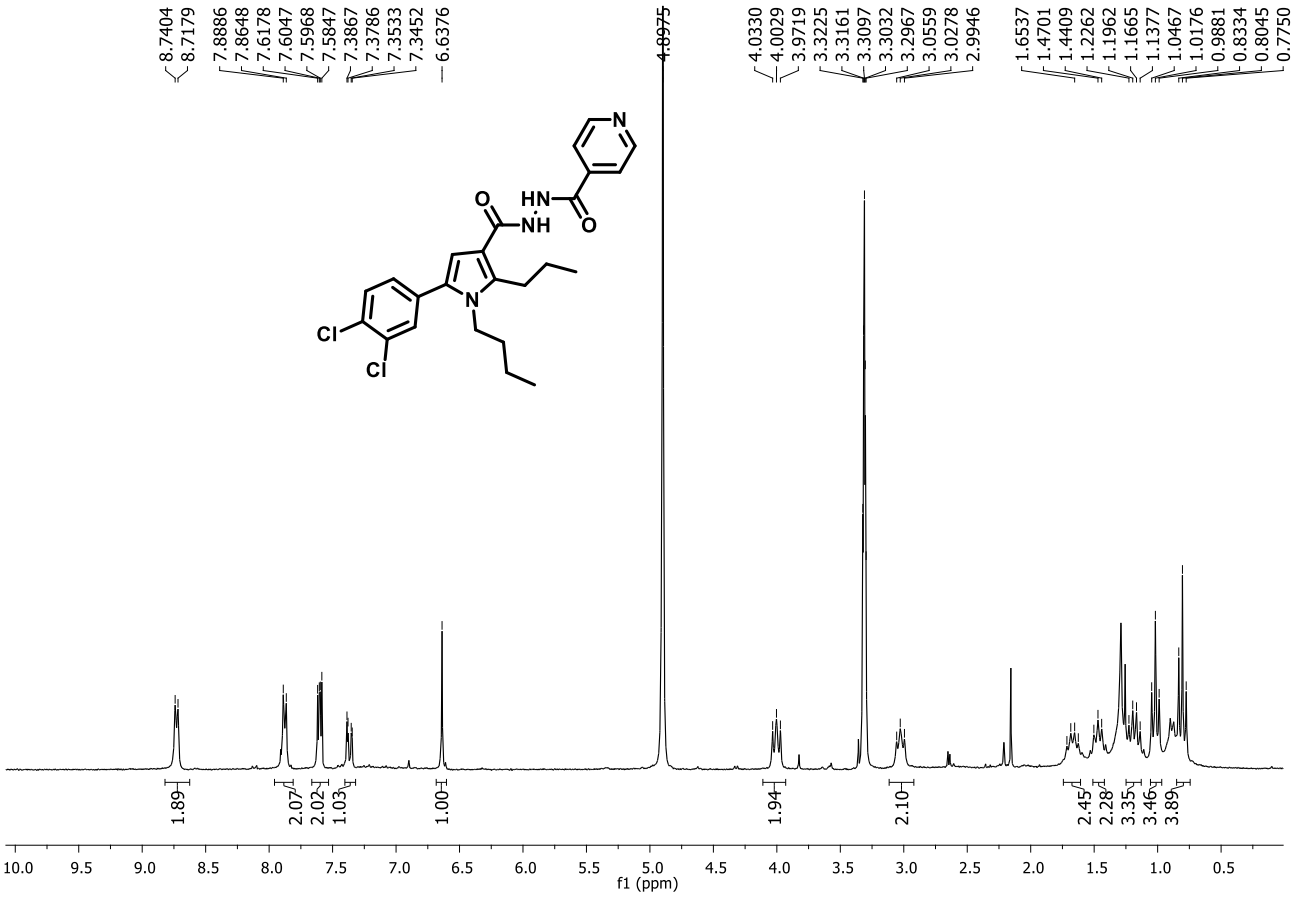
8.7404
8.7179
7.8886
7.8648
7.6178
7.6047
7.5968
7.5847
7.3867
7.3786
7.3533
7.3452
6.6376
4.8975
4.0330
4.0029
3.9719
3.3225
3.3161
3.3097
3.3032
3.2967
3.0559
3.0278
2.9946
1.6537
1.4701
1.4409
1.2262
1.1962
1.1665
1.1377
1.0467
1.0176
0.9881
0.8334
0.8045
0.7750
1.89
2.07
2.02
1.03
1.00
1.94
2.10
2.45
2.28
3.35
3.46
3.89
f1 (ppm)

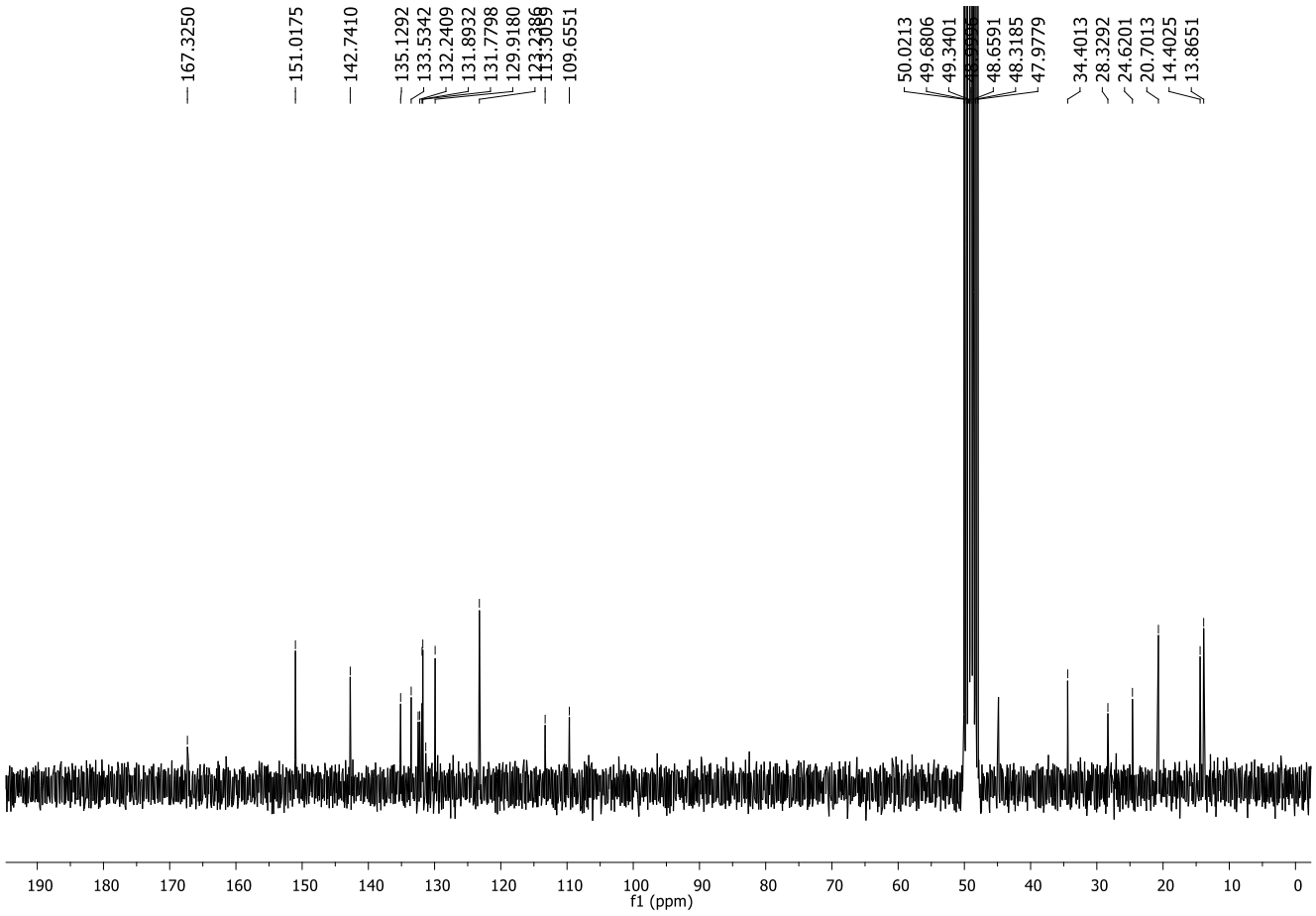
167.3250
151.0175
142.7410
135.1292
133.5342
132.2409
131.8932
131.7798
129.9180
109.6551
50.0213
49.6806
49.3401
48.6591
48.3185
47.9779
34.4013
28.3292
24.6201
20.7013
14.4025
13.8651
f1 (ppm)

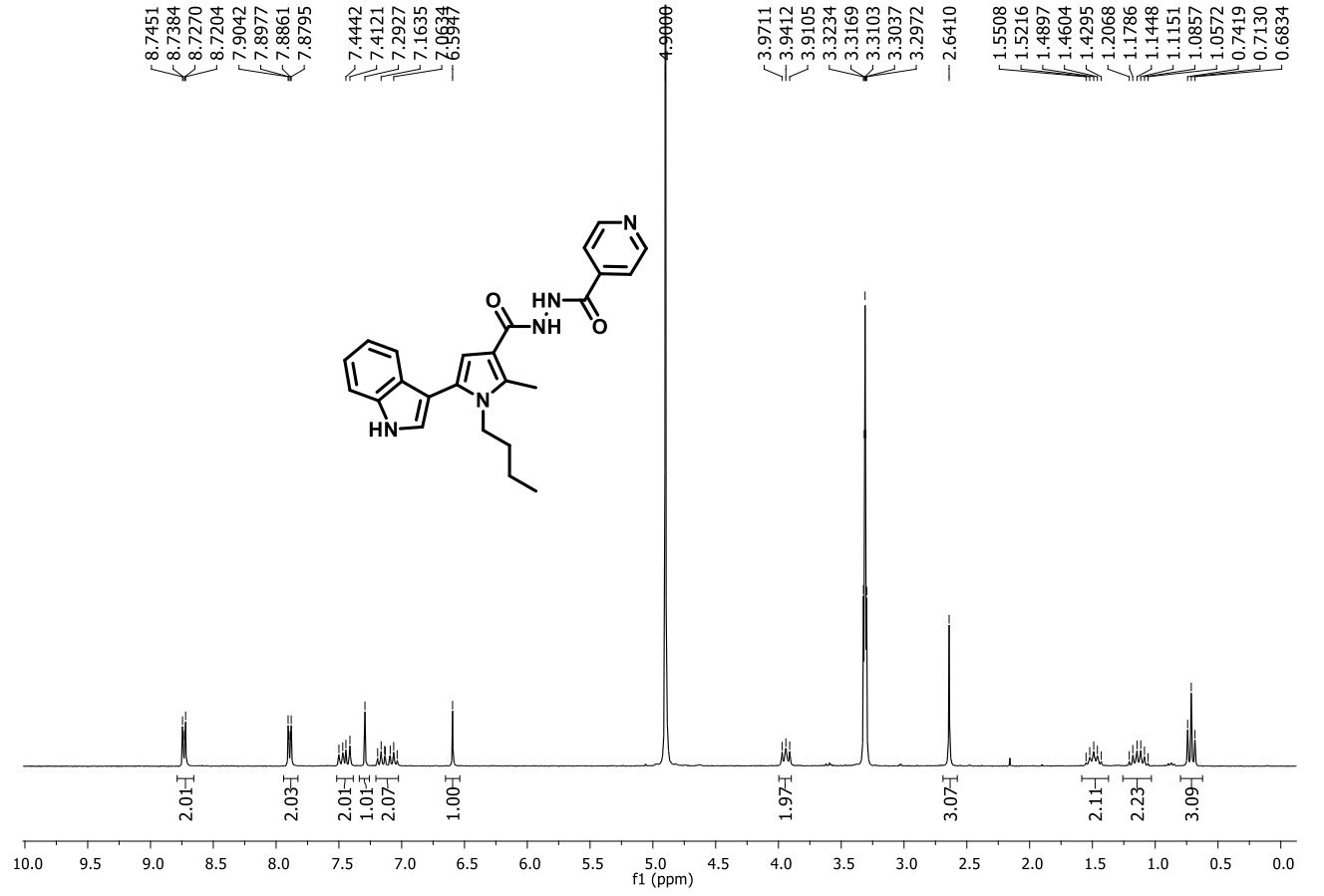
8.7451
8.7384
8.7270
8.7204
7.9042
7.8977
7.8861
7.8795
7.4442
7.4121
7.2927
7.1635
7.0634
6.9947
4.0000
3.9711
3.9412
3.9105
3.3234
3.3169
3.3103
3.3037
3.2972
2.6410
1.5508
1.5216
1.4897
1.4604
1.4295
1.2068
1.1786
1.1448
1.1151
1.0857
1.0572
0.7419
0.7130
0.6834
2.01
2.03
2.01
1.01
2.07
1.00
1.97
3.07
2.11
2.23
3.09
f1 (ppm)

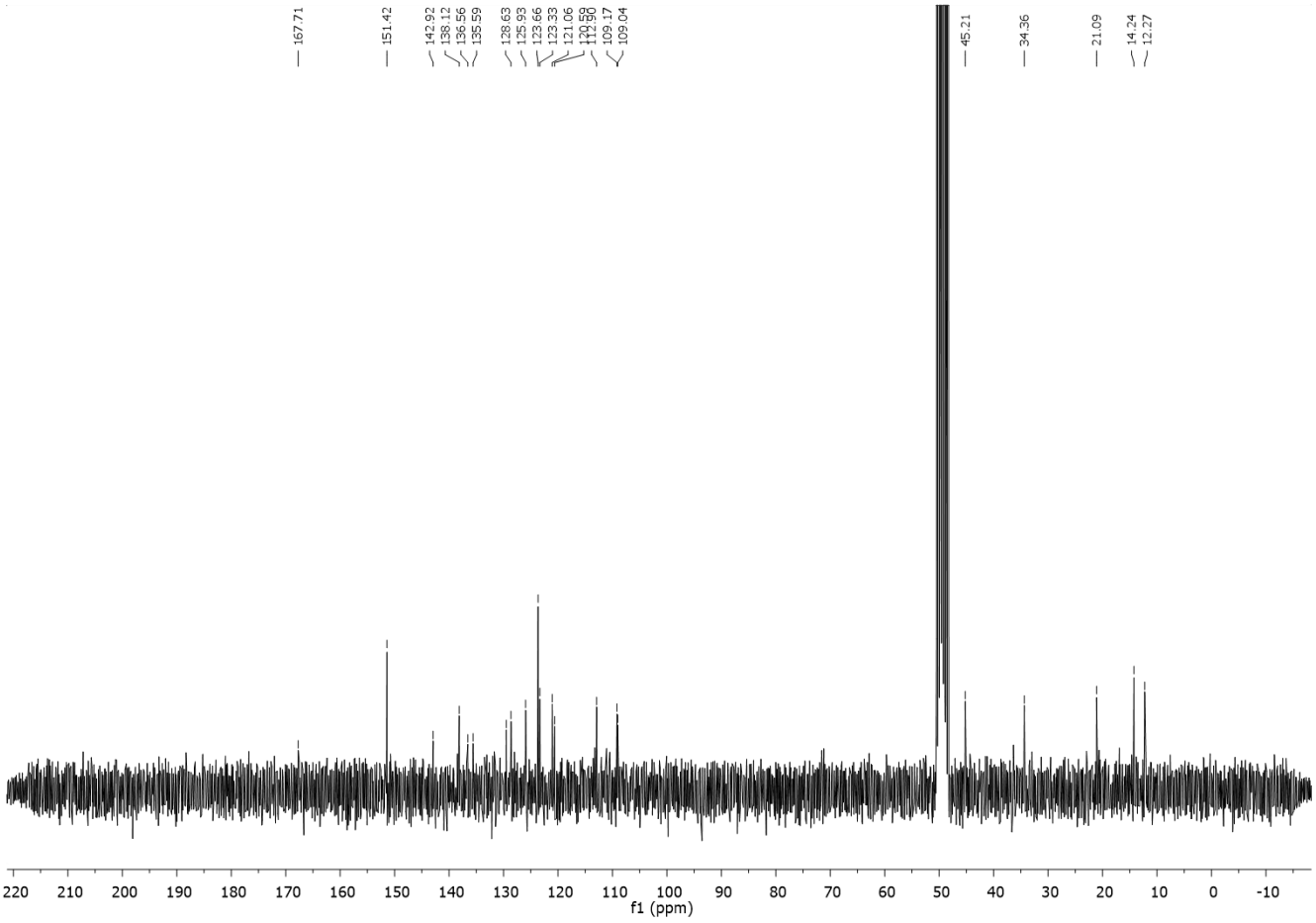
167.71
151.42
142.92
138.12
136.56
135.59
128.63
125.93
123.66
123.33
121.06
109.17
109.04
45.21
34.36
21.09
14.24
12.27
f1 (ppm)